CONJUNCTIVE MANAGEMENT OF SURFACE WATER AND GROUNDWATER RESOURCES

VOLUME I

A Dissertation Presented to
The Academic Faculty

By

Malek Abu Rumman

In Partial Fulfillment of the
Requirements for the Degree
Doctor of Philosophy in Civil Engineering

Georgia Institute of Technology
May 2005

CONJUNCTIVE MANAGEMENT OF SURFACE WATER AND GROUNDWATER RESOURCES

Approved by:

Dr. Aris Georgakakos, Advisor
School of Civil and Environmental Engineering
Georgia Institute of Technology

Dr. Alex Shapiro
School of Industrial Systems and Engineering
Georgia Institute of Technology

Dr. Philip Roberts
School of Civil and Environmental Engineering
Georgia Institute of Technology

Dr. Clifford Voss
Research Hydrologist
U.S. Geological Survey

Dr. Fotis Sotiropoulos
School of Civil and Environmental Engineering
Georgia Institute of Technology

Date Approved: 04/11/ 2005

Acknowledgements

I would like to extend my sincere thanks and appreciation to all those who have made this work possible. First, I express my gratitude to Dr. Aris Georgakakos, GWRI Director, for his advice and strong support throughout my time at Georgia Tech. His high research standards have been an excellent guide and an inspiration. In addition, I extend thanks to my colleagues at Georgia Tech. Their friendship and help have made my time and work here a positive and rewarding experience.

Special thanks are due to the United States Geological Survey for their financial support through a series of GWRI internships. The experience gained through my participation in various groundwater projects at USGS has been enriching. I also wish to thank my colleagues at USGS for their support and friendship.

I am most indebted to my family for their continuous encouragement during my years of study and research. My parents have been endlessly supportive, loving, and ever-patient. The love and dedication of my wife and daughter have been a constant source of support and inspiration.

Table of Contents

Acknowledgements iii

List of Tables viii

List of Figures x

Summary xxxi

Chapter 1. Introduction 1

Chapter 2. Literature Review 4

2.1 Introduction 4

2.2 Groundwater Management 5

2.3 Conjunctive Groundwater and Surface Water Management 15

2.4 Groundwater Modeling under Uncertainty 17

2.4.1 Geostatistical Approach 17

2.4.2 Other Statistical Approaches 29

2.5 Concluding Remarks on Literature Review 38

2.6 Conjunctive Management: Challenges and Issues To be Addressed 41

Chapter 3. Groundwater Modeling Under Uncertainty 42
3.1 Introduction 42
3.2 Deterministic Transfer Functions 43
3.2.1 Groundwater Simulation Model 43
3.2.2 Model Calibration 46
3.2.3 State Space Representation of Transfer Functions 48
3.2.4 Application 60
3.3 Parameter Uncertainty 65
3.3.1 Overview 65
3.3.2 Methodology 65
3.3.3 Application 69
3.3.3.1 Effect of Spatial Correlation, Global test and hydraulic head realizations 71
3.4 Effective Groundwater Parameters 74
3.4.1 Application 86
3.5 Mean Drawdown and Uncertainty Characterization 91
3.6 Regional Approximation of Drawdown Sequences 92
3.7 Application 99
3.7.1 Determination of Base Locations 99
3.7.2 Mean Drawdown and Uncertainty Characterization 106
3.8 Summary of Groundwater Drawdown Uncertainty Characterization 115
3.9 Conclusions 116

Chapter 4. Conjunctive Surface Water and Groundwater Management 118
4.1 Introduction 118
4.2 Conjunctive Water Resources Management: State Space Formulation 118
4.2.1 The Jordanian Water Resources System 119
4.2.1.1 Introduction 119
4.2.1.2 Surface Water Resources System 120
4.2.1.3 Groundwater System 130
4.2.2 Conjunctive Water Resources Management: Problem Formulation 134
4.2.2.1 System Dynamics 137
4.2.2.2 System Constraints 143
4.2.2.3 Objective Function (Performance Index) 144
4.3 Solution Approach: The Extended Linear Quadratic Gaussian (ELQG) 148
4.3.1 ELQG Control Method 149
4.3.2 Overview of the Conjunctive Management Procedure 150
4.4 Application to Jordan 151
4.4.1 Control Model Inputs and Outputs 152
4.4.2 Inflow and Boundary Condition Realizations 153
4.4.3 Case Study 160
4.5 Concluding Remarks 179

Chapter 5. Assessment Scenarios 180
5.1 Introduction 180
5.2 Scenario Definition 181
5.3 Scenario Assessment Criteria 191

5.4 Scenario Assessments 193

5.5 Conclusions and Recommendations 229

Chapter 6. Conclusions and Future Work Recommendations 232

Appendix A. State Space Representation of Transfer Functions with Different Coefficients Ratios 236

Appendix B. ELQG Control Method 243

Appendix C. The Analog ESP Forecast Model 248

Appendix D. Baseline Case 251

Appendix E. Scenario1: Existing conditions 266

Appendix F. Scenario2: Existing conditions+ Al Wehdah Dam 281

Appendix G. Scenario3: Syrian irrigation withdrawals 296

Appendix H. Scenario4: Residual flow to Dead Sea 325

Appendix I. Scenario5: M&I demands increase 354

Appendix J. Scenario6: Agricultural demands increase 383

Appendix K. Perfect forecast scenario 412

Appendix L. Non-conjunctive Management scenario 427

References 442

Vita 447

List of Tables

3.1 Perturbed groundwater parameters ranges. 72

3.2 Effective groundwater parameters at the monitoring locations. 104

5.2.1 Assessment Focus; Scenario1, existing conditions. 183

5.2.2 Assessment Focus; Scenario2, value of Al Wehdah Dam. 184

5.2.3 Assessment Focus; Scenario3, effect of Syrian irrigation Withdrawals. 185

5.2.4 Assessment Focus; Scenario4, residual flow to the Dead Sea. 187

5.2.5 Assessment Focus; Scenario5, M&I demands increase. 188

5.2.6 Assessment Focus; Scenario6, agricultural demands increase. 190

5.4.1 Baseline case, constrained and unconstrained GW drawdown Runs. 194

5.4.2a Existing conditions, constrained GW drawdown. 195

5.4.2b Existing conditions, unconstrained GW drawdown. 196

5.4.3a Existing conditions and WD, constrained GW drawdown. 200

5.4.3b Existing conditions and WD, unconstrained GW drawdown. 201

5.4.4a Syrian irrigation withdrawals, constrained GW drawdown. 204

5.4.4b Syrian irrigation withdrawals, unconstrained GW drawdown. 205

5.4.5a Dead Sea residual flow, constrained GW drawdown. 207

5.4.5b Dead Sea residual flow, unconstrained GW drawdown. 208

5.4.6a Municipal and industrial demands increase, constrained GW drawdown. 210

5.4.6b Municipal and industrial demands increase, unconstrained GW drawdown. 211

5.4.7a Agricultural demands increase, constrained GW drawdown. 214

5.4.7b Agricultural demands increase, unconstrained GW drawdown. 215

5.4.8a Perfect forecast scenario, constrained GW drawdown. 218

5.4.8b Perfect forecast scenario, unconstrained GW drawdown. 219

5.4.9a Non-conjunctive management scenario, constrained GW drawdown. 223

5.4.9b Non-conjunctive management scenario, unconstrained GW drawdown. 224

List of Figures

3.2.1.1 Amman-Wadi Sir aquifer. 44

3.2.1.2 Amman-Wadi Sir aquifer, finite difference scheme. 45

3.2.2.1 Amman-Wadi Sir aquifer, calibrated hydraulic conductivity and storage coefficients zones. 49

3.2.2.2 Amman-Wadi Sir aquifer, simulated and observed piezometric heads. 50-52

3.2.2.3 Amman-Wadi Sir aquifer,simulated and interpolated head at the no flow boundary clusters. 53

3.2.3.1 Groundwater transfer functions. 54

3.2.3.2a Transfer functions coefficients ratio. 57

3.2.3.2b Transfer functions coefficients ratio. 58

3.2.4.1 Groundwater transfer functions, application. 61

3.2.4.2 Groundwater transfer functions, pumping and boundary perturbations sequences. 62

3.2.4.3 Groundwater transfer functions, application of dynamical equation. 63-64

3.3.3.1 Calibrated groundwater model parameters. 70

3.3.3.1.1 Statistical procedure, null distribution 95% reliability level. 73

3.3.3.1.2 Statistical procedure, null distribution 80% reliability level. 75

3.3.3.1.3(a-c) Statistical procedure, head realizations 95% reliability level. 76-78

3.3.3.1.4(a-c) Statistical procedure, head realizations 80% reliability level. 79-81

3.4.1 Transfer functions realizations at the monitoring locations. 83

3.4.1.1 Effective groundwater parameters. 87

3.4.1.2a Effective parameters, estimated transfer functions and drawdown sequences. 88

3.4.1.2b Effective parameters, estimated transfer functions and drawdown sequences. 89

3.4.1.2c Effective parameters, estimated transfer functions and drawdown sequences. 90

3.5.1a Estimation of mean draw down. 93

3.5.1b Estimation of mean draw down. 94

3.5.2 Ensemble statistics. 95

3.7.1.1 Monitoring locations, and calibrated zones of groundwater parameters. 101

3.7.1.2 Transfer functions realizations at some monitoring locations. 102-103

3.7.1.3 Base locations selection. 105

3.7.2.1 Estimation of mean drawdown at base locations. 107

3.7.2.2 Estimation of mean drawdown at some monitoring locations. 108-109

3.7.2.3 Ensemble drawdown and ensemble statistics. 110-114

4.2.1.2.1 The Jordan-Yarmouk-Zarqa system. 121

4.2.1.2.2 Hydrographs of the Yarmouk River, Zarqa River, NJV Side Wadis and C/S JV Side Wadis. 124

4.2.1.2.3 System Layout and Water Demands. 127

4.2.1.2.4 Al Samra Effluent Flow (Jan1986- Sep 2000), And Al Baqa Effluent Flow (Jan 1994- Sep 2000). 131

4.2.1.3.1 Monthly Pumping From Mukheiba Wells. 133

4.2.2.1 System schematic. 135

4.4.2.1(a,b) Stream flow realizations. 154

4.4.2.2a Boundary clusters and monitoring locations. 156

4.4.2.2b Boundary perturbations. 157

4.4.2.3(a-c) Boundary perturbations realizations. 158-159

4.4.3.1(a-f) Mean storages and releases sequences. 161-163

4.4.3.2(a-d) WD and KTD storage realizations. 164-165

4.4.3.3(a-d) Cumulative deficits and releases at supply-demand nodes. 167-168

4.4.3.4(a-e) Mean GW drawdown and pumping sequences. 169-171

4.4.3.5(a-h) GW drawdown realizations at selected monitoring locations. 173-176

4.4.3.6 Disi Aquifer water transfer to Amman-Zarqa Area. 177

4.4.3.7(a-c) Energy realizations. 178

5.4.1a Non conjunctive management scenario, constrained GW draw down. 226

5.4.1b Non-conjunctive management scenario, unconstrained GW drawdown. 228

D.1 Assessment model, baseline case, constrained GW drawdown, WD, KTD, and KD storage and release sequences. 252

D.2 Assessment model, baseline case, constrained GW drawdown, AD, ZD, and KafD storage and release sequences. 253

D.3 Assessment model, baseline case, constrained GW drawdown, monthly water deficit and release sequences at Adasiya and North Jordan Valley nodes. 254

D.4 Assessment model, baseline case, constrained GW drawdown, monthly water deficit and release sequences at Amman-Zarqa and C/S Jordan Valley nodes. 255

D.5 Assessment model, baseline case, constrained GW drawdown monthly pumping, draw down and Disi transfer sequences. 256

D.6 Assessment model, baseline case, constrained GW drawdown, WD, KTD and pumping energy sequences. 257

D.7 Assessment model, baseline case, constrained GW drawdown, annual deficits, storages, and draw downs frequency curves. 258

D.8 Assessment model, baseline case, unconstrained GW drawdown, WD, KTD, and KD storage and release sequences. 259

D.9 Assessment model, baseline case, unconstrained GW drawdown, AD, ZD, and KafD storage and release sequences. 260

D.10 Assessment model, baseline case, unconstrained GW drawdown, monthly water deficit and release sequences at Adasiya and North Jordan Valley nodes. 261

D.11 Assessment model, baseline case, unconstrained GW drawdown, monthly water deficit and release sequences at Amman-Zarqa and C/S Jordan Valley nodes. 262

D.12 Assessment model, baseline case, unconstrained GW drawdown, monthly pumping, drawdown and Disi transfer sequences. 263

D.13 Assessment model, baseline case, unconstrained GW drawdown , WD, KTD and pumping energy sequences. 264

D.14 Assessment model, baseline case, unconstrained GW drawdown, annual deficits, storages, and draw downs frequency curves. 265

E.1 Assessment model, scenario1, constrained GW drawdown , WD, KTD, and KD storage and release sequences. 267

E.2 Assessment model, scenario1, constrained GW drawdown, AD, ZD, and KafD storage and release sequences. 268

E.3 Assessment model, scenario1, constrained GW drawdown , monthly water deficit and release sequences at Adasiya and North Jordan Valley nodes. 269

E.4 Assessment model, scenario1, constrained GW drawdown, monthly water deficit and release sequences at Amman-Zarqa and C/S Jordan Valley nodes. 270

E.5 Assessment model, scenario1, constrained GW drawdown, monthly pumping, draw down and Disi transfer sequences. 271

E.6 Assessment model, scenario1, constrained GW drawdown ,WD, KTD and pumping energy sequences. 272

E.7 Assessment model, scenario1, constrained GW drawdown, annual deficits, storages, and drawdowns frequency curves. 273

E.8 Assessment model, scenario1, unconstrained GW drawdown , WD, KTD, and KD storage and release sequences. 274

E.9 Assessment model, scenario1, unconstrained GW drawdown, AD, ZD, and KafD storage and release sequences. 275

E.10 Assessment model, scenario1, unconstrained GW drawdown , monthly water deficit and release sequences at Adasiya and North Jordan Valley nodes. 276

E.11 Assessment model, scenario1, unconstrained GW drawdown, monthly water deficit and release sequences at Amman-Zarqa and C/S Jordan Valley nodes. 277

E.12 Assessment model, scenario1, unconstrained GW drawdown, monthly pumping, drawdown and Disi transfer sequences. 278

E.13 Assessment model, scenario1, unconstrained GW drawdown , WD, KTD and pumping energy sequences. 279

E.14 Assessment model, scenario1, unconstrained GW drawdown, annual deficits, storages, and drawdowns frequency curves. 280

F.1 Assessment model, scenario2, constrained GW drawdown, WD, KTD, and KD storage and release sequences. 282

F.2 Assessment model, scenario2, constrained GW drawdown, AD, ZD, and KafD storage and release sequences. 283

F.3 Assessment model, scenario2, constrained GW drawdown, monthly water deficit and release sequences at Adasiya and North Jordan Valley nodes. 284

F.4 Assessment model, scenario2, constrained GW drawdown , monthly water deficit and release sequences at Amman-Zarqa and C/S Jordan Valley nodes. 285

F.5 Assessment model, scenario2, constrained GW drawdown, monthly pumping, drawdown and Disi transfer sequences. 286

F.6 Assessment model, scenario2, constrained GW drawdown , WD, KTD and pumping energy sequences. 287

F.7 Assessment model, scenario2, constrained GW drawdown, annual deficits, storages, and drawdowns frequency curves. 288

F.8 Assessment model, scenario2, unconstrained GW drawdown, WD, KTD, and KD storage and release sequences. 289

F.9 Assessment model,scenario2, unconstrained GW drawdown, AD, ZD,and KafD storage and release sequences. 290

F.10 Assessment model, scenario2, unconstrained GW drawdown, monthly water deficit and release sequences at Adasiya and North Jordan Valley nodes. 291

F.11 Assessment model, scenario2, unconstrained GW drawdown, monthly water deficit and release sequences at Amman-Zarqa and C/S Jordan Valley nodes. 292

F.12 Assessment model, scenario2, unconstrained GW drawdown, monthly pumping, drawdown and Disi transfer sequences. 293

F.13 Assessment model, scenario2, unconstrained GW drawdown , WD, KTD and pumping energy sequences. 294

F.14 Assessment model, scenario2, unconstrained GW drawdown, annual deficits, storages, and drawdowns frequency curves. 295

G.1 Assessment model, scenario3, Syrian withdrawals 20%, constrained GW drawdown, WD, KTD, and KD storage and release sequences. 297

G.2 Assessment model, scenario3, Syrian withdrawals 20%, constrained GW drawdown, AD, ZD, and KafD storage and release sequences. 298

G.3 Assessment model, scenario3, Syrian withdrawals 20%, constrained GW drawdown, monthly water deficit and release sequences at Adasiya and North Jordan Valley nodes. 299

G.4 Assessment model, scenario3, Syrian withdrawals 20%, constrained GW drawdown, monthly water deficit and release sequences at Amman-Zarqa and C/S Jordan Valley nodes. 300

G.5 Assessment model, scenario3, Syrian withdrawals 20%, constrained GW drawdown, monthly pumping, drawdown and Disi transfer sequences. 301

G.6 Assessment model,scenario3,Syrian withdrawals 20%,constrained GW drawdown, WD, KTD and pumping energy sequences. 302

G.7 Assessment model, scenario3, Syrian withdrawals 20%, constrained GW drawdown, annual deficits, storages, and drawdowns frequency curves. 303

G.8 Assessment model, scenario3, Syrian withdrawals 30%, constrained GW drawdown, WD, KTD, and KD storage and release sequences. 304

G.9 Assessment model, scenario3, Syrian withdrawals 30%, constrained GW drawdown, AD, ZD, and KafD storage and release sequences. 305

G.10 Assessment model, scenario3, Syrian withdrawals 30%, constrained GW drawdown, monthly water deficit and release sequences at Adasiya and North Jordan Valley nodes. 306

G.11 Assessment model, scenario3, Syrian withdrawals 30%, constrained GW drawdown, monthly water deficit and release sequences at Amman-Zarqa and C/S Jordan Valley nodes. 307

G.12 Assessment model, scenario3, Syrian withdrawals 30%, constrained GW draw down, monthly pumping, drawdown and Disi transfer sequences. 308

G.13 Assessment model, scenario3, Syrian withdrawals 30%, constrained GW draw down, WD, KTD and pumping energy sequences. 309

G.14 Assessment model, scenario3, Syrian withdrawals 30%, constrained GW drawdown, annual deficits, storages, and drawdowns frequency curves. 310

G.15 Assessment model, scenario3, Syrian withdrawals 20%, unconstrained GW drawdown, WD, KTD, and KD storage and release sequences. 311

G.16 Assessment model, scenario3, Syrian withdrawals 20%, unconstrained GW drawdown, AD, ZD, and KafD storage and release sequences. 312

G.17 Assessment model, scenario3, Syrian withdrawals 20%, unconstrained GW drawdown, monthly water deficit and release sequences at Adasiya and North Jordan Valley nodes. 313

G.18 Assessment model, scenario3, Syrian withdrawals 20%, unconstrained GW drawdown, monthly water deficit and release sequences at Amman-Zarqa and C/S Jordan Valley nodes. 314

G.19 Assessment model, scenario3, Syrian withdrawals 20%, unconstrained GW drawdown, monthly pumping, drawdown and Disi transfer sequences. 315

G.20 Assessment model, scenario3, Syrian withdrawals 20%, unconstrained GW drawdown, WD, KTD and pumping energy sequences. 316

G.21 Assessment model, scenario3, Syrian withdrawals 20%, unconstrained GW drawdown, annual deficits, storages, and drawdowns frequency curves. 317

G.22 Assessment model, scenario3, Syrian withdrawals 30%, unconstrained GW drawdown, WD, KTD, and KD storage and release sequences. 318

G.23 Assessment model, scenario3, Syrian withdrawals 30%, unconstrained GW drawdown, AD, ZD, and KafD storage and release sequences. 319

G.24 Assessment model, scenario3, Syrian withdrawals 30%, unconstrained GW drawdown, monthly water deficit and release sequences at Adasiya and North Jordan Valley nodes. 320

G.25 Assessment model, scenario3, Syrian withdrawals 30%, unconstrained GW drawdown, monthly water deficit and release sequences at Amman-Zarqa and C/S Jordan Valley nodes. 321

G.26 Assessment model, scenario3, Syrian withdrawals 30%, unconstrained GW drawdown, monthly pumping, drawdown and Disi transfer sequences. 322

G.27 Assessment model, scenario3, Syrian withdrawals 30%, unconstrained GW drawdown, WD, KTD and pumping energy sequences. 323

G.28 Assessment model, scenario3, Syrian withdrawals 30%, unconstrained GW drawdown, annual deficits, storages, and drawdowns frequency curves. 324

H.1 Assessment model, scenario4, residual flow to Dead Sea 5%, constrained GW draw down, WD, KTD, and KD storage and release sequences. 326

H.2 Assessment model, scenario4, residual flow to Dead Sea 5%, constrained GW draw down, AD, ZD, and KafD storage and release sequences. 327

H.3 Assessment model, scenario4, residual flow to Dead Sea 5%, constrained GW drawdown, monthly water deficit and release sequences at Adasiya and North Jordan Valley nodes. 328

H.4 Assessment model, scenario4, residual flow to Dead Sea 5%, constrained GW drawdown, monthly water deficit and release sequences at Amman-Zarqa and C/S Jordan Valley nodes. 329

H.5 Assessment model, scenario4, residual flow to Dead Sea 5%, constrained GW drawdown, monthly pumping, drawdown and Disi transfer sequences. 330

H.6 Assessment model, scenario4, residual flow to Dead Sea 5%, constrained GW drawdown, WD, KTD and pumping energy sequences. 331

H.7 Assessment model, scenario4, residual flow to Dead Sea 5%, constrained GW drawdown, annual deficits, storages, and drawdowns frequency curves. 332

H.8 Assessment model, scenario4, residual flow to Dead Sea 10%, constrained GW drawdown, WD, KTD, and KD storage and release sequences. 333

H.9 Assessment model, scenario4, residual flow to Dead Sea 10%, constrained GW drawdown, AD, ZD, and KafD storage and release sequences. 334

H.10 Assessment model, scenario4, residual flow to Dead Sea 10%, constrained GW drawdown, monthly water deficit and release sequences at Adasiya and North Jordan Valley nodes. 335

H.11 Assessment model, scenario4, residual flow to Dead Sea 10%, constrained GW drawdown, monthly water deficit and release sequences at Amman-Zarqa and C/S Jordan Valley nodes. 336

H.12 Assessment model, scenario4, residual flow to Dead Sea 10%, constrained GW drawdown, monthly pumping, drawdown and Disi transfer sequences. 337

H.13 Assessment model, scenario4, residual flow to Dead Sea 10%, constrained GW drawdown, WD, KTD and pumping energy sequences. 338

H.14 Assessment model, scenario4, residual flow to Dead Sea 10%, constrained GW drawdown, annual deficits, storages, and drawdowns frequency curves. 339

H.15 Assessment model, scenario4, residual flow to Dead Sea 5%, unconstrained GW drawdown, WD, KTD, and KD storage and release sequences. 340

H.16 Assessment model, scenario4, residual flow to Dead Sea 5%, unconstrained GW draw down, AD, ZD, and KafD storage and release sequences. 341

H.17 Assessment model, scenario4, residual flow to Dead Sea 5%, unconstrained GW drawdown, monthly water deficit and release sequences at Adasiya and North Jordan Valley nodes. 342

H.18 Assessment model, scenario4, residual flow to Dead Sea 5%, unconstrained GW drawdown, monthly water deficit and release sequences at Amman-Zarqa and C/S Jordan Valley nodes. 343

H.19 Assessment model, scenario4, residual flow to Dead Sea 5%, unconstrained GW drawdown, monthly pumping, drawdown and Disi transfer sequences. 344

H.20 Assessment model, scenario4, residual flow to Dead Sea 5%, unconstrained GW drawdown, WD, KTD and pumping energy sequences. 345

H.21 Assessment model, scenario4, residual flow to Dead Sea 5%, unconstrained GW drawdown, annual deficits, storages, and drawdowns frequency curves. 346

H.22 Assessment model, scenario4, residual flow to Dead Sea 10%, unconstrained GW drawdown, WD, KTD, and KD storage and release sequences. 347

H.23 Assessment model, scenario4, residual flow to Dead Sea 10%, unconstrained GW drawdown, AD, ZD, and KafD storage and release sequences. 348

H.24 Assessment model, scenario4, residual flow to Dead Sea 10%, unconstrained GW drawdown, monthly water deficit and release sequences at Adasiya and North Jordan Valley nodes. 349

H.25 Assessment model, scenario4, residual flow to Dead Sea 10%, unconstrained GW drawdown, monthly water deficit and release sequences at Amman-Zarqa and C/S Jordan Valley nodes. 350

H.26 Assessment model, scenario4, residual flow to Dead Sea 10%, unconstrained GW drawdown, monthly pumping, drawdown and Disi transfer sequences. 351

H.27 Assessment model, scenario4, residual flow to Dead Sea 10%, unconstrained GW drawdown, WD, KTD and pumping energy sequences. 352

H.28 Assessment model, scenario4, residual flow to Dead Sea 10%, unconstrained GW drawdown, annual deficits, storages, and drawdowns frequency curves. 353

I.1 Assessment model, scenario5, M&I demand increase 10%, constrained GW drawdown, WD, KTD, and KD storage and release sequences. 355

I.2 Assessment model, scenario5, M&I demand increase 10%, constrained GW drawdown, AD, ZD, and KafD storage and release sequences. 356

I.3 Assessment model, scenario5, M&I demand increase 10%, constrained GW drawdown, monthly water deficit and release sequences at Adasiya and North Jordan Valley nodes. 357

I.4 Assessment model, scenario5, M&I demand increase 10%, constrained GW drawdown, monthly water deficit and release sequences at Amman-Zarqa and C/S Jordan Valley nodes. 358

I.5 Assessment model, scenario5, M&I demand increase 10%, constrained GW drawdown, monthly pumping, drawdown and Disi transfer sequences. 359

I.6 Assessment model, scenario5, M&I demand increase 10%, constrained GW drawdown, WD, KTD and pumping energy sequences. 360

I.7 Assessment model, scenario5, M&I demand increase 10%, constrained GW drawdown, annual deficits, storages, and drawdowns frequency curves. 361

I.8 Assessment model, scenario5, M&I demand increase 20%, constrained GW drawdown, WD, KTD, and KD storage and release sequences. 362

I.9 Assessment model, scenario5, M&I demand increase 20%, constrained GW drawdown, AD, ZD, and KafD storage and release sequences. 363

I.10 Assessment model, scenario5, M&I demand increase 20%, constrained GW drawdown, monthly water deficit and release sequences at Adasiya and North Jordan Valley nodes. 364

I.11 Assessment model, scenario5, M&I demand increase 20%, constrained GW drawdown, monthly water deficit and release sequences at Amman-Zarqa and C/S Jordan Valley nodes. 365

I.12 Assessment model, scenario5, M&I demand increase 20%, constrained GW drawdown, monthly pumping, drawdown and Disi transfer sequences. 366

I.13 Assessment model, scenario5, M&I demand increase 20%, constrained GW drawdown, WD, KTD and pumping energy sequences. 367

I.14 Assessment model, scenario5, M&I demand increase 20%, constrained GW drawdown, annual deficits, storages, and drawdowns frequency curves. 368

I.15 Assessment model, scenario5, M&I demand increase 10%, unconstrained GW drawdown, WD, KTD, and KD storage and release sequences. 369

I.16 Assessment model, scenario5, M&I demand increase 10%, unconstrained GW drawdown, AD, ZD, and KafD storage and release sequences. 370

I.17 Assessment model, scenario5, M&I demand increase 10%, unconstrained GW drawdown, monthly water deficit and release sequences at Adasiya and North Jordan Valley nodes. 371

I.18 Assessment model, scenario5, M&I demand increase 10%, unconstrained GW drawdown, monthly water deficit and release sequences at Amman-Zarqa and C/S Jordan Valley nodes. 372

I.19 Assessment model, scenario5, M&I demand increase 10%, unconstrained GW drawdown, monthly pumping, drawdown and Disi transfer sequences. 373

I.20 Assessment model, scenario5,M&I demand increase 10%, unconstrained GW drawdown, WD, KTD and pumping energy sequences. 374

I.21 Assessment model, scenario5, M&I demand increase 10%, unconstrained GW drawdown, annual deficits, storages, and drawdowns frequency curves. 375

I.22 Assessment model, scenario5, M&I demand increase 20%, unconstrained GW drawdown, WD, KTD, and KD storage and release sequences. 376

I.23 Assessment model, scenario5, M&I demand increase 20%, unconstrained GW drawdown, AD, ZD, and KafD storage and release sequences. 377

I.24 Assessment model, scenario5, M&I demand increase 20%, unconstrained GW drawdown, monthly water deficit and release sequences at Adasiya and North Jordan Valley nodes. 378

I.25 Assessment model, scenario5, M&I demand increase 20%, unconstrained GW drawdown,monthly water deficit and release sequences at Amman-Zarqa and C/S Jordan Valley nodes. 379

I.26 Assessment model, scenario5, M&I demand increase 20%, unconstrained GW drawdown, monthly pumping, drawdown and Disi transfer sequences. 380

I.27 Assessment model, scenario5, M&I demand increase 20%, unconstrained GW drawdown, WD, KTD and pumping energy sequences. 381

I.28 Assessment model, scenario5, M&I demand increase 20%, unconstrained GW drawdown, annual deficits, storages, and drawdowns frequency curves. 382

J.1 Assessment model, scenario6, agricultural demand increase 10%, constrained GW drawdown, WD, KTD, and KD storage and release sequences. 382

J.2 Assessment model, scenario6, agricultural demand increase 10%, constrained GW drawdown, AD, ZD, and KafD storage and release sequences. 384

J.3 Assessment model, scenario6, agricultural demand increase 10%, constrained GW drawdown, monthly water deficit and release sequences at Adasiya and North Jordan Valley nodes. 386

J.4 Assessment model, scenario6, agricultural demand increase 10%, constrained GW drawdown, monthly water deficit and release sequences at Amman-Zarqa and C/S Jordan Valley nodes. 387

J.5 Assessment model, scenario6, agricultural demand increase 10%, constrained GW drawdown, monthly pumping, drawdown and Disi transfer sequences. 388

J.6 Assessment model, scenario6, agricultural demand increase 10%, constrained GW drawdown, WD, KTD and pumping energy sequences. 389

J.7 Assessment model, scenario6, agricultural demand increase 10%, constrained GW drawdown, annual deficits, storages, and drawdowns frequency curves. 390

J.8 Assessment model, scenario6, agricultural demand increase 20%, constrained GW drawdown, WD, KTD, and KD storage and release sequences. 391

J.9 Assessment model, scenario6, agricultural demand increase 20%, constrained GW drawdown, AD, ZD, and KafD storage and release sequences. 392

J.10 Assessment model, scenario6,agricultural demand increase 20%, constrained GW drawdown, monthly water deficit and release sequences at Adasiya and North Jordan Valley nodes. 393

J.11 Assessment model, scenario6,agricultural demand increase 20%, constrained GW drawdown, monthly water deficit and release sequences at Amman-Zarqa and C/S Jordan Valley nodes. 394

J.12 Assessment model, scenario6,agricultural demand increase 20%, constrained GW drawdown, monthly pumping, drawdown and Disi transfer sequences. 395

J.13 Assessment model, scenario6,agricultural demand increase 20%, constrained GW drawdown, WD, KTD and pumping energy sequences. 396

J.14 Assessment model, scenario6,agricultural demand increase 20%, constrained GW drawdown, annual deficits, storages, and drawdowns frequency curves. 397

J.15 Assessment model, scenario6,agricultural demand increase 10%, unconstrained GW drawdown, WD, KTD, and KD storage and release sequences. 398

J.16 Assessment model, scenario6,agricultural demand increase 10%, unconstrained GW drawdown, AD, ZD, and KafD storage and release sequences. 399

J.17 Assessment model, scenario6,agricultural demand increase 10%, unconstrained GW drawdown, monthly water deficit and release sequences at Adasiya and North Jordan Valley nodes. 400

J.18 Assessment model, scenario6,agricultural demand increase 10%, unconstrained GW drawdown, monthly water deficit and release sequences at Amman-Zarqa and C/S Jordan Valley nodes. 401

J.19 Assessment model, scenario6,agricultural demand increase 10%, unconstrained GW drawdown, monthly pumping, drawdown and Disi transfer sequences. 402

J.20 Assessment model, scenario6,agricultural demand increase 10%, unconstrained GW drawdown, WD, KTD and pumping energy sequences. 403

J.21 Assessment model, scenario6,agricultural demand increase 10%, unconstrained GW drawdown, annual deficits, storages, and drawdowns frequency curves. 404

J.22 Assessment model, scenario6,agricultural demand increase 20%, unconstrained GW drawdown, WD, KTD, and KD storage and release sequences. 405

J.23 Assessment model, scenario6,agricultural demand increase 20%, unconstrained GW drawdown, AD, ZD, and KafD storage and release sequences. 406

J.24 Assessment model, scenario6,agricultural demand increase 20%, unconstrained GW drawdown, monthly water deficit and release sequences at Adasiya and North Jordan Valley nodes. 407

J.25 Assessment model, scenario6,agricultural demand increase 20%, unconstrained GW drawdown, monthly water deficit and release sequences at Amman-Zarqa and C/S Jordan Valley nodes. 406

J.26 Assessment model, scenario6,agricultural demand increase 20%, unconstrained GW drawdown, monthly pumping, drawdown and Disi transfer sequences. 409

J.27 Assessment model, scenario6,agricultural demand increase 20%, unconstrained GW drawdown, WD, KTD and pumping energy sequences. 410

J.28 Assessment model, scenario6,agricultural demand increase 20%, unconstrained GW drawdown, annual deficits, storages, and drawdowns frequency curves. 411

K.1 Assessment model, perfect forecast scenario, constrained GW drawdown, WD, KTD, and KD storage and release sequences. 413

K.2 Assessment model, perfect forecast scenario, constrained GW drawdown, AD, ZD, and KafD storage and release sequences. 414

K.3 Assessment model, perfect forecast scenario, constrained GW drawdown, monthly water deficit and release sequences at Adasiya and North Jordan Valley nodes. 415

K.4 Assessment model, perfect forecast scenario, constrained GW drawdown, monthly water deficit and release sequences at Amman-Zarqa and C/S Jordan Valley nodes. 416

K.5 Assessment model, perfect forecast scenario, constrained GW drawdown, monthly pumping, drawdown and Disi transfer sequences. 417

K.6 Assessment model, perfect forecast scenario, constrained GW drawdown, WD, KTD and pumping energy sequences. 418

K.7 Assessment model, perfect forecast scenario, constrained GW drawdown, annual deficits, storages, and drawdowns frequency curves. 419

K.8 Assessment model, perfect forecast scenario, unconstrained GW drawdown, WD, KTD, and KD storage and release sequences. 420

K.9 Assessment model, perfect forecast scenario, unconstrained GW drawdown, AD, ZD, and KafD storage and release sequences. 421

K.10 Assessment model, perfect forecast scenario, unconstrained GW drawdown, monthly water deficit and release sequences at Adasiya and North Jordan Valley nodes. 422

K.11 Assessment model, perfect forecast scenario, unconstrained GW drawdown, monthly water deficit and release sequences at Amman-Zarqa and C/S Jordan Valley nodes. 423

K.12 Assessment model, perfect forecast scenario, unconstrained GW drawdown, monthly pumping, drawdown and Disi transfer sequences. 424

K.13 Assessment model, perfect forecast scenario, unconstrained GW drawdown, WD, KTD and pumping energy sequences. 425

K.14 Assessment model, perfect forecast scenario, unconstrained GW drawdown, annual deficits, storages, and drawdowns frequency curves. 426

L.1 Assessment model, non-conjunctive management scenario, constrained GW drawdown ,WD, KTD, and KD storage and release sequences. 428

L.2 Assessment model, non-conjunctive management scenario, constrained GW drawdown ,WD, KTD, and KD storage and release sequences. 429

L.3 Assessment model, non-conjunctive management scenario, constrained GW drawdown ,WD, KTD, and KD storage and release sequences. 430

L.4 Assessment model, non-conjunctive management scenario, constrained GW drawdown ,WD, KTD, and KD storage and release sequences. 431

L.5 Assessment model, non-conjunctive management scenario, constrained GW drawdown ,WD, KTD, and KD storage and release sequences. 432

L.6 Assessment model, non-conjunctive management scenario, constrained GW drawdown ,WD, KTD, and KD storage and release sequences. 433

L.7 Assessment model, non-conjunctive management scenario, constrained GW drawdown ,WD, KTD, and KD storage and release sequences. 434

L.8 Assessment model, non-conjunctive management scenario, constrained GW drawdown ,WD, KTD, and KD storage and release sequences. 435

L.9 Assessment model, non-conjunctive management scenario, constrained GW drawdown ,WD, KTD, and KD storage and release sequences. 436

L.10 Assessment model, non-conjunctive management scenario, constrained GW drawdown ,WD, KTD, and KD storage and release sequences. 437

L.11 Assessment model, non-conjunctive management scenario, constrained GW drawdown, WD, KTD, and KD storage and release sequences. 438

L.12 Assessment model, non-conjunctive management scenario, constrained GW drawdown ,WD, KTD, and KD storage and release sequences. 439

L.13 Assessment model, non-conjunctive management scenario, constrained GW drawdown ,WD, KTD, and KD storage and release sequences. 440

L.14 Assessment model, non-conjunctive management scenario, constrained GW drawdown ,WD, KTD, and KD storage and release sequences. 441

Summary

Surface water and groundwater systems consist of interconnected reservoirs, rivers, and confined and unconfined aquifers. The integrated management of such resources faces several challenges:

High dimensionality refers to the requirement of the large number of variables that need to be considered in the description of surface water and groundwater systems. These variables are needed to model reservoirs, river reaches, aquifer piezometric heads, and management objectives, among others, and can easily number in the thousands. Especially taxing is the extent and distributed nature of groundwater aquifers. As the number of these variables increases, the computational requirements quickly saturate the capabilities of the existing management methods.

Uncertainty relates to the imprecise nature of many system inputs and parameters, including reservoir and tributary inflows, precipitation, evaporation, aquifer parameters (e.g., hydraulic conductivity and storage coefficient), and various boundary and initial conditions. System modeling under uncertainty not only entails difficult challenges in its own right, but it also complicates very significantly the development and application of efficient management models.

Nonlinearity is intrinsic to some physical processes and also enters through various facility and operational constraints on reservoir storages, releases, and aquifer drawdown and pumping. Nonlinearities compound the previous difficulties.

Multiple objectives pertain to the process of optimizing the use of the integrated surface and groundwater resources to meet various water demands, generate sufficient

energy, maintain adequate instream flows, and protect the environment and the ecosystems. Multi-objective decision models and processes continue to challenge professional practice.

Although surface and ground water systems are traditionally managed separately they are almost always coupled because of hydraulic linkages, the need to meet common management objectives, or both. The aim of this research is to develop efficient methods for conjunctive management of interconnected surface water and groundwater systems.

This research draws on several disciplines including groundwater flow modeling, hydrology and water resources systems, uncertainty analysis, estimation theory, stochastic optimization of dynamical systems, and policy assessment. A summary of the research contributions made in this work follows:

1. High dimensionality issues related to groundwater aquifers system have been mitigated by the use of transfer functions and their representation by state space approximations.
2. Aquifer response under uncertainty of inputs and aquifer parameters is addressed by a new statistical procedure that is applicable to regions of relatively few measurements and incorporates management reliability considerations.
3. The conjunctive management problem is formulated in a generally applicable way, taking into consideration all relevant uncertainties and system objectives. This problem is solved via an efficient stochastic optimization method that overcomes dimensionality limitations.

4. The methods developed in this Thesis are applied to the Jordanian water resources system, demonstrating their value for operational planning and management. The application demonstrates a clear advantage and necessity of conjunctive surface and groundwater resources management.

CHAPTER 1

INTRODUCTION

Surface water and groundwater resources sustain all human and ecological water uses. Worldwide, surface water resources provide less than 1 percent of total water supply, Freeze and Cherry (1979), while the rest is provided by groundwater. Surface water resources are regulated by storage facilities (reservoirs) that support various water uses including water supply to urban, agricultural, and industrial areas, energy generation, flood protection, navigation, recreation, and environmental and ecological sustainability. Groundwater resources are associated with groundwater aquifers (water bearing soil layers) that are exploited by pumping to supply water for human use.

Surface water and/or groundwater management aims at developing and implementing strategies for water resources utilization with due consideration of spatial and temporal interdependencies among natural processes and water uses. Management may include supply side decisions such as reservoir and aquifer regulation as well as demand side strategies such as water conservation and recycling.

Surface and groundwater management is a challenging undertaking. In surface water systems, complicating factors include uncertain river flows and water demands, multiple water uses and management objectives, nonlinear dynamics, and complex interdependences of natural processes and water uses. Likewise, groundwater systems are

characterized by various uncertainty sources (recharge rates, boundary conditions, and parameter heterogeneity), nonlinear response, and large dimensionality due to their spatial extent.

Conjunctive surface water and groundwater management becomes necessary when there is strong coupling between the two subsystems. Coupling may be due to interaction of natural processes, interaction of management objectives, or both. An example of the former occurs when aquifers and streams are hydraulically connected. In such cases, water is transferred to the streams from the aquifers when aquifer levels are high and streamflows are low. Water transfer is reversed when aquifer levels experience drawdowns and streams experience normal or high flows. Coupling of management objectives occurs when certain water uses may be met by either surface water or groundwater. In such cases, virtual transfers of water can occur between the two subsystems by preferentially using one or the other to meet the water uses.

Conjunctive management compounds the challenges of managing either surface water or groundwater separately. The difficulty increases as one must represent the response of both systems and their interactions, and develop management strategies that simultaneously address reservoir and aquifer regulation.

The objective of this work is to formulate and solve the conjunctive surface water/ groundwater management problem in a computationally efficient manner. The main challenges that this research addresses are as follows:

1. Dimensionality of groundwater systems and development of consistent surface water and groundwater models.
2. Uncertainty of groundwater parameters and stresses.

3. Computational efficiency of conjunctive management methods.

A review of the literature pertaining to surface water and groundwater management, and to methods developed to address parameter uncertainty is presented in Chapter 2. Chapter 3 considers the problem of modeling the response of large groundwater systems in a stochastic framework. Chapter 4 describes the formulates the conjunctive management problem and develops a computationally efficient procedure for its solution. Chapter 5 presents various case studies and assessments pertaining to the Jordanian water resources system. Chapter 6 concludes the Thesis with a summary of general conclusions and a short list of future research recommendations. Mathematical derivations and detailed algorithm descriptions are delegated to appendices.

CHAPTER 2

LITERATURE REVIEW

2.1 Introduction

Groundwater and surface water management modeling can be viewed as the coupling of two techniques from two broader and distinct scientific disciplines: groundwater and surface water modeling (watershed, river, reservoir, and aquifer hydrology) from hydrological sciences, and mathematical optimization from operation research and management science. Watershed, river, and reservoir hydrology describes the relationships between all surface water processes including precipitation, evapotranspiration, streamflow, and reservoir storage. Groundwater hydrology provides the relationships between aquifer recharge, flow, and levels. Mathematical optimization aims to identify best management strategies based on (1) surface water and groundwater models and (2) water use levels.

Uncertainty is inherent in groundwater and surface water systems. In groundwater systems, uncertainty arises from the boundary conditions the aquifer parameters (e.g., hydraulic conductivity and storage coefficients), the latter also known as model uncertainty. In surface water systems, uncertainty stems from the natural variability of the climatic inputs and, to a lesser degree, from model parameters. It is important that uncertainty be addressed because it not only affects the ability to predict the system response but also determines the type of management policies appropriate to apply.

The literature review done in this chapter covers published works on groundwater management, conjunctive groundwater and surface water management, and groundwater modeling under parameter uncertainty. The review begins with mathematical programming techniques that have been proposed for groundwater management or conjunctive surface water and groundwater management problems (Sections 2 and 3). Generally, the literature of the former is much larger than the literature of the latter. The fourth section focuses on some of the methods used to model groundwater aquifers under parameter uncertainty, including geostatistical and statistical methods. The fifth section summarizes the conclusions of the literature review, and the sixth section goes over the challenges addressed by this research

2.2 Groundwater Management

Groundwater management problems can be divided into two categories depending on the form in which the groundwater system is simulated as part of the management model.

1. The embedding approach uses finite element or finite difference approximations of the flow equations for all nodes or grid points in the management model. These equations are incorporated in the set of constraints.
2. The response matrix approach: requires developing hydraulic head responses due to unit perturbations of the pumping variables. These responses are assembled in a response matrix and are included in the management model.

Ahlfeld et al (1997) describes a heuristic algorithm for solving problems that include water quality constraints (contaminant concentrations) in addition to constraints pertaining to hydraulic heads and pumping extraction rates. The formulations are for

confined aquifers. The method is based on decoupling the concentration constraints from the hydraulic management problem as follows: The full problem is solved using an iterative technique. At each iteration, the hydraulic constraints are adjusted heuristically, with the adjustment based on a contaminant transport simulation using the optimal pumping rates obtained from the solution of the previous stage of the hydraulic management problem. Iterations terminate when pumping rates converge. The approach essentially amounts to calibrating the constraints of the hydraulic management problem by examining the response of the transport solution. The management problem is solved using linear programming, Chvatal (1980).

The authors mention several possible limitations of the algorithm. These relate to limitations of the general nature of the relationship between hydraulic control constraints and concentration constraints. The algorithm assumes that changing a hydraulic constraint does not significantly affect those concentration values that are not associated with that hydraulic constraint. Furthermore, all concentrations that are affected by a given hydraulic head constraint are affected consistently, i.e., the concentrations increase or decrease simultaneously. If these assumptions are not valid, the algorithm tends to oscillate and not converge.

Herrling et al (1986) also used a linear optimization procedure (simplex algorithm) to solve the groundwater management problem. The paper considered only steady state horizontal 2-dimensional groundwater flow, where the transmissivities are independent of groundwater levels (confined aquifer). A finite element scheme was used to solve the governing differential equations with the appropriate boundary conditions. The hydraulic head at each node was explicitly expressed in terms of boundary

conditions, pumping stresses, and heads in the other nodes by applying the cholesky solution method to the finite element equations for all nodes. The authors refer to the equations that explicitly relate the heads to the pumping stresses as "influence functions." The influence functions are then included in the objective function and the constraint set. The authors did not discuss how the procedure can be modified to account for uncertainties in groundwater parameters and boundary conditions. Furthermore, the authors report high computational requirements when applying this procedure to management problems under transient (unsteady) conditions.

Jones et al (1987) used the embedding approach and differential dynamic programming to solve a deterministic and nonlinear groundwater management problem for a hypothetical unconfined aquifer. The objective function was quadratic, and the system constraints were included in the objective function using Lagrange multipliers. A finite difference scheme was used to approximate the groundwater dynamics for an unconfined aquifer, with the nonlinear equations linearized around a nominal pumping sequence. The management problem was then solved iteratively to get new nominal pumping sequences. The technique terminated when the change in the objective function from one iteration to the next was small. This article uses the embedding approach in the management model. This approach creates a heavy computational burden if large groundwater systems are considered. The article does not account for uncertainty in boundary conditions and groundwater parameters.

Wagner and Gorelick (1987) solve a stochastic groundwater quality management problem. They used the first and second statistical moment approach to formulate the management problem. The formulation included chance constraints with respect to

concentrations at the desired monitoring locations. First, they used nonlinear least square regression analysis to estimate the effective porosity, hydraulic conductivity, and longitudinal and transverse dispersivities. Second, the covariance matrix for these parameters was also estimated by computing the jacobian of the simulated heads and concentrations at the observation locations with respect to groundwater parameters. Third, the uncertainty of in the groundwater parameters was translated to uncertainty of the concentrations by computing the first and second moments of the simulated concentrations using the computed first and second moments of the aquifer parameters. Finally, this nonlinear and chance-constrained optimization problem was solved using an optimization package called NPSOL combined with the simulation model SUTRA. This approach also employs the embedding technique, the basis of which is the simulation model SUTRA. SUTRA is called repeatedly by the optimization procedure and can potentially introduce heavy computational requirements in regional, multi aquifer systems. Unsteady conditions add to the complication as they require the optimization model to consider several time steps. The authors report that it took approximately 8 hours of CPU time on a Prime 9955 minicomputer to solve the steady state stochastic aquifer reclamation problem.

Gorelick and Voss (1984) combined a solute transport simulation model (SUTRA), with a nonlinear optimization solver (MINOS) to produce a methodology for aquifer rehabilitation. The simulation-optimization model was used to determine pumping and injection rates and well locations for groundwater quality control. The model was applied to a hypothetical confined aquifer that has two contaminated areas. Examples were shown aiming to find minimum pumping rates such that the

contamination concentrations at the monitoring locations are maintained below a groundwater quality standard. The constraint set included nonlinear concentration constraints and linear hydraulic heads. The article does not consider uncertainty analysis in the aquifer rehabilitation solution.

Gorelick and Remson (1982) use a linear programming-superposition method for managing multiple sources of groundwater pollution over time. The methodology is applied to a one dimensional confined aquifer with 3 water supply pumping locations and potentially 3 disposal sites. The objective is to maximize the total disposal of waste solutes into the system, while maintaining a solute concentration at each water supply well below a certain water quality standard. For the described system the relation between the injection rate and the concentration is linear. A unit source-concentration response matrix was developed using the simulation model. This matrix shows the concentrations that result at particular water supply wells from unit solute injections at each of the disposal sites over time. The management problem is to maximize the solute injection rates, subject to the concentration constraints. Concentrations at the water supply locations are obtained by multiplying the unit source-concentration response matrix with the injection rates (control variables). This article does not take into consideration the uncertainties in the specified head boundary conditions and the uncertainty in the flow and solute transport parameters. In addition, the procedure is based on a relatively simple system (one dimensional) and is not realistic in most aquifer management problems.

Georgakakos and Vlasta (1991) formulate a stochastic groundwater management problem where the uncertainty stems from groundwater parameters (transmissivity) and

boundary conditions. Their methodology was applied to two confined aquifer layers separated by a semipervious leaky layer. Uncertainty was introduced in the transmissivity and the boundary conditions and was then transferred to the groundwater dynamical equation by means of the first and second moment approach. The management problem was then formulated with an objective function that includes quadratic terms for aquifer head targets, energy targets, supply-demand targets and pumping rates targets. Aquifer heads (state variables) were expressed in terms of the mean and covariance terms in the performance index. The open loop feedback control method (OLF) was used to solve the management problem. Main results from the case studies showed that by doubling the nodes of the finite element grid, the computational time increased by 6- 7 times. Also by excluding the covariance terms from the performance index the resulting pumping differed from the optimal pumping (when the covariance terms were in the performance index) by less than 10%. Hence, excluding the covariance terms would reduce the problem dimensionality and lead to a reasonable approximation.

Yazicigil and Rasheedudin (1987) coupled a simulation model with an optimization model (embedding technique), where the management problem was solved using linear programming. The combined management model was used to determine the optimal pumping rates for a multi-aquifer system under transient and steady state conditions. The groundwater system consisted of 2 confined aquifers separated by a leaky confining unit and 9 pumping wells in each layer. The management period for the system was for 1 year on a seasonal basis (4 seasons). The management problem objective was to maximize the piezometic heads in both aquifers, and the constraints were supply-demand constraints, head constraints for water quality purposes, and pumping constraints. The

authors performed a multi-objective analysis for the same system under steady state conditions. This approach produced trade-off curves associated with conflicting system objectives such as maximizing the sum of hydraulic heads while satisfying a prescribed demand for water. The purpose of the multi-objective analysis is to enhance the decision makers ability to select a development policy from a set of alternative policies.

Ahlfeld (1994) formulated the groundwater supply management problem as a linear program. The formulation was based on confined aquifers. Ahlfeld used the response functions technique to represent the aquifer heads as function of the unknown pumping. The objective function was to minimize the pumping or recharge costs, with linear constraints over the aquifer hydraulic heads at the monitoring locations, horizontal or vertical hydraulic gradients constraints (head differences), and pumping/ recharge rate constraints.

Wagner (1999) presented an approach for assessing the value of groundwater sampling within the context of groundwater management under uncertainty. The procedure couples two optimization models; a chance-constrained groundwater management model and an integer-programming sampling network design model. The methodology consists of the following steps: (1) The optimal groundwater management strategy for the present level of model uncertainty is determined using a chance constrained management model (Wagner and Gorelick 1987); (2) For a specified data collection budget, the monitoring network design model identifies the sampling strategy that will minimize model uncertainty; (3) Find the optimal groundwater management strategy on the basis of the projected model uncertainty after sampling; (4) The worth of the monitoring strategy is assessed by comparing the value of the sample information

(reduction in management cost) with the cost of data collection. A monitoring strategy is justified only if the value of sample information exceeds the cost of data collection. The methodology was applied to a hypothetical aquifer system with the following properties: confined aquifer, 2 zones of hydraulic conductivity, steady conditions for the flow model, uniform longitudinal and transverse dispersivities and uniform effective porosity. A source of contamination was introduced to the aquifer and the management goal is to reduce the contamination concentrations at the monitoring locations below a certain water quality standards with the minimum pumping costs. Sampling budget ranged from $5000 to $150000. The results showed that when only hydraulic heads and concentrations are sampled the optimal sampling strategy to minimize the overall management and monitoring cost requires a sampling budget of $25000. On the other hand, adding 2 additional aquifer pumping tests (for hydraulic conductivity sampling) resulted in two more sampling strategy budgets of $35000 and $50000.

Lefkoff and Gorelick (1986) formulated an aquifer restoration management problem under transient conditions. The methodology was applied to a hypothetical confined aquifer which is heterogeneous and isotropic. The aquifer is polluted by a contaminant plume. The objective is to remove the aquifer contamination within 4 years with the lowest pumping and injection costs. The constraints included hydraulic head constraints at the pumping and injection well locations and retarded seepage velocity constraints at the plume boundaries. The constraints were represented as linear functions of the unknown pumping and injection rates (response matrix approach). The objective function was not linear because of nonlinear cost terms from pumping. The nonlinear management problem was solved by the nonlinear optimization solver (MINOS). The

authors emphasize that their management model ignores dispersion and chemical reactions and incorporates only retardation. The authors conducted sensitivity analyses on the effect of the type of treatment processes used (injection treatment types), maximum allowable pumping and injection rates, and the number of potential well sites.

Maddock (1973) formulated a stochastic management problem for an irrigated farm subject to variations in economic factors such as pumping costs and crop prices, and groundwater parameters including transmissivity and storage coefficients. The objective was to maximize the net revenues, the objective function formulated in quadratic form due to pumping cost terms. Maddock used the response functions approach to express groundwater drawdowns in terms of pumping rates (Maddock, 1972). He analyzed the effect of the economic and hydrologic parameters by developing regret functions, which represent the net losses in the revenues when values other than the correct parameter values were used in the planning model. By assuming a certain distribution for the parameters uncertainties, he computed the expected value for the mean regret function with respect to parameter uncertainty, and also ranked the parameters by priority for further data collection activities. His analysis showed that the expected regret was more sensitive to economic parameters than hydrologic parameters, and his conclusion was that priority should be given to gather more data for economic factors.

Wagner and Gorelick (1989) formulated a stochastic groundwater management problem using a geostatistical approach to represent the uncertainty of hydraulic conductivity. They assumed a second order stationary process where log-conductivity was a random field with a certain mean and covariance function. Conditional simulations were used to generate realizations of the hydraulic conductivity field. The objective of the

management problem was to find the minimum pumping required to reach certain water quality standards in a hypothetical confined aquifer. Gorlelick and Wagner approached the problem in two ways: Their first approach was to generate a limited number of hydraulic conductivity realizations (30 realizations) which were considered simultaneously in the solution of the management problem. The second approach was to use Monte Carlo to find the optimal pumping probability density distribution by solving the management problem separately for each hydraulic conductivity realization and repeating for each realization.

Willis and Finney (1985) used a quasilinearization approach to solve the management problem for a hypothetical unconfined aquifer. The quasilinearization approach used a generalized Newton Raphson approximation to linearize the nonlinear flow equations for unconfined aquifers (Boussinesq equation) around a trial pumping sequence. The quasilinearization optimization algorithm generates a sequence of suboptimal solutions of pumping that will converge eventually to at least a local solution to the control problem. The management model was applied to 2 examples where in the first the objective function was to maximize the hydraulic heads, and in the second was to minimize the pumping cost. Willis and Finney compared their results from the two examples to the results from solving the same problems using projected Lagrangian methods. Both results compared well.

Keshari and Datta (1995) incorporated the finite difference forms of the coupled set of flow and pollutant transport in confined aquifers into the management model using the embedding technique. The objective was to maximize the sum of the pumping rates temporally and spatially, and the system constraints were related to hydraulic heads,

pumping, and contaminant concentrations. The nonlinear optimization problem was solved using the exterior penalty function method combined with the searching algorithm by Hooke and Jeeves (1966). The management model was applied to a hypothetical confined aquifer with constant properties for the storage coefficient, effective porosity, and longitudinal and transverse dispersivities. Management scenarios were conducted to see the effect of the uncertainty in hydraulic conductivity and boundary conditions on the optimal pumping sequence. The hydraulic conductivity was assumed to be constant, or vary exponentially across the aquifer, or vary randomly following a gaussian distribution. The results showed significant difference in the optimal pumping sequence either due to incorrect boundary conditions or different hydraulic conductivity distribution across the aquifer. Other management scenarios included sensitivities on hydraulic head constraints and man made activities (waste injection).

2.3 Conjunctive Groundwater and Surface Water Management

Haimes and Dreizin (1977) developed a decentralized formulation for the conjunctive groundwater / surface water management problem. The problem set up consists of certain number of users pumping groundwater for agricultural or industrial purposes. All users are connected to a regional authority (RA) that controls the surface water systems (reservoirs) and distributes surface water to the users based on their demands. The conjunctive management problem was formulated as a two level interactive problem as follows:

In the first level and for each user, a nonlinear optimization problem is considered to maximize his profit due to groundwater pumping surface water supply and artificial

recharge to the aquifer, subject to pumping, recharge and drawdown constraints. Since this optimization problem is solved individually for each user, information including the drawdown at the user's wells due to aggregate pumpage and recharge from the other users is not known. Furthermore, the actual supply of surface water from the RA is not known at this stage. However both pieces of information will be provided to each user iteratively by the second level.

Results from the optimization problem from each user are: the quantity of water pumped, quantity of water used to recharge the aquifer and the quantity of water the user demands from the surface water system, all will be provided to the second level of the management model.

In the second level, two stages are defined: In the first stage, the model computes for each user the drawdown at his wells due to aggregate pumpage and recharge from all other users. Also the model computes the total amount of water induced from the stream into the aquifer cells, the latter quantity being useful in the optimization for the surface water system.

In the second stage, the model solves the optimization problem for the surface water system, which is to minimize the cost of surface water allocation, subject to physical constraints (reservoir capacity and water availability). Results from this stage provide each user with the amount of his surface water share.

The management problem described above is solved iteratively and interactively between the first and second levels of the management model. Convergence is achieved when the change in the objective function value for each user from one iteration to the next is small. The authors state that the hierarchical structure by multilevel optimization

circumvents the dimensionality problem and the need for much more computational requirements.

Reichard (1995) used a response matrix approach to formulate the conjunctive use management problem, and applied it to the Santa Clara- Calleguas Basin in California. The elements of the surface water include a water transfer to the basin from the Santa Clara River through a diversion facility, which was treated as a stochastic element in the management problem, and the possibility of providing supplemental water to the basin from water that has been reclaimed or imported. The supplemental water amount was assumed to be a fraction of the diverted water. The groundwater elements include groundwater pumped to meet the agricultural demands and artificial recharge from two aquifers.

The optimization model considered three possible objective functions: (1) minimizing the relative amount of supplemental water obtained for a specified reduction in water use (water demand); (2) minimizing the imposed water use reduction for a specified amount of supplemental water, or (3) minimizing the deviation of pumping from a current average pumping based on a specified reduction in water use. Constraints were applied to groundwater levels, groundwater hydraulic gradients, water demands, pipeline capacities, and groundwater hydraulics. The nonlinear management problem was solved using MINOS (Murtagh and Saunders, 1987).

2.4 Groundwater Modeling under Uncertainty

2.4.1 Geostatistical Approach

Groundwater system uncertainty stems from the spatial heterogeneity of groundwater flow parameters including hydraulic conductivity, transmissivity and storage coefficients. The ways in which this uncertainty has been accounted for in the past are reviewed below. The review focuses on the work by Hoeksema and Kitanidis whose work provides a comprehensive treatment of this subject.

Hoeksema and Kitanidis (1984) developed a geostatistical approach to estimate transmissivities. Their work dealt with steady two-dimensional flow with Diriclet (given head) boundary conditions and no pumping or accretion terms. Their approach included the following steps: First, a selection of a model for the structure of the field of log transmissivity is made. Second, the random structure of the hydraulic head is related to the random structure of the log transmissivities through analytically derived relationships, Monte Carlo simulation, or linearization of the flow equations. Third, the unknown statistical parameters of the assumed log transmissivity model are estimated based on measurements of log transmissivity and hydraulic head. And fourth, point or block-averaged values of the field log transmissivity anywhere in the model are predicted using a minimum variance unbiased linear estimation approach, i.e., kriging or cokriging. More specifically, the above steps were carried out as follows:

Step 1: The auto-covariance of the log transmissivity is:

$$Cov(Y_i,Y_j)=\theta_1\delta_{ij} + \theta_2 d_{ij} \quad (2.1)$$

Where δ_{ij} is Kronecker's delta (1 if i=j; 0 otherwise); d_{ij} is the scalar distance between the locations of the point log transmissivity values Y_i and Y_j; and $\theta_1 \geq 0$, $\theta_2 \leq 0$ are parameters to be estimated.

Step2: Parameters θ_1 and θ_2 are estimated from measurements of log transmissivity y and hydraulic head ϕ. Thus, the generalized covariance matrix φ can be constructed as follows:

$$\varphi = \begin{pmatrix} \varphi_{\phi\phi} & \varphi_{\phi y} \\ \varphi_{y\phi} & \varphi_{yy} \end{pmatrix} = \theta_1 \begin{pmatrix} R_{\phi\phi} & R_{\phi y} \\ R_{y\phi} & R_{yy} \end{pmatrix} + \theta_2 \begin{pmatrix} S_{\phi\phi} & S_{\phi y} \\ S_{y\phi} & S_{yy} \end{pmatrix} + \begin{pmatrix} P_{\phi\phi} & 0 \\ 0 & 0 \end{pmatrix} \quad (2.2)$$

where $\varphi_{\phi\phi}$ is the head measurement covariance matrix, $\varphi_{\phi y}$ is the head - log transmissivity measurement generalized cross covariance matrix, and φ_{yy} is the log transmissivity measurement generalized covariance matrix. The submarices with the "R" designation represent the nugget effect variability; namely, variability which can not be attributed to significant spatial separation of the measurement points. The submatrices with the "S" designation represent the structured variability; namely, the variability attributable to spatial separation between measurement points. The submatrix $P_{\phi\phi}$ is the head measurement errors submatrix.

Matrices including ϕ in their subscripts are computed using the partial differential equation relating piezometric head to log transmissivity. For a two-dimensional, nonhomogeneous, isotropic, and confined aquifer with no inflow and prescribed head boundary conditions, the hydraulic head ϕ and the aquifer transmissivity T must satisfy the following partial differential equation (PDE):

$$(\partial T/\partial x)(\partial\phi/\partial x) + T(\partial^2\phi/\partial x^2) + (\partial T/\partial y)(\partial\phi/\partial y) + T(\partial^2\phi/\partial y^2) = 0 \quad (2.3)$$

This equation can also be written in terms of the log-transmissivity Y=ln T, and can then be separated into a deterministic and a stochastic form. The following substitutions are made:

$$\phi = H + h \tag{2.4}$$

$$Y = F + f \tag{2.5}$$

Linearizing the resulting equation by eliminating second order terms results in:

$$(\partial f/\partial x)(\partial H/\partial x) + (\partial^2 H/\partial x^2) + (\partial^2 h/\partial x^2) + (\partial f/\partial y)(\partial H/\partial y) + (\partial^2 H/\partial y^2) + (\partial^2 h/\partial y^2) = 0 \tag{2.6}$$

Taking the expected value of the above equation results in:

$$(\partial^2 H/\partial x^2) + (\partial^2 H/\partial y^2) = 0 \tag{2.7}$$

Then subtracting the last equation from the one before it results in:

$$(\partial^2 h/\partial x^2) + (\partial^2 h/\partial y^2) = -(\partial f/\partial x)(\partial H/\partial x) - (\partial f/\partial y)(\partial H/\partial y) \tag{2.8}$$

The above equation can be written in a finite difference form:

$$h_{j-1} + h_{i-1} - 4h_{j+1} + h_{i+1} = \Delta x/2(f_{j-1} - f_{j-1})(\partial H/\partial x) - \Delta x/2(f_{j+1} - f_{j+1})(\partial H/\partial y) \tag{2.9}$$

The above equation can be written for each grid point to evaluate the head perturbations. Now the above sub matrices can be evaluated:

$$\varphi_{\phi\phi} = E(\mathbf{h}_p \mathbf{h}_p) \tag{2.10}$$

$$\varphi_{\phi y} = E(\mathbf{h}_p \mathbf{f}_p) \tag{2.11}$$

where the bold letters refer to vectors, and the subscript "p" refers to point head or log transmissivity perturbations (where we have measurements). $\mathbf{h}_p$ can be evaluated by interpolation from the closest 4 block head perturbations evaluated by the finite difference equation for head perturbations mentioned earlier.

Also the remaining sub matrices can be evaluated: $S_{\phi\phi}$, $S_{\phi y}$, $P_{\phi\phi}$ and $S_{y\phi}$

Step3: Involves the estimation of θ_1 and θ_2 given the measurements [$\phi_1,\phi_2,\ldots..\phi_n$, $Y_1,Y_2,\ldots.Y_m$]

This step involves determining the n measurement point expected heads H_1, H2…. Hn via a numerical simulation model of the aquifer with assumed boundary condition and constant transmissivity, this produces expected head values for discrete points throughout the aquifer. The measurement point values are then obtained by using interpolation procedures. Next the measurement covariance matrix is constructed as a function of θ_1 and θ_2, and the maximum likelihood parameter estimation procedure is used to determine the most probable values of θ_1 and θ_2 given the measurements.

Step4: Linear, minimum variance, unbiased estimation theory is used to predict values of log transmissivity at any point in the field. The unbiased estimator used is cokriging. Let the estimate of log transmissivity at any point or over any location in the field be X_0. X_0 is considered to be a linear combination of the n head measurements and (m) log transmissivity measurements.

$$X_0 = \Sigma_{i=1,\ldots n}\mu_i\phi_i + \Sigma_{j=1,\ldots m}\lambda_j Y_j + \xi \qquad (2.12)$$

If "Y_0" is the true value of log transmissivity at any point or block of estimation then the variance of the estimate can be expressed as:

$$E[(Y_0 - X_0)^2] = E[(Y_0 - \Sigma_{i=1,\ldots n}\mu_i\phi_i + \Sigma_{j=1,\ldots m}\lambda_j Y_j + \xi)^2] \qquad (2.13)$$

Next the estimate of the variance must be minimized. Define

$$Z = E[(Y_0 - X_0)^2] + 2\nu(1-\Sigma_{j=1,\ldots m}\lambda_j) \qquad (2.14)$$

where ν is the Lagrange multiplier. Then, the estimate variance is minimized if the following is true:

$$(\partial Z/\partial\mu_i)=0 \quad i=1,\ldots,n \qquad (2.15)$$

$(\partial Z/\partial \lambda_j)=0 \quad j=1,\ldots,m$ (2.16)

$(\partial Z/\partial \nu)=0$ (2.17)

$(\partial Z/\partial \xi)=0$ (2.18)

The above 4 minimization equations give a set of n+m+1 linear equations in n+m+1 unknowns:

$\mu_{1,\ldots..}, \mu_n, \lambda_{1,\ldots}, \lambda_m$, and ν

This set of equations can be solved at each point or block where the log transmissivity is to be estimated.

This procedure was applied to a test case in which the values of log transmissivity and head were generated with known values of the geostatistical parameters. The test aquifer is square with 300-km sides and constant head boundaries. To investigate the effect of discretization (or grid averaging) and interpolation (head measurement not coinciding with grid nodes) on the estimates of log tarnsmissivity and hydraulic head, three levels of discretization were investigated (fine: Δx = 25 km; medium Δx=50 km; and coarse: Δx=100 km). The simulation results showed that the coarse grid does not give useful results. The medium discretization level gave reasonable results, while the fine discretization level provided the best approximation.. Furthermore the use of head measurements was shown to improve the log transmissivity estimates, although the degree of improvement varied widely from case to case.

This methodology was applied to estimate the transmissivity field in the Jordan aquifer in Iowa. It is considered a confined aquifer, the original data contained 31 head and 56 log transmissivity measurements. Four runs were performed. The first run used 56 log transmissivity measurements to estimate the linear model parameters θ_1 and θ_2.

The fitted linear model represented the spatial variability of the log transmissivity of the Jordan aquifer adequately, and these parameters were then used for the estimation through kriging of grid averaged log transmissivity.

The second run used the geostatistical solution developed above, by using the entire set of 31 head and 56 transmissivity measurements. It was assumed that no accretion, pumping or leakage occurred. The estimated θ_1 and θ_2 did not change drastically from the values obtained by the first run. When the fitted linear model was applied, it resulted in a larger sum of squares of residuals than the sum of squares of residuals resulting from the first run.

The third run also used the geostatistical solution developed above, but accounted for the leakage effect that may occur. The results of this run also gave a sum of square residuals similar to the second run.

Hoeksema and Kitanidis (1989) also applied a geostatistical approach to solve the inverse problem of the groundwater equation. Their approach mainly included the following steps: choosing a geostatistical model for spatial variability of log-transmissivity, obtaining a measurement covariance matrix, estimation of covariance function variables, and finally applying linear estimation to estimate the transmissivity random field. Furthermore they also used conditional simulations to generate many probable sets of the estimated random field. At the end, they evaluated their methodology through application to hypothetical data.

Details of the above steps are similar to their work in 1984, with the following differences: The measurement covariance matrix is obtained by

$$\varphi = \begin{pmatrix} \varphi_{\phi\phi} & \varphi_{\phi y} \\ \varphi_{y\phi} & \varphi_{yy} \end{pmatrix} = \theta_1 \begin{pmatrix} \mathbf{0} & \mathbf{0} \\ \mathbf{0} & \mathbf{I} \end{pmatrix} - \theta_2 \begin{pmatrix} \varphi_{\phi\phi D} & \varphi_{\phi yD} \\ \varphi_{y\phi D} & \varphi_{yyD} \end{pmatrix} - \theta_3 \begin{pmatrix} \mathbf{I} & \mathbf{0} \\ \mathbf{0} & \mathbf{0} \end{pmatrix} + \begin{pmatrix} \varphi_{PB} & \mathbf{0} \\ \mathbf{0} & \mathbf{0} \end{pmatrix} \quad (2.19)$$

where any submatrix with a subscript that includes "D" refers to a derivative sub matrix. Like an example $\varphi_{\phi\phi D}$ is the derivative sub matrix of the covariance sub matrix for point observations of head, φ_{PB} is the covariance sub matrix for point observation of head due to uncertainty in boundary conditions, and the remaining sub matrices on the left hand side are as in their earlier work. θ_3 is the variance associated with heads due to measurements error.

The linear estimation in this approach was applied through cokriging and ordinary kriging. Linear estimation was applied to estimate log transmissivities, piezometric heads, and seepage velocities. Therefore covariance matrices between the measurements and log transmissivities, piezometric heads, and seepage velocities were developed. In the case of seepage velocity, linearization of the seepage velocity equation was first applied and the perturbation from the mean seepage velocity was next obtained to arrive at a nondimentional, zero-mean term used to derive the velocity- measurement covariance matrix and the unconditional velocity covariance matrix.

After estimating the log transmissivity, piezometric head and velocity fields, conditional simulations were used to generate many probable sets of the preceding fields. Each of these sets is consistent with the governing flow equations, the observations, and the model of spatial variability of transmissivity.

For example, let the matrix $\mathbf{G}_n$ contain the new set of log transmissivity and boundary head vectors based on conditional simulations, and the matrix $\mathbf{G}_k$ contain the estimated

log transmissivity vector and boundary head vector. Also let $\mathbf{V}_{GG}$ be the covariance matrix associated with $\mathbf{G}_k$.

Then: $\mathbf{G}_n = \mathbf{G}_k + \mathbf{R}_{GG}\,\mathbf{S}$ (2.20)

where $\mathbf{R}_{GG}$ is a decomposition of $\mathbf{V}_{GG,}$ and $\mathbf{S}$ is a vector of random numbers which are uncorrelated, normally distributed, and have a zero mean and unit variance.

The methodology was applied to artificial data, namely to a hypothetical aquifer model, and log transmissivity values where generated based on an assumed covariance relation with known parameters. A numerical model was used to simulate piezometric heads. The generated log transmissivities and the simulated heads were considered as true values and were taken as measurements. Then, ordinary kriging and cokriging were used to estimate the log transmissivity field and gave good results. However, the mean squared error (MSE) ciriterion value was less in the case of cokriging, indicating better estimation. Ordinary kriging and cokriging where also used to estimate the piezometric head field, with the cokriging MSE being less than that of ordinary kriging.

Hoeksema and Kitanidis (1985) made a comparison between the Gaussian conditional mean and kriging estimates in the geostatistical solution of the inverse problem. Their solution provided for vertical flow (leakage or pumping) occurring in confined aquifers with steady, two dimensional flows. Their kriging application is new in that it uses linearized mean heads to avoid use of an estimated log-transmissivity mean in the kriging equation. For the Gaussian conditional mean estimate, the log transmissivity field is assumed to be normally distributed. This estimate is based on available estimates for the drift (mean) of log transmissivity, the cross covariance matrix between the grid-averaged log-transmissivity being estimated and each measurement,

measurement vector, measurement expectation vector, and the measurement covariance matrix. The primary difficulty associated with using the Gaussian conditional mean approach is that the computed variance tends to underestimate the true squared log transmissivity prediction error.

The cokriging estimate of the log transmissivity field used an iterative procedure to estimate the drift (mean) measurement parameters, by first estimating the measurement covariance parameters using the Gauss-Newton method of maximum likelihood estimation. Then, the new drift parameters were estimated using weighted least squares. Next, the new drift parameter estimates were used in the next iteration to obtain the new measurement covariance matrix to be used to estimate the covariance parameters as in the first step. This iterative procedure terminates when the negative log likelihood (in the procedure to estimate covariance parameters) reaches a stationary value.

The methodology in this article was applied to two hypothetical aquifers showing that good estimates of the transmissivity field can be obtained (through Gaussian conditional mean or cokriging estimation) even in the presence of leakage into (or out of) aquifer. The methodology was also applied to the Jordan aquifer in Iowa, [Hoeksema and Kitanidis, 1984], for which the estimated predicted transmissivity field was quite similar to that of the previous article.

Hoeksema and Kitanidis (1985) also analyzed the horizontal spatial variability of some aquifer properties (transmissivity, hydraulic conductivity, and storage coefficients) based on point measurements from each of several aquifers. The purpose was to quantify for each parameter the integral scale and structured and unstructured variability and provide evidence for or against the normal and lognormal probability density function.

Their work examined aquifer properties that govern aquifer behavior at the scale of kilometers or tens of kilometers. Three models were proposed to describe the spatial structure of the hydrogeologic properties of interest, each model describing the spatial distribution of the property (or its natural logarithm) mean and covariance. The models included:

1. Constant mean, log transformation of data: The log transformation is applied to the spatial property of interest. The mean of the log transformed property is represented by a constant, and the spatial covariance function of the log transformed property is represented by an exponential function. The exponential function includes the nugget effect coefficient, structured variability coefficient, and the integral scale of the property.
2. Linear drift, log transformation of data: Similar to Model 1 but the mean of the property is varied linearly across the spatial field.
3. Linear drift and untransformed data: Similar to model 2 but the log transformation is not applied to the property of interest .

For each model, there are three parameters to be estimated. These include the integral scale coefficient ι (distance over which two measurements of the quantity of interest become uncorrelated), the unstructured variability coefficient V_n (variability which can not be attributed to significant spatial separation of measurement points), and structured variability coefficient V_s, (the variance of fluctuations attributable to spatial separation using the exponential form. The preceding coefficients were estimated using the maximum likelihood (ML) estimation approach. The estimation process included the transformation of the data so that the unknown mean is filtered out (to avoid

underestimating ι and V_s). The covariance matrix of the transformed data is then obtained, and ML estimation is applied. The third goal of this paper is to provide some evidence for or against two specific probability density models. The two considered models are (1) Gaussian using the original data or (2) Gaussian using the log transformed data. This was achieved using various statistical tests, including tests on the mean, variance, skewness coefficient, coefficient of Kurtosis, and the Kolmogorov-Smirnov test for normality.

To find which parameter model fits the spatial variability for a given data set, the Akaike Information Criterion (AIC) was used. This criterion is based on the estimation of the negative log likelihood for the fitted model and the number of independently adjusted coefficients within the model. The best model is the one that minimizes the AIC value.

This methodology was applied to 20 aquifers to analyze the spatial variability of transmissivity for aquifers in consolidated and unconsolidated materials, hydraulic conductivity for aquifers in unconsolidated materials, and the storage coefficient. The results of the analyses led to the following conclusions:

1. Precise estimates of the integral scale are difficult to obtain in all cases; The median value for the transmissivity integral scale for consolidated materials was estimated at 9.2 miles and for unconsolidated materials at 7.4 miles. The median value for the hydraulic conductivity in unconsolidated materials was estimated at 3.9 miles, while the median value for the storage coefficient was not determined because of convergence problems.

2. The results suggest that the lognormal distribution is a better choice than the normal distribution for all three parameters.
3. Models 1 and 2 were deemed most useful to analyze the spatial variability of the above-mentioned parameters.

2.4.2 Other Statistical Approaches

Wagner and Gorelick (1986) applied a statistical methodology to estimate the parameters of a one-dimensional linear solute transport model. Their approach was to combine solute transport simulation with nonlinear regression. Parameters are estimated by minimizing the weighted sum of squared differences between simulated and observed concentrations.

More specifically, this approach consists of the following steps: A nonlinear regression function estimates the solute transport parameters in the governing equation. Nonlinear regression is used because the unknown parameters in the governing solute transport equation are multiplied directly with either the solute concentrations or the first and second derivatives of these concentrations with respect to time or location. The parameters are estimated by minimizing the sum of squared residuals between observed and simulated concentrations. The simulated concentrations were obtained by developing a finite difference approximation to the governing equation using a Crank-Nicolson finite difference scheme. The solution of the unconstrained minimization problem is solved by the Newton method or the Gauss-Newton method. The solution procedure includes applying a Taylor-series expansion to the objective function, so that a quadratic model of the objective function about the current parameter estimates is developed.

The methodology was applied to a hypothetical one-dimensional case consisting of solute transport in a 100 meter soil column with the following unknown parameters:

average pore water velocity, hydrodynamic dispersion coefficient, first order decay coefficient, and zero order production coefficient. The study showed that the bias and standard deviation associated with the parameter estimates are significantly affected by the spatial and temporal location of the concentration data.

Kunstmann et al (2002) used a conditional and unconditional first order/second-moment (FOSM) analysis to quantify the uncertainty in groundwater modeling. Their work is an extension to work done by Dettinger and Wilson, 1981, Townley and Wilson, 1985, James and Oldenburg, 1997, and others. Second moment analysis was performed to derive the covariance matrices for heads and concentrations from the relevant governing equations. The analysis was performed for steady state conditions, with hydraulic conductivity and recharge considered random. The term "first order" refers to the use of Taylor expansion to linearize the expressions that relate hydraulic heads or concentrations to variations of log hydraulic conductivity or log recharge. Conditional first order second moment analysis was used assuming the availability of head or concentration measurements.

Polmann et al (1991) applied a stochastic modeling approach to evaluate large scale flow in heterogeneous unsaturated soils. A simulation experiment is designed to test the performance of a mean flow model based on the Mantoglou and Gelhar theory [1987a, b, c]. This experiment is done by comparing the predictions of the mean flow model (mean and variance of soil-water tension) to soil-water tension distributions obtained from a detailed three-dimensional model with spatially variable unsaturated hydraulic conductivity functions [Ababou, 1988]. The parameters which define these

functions are synthetically generated random fields which vary in a realistic way over all three dimensions.

The mean unsaturated flow model is based on expressing the Richards equation in a stochastic partial differential form. The steps to do that are as follows:

The Richards equation is expressed by

$$C(\Psi)\frac{\partial \Psi}{\partial t} = \frac{\partial}{\partial x_i}\left[K(\Psi)\frac{\partial (\Psi + x_1)}{\partial x_i}\right] \tag{2.21}$$

Where ψ is the (positive) soil-water tension at location x and time t. x_1 is the depth (increasing downward), $c(\psi) = -\partial\theta/\partial\Psi$ is the specific moisture capacity, θ is the volumetric soil moisture content, and $K(\psi)$ is an isotropic unsaturated hydraulic conductivity function. Tensor notation is used to represent spatial vectors, and is understood to be summed from 1 to 3.

In this article, the specific capacity in equation (2.21) is assumed to be a known invariant function of tension. The hydraulic conductivity function is assumed to have a log linear form:

$$\ln K(\psi) = \ln K_s - \alpha\,\psi \tag{2.22}$$

where K_s is the saturated hydraulic conductivity and α is the slope of the unsaturated log conductivity function. It should be noted that the coefficients $\ln K_s$ and α do not depend on tension and may vary over space. The effects of spatial variability are accounted for by assuming that $\ln K_s$ and α are stationary random with known statistical properties. More specifically, each of these parameters is decomposed into a mean and a random component:

$$\alpha = A + a \tag{2.23a}$$

$$\ln K_s = F + f \tag{2.23b}$$

Where A and F are ensemble means and a and f are random fluctuations. If the soil properties are assumed to be locally stationary, the variables A and F can be viewed as large-scale, slowly varying trends, while the fluctuations a and f can be viewed as local deviations from these trends.

If we substitute equations (2.22) and (2.23) into (2.21), we obtain the stochastic partial differential equation of the Richards equation. The mean soil-water tension can be expressed as follows:

$$C(H)\frac{\partial H}{\partial t} = \frac{\partial}{\partial x_i}\left[\hat{K}_{ij}\frac{\partial (H + x_1)}{\partial x_j}\right] \tag{2.24}$$

Where H is the mean tension and $\hat{K}_{ij}$ is an anisotropic hydraulic conductivity function which depends on the mean tension, the time and space derivatives of the mean tension, and the statistical properties of f and α. C(H) is the effective specific capacity.

The mean moisture content Θ can also be expressed as :

$$\Theta = \theta(H) \tag{2.25}$$

Equation (2.24) may be solved for the mean tension distribution once initial and boundary conditions have been specified for H.

The mean tension H is related to the random tension ψ by a relationship analogously to (2.23)

$$\psi = H + h \tag{2.26}$$

where h is a random fluctuation.

In order to solve equation (2.24) general functional expressions have to be substituted for the hydraulic conductivity and tension variances [Mantoglou and Gelhar, 1987a, b, c].

Unfortunately these general functions are quite complex and must be solved iteratively when they are substituted into (2.24). However these expressions can be simplified considerably if the following assumptions are used:

1. The random fields f and a have exponential autocorrelation functions with common vertical scale λ_1 and variances σ_f^2 and σ_a^2 respectively;
2. The random fields f and a are uncorrelated;
3. The dependence of $\hat{K}_{ij}$ and the tension variance σ_h^2 on the mean tension gradient $\frac{\partial (H)}{\partial x_i}$ is negligible;

Under these assumptions, the Mantoglou and Gelhar [1987a, b, c] expressions for $\hat{K}_{ij}$ and σ_h^2 are as follows:

$$\hat{K}_{11} = K_G \exp\left[- AH - E(ah) - \frac{\sigma_\varepsilon^2}{2} \right] \tag{2.27a}$$

$$\hat{K}22 = K_G \exp\left[- AH - E(ah) + \frac{\sigma_\varepsilon^2}{2} \right] \tag{2.27b}$$

$$\hat{K}12 = \hat{K}21 = 0 \tag{2.27c}$$

$$\sigma_h^2 = 2 \frac{\sigma_f^2 \lambda_1}{\pi} I_{hh} \tag{2.28}$$

In the above equations, K_G is the geometric mean of the saturated hydraulic conductivity, defined as $K_G = \exp(F)$. In equations (2.27a and 2.27b), E(ah) is the expected value of

the perturbation interactions of a and h. The term σ_ε^2 depends on σ_f^2, σ_a^2, σ_h^2, E(ah), and E(fh) . I_{hh} is an integral term defined by Mantoglou and Gelhar [1987a, b, c]. Equations (2.24)- (2.28) represent a complete set to evaluate the mean and variability of the soil-water tension due to the spatial variability of the unsaturated hydraulic conductivity parameter.

This approach was then applied to represent the mean and variability of the soil-water tension, for a defined synthetic problem by Ababou (1988):

1. Detailed model simulation: Equation (2.21) is solved for a three dimensional field 15 m (length) by 15 m (width) by 5 m (depth). The domain geometry is based on the first Las Cruces trench experiment [Weirenga et al., 1986]. The spatially variable parameters ln K_s and ln α, which define the unsaturated hydraulic conductivity functions, are obtained from two independent normally distributed random fields produced by the turning bands algorithm [Mantoglou, 1987]. Equation (2.21) is then solved for the soil-water tension field using a finite difference approximation scheme.
2. The mean flow simulation: Equations (2.24)- (2.28) are then solved for the same field, as above, using a finite element scheme.

Results from the two simulation experiments, show that the mean and variability of the soil-water tension from the detailed model simulation are represented well using the mean flow simulation.

The authors refer to few limitations to their approach as follows:

1. Their experiment is based on a simplified model of unsaturated hydraulic conductivity which cannot be valid over a wide range of tensions;

2. The mean flow model and detailed simulation both assume that the random hydraulic conductivity parameters f and a are uncorrelated. In a real field problem these parameters tend to be correlated;
3. The mean flow model and detailed simulation both assume that the variability in soil water tension is only due to the hydraulic conductivity variability. This assumption ignores other important sources of heterogeneity which may influence large scale moisture movement. For example, the volumetric soil moisture content was treated deterministically based on an invariant moisture retention curve.
4. The mean model is based on perfect knowledge of the statistical parameters used to generate the detailed models soil properties. These statistical parameters include, for example, the autocorrelation functions for ln K_s and ln α. In reality, this model would have to rely on approximate statistics estimated from a limited number of soil samples.

Kapoor and Gelhar (1994), followed an analytical approach to asses the concentration variability in three-dimensionally heterogeneous aquifers. The partial differential equations of the mean and variance of the concentration are developed based on the governing solute transport equation. Mathematical analysis is applied for the macrodispersive terms and variance dissipation term in the developed mean and variance of the concentration partial differential equations. The purpose of this analysis is to understand the effect of these terms on the dynamics of the concentration fluctuations. Their analysis is as follows:

The transport of a passive scalar with concentration c, undergoing local dispersion and advection in a velocity field with a mean ν in the x_1 direction, and a zero-mean, three-

dimensional, divergence free, and spatially varying component v_i' is governed by the parabolic equation

$$\frac{\partial c}{\partial t} + v \frac{\partial c}{\partial x_1} + v_i' \frac{\partial c}{\partial x_i} - v \alpha_{ij} \frac{\partial^2 c}{\partial x_i \partial x_j} = 0 \qquad (2.29)$$

Summation over repeated indices is implied in (2.29). The local dispersivities α_{ij} have different longitudinal and transverse values.

In equation (2.29):

$$c = \bar{c} + c' \qquad (2.30)$$

Where $\bar{c}$ is the mean concentration and c' is concentration perturbation.

Substituting (2.30) in (2.29), using the divergence-free condition of the velocity fields $\frac{\partial v_i'}{\partial x_i} = 0$ (continuity equation), and then taking the expectation, they get the mean concentration equation:

$$\frac{\partial \bar{c}}{\partial t} + v \frac{\partial \bar{c}}{\partial x_1} - v \alpha_{ij} \frac{\partial^2 \bar{c}}{\partial x_i \partial x_j} + \frac{\partial \overline{c' v_i'}}{\partial x_i} = 0 \qquad (2.31)$$

By subtracting equation (2.31) from (2.29), they derive the concentration perturbation equation:

$$\frac{\partial c'}{\partial t} + v \frac{\partial c'}{\partial x_1} - v \alpha_{ij} \frac{\partial^2 c'}{\partial x_i \partial x_j} + \frac{\partial}{\partial x_i}(c' v_i' - \overline{c' v_i'}) = - v_i' \frac{\partial \bar{c}}{\partial x_i} \qquad (2.32)$$

To analyze the concentration variance, i.e., $\sigma_c^2 = E[\, c' \,]$, Equation (2.32) is multiplied by another concentration perturbation. After taking the mean, we get the exact concentration variance equation (2.33):

$$\frac{\partial \sigma_c^2}{\partial t} + v \frac{\partial \sigma_c^2}{\partial x_1} - v \alpha_{ij} \frac{\partial^2 \sigma_c^2}{\partial x_i \partial x_j} + \frac{\partial}{\partial x_i}(\overline{v' c_i'^2}) = -2(\overline{v' c_i'}) \frac{\partial \bar{c}}{\partial x_i} - 2 v \alpha_{ij} \overline{\frac{\partial c'}{\partial x_i} \frac{\partial c'}{\partial x_j}}$$

Kapoor and Gelhar then analyzed the following terms from the mean and variance concentration equations:

1. $\frac{\partial \overline{c' v_i'}}{\partial x_i}$, which is the last term on the left hand side of equation (2.31). This term is noted in the article as the macrodispersive flux term for the mean concentration.
2. $\frac{\partial}{\partial x_i}(\overline{v' c_i'^2})$, the last term on the left hand side of equation (2.33). This term is noted in the article as the macrodispersive flux term for the variance concentration.
3. $2 v \alpha_{ij} \overline{\frac{\partial c'}{\partial x_i} \frac{\partial c'}{\partial x_j}}$, the last term on the right hand side of equation (2.33). This term is nonnegative and therefore acts as a sink for the concentration variance. This term is noted in the article as the dissipation/destruction of variance concentration term.

Mathematical analysis for the above three terms using mainly the Green's function for the advection- dispersion operator, resulted in the following estimates for the above terms:

1. $$(\overline{v' c_i'}) = -v A_{mi}(t) \frac{\partial \bar{c}(x,t)}{\partial x_i} \qquad (2.34)$$

where the "macrodispersivities" $A_{mi}(t)$ are calculated based on the Green's function for the advection- dispersion operator governing the macrodispersive flux term

2. $\overline{(\nu' c_i'^2)} = -\nu A_{mi} \frac{\partial \sigma_c^2}{\partial x_i}$ (2.35)

3. $2 \nu \alpha_{ij} \overline{\frac{\partial c'}{\partial x_i} \frac{\partial c'}{\partial x_j}} \approx \langle \frac{2 \nu \alpha_{ij}}{\Delta_i^c \Delta_j^c} \rangle \sigma_c^2$ (2.36)

The reason for using the approximation sign $\approx$ in the above equation is because of applying the stationarity assumption for the covariance field. This means that the covariance function between any two locations like x_i and x_j is a function of the distance between the two locations: x_j-x_i . In equation (2.36), Δ_i^c is called the microscale of the concentration perturbation field. It is the scale that characterizes the derivatives of the concentration perturbation field. The term $\langle \frac{2 \nu \alpha_{ij}}{\Delta_i^c \Delta_j^c} \rangle$ is called the " variance decay coefficient."

Equations (2.34) – (2.36) are then substituted in the mean and variance of concentration equations. The authors concluded their article by comparing their analytical results with results obtained by Dagan [1982, 1990]. Their conclusion is that their approach compares favorably with Dagan's results.

2.5 Concluding Remarks on Literature Review

From the review of the previous literature, the following research challenges can be identified in the area of conjunctive groundwater and surface water management:

(1) Dimensionality: The representation of groundwater system response requires the use of finite element or finite difference numerical schemes. However, accurate

representation requires a large number of nodes (in finite element schemes) or grid points (in finite difference schemes), with this number rising to more than 10000 nodes or grid points in multi layer systems. In this regard, the response matrix approach has a definite advantage over the embedding method. However, even the response matrix approach faces challenges in view of the need to represent system uncertainties and transient flow and contaminant dynamics.

(2) Uncertainty analysis: Geostatistical approach provides a comprehensive framework to incorporate groundwater parameter uncertainty. However, the following disadvantages have been noted:

1. The geostatistical approach requires the use of many measurement points to identify the spatial structure of the hydrogeological properties of the aquifers including transmissivity, hydraulic conductivity, specific storage, and specific yield. The spatial structure of these properties is described by models that preserve the mean and the covariance. Accurate representation of these models requires accurate assessment of the coefficients these models depend on such as the integral scale, structured variability and the nugget effect coefficient. In large ground water models, however, many measurement points must be taken at different locations and depths to accurately estimate the above-mentioned coefficients. This requires expensive field tests that are seldom available. Therefore, other approaches must be considered to characterize parameter uncertainty when dealing with large aquifer systems.
2. The geostatistical approach represents parameter uncertainty by generating point realizations of groundwater parameters. However, in groundwater models

groundwater parameters are represented in zones, and the use of geostatistical approaches to generate realizations of these zones requires modifications of the basic geostatistical theory including the generation of the variogram functions.

The issues associated with conditional and unconditional first order second-moment analysis echo those indicated above:

1. Dimensionality: The size of the covariance matrices can become infeasibly large as the nodes of the numerical scheme increase. Transient simulation adds more burden because the large covariance matrices have to be propagate in time.
2. Uncertainty: Parameter uncertainty must be moderate as the method is inherently a linear method. Cornell (1972) suggests that the coefficient of variation of the parameters should be $\leq .2$.

(3) Management algorithms:

1. The management algorithms reported in the literature review do not guarantee convergence to globally optimal solutions. For example, in the article by Wagner and Gorelick (1987), where the nonlinear optimization solver NPSOL is used, the authors mention that global optimality cannot be guaranteed. Likewise, Gorelick and Voss (1984) used MINOS; these authors mention that any practical solution for the optimization problem using MINOS can guarantee only a local optimum.
2. Linear programming (LP) has been used widely in groundwater management problems. While efficient, this optimization method has certain disadvantages: First, the objective function and the constraints have to be linear. In conjunctive management problems, however, nonlinearities are embedded in the problem formulation. Therefore, the use of linear programming limits the management

problem formulation. Second, according to Ahlfeld and Mulligan (2000), in large regional systems with many constraints, the LP can be computationally challenging. This is because LP requires the calculation of the inverse basis matrix (the matrix that includes the constraints coefficients) periodically during the solution process.

3. The management algorithms reported in the literature do not fully account for system uncertainty. The reason is that the computational requirements increase significantly when uncertainty and stochastic analysis is included (Wagner and Gorelick (1987)).

2.6 Conjunctive Management: Challenges and Issues to be Addressed

Dimensionality: This issue is addressed by developing parsimonious state space representations of aquifer response. The associated equations are included explicitly in the optimization model.

Uncertainty: A new statistical procedure to asses the uncertainty in groundwater parameters is developed assuming that the aquifer consists of distinct zones with constant but uncertain parameters. This procedure has a fairly general applicability including systems with scarce measurements. Aquifer response uncertainty is characterized through the generation of ensembles reflect various uncertainty sources.

Management Method: The conjunctive management problem is solved using efficient stochastic control theory methods. The case studies demonstrate that the overall approach is able to handle all previous aspects with high reliability and efficiency.

CHAPTER 3

GROUNDWATER MODELING UNDER UNCERTAINTY

3.1 Introduction

In this chapter, the goal is to develop models of groundwater aquifer response that (1) account for input and parameter uncertainty and (2) are sufficiently computationally efficient to be used with management models. The development focuses on confined aquifers, but the methodology can potentially be extended to unconfined aquifers. Some comments in this regard are offered at the end of the chapter.

Past research experience (literature review section) shows that the response matrix approach has several advantages over the embedding method. However, it too suffers from conceptual and computational difficulties, the former related to its ability to correctly represent uncertainties and the latter to dimensionality issues.

This chapter addresses these difficulties in the following progressive manner: First, a state space representation of the transfer function approach is developed that reduces the dimensionality of the variables necessary to represent aquifer response. Second, parameter uncertainty is modeled using a statistical approach. Third, parameter uncertainty is incorporated in the transfer function representation. Fourth, a Monte Carlo approach is used to generate transfer function ensembles to be used in the management

model. The Amman-Wadi Sir aquifer in Jordan serves as a case study for the application of the methods developed herein.

3.2 Deterministic Transfer Functions

3.2.1 Groundwater Simulation Model

Transfer functions can be developed by any groundwater model that simulates aquifer flow. This study uses MODFLOW, a well known groundwater model developed by the United States Geological Survey (USGS), Mcdonald and Harbaugh (1988). MODFLOW employs a finite difference scheme to approximate the three dimensional groundwater flow equation. The grid size used to model the Amman-Wadi Sir aquifer (the most important aquifer of the Amman-Zarqa basin in Jordan) is 2 km by 2 km applied over an area of 50 km by 108 km. (Namely, the grid consists of 25 rows 54 columns.) Eleven observational wells and 25 pumping centers exist within the basin. Data from these wells and pumping areas are available from February, 1989, to December, 2000, on monthly time resolution.

Figure 3.2.1.1 shows the Amman-Zarqa basin, the geological layers within the basin, and the conceptual groundwater flow model for the Amman-Wadi Sir Aquifer. Figure 3.2.1.2 shows the finite difference grid scheme to simulate the flow within the Amman-Wadi Sir Aquifer, including the locations of the specified head (lateral boundary condition) grid points, pumping well locations, observation well locations and names (P(i),i=1,…,11), recharge area, and inactive area.

Amman-Wadi Sir Aquifer:

- Most Important Aquifer in the Amman-Zarqa Basin (AZB)
- Principal Source of Fresh Water For Amman
- Relatively High Hydraulic Conductivity

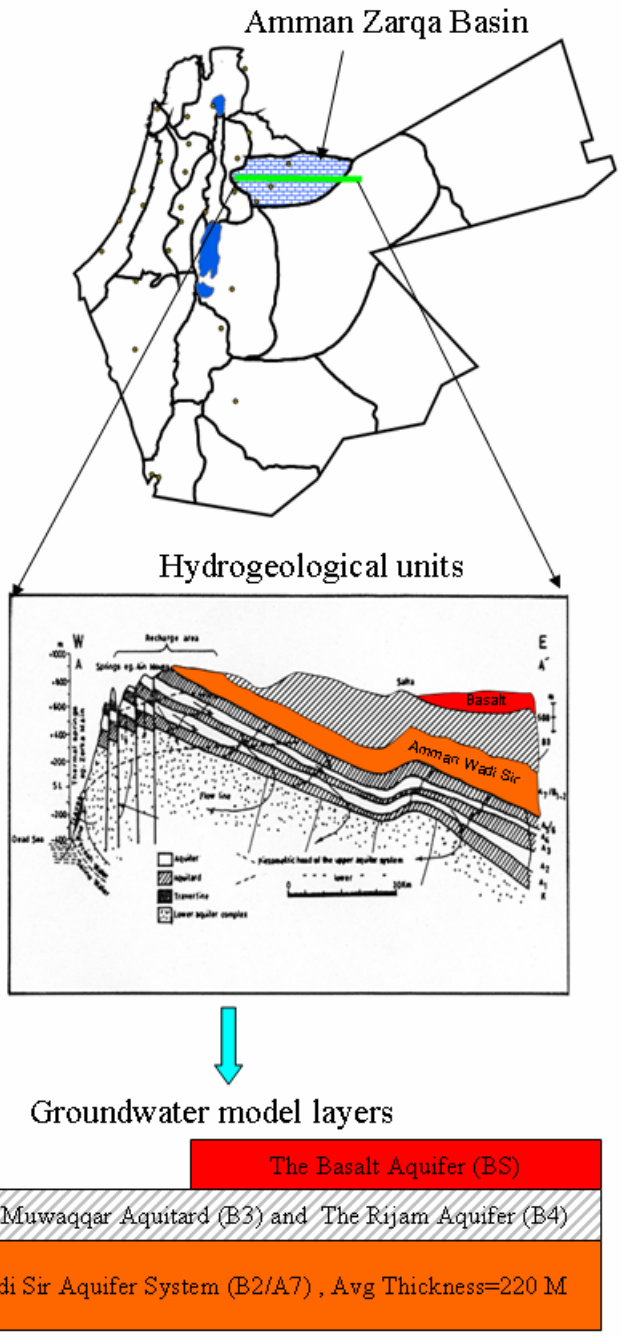

Figure 3.2.1.1: Amman-Wadi Sir aquifer

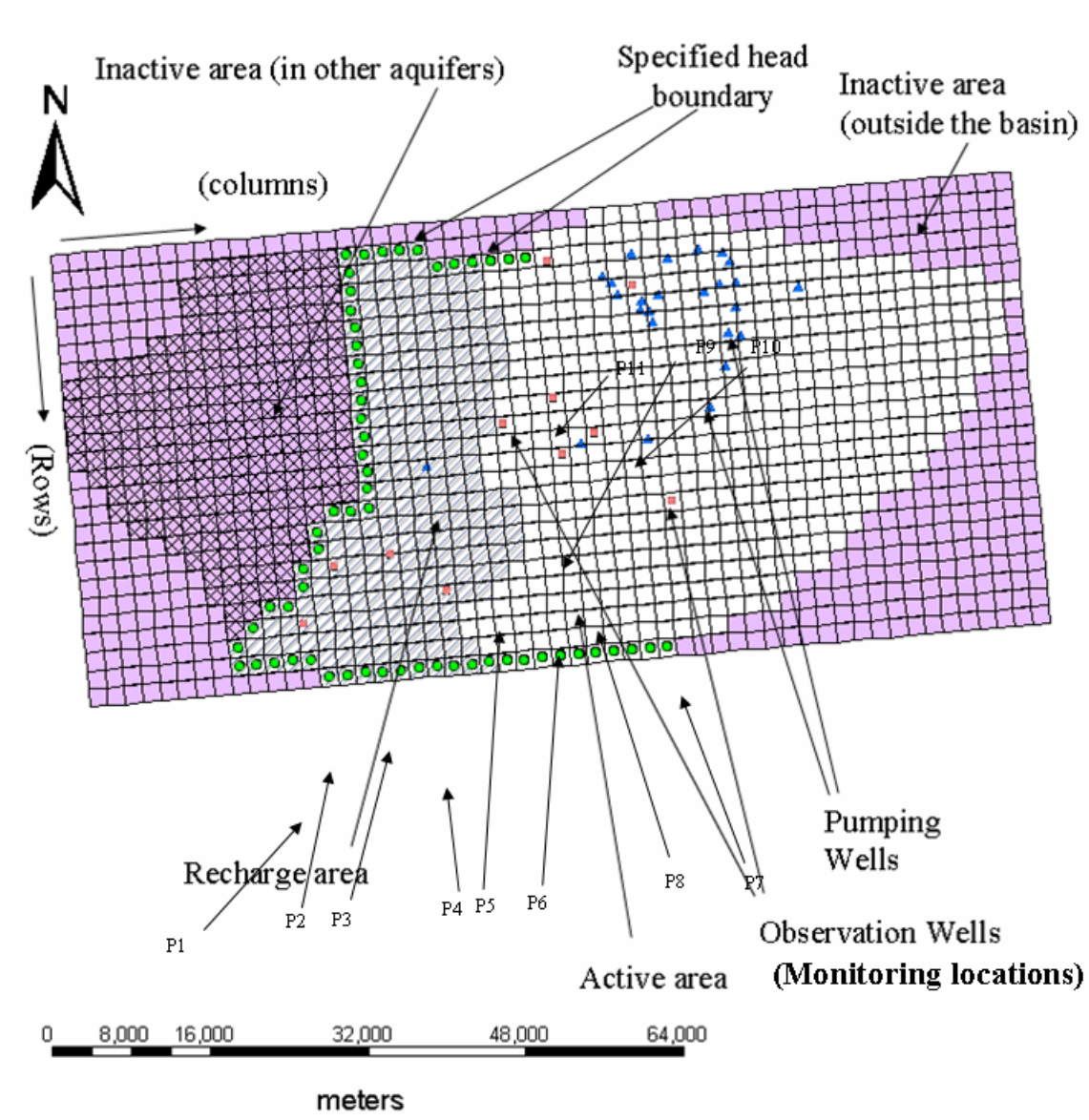

Figure 3.2.1.2: Amman-Wadi Sir aquifer, finite difference scheme

Specified head boundaries at the boundary grid points were determined based on interpolating hydraulic heads at the observational well locations (qrtificial boundary method, Anderson and Woessner, 1992). No flow boundary condition was applied at the eastern parts of the aquifer based on current information about the aquifer hydrogeological boundaries (Overview of Middle East Water Resources, USGS publication; 1998). The assumption of no flow boundary was verified during the calibration process by comparing simulated and interpolated heads at these grid nodes. The results are shown in the next section and support this assumption.

Model inputs are boundary conditions, aquifer thickness, hydraulic conductivity and specific storage coefficients, pumping and recharge. Model outputs are simulated hydraulic heads at each grid point. The calibration data set consists of hydraulic head observations at the monitoring locations. Model calibration is based on a two step approach: First, the root mean squared error (RMSE), i.e., the square root of the mean sum of squared residuals (difference between observed and simulated heads) at all monitoring wells, is minimized. Second, a statistical test is applied at each location to check if calibrated and observed head sequences are statistically similar. This process is described in more detail next.

3.2.2 Model Calibration

The calibration process aimed at defining an adequate number of constant hydraulic conductivity and storage coefficient zones such that an acceptable match between observed and simulated piezometric heads is achieved at the monitoring locations. The "acceptability" of matching was evaluated based on the following criterion:

[RMSE / Head difference across the basin] * 100% ≤ 10%. (3.1)

This criterion is used by USGS for regional model calibrations.

The resulting RMSE for the calibrated model is 3.22 m, while the head difference across the Amman-Wadi Sir aquifer is 275 m.

The "acceptability" of the calibration process was further evaluated at each monitoring location by checking if the observed head and calibrated head sequences are statistically similar. This test was carried out using the Wilcoxon signed-rank statistical test, as explained in section 3.3. The purpose of this test is to check if the observed and simulated head sequences belong to the same statistical population. The test null and alternative hypotheses were formulated as follows:

H_0: Simulated and observed head sequences belong to the same population;

H_a: Simulated and observed head sequences do not belong to the same population.

Under the null hypothesis the distribution of the Wilcoxon signed-rank test statistic is Gaussian, and the null hypothesis is evaluated. The significance level was taken equal to 5% .

In the calibrated model, the number of monitoring locations passing the statistical test was 10. The test accounts for the effect of spatial correlation expected to exist in this case. Generally, spatial correlation may lead to more monitoring locations failing the test than under spatial independence. However, 10 out of 11 locations passing the statistical test is clearly inside the rejection region of the null hypothesis, and the conclusion is that the simulated and observed heads are statistically similar.

The calibration process started off by a number of zones where hydraulic conductivity and storage coefficients were thought to be constant based on hydrogeologic aquifer data. Further refinement of the zones proceeded by zone subdivision or

aggregation. For each zone configuration, a direct search approach was used to identify the optimal hydraulic conductivity and storage coefficient values. The calibration process ended when the acceptability criterion was met.

Figure 3.2.2.1 shows the identified zones of hydraulic conductivity and storage coefficients. Figure 3.2.2.2 shows observed and simulated head sequences at some of the observational wells over the 1989 to 2002 calibration period.

The no flow boundary condition was verified by comparing the simulated head at the no flow boundary nodes with the interpolated head from well observations. The no flow boundary nodes were divided into two clusters based on the patterns of the interpolated head at theses grid points. For each cluster, the mean head from all grid points within the cluster is computed for the interpolated and simulated heads. The interpolated and simulated mean heads compare favorably at both clusters (Figure 3.2.2.3).

3.2.3 State Space Representation of Transfer Functions

A transfer function is the groundwater response (drawdown) at a particular location resulting from the application of a unitary pulse stress (such as pumping at another location or boundary condition change). Figure (3.2.3.1) shows 3 transfer functions at two different monitoring locations. Two of the transfer functions are due to pumping pulses, whereas the third corresponds to a boundary perturbation.

In confined aquifers, the relation between pumping or boundary stresses and drawdown is linear. Mathematically, this can be expressed as follows:

Pumping Stress:

$$d_P(k+1)= T_P(1)\, P(k) + T_P(2)\, P(k-1) + T_P(3)\, P(k-2)+\ldots+ T_P(n)\, P(k-n+1) \qquad (3.2)$$

Boundary Stress:

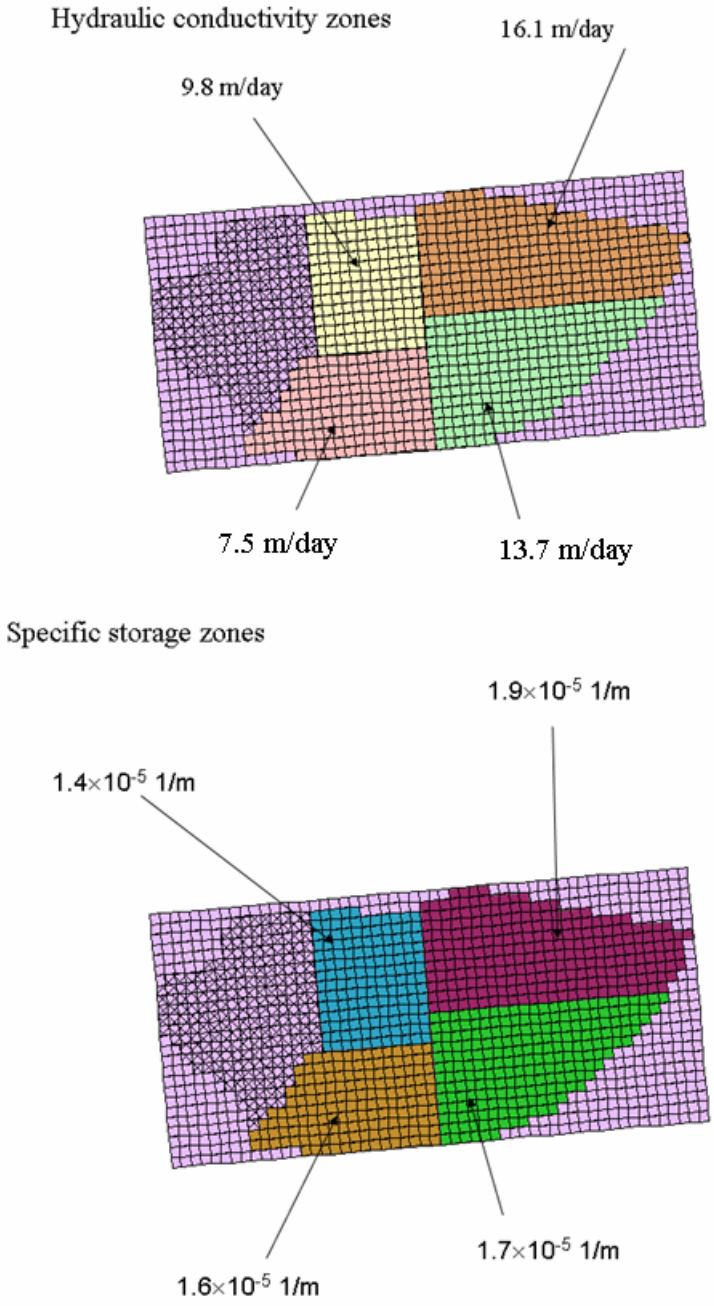

Figure 3.2.2.1: Amman-Wadi Sir aquifer, calibrated hydraulic conductivity and storage coefficients zones

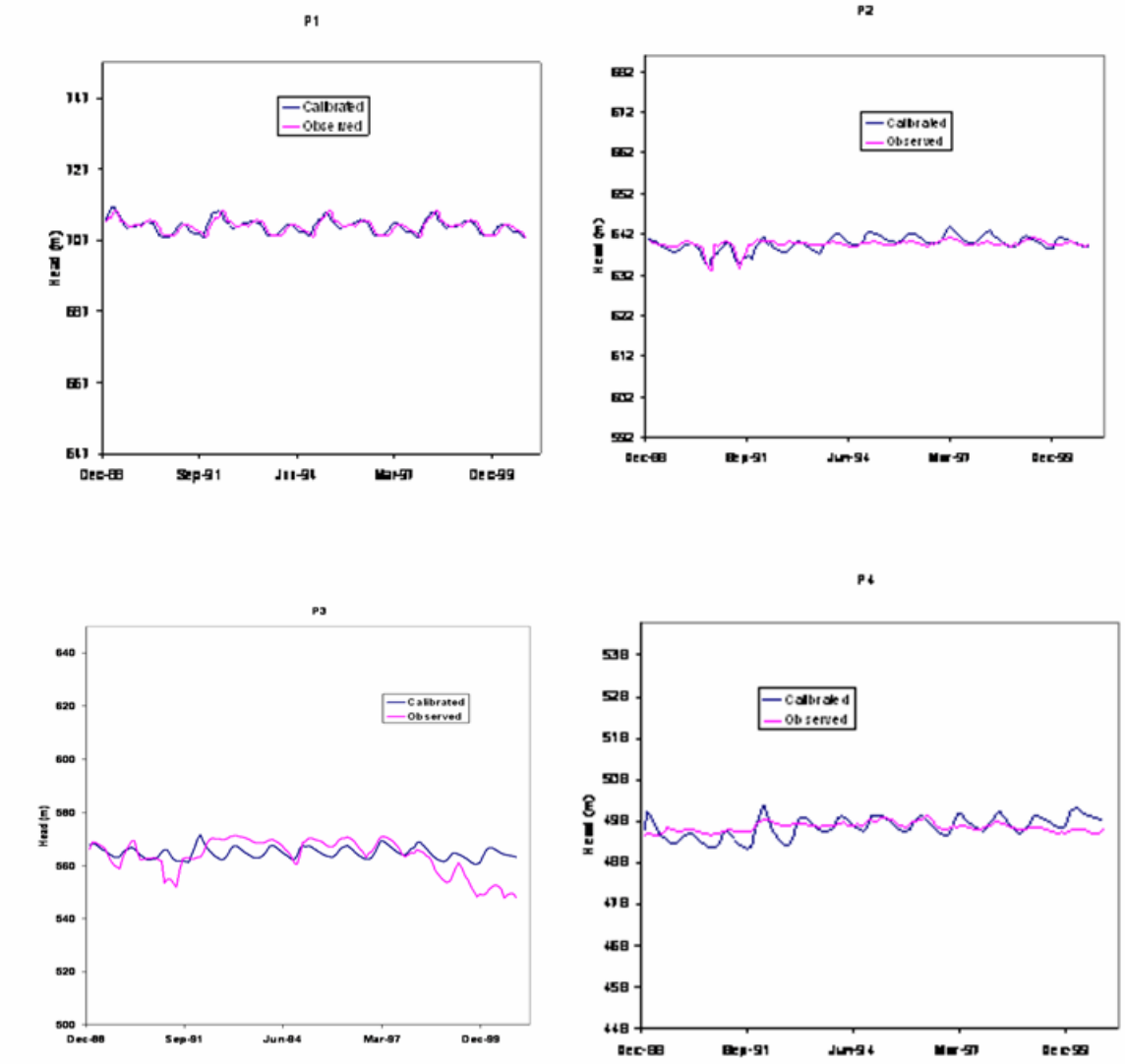

Figure 3.2.2.2: Amman-Wadi Sir aquifer, simulated and observed piezometric heads

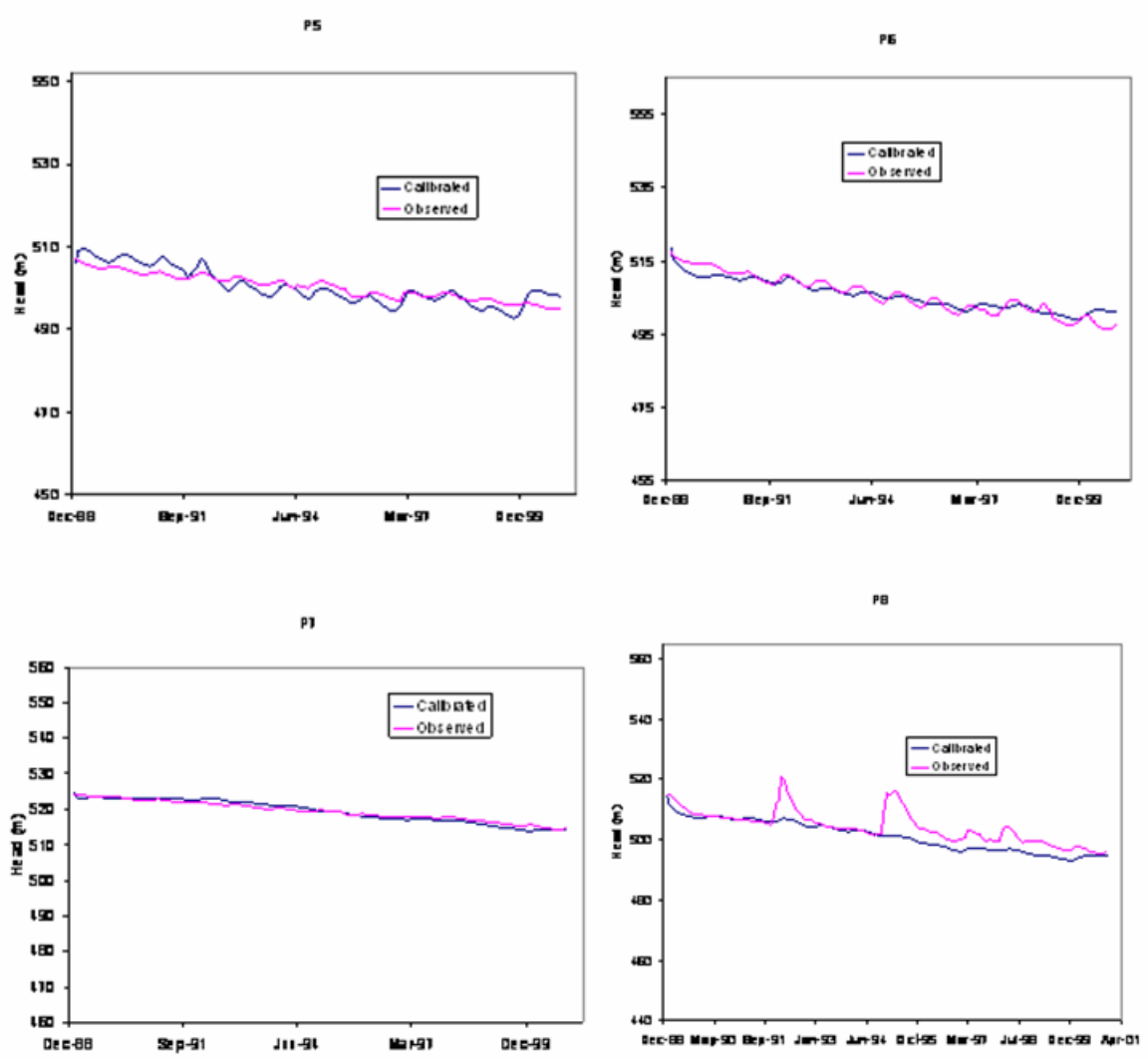

Figure 3.2.2.2: Amman-Wadi Sir aquifer, simulated and observed piezometric heads

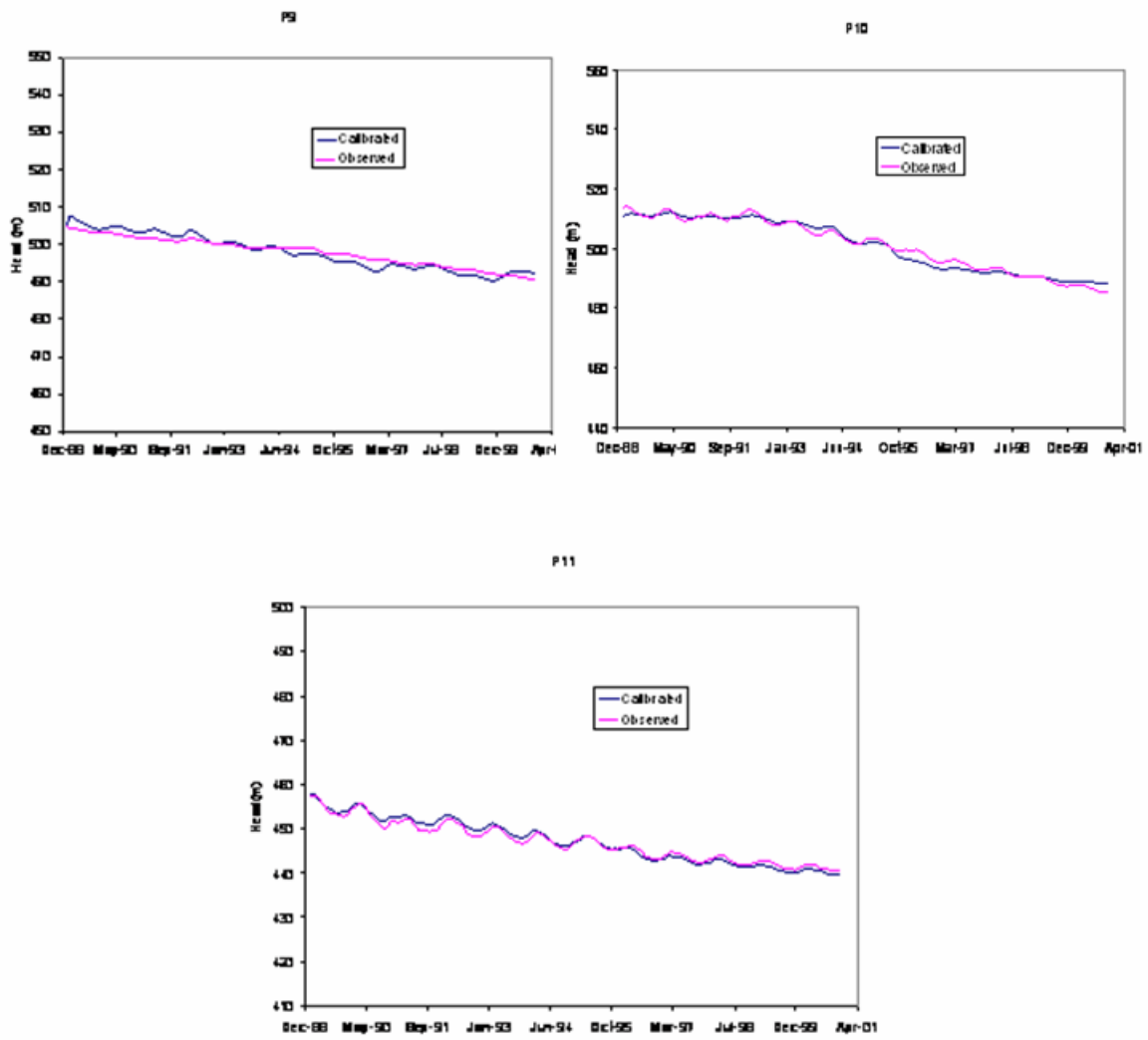

Figure 3.2.2.2: Amman-Wadi Sir aquifer, simulated and observed piezometric heads

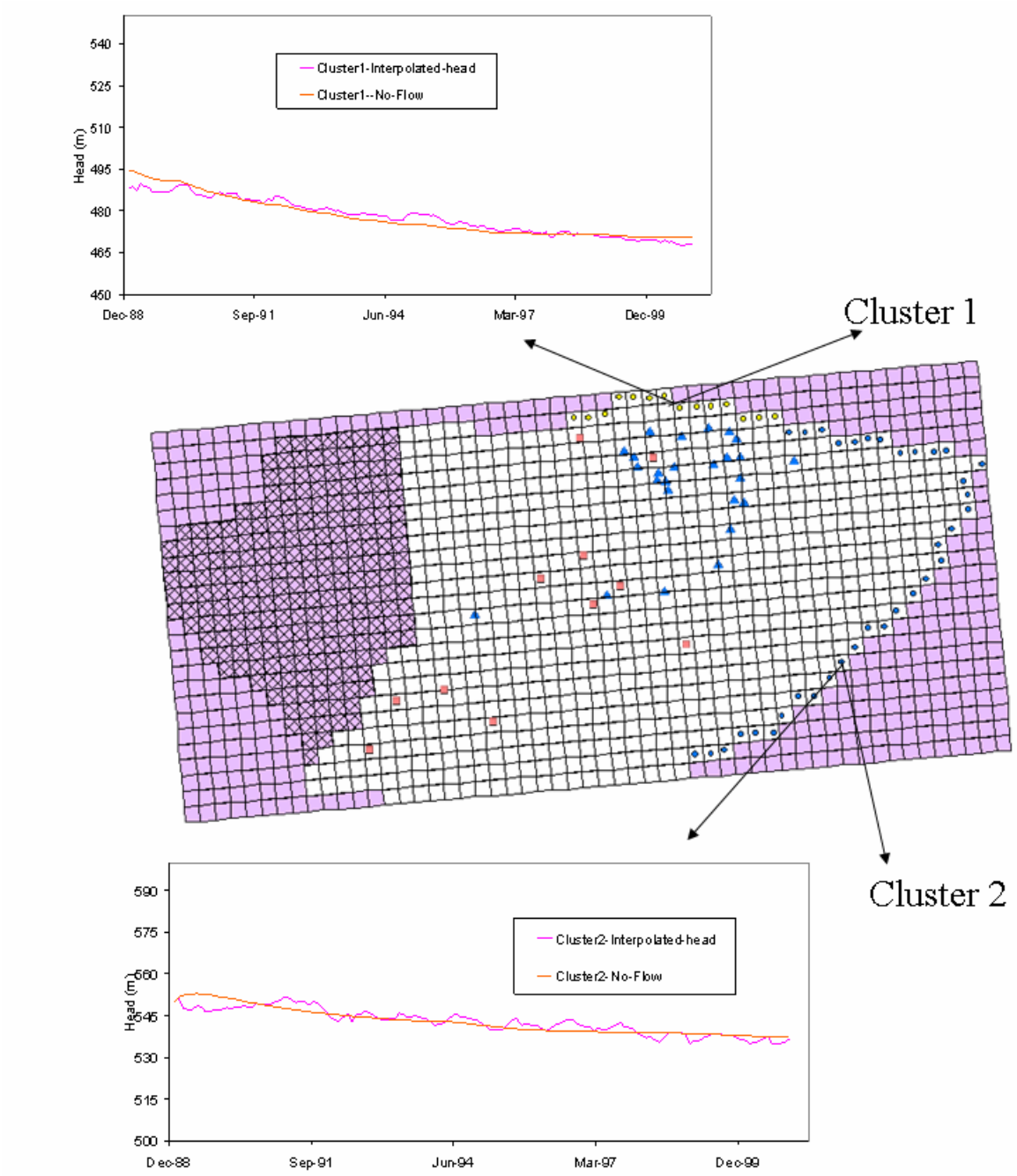

Figure 3.2.2.3: Amman-Wadi Sir aquifer, simulated and interpolated heads at the no flow boundary clusters

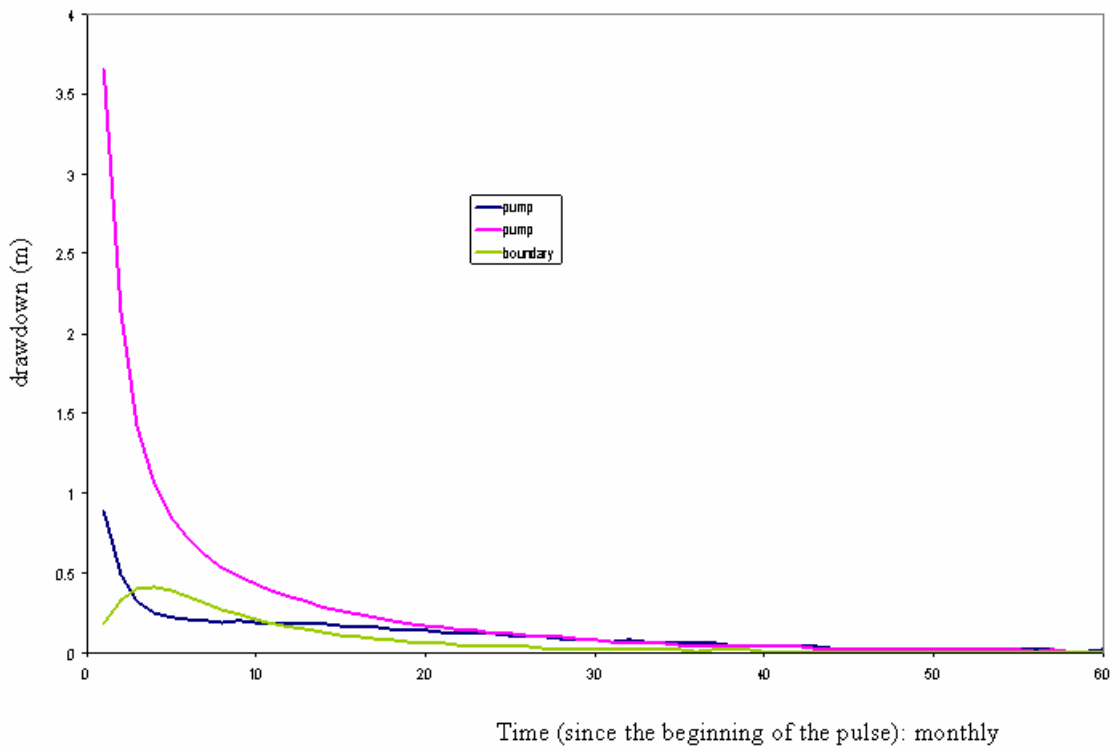

Figure 3.2.3.1: Groundwater transfer functions

$$d_b(k+1)= T_b(1)\, b(k) + T_b(2)\, b(k-1) + T_b(3)\, b(k-2)+\ldots.+ T_b(n)\, b(k-n+1) \qquad (3.3)$$

where:

$d_p(k+1)$ and $d_b(k+1)$ are drawdowns due to pumping and boundary stresses respectively, at the beginning of time step (k+1);

P(i) and b(i): are pumping and boundary stresses respectively, at time step i,

i = k, k-1,…., k-n+1;

n is the number of time periods over which the transfer function is defined; and

T_p (j) and T_b(j), j=1,….,n, are transfer function coefficients corresponding to pumping and boundary stresses respectively.

Equations (3.2) and (3.3) determine aquifer drawdown as a function of stresses that might have occurred several time periods earlier. From a management standpoint, this is a complicating feature as it leads to dimensionality complications. It is thus desirable to try to convert the transfer function into a simpler form that depends on fewer variables. The approach taken here is to develop a state space approximation of the transfer function drawdown. The following development motivates this approach. Consider equation (3.2), the transfer function pertaining to pumping, for two time steps k and k+1:

Time step (k):

$$d_p(k+1)= T_p(1)\, P(k) + T_p(2)\, P(k-1) + T_p(3)\, P(k-2)+\ldots+ T_p(n)\, P(k-n+1)$$

Time step (k+1):

$$d_p(k+2)= T_p(1)\, P(k+1) + T_p(2)\, P(k) + T_p(3)\, P(k-1)+\ldots+ T_p(n)\, P(k-n+2) \qquad (3.4)$$

Equation (3.4) can be written as follows:

$$d_p(k+2)- T_p(1)\, P(k+1) = T_p(2)\, P(k) + T_p(3)\, P(k-1)+\ldots+T_p(n)\, P(k-n+2) \qquad (3.5)$$

Dividing (3.5) by (3.3) yields:

$$\frac{dp(k+2) - Tp(1)\,P(k+1)}{dp(k+1)} = \frac{Tp(2)\,P(k) + Tp(3)\,P(k-1) + \ldots + Tp(n)\,P(k-n+2)}{Tp(1)\,P(k) + Tp(2)\,P(k-1) + \ldots + Tp(n)\,P(k-n+1)} \qquad (3.6)$$

For large enough n, $T_p(n)$ becomes small and P(k-n+1) can be neglected in the denominator:

$$\frac{dp(k+2) - Tp(1)\,P(k+1)}{dp(k+1)} = \frac{Tp(2)\,P(k) + Tp(3)\,P(k-1) + \ldots + Tp(n)\,P(k-n+2)}{Tp(1)\,P(k) + Tp(2)\,P(k-1) + \ldots + Tp(n-1)\,P(k-n+2)} \qquad (3.7)$$

If the ratios $T_p(k+1)/ T_p(k)$, k=1,2,…,n-1, were all equal to a constant α, then,

$$\frac{dp(k+2) - Tp(1)\,P(k+1)}{dp(k+1)} = \frac{\alpha(Tp(1)\,P(k) + Tp(2)\,P(k-1) + \ldots + Tp(n-1)\,P(k-n+2))}{Tp(1)\,P(k) + Tp(2)\,P(k-1) + \ldots + Tp(n-1)\,P(k-n+2)} \qquad (3.8)$$

and the result would be

$$\frac{dp(k+2) - Tp(1)\,P(k+1)}{dp(k+1)} = \alpha \quad . \qquad (3.8a)$$

The above equation can also be written as

$$d_p(k+2) = T_p(1)\,P(k+1) + \alpha\, d_p(k+1) \quad . \qquad (3.9)$$

In this equation, quantity $d_p(k+1)$ is the state variable and represents the information needed at time k to predict the future evolution of the drawdown in response to a certain pumping stress sequence [P(k+1), P(k+2), P(k+3), …]. Equation (3.9) is said to be in state space form. This equation is computationally simpler than the original transfer function as it substitutes all terms prior to time k+1 by the term $\alpha\, d_p(k+1)$.

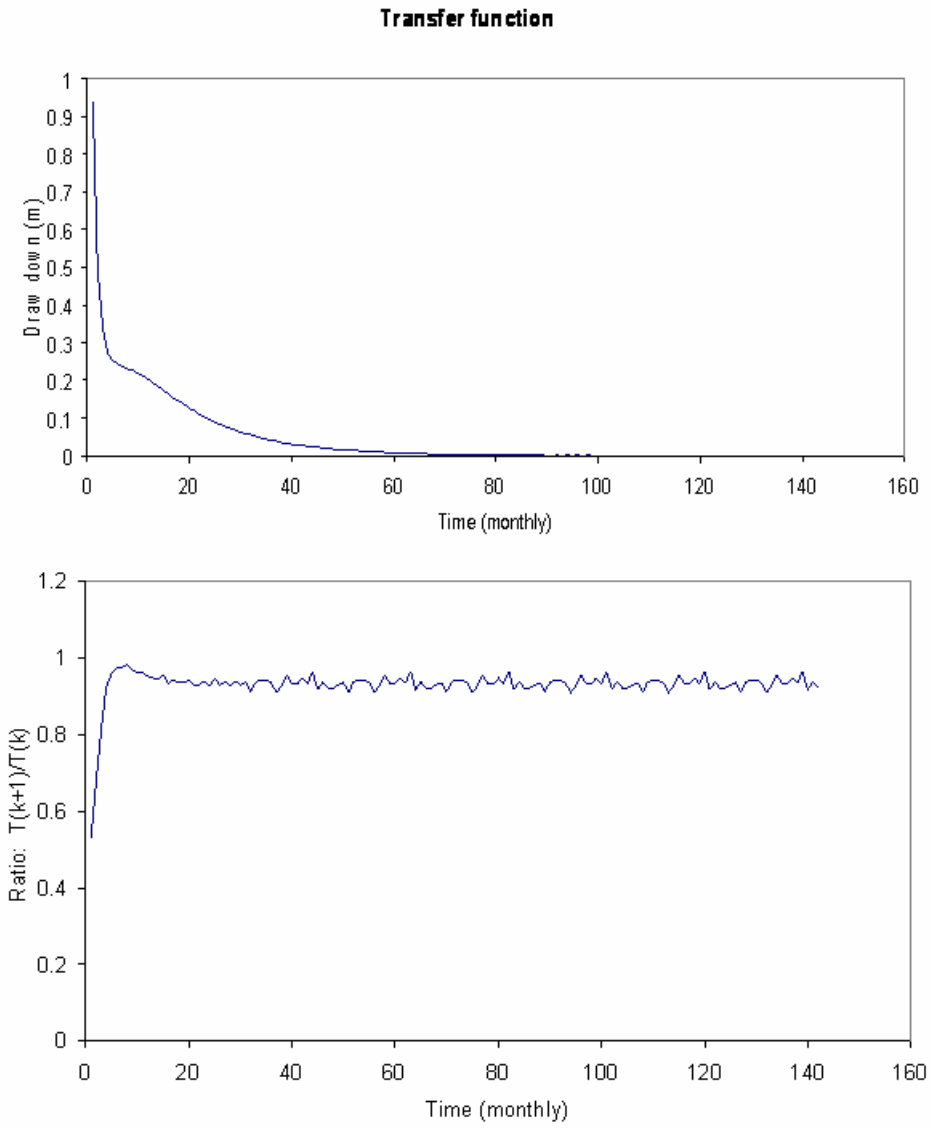

Figure 3.2.3.2a: Transfer functions coefficients ratio

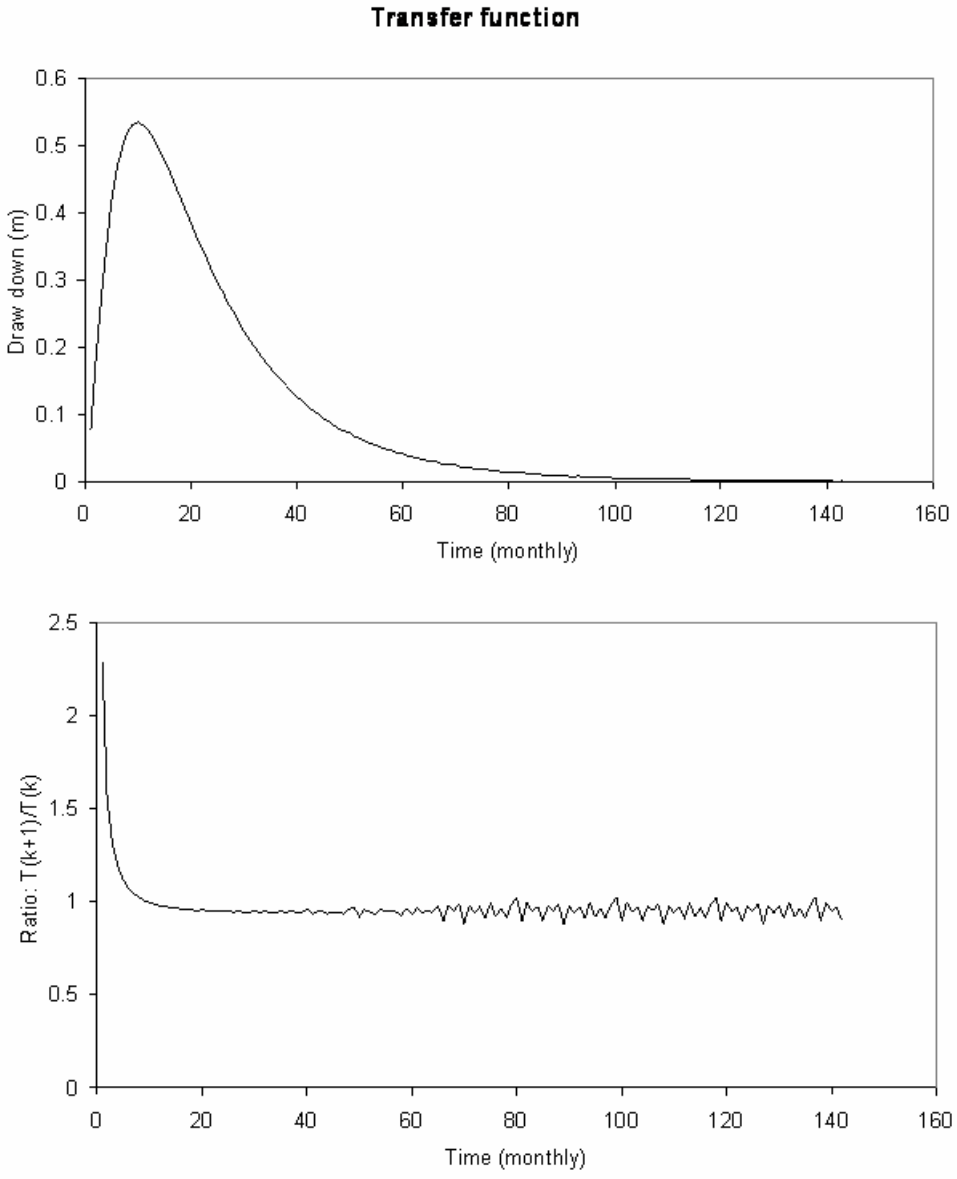

Figure 3.2.3.2b: Transfer functions coefficients ratio

Returning to the assumption that led to equation (3.9), the form of the transfer functions is such that after an initial period, the ratio $T_p(k+1)/ T_p(k)$ settles to an approximately constant value. Figures 3.2.3.2a and 3.2.3.2b show this ratio for two different transfer functions and verify that after an initial period the ratio is approximately constant. Thus, in this region (i.e., in the long tail of the transfer function), the state space formulation provides a very good approximation. However, to account for the initial period during which α fluctuates, the formulation needs to be expanded. The modification could be derived by repeating the previous analysis assuming that $T_p(k+1)/ T_p(k) = \alpha$ if $k > m$, and $T_p(k+1)/ T_p(k) = \alpha + \Delta\alpha$ for $k \leq m$. Namely, one approach is to assume that α is constant over a certain portion of the transfer function and gradually shifts to different values as time nears the origin (i.e., the instant that the stress pulse is applied). The effect on the resulting equation would be to include more $P(k)$ and $d_p(k)$ terms at different times. The associated mathematical derivation is included in Appendix A.

Thus, aquifer drawdown due to pumping or boundary stresses, can potentially be represented by state space dynamical equations of the following form:

Pumping at site i:

$$d_p(k+1,i) = \alpha_p(i)\, P(k,i) + \beta_p(i)\, P(k-1,i) + \gamma_p(i)\, d_p(k,i) + \theta_p(i)\, d_p(k-1,i) \qquad (3.10)$$

where $[\alpha_p(i), \beta_p(i), \gamma_p(i), \text{and } \theta_p(i)]$ are coefficients to be estimated.

Compared to equation (3.9), equation (3.10) includes two additional terms. More terms could be added depending on the "goodness" of the approximation. Equation (3.10) includes three state variables, $P(k-1,i)$, $d_p(k,i)$, and $d_p(k-1,i)$, significantly reducing the dimensionality of the original transfer function.

Using the property of superposition, the total drawdown due to pumping and boundary stresses can be computed by

$$d(k+1)=\sum_i d_p(k+1,i) + \sum_j d_b(k+1,j) \quad (3.11)$$

$i=1,\ldots,L$, and $j=1,\ldots,M$,

where L and M are the number of pumping and boundary stress sites respectively.

3.2.4 Application

This application uses the previous approach to estimate the drawdown at a particular monitoring location due to pumping and boundary stresses. Figure 3.2.4.1 shows the monitoring location, pumping locations, and boundary locations. The boundary locations are grouped into two clusters, and the pumping locations are grouped into one. The drawdown at the monitoring location can be estimated as the sum of the drawdowns due to the pumping cluster and the two boundary stresses (superposition principle). Figure 3.2.4.1 also shows the transfer functions at the monitoring location due to the pumping and boundary stresses. The stresses applied at each cluster are shown in Figure 3.2.4.2. Pumping ranges from 0 m^3/day to 1000 m^3/day, and the head perturbations at each boundary cluster range from –15 m to 15 m. These ranges for the pumping stress and boundary head perturbations are based on the historical record of pumping sequences and estimated head fluctuations at the boundary nodes for the period from February, 1989, to December, 2000.

Figure 3.2.4.3 compares the drawdowns due to the above stresses computed by direct application of the transfer functions and by the state space equation developed above. As can be seen from this figure, the drawdown estimates correspond well and support the validity of the state space transfer function model.

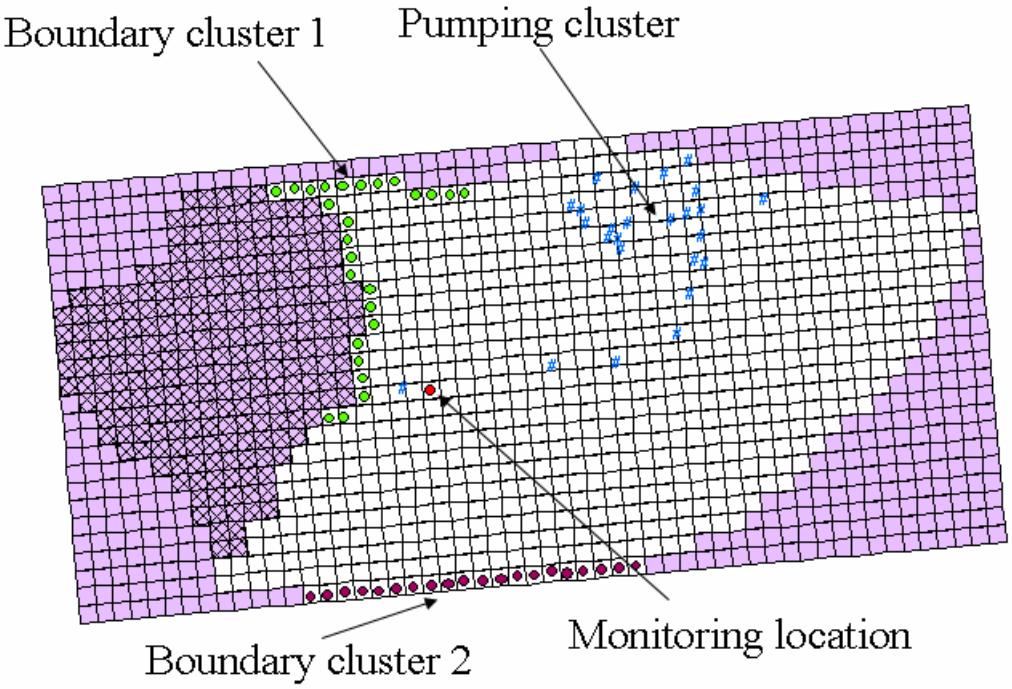

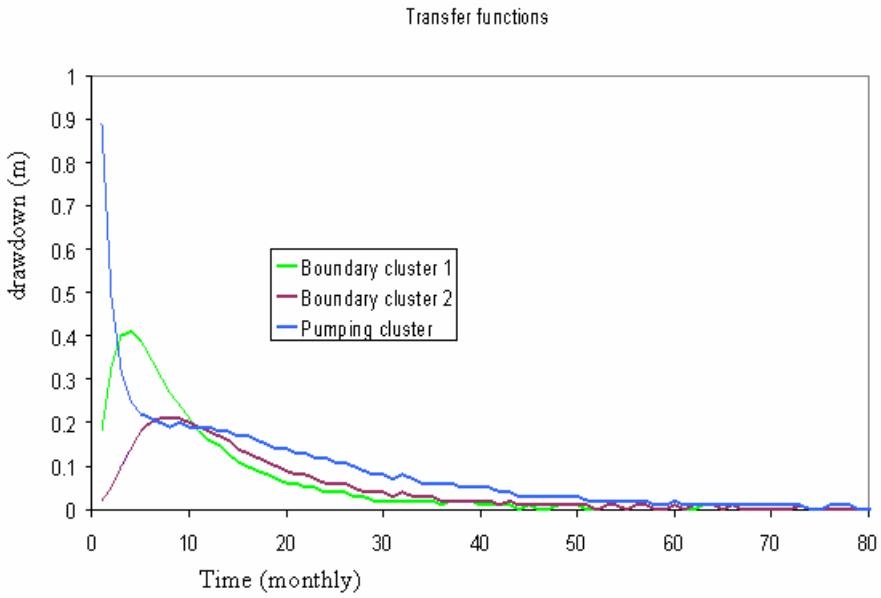

Figure 3.2.4.1: Groundwater transfer functions, application

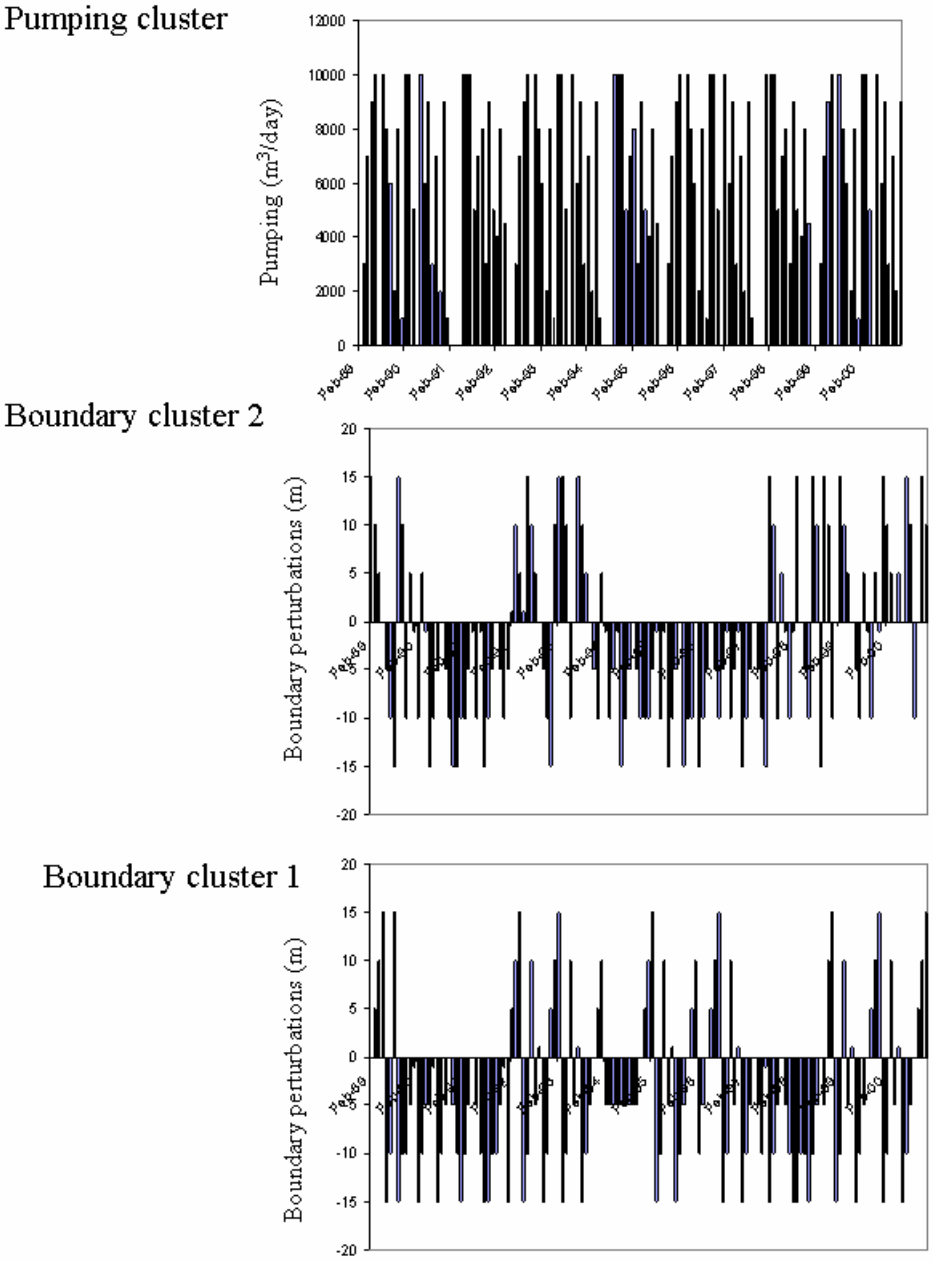

Figure 3.2.4.2: Groundwater transfer functions, pumping and boundary perturbations sequences

- drawdown due to pumping cluster

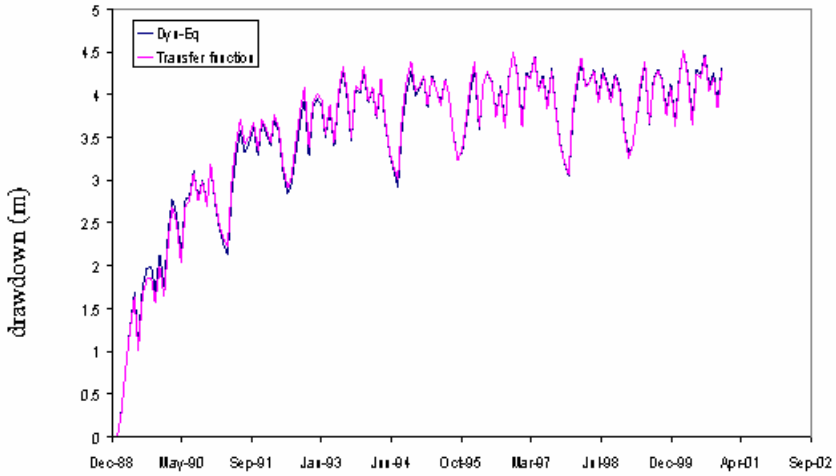

- drawdown due to boundary cluster 2

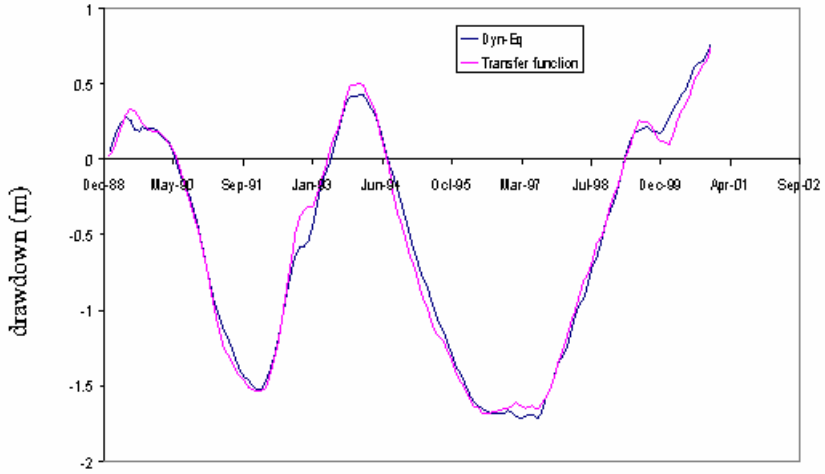

Figure 3.2.4.3: Groundwater transfer functions, application of dynamical equation

- drawdown due to boundary cluster 1

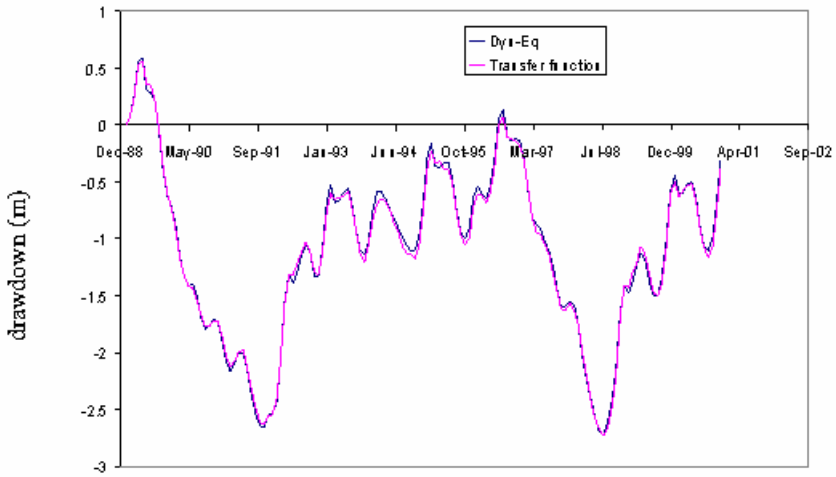

- Total drawdown

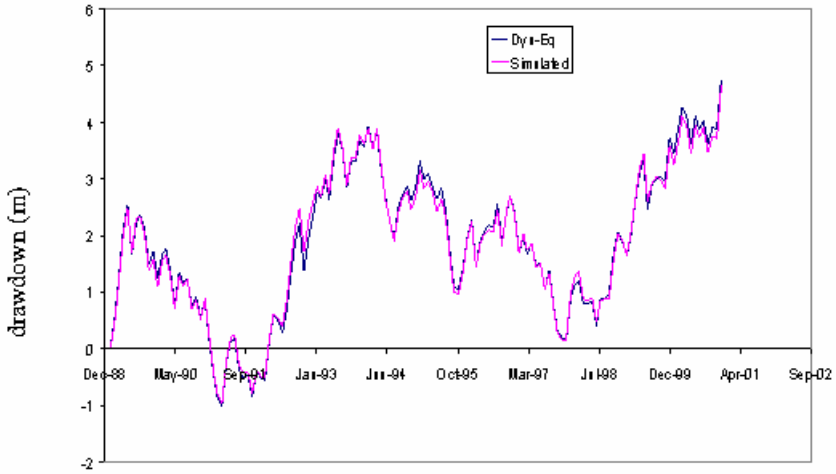

Figure 3.2.4.3: Groundwater transfer functions, application of dynamical equation

3.3 Parameter Uncertainty

3.3.1 Overview

In this section, a statistical approach is developed to model the uncertainty of aquifer parameters. Geostatistical methods do not lend themselves in cases where aquifers consist of distinct zones with constant parameter values. Alternatively, the approach taken here is to assume that the aquifer consists of a number of such zones and generate simultaneous parameter realizations for these zones such that modeled and observed data are in good agreement. The procedure includes a sequence of statistical tests to ensure compliance with local and field (global) conditions.

3.3.2 Methodology

MODFLOW and other groundwater models can represent the variation of aquifer heads through numerical integration of the flow equations. For this representation to be adequate, groundwater parameters (hydraulic conductivity and storage coefficients) are usually calibrated using observed data. However the calibrated parameters are but one of many possible parameter sets that result in similar simulated heads and aquifer flow regimes. Thus, aquifer parameters should be viewed as uncertain quantities. The purpose of this section is to develop a valid statistical procedure to quantify parameter uncertainty. The concept of the approach adopted in this work is as follows:

1. Determine the reliability level that the management process requires relative to aquifer head fluctuations. Namely, determine the confidence with which aquifer head predictions should be characterized. For example, it may be required that that actual aquifer heads should not fall outside their predicted range more than

10% of the time. This determination incorporates the requirements of the management process, and conditions the level of uncertainty that needs to be addressed in the modeling process. If the management process sets the error tolerance to 1% rather than 10%, the aquifer head forecast band (and consequently the uncertainty of the aquifer parameters) will have to be increased.

2. Define an RMSE range (away from the optimal calibration value) within which the estimation process will search for parameter sets with desirable uncertainty characteristics. For example, this RMSE range can within 30% of the optimal RMSE value. Define ranges of the individual model parameters such that individual parameter perturbations away from their optimal estimates give rise to RMSE values within the previous range.
3. Randomly and simultaneously select parameters within the ranges defined in step 2 and evaluate whether the resulting aquifer heads at the monitoring locations are statistically similar to the observed data. If a parameter set meets this criterion, consider it as a possible parameter set, and repeat the process until enough parameter sets have been identified.

The last step in this procedure involves the application of a statistical test at each monitoring location to test if the generated and observed heads are statistically similar. This process requires a two level statistical test, one pertaining to each monitoring well (local test) and a second pertaining to the all monitoring wells simultaneously (global or field test). The global statistical test is necessary due to the effects of spatial correlation.

Local Statistical Test:

At the local level the null and alternative hypotheses are as follows:

H_o: The generated and observed hydraulic heads belong to the same population;

H_a: The generated and observed hydraulic heads do not belong to the same population.

The null hypothesis is a two sided hypothesis. The local test is carried out using the Wilcoxon signed-rank non-parametric test Wilks (2000). This test applies to correlated paired samples and includes the following steps:

1. For each data pair {X(i), Y(i)}, i=1,…,n, where n is the number of data pairs, find the difference d(i)= X(i) - Y(i);
2. Rank the absolute differences of the data values:

   rank $|d(i)|$, i=1, 2, ..., n;
3. Calculate the test statistic (t) which is the sum of the ranks of either the negative or the positive differences; Commonly, statistical tables require choosing the smaller number between

   $$t = \sum_{d(i)>0} \text{rank}\,|d(i)| \quad \text{or} \quad t = \sum_{d(i)<0} \text{rank}\,|d(i)|$$
4. The null distribution of t for moderately large samples (n greater than 20) is Gaussian with

   mean $\mu_t = \frac{n(n+1)}{4}$ and variance $\sigma_t^2 = \frac{n(n+1)(2n+1)}{24}$.

Any cases of d(i)=0 are allocated equally between the sum of ranks for the positive and negative d(i).

Under the null hypothesis, both samples X and Y belong to the same population. Thus, the number of positive and negative differences between their pairs of data should be comparable. If there are considerable differences between the values of X and Y, the

differences d(i) would tend to be positive or negative. As a consequence, the test statistic, t, will tend to be either too small or too large as compared to the mean of the ranks μ_t, and the null hypothesis will be rejected.

The second testing level (global significance) is necessary because failure to pass some local tests does not necessarily imply global rejection of the null hypothesis. The null and alternative hypotheses of the global test are as follows:

H_o: The generated and observed hydraulic heads at the monitoring locations are statistically different;

H_a: The generated and observed hydraulic heads at the monitoring locations are not statistically different.

To carry out this test, an appropriate test statistic has to be defined. The test statistic used herein is the number of monitoring locations that pass the local tests T or, as defined in the literature, the "counting norm statistic," Zwiers (1987).

Groundwater hydraulic heads are most likely to be spatially correlated, and local tests will have the tendency to fail or pass in clusters. Under the assumption of spatial independence, the null distribution of the global test statistic--the number of monitoring locations that passed the test T--, is Binomial $B(n,1-\alpha)$, where n is the number of local tests and α is the significance level at which the local tests were conducted, Livezey and Chen (1983). However, if the local tests are not spatially independent, the null distribution of the global statistic T remains to be established. This can be accomplished via a bootstrap approach, Conover (1999). The bootstrap procedure generates many random parameter sets (as in step 1), and simulates the resulting heads at the monitoring locations. A local test is applied at each monitoring location, and the number of

monitoring locations that pass the local test is found. Since the parameters are selected randomly, the bootstrap procedure generates the distribution of the statistic under the null hypothesis This distribution serves to evaluate the field significance of the local test failure rate.

More details on bootstrap procedures can be found in Wilks, 2000, and Efron and Tibishirani, 1993. Another application of the bootstrap on a similar problem can be found in Livezey and Chen, 1983.

For a given significance level (α) the above hypothesis is evaluated as a one sided hypothesis (upper tailed test). The rejection of the null hypothesis implies that the number of locations that passed the test is statistically large enough to conclude that the calibrated and generated sets of groundwater parameters are statistically similar.

3.3.3 Application

In this study, Groundwater parameters include hydraulic conductivity and specific storage for all zones identified during model calibration (Figure (3.3.3.1). The statistical test is run for two reliability levels, 95% and 80%.

At the 95% reliability level, the significance level for the local and global tests is 5%, the reliability level for the resulting hydraulic head realizations is equal to 95%, and the RMSE range is such that the observed heads at the monitoring locations are contained within the forecasted band 95% of the time.

At the 80% reliability level, the significance level for the local and global tests is 20%, the reliability level for the resulting hydraulic head realizations is 80%, and the

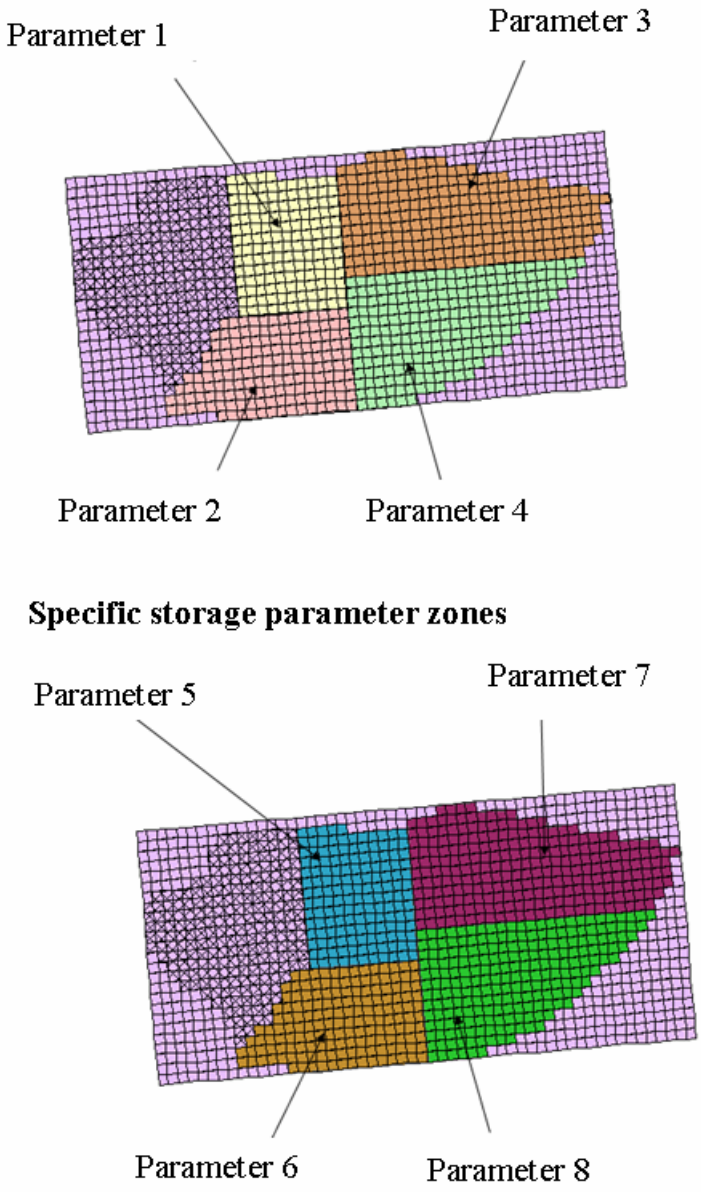

Figure 3.3.3.1: Calibrated groundwater model parameters

RMSE range is such that the observed heads at the monitoring locations are contained within the forecsted bands 80% of the time.

The RMSE perturbation range found to meet the 95% and 80% reliability level requirement is 45% and 30% respectively. For each perturbation level, a range for each individual parameter is defined such that any perturbation of this parameter within this range leads to an RMSE perturbation within 45% or 30% respectively. In this analysis, all other parameters are assumed to be equal to their optimal calibration values. For example, the hydraulic conductivity range for zone 4 was found to be between 10.75 m/day and 20 m/day at the 30% range of the optimal RMSE. Generally, the hydraulic conductivity ranges of all zones varies between .01 and 20 m/day, the soil type being predominantly silty sand. Specific storage ranges vary between 10^{-3} (1/m) and 10^{-5} (1/m), (Freeze and Cherry (1979), and Anderson and Woessner (1992)). Table (3.1) shows the ranges of all groundwater parameters for the Amman-Wadi Sir aquifer.

3.3.3.1 Effect of Spatial Correlation, Global Test, and Hydraulic Head Realizations

To find the global test null distribution, a bootstrap approach was employed. Many sets of groundwater parameters were generated, and the groundwater model was run for each set to generate the hydraulic head sequences, as described in the previous section. Figure (3.3.3.1.1) shows the null distribution of the number of monitoring points that failed at 95% reliability level. As mentioned above, the RMSE range for the 95% reliability level is found to be 45% from the optimal value. The figure also shows 50

Table 3.1: Perturbed groundwater parameters ranges

Hydraulic conductivity: (m/day)

parameter	Calibrated value	Upper bound		Lower bound	
number	0%	30%	45%	30%	45%
1	9.8	20	20	4.3	3.5
2	7.5	20	20	3.3	3
3	16.1	20	20	9.25	7.5
4	13.7	20	20	10.75	8.77

Specific storage: (1/m)

parameter	Calibrated value	Upper bound		Lower bound	
number	0%	30%	45%	30%	45%
5	0.000014	0.00021	0.00031	0.00001	0.00001
6	0.000016	0.00024	0.00033	0.00001	0.00001
7	0.000019	0.00026	0.00037	0.00001	0.00001
8	0.000017	0.00027	0.00041	0.00001	0.00001

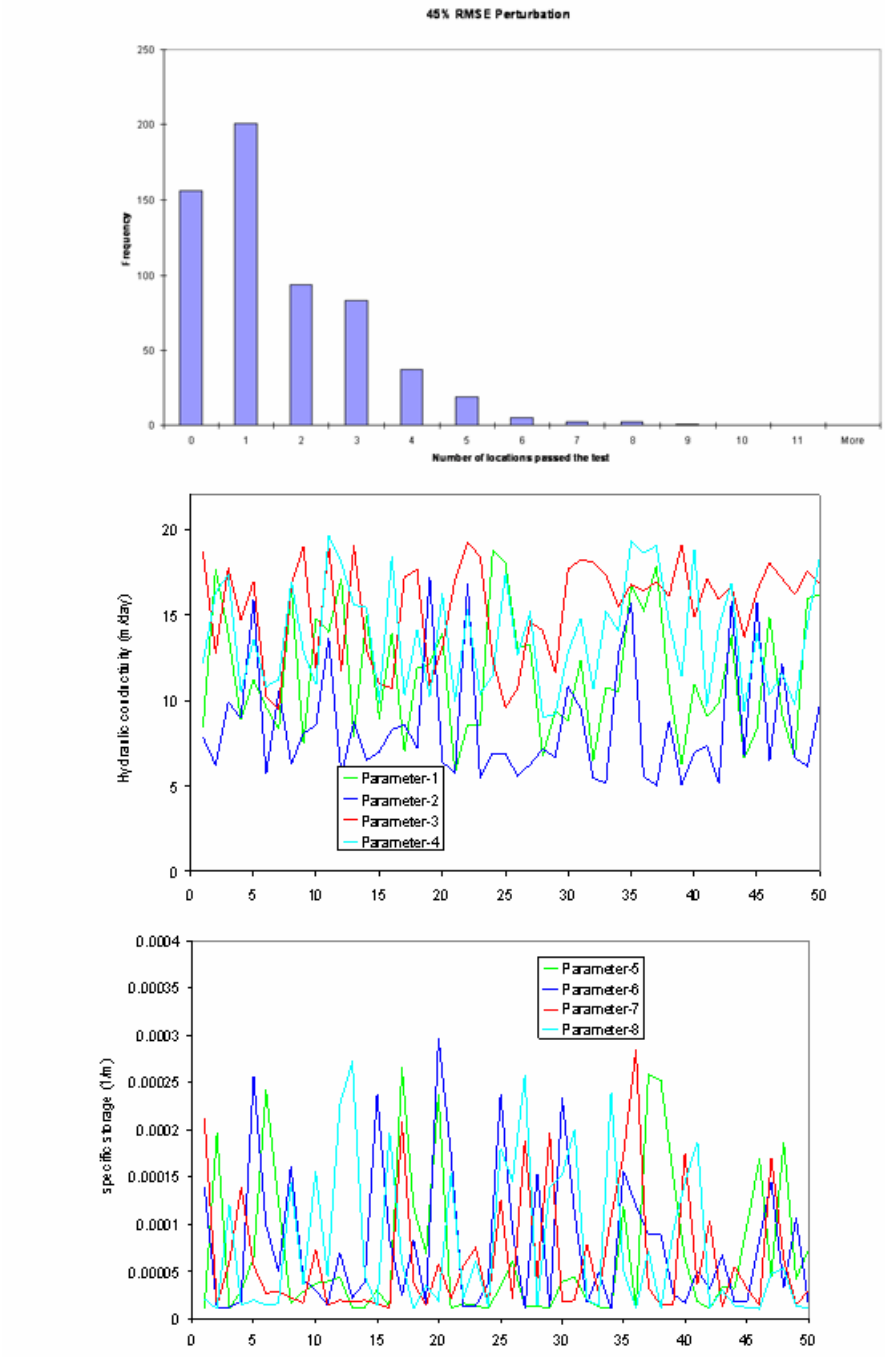

Figure 3.3.3.1.1 : Statistical procedure, null distribution 95% reliability level

realizations that pass the statistical test. Each realization consists of 4 parameters of hydraulic conductivity and 4 parameters of specific storage.

Figure (3.3.3.1.2) shows the null distribution of the number of monitoring points that failed at the 80% reliability level. The RMSE perturbation for the 80% reliability level is 30% from the optimal value. The figure also shows 50 realizations that pass the statistical test.

Figures (3.3.3.1.3a- 3.3.3.1.3c) show the resulting head sequences for 100 realizations generated at the 95% reliability level . At almost all wells, the observed head sequences are within the generated head sequences. The percentage of time at which violations occur is about 4.8%.

Figures (3.3.3.1.4a- 3.3.3.1.4c) show the resulting head sequences at the 80% reliability level. The 80% reliability level is not met 19.2% of the time collectively at all monitoring locations. This rate is compatible with the statistical test specifications. Since the reliability level is lower than in the previous case, it is expected that the head realization band is narrower than before. This can be seen by comparing Figures (3.3.3.1.4a- 3.3.3.1.4c) with Figures (3.3.3.1.3a- 3.3.3.1.3c).

3.4 Effective Groundwater Parameters

Transfer functions realizations can be created by running the groundwater model for the generated parameter sets. An example of such an ensemble is shown on Figure (3.4.1). For a particular transfer function, most of the ensemble variability may be related to a smaller subset of the parameters. For example, a parameter of a zone far away from the stress and impact sites of a particular transfer function may have no influence on the

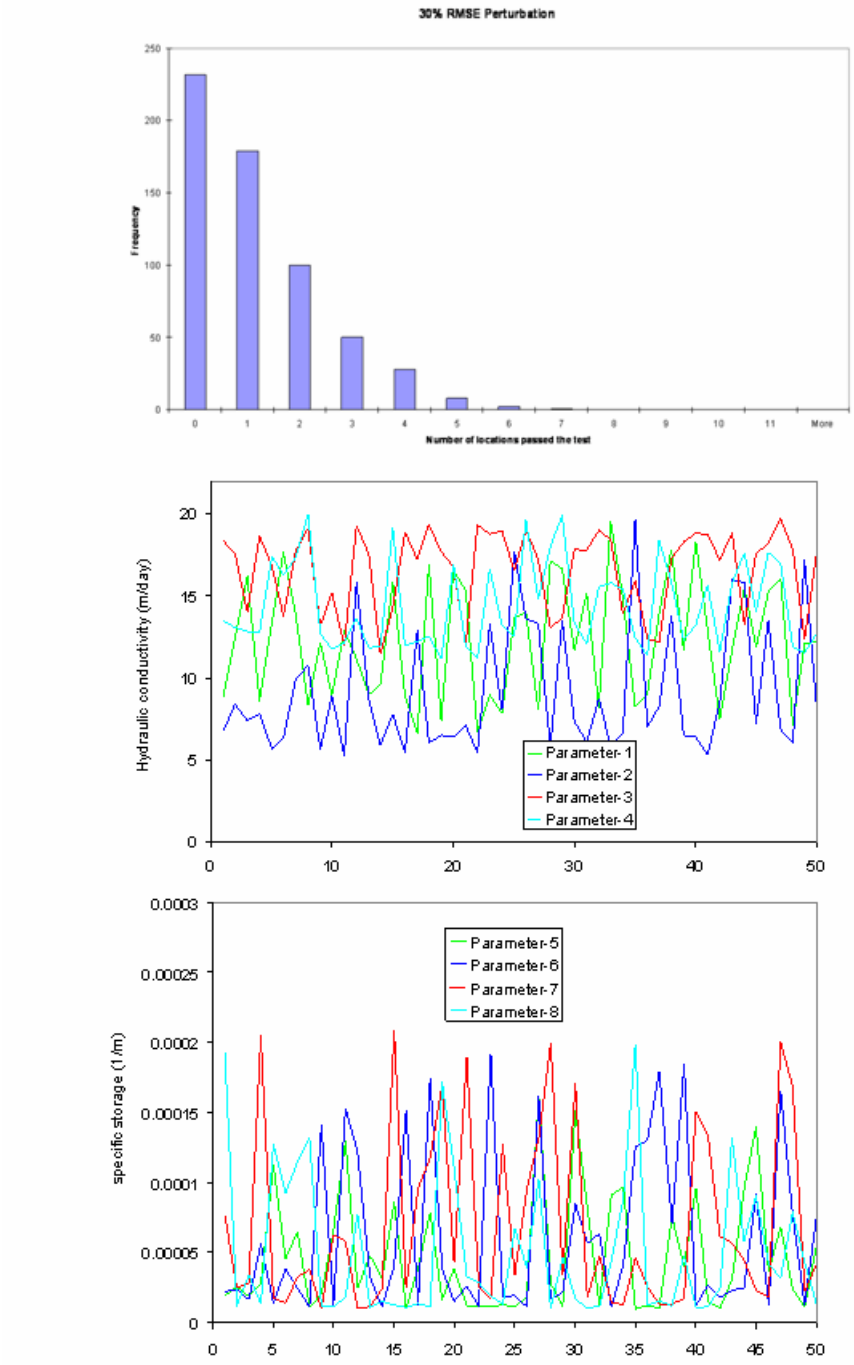

Figure 3.3.3.1.2: Statistical procedure , null distribution 80% reliability level

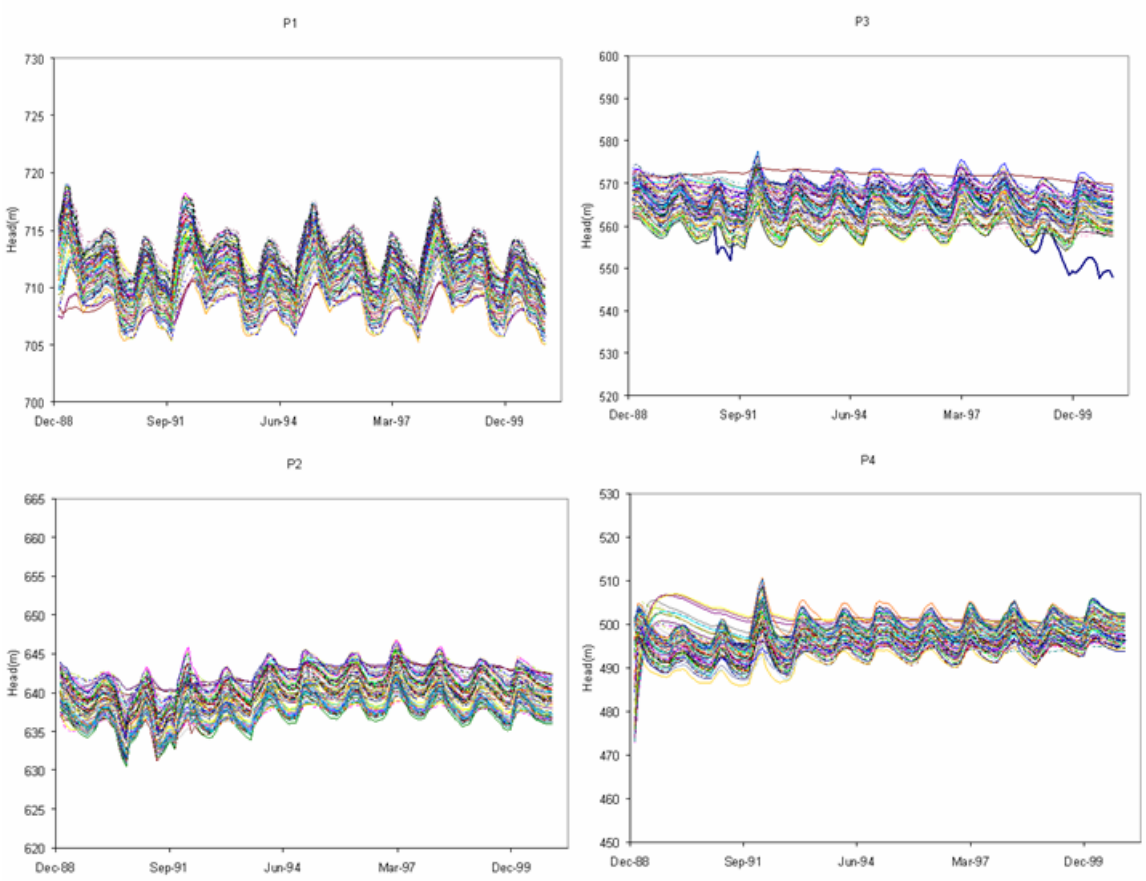

Figure 3.3.3.1.3a: Statistical procedure, head realizations 95% reliability level

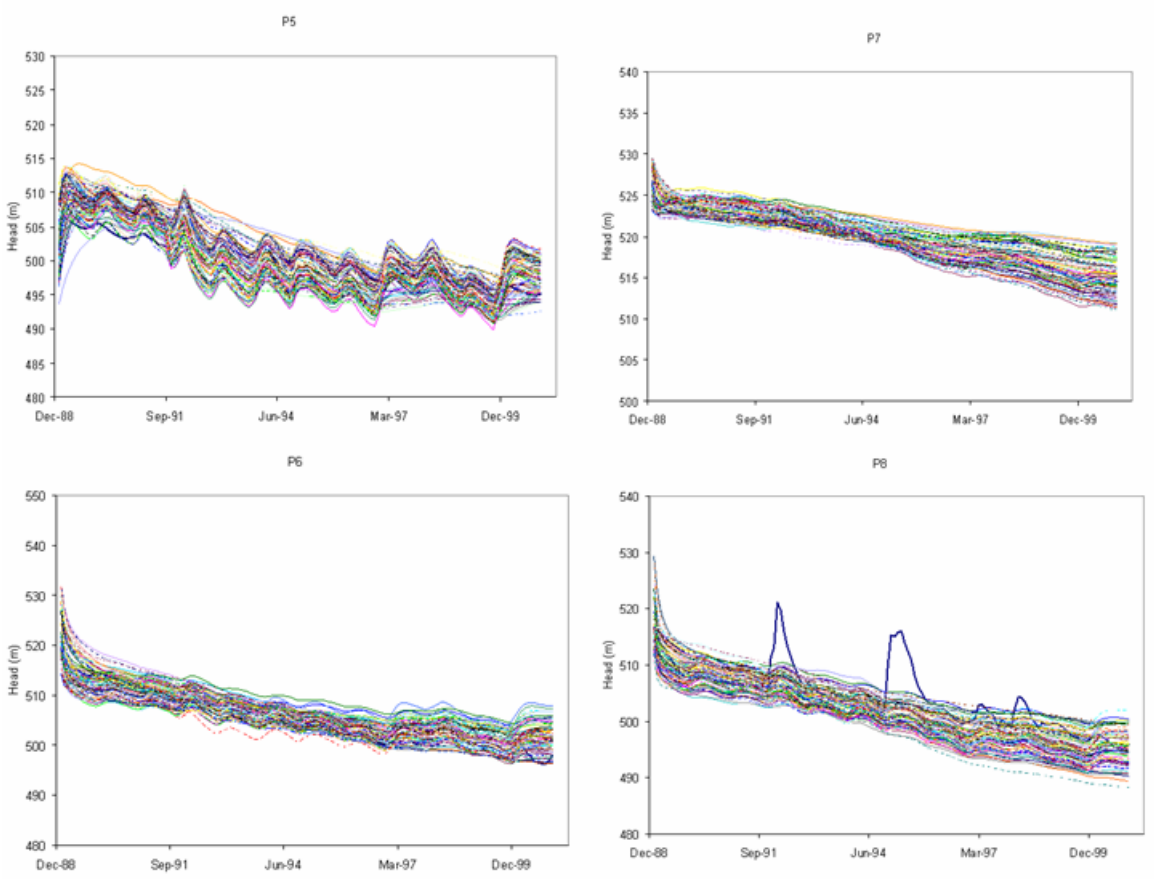

Figure 3.3.3.1.3b: Statistical procedure, head realizations 95% reliability level

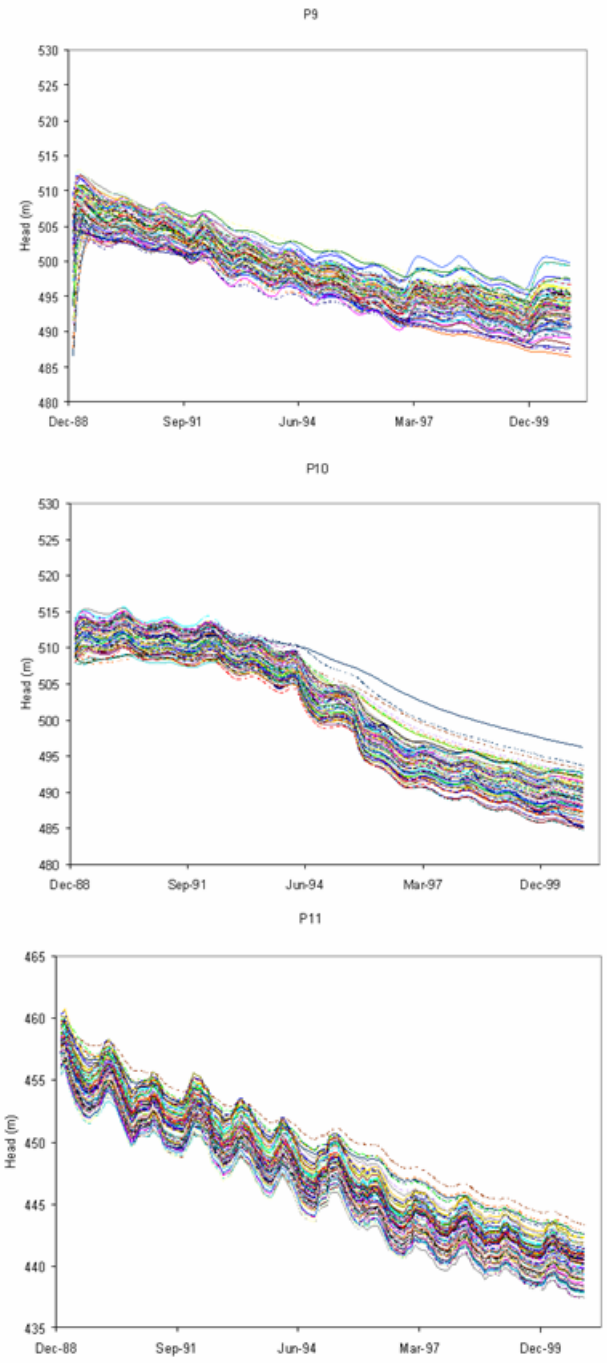

Figure 3.3.3.1.3c: Statistical procedure, head realizations 95% reliability level

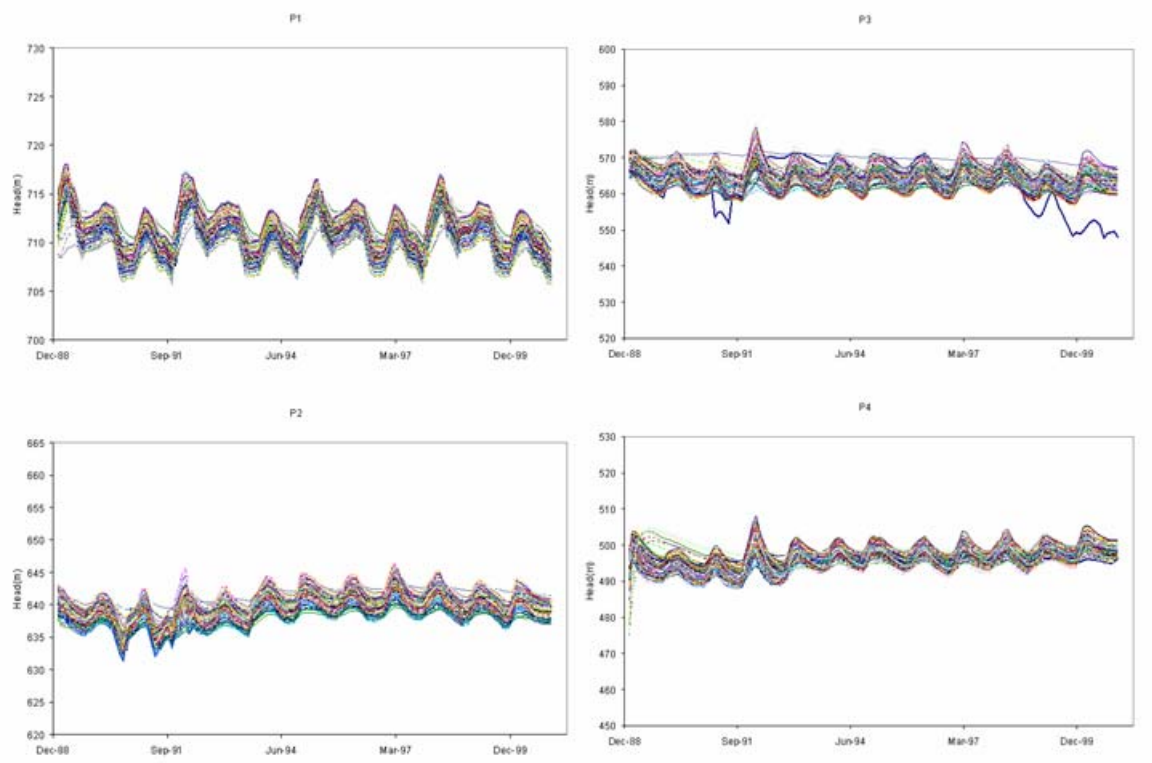

Figure 3.3.3.1.4a: Statistical procedure, head realizations 80% reliability level

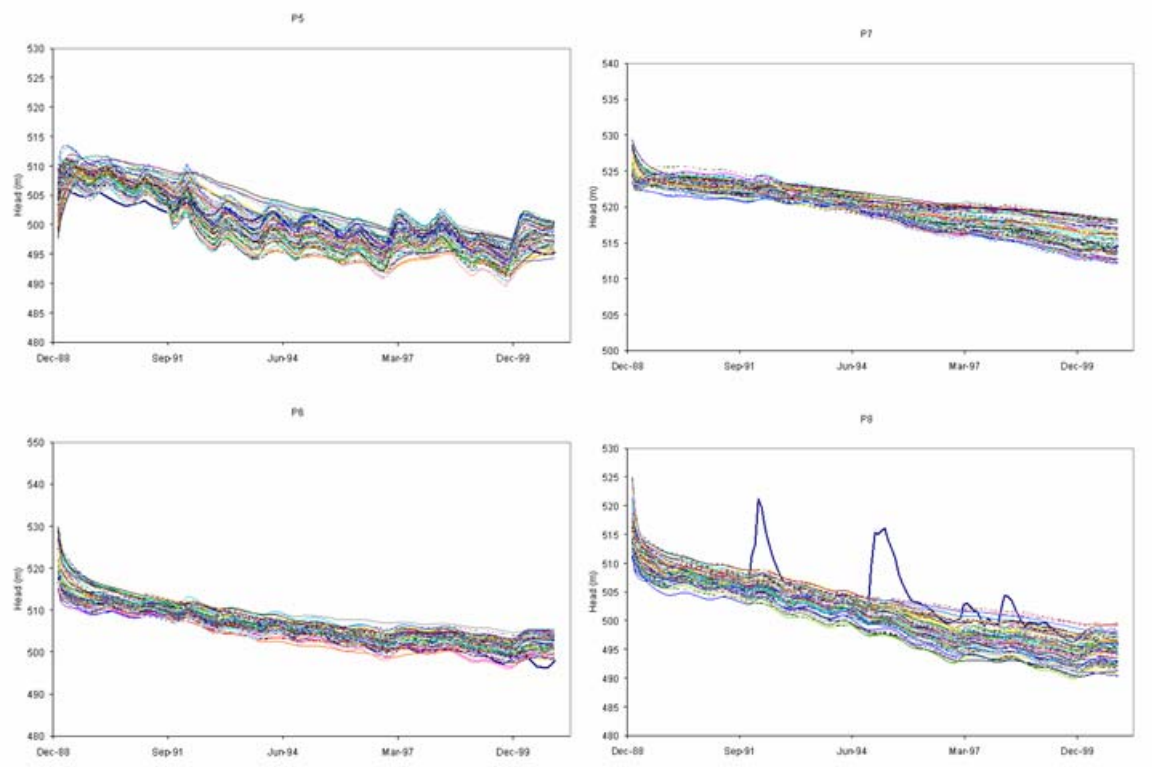

Figure 3.3.3.1.4b: Statistical procedure, head realizations 80% reliability level

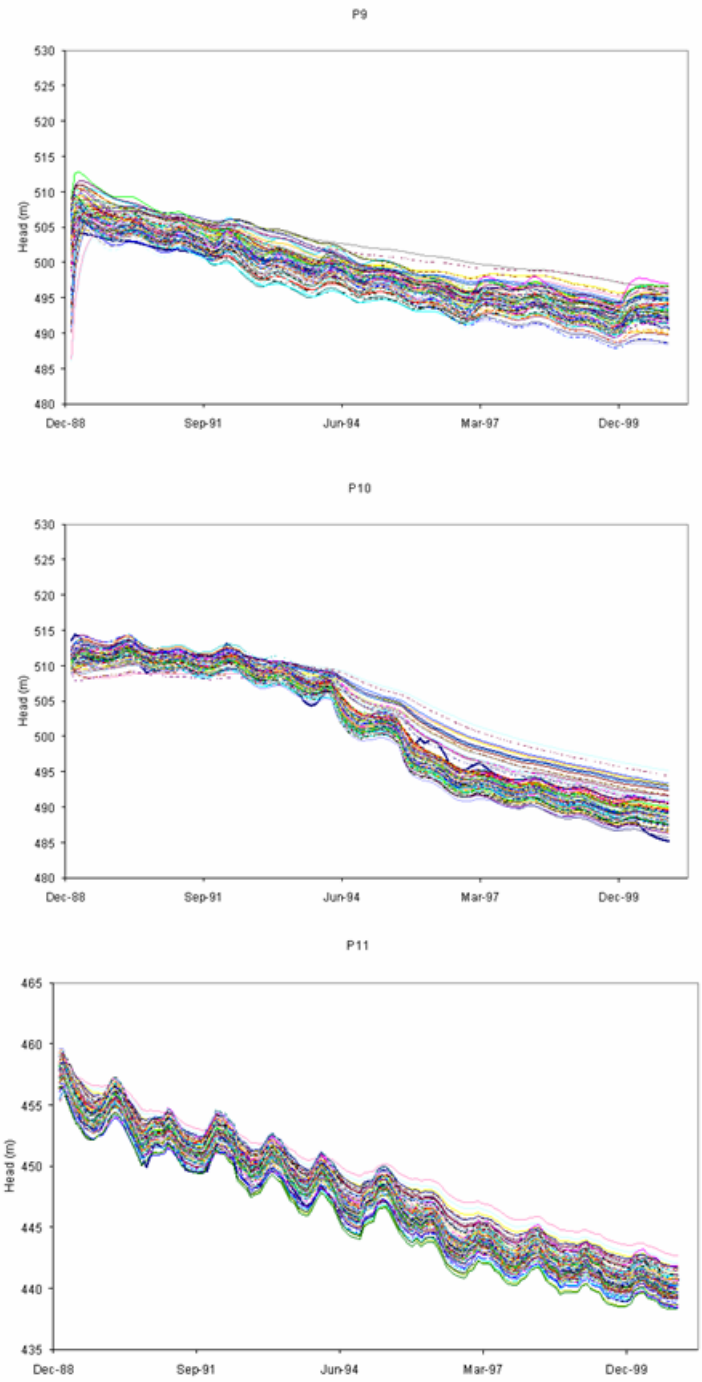

Figure 3.3.3.1.4c: Statistical procedure, head realizations 80% reliability level

form of this function. Thus, knowledge of this effective parameter set can simplify the process of generating transfer function ensembles. Additional analysis of the transfer functions ensembles shown in figure (3.4.1) will be undertaken in subsection 3.4.1, where effective parameter sets will be computed for the three locations.

Since the variability in the transfer function realizations is due to the variability of groundwater parameters, the effective parameters set can be identified and used to estimate the transfer functions realizations.

For a given transfer function ensemble and a groundwater parameter set, let the index (m) denote the realization number within each ensemble, m = 1, 2, …, M with M being the total number of transfer function realizations or generated groundwater parameter sets. Using the natural logs of groundwater parameters as predictors, the form of the function used to estimate the transfer function coefficients is:

$$\hat{T}_{(i,m)} = a_{(i,0)} + a_{(i,1)} \text{ Ln } K_{(1,m)} + a_{(i,2)} \text{ Ln } K_{(2,m)} + \ldots + a_{(i,p)} \text{ Ln } K_{(p,m)} \qquad (3.12)$$

Where:

p: refers to the number of effective parameters

i: refers to the transfer function coefficient number, i = 1, 2, …, n, where n is the total number of transfer function coefficients;

m: refers to the generated realization of transfer function or groundwater parameter set.

$a_{(i,0)}$, $a_{(i,1)}$, $a_{(i,2)}$,…, $a_{(i,p)}$: are coefficients to be determined;

$K_{(1,m)}$, $K_{(2,m)}$,…, $K_{(p,m)}$: are the unknown effective parameters subset;

Ln: refers to the natural log transformation;

$\hat{T}_{(i,m)}$: refers to the estimated transfer function coefficient (i), for the transfer function realization (m);

Transfer functions realizations at i=14, j=22

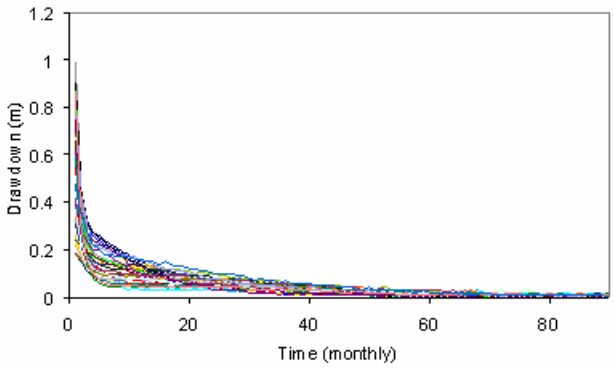

Transfer functions realizations at i=10, j=34

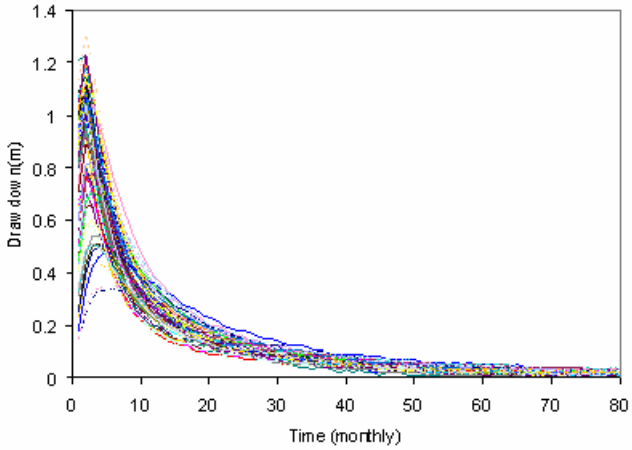

Transfer functions realizations at i=6, j=35

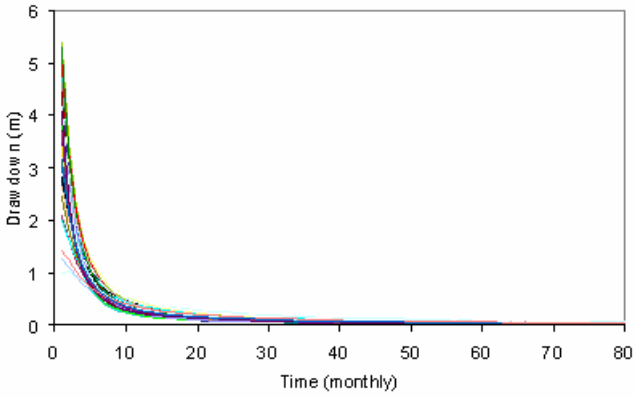

Figure 3.4.1: Transfer functions realizations at the monitoring locations

In equation (3.12), it should be noted that coefficients $a_{(i,0)}$, $a_{(i,1)}$, $a_{(i,2)}$,…,$a_{(i,p)}$ are different based on the coefficient number of the transfer function. So for the first transfer coefficient the estimated coefficients are $a_{(1,0)}$, $a_{(1,1)}$, $a_{(1,2)}$,…,$a_{(1,p)}$; for the second $a_{(2,0)}$, $a_{(2,1)}$, $a_{(2,2)}$,…,$a_{(2,p)}$ etc.

Our goal from estimating the transfer function coefficients has two motivations: first is to find the effective parameters subset, secondly to make sure that the estimated transfer function coefficients provide a good estimate of the resulting drawdown sequences.

In order to find the unknowns in equation (3.12) the following minimization problem must be solved:

$$\text{Min} \quad J = \sum_{\substack{k=1,...,N \\ m=1,...,M}} \sum \{\hat{d}(m,k+1) - d(m,k+1)\}^2 \quad . \tag{3.13}$$

$$\hat{d}(m,k+1) = \overline{T}_{(1,m)}\, p(k) + \overline{T}_{(2,m)}\, p(k-1) + \overline{T}_{(2,m)}\, p(k-1) + \ldots + \overline{T}_{(n,m)}\, p(k-n+1) \tag{3.13a}$$

$$d(m,k+1) = T_{(1,m)}\, p(k) + T_{(2,m)}\, p(k-1) + T_{(2,m)}\, p(k-1) + \ldots + T_{(n,m)}\, p(k-n+1) \tag{3.13b}$$

$$\overline{T}_{(i,m)} = a_{(i,0)} + a_{(i,1)} \text{ Ln } K_{(1,m)} + a_{(i,2)} \text{ Ln } K_{(2,m)} + \ldots + a_{(i,p)} \text{ Ln } K_{(p,m)} \tag{3.13c}$$

where:

$\hat{d}(m,k+1)$: is the estimated drawdown at time step (k+1) using the estimated transfer functions realization (m);

$d(m,k+1)$: is the drawdown at time step (k) using the actual transfer function realization (m);

p(k), p(k-1), .., p(k-n+1) : pumping sequence (or boundary perturbation sequence);

$T_{(1,m)}$, $T_{(2,m)}$, $T_{(2,m)}$,…, $T_{(n,m)}$: coefficients for transfer function realization (m);

$\overline{T}_{(1,m)}$, $\overline{T}_{(2,m)}$, $\overline{T}_{(2,m)}$,…+ $\overline{T}_{(n,m)}$: estimated coefficients for transfer function realization (m);

N: Period over which the drawdown is computed.

The minimization problem in (3.13) can be viewed as minimizing the squared errors between the estimated and computed drawdown sequences. This minimization is a nonlinear minimization problem. The procedure to solve for the unknowns $a_{(i,1)}$, $a_{(i,2)}$,…, and $a_{(i,p)}$ and $K_{(1,m)}$, $K_{(2,m)}$,…, and $K_{(p,m)}$ is as follows:

1. Determine a single groundwater parameter that minimizes (3.13). In this case, $\overline{T}_{(i,m)} = a_{(i,0)} + a_{(i,1)} \text{ Ln } K_{(1,m)}$ where the variables are $a_{(i,0)}$, $a_{(i,1)}$,and $\text{Ln } K_{(1,m)}$. Find the minimum value of the objective function (J) and store it as (J_1)
2. Determine two groundwater parameters that minimize (3.13). In this case, $\overline{T}_{(i,m)} = a_{(i,0)} + a_{(i,1)} \text{ Ln } K_{(1,m)} + a_{(i,2)} \text{ Ln } K_{(2,m)}$. Find the minimum value of the objective function and store it as (J_2)
3. Repeat the previous procedure for three, four, etc. parameters until all parameters are selected. In each case find the minimum value of the objective function (J_i , i = 3, 4, ...S), where S refers to the total number of parameters.

It is clear that by adding more parameters the (J_i) value decreases; however, this decrease becomes increasingly smaller as the number of parameters increase. Thus, the effective parameter set can be identified as the subset for which any further reduction in (J_i) by adding any additional parameter is negligibly small:

$$\left(\frac{J_{i-1} - J_i}{J_{i-1}} \right) \times 100\% \leq \lambda \qquad (3.14)$$

where λ is a small percentage such as 1% ,3%, or 5%.

The effective parameter subset can be used to describe the transfer function ensemble. Namely, instead of running the aquifer model for different parameter sets, one

can determine the transfer function coefficients from the previous relationships and then create the ensemble.

3.4.1 Application

The problem is to find the effective parameters at the monitoring locations shown in Figure (3.4.1.1). These locations include {i=14,j=22}, {i=10,j=34}, and {i=6,j=35}.. The figure also shows the zones of constant groundwater parameters and the pumping cluster.

Figure (3.4.1) shows the transfer functions realizations at the monitoring locations due to pumping. The squared errors of the solution of 3.13, 3.13a, 3.13b, and 3.13c are shown in Figures (3.4.1.2a), (3.4.1.2b), and (3.4.1.2c). The error plots show that significant error reduction is achieved by the effective parameters. The effective parameters for the monitoring locations are as follows:

Location	Eff. Parameters
{i=14,j=22}:	1, 7, 2, 5, 8
{i=10,j=34}:	7, 4, 8, 3,1,5
{i=6,j=35}:	7, 3,8,4,5,6

Figures (3.4.1.2a), (3.4.1.2b), and (3.4.1.2c) compare the drawdown sequences and transfer functions estimated according to the effective parameters approach with the actual transfer functions and drawdown sequences computed using the groundwater model. All graphs indicate a favorable comparison.

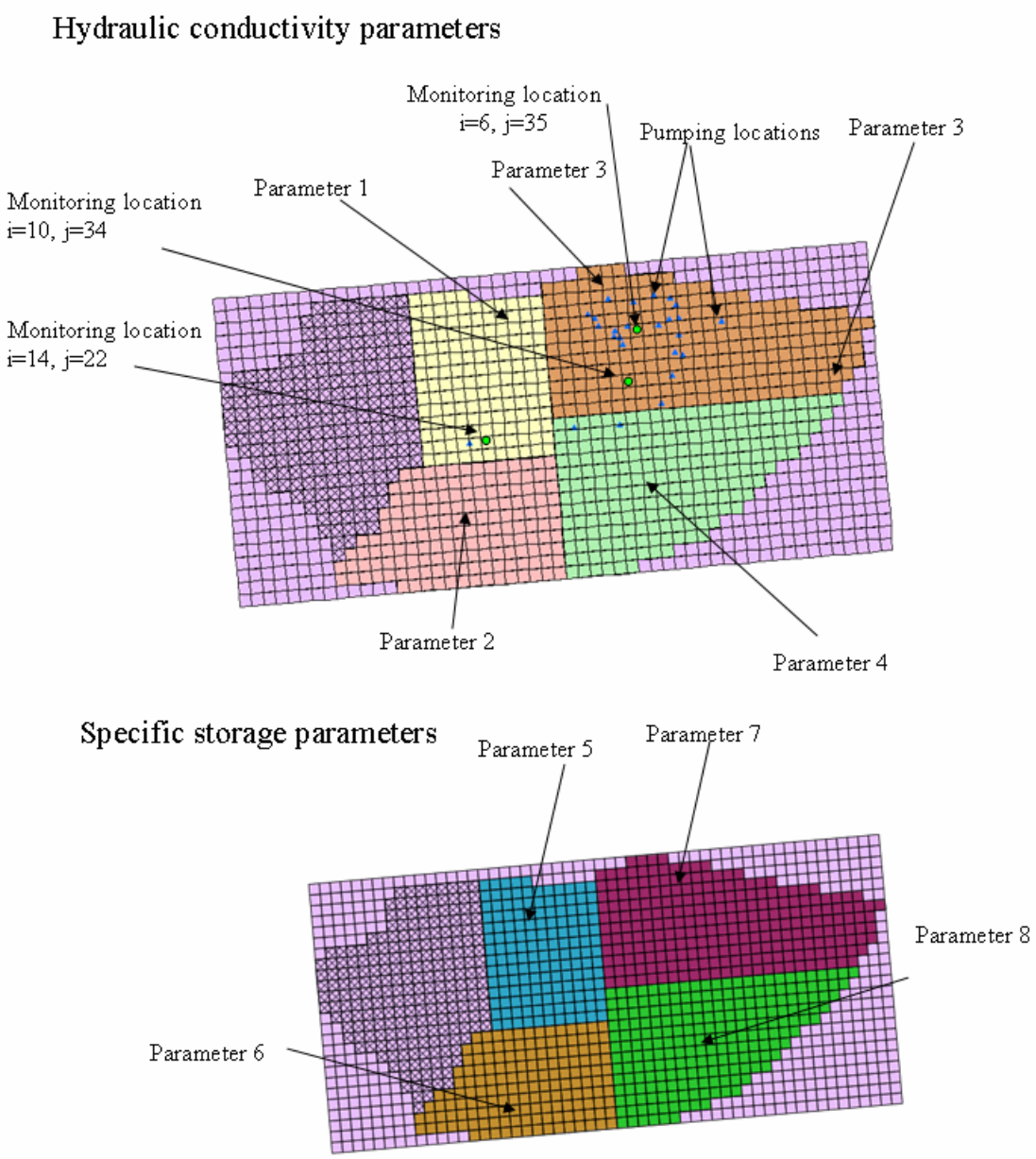

Figure 3.4.1.1 : Effective groundwater parameters

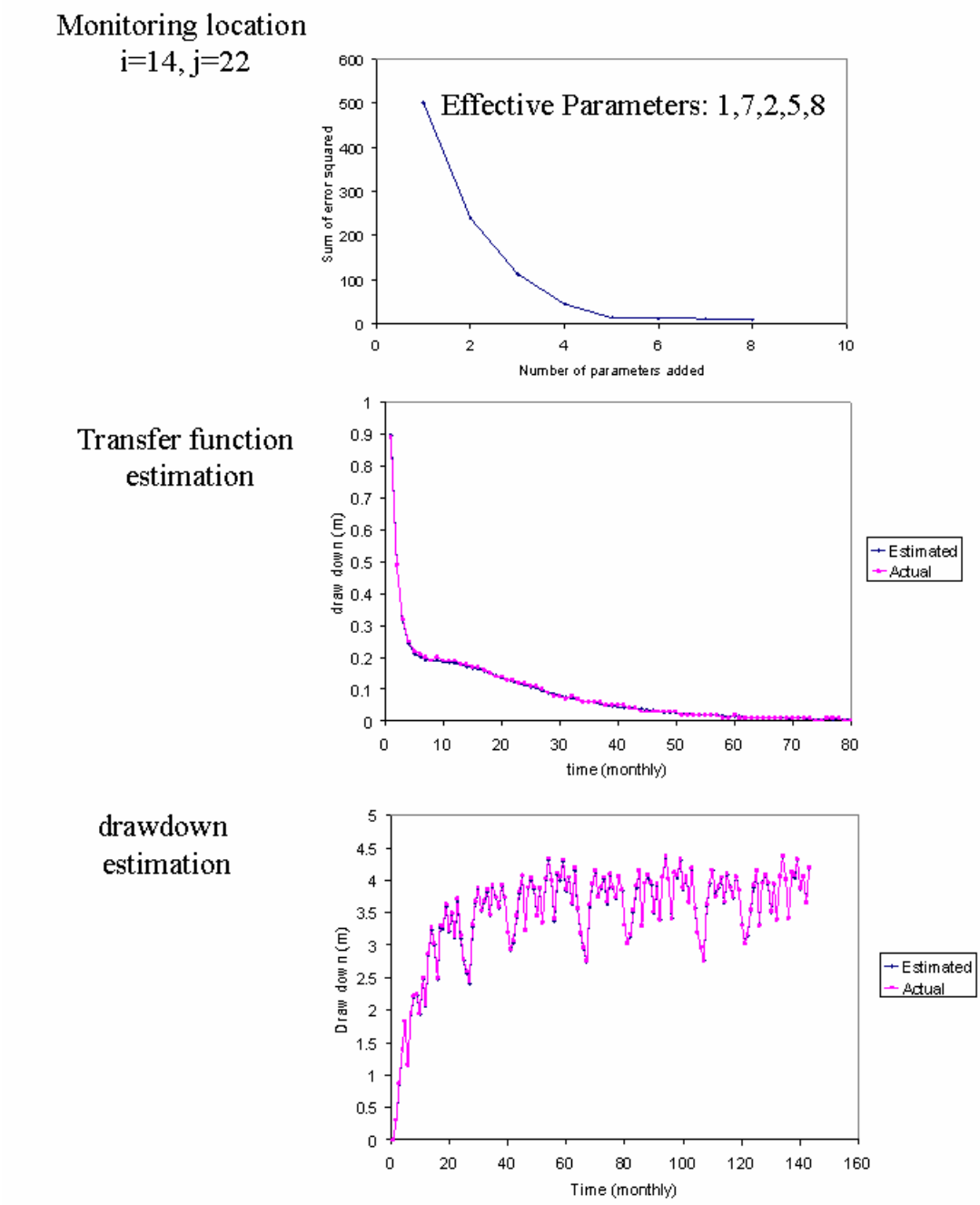

Figure 3.4.1.2a: Effective parameters, estimated transfer functions and drawdown sequences

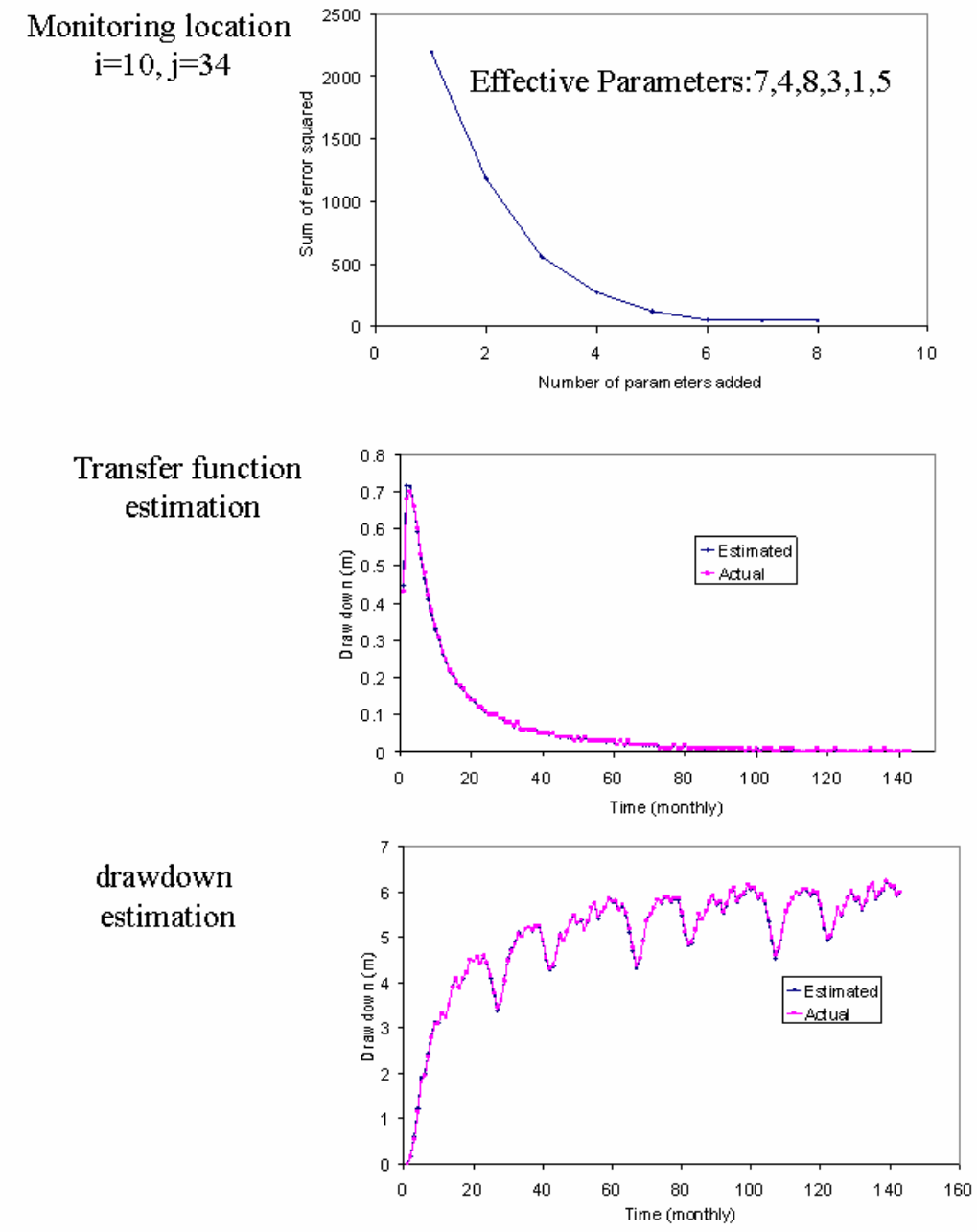

Figure 3.4.1.2b: Effective parameters, estimated transfer functions and drawdown sequences

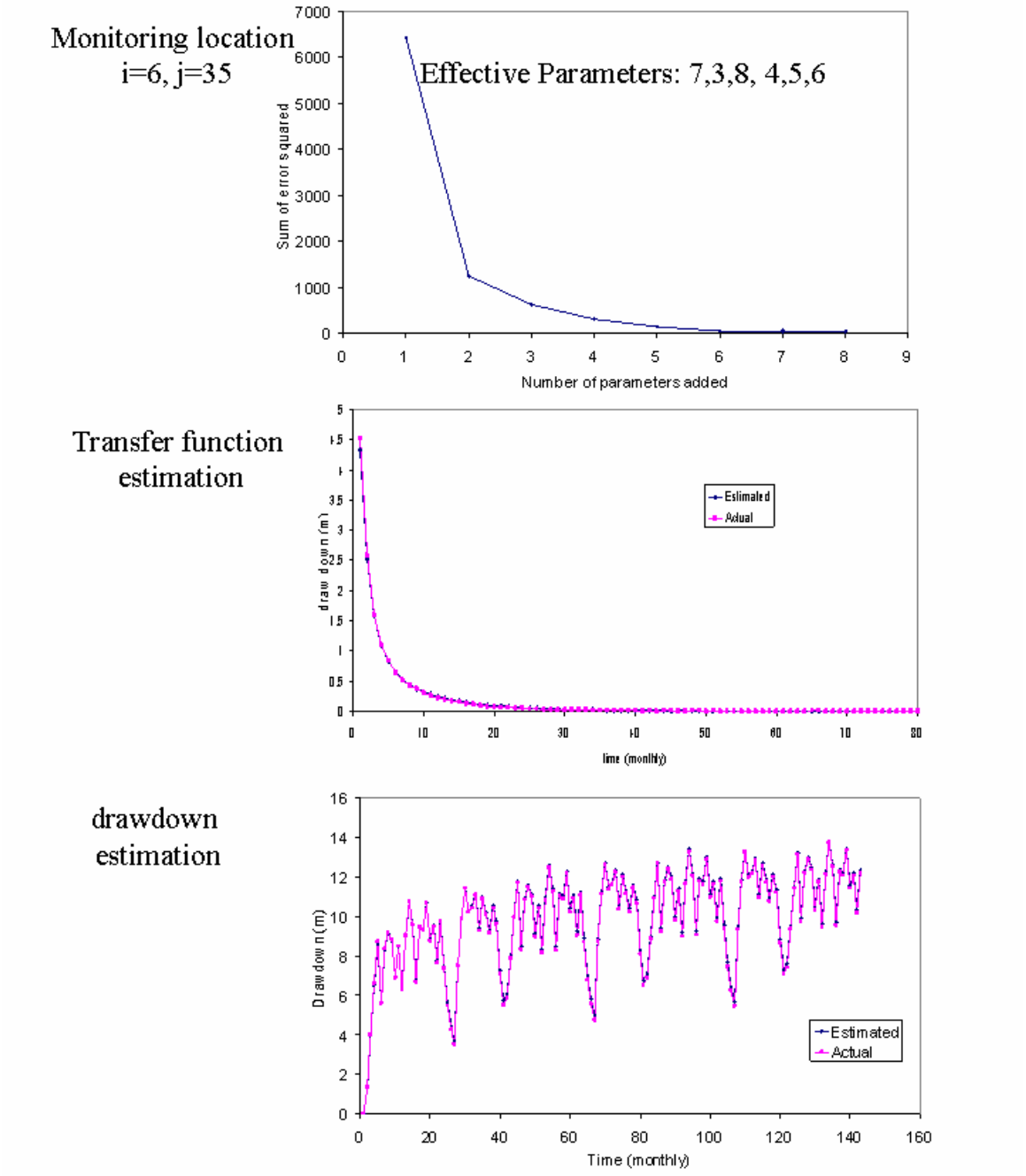

Figure 3.4.1.2c: Effective parameters, estimated transfer functions and drawdown sequences

3.5 Mean Drawdown and Uncertainty Characterization

Parameter uncertainty implies many possible groundwater drawdowns for the same pumping sequence. To describe this uncertainty, the approach taken herein is to develop

a representative ensemble of transfer functions and drawdown realizations at each location. Statistical measures of particular interest include the ensemble mean and various percentiles reflecting the spread of the ensemble about the mean.

The drawdown ensemble mean can be readily generated by taking the expected value of equation (3.2):

$$E\{d_P(k+1)\} = E\{T_P(1)\,P(k) + T_P(2)\,P(k-1) + T_P(3)\,P(k-2) + \ldots + T_P(N)\,P(k-N+1)\}$$

where the uncertainty of the right hand side stems from the transfer function coefficients. Thus,

$$E(d_P(k+1)) = E(Tp(1))\,P(k) + E(Tp(2))\,P(k-1) + E(Tp(3))\,P(k-2) + \ldots + E(Tp(N))\,P(k-N+1) \quad (3.15)$$

where:

$E(Tp(i))$ can be estimated by the ensemble mean, $\sum(T(i,m))/M$,

i is the transfer function coefficient number, $i=1,\ldots,n$,

m is the realization number, $m=1,\ldots, M$, and

$E(\,)$ is the expectation operator.

As shown earlier, the above mean drawdown equation can be approximated by the following dynamical equation:

$$E(d_P(k+1)) = \alpha\,P(k) + \beta\,P(k-1) + \gamma\,E(d_P(k)) + \theta\,E(d_P(k-1)) \quad (3.16)$$

To illustrate the accuracy of the approximation (3.16), the mean drawdown is estimated for two of the monitoring locations described in the previous section (3.4.1), {i=10, j=34} and {i=7,j=33}. Figures (3.5.1a) and (3.5.1b) show for each location the drawdown ensemble and the estimated and the computed (using transfer function) mean drawdown. The figures indicate that estimated and computed drawdowns compare favorably for both locations.

Equation 3.16 is a key element of the conjunctive management model, as it enables the inclusion of a state space representation of the groundwater system. The rest of the drawdown probability band can be represented by the percentile distances from the mean sequence. These distances are estimated directly using the ensemble traces.

Depending on the risk attitude of the decision maker, the percentile levels may be set to 95%, 90%, or any other value. For any percentile level, the goal of the management model will be to ensure that the specified percentage of drawdown traces observe the stated constraints. Figure (3.5.2) shows the mean drawdown and the 95, 90, and 80 percentiles for the ensembles in figure (3.5.1).

3.6 Regional Approximation of Drawdown Sequences:

It has been shown that it is possible to estimate the drawdown at a certain monitoring location (m1) using this state dynamical equation :

$$d_{m1}(k+1)= \alpha P(k) + \beta P(k-1) + \gamma d_{m1}(k) + \theta d_{m1}(k-1) \qquad (3.17)$$

The above dynamical equation includes only 3 state variables, P(k-1) , d_{m1} (k), and d_{m1} (k-1). The drawdown at other monitoring locations, m2 ,m3 , m4, m5, and m6 for example, can also be estimated from similar dynamical equations:

Monitoring location i=10, j=34

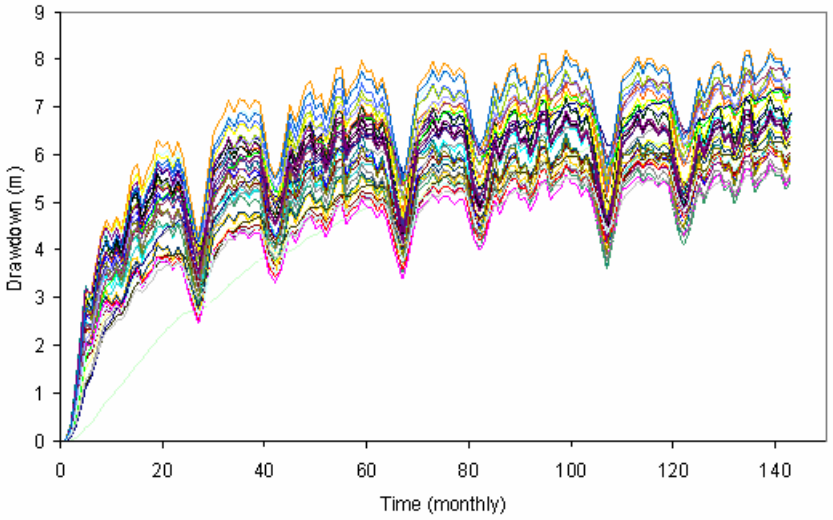

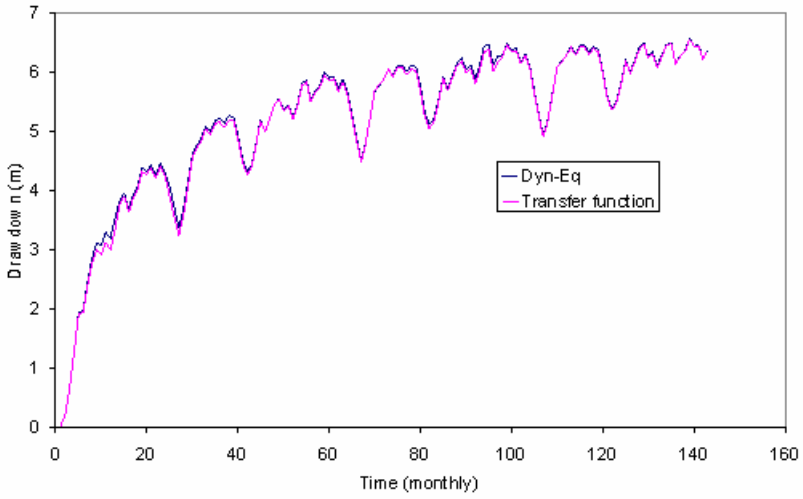

Figure 3.5.1a: Estimation of mean drawdown

Monitoring location i=7, j=33

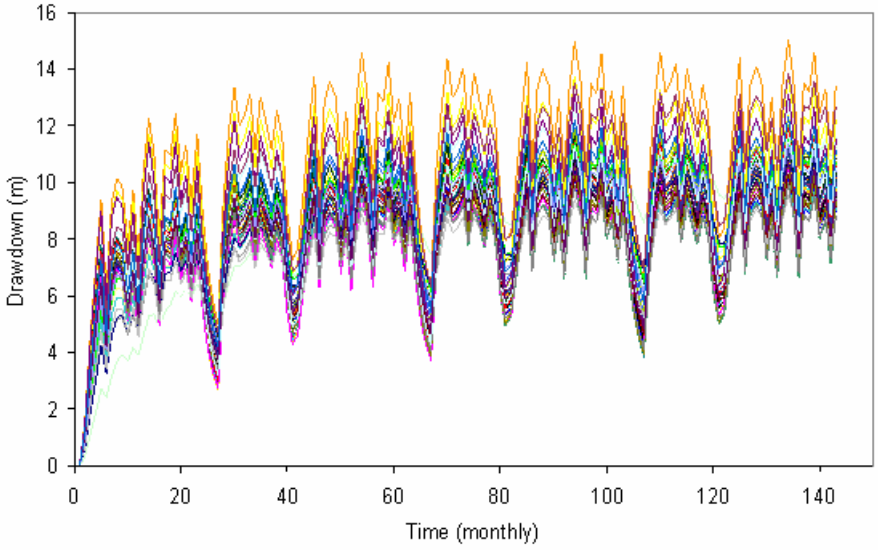

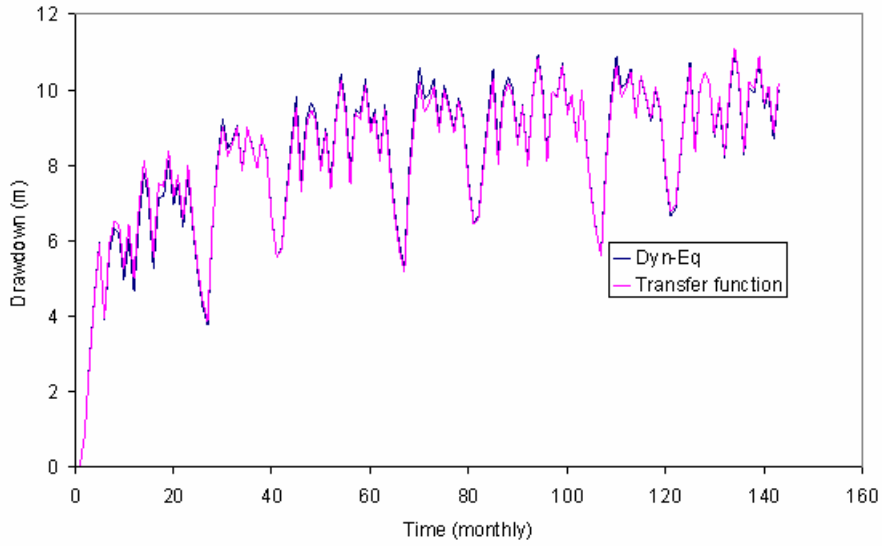

Figure 3.5.1b: Estimation of mean drawdown

Monitoring location i=10, j=34

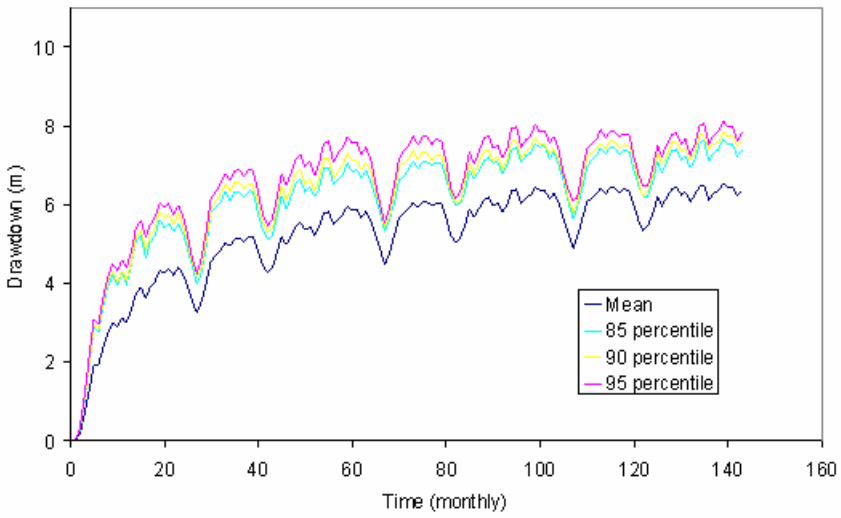

Monitoring location i=7, j=33

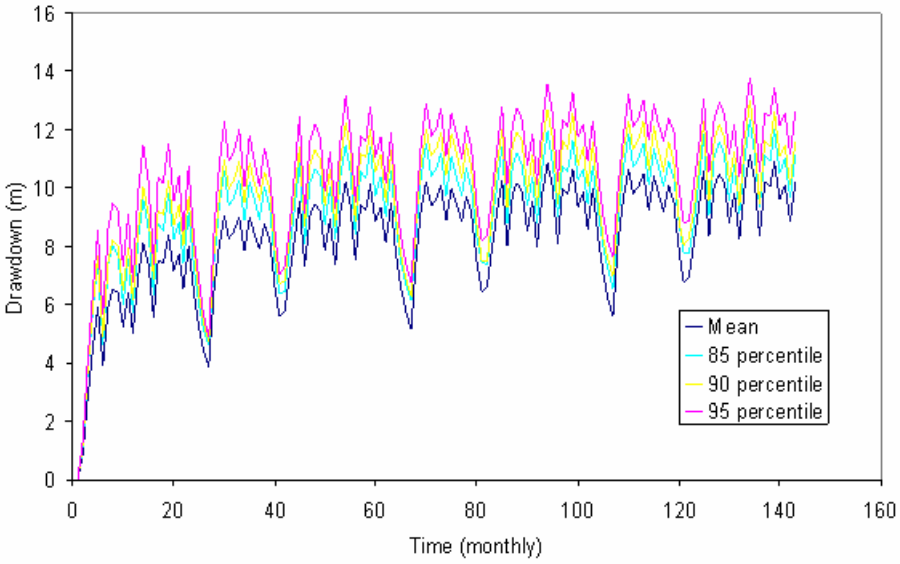

Figure 3.5.2: Ensemble statistics

$$d_{m2}(k+1)= \alpha P(k) + \beta P(k-1) + \gamma d_{m2}(k) + \theta d_{m2}(k-1) \quad (3.18)$$

$$d_{m3}(k+1)= \alpha P(k) + \beta P(k-1) + \gamma d_{m3}(k) + \theta d_{m3}(k-1) \quad (3.19)$$

$$d_{m4}(k+1)= \alpha P(k) + \beta P(k-1) + \gamma d_{m4}(k) + \theta d_{m4}(k-1) \quad (3.20)$$

$$d_{m5}(k+1)= \alpha P(k) + \beta P(k-1) + \gamma d_{m5}(k) + \theta d_{m5}(k-1) \quad (3.21)$$

$$d_{m6}(k+1)= \alpha P(k) + \beta P(k-1) + \gamma d_{m6}(k) + \theta d_{m6}(k-1) \quad (3.22)$$

where each location has distinct coefficients α , β, γ, and θ. The above equations include ten additional state variables (two state variables per equation): $d_{m2}(k)$, $d_{m2}(k-1)$, $d_{m3}(k)$, $d_{m3}(k-1)$, $d_{m4}(k)$, $d_{m4}(k-1)$, $d_{m5}(k)$, $d_{m5}(k-1)$, $d_{m6}(k)$, and $d_{m6}(k-1)$.

Thus, from a management model perspective, the addition of monitoring locations increases the problem dimensionality and complicates its solution.

The goal of this section is to investigate the possibility of approximating the drawdown at any monitoring location of interest using the drawdown at few monitoring locations which will be referred to as base locations. If shown to be possible, regional approximation can further reduce the dimensionality of the management problem and facilitate its solution. For example, if the drawdown sequences (3.18) through (3.22) could be expressed in terms of the drawdown sequences at two locations m2 and m3, the original requirement of 13 state variables would be reduced to five without loss of modeling accuracy This simplification would have very significant implications in regional models where hundreds of monitoring locations may be relevant to the management process.

The regional approximation procedure seeks to develop the following representation for the drawdown at any monitoring location:

$$d_{m1}(k+1)=a_{m1,1}\,p(k)+a_{m1,2}\,p(k-1)+a_{m1,3}\,d_1(k)+a_{m1,4}\,d_1(k-1)+a_{m1,5}\,d_2(k)+a_{m1,6}\,d_2(k-1)+\ldots..+a_{m1,(2n+1)}\,d_n(k)+a_{m1,(2n+2)}\,d_n(k-1) \quad (3.21)$$

where :

$d_{m1}(k+1)$: drawdown at a monitoring location of interest (m1) at time step (k+1);

$p(k)$, $p(k-1)$: pumping rates at time (k) and (k-1);

$d_1(k)$, $d_2(k)$, …, $d_n(k)$: drawdown at time step (k) at base locations 1,2,…, n;

$d_1(k-1)$, $d_2(k-1)$,…, $d_n(k-1)$: drawdown at time step (k-1) at base locations 1,2,…, n;

$a_{m1,1}$, $a_{m1,2}$, $a_{m1,3}$, $a_{m1,4}$, $a_{m1,5}$, $a_{m1,6}$, ….., $a_{m1,(2n+1)}$, $a_{m1,(2n+2)}$: unknown coefficients to be estimated.

To fully define equation (3.21) one needs to determine the base locations and estimate the coefficients $a_{m1,1}$, $a_{m1,2}$, $a_{m1,3}$, $a_{m1,4}$, $a_{m1,5}$, $a_{m1,6}$, ….., $a_{m1,(2n+1)}$, and $a_{m1,(2n+2)}$.

Let (J) denote the set of the base locations and (I) the set of the remaining monitoring locations. Then the problem stated earlier amounts to minimizing the objective function:

$$J=\sum_{\substack{i\in I\\ m=1,\ldots,M\\ k=1,\ldots,N}}\sum\sum\{\hat{d}(i,m,k+1)-d(i,m,k+1)\}^2 \quad (3.22)$$

where

$d(i,m,k+1)$: the drawdown at monitoring location (i), time step (k+1), for transfer function realization (m);

$\hat{d}(i,m,k+1)$: the estimated drawdown at monitoring location (i) at time step (k+1) for transfer function realization (m), using the drawdown at base locations $\{1, 2, ..,j\} \in J$;

$\hat{d}(i,m,k+1) = a_{m,i,1}\, p(k) + a_{m,i,2}\, p(k-1) + a_{m,i,3}\, d_{m,1}(k) + a_{m,i,4}\, d_{m,1}(k-1) + a_{m,i,5}\, d_{m,2}(k) + a_{m,i,6}\, d_{m,2}(k-1) + \ldots\ldots + a_{m,i,(2j+1)}\, d_{m,j}(k) + a_{m,i,(2j+2)}\, d_{m,j}(k-1)$ (3.22a)

where

$d_{m,1}(k)$, $d_{m,2}(k)$, ….., $d_{m,j}(k)$: drawdowns at base locations 1, 2, …, $j \in J$ at time step (k), for transfer function realization (m);

$a_{m,i,1}$, $a_{m,i,2}$, $a_{m,i,3}$, $a_{m,i,4}$, $a_{m,i,5}$, $a_{m,i,6}$, ….., $a_{m,i,(2j+1)}$, and $a_{m,i,(2j+2)}$: are coefficients specific for the monitoring location (i) and transfer function realization (m).

This is a nonlinear optimization problem with the following unknowns:

1. The base locations with drawdowns $d_{m,1}(k)$, $d_{m,1}(k-1)$, $d_{m,2}(k)$, $d_{m,2}(k-1)$, ….., $d_{m,j}(k)$ and $d_{m,j}(k-1)$.
2. The coefficients: $a_{m,i,1}$, $a_{m,i,2}$, $a_{m,i,3}$, $a_{m,i,4}$, $a_{m,i,5}$, $a_{m,i,6}$, ….., $a_{m,i,(2j+1)}$, and $a_{m,i,(2j+2)}$.

Finding the base locations among many monitoring locations can be a computationally complex proposition. However, the concept of the effective parameters can be used to simplify the search. Transfer functions with the same effective parameters are linear transformations of the same input variables and parameter values. Thus, in searching for independent base locations, transfer functions with the same effective parameters can be grouped together and be represented through one group member. Thus, the following direct search approach can be implemented to determine the set of base locations:

1. Assuming there are N monitoring locations, determine the effective parameters at each location.

2. Assign monitoring locations that have the same effective parameters to a group, {group (1), group (2),...., group (m)}.
3. Select any monitoring location from within the group as a group representative; Namely, select m monitoring locations as candidates for base locations.
4. Among the m base location candidates, determine the base location that minimizes (3.22). In this case, equation (3.23) can be written as $d_{m,i}(k+1)=a_{m,i,1}$ $p(k)+ a_{m,i,2}$ $p(k-1)+ a_{m,i,3}$ $d_{m,1}(k)+ a_{m,i,4}$ $d_{m,1}$ $(k-1)$. Denote by J_1 the minimum value of the objective function.
5. Next, among the m base locations, determine the two base locations that minimize (3.22). In this case, equation (3.23) can be written as : $d_{m,i}(k+1)=a_{m,i,1}$ $p(k)+ a_{m,i,2}$ $p(k-1)+ a_{m,i,3}$ $d_{m,1}(k)+ a_{m,i,4}$ $d_{m,1}$ $(k-1)+ a_{m,i,5}$ $d_{m,2}(k)+ a_{m,i,6}$ $d_{m,2}(k-1)$. Denote the minimum value of the objective as J_2.
6. Repeat this process for three, four, etc., base locations and determine the corresponding objective function values: J_3 , J_4 $_{,....,}$ J_i Terminate when

$\left(\frac{J_{i-1} - J_i}{J_{i-1}}\right) \times 100\% \leq \lambda$, where λ is a small percentage.

The following applications show that the above-described approach successfully identifies the base locations that provide good transfer function regional approximations.

3.7 Applications

3.7.1 Determination of Base Locations

In this case, aquifer drawdown is to be estimated at 19 monitoring locations. The pumping sites were assumed to form one cluster, as shown in Figure 3.2.1.2. Figure

3.7.1.1 shows the monitoring locations, and the calibrated hydraulic conductivity and storage coefficients zones. (Index i refers to the row number and index j refers to the column number.) Figure 3.7.1.2 shows some of the transfer functions realizations at some of the monitoring locations. Table 3.2, shows the effective parameters at the monitoring locations found based on the procedure outlined earlier. Four subsets of monitoring locations have the same effective parameters. (These are marked by different colors.) Thus, only one monitoring well from each subset is used in the procedure to find the base locations. These four locations were (i=16, j=35), (i=14, j=22), (i=5, j=34),and (i=3, j=30). Figure 3.7.1.3, shows the number of monitoring locations needed to be used as base locations. Two base locations were identified (i=7, j=33) and (i=13, j=43). The table in the figure shows that when using three base locations the overall error reduction at the remaining monitoring locations is negligible. In the table, the monitoring locations marked in black color are basically the base locations found when selecting all 19 monitoring locations. This represents the optimal solution. By contrast, the base locations marked by pink color are base location found using the procedure in the previous section. When the same base location is found by the optimal and sub-optimal procedures only one entry is shown in the table. It can be seen that the base locations found using the procedure in the previous section are almost always the same as the optimal locations. In this case, only two base locations are needed, the optimal solution is the same as the solution provided by the search procedure described earlier. The reason for the agreement of the two solution procedures is related to the grouping of the monitoring locations based on their effective parameters. The transfer function candidates

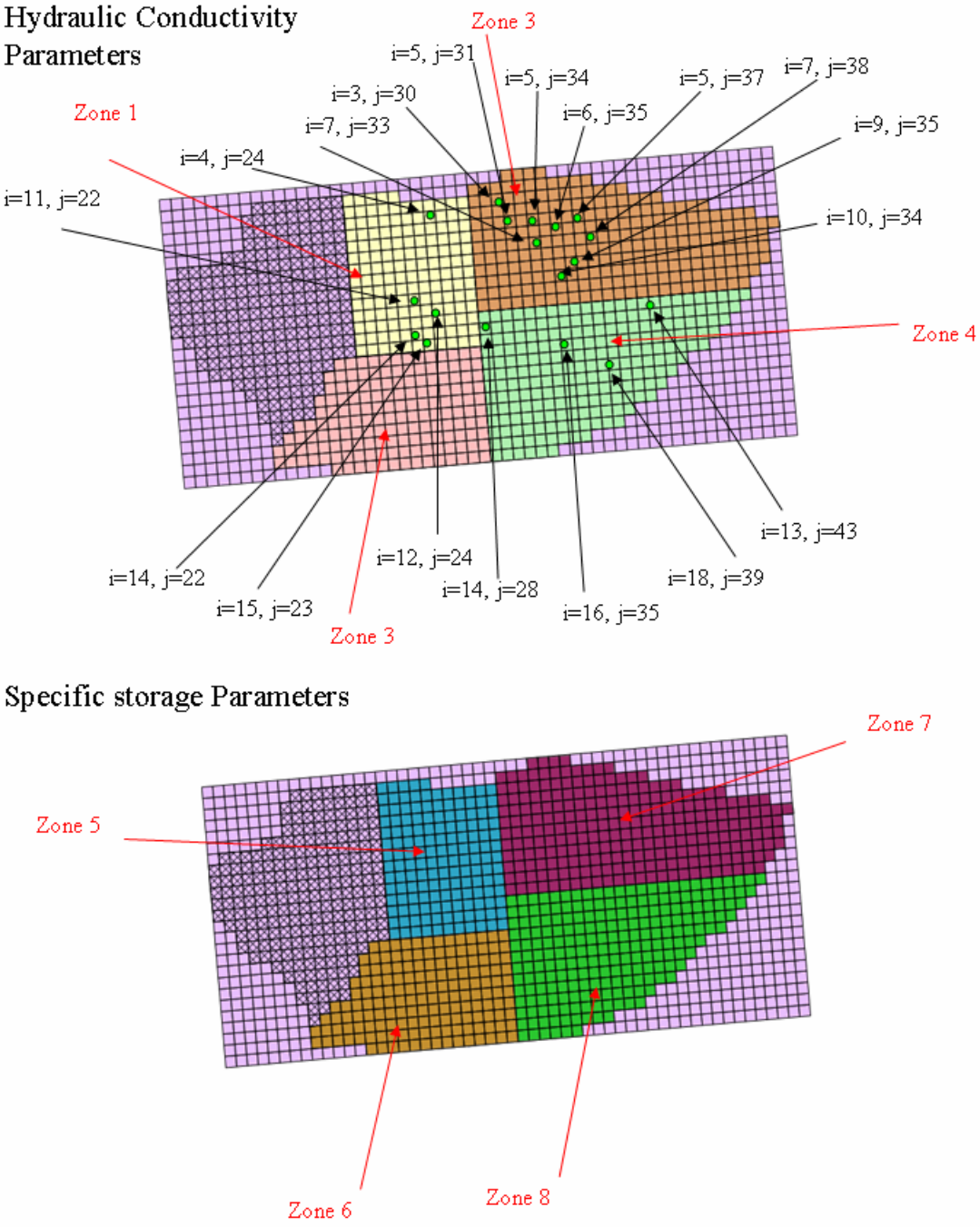

Figure 3.7.1.1: Monitoring locations, and calibrated zones of groundwater parameters

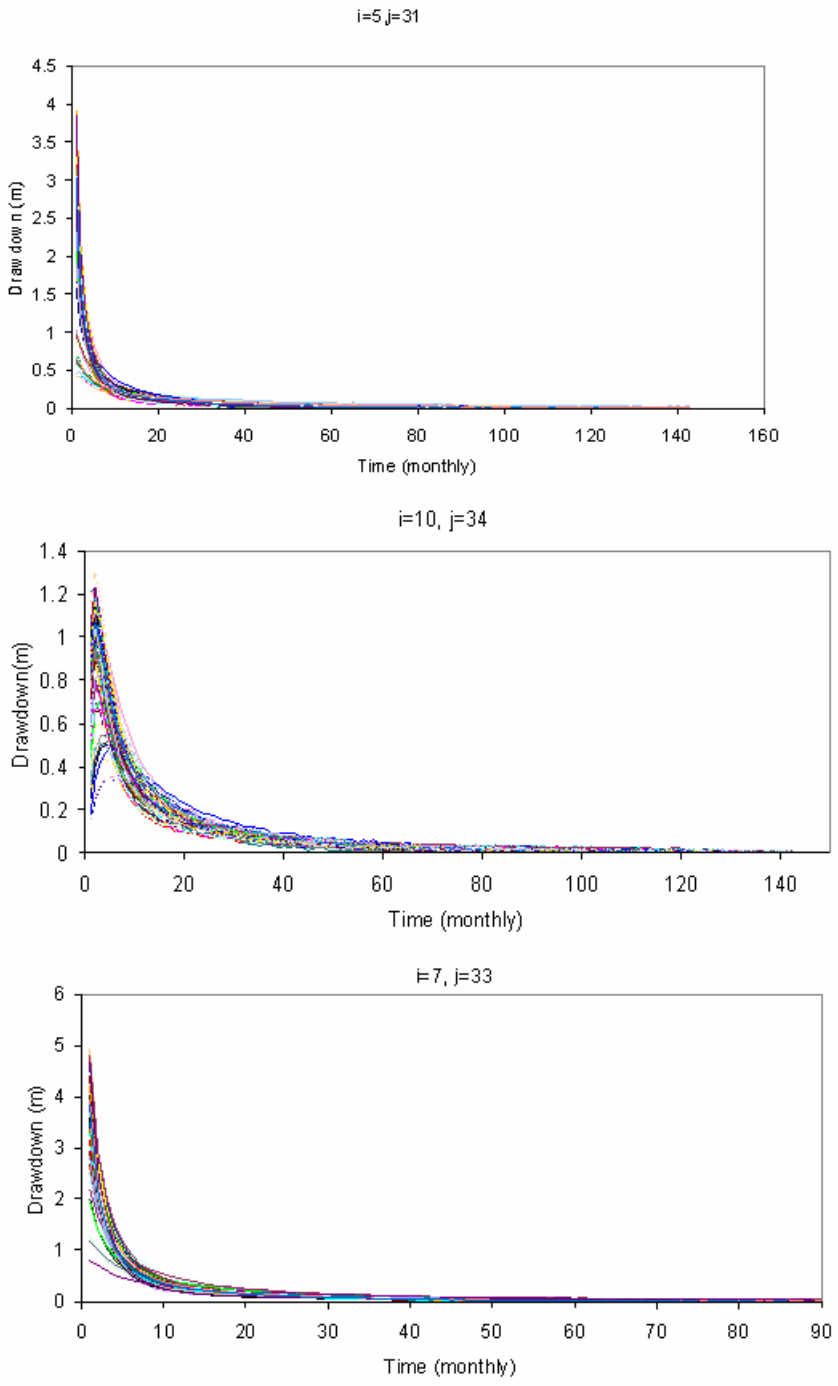

Figure 3.7.1.2: Transfer function realizations at some monitoring locations

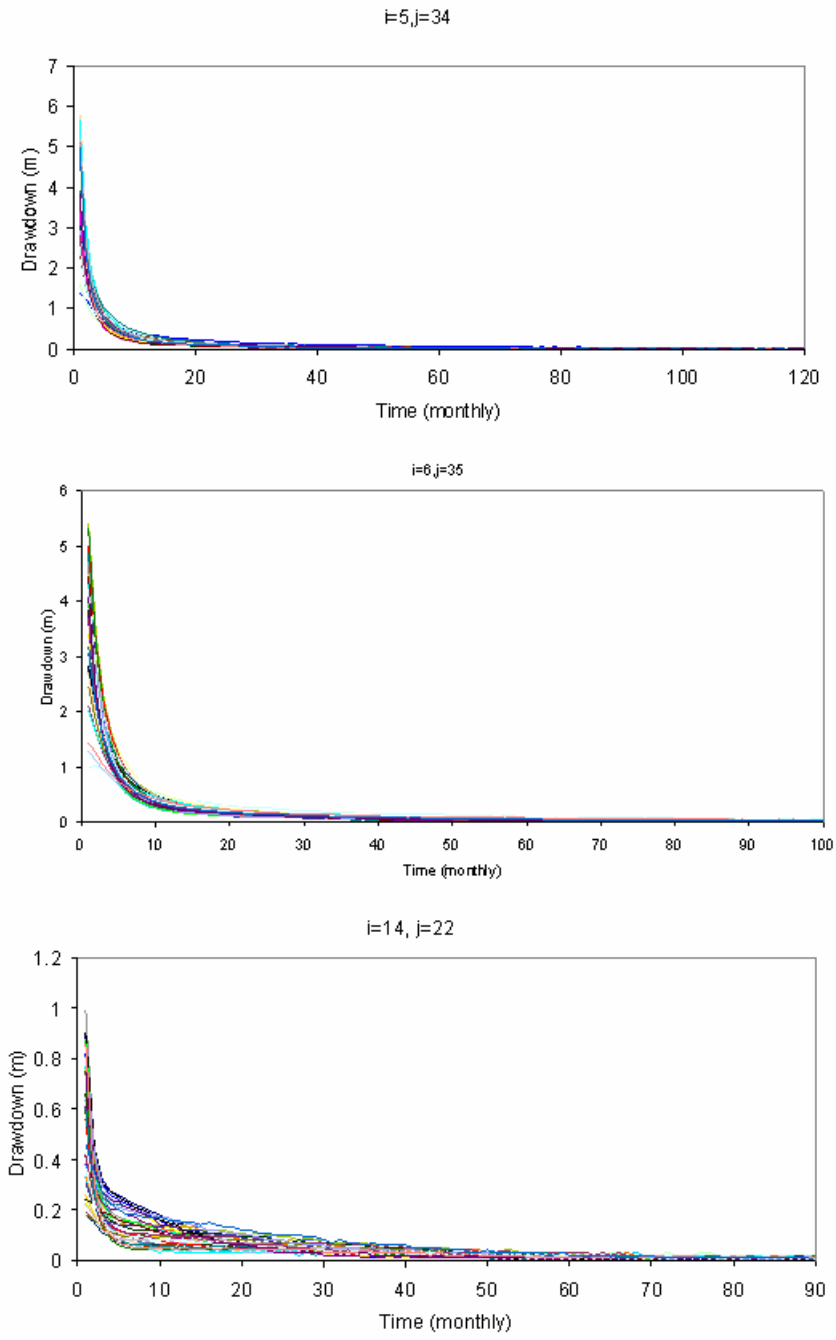

Figure 3.7.1.2: Transfer functions realizations at some monitoring locations

Table 3.2: Effective groundwater parameters at the monitoring locations

Monitoring locations	Effective parameter zones					
i=16, j=35	7	8	4	3	5	
i=18, j=39	7	8	4	3	5	
i=14, j=22	1	7	2	5	8	
i=13, j=23	1	7	2	5	8	
i=15, j=23	1	7	2	5	8	
i=11, j=22	1	7	2	5	8	
i=12, j=24	1	7	2	5	8	
i=5, j=34	7	3	8	4	5	6
i=5, j=37	7	3	8	4	5	6
i=7, j=38	7	3	8	4	5	6
i=6, j=35	7	3	8	4	5	6
i=9, j=35	7	3	8	4	5	6
i=3, j=30	7	3	1	8	4	5
i=5, j=31	7	3	1	8	5	4
i=10, j=34	7	4	8	3	1	5
i=7, j=33	7	3	8	4	6	1
i=13, j=43	7	8	4	3		
i=14, j=28	7	8	4	1	3	2
i=4, j=24	1	7	5	8	4	

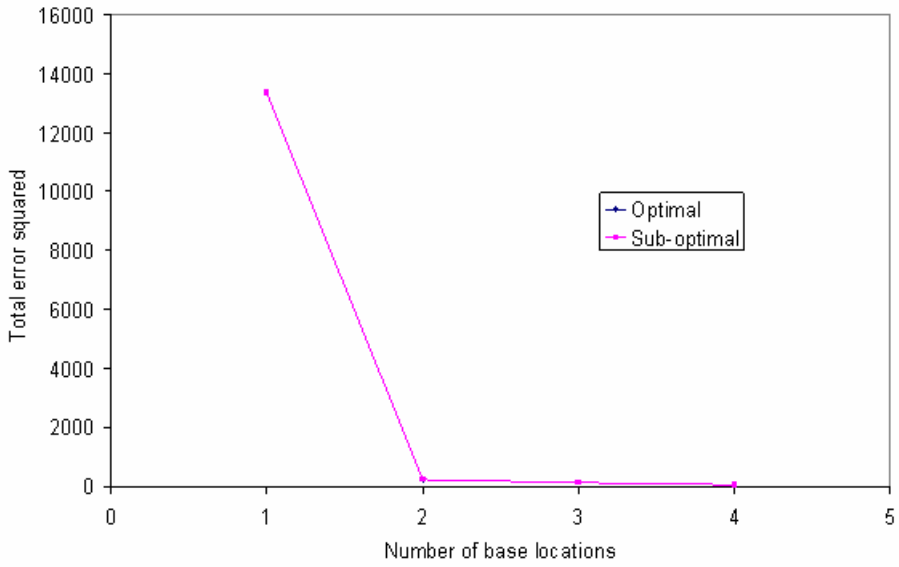

l=7,j=33	l=13,j=43	l=13,j=43	l=7,j=33
	l=7, j=33	l=10, j=34, l=3,j=30	l=13, j=43
		l=7, j=38, l=5,j=34	l=18, j=39, l=14,j=22
			l=14,j=28, l=16,j=35

Figure 3.7.1.3: Base locations selection

from the grouped monitoring locations represent all effective parameters that are needed to represent all transfer functions at the other monitoring locations.

3.7.2 Mean Drawdown and Uncertainty Characterization

After determining the base locations, the next step is to estimate the drawdown at all other monitoring locations of interest (regional approximation). The mean drawdown is computed as described in section 3.5. Figure 3.7.2.1 shows the mean drawdown at the base locations (i=7, j=33) and (i=13, j=43) for a given pumping sequence. As initial conditions, the model uses zero drawdowns everywhere in the field. This is the reason for the initial portion of the drawdown curve continuously ascending from zero. As time progresses, all transfer function coefficients contribute to estimating the drawdown, and the curve stabilizes and begins to fluctuate based on the pumping stresses. As can be seen from both graphs, the dynamical equation (3.16) estimates the mean drawdown very well. The regional approximation of drawdown sequences procedure is then used to estimate the mean drawdown at the remaining monitoring locations (figure 3.7.2.2). The figure compares the mean drawdown obtained via the regional approximation with the mean drawdown obtained directly from the transfer functions. The results are in good agreement.

Figure (3.7.2.3) shows the ensemble drawdown traces and associated statistics at different monitoring locations. It is noted that the ensemble uncertainty range depends on the pumping sequence. This can be concluded by examining equation (3.2). Thus, different pumping sequences give rise to different drawdown ranges. In this particular example, the pumping sequence is similar to the sequence in figure (3.2.4.2). The ensemble statistics of figure (3.7.2.3) show that the 95 percentile drawdown point can be

- Mean drawdown due to pumping: at base location 1:I=13, j=43, using
  $E(d1(k+1)) = \alpha 1\, P(k) + \beta 1\, P(k-1) + \gamma 1\, E(d1(k)) + \theta 1\, E(d1(k-1))$

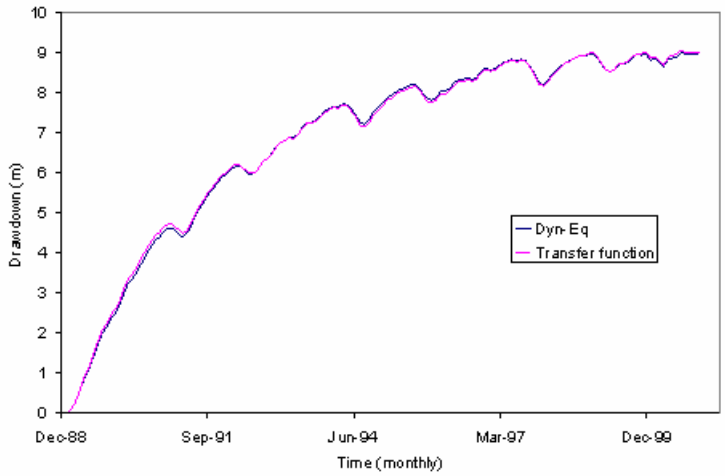

- Mean drawdown due to pumping: at base location 1: I=7, j=33, using
  $E(d2(k+1)) = \alpha 2\, P(k) + \beta 2\, P(k-1) + \gamma 2\, E(d2(k)) + \theta 2\, E(d2(k-1))$

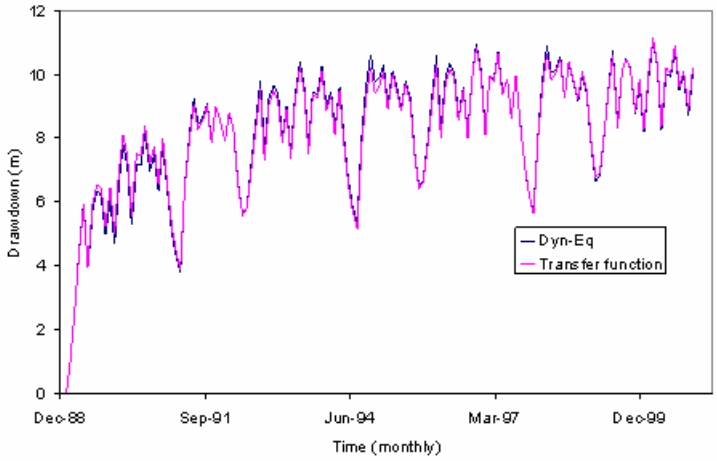

Figure 3.7.2.1: Estimation of mean drawdown at base locations

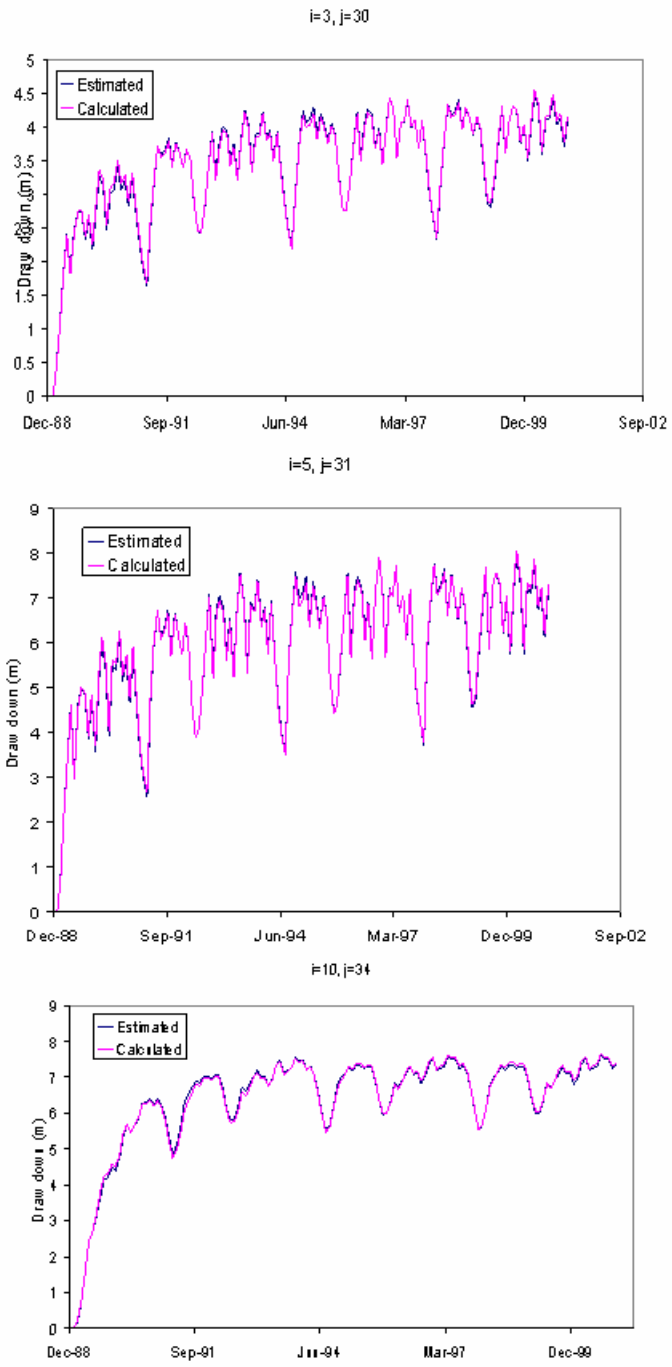

Figure 3.7.2.2: Estimation of mean drawdown at some monitoring locations

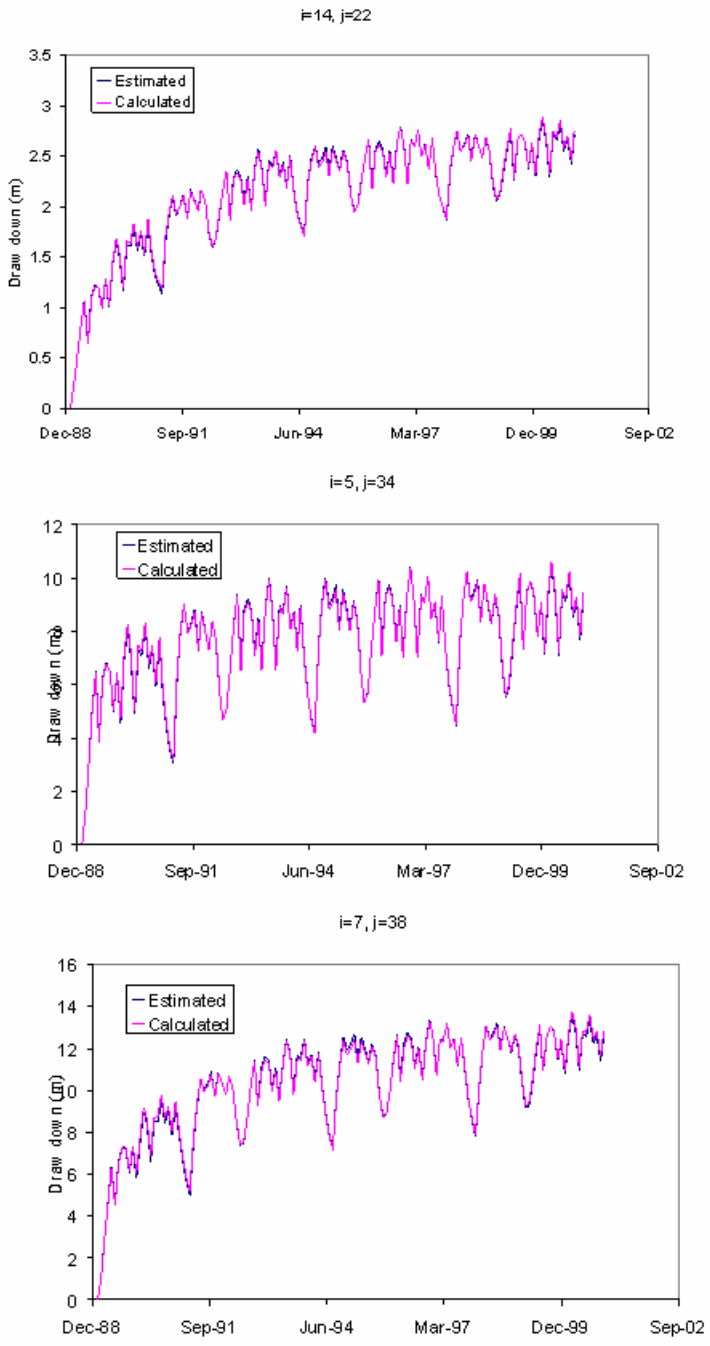

Figure 3.7.2.2: Estimation of mean drawdown at some monitoring locations

Monitoring location i=14, j=22

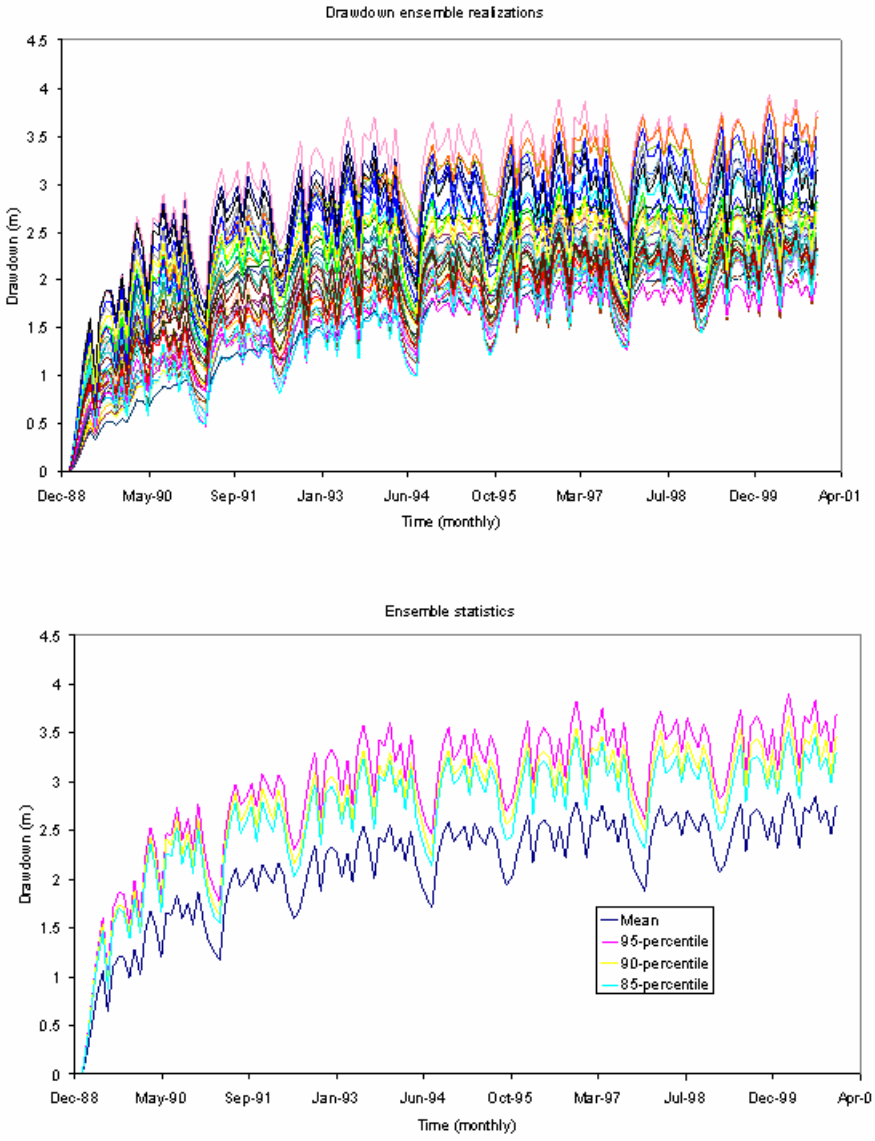

Figure 3.7.2.3: Ensemble drawdown and ensemble statistics

Monitoring location i=5, j=34

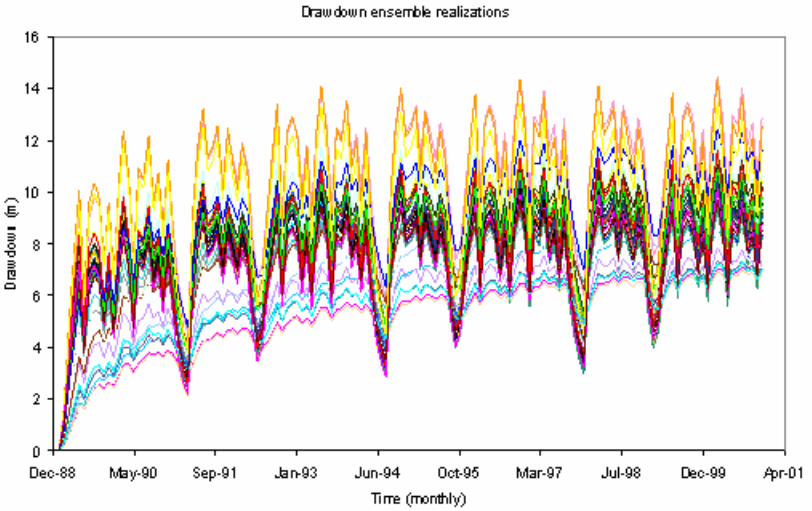

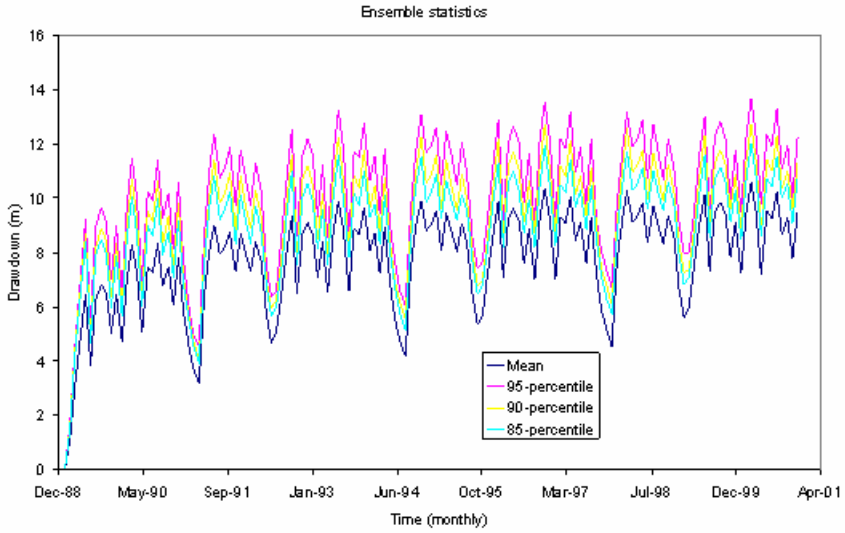

Figure 3.7.2.3: Ensemble drawdown and ensemble statistics

Monitoring location i=3, j=30

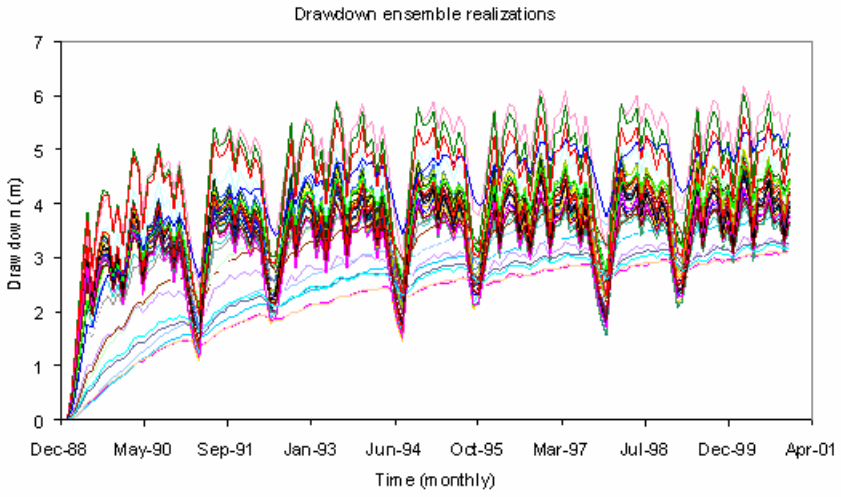

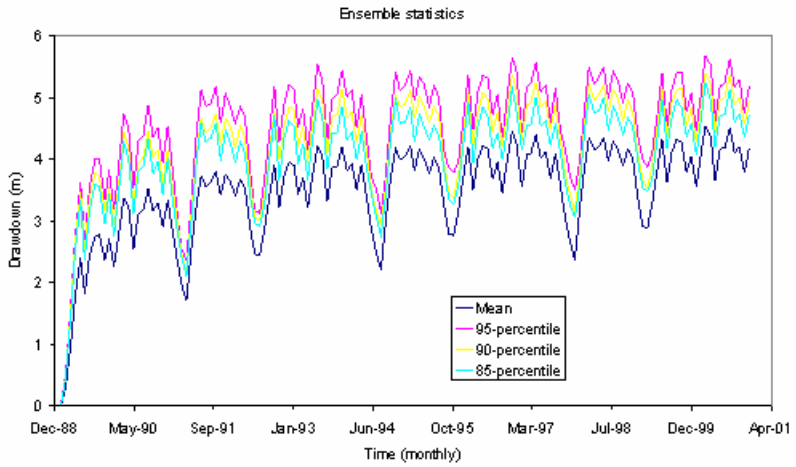

Figure 3.7.2.3: Ensemble drawdown and ensemble statistics

Monitoring location i=5, j=31

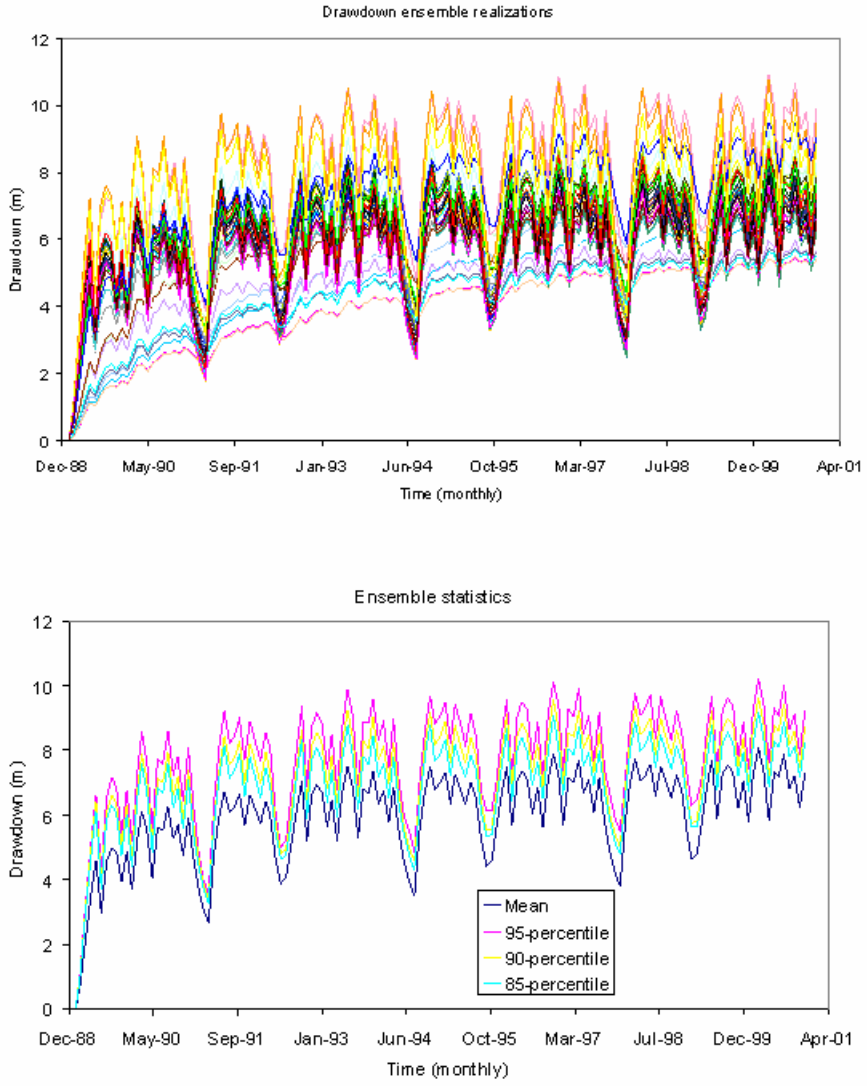

Figure 3.7.2.3: Ensemble drawdown and ensemble statistics

Monitoring location i=7, j=38

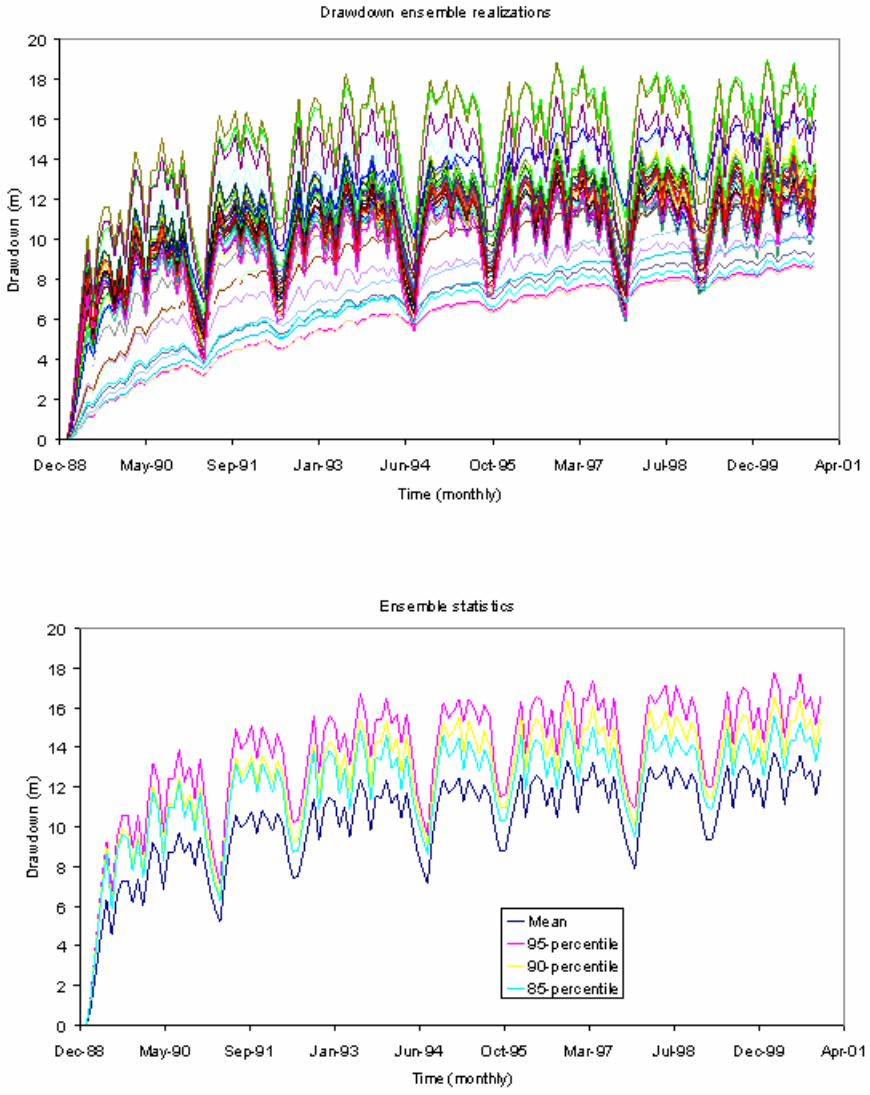

Figure 3.7.2.3: Ensemble drawdown and ensemble statistics

several meters away from the mean drawdown. In aquifer management, therefore, considering only the mean drawdown sequence may lead to frequent aquifer depletion and water quality deterioration

3.8 Summary of Groundwater Drawdown Uncertainty Characterization

The aim of the previous procedures is to reduce the dimensionality in the groundwater representation. It was shown that the drawdown sequences at any monitoring location of interest can be represented using only few state variables.

Following is a conceptual summary of the procedures developed in this chapter to be used as part of the conjunctive management model.

1. Use the statistical procedure to produce realizations of groundwater parameters that are consistent with the uncertainties in the groundwater aquifer. Develop sets of parameters and generate the transfer function ensembles.
2. Determine the base locations using the procedure of section 3.6. Develop the state dynamical equation at each base location to estimate its mean drawdown using equation (3.16):

   $$E(d_{Bas(i)}(k+1)) = \alpha_{Bas(i)}P(k) + \beta_{Bas(i)}P(k-1) + \gamma_{Bas(i)}E(d_{Bas(i)}(k)) + \theta_{Bas(i)}E(d_{B(i)}(k-1))$$

   where index (i) refers to the base locations.

   At the remaining monitoring locations, use equation (3.21) to estimate the mean drawdown:

   $$d_{m1}(k+1)=a_{m1,1}\,p(k)+ a_{m1,2}\,p(k-1)+ a_{m1,3}\,d_1(k)+ a_{m1,4}\,d_1\,(k-1)+ a_{m1,5}\,d_2(k)+ a_{m1,6}\,d_2(k-1)+ \ldots..+ a_{m1,(2n+1)}\,d_n(k)+ a_{m1,(2n+2)}\,d_n(k-1)$$

   where subscript (m1) refers to the monitoring location.

3. For a nominal pumping sequence (control sequence), or boundary stress sequence use the transfer function ensembles to characterize the uncertainty of the drawdown around the mean sequence. Namely, for each drawdown ensemble find the distance between the 95%, 90%, etc. percentiles from the mean: $G_{m1}(k+1)$, k=0,..,N-1, where m1 refers to the monitoring location number, and N is the control horizon.
4. Use equations (3.16) and (3.21) along with $G_{m1}(k+1)$ in the control model formulation to identify new pumping sequences that meet the management objectives.
5. Compute the new mean drawdown sequences and associated ensembles; Update the distances $G_{m1,new}(k+1)$, k=0,..,N-1, and repeat the previous steps until convergence.

3.9 Conclusions

This chapter describes a new procedure to model aquifer response under uncertainties related to groundwater parameters and boundary stresses. The following conclusions can be draw from these procedures:

1. The state space formulation of the transfer functions reduces the number of variables needed to describe aquifer response at a particular location.
2. The regional approximation of transfer functions and aquifer drawdowns reduces the spatial dimensionality of the problem even further.
3. Parameter uncertainty is incorporated through transfer function ensembles. This is important for providing risk based management policies.

4. The previous procedures are implemented here for a confined aquifer. However, it can also be extended for unconfined aquifers. In such cases, one could develop linearized drawdown state equations around a nominal pumping and boundary stress sequence and precede with the control model iterations.

CHAPTER 4

CONJUNCTIVE SURFACE WATER AND GROUNDWATER MANAGEMENT

4.1 Introduction

The purpose of this chapter is to formulate and solve the surface water and groundwater management problem using the concepts developed in chapter 3. The problem is formulated in state space form with explicit account of uncertainty through ensemble characterization of all random quantities. The objective of the optimization module is to determine reservoir release and groundwater pumping sequences that meet water demands as best as possible. This is a dynamic optimization problem that is solved using control theory methods.

To this end, section 4.2 develops the conjunctive management problem formulation using Jordan as a typical water resources system; Section 4.3 presents a control method suitable for its solution; Section 4.4 discusses the application of this method to the Jordanian case study, and section 4.5 summarizes the developments in this chapter.

4.2 Conjunctive Water Resources Management: State Space Formulation

Conjunctive water resources management implies the simultaneous regulation of surface water and groundwater systems. Such regulation is appropriate when the two subsystems are linked hydraulically or by the need to meet common water demands. In

either case and for any region, the conjunctive management problem can be cast in a very similar form. In this work, the water resources system in Jordan is used as a typical case study to develop the conjunctive management formulation. It will be seen that this formulation has a general and flexible structure able to accommodate practically all problem variations.

4.2.1 The Jordanian Water Resources System

4.2.1.1 Introduction

Water resources planning and management is a top national priority and necessity in Jordan. There are several compelling reasons for this, as evidenced by the following facts:

1. The per capita water supply is 150 cubic meters per year, which is much below the 1000 cubic meters per year considered to be the threshold of water scarcity (FAO, 1993).
2. Water supply is seriously deficient relative to the rapidly rising demand, in spite of significant infrastructure investments in the water sector (El-Naser, 1997). Presently, the deficit is covered by over-exploiting groundwater aquifers at rates far beyond their sustainable range (i.e., 146 to 235%, El-Naser, 1997). The over-exploitation of surface and groundwater has caused a historically unprecedented decline of the Dead Sea level (of over 21 meters since 1930).
3. The population of Jordan, presently about 4.5 million, is growing at a very high rate of 3.4 percent annually, intensifying the stress on the country's water resources and placing serious limitations on its economic growth.

4. Jordan's primary surface water resources are shared with neighboring countries, including the Yarmouk River (on the Syrian border) and the Jordan River (on the border with Israel).

4.2.1.2 Surface Water Resources System

The Jordanian river system is formed by the Jordan, Yarmouk, and the Zarqa Rivers (Figure 4.2.1.2.1). In addition to these rivers, the system includes the King Talal Dam on the Zarqa river, the King Abdullah Canal that runs parallel to the Jordan River, the North Jordan Valley side tributaries called "wadis" (Wadi Ziglab, Wadi Yabis, Wadi Rajib, and Wadi Arab), the Central/Southern Jordan Valley side wadis (Wadi Shueib, Wadi Kafrein and Wadi Hisban), the Mukheiba Wells, the Al Karameh Dam, the Wadi Ziglab Dam, the Wadi Arab Dam, the Wadi Kafrein Dam, and a proposed dam on the Yarmouk River known as the Al Wehdah Dam.

A short description of these elements follows. Data for the modeling of these elements were provided by the Jordanian Ministry of Water and Irrigation.

Hydrologic Data

Hydrologic data include

1. unimpaired streamflow data for the Zarqa River and the Yarmouk River at Maqaren from October 1963 to September 2000.
2. Streamflows for the North Jordan Valley Side Wadis and Central/ Southern Jordan Valley Side Wadis from October 1984 to September 1995.

Figure 4.2.1.2.1: The Jordan-Yarmouk-Zarqa system

3. Average monthly evaporation data at Al Wehdah and King Talal Dams.

The monthly flows for the Zarqa River and the Yarmouk River at Maqaren were adjusted to account for the changes in their flows due to return flows from two treatment plants and the Syrian water withdrawals. For the Zarqa River, the monthly effluent flow from the Al Samra and Al Baqa treatment plants was subtracted from the Zarqa River monthly flows from 1986 until 2000—the time period during which the plants were operational—and the resulting monthly Zarqa River flow sequence was considered to be the unimpaired Zarqa River flow. This adjustment was necessary because these plants serve Amman which receives its water supply from sources outside the Zarqa River Basin. The monthly effluent flows for 2000 were taken as the representative monthly effluent flows to the Zarqa River.

For the Yarmouk River at Al Maqaren, the adjustment of the monthly flows was based on assessing the annual Syrian withdrawals from the Yarmouk Basin. The annual Syrian withdrawals are implemented through the Syrian storage facilities built on the Yarmouk River tributaries since 1970. The storage capacity of the Syrian dams built on Wadi Raggad is 61 MCM, while the storage capacity of the dams built on the Yarmouk tributaries upstream of Al Maqaren is 95 MCM. Therefore, the annual Syrian withdrawals since 1970 are taken to be 95 MCM/year from the Yarmouk River tributaries upstream of Al Maqaren and 61 MCM/year from Wadi Raggad respectively. Hence to re-construct the unimpaired flows of the Yamouk River at Al Maqaren, the annual Syrian withdrawals of 95 MCM/year are added to the Yarmouk River flow at Al Maqaren on a monthly basis. Prior to 1970 (1963 to 1970) no adjustment was applied to the Yarmouk River flows as the Syrian withdrawals were considered negligible. The unimpaired flows

of the Yarmouk River at Al Maqaren are used as hydrologic input to the model. Furthermore, the 95 MCM/year is assumed to represent the Syrian monthly withdrawals from the Yarmouk basin after 1970.

Figure 4.2.1.2.2 depicts the monthly streamflows of the Yarmouk River, the Zarqa River, the North Jordan Valley Wadis, and the Central/Southern Jordan Valley Side Wadis.

Al Wehdah Dam

The proposed Al Wehdah Dam is a joint project between Jordan and Syria and has the following characteristics, (Harza, 1988a):

Dead storage: 30 MCM

Normal pool Storage: 225 MCM

Active Storage: 195 MCM

Max release: 30 MCM/month

Power Capacity: assumed to equal 11.5 MW

The hydrologic input to Al Wehdah Dam is the flow of the Yarmouk as measured at Al-Maqaren, a location close to the proposed dam site. The main project purposes include irrigation, municipal and industrial water supply, and power generation. The benefits of the Al-Wehdah Dam will be shared by Jordan, Syria, and, to a lesser extent, by Israel who is a downstream riparian and is also entitled some share of the Yarmouk flow. The multinational interest in the planning and management of the new dam creates the need for shared-vision agreements among the countries. In this regard, some important questions that need to be addressed include: What is the regulatory capability

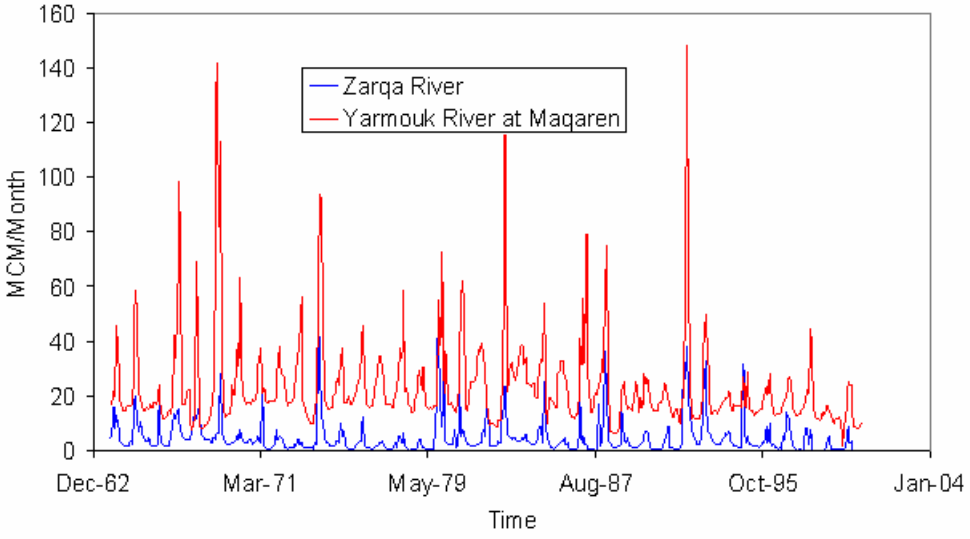

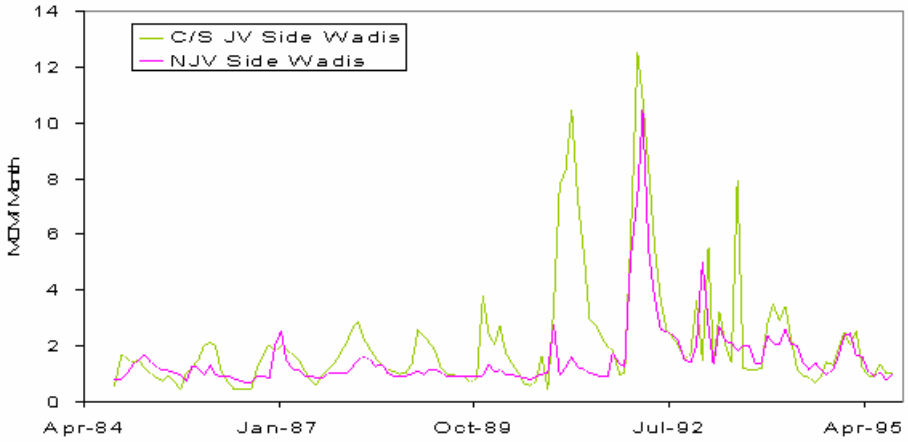

Figure 4.2.1.2.2: Hydrographs of the Yarmouk River, Zarqa River, NJV Side Wadis and C/S JV Side Wadis

of the Al-Wehdah Dam relative to the seasonality of the Yarmouk flow and the downstream water uses? How should it be operated to best meet the agricultural,municipal, and industrial water needs of Jordan, Syria, and Israel? Quantitative answers to these questions can only be provided by a holistic analysis of the Jordanian water resources system. This is the practical utility of the decision support system developed herein.

King Talal Dam

The characteristics of the King Talal Dam (KTD) are as follows, (Harza, 1988b):

Elevation at the top of the Dam:	185 m
Normal Pool Level:	179.0 m
Storage at Normal Pool Level:	85 MCM
Minimum Reservoir Level:	123.0 m
Live Storage Capacity:	75 MCM
Max release from KTD:	17 MCM per month
Install Power Capacity:	6 MW (2 turbines)

The hydrologic inputs to King Talal Dam are the Zarqa River flow and the effluent from the Al Samra and Al Baqa Plants. KTD's main purposes are (1) the provision of irrigation water supply for Central and Southern Jordan Valley and (2) energy generation. The construction of the Al Wehdah Dam raises the need for a coordinated management strategy between the two storage projects.

Al Karameh and Side Wadis dams

The Al Karameh and side wadis dams are storage impoundments with the following characteristics:

Al Karameh Dam Live Storage: 55 MCM

Al Kafrein Dam Live Storage: 8.5 MCM

Wadi Ziglab Dam Live Storage: 3 MCM

Wadi Arab Dam Live Storage: 17 MCM

King Abdullah Canal (KAC)

The King Abdullah Canal (KAC) was constructed to provide irrigation water to the Jordan valley. KAC connects with the Yarmouk River at Adasiya. The canal capacity at the intake (Adasiya) is 20 m^3/sec, and it is reduced to 12 m^3/sec at the location of the Zarqa River and 3 m^3/sec at its end point.

Demands, water transfers, and return flows

The major irrigation areas are located in the North Jordan Valley region extending from the Yarmouk River to Wadi Ragib (approximately 11500 hectares) and in the Central/ Southern Jordan Valley region extending from Wadi Rajib to the Dead Sea (approximately 19660 hectares). Municipal water demand is mainly associated with Amman, the Jordanian Capital, and Zarqa, the second largest city after Amman. The current monthly demands for these areas are plotted on Figure 4.2.1.2.3.

A transfer from Lake Tiberias to King Abdulla Canal has been included based on the Jordanian Quota from the Jordan/ Israel Peace Treaty. The agreement stipulates that the transfer amount would be 20 million cubic meters (MCM) during the summer period (May-September), and 10 MCM from the Jordan River (desalinated water from saline

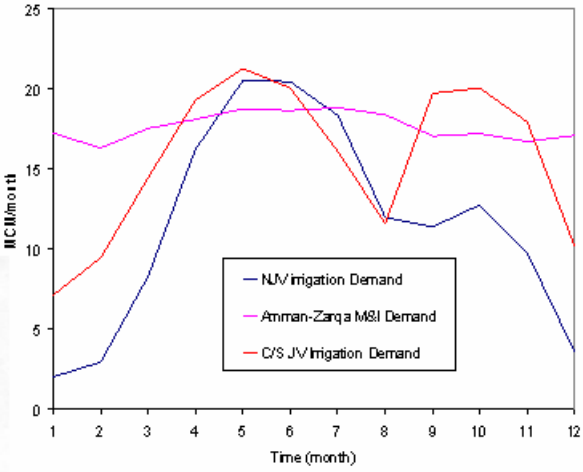

Peace Treaty Shares

Jordan: 20 MCM (Lk. Tiberias; summer)

10 MCM (desalinated; winter)

25 MCM (additional supplies)

Israel: 12 MCM (Yarmouk; summer)

33 MCM (Yarmouk; winter)

Assumed Syrian water allocation (withdrawals) from Al Wehdah Dam: 10%-30% of NJV Irrigation Demand

Figure 4.2.1.2.3: System Layout and Water Demands

springs) for the winter period (October-April). An additional 25 MCM will also be provided to Jordan as part of the treaty (Figure 4.2.1.2.3). The Jordanian quota is assumed to be distributed based on North Jordan Valley irrigation demands. By the Peace Treaty, Israel also accrues water from the Yarmouk River as follows: During the summer period (May-September), Israel can pump 12 MCM over the 5 months of summer period. During winter (October-April), Israel can pump a total of 33 MCM from the Yarmouk of which 13 MCM is the Israeli quota from the Yarmouk and 20 MCM is the Jordanian transfer to be stored in lake Tiberias and then pumped back to Jordan during summer.

Syrian allocation from Al Wehdah Dam is assessed based on the Syrian/ Jordanian agreement. The main points of the agreement that relate to this work are as follows:

1. The constructed dam will be built on the Syrian-Jordanian territories near the site of Al Maqaren Gage station. The dam will be used for power generation; irrigation of Jordanian lands; provision of water for any other Jordanian water needs; irrigation of Syrian Lands in areas down stream of the dam that are contiguous to the Yarmouk River and have an elevation up to 200 m above sea level.
2. Jordan is responsible to finance fully the project in all its stages; this includes the studies and the designs for the project, also construction, operation and maintenance of the dam. On the other hand, Syria is responsible to provide the required help and assistance for the workers in the project in order for them to

enter the Syrian territories within the project area and do the related work during all the project stages.

3. Jordan is to design and construct Al Wehdah Dam with a total height of 100 m, (including the spillage gates). This dam will be used to store the Yarmouk River water that is left after filling all the Syrian dams, and Syria has the right to fully keep all the water stored in its dams.

4. Syria has the right to fully use all the springs that are in the Yarmouk Basin within its territories, except for all the springs that are located upstream of the dam and are below the dam elevation by 250 m. Syria also has the right to fully utilize all the Yarmouk tributaries downstream of the dam which are in its territories and to irrigate all the lands which are contiguous to the Yarmouk River watercourse.

5. Both countries (Jordan and Syria), each at its own side, have to take all the necessary procedures to prevent the accumulation of the sediments in the reservoir, and to conserve the soil at the dam site from erosion. Jordan is responsible for all the cost that is resulting from such works.

6. Both countries have the right to benefit from the reservoir for tourism and fishing purposes under the condition that such use will not impede management of the reservoir.

The Syrian share from the Al Wehdah Dam was interpreted to apply downstream of Al Wehdah Dam as part of the dam's release. However, it was not quantitatively determined due to lack of detailed information (such as topographic maps that show the area of the Syrian lands along the Yarmouk River with elevation less than 200 m below

sea level). Thus, the Syrian share from Al Wehdah Dam was estimated as a certain percentage of the irrigation demand in the North Jordan Valley region. A sensitivity analysis on this percentage can be used to assess the ability of the system to meet various demand levels.

Return flows pertain to the Al Samra and Al Baqa Treatment Plants. The Al Samra Treatment Plant discharges the effluent to Wadi Dulayl which flows into the Zarqa River. Thus, the Al Samra Plant effluent becomes part of the Zarqa River flow that flows into the King Talal Dam. The annual effluent volume from the plant was almost 20 MCM in 1986, and increased to 50 MCM in 2000. For the last few years, the plant has been operating over its design capacity by almost 334% due to the large influent volumes of sewage from Amman and Zarqa. Unfortunately, the quality of the treated effluent is not within the required standards. The Al Baqa plant is a much smaller plant than Al Samra. Its effluent flow is discharged to Wadi Rumaymeen and from there it also flows into the King Talal Dam. The Al Baba effluent volume in 2000 was almost 3.5 MCM. Figure 4.2.1.2.4 shows the monthly effluent flows from both plants. These effluent flows augment the natural inflow of the Zarqa river because water supply for Amman comes from outside the Zarqa River basin (i.e., the Jordan River, the Yarmouk, or from aquifers). Based on historical data, the return flow is estimated at 35% of the water supplied to Amman.

4.2.1.3 Groundwater System

The groundwater system consists of several aquifers. From north to south, these aquifers are the Yarmouk Basin aquifer tapped by the Mukheibah wells, the Amman-

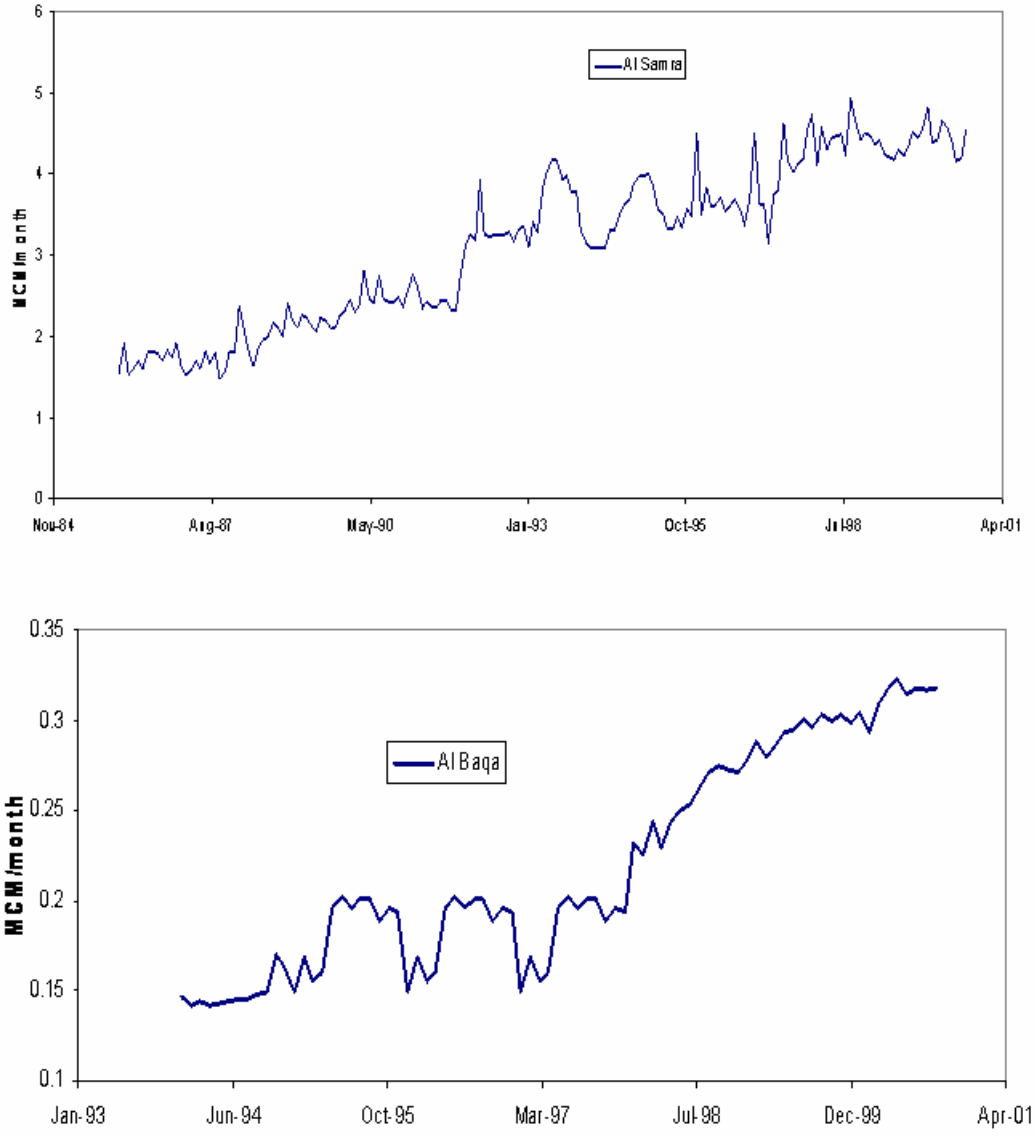

Figure 4.2.1.2.4: Al Samra Effluent Flow (Jan1986- Sep 2000), And Al Baqa Effluent Flow (Jan 1994- Sep 2000)

Wadi sir Aquifer in the Amman-Zarqa Basin, and the Disi Aquifer in the southern part of the country.

At the present time, flow from the Mukheiba Wells is diverted into the King Abdulla Canal just south of the intake from the Yarmouk River (Adasiya diversion). The long term yield is estimated to be about 20 MCM/year. Although the Mukheiba Wells are located in the Yarmouk Basin, the aquifer exploited by the wells is isolated from the Yarmouk River by an impervious layer. This same aquifer is the source for the springs in the Wadi Arab and, therefore, pumping has a direct effect on the flows in Wadi Arab.

Again due to lack of detailed data, this hydraulic connection could not be fully modeled. Thus, the assumption made herein is that the Mukheiba Wells represent an independent water source that can supply up to 20MCM/year. Figure 4.2.1.3.1 shows a historical monthly pumping sequence from the Mukheiba Wells.

The Amman-Wadi Sir Aquifer is the main aquifer in the Amman- Zarqa Basin, and it is the major source of water supply for the 2.5 million people that live in the cities of Amman and Zarqa. This aquifer covers the entire basin, with its eastern part extending into Syria. The aquifer has the following characteristics (Hydrogeology of the Amman-Zarqa Groundwater Basin, Ministry of water and Irrigation, Jordan 2000):

Aquifer average depth : 220 m

Aquifer soil type: Sandy silty soil

Estimated transmissivity: 9.0 m^2/day to 1000.0 m^2/day

Estimated specific storage coefficient: 2.5×10^{-5} m^{-1} to .0012 m^{-1}

Total number of pumping centers: 25

Hydraulic head: Ranges from 400 m to 750 m across the aquifer

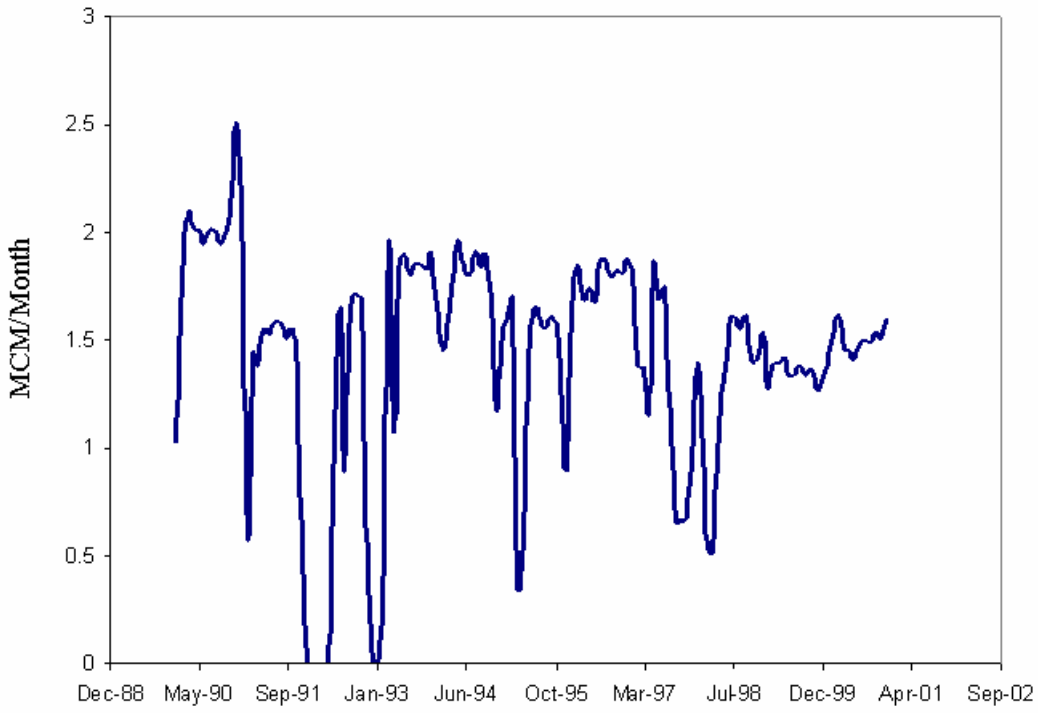

Figure 4.2.1.3.1: Monthly Pumping From Mukheiba Wells

The Amman-Wadi Sir aquifer is modeled according to the procedures established in Chapter 3.

The Disi Aquifer is also a major aquifer in Jordan. The Disi was formed during the early geologic ages and contains fossil, unreplenishable water. This aquifer has the following characteristics (Ministry of Water and Irrigation, "Groundwater Uses 1999"):

Aquifer Depth:	150 m
Aquifer Safe extraction rate:	125 MCM/Year
Total number of wells:	71
Current pumping for irrigation and M&I:	66.26 MCM/Year
Current Extraction as percentage of safe yield:	53%

A water transfer from the Disi to Amman was also considered to assess the benefits of the Disi Aquifer Conveyor project. This transfer is assumed to occur within a certain conveyance capacity range, and it is dedicated to meeting Amman's municipal and industrial demands. The Dici-Amman transfer was taken as 75 MCM/year. Due to lack of detailed data, the Disi aquifer could not be modeled using the methods developed in Chapter 3.

4.2.2 Conjunctive Water Resources Management: Problem Formulation

In developing the management problem formulation, it is helpful to view the water resources system as a network of nodes representing hydrologic inputs, storage (regulation) elements, and demand areas (figure 4.2.2.1).

In addition to the Yarmouk and Zarqa rivers that represent the inflows to the Al Wehdah and King Talal reservoirs, hydrologic inputs also include the following side wadis: Wadi Raggad, Wadi Arab, Wadi Ziglab, Wadi Yabis, and Wadi Rajib. For

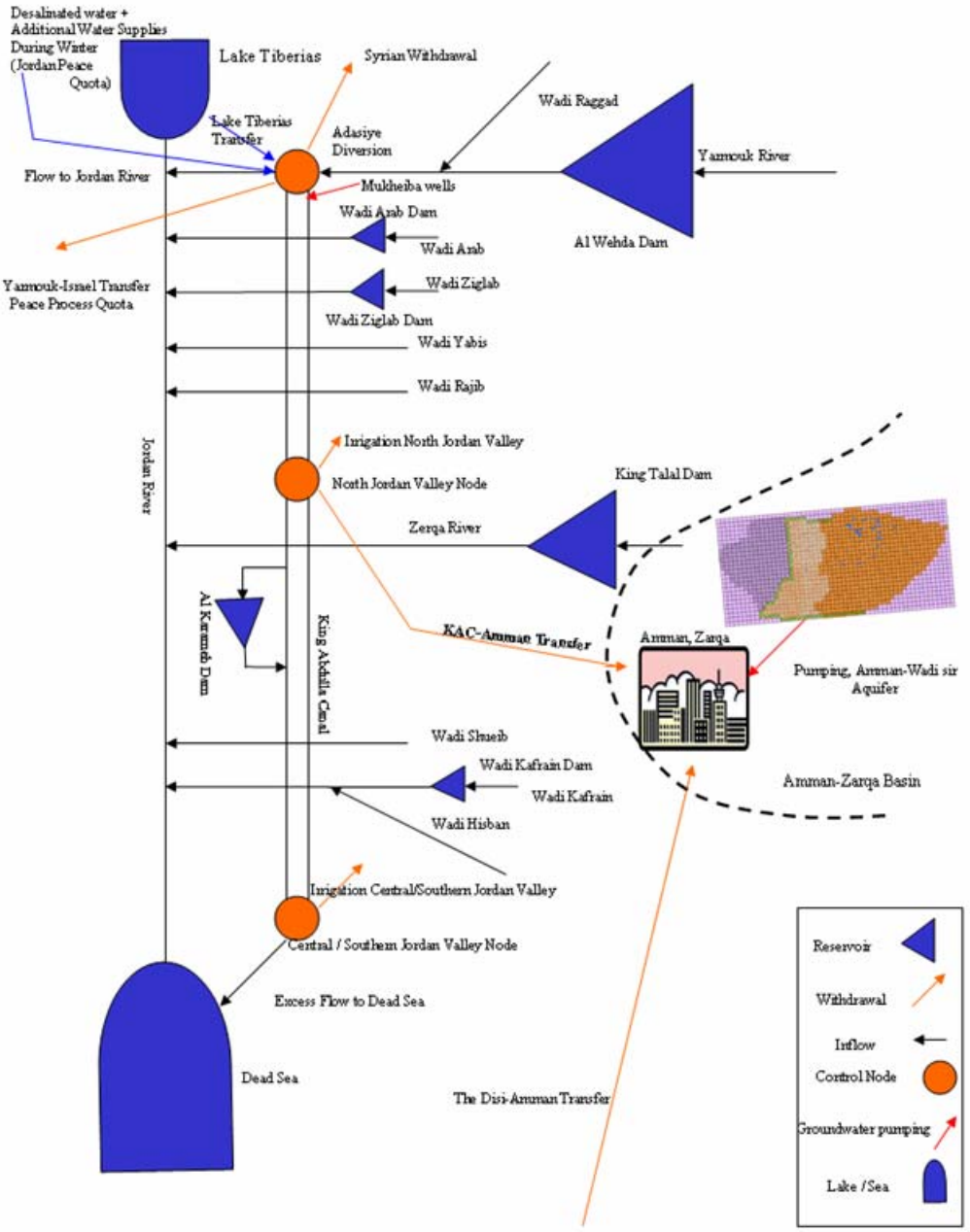

Figure 4.2.2.1: System schematic

modeling purposes, the flows of Wadi Yabis and Wadi Rajib are aggregated into one hydrologic input referred to as the North Jordan Valley side wadis. All reservoirs and side wadis provide water to King Abdullah canal, which is an open conduit intended to meet the water demands along the Jordan Valley.

The main surface reservoir nodes in the system are the Al Wehdah Dam, Arab Dam, Ziglab Dam, King Talal Dam, Karameh Dam, and Kafrein Dam. The Al Wehdah and King Talal dams are the major dams in Jordan. Karameh Dam is the third largest reservoir and together with the Kafrein Dam and the side tributaries called Wadi Shuieb and Wadi Hisban provide irrigation water to the Central and South Jordan Valley.

The main groundwater reservoir considered herein is the Amman Wadi-Sir aquifer, which is the major aquifer in the Amman-Zarqa Basin. The aquifer is regulated through pumping and provides water to the Amman-Zarqa region. The Disi Aquifer and the aquifer associated with the Mukheiba well field are considered as water sources.

Nodes of water demand include the Adasiya (which is the node associated with the Israeli peace quota and the Syrian quota from Al Wehdah Dam), North Jordan Valley (associated with agricultural demands), Amman-Zarqa (municipal and industrial demands), and Central and South Jordan Valley (agricultural demands). The Adasiya node receives water from the Al Wehdah Dam, Wadi Raggad, and any water transfer from Lake Tiberias as part of the peace process quota. The Adasiya node provides water to the North Jordan Valley, Israel (peace process quota from the Yarmouk River), and to Syria as part of the Al Wehdah Dam agreement.

The North Jordan Valley node receives its water supply from the Adasiya node, Wadi Arab Dam, Wadi Ziglab Dam, Mukheiba Wells, and North Jordan Valley side

wadis. In turn, the North Jordan Valley node provides water to Karameh Dam and to the Amman-Zarqa node.

The Central and South Jordan valley node receives water from the Karameh Dam and supplies the Dead Sea as part of environmental demand. Because system water demand is higher than supply, however, residual flow from the canal to the Dead Sea is only permitted during floods when the available storage is completely filled.

The Amman-Zarqa node also receives water from the Disi Aquifer as well as the surface water system through the King Abdullah Canal. Due to the high cost of pumping and transporting water from the Disi to Amman, the Disi water transfer is used as a last option in the management model. The municipal and industrial demands for the Amman-Zarqa node were considered to be twice the demands of Amman to account for the demand in other cities in the Amman-Zarqa Basin (i.e., Zarqa, Al-Mafraq, and others).

4.2.2.1 System Dynamics

The system dynamics consist of the response of the reservoir and groundwater storages. These can be represented by continuity equations as shown below:

Surface water system:

Al Wehdah Dam (WD):

$$S_{WD}(k+1)= S_{WD}(k)+ w_{Yarmouk}(k) – u_{WD}(k)-e_{WD}(k) \quad (4.1)$$

Adasiya node (AdN):

$$S_{AdN}(k+1) = S_{AdN}(k)+ u_{WD}(k) + w_{Rag}(k) + T_{JOR}(k)- u_{AdN}(k)- D_{AdN}(k) \quad (4.2)$$

Wadi Arab Dam (AD):

$$S_{AD}(k+1)= S_{AD}(k)+ w_{AD}(k)- u_{AD}(k) -e_{AD}(k) \quad (4.3)$$

Wadi Ziglab Dam (ZD):

$$S_{ZD}(k+1)= S_{ZD}(k)+ w_{ZD}(k)- u_{ZD}(k) -e_{ZD}(k) \quad (4.4)$$

NJV node (NJVN):

$$S_{NJVN}(k+1) = S_{NJVN}(k)+ u_{AdN}(k) +u_{AD}(k) + u_{ZD}(k)+ P_{Muk}(k) + w_{NSW}(k)- D_{NJVN}(k) - u_{AZB}(k) - u_{NJVN}(k) \quad (4.5)$$

Amman-Zarqa Basin node (AZBN):

$$S_{AZBN}(k+1) = S_{AZBN}(k)+ P(k) + u_{AZB}(k) - D_{AZBN}(k)+ u_{DAN}(k) \quad (4.6)$$

Disi Aquifer node (DAN):

$$S_{DAN}(k+1) = S_{DAN}(k)+ u_{DAN}(k) \quad (4.7)$$

King Talal Dam (KTD):

$$S_{KTD}(k+1)= S_{KTD}(k)+ w_{Zarqa}(k)- u_{KTD}(k) +C_R(u_{AZB}(k)+ u_{DAN}(k)+ P(k)) -e_{KTD}(k) \quad (4.8)$$

Karameh Dam (KD):

$$S_{KD}(k+1)= S_{KD}(k) + u_{KTD}(k)+ u_{NJV}(k) - u_{KD}(k) -e_{KD}(k) \quad (4.9)$$

Wadi Kafrein Dam (KafD):

$$S_{KafD}(k+1)= S_{KafD}(k)+ w_{KafD}(k)- u_{KafD}(k) -e_{KafD}(k) \quad (4.10)$$

Central and South Jordan Valley node (CSJVN):

$$S_{CSJVN}(k+1) = S_{CSJVN}(k)+ u_{KD}(k) + w_{Shueib}(k) + w_{Hisban}(k) + u_{KafD}(k) - D_{CSJVN}(k) - D_{Env}(k) - u_{CSJVN}(k) \quad (4.11)$$

In the above equations,

$S_X(k)$: storage at the beginning of time step (k) for reservoir or node (X);

$w_X(k)$: inflow from river or side wadi (X) during time step (k);

u_X (k): release from reservoir or node (X) during time step (k);

e_X (k): evaporation from reservoir (X) during time step (k);

D_X (k): demand at node (X) during time step (k);

P(k): pumping from the Amman-Zarqa Basin to Amman-Zarqa node during time k;

C_R : constant to represent the fraction of the return flow to King Talal Dam;

P_{Muk}(k): pumping from Mukheiba wells during time k;

u_{AZB}(k): water transfer from the canal at North Jordan Valley node to Amman-Zarqa node during time k;

T_{JOR}(k): Jordanian peace process quota from the Jordan river;

D_{Env}(k): environmental demand at time step (k).

Groundwater system:

Aquifer drawdown at any monitoring location of interest is due to pumping and boundary condition stresses. All pumping centers in the Amman-Wadi sir aquifer are used for domestic and industrial water supply purposes, and most of them are located in the eastern part of the aquifer as indicated in Chapter 3. For the purposes of the management model, all pumping wells are grouped together and are considered to be one cluster.

As mentioned in Chapter 3, specified head is used as a lateral boundary condition on almost the western parts of the aquifer. Boundary condition grid points are grouped into 3 clusters based on the historical piezometric head patterns along the boundary. The hydraulic head at the boundary grid points of a particular cluster are perturbed

simultaneously. More details regarding the boundary cluster locations and their perturbations are included in section 4.4.

The procedures of Chapter 3 are used to estimate the drawdowns associated with pumping and boundary perturbations at monitoring locations of interest. The monitoring locations are selected to ensure that drawdowns do not exceed certain maximum ranges to avoid overexploitation of groundwater resources.

The groundwater dynamics can be represented as follows (1 pumping cluster, 4 boundary clusters, and 21 monitoring locations):

Base locations: (2 base locations)

$$d_1(k+1)= \alpha_1\, p(k)+ \beta_1\, y(k)+ \gamma_1 d_1\,(k)+\theta_1\, f_1\,(k) \quad (4.12)$$

$$y(k+1)= p(k) \quad (4.13)$$

$$f_1\,(k+1)= d_1\,(k) \quad (4.14)$$

$$d_2\,(k+1)= \alpha_2\, p(k)+ \beta_2\, y(k)+ \gamma_2\, d_2\,(k)+ \theta_2\, f_2\,(k) \quad (4.15)$$

$$f_2\,(k+1)= d_2(k) \quad (4.16)$$

Regional approximation:

$$d_3(k+1)=a_{3,1}p(k)+a_{3,2}\, y(k)+a_{3,3}\, d_1(k)+a_{3,4}\, f_1(k)+ a_{3,5}\, d_2(k) + a_{3,6}\, f_2(k) \quad (4.17)$$

$$d_4(k+1)= a_{4,1}p(k)+a_{4,2}\, y(k)+a_{4,3}\, d_1(k)+a_{4,4}\, f_1(k)+ a_{4,5}\, d_2(k) + a_{4,6}\, f_2(k) \quad (4.18)$$

$$d_5(k+1))= a_{5,1}p(k)+a_{5,2}\, y(k)+a_{5,3}\, d_1(k)+a_{5,4}\, f_1(k)+ a_{5,5}\, d_2(k) + a_{5,6}\, f_2(k) \quad (4.19)$$

.

.

.

$$d_{21}(k+1)= a_{21,1}p(k)+a_{21,2}\, y(k)+a_{21,3}\, d_1(k)+a_{21,4}\, f_1(k)+ a_{21,5}\, d_2(k) + a_{21,6}\, f_2(k) \quad (4.20)$$

In the above equations,

p(k): pumping at time step k;

y(k): pumping at time step k-1;

d_1 (k): drawdown at the beginning of time step k at base location 1;

f_1 (k): drawdown at the beginning of time step k-1 at base location 1;

d_2 (k): drawdown at the beginning of time step k at base location 2;

f_2 (k): drawdown at the beginning of time step k-1 at base location 2;

α_i, β_i, γ_i, θ_i : coefficients for base location i;

$a_{j,1}$, $a_{j,2}$, $a_{j,3}$, $a_{j,4}$, $a_{j,5}$, $a_{j,6}$: constants for monitoring location j.

Assembling all previous relationships, one obtains the surface water and groundwater system dynamics as follows:

$$X(k+1)= A(k)\, X(k) + B(k)\, U(k)+ C(k)\, W(k) \qquad (4.21)$$

Where

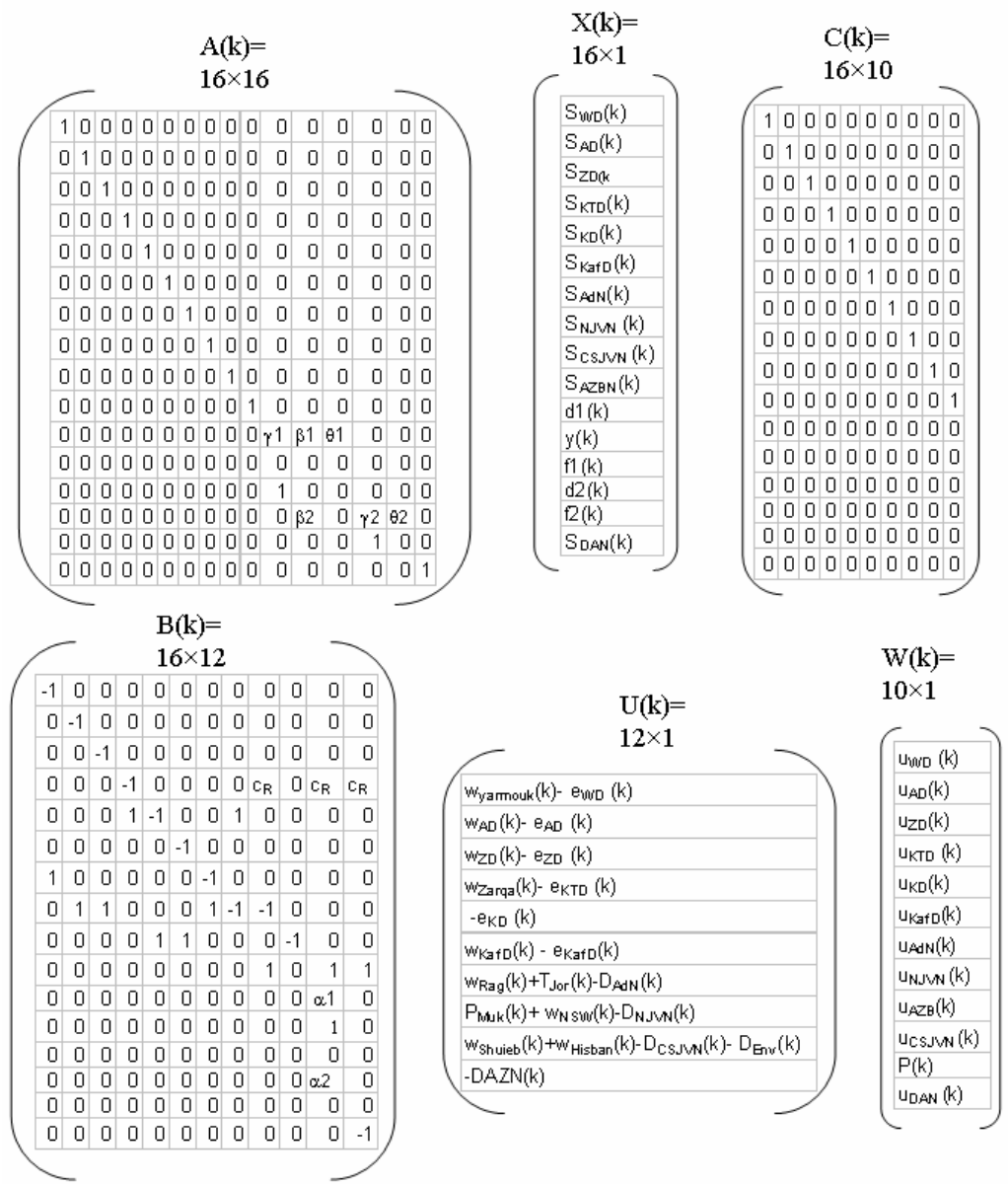

In equation (4.21), vector X(k) represents the system state variables, vector U(k) represents the system control variables, and vector W(k) represents the system inputs, including rivers and side wadi inflows, aquifer boundary conditions, water transfers, and system demands. The matrices A(k), B(k) and C(k) represent the coefficients that of the system dynamical equations. The purpose of the management model is to determine control variable sequences that generate desirable state variable sequences. Desirable

sequences are those sequences that satisfy various operational constraints and optimize the management goals. These elements are discussed next.

4.2.2.2 System Constraints

State variable constraints:

State variable constraints include constraints on reservoirs storages, supply-demand node storages, and monitoring location drawdowns. Each reservoir storage, for example, is required to be between an upper and lower bound. Furthermore, the monitoring location drawdown is required to be less than a certain value for environmental and aquifer remediation purposes. Thus, the state variable constraint set is as follows:

$$S_{KTDmin} \le S_{KTD}(k) \le S_{KTDmax} \quad (4.22)$$

$$S_{WDmin} \le S_{WD}(k) \le S_{WDmax} \quad (4.23)$$

$$S_{ADmin} \le S_{AD}(k) \le S_{ADmax} \quad (4.24)$$

$$S_{ZDmin} \le S_{ZD}(k) \le S_{ZDmax} \quad (4.25)$$

$$S_{KDmin} \le S_{KD}(k) \le S_{KDmax} \quad (4.26)$$

$$S_{KafDmin} \le S_{KafD}(k) \le S_{KafDmax} \quad (4.27)$$

$$-\varepsilon \le S_{AdN}(k) \le \varepsilon \quad (\varepsilon \text{ is a small positive number}) \quad (4.28)$$

$$-\varepsilon \le S_{NJVN}(k) \le \varepsilon \quad (4.29)$$

$$-\varepsilon \le S_{CSJVN}(k) \le \varepsilon \quad (4.30)$$

$$-\varepsilon \le S_{AZBN}(k) \le \varepsilon \quad (4.31)$$

$$d_i(k) \le d_{max}, \ i=1,\ldots,21 \quad (4.32)$$

Control variable constraints:

Control variables are reservoir releases (at all reservoir nodes) and aquifer pumping rates. Control variables are bounded by lower and upper limits associated with hydraulic capacities and minimum operational requirements.

$$0 \le u_{KTD}(k) \le u_{KTDmax} \quad (4.33)$$

$$0 \le u_{WD}(k) \le u_{WDmax} \quad (4.34)$$

$$0 \le u_{AD}(k) \le u_{ADmax} \quad (4.35)$$

$$0 \le u_{ZD}(k) \le u_{ZDmax} \quad (4.36)$$

$$0 \le u_{KD}(k) \le u_{KDmax} \quad (4.37)$$

$$0 \le u_{KafD}(k) \le u_{KafDmax} \quad (4.38)$$

$$0 \le u_{AdN}(k) \le u_{AdNmax} \quad (4.39)$$

$$0 \le u_{NJVN}(k) \le u_{NJVNmax} \quad (4.40)$$

$$0 \le u_{AZB}(k) \le u_{AZBmax} \quad (4.41)$$

$$0 \le u_{CSVN}(k) \le u_{CSVNmax} \quad (4.42)$$

$$0 \le u_{DAN}(k) \le u_{DANmax} \quad (4.43)$$

$$0 \le P(k) \le Pmax \quad (4.44)$$

4.2.2.3 Objective Function (Performance Index)

The objective function, or performance index, is a measure of the system performance relative to its water uses. In this formulation, the objective function includes terms which enforce agricultural, municipal, and industrial requirements, and ensure that state and control variables stay within prescribed limits.

The performance index (J) has the following general form:

$$J_k(s(k)) = \sum_{k=n}^{k=N-1} \sum_{m=1}^{m=L} g_m(s(k),u(k),w(k)) + \sum_{m=1}^{m=L} g_m(s(N)) \text{ , } k=0,1,\ldots N-1 \quad (4.45)$$

where k represents the periods of the control horizon N, and m the terms at each time step k.

More specifically, the performance index used in this work has the following form:

Minimize:

$$J_k(s(k)) = \sum_{k=n,\ldots,N-1} \{g_1(s_{KTD}(k)) + g_2(s_{WD}(k)) + g_3(s_{AD}(k)) +$$

$$g_4(s_{ZD}(k)) + g_5(s_{KD}(k)) + g_6(s_{KafD}(k)) + \sum_i g_{7,i}(d_i(k)), i=1,..,21 + g_8(s_{WD}(k), s_{KTD}(k)) + \sum_i g_{9,i}(d_i(k)), i=1,..,21 + g_{10}(s_{WD}(k)) + g_{11}(s_{KTD}(k)) + g_{12}(s_{AD}(k)) + g_{13}(s_{ZD}(k)) + g_{14}(s_{KD}(k)) + g_{15}(s_{KafD}(k)) + g_{16}(S_{AdN}(k)) + g_{17}(S_{NJVN}(k)) + g_{18}(S_{CSJVN}(k)) + g_{19}(S_{AZBN}(k)) + g_{20}(S_{DAN}(k)) + g_{21}(s_{WD}(k),u_{WD}(k)) + g_{22}(s_{KTD}(k),u_{KTD}(k)) + \sum_i g_{23,i}(P(k),d_i(k)), i=1,..,21 + g_{24}(u_{WD}(k), u_{AD}(k), u_{ZD}(k), u_{KTD}(k), u_{KD}(k), u_{KafD}(k), u_{AdN}(k), u_{NJVN}(k), u_{CSJVN}(k), u_{DN}(k), P(k)) \} \quad (4.46)$$

The meaning of each term in the above expression is as follows:

$g_i(S_X(k))$: a barrier function term to penalize state variable X if it is less than the lower limit or higher than the upper limit, i=1,…,6. Using as an example the storage of the King Talal Dam, $S_{KTD}(k)$, this term has the following mathematical form:

$$g_i(S_{KTD}(k)) = \frac{\varepsilon \left[S_{KTD}(k) - S_{KTD}\,Min\right]^2}{1 + \exp\left(\frac{S_{KTD}(k) - S_{KTD}\,Min}{T}\right)} + \frac{\varepsilon \left[S_{KTD}(k) - S_{KTD}\,Max\right]^2}{1 + \exp\left(\frac{S_{KTD}\,Max - S_{KTD}(k)}{T}\right)} \quad (4.47)$$

where ε and T are coefficients with typical values 100 and 0.1 respectively. The first term in Equation (4.47) becomes significant if storage becomes less than its minimum

bound S_{KTD}^{Min}, while the second term becomes significant if storage exceeds its maximum value S_{KTD}^{Max}.

$g_7(d_i(k))$, i=1,..,21: nonlinear terms that ensure that aquifer drawdowns at the monitoring locations are less than a maximum drawdown. This term has a functional form similar to (4.47). In this case, however, the expression only includes the second term penalizing aquifer drawdown only if it exceeds some upper bound.

$g_8(S_{WD}(k), S_{KTD}(k))$: a quadratic term intended to coordinate the Al Wehdah and King Talal Dams so that their storages increase or decrease uniformly. This term has the following form,

$g_8(s_{WD}(k), s_{KTD}(k)) =$

$$\left[\frac{(S_{WD}(k) - S_{WD}\,Min)}{(S_{WD}\,Max - S_{WD}\,Min)} - \frac{(S_{KTD}(k) - S_{KTD}\,Min)}{(S_{KTD}\,Max - S_{KTD}\,Min)}\right]^2 \qquad (4.48)$$

The above term is minimized when the proportion of the actual storage value relative to its respective range is the same for both reservoirs.

$g_{9,i}(d_i(k))$, i = 1, ..., 21: a quadratic term for the drawdown at monitoring location (i) that penalizes drawdown deviations from a particular drawdown target sequence. This term has the following form:

$$g_{9,i}(d_i(k)) = (d_i(k) - d_{j,Target})^2 \qquad (4.49)$$

where $(d_{j,Target})$ is the target drawdown sequence for monitoring location (j).

$g_i(S_X(k))$, i = 10,…, 15: a quadratic term for the storage at reservoir (X) that penalizes storage deviations from a particular target sequence. This term has the following form:

$$g_i(S_X(k)) = (S_X(k) - S_{X,Target})^2 \qquad (4.50)$$

where $(S_{X,Target})$ is the target sequence for reservoir (X).

$g_i(S_X(k))$, i = 16, …, 20: a quadratic term to penalize the storage of the hypothetical reservoir associated with a supply or demand node X. This term has the following form:

$$g_i(S_X(k)) = (S_X(k))^2 \quad (4.51)$$

It is noted that this term penalizes storage deviations away from zero, so that inputs equal outputs at the node.

$g_{21}(S_{WD}(k),u_{WD}(k))$, $g_{22}(S_{KTD}(k),u_{KTD}(k))$, and $g_{23}(P(k),d(k))$: quadratic terms to meet certain energy generation or consumption targets at Al Wehdah Dam, King Talal Dam, and the Amman-Wadi Sir Aquifer (pumping). The energy term for the King Talal Dam has the following form:

$$g_{21}(S_{KTD}(k),u_{KTD}(k)) = (\text{Energy}_{KTD}(S_{KTD}(k),u_{KTD}(k)) - \text{Energy}_{Target,KTD})^2 \quad (4.52)$$

In the above equation, the energy generation at the King Talal Dam, $\text{Energy}_{KTD}(S_{KTD}(k),u_{KTD}(k))$, is a function of its storage (creating the hydraulic head) and release. The form of this function is based on the storage-stage relation, power-stage relation, and discharge-stage relation. $\text{Energy}_{Target,KTD}$ is the target energy sequence at King Talal Dam. The target sequence could simply be the maximum energy generation or any other energy demand sequence. The Al Wehdah energy function has a similar form.

The energy required for pumping (term $g_{23}(P(k),d(k))$) is a function of the pumping rate and of the lift. The latter is the distance between the ground surface elevation and the piezometric head at the pumping location. Generally, since the goal is to reduce the energy required for pumping, the term $g_{23}(P(k),d(k))$ has the following form:

$$g_{23}(P(k),d(k)) = (C\,P(k)\,(L'+d(k)))^2 \quad (4.53)$$

In the above equation, the constants C and L′ are respectively included to account for energy conversion units and the vertical distance (L′) between the ground surface and the piezometric head at the pumping location when no pumping takes place. P(k) and d(k) are the pumping and drawdown at this location due to pumping. The total lift "L(k)" equals : L(k) = L′+d(k) . For the Amman- Wadi sir Aquifer L′ is approximately 100m.

$g_{24}(u_{WD}(k),u_{AD}(k),u_{ZD}(k),u_{KTD}(k),u_{KD}(k),u_{KafD}(k),u_{AdN}(k),u_{NJVN}(k),u_{CSJVN}(k),u_{DN}(k),P(k))$: a quadratic term for reservoirs releases, node releases, and pumping to meet various release targets. For example, if the Al Wehdah and King Talal releases are to follow a certain target sequence,

$$g_{24}(u_{WD}(k),u_{KTD}(k)) = (u_{WD}(k) - u_{WD,Target}(k))^2 + (u_{KTD}(k) - u_{KTD,Target}(k))^2 \quad (4.54)$$

where $u_{WD,Target}(k)$ and $u_{KTD,Target}(k)$ are the target values for the Al Wehdah and King Talal Dam releases.

Each of the above-described terms is multiplied by a weighing coefficient that establishes its overall objective priority. In the Jordan application, the weights give highest priority to the state and control ranges followed by the water supply requirements at the demand nodes and the energy generation/pumping requirements.

4.3 Solution Approach: The Extended Linear Quadratic Gaussian (ELQG) Control Method

The purpose of the control method is to determine the reservoir release and aquifer pumping sequences $\{u_j(k), j=1,\ldots,m, k=0,1,\ldots, N\}$ that minimize the **performance index**:

$$J=E\left[\ \sum_k\ \{g_1(s(k),u(k),k)+ g_2(s(k),u(k),k)+ \ldots.+g_L(s(k),u(k),k)\ ,\ k=0,1,\ldots,\ N-1\ \}\right.$$

$$\left.+\ g_1(s(N),N)+ g_2(s(N),N)+ g_3(s(N),N)+ \ldots.+g_L(s(N))\ \right] \qquad (4.55)$$

Subject to the,

state dynamics:

$$\mathbf{X}(k+1)=A(k)\mathbf{X}(k)+ B(k)\mathbf{U}(k)+ \Gamma(k)\mathbf{W}(k)+ \Delta(k)\mathbf{d}(k) \qquad (4.56)$$

and control and state variable constraints:

$$u_j(k)^{min} \le\ u_j(k) \le u_j(k)^{max}\ ,\ j=1,\ldots.,m\ ,\ k=0,1,2\ldots,N \qquad (4.57)$$

$$s_i(k)^{min} \le\ s_i(k) \le s_i(k)^{max}\ ,\ i=1,\ldots.,n\ ,\ k=0,1,2\ldots,N \qquad (4.58)$$

Since this is an uncertain system, (4.58) implies the following reliability constraints:

$$\text{Prob}\ [S_i(k) \le\ S_i(k)^{min}\ ] \le \gamma_i(k)^{min},\ i=1,\ldots.,n\ ,\ k=0,1,2\ldots,N \qquad (4.58a)$$

$$\text{Prob}\ [S_i(k) \ge\ S_i(k)^{max}\ ] \le \gamma_i(k)^{max},\ i=1,\ldots.,n\ ,\ k=0,1,2\ldots,N \qquad (4.58b)$$

where $\gamma_i(k)^{min}$ and $\gamma_i(k)^{max}$ represent reliability thresholds reflective of the managers' risk taking or aversion attitude. The rest of the symbols represent the quantities defined in the previous section.

4.3.1 ELQG Control Method:

ELQG (Extended Linear Gaussian Quadratic control) is a trajectory iteration algorithm for optimization of stochastic dynamical systems (Georgakakos, 1987, 89, 1998, Yao and Georgakakos, 2001.) The solution process begins from a nominal control sequence and the corresponding probabilistic state sequence. Next, the control sequence is updated using a local quadratic approximation of the performance index and analytically derived optimization directions. Control constraints are accounted for using a projected Newton approach and state constraints are handled through barrier functions.

ELQG quantifies the uncertainty of the state variables by generating an ensemble of possible traces. A step-by-step description of the ELQG algorithm is included in appendix B.

4.3.2 Overview of the Conjunctive Management Procedure

Combining the developments of the last two chapters, the conjunctive management approach can be summarized as follows:

1. Generate multiple sets of groundwater parameters to characterize the uncertainty of the groundwater aquifer. Furthermore, generate multiple inflow realizations and realizations of the possible aquifer boundary conditions. Define the nominal release and pumping sequences.

2. Find the aquifer base locations, and develop the state dynamical equation at each base location to estimate the mean drawdown using

$$E(d_{Bas(i)}(k+1)) = \alpha_{Bas(i)}P(k) + \beta_{Bas(i)}P(k-1) + \gamma_{Bas(i)}E(d_{Bas(i)}(k)) + \theta_{Bas(i)}E(d_{B(i)}(k-1)) \quad (4.59)$$

where index (i) refers to the base location number.

At the remaining monitoring locations, use the regional drawdown approximation to estimate the mean drawdown:

$$d_{m1}(k+1)=a_{m1,1}\,p(k)+ a_{m1,2}\,p(k-1)+ a_{m1,3}\,d_1(k)+ a_{m1,4}\,d_1\,(k-1)+ a_{m1,5}\,d_2(k)+ a_{m1,6}\,d_2(k-1)+ \ldots..+ a_{m1,(2n+1)}\,d_n(k)+ a_{m1,(2n+2)}\,d_n(k-1) \quad (4.60)$$

where subscript (m1) refers to the monitoring location number. All variables and constants in equations 4.59 and 4.60 are defined in Chapter 3.

3. Compute the mean reservoir storage sequences using the following dynamical equation:

$$E(S_{(j)}(k+1)) = E(S_{(j)}(k)) + u(k) + E(w_{(j)}(k)) - e_{(j)}(k) \quad (4.61)$$

Where the index (j) refers to the reservoir number, $E(S_{(j)}(k))$ is the expected value of the storage at the beginning of time step k, u(k) is the release during the current time step, $E(w_{(j)}(k))$ is the expected inflow for reservoir (j), and e(k) is the monthly mean evaporation from reservoir (j).

4. Use the resulting transfer function realizations, boundary perturbations realizations, and inflow realizations to construct the corresponding realizations of groundwater drawdowns at the monitoring locations and storage realizations at the reservoirs.

5. For each ensemble realization, determine the distance of the percentiles associated with the reliability thresholds from the mean. Denote this distance $G_m(k+1)$, k=0,..,N-1, where (N) refers to the control horizon, and subscript m refers to the reservoir or drawdown location.

6. Use G_m (k+1), k=0,.., N-1, and equations (4.59-4.61) in the ELQG control algorithm to obtain updated reservoir release and pumping sequences.

7. Repeat the above steps until convergence. Namely, repeat this process until the resulting control, state variables, and percentile distances from one iteration to the next are negligibly small.

4.4 Application to Jordan

The above optimization procedure is applied to the Jordanian water resources system (Figure (4.2.2.1). The management purpose is to meet as much of the water demands as possible subject to the physical system constraints and other operational

requirements. In the applications that follow, the control model is implemented with a monthly time resolution and a horizon of one year.

4.4.1 Control Model Inputs and Outputs

The inputs of the control model include:

1. Monthly water demands in the Amman-Zarqa Basin, North Jordan Valley, and Central and South Jordan Valley.
2. Monthly flows at Yarmouk and Zarqa rivers, and side wadis.
3. Reservoirs characteristics; minimum storages, maximum storages, stage-volume and stage-area relations, and evaporation rates.
4. Peace process Jordanian quota from Lake Tiberias; Monthly pumping from Mukheiba wells.
5. Peace process Israeli quota and Syrian irrigation withdrawals from the Al-Wehdah Dam.
6. Groundwater transfer functions realizations, at the monitoring locations, due to pumping and boundary conditions.
7. Boundary perturbations at the boundary clusters.

The outputs of the control model include:

1. Monthly reservoir releases and storages.
2. Monthly aquifer pumping and drawdown sequences at the monitoring locations.
3. Monthly water deficits and releases from the supply-demand nodes, namely, Adasiya, North Jordan Valley node, Amman-Zarqa node, and Central and South Jordan Valley node.

4. Energy generation at the Al-Wehdah and King Talal Dams; energy required for aquifer pumping.

4.4.2 Inflow and Boundary Condition Realizations

A historical analog model (Yao and Georgakakos, 2001) is used to produce realizations of stream flows for the surface water system. The underlying premise of this model is that streamflows materialize as a result of a nonlinear hydro-climatic process orbiting around an unknown attractor set. Although this set is not easily definable, this premise leads to the following conjecture: If the process is presently at a certain point in its orbit, its position in the near future can potentially be inferred by observing the movement it experienced on similar occasions in the past. More specifically, streamflows are the result of the rainfall-runoff process, and the values they assume over a certain time period depend on various hydro-climatic factors including watershed rainfall, temperature, and soil moisture conditions. Thus, if the climate-watershed system tends to revisit the neighborhood of certain conditions (states), it should also tend to generate similar streamflow patterns. A detailed explanation of this forecast method is shown is appendix C.

The historical analog model was herein used to generate forecasts consisting of 15 streamflow realizations for the upcoming 12 months. Figures (4.4.2.1a) and (4.4.2.1b) show the forecast realizations for the Yarmouk and Zarqa Rivers, the main rivers in Jordan. For the side wadis, complete records are not available, and the monthly average values are used instead.

For the groundwater system, the historical analog model is used to produce realizations of boundary head perturbations. As mentioned in Chapter 3, specified head is

Figure 4.4.2.1a: the Yarmouk river stream flow forecast realizations

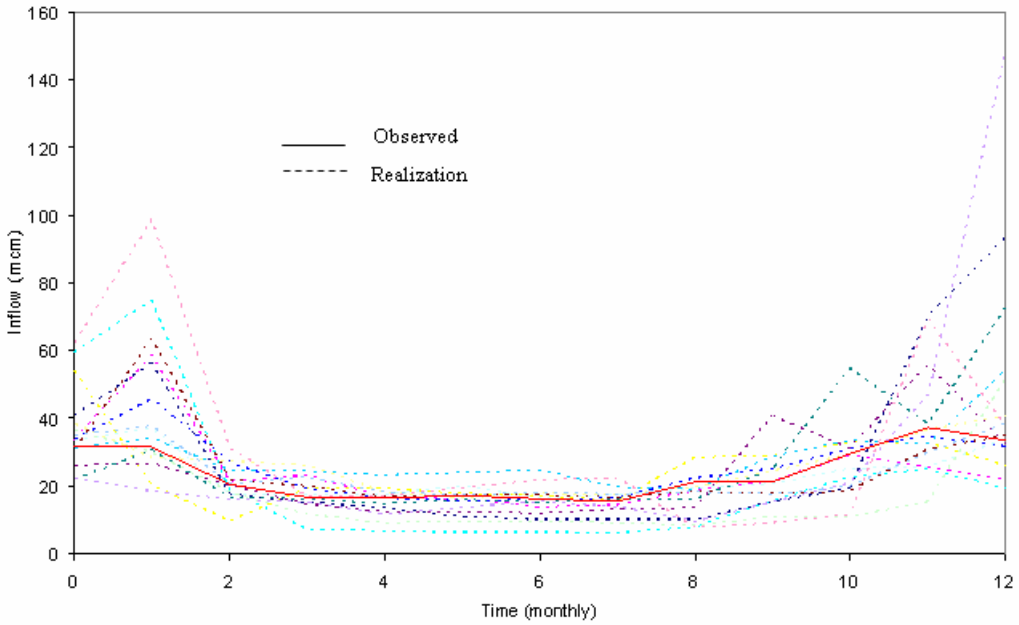

Figure 4.4.2.1b: the Zarqa river stream flow forecast realizations

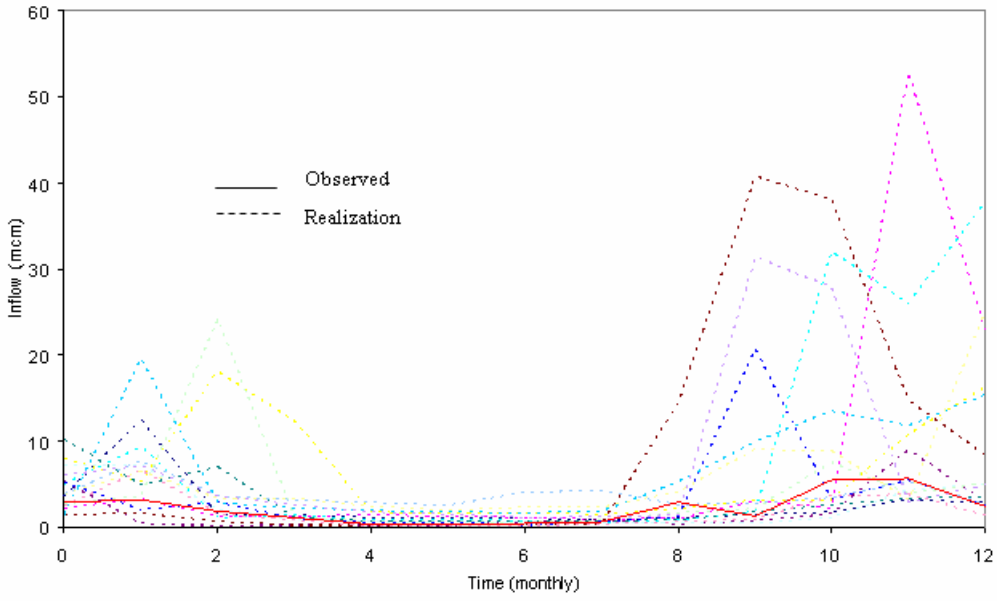

Figure 4.4.2.1(a,b) : Stream flow realizations

used as a lateral boundary condition mostly at the western parts of the aquifer (figure 3.2.1.2). Boundary grid points with similar specified head boundary condition are grouped together into one cluster. The specified head boundary grid points were grouped into three clusters. The reason for this grouping is to simplify the computations in the control model later on. Figure (4.4.2.2a) shows the locations of the three boundary clusters and the locations of the monitoring wells. For each boundary cluster, the average piezometric head is computed over all grid points within the cluster. Uncertainty in the boundary head is expressed in terms of head perturbation around the average seasonal mean head. To characterize the uncertainty of the boundary piezometric heads for each cluster, , boundary perturbations are generated by subtracting the piezometric head value from the average seasonal piezometric head for the cluster.. Figure (4.4.2.2b) shows the boundary perturbations for clusters 1 through 3. . Finally, similarly to the streamflow forecasts, the historical analog model is used to produce realizations of boundary perturbations. The forecasts are also issued for the next 12 months and consist of 10 boundary head sequences for each cluster. The forecasts are shown on Figures (4.4.2.3a) to (4.4.2.3c).

Transfer functions realizations are produced using the statistical procedure developed in Chapter 3. At the 21 monitoring locations of interest, 10 transfer functions are produced for each pumping or boundary cluster. As mentioned earlier, there are four boundary clusters and one pumping center. (All pumping wells are located relatively close to each other in the eastern part of the basin.)

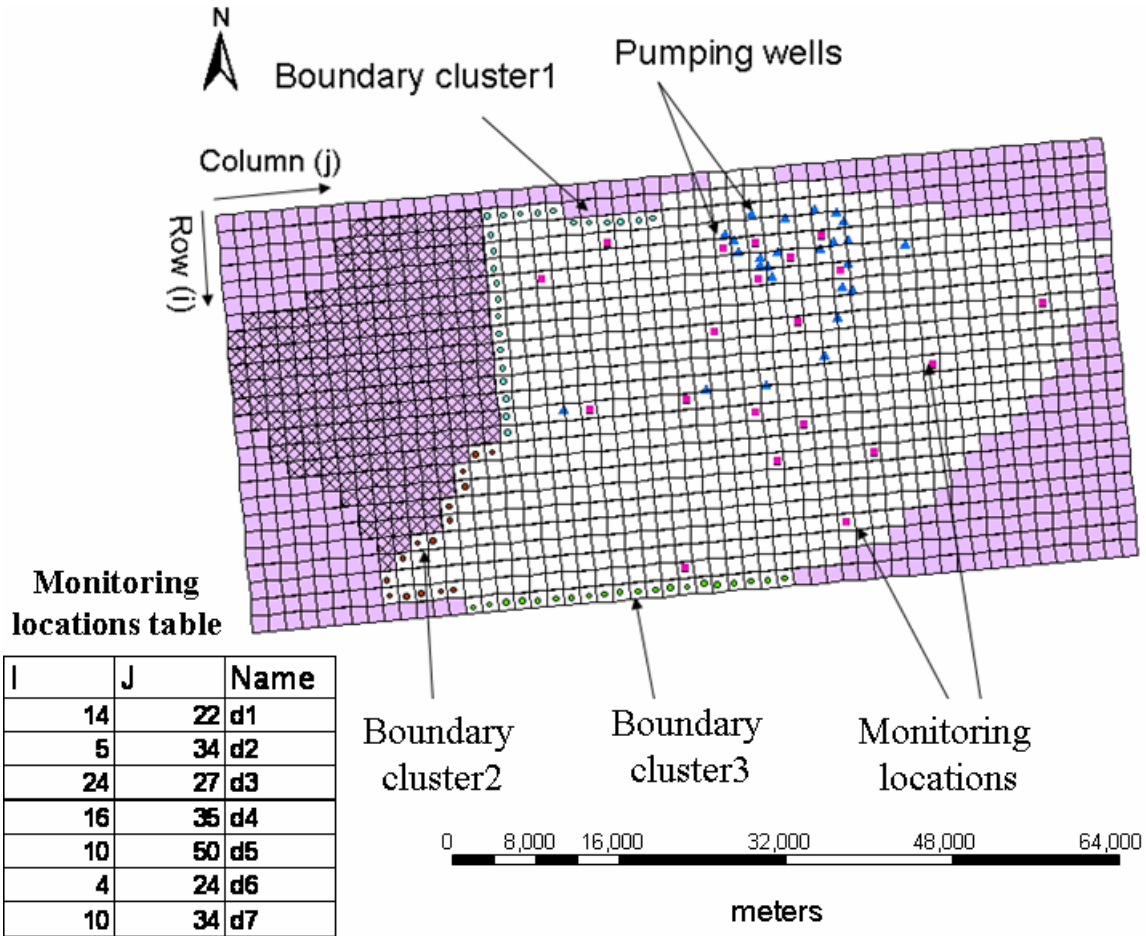

Monitoring locations table

I	J	Name
14	22	d1
5	34	d2
24	27	d3
16	35	d4
10	50	d5
4	24	d6
10	34	d7
18	39	d8
22	37	d9
6	20	d10
5	33	d11
9	35	d12
5	31	d13
3	30	d14
15	32	d15
14	28	d16
6	35	d17
5	37	d18
7	38	d19
13	43	d20
7	33	d21

Figure 4.4.2.2a : Boundary clusters and monitoring locations

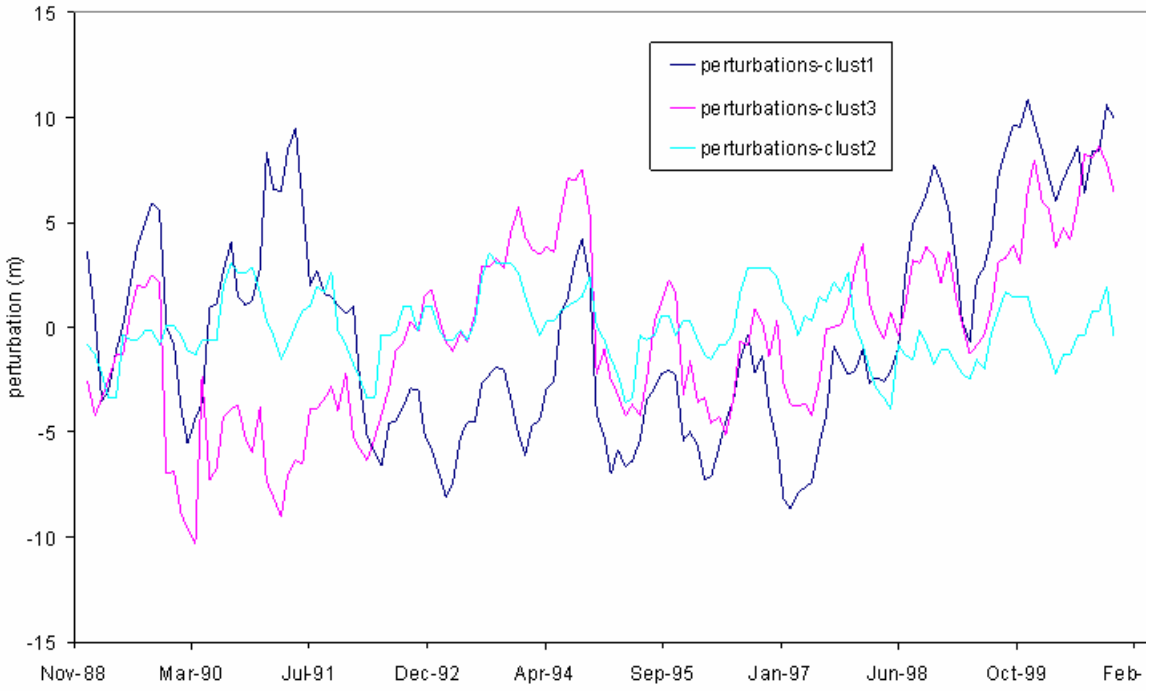

Figure 4.4.2.2b : Boundary perturbations

Figure 4.4.2.3a: boundary cluster 1, forecast realizations

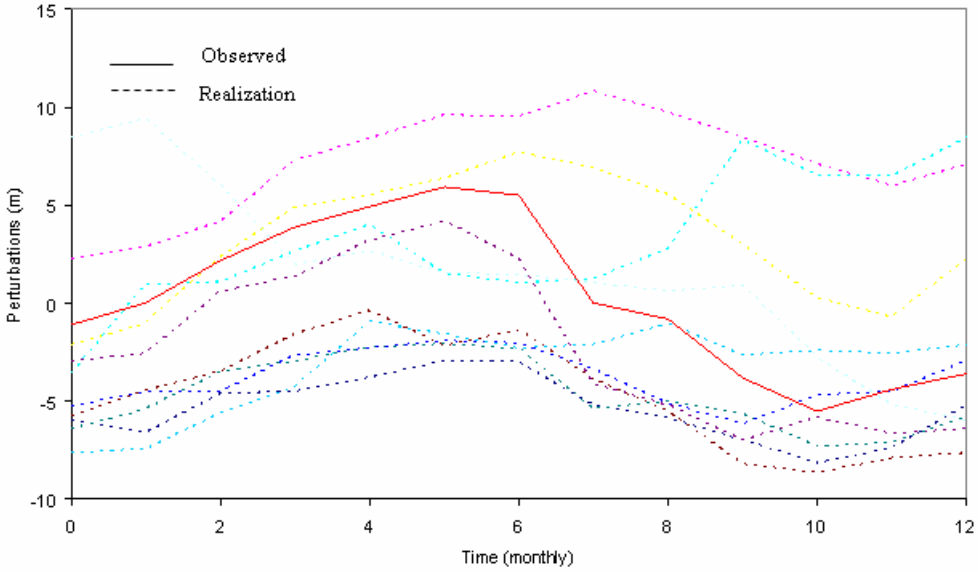

Figure 4.4.2.3b: boundary cluster 2, forecast realizations

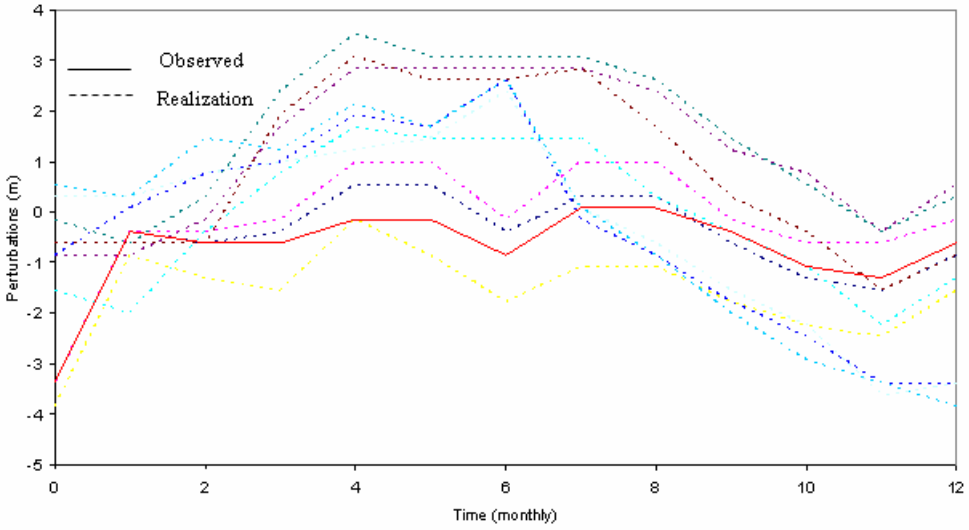

Figures 4.4.2.3(a-c): Boundary perturbations realizations

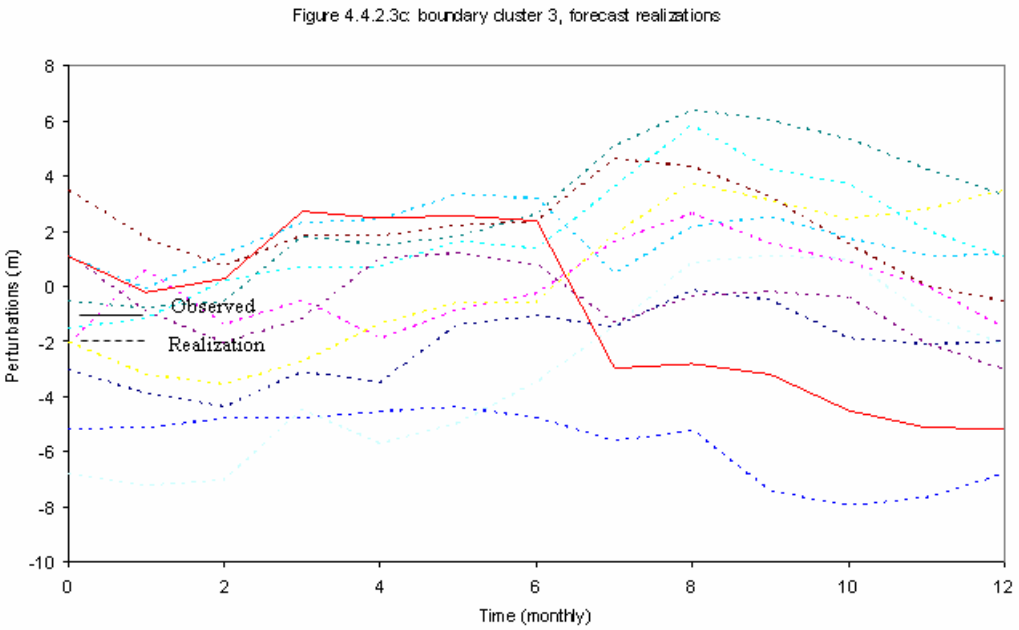

Figures 4.4.2.3(a-c): Boundary perturbations realizations

4.4.3 Case Study

In this case study, the system configuration is assumed to include all existing dams and diversions as well as the Al Wehdah Dam and the Disi water transfer. The management purpose is to determine the release and pumping sequences that over the forthcoming 12 months minimize the water supply deficits while meeting all prescribed physical capacity limits and operational requirements.

Figures (4.4.3.1a), (4.4.3.1b), (4.4.3.1c), (4.4.3.1d), (4.4.3.1e), and (4.4.3.1f) show the resulting mean storage and release sequences for all reservoirs. The red lines in these figures demarcate the minimum and maximum bounds for each variable. The upper and lower percentiles for the state reliability constraints were equal to 90% and 10% respectively.

Figures (4.4.3.2a), (4.4.3.2b), (4.4.3.2c), and (4.4.3.2d) show the storage realizations for Al Wehdah and King Talal Dams. For Al Wehdah, figure (4.4.3.2a) shows the storage realizations corresponding to the initial release sequence. The figure shows that the storage reliability constraint (90%) is not binding. By contrast, Figure (4.4.3.2b) shows the final storage sequence, after convergence of the algorithm, where this constraint is binding and only two storage traces exceed the upper bound.

The same can be noted for the King Talal Dam (figures (4.4.3.2c) and (4.4.3.2d)). In this case, however, the initial storage realizations (4.4.3.2c) exceed the upper bound more than 90%. At the optimal sequences, however (figure (4.4.3.2d)), all storage realizations meet the reliability constraint.

The previous comments indicate the principles that ELQG follows to solve the management problem. The method translates the input forecasts into state variable

Figure 4.4.3.1a: Al-Wehdah dam storage and realease sequences

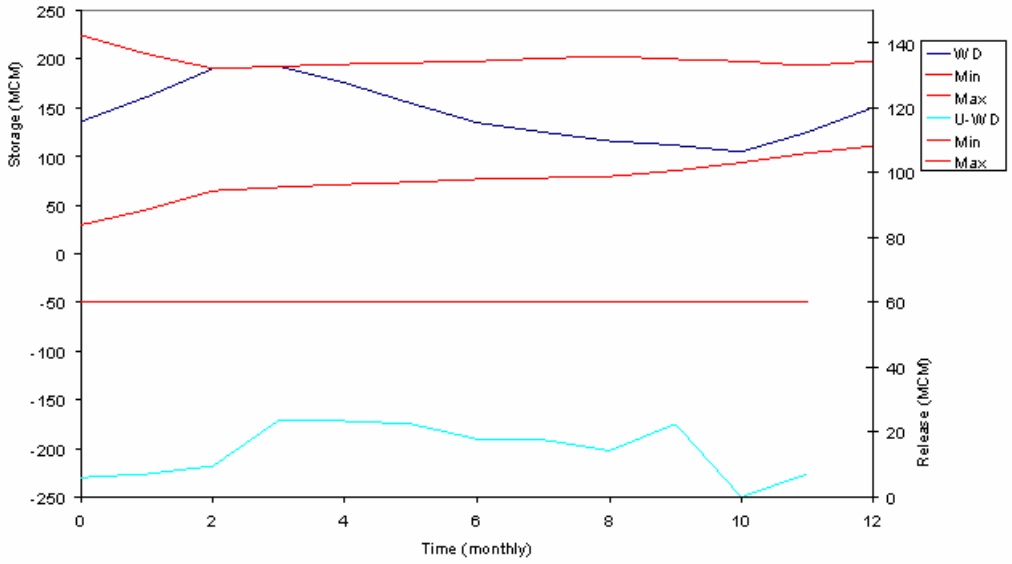

Figure 4.4.3.1b: King Talal dam storage and realease sequences

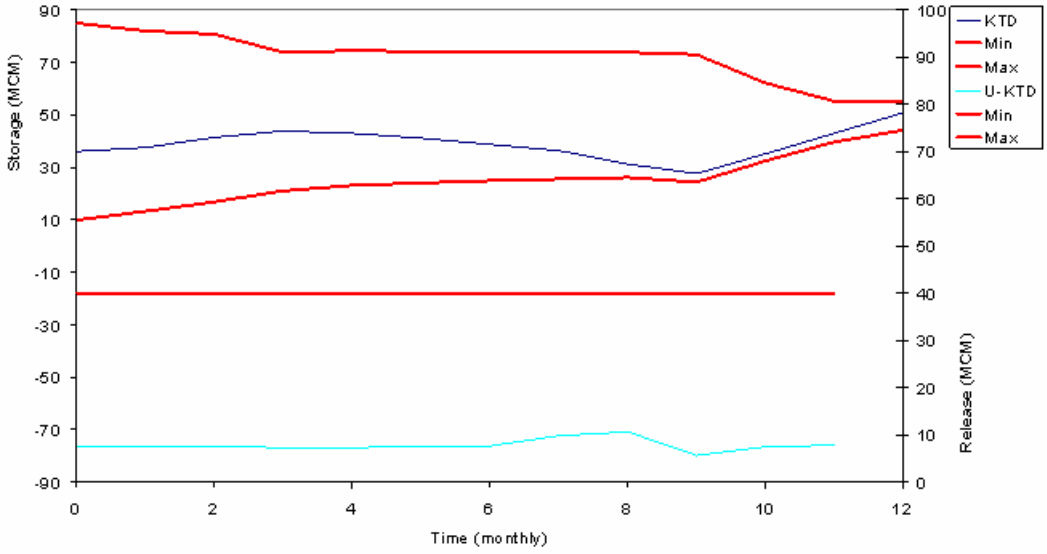

Figures 4.4.3.1(a-f): Mean storages and releases sequences

Figure 4.4.3.1c: Karameh dam storage and realease sequences

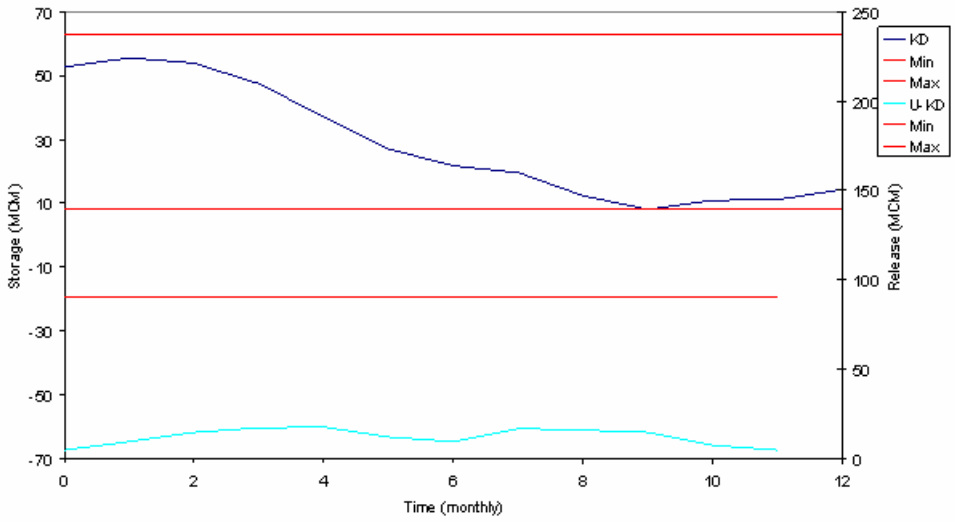

Figure 4.4.3.1d: Arab dam storage and realease sequences

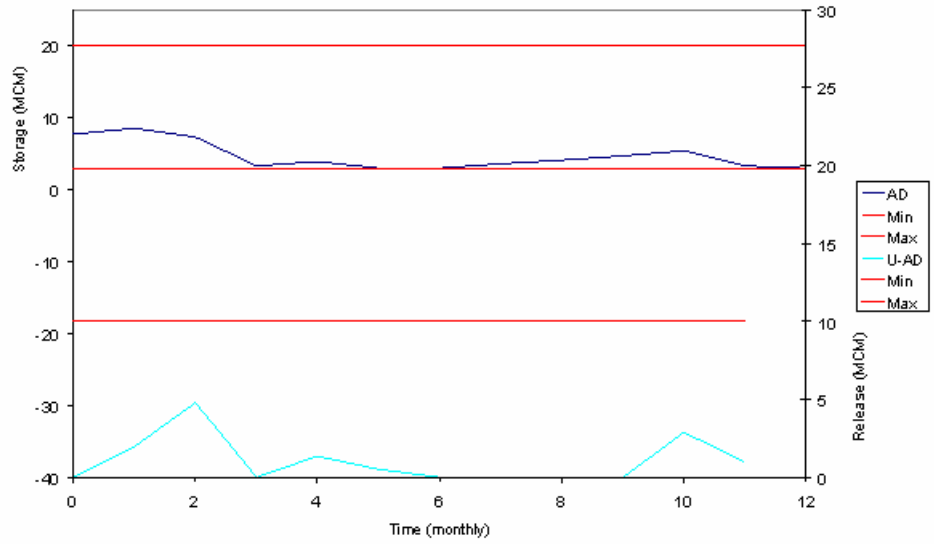

Figures 4.4.3.1(a-f): Mean storages and releases sequences

Figure 4.4.3.1e: Ziglab dam storage and realeases equences

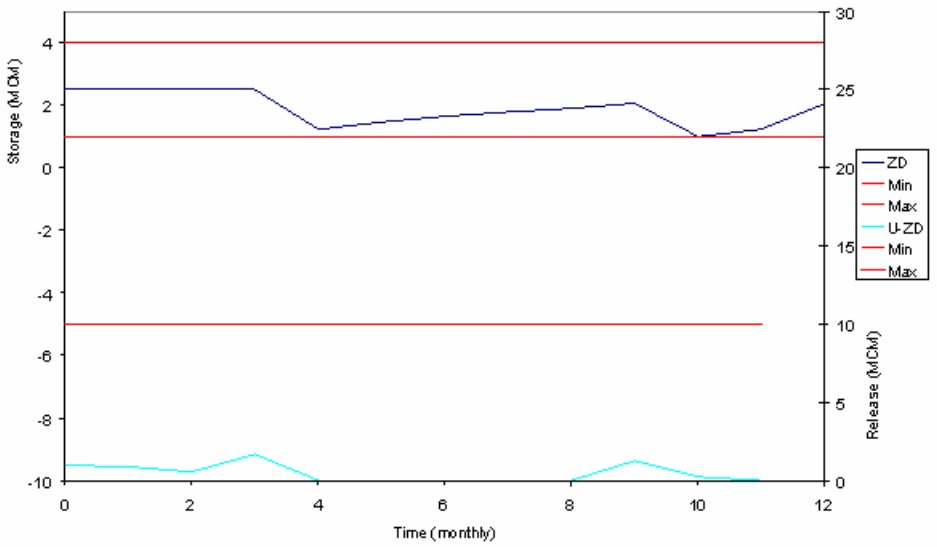

Figure 4.4.3.1f: Kafrein dam storage and realeases equences

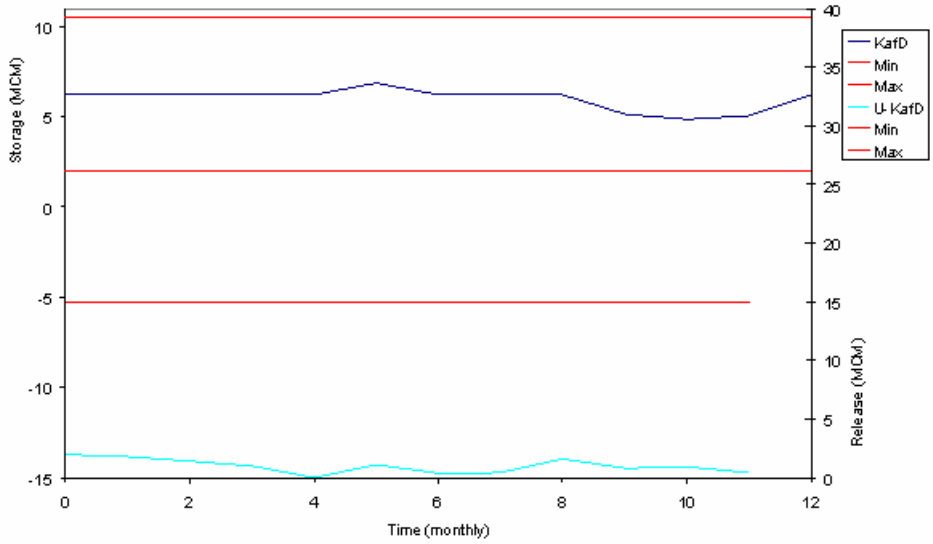

Figures 4.4.3.1(a-f): Mean storages and releases sequences

Figure 4.4.3.2a: Al Wehdah dam initial storage realizations

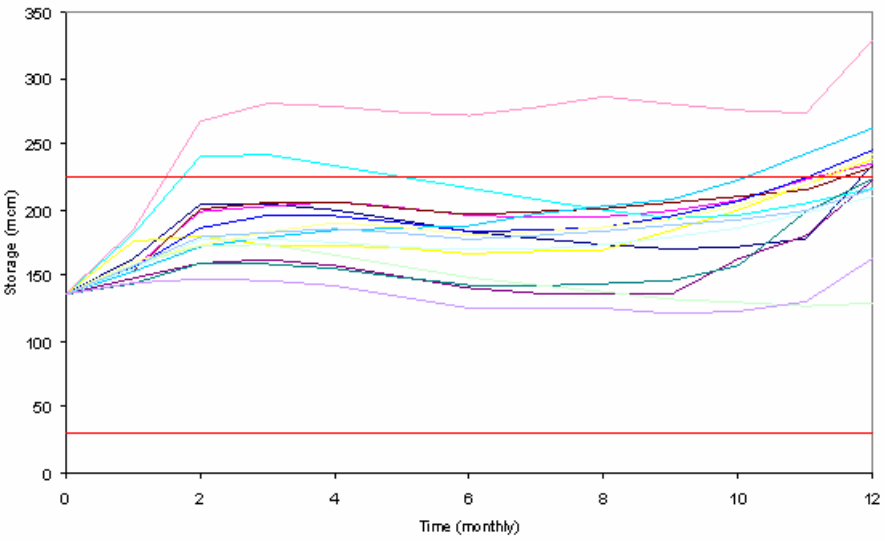

Figure 4.4.3.2b: Al Wehdah dam final storage realizations

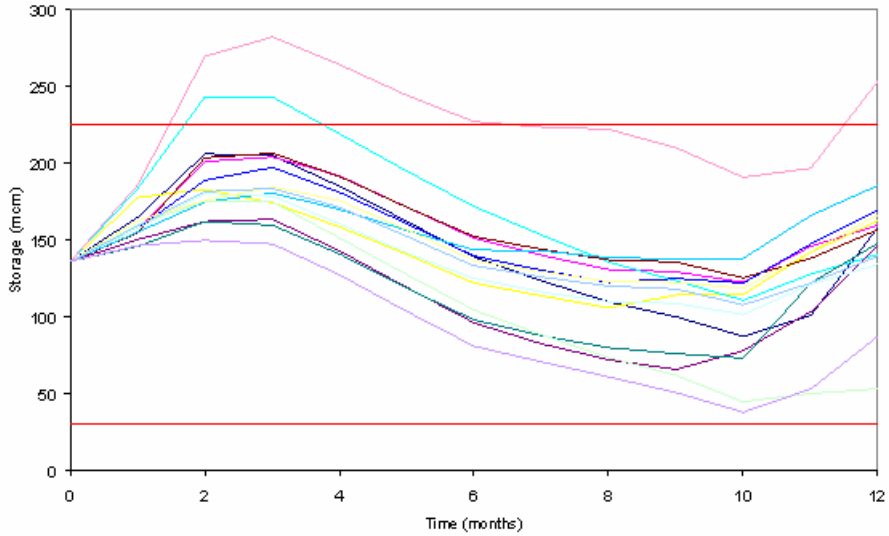

Figures 4.4.3.2(a-d): WD and KTD storage realizations

Figure 4.4.3.2c: King Talal dam initial storage realizations

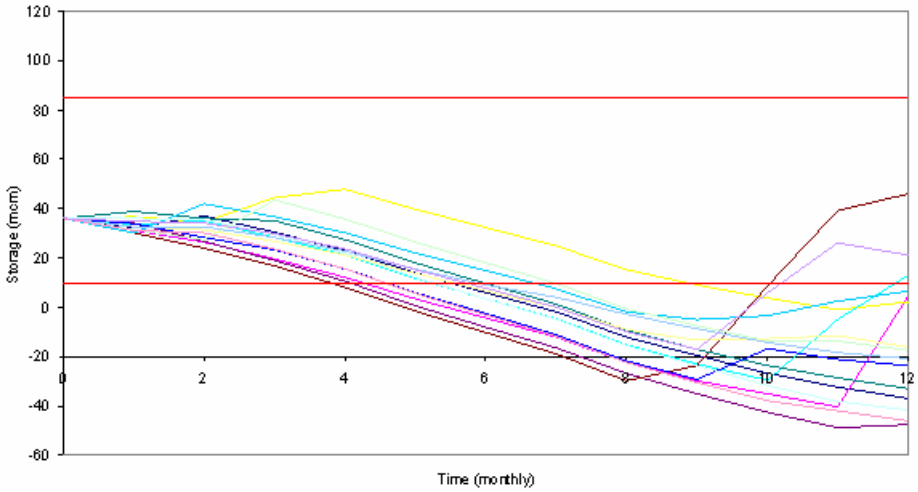

Figure 4.4.3.2d: King Talal dam final storage realizations

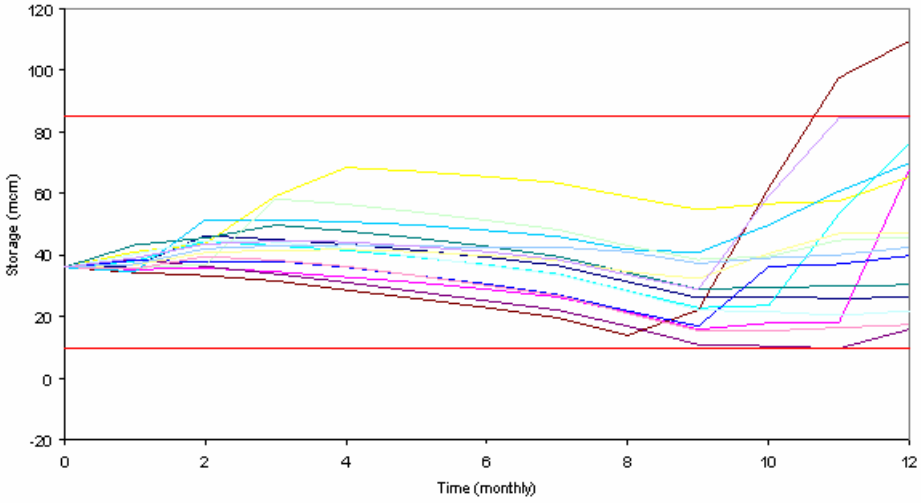

Figures 4.4.3.2(a-d): WD and KTD storage realizations

forecasts and proceeds to identify increasingly better sequences that meet the stated constraints while optimizing the performance index.

Figures (4.4.3.3a), (4.4.3.3b), (4.4.3.3c), (4.4.3.3d) show the cumulative water deficits (demand minus supply) at Adasiya, North Jordan Valley, Amman-Zarqa, and Central and South Jordan Valley nodes. For all system nodes, water demands are met in full. The figures also show the releases from each node to the downstream system with some reaching their maximum capacity limits (red lines). The release of the Central and South Jordan Valley node to the Dead Sea is nearly zero for all months. This is because in this control run, the minimum residual flow to the Dead Sea was set to zero. In an actual application, however, this minimum flow constraint can be increased to explore the capacity of the system to meet all water uses including environmental protection of the Dead Sea. This would be the appropriate operational mode of the decision system developed herein: to first assess the applicable water use tradeoffs and then determine the most appropriate management policy.

Figures (4.4.3.4a), (4.4.3.4b), (4.4.3.4c), (4.4.3.4d), and (4.4.3.4e) show the mean groundwater drawdown at selected groundwater monitoring locations. The maximum drawdown limit at any monitoring location is taken to be 10 m; the lower limit being zero. As seen from figure (4.4.3.4a), the mean drawdown at any time step does not reach the maximum limit of 10 m. This is because the model ensures that 90% of the drawdown ensemble is below the maximum limit. Figure (4.4.3.4b), (4.4.3.4c), (4.4.3.4d) and (4.4.3.4d) show the mean drawdown at selected wells together with the feasible region for it based on the 90% reliability constraint. As can be seen, the mean drawdown stays within the feasible range. Figure (4.4.3.4e) shows that a certain location experiences a

Figure 4.4.3.3a: cumulative deficits and release at Adasiya node

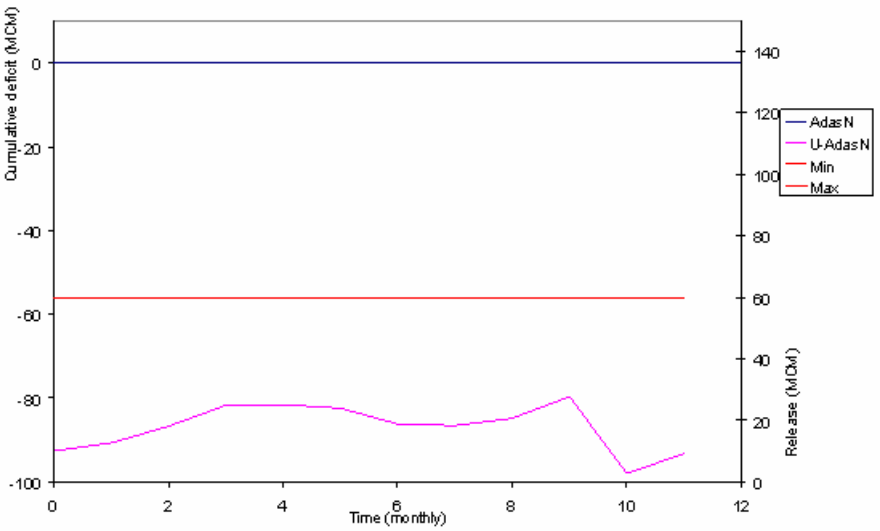

Figure 4.4.3.3b: Cumulative deficits and release at North Jordan Valley node

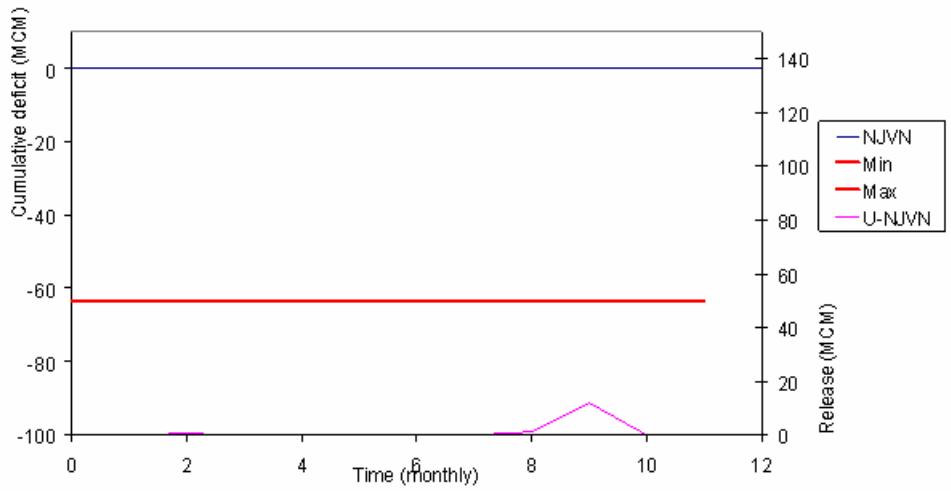

Figures 4.4.3.3(a-d): Cumulative deficits and releases at supply-demand nodes

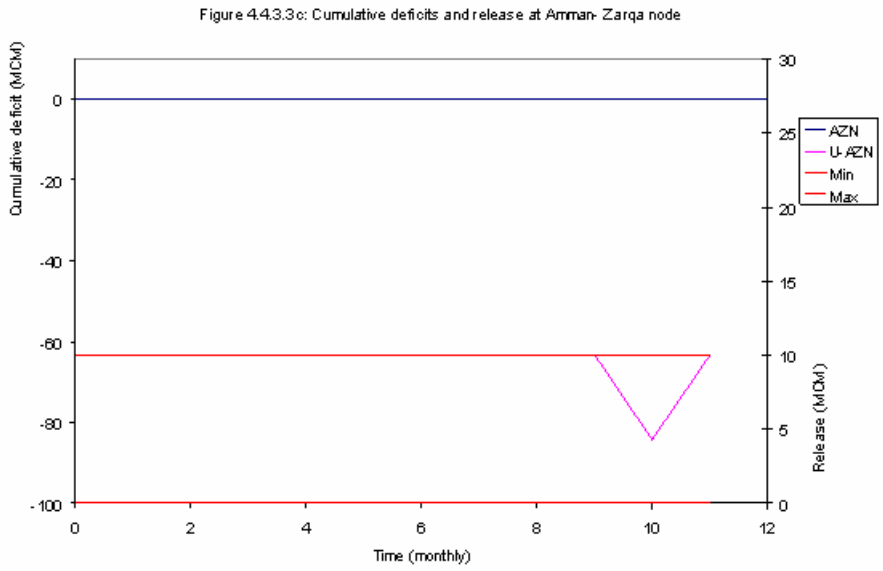

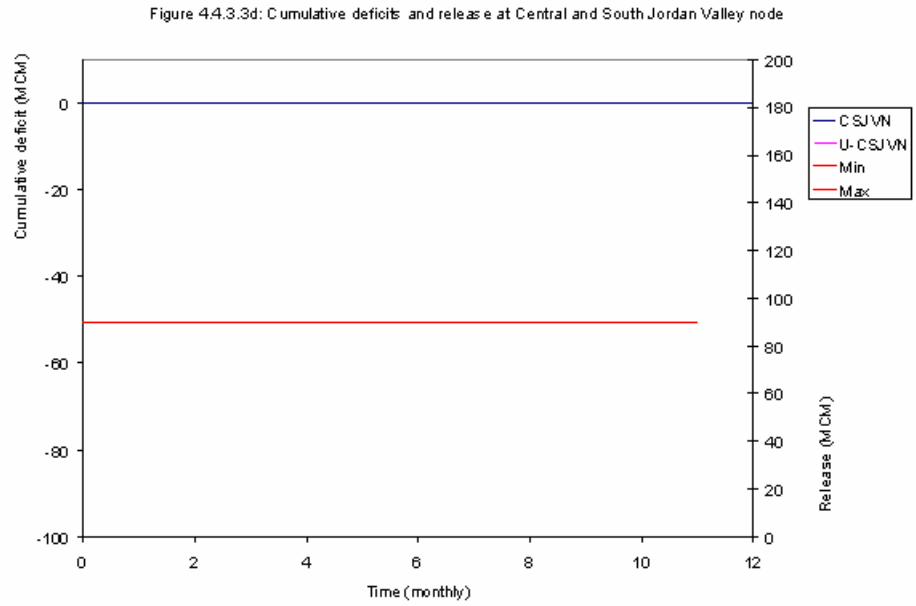

Figures 4.4.3.3(a-d): Cumulative deficits and releases at supply-demand nodes

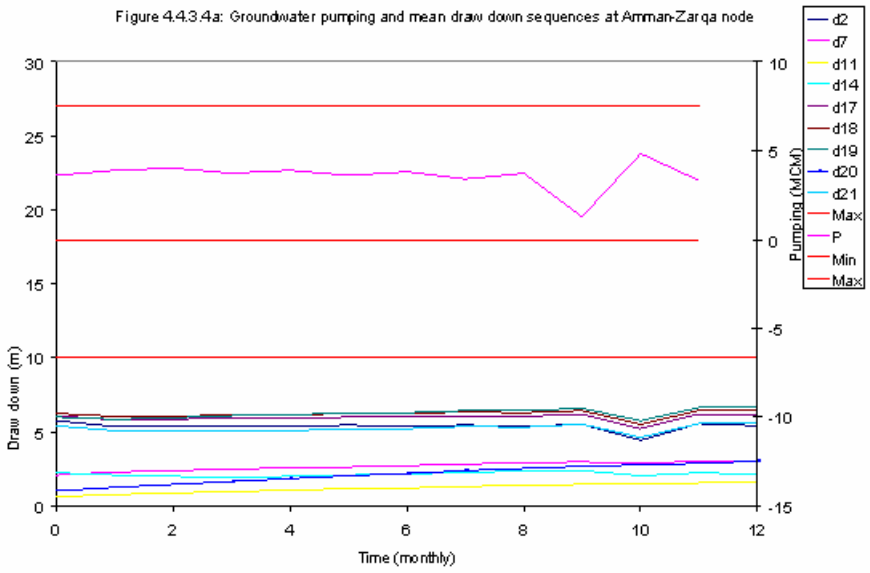

Figure 4.4.3.4b: groundwater mean drawdown at monitoring location d19

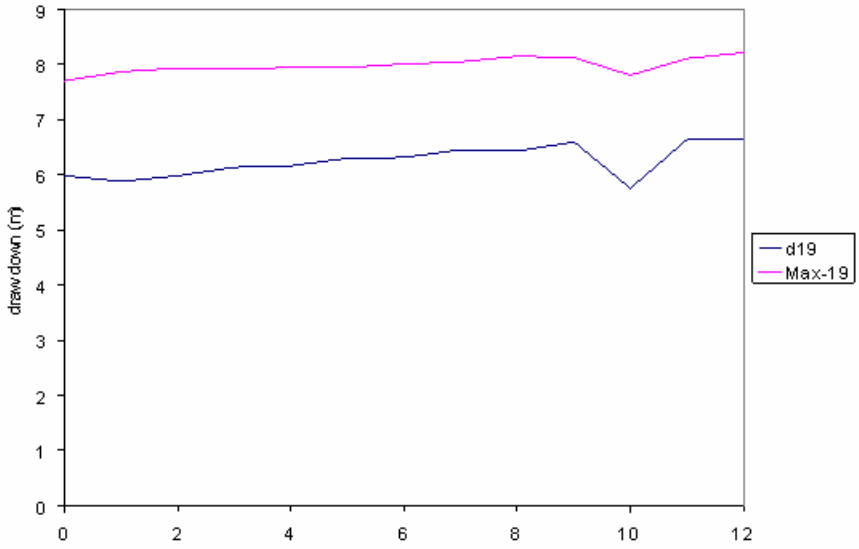

Figures 4.4.3.4(a-e): Mean GW drawdown and pumping sequences

Figure 5.4.1.4c: groundwater mean drawdown at monitoring location d18

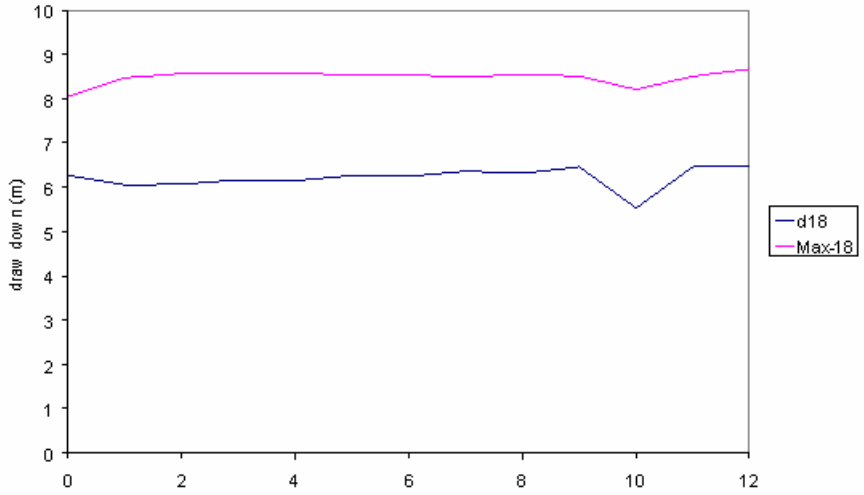

Figure 4.4.3.4d: groundwater mean draw down at monitoring location d17

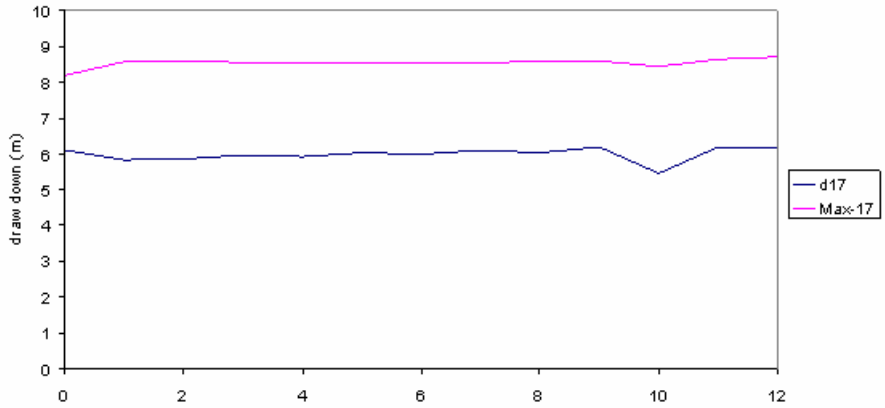

Figures 4.4.3.4(a-e): Mean GW drawdown and pumping sequences

Figure 4.4.3.4e: groundwater mean drawdown at monitoring location d6

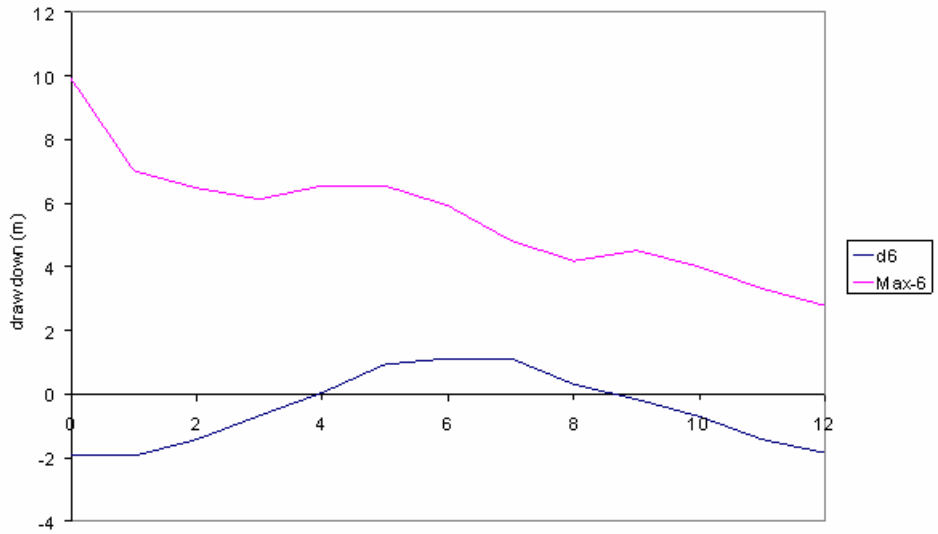

Figures 4.4.3.4(a-e): Mean GW drawdown and pumping sequences

negative drawdown. This implies an increase in the mean piezometric head due to an unusually high boundary condition.

Figures (4.4.3.5a), (4.4.3.5b), (4.4.3.5c), (4.4.3.5d), (4.4.3.5e), (4.4.3.5f), (4.4.3.5g), and (4.4.3.5h) show drawdown realizations at 4 different monitoring locations. Figures (4.4.3.5a) and (4.4.3.5b) show the initial and final drawdown realizations at monitoring location d11 respectively. The first of these figures show that the 90^{th} percentile reliability constraint is clearly violated. However the final drawdown realizations meet this constraint. Similar observations can be made for the remaining figures.

Figure (4.4.3.6) shows the final pumping sequence from the Disi Aquifer to the Amman-Zarqa node. Water from the Disi Aquifer is only used when the demands of Amman- Zarqa node are not met by the surface or by the ground water system.

Finally, figures (4.4.3.7a), (4.4.3.7b), and (4.4.3.7c) show the energy generation realizations from the AL-Wehdah and King Talal Dams and the energy consumption for groundwater pumping. Each realization corresponds to a different realization of the associated state variable. In the objective function, the energy term is not given a large weight as compared to the water deficits and state constraint terms. Thus, in this run, water management takes precedence and energy generation follows. It is, of course, possible to change the objective function weights and investigate the water-energy tradeoff. Pumping energy sequences do not display much variability because the lift is dominated by the distance of the ground surface to the piezometric head. This distance is 100 meters while the maximum drawdown is 10 meters.

Figure 4.4.3.5a: draw down initial realizations, d19

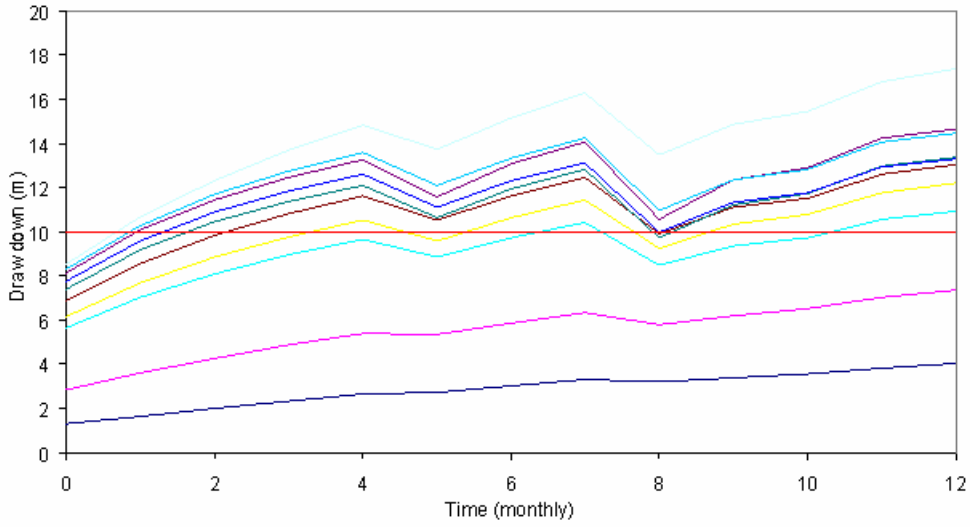

Figure 4.4.3.5b: Draw down final realizations, d19

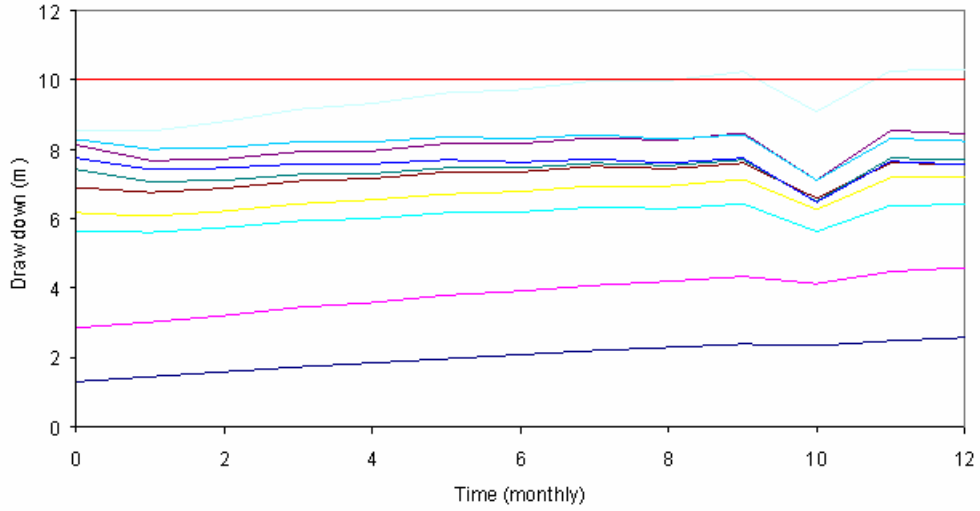

Figures 4.4.3.5(a-h): GW drawdown realizations at selected monitoring locations

Figure 4.4.3.5c: draw down initial realizations, d18

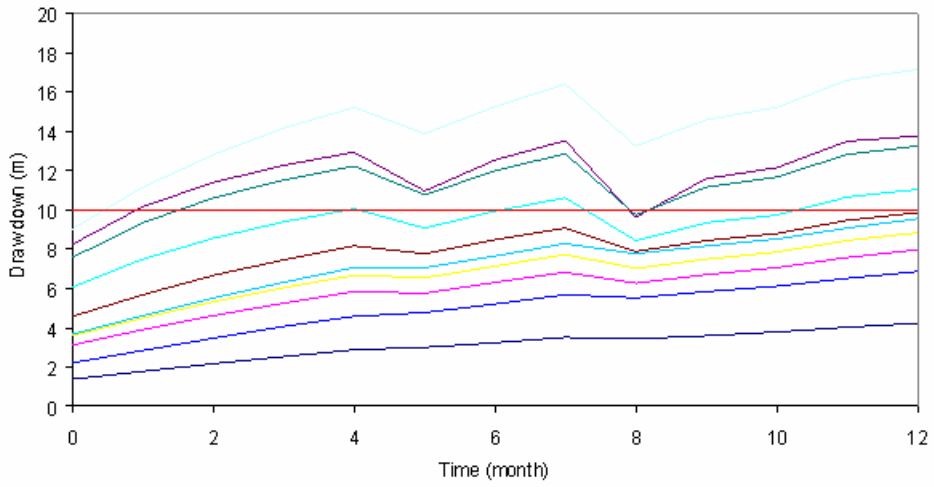

Figure 4.4.3.5d: Draw down final realizations, d18

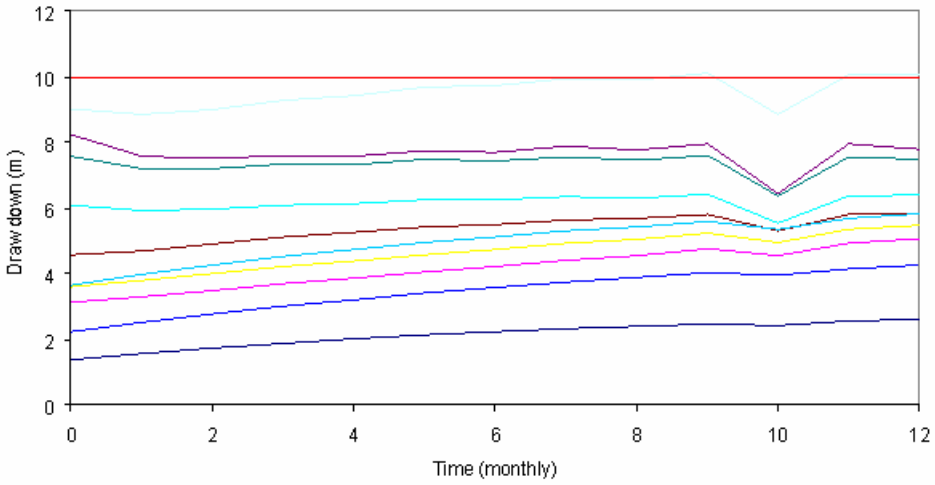

Figures 4.4.3.5(a-h): GW drawdown realizations at selected monitoring locations

Figure 4.4.3.5e: draw down initial realizations, d17

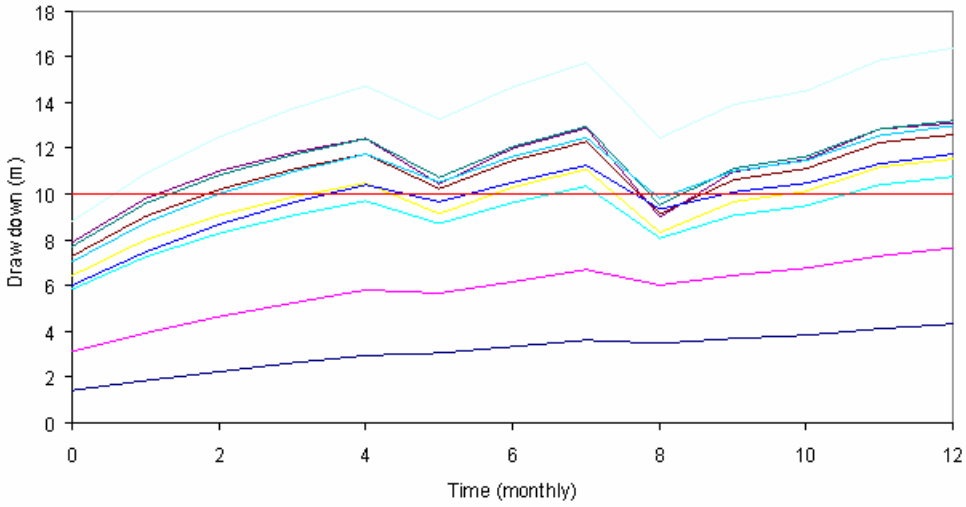

Figure 4.4.3.5f: Draw down final realizations, d17

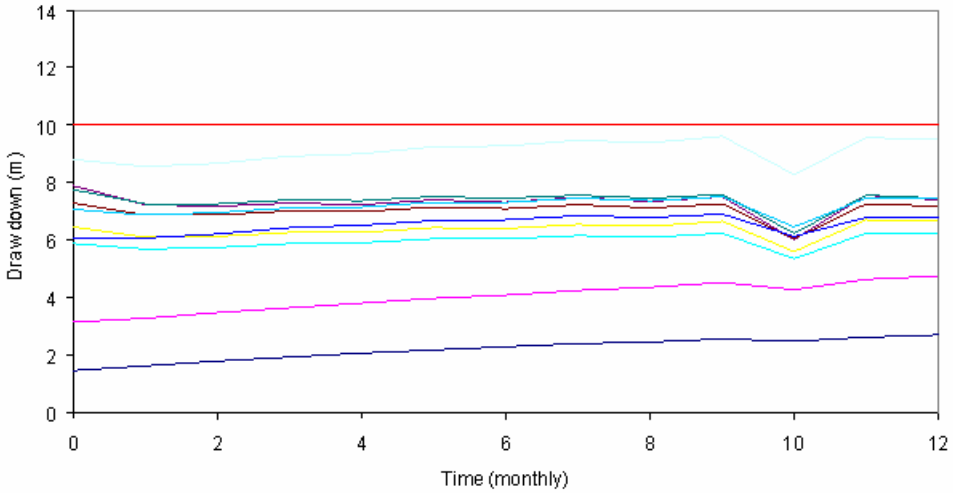

Figures 4.4.3.5(a-h): GW drawdown realizations at selected monitoring locations

Figure 4.4.3.5g: draw down initial realizations, d6

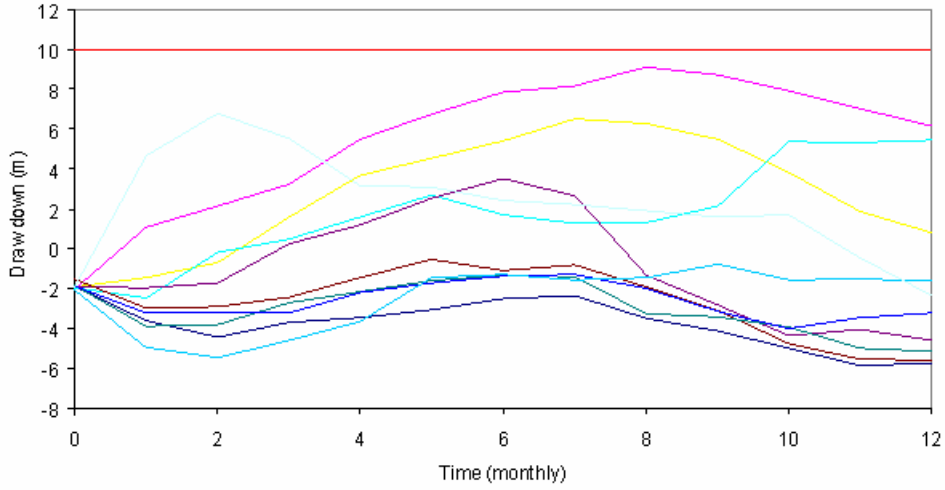

Figure 4.4.3.5h: Draw down final realizations, d6

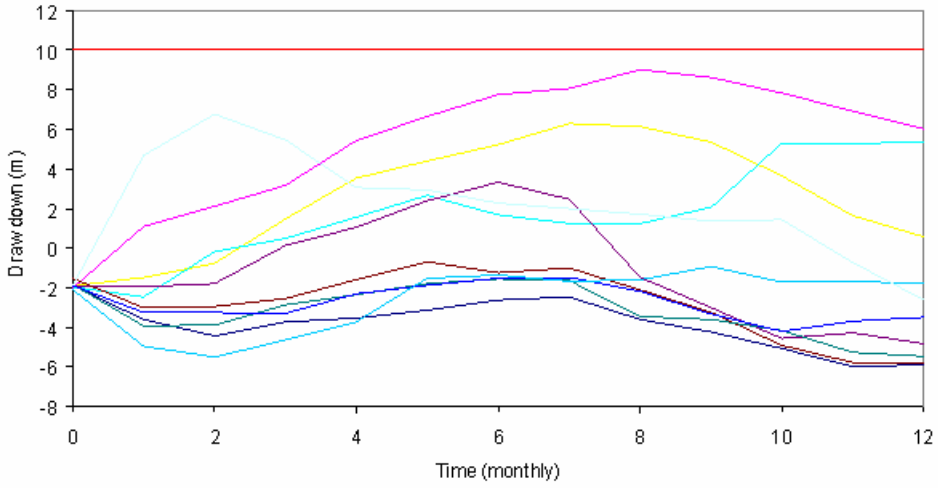

Figures 4.4.3.5(a-h): GW drawdown realizations at selected monitoring locations

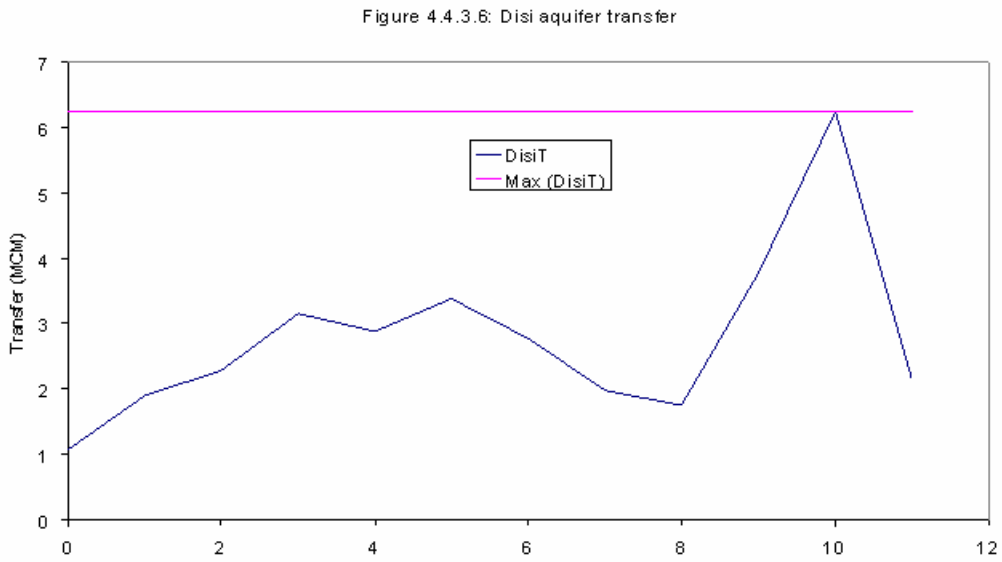

Figure 4.4.3.6: Disi Aquifer water transfer to Amman-Zarqa Area

Figure 4.4.3.7a: WD energy realizations

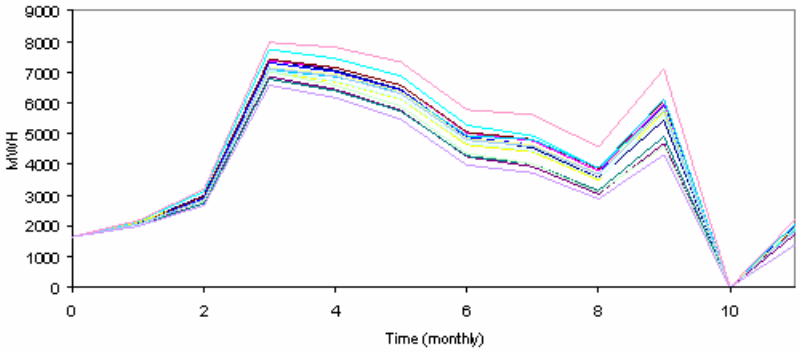

Figure 4.4.3.7b: KTD energy realizations

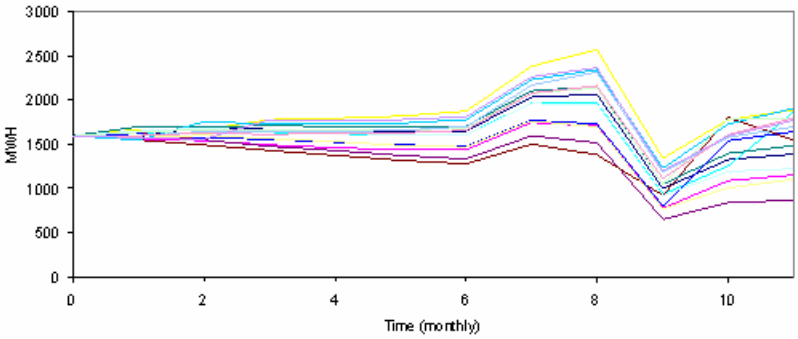

Figure 4.4.3.7c: Pumping energy realizations

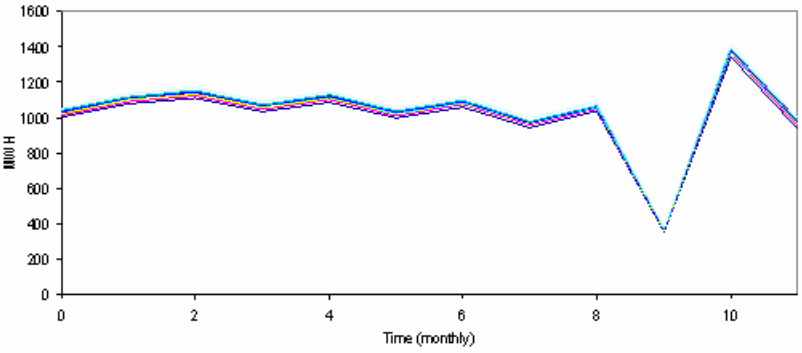

Figures 4.4.3.7(a-c): Energy realizations

4.5 Concluding Remarks

In this chapter, the conjunctive surface and ground water management problem was formulated and solved using an optimal control methodology. The case study shows that the methods developed herein enable the analysis and management of large, multi-objective, and uncertain surface and groundwater systems. Specifically, the solutions discussed earlier for the Jordanian system (of 16 state variables) were derived on a personal computer in less than two minutes.

In the next chapter the conjunctive control model will be used to analyze various operational scenarios and demonstrate the value of conjunctive water resources management.

CHAPTER 5

ASSESSMENT SCENARIOS

5.1 Introduction

The decision model described in chapter 4 is employed in this chapter to investigate several issues relevant to water resources planning in Jordan. These issues include:

1. The reliability with which the existing system can meet water demands;
2. The benefit of adding the Al-Wehdah Dam and Disi Aquifer;
3. The benefit of conjunctive management of surface water and groundwater;
4. The impact of water demand increases; and
5. The value of better forecasting and management systems.

The above issues are investigated by simulating the system response for the period from October, 1976, to September, 2000. More specifically, at each month of the simulation horizon, the management model is run with a control horizon of 6 months using forecasted inflows and groundwater boundary conditions. The forecasts assume knowledge of data *prior* to that month. The optimal releases and pumping levels corresponding to the first month of the control horizon are applied, and the system response is simulated based on inflows and boundary conditions that actually occurred in this month. The process is repeated for all months of the simulation horizon. At the end of the control-simulation process, reservoir levels, reservoir releases, groundwater levels, groundwater pumping amounts, water supply deficits, energy generation, and other

quantities) are analyzed and compared to assess the relative system performance across the scenarios.

5.2 Scenario Definition

Baseline Scenario

The baseline scenario is the scenario against which all other scenarios will be compared and their relative performance will be assessed. For this reason, it is usually defined as the scenario of the existing conditions. In Jordan's case, however, the existing water infrastructure and supplies are grossly inadequate to meet the current demands, and all other development scenarios result in drastic changes in system response. For this reason, the baseline scenario is herein defined assuming that two major projects, the Al-Wehdah Dam and the Disi Aquifer, are on line. As will be seen, this definition allows for more meaningful comparisons. The main elements of the baseline scenario are listed below:

1. Al-Wehdah Dam on line.
2. Disi Aquifer on line.
3. Groundwater drawdown constraints: (1) not to exceed 10 meters or (2) unconstrained.
4. Syrian irrigation withdrawals from Al Wehdah Dam equal 10% of North Jordan Valley irrigation demands.
5. Current water demands are used for Amman-Zarqa node (municipal and industrial) and for the Jordan Valley (agricultural).
6. No residual flow required for the Dead Sea. However, flow to the Dead Sea may occur during floods when the system storage is insufficient to regulate the flow.

Scenario 1: Existing conditions (Table 5.2.1)

This scenario is to assess the capability of the existing system to meet the existing water demands

1. Al-Wehdah Dam not on line.
2. Disi Aquifer not no line.
3. Groundwater drawdown constraints: (1) not to exceed 10 meters or (2) unconstrained.
4. Water demands as in baseline.

Scenario 2: (Table 5.2.2)

This scenario aims to assess the benefits of the Al Wehdah Dam with respect to the existing conditions. Furthermore, by comparing this scenario with the baseline, the effect of the Disi Aquifer on the system can also be assessed

1. Disi Aquifer not on line.
2. Al-Wehdah Dam on line.
3. Groundwater drawdown constraints: (1) not to exceed 10 meters or (2) unconstrained.
4. Water demands as in baseline.

Scenario 3: (Table 5.2.3)

This scenario aims to assess the impacts of increasing the Syrian irrigation withdrawals.

1. Al-Wehdah Dam on line.
2. Disi Aquifer on line.

Table 5.2.1: Assessment Focus; Scenario1, existing conditions

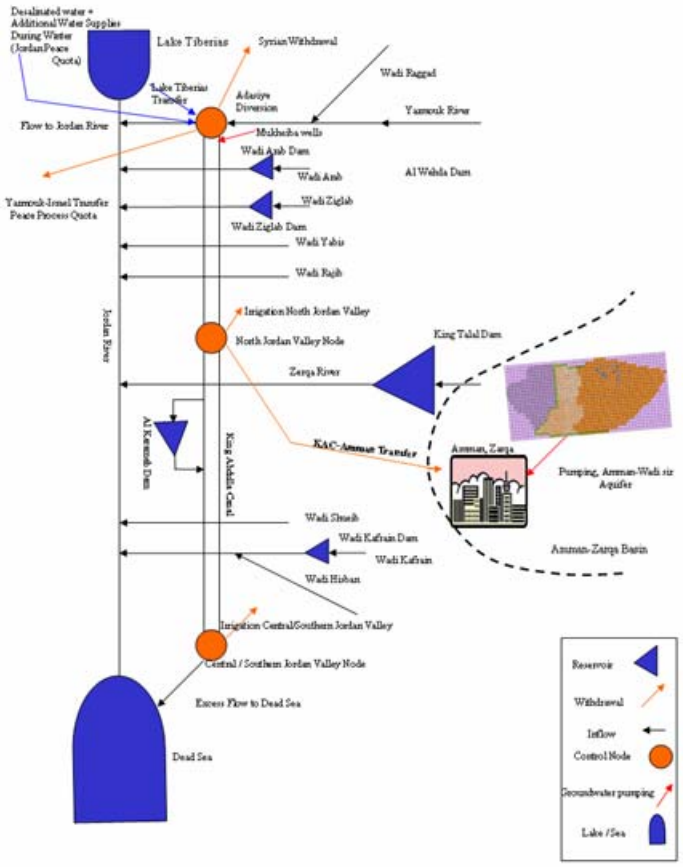

	Scenario Runs
A	Baseline Case: Al Wehdah On-line Disi Aquifer is in the system Syrian allocation: 10 % NJV No residual flow to Dead Sea
B	Existing Conditions

Table 5.2.2: Assessment Focus; Scenario2, value of Al Wehdah Dam

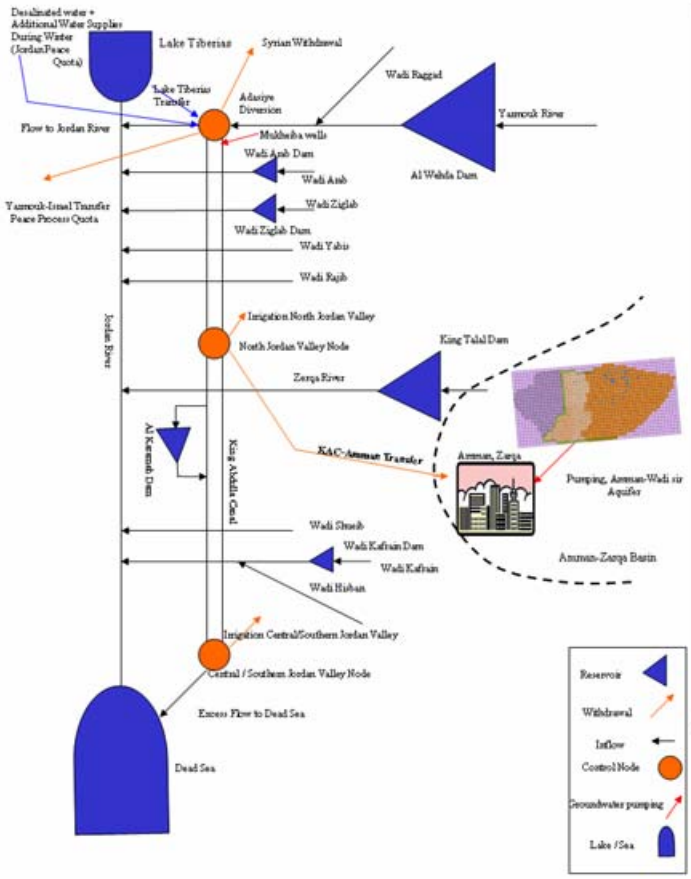

	Scenario Runs
A	Baseline Case: Al Wehdah On-line Disi Aquifer is in the system Syrian Allocation: 10 % NJV No residual flow to Dead Sea
B	No Disi transfer to Amman-Zarqa Basin

Table 5.2.3: Assessment Focus; Scenario3, effect of Syrian irrigation withdrawals

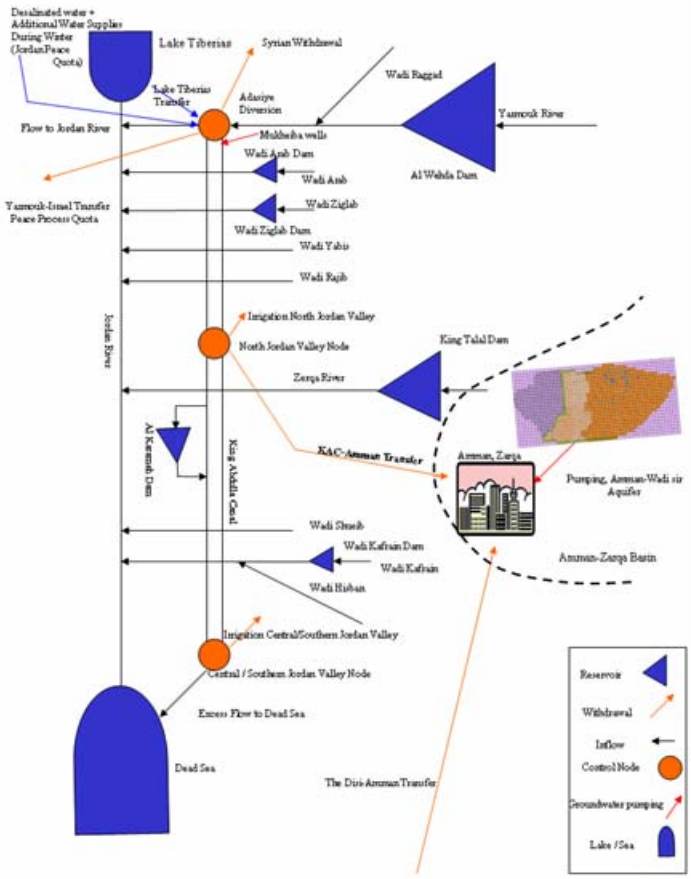

	Scenario Runs
A	Baseline Case: Al Wehdah On-line Disi Aquifer is in the system Syrian allocation: 10 % NJV No residual flow to Dead Sea
B	Syrian allocation: 20 % NJV
C	Syrian allocation: 30 % NJV

3. Groundwater drawdown constraints: (1) not to exceed 10 meters or (2) unconstrained.
4. Syrian irrigation withdrawals equal 20% or 30% of North Jordan Valley irrigation demands.
5. All other demands as in baseline.

Scenario 4: (Table 5.2.4)

This scenario aims to assess the implications of a minimum residual flow to the Dead Sea for environmental protection.

1. Al-Wehdah Dam on line.
2. Disi Aquifer on line.
3. Groundwater drawdown constraints: (1) not to exceed 10 meters or (2) unconstrained.
4. Minimum monthly flow to the Dead Sea equals 5% of the seasonal average surface water inflows (all system rivers and side wadis).
5. Minimum monthly flow to Dead Sea equals 10% of the seasonal average surface water inflows.
6. All other demands as in baseline.

Scenario 5: (Table 5.2.5)

This scenario aims to assess the impact of increasing the municipal and industrial water demand of Amman.

1. Al-Wehdah Dam on line.
2. Disi Aquifer on line.

Table 5.2.4: Assessment Focus; Scenario4, residual flow to the Dead Sea

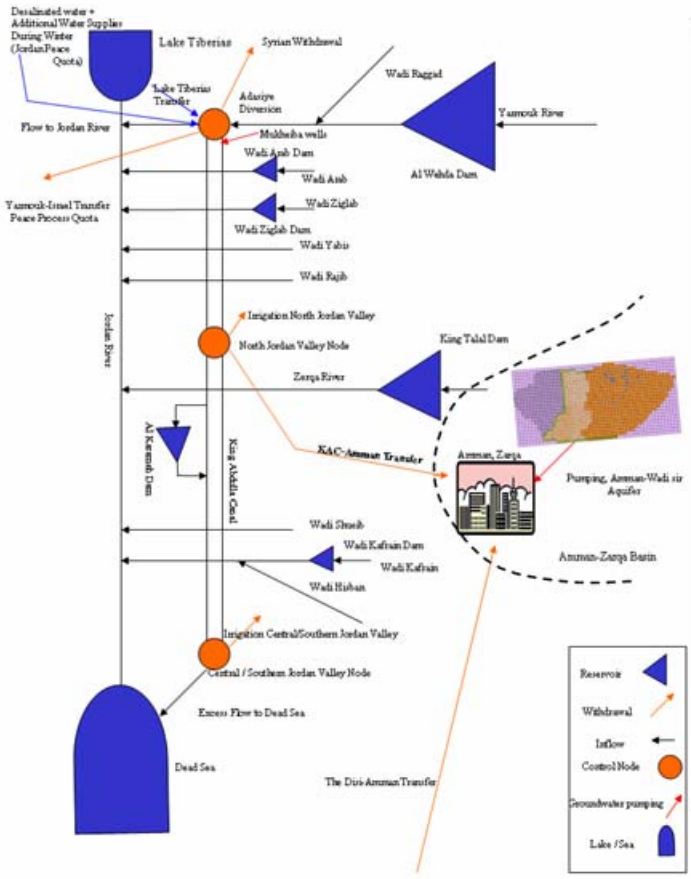

	Scenario Runs
A	Baseline Case: Al Wehdah On-line Disi Aquifer is in the system Syrian allocation: 10 % NJV No residual flow to Dead Sea
B	Residual flow to Dead Sea: 5 %
C	Residual flow to Dead Sea: 10%

Table 5.2.5: Assessment Focus; Scenario5, M&I demands increase

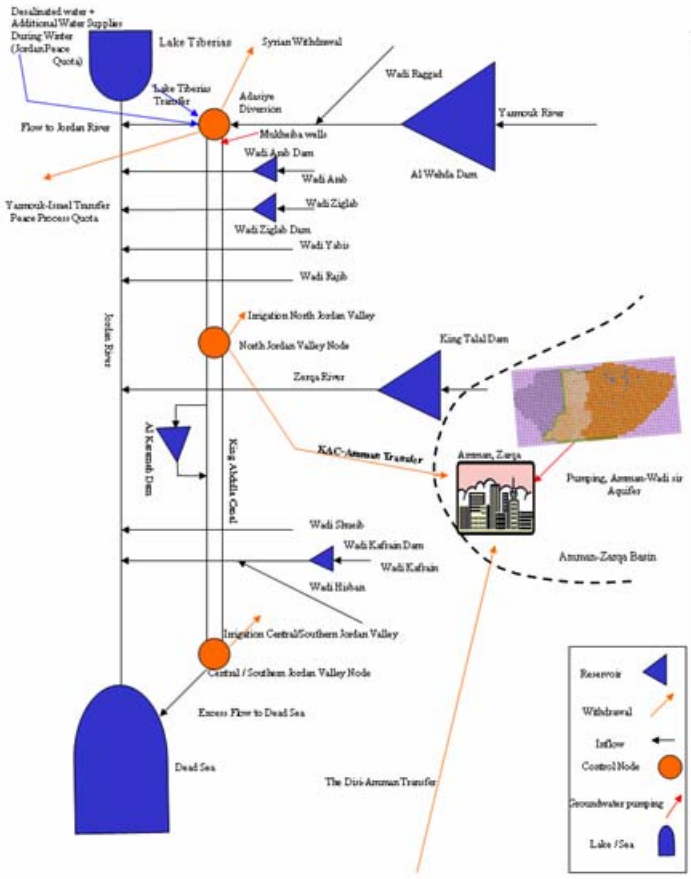

	Scenario Runs
A	Baseline Case: Al Wehdah On-line Disi Aquifer is in the system Syrian allocation: 10 % NJV No residual flow to Dead Sea
B	M&I demands increase: 10 %
C	M&I demands increase : 20%

3. Groundwater drawdown constraints: (1) not to exceed 10 meters or (2) unconstrained.
4. Municipal and industrial water demands for Amman increased by 10% or 20%.
5. All other demands as in baseline.

Scenario 6: (Table 5.2.6)

This scenario aims to assess the impacts of agricultural water demand increases.

1. Al-Wehdah Dam on line.
2. Disi Aquifer on line.
3. Groundwater drawdown constraints: (1) not to exceed 10 meters or (2) unconstrained.
4. Agricultural water demands increased by 10% or 20%.
5. All other demands as in baseline.

Perfect Forecast Scenario:

This scenario is similar to the baseline, with the important difference that perfect knowledge of the uncertain system components is assumed. Namely, the actually observed river flows, the boundary conditions, and the parameters are assumed to be equal to their observed values.

Non-conjunctive Management Scenario:

The purpose of this scenario is to assess the system performance assuming that surface water and groundwater resources are managed separately. A comparison of this scenario with conjunctive management will indicate the benefits, if any, of holistic water resources management.

Table 5.2.6: Assessment Focus; Scenario6, agricultural demands increase

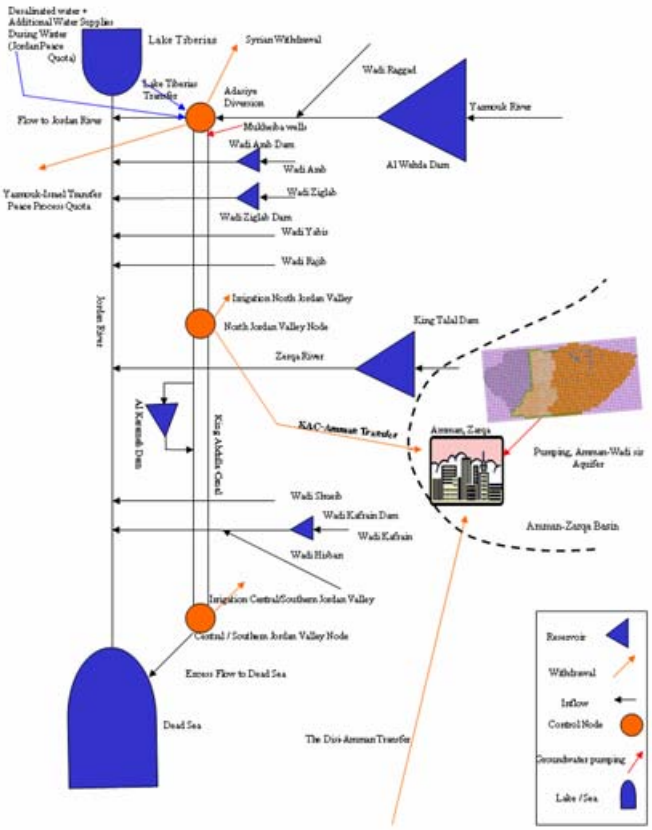

	Scenario Runs
A	Baseline Case: Al Wehdah On-line Disi Aquifer is in the system Syrian allocation: 10 % NJV No residual flow to Dead Sea
B	Agricultural demands increase: 10 %
C	Agricultural demands increase : 20%

In the Jordanian system, the King Abdullah Canal provides drinking water to Amman through a diversion at the North Jordan Valley node. This water transfer is a control variable in the conjunctive management model. In this scenario, the Amman water transfer is taken to follow a fixed sequence based on the current practices. Presently, about 20% of the Amman-Zarqa area demands (on a monthly basis) is covered by this diversion. The annual water transfer is about 45 MCM/year (Ministry of Water and Irrigation, Web site: www.water-technology.net/projects/greater_amman/specs.html) All the other surface water and groundwater elements of this scenario are as in the baseline.

5.3 Scenario Assessment Criteria

The system performance is assessed with respect to the following criteria:

1. North Jordan Valley irrigation deficits;
2. Central/ South Jordan Valley irrigation deficits;
3. Amman-Zarqa node municipal and industrial water supply deficits;
4. Total water deficits (agricultural, municipal and industrial);
5. Energy generation from Al-Wehdah Dam;
6. Energy generation from King Talal Dam;
7. Energy required for pumping from the Amman-Zarqa node;
8. Residual flow to the Dead Sea;
9. Water transfer from the Disi Aquifer.

For all scenarios, the state reliability constraints were implemented with a 90% upper limit requirement and a 10% lower limit requirement. Namely, all reservoir

storages and aquifer drawdowns are required to stay below their upper bound at least 90% of the time. In addition, reservoir storages are required to be greater than their lower bound at least 10% of the time. If these requirements could not be met, the reliability constraints are relaxed and the reliability thresholds are adjusted to 80% and 20%. If a third adjustment is necessary, the reliability thresholds are set to 70% and 30%. No further adjustments were necessary in the scenario runs performed.

The outputs of the scenario assessment model run include:

1. Storage and release sequences at all dams (Al-Wehdah Dam, King Talal Dam, Karameh Dam, Arab Dam, Ziglab Dam, and Kafrein Dam);
2. Water deficits and releases at the control nodes (Adasiya node, North Jordan Valley node, Central/South Jordan Valley node, and Amman-Zarqa node);
3. Groundwater pumping and mean drawdown sequences at the monitoring locations in the Amman-Zarqa Basin;
4. Energy generation at the Al-Wehdah and King Talal Dams, and energy required for pumping;
5. Groundwater transfer from the Disi Aquifer to Amman-Zarqa node;
6. Frequency curves for annual deficits at Adasiya node, North Jordan Valley node, Central/South Jordan Valley node, and Amman-Zarqa node; Frequency curves for the total annual deficits;
7. Frequency curves for monthly reservoir storages and monthly drawdowns at the monitoring locations;

A discussion of the scenario assessments follows. Detailed numerical results for each scenario are reported in appendices (D through L).

5.4 Scenario Assessments

Baseline

Detailed results of the baseline scenario are included in Appendix D. Table 5.4.1 shows the annual average water supply deficits for the groundwater constrained and unconstrained runs. The table shows that there are still deficits in all demand areas despite the presence of the Al-Wehdah Dam and Disi Aquifer projects. The Amman-Zarqa node demands are reduced significantly in the unconstrained drawdown run compared to the constrained run. However, the resulting unconstrained drawdowns exceeded 20 m at some locations. Such high drawdowns can cause water quality problems due to intrusion of salty water from the aquifers above and below.

The energy generation of the Al-Wehdah and King Talal dams are almost similar for the constrained and unconstrained runs, however the pumping energy in the unconstrained case is significantly higher than pumping energy in the constrained case. The resulting residual flow to the Dead Sea is similar in both cases. Finally the Disi Aquifer water transfer to the Amman-Zarqa node is significantly reduced for the unconstrained case by an average of almost 39 MCM/year. However the issue of concern for the Amman-Zarqa Basin is the deterioration of its water quality and quantity.

Scenario 1: Existing conditions

Detailed results of this scenario are shown in Appendix E and Tables 5.4.2a and 5.4.2b for the constrained and unconstrained runs respectively. The values between brackets represent the percentage change of the criterion value in this scenario versus the value of the criterion in the baseline. More specifically,

Table 5.4.1: Baseline case, constrained and unconstrained GW drawdown

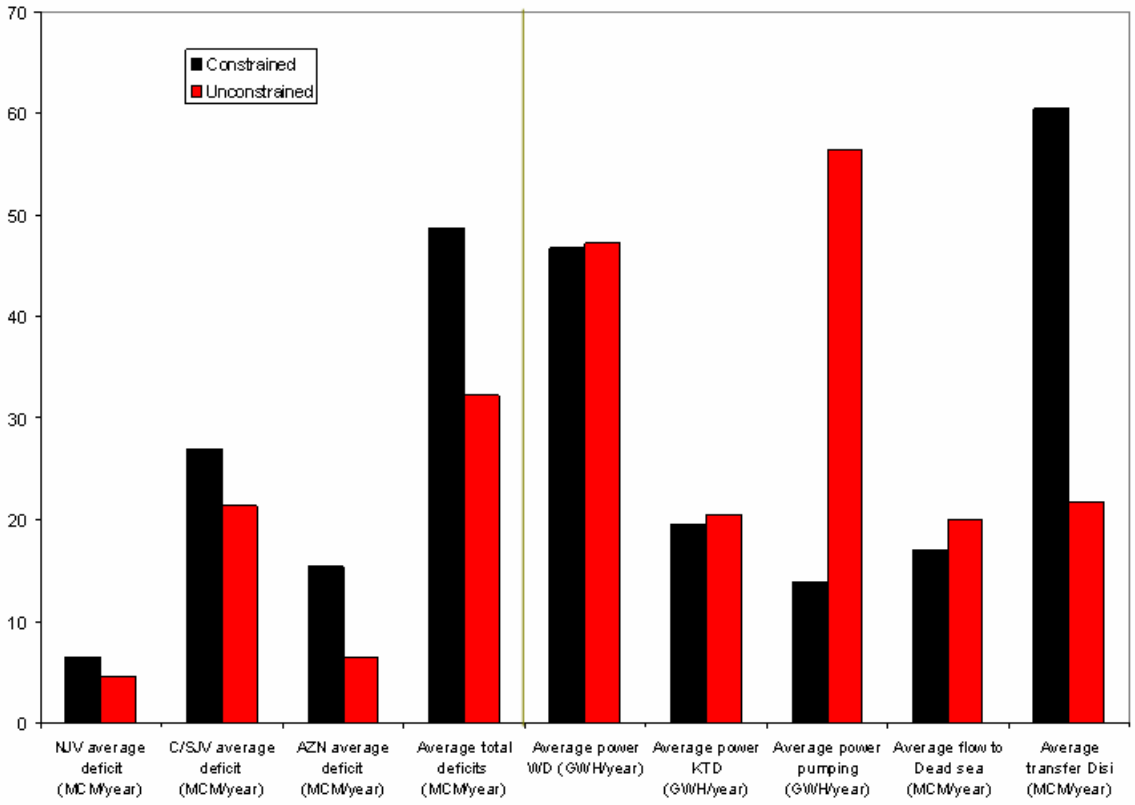

Criteria / Run	NJV average deficit (MCM/year)	C/SJV average deficit (MCM/year)	AZN average deficit (MCM/year)	Average total deficits (MCM/year)	Average power WD (GWH/year)	Average power KTD (GWH/year)	Average power pumping (GWH/year)	Average flow to Dead sea (MCM/year)	Average transfer Disi (MCM/year)
Constrained	6.48	26.92	15.38	48.79	46.73	19.52	13.79	17.0	60.44
Unconstrained	4.43	21.32	6.46	32.23	47.26	20.49	56.40	19.91	21.74

Table 5.4.2a: Existing conditions, constrained GW drawdown

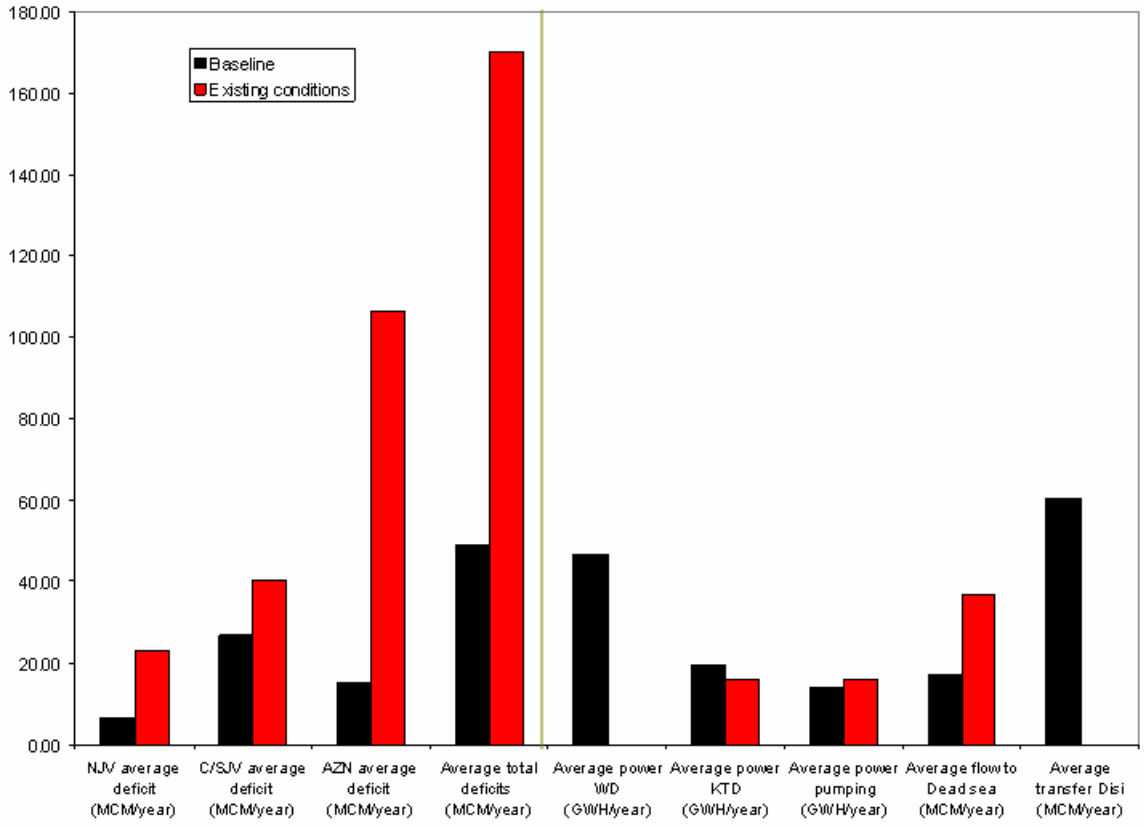

Criteria / Run	NJV average deficit (MCM/year)	C/SJV average deficit (MCM/year)	AZN average deficit (MCM/year)	Average total deficits (MCM/year)	Average power WD (GWH/year)	Average power KTD (GWH/year)	Average power pumping (GWH/year)	Average flow to Dead sea (MCM/year)	Average transfer Disi (MCM/year)
Baseline	6.48	26.92	15.38	48.79	46.73	19.52	13.79	17.0	60.44
Existing conditions	23.13 (256.8%)	40.41 (50.11%)	106.54 (592.4%)	170.09 (248.62%)	0	15.8 (-18.83%)	16.23(17.69%)	36.70 (115.32%)	0

Table 5.4.2b: Existing conditions, unconstrained GW drawdown

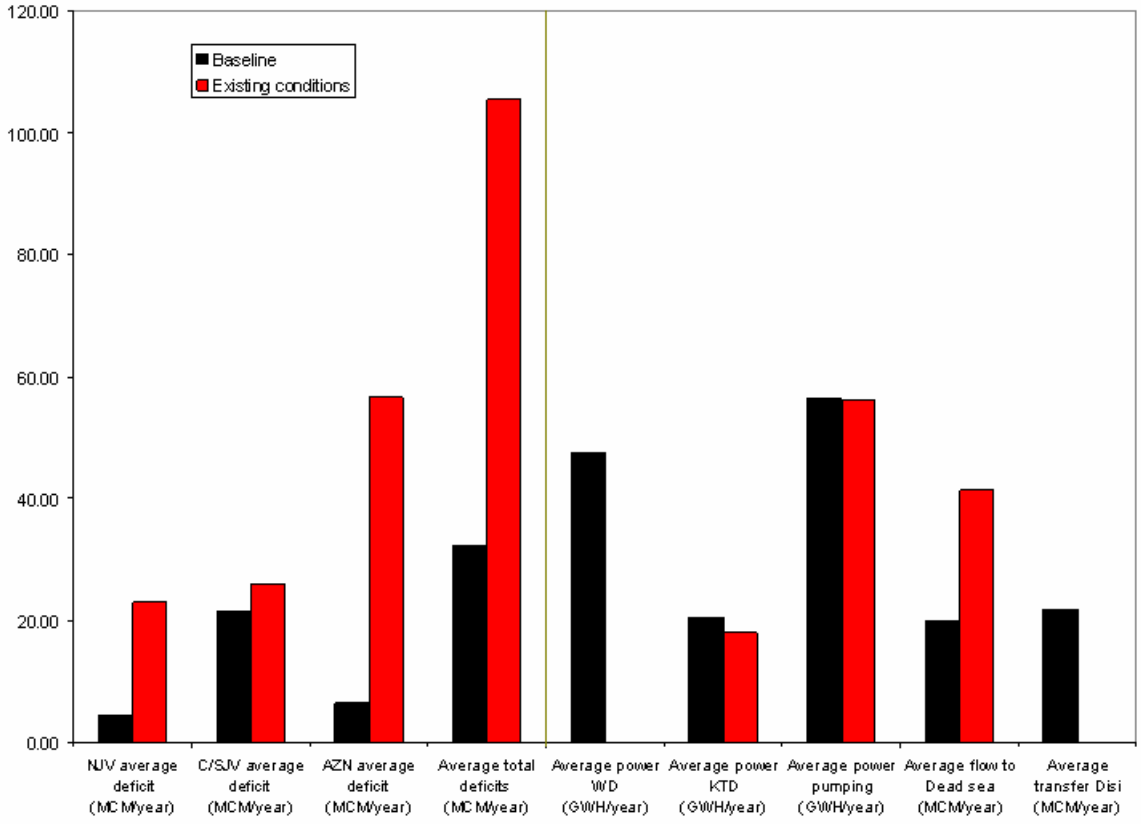

Criteria / Run	NJV average deficit (MCM/year)	C/SJV average deficit (MCM/year)	AZN average deficit (MCM/year)	Average total deficits (MCM/year)	Average power WD (GWH/year)	Average power KTD (GWH/year)	Average power pumping (GWH/year)	Average flow to Dead sea (MCM/year)	Average transfer Disi (MCM/year)
Baseline	4.43	21.32	6.46	32.23	47.26	20.49	56.40	19.91	21.74
Existing conditios	22.99 (418.19%)	25.82 (21.07%)	56.46 (773.33%)	105.28 (226.64%)	0 (-100%)	18.01 (-12.10%)	56.11 (-.51%)	41.22 (106.95%)	0 (-100%)

$$(Y)\% = ((X_{scenario} - X_{Baseline}) / X_{Baseline}) * 100\% \quad (5.1)$$

Where :

$X_{scenario}$: criterion value in this scenario;

$X_{Baseline}$: criterion value in the baseline;

Y: percentage change.

The following comments are noted for the constrained case:

Constrained groundwater case:

1. All demand areas show an increase in water deficits. The increase is most prominent in the North Jordan Valley area where the water deficits increase by 256% and in the Amman-Zarqa area where the increase is 592%.
2. Energy generation at King Talal Dam shows a reduction of 19%. The reason for this is the reduction in the return flow from the Amman-Zarqa node to King Talal Dam as there is no water transfer from the Disi aquifer to Amman in this scenario. An increase in pumping energy (18%) is recorded indicating an increase of pumping to meet the demands of the Amman-Zarqa node.
3. Finally, the residual flow to the Dead Sea shows a percentage increase by about 115% with respect to the baseline case. This occurs because Al-Wehdah Dam is not on line, and the system cannot store and utilize inflows for meeting the stated demands. As a result, a significant portion of high flow episodes in the Yarmouk pass through the system and enter the Dead Sea.

Unconstrained groundwater case:

In the unconstrained groundwater scenario, total water deficits are reduced by 38% with respect to the constrained case. In particular, the Amman-Zarqa water deficits

are reduced by 47% with respect to the constrained case. However, this reduction is achieved at by overdrawing the groundwater resources in the Amman-Zarqa Basin (Figures, Appendix E), a clearly unsustainable practice.

A comparison of this scenario (unconstrained case) and the unconstrained baseline case leads to the following observations:

1. Water deficits increase mainly in the North Jordan Valley and Amman-Zarqa areas, similar to the constrained case.
2. Energy generation at King Talal Dam is reduced by 2% as a result of the reduction in the return flow from the Amman-Zarqa area. No change is noted in pumping energy as drawdowns are unconstrained in both cases.
3. The residual flow to the Dead Sea shows a 107% percent increase with respect to the baseline for the reason mentioned earlier.

Scenario 2: Impact of the Al Wehdah Dam and the Disi Aquifer

This scenario is designed to quantify the benefit of constructing the Al-Wehdah Dam and the Disi Aquifer. The Disi Aquifer water transfer is not assumed operational. Thus, comparison of this scenario with the scenario of existing conditions will indicate the benefits of the Al Wehdah, while comparison with the baseline will indicate the benefits of the Disi. Detailed results from this scenario are shown in Appendix F for the constrained and unconstrained groundwater drawdown runs.

Comparison with Existing Conditions; Constrained groundwater case:

1. North Jordan Valley and Amman- Zarqa deficits are reduced by 65% and 27% respectively compared to the existing conditions scenario. Total deficits are reduced by 28% relative to the same scenario.

2. Energy generation at the King Talal Dam increased by about 6% with respect to the existing conditions scenario. This increase is due to the increase in return flow from the Amman-Zarqa area.
3. The residual flow to the Dead Sea is reduced after adding Al Wehdah Dam to the system (67% reduction). This occurs because the large storage of the new dam facilitates more efficient transfer of the flows from wet periods to droughts and enables the utilization of more water.

Comparison with Existing Conditions; Unconstrained groundwater case:

Comparing the unconstrained cases of this and the existing conditions scenario, similar results are observed as above. The main observations follow:

1. North Jordan Valley and Amman- Zarqa deficits are reduced by 71% and 56% respectively compared to the existing conditions. Total deficits are reduced by 46% relative to existing conditions.
2. Energy generation at the King Talal Dam increased by 18% with respect to the existing conditions scenario.
3. The residual flow to the Dead Sea is reduced after adding Al Wehdah Dam to the system (60% reduction).

The previous comparisons were against the existing conditions scenario. Comparison of this scenario with the baseline assesses the effect of adding the Disi Aquifer project. Tables 5.4.3a and 5.4.3b show the results for the constrained and unconstrained cases. The following observations are noted for the constrained groundwater case:

Comparison with Baseline; Constrained groundwater case:

Table 5.4.3a: Existing conditions and Al Wehdah Dam, constrained GW drawdown

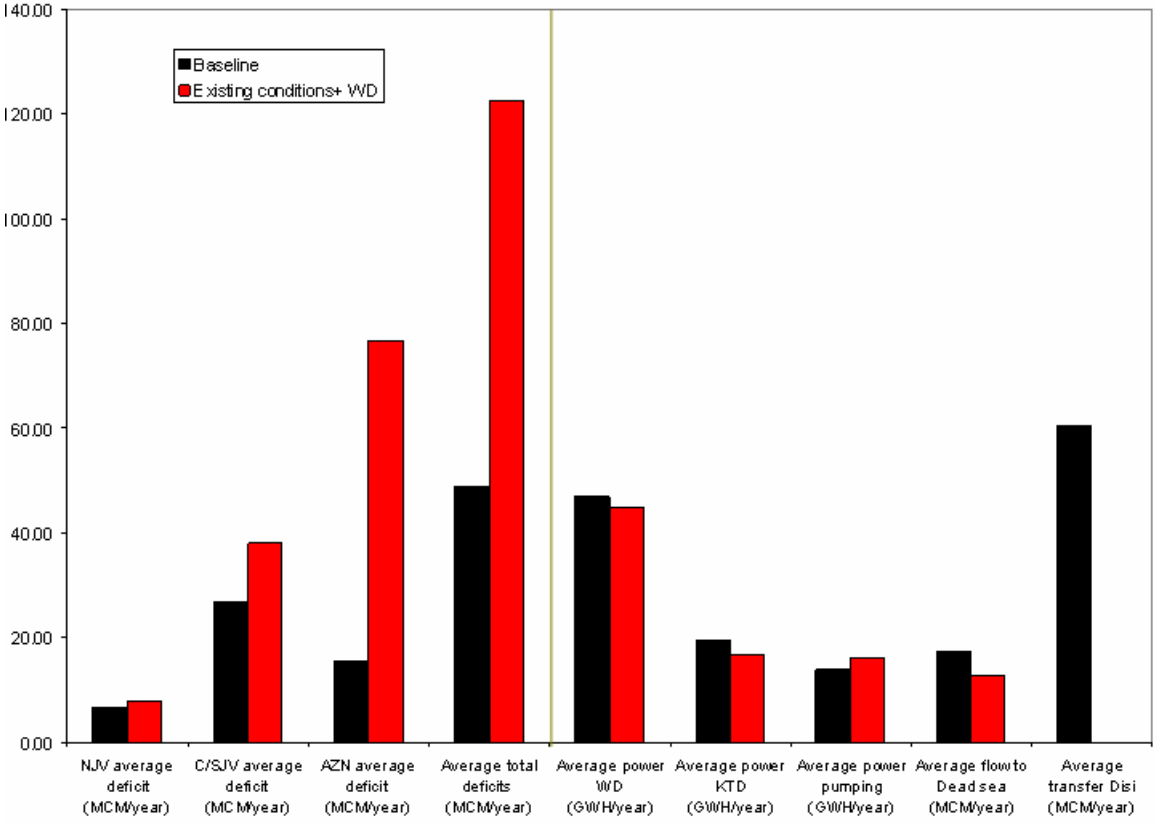

Criteria / Run	NJV average deficit (MCM/year)	C/SJV average deficit (MCM/year)	AZN average deficit (MCM/year)	Average total deficits (MCM/year)	Average power WD (GWH/year)	Average power KTD (GWH/year)	Average power pumping (GWH/year)	Average flow to Dead sea (MCM/year)	Average transfer Disi (MCM/year)
Baseline	6.48	26.92	15.38	48.79	46.73	19.52	13.79	17.0	60.44
Existing conditions+WD	7.92 (22.21%)	38.00 (41.15%)	76.74 (398.75%)	122.67 (151.43%)	44.83 (-4.06%)	16.79 (-13.97%)	16.00 (16.04%)	12.85 (-24.57%)	0

Table 5.4.3b: Existing conditions and Al Wehdah Dam, unconstrained GW drawdown

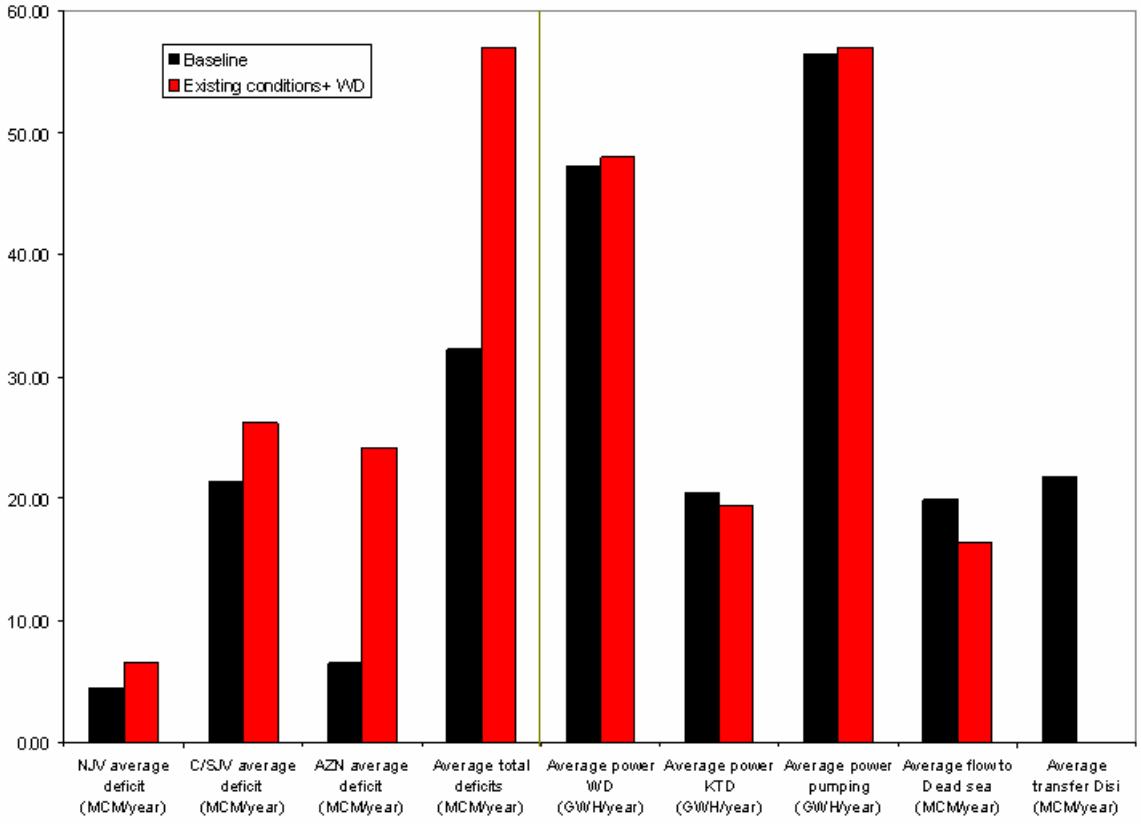

Criteria / Run	NJV average deficit (MCM/year)	C/SJV average deficit (MCM/year)	AZN average deficit (MCM/year)	Average total deficits (MCM/year)	Average power WD (GWH/year)	Average power KTD (GWH/year)	Average power pumping (GWH/year)	Average flow to Dead sea (MCM/year)	Average transfer Disi (MCM/year)
Baseline	4.43	21.32	6.46	32.23	47.26	20.49	56.40	19.91	21.74
Existing conditios+WD	6.58 (48.33%)	26.19 (22.83%)	24.10 (272.88%)	56.89 (76.50%)	47.96 (1.47%)	19.44 (-5.12%)	57.00 (1.04%)	16.45 (-17.40%)	0 (-100%)

1. The Amman-Zarqa area shows an increase in deficits by 398% compared to the constrained baseline case, the main reason being the absence of the Disi Aquifer water transfer. The Central/South Jordan Valley shows a deficit increase by 41% due to the reduced return flow in the Amman-Zarqa area. The North Jordan Valley area also experiences a slight increase in deficits with respect to the baseline run, the reason again being the absence of the Disi Aquifer transfer to Amman. Because of this, the Al-Wehdah Dam is forced to release more to make up for the Disi Aquifer transfer and, in the long run, fails to maintain the reliability of water supply to the North Jordan Valley.
2. Energy generation at the King Talal Dam is reduced by about 14% with respect to the baseline run, as a consequence of the reduced return flow to the Zarqa River. Energy generation at Al-Wehdah Dam is practically the same as in the baseline run. Pumping energy is increased by 16%.
3. Residual flow to the Dead Sea is reduced by 24% with respect to the baseline case, as a result of the reduced Zarqa River flows.

Comparison with Baseline; Unconstrained groundwater case:

A comparison of this scenario and the baseline (unconstrained cases) leads to the following observations:

1. Water deficits in the North Jordan Valley are increased by 48%, in the Central/South Jordan Valley by 22%, and in the Amman-Zarqa area by 272%. The total deficits are increased by 76%.

2. Energy generation from the Al-Wehdah and King Talal Dams are not significantly different with respect to the baseline. The same applies to pumping energy.
3. The flow to the Dead Sea is reduced by 17% with respect to the baseline. However, relative to the constrained run, residual flow increases by 26%.

Finally, it is noted that the unconstrained groundwater scenario reduces total deficits by 50% and the Amman-Zarqa deficits by 64% compared to the constrained scenario.

Scenario 3: Impacts of Syrian Agricultural Withdrawals

This scenario aims to assess the implications of increased Syrian agricultural withdrawals downstream of the Al-Wehdah Dam. Detailed results for this scenario are shown in appendix G for both the constrained and unconstrained groundwater runs. Tables 5.4.4a and 5.4.4b compare these scenarios to the baseline.

Notable observations for the constrained groundwater case are as follows:

1. Syrian withdrawal increases of 20% and 30% lead to increased water deficits in all demand areas in Jordan, with the North Jordan Valley impacted most. This is because most of the water used in the North Jordan Valley comes from the Yarmouk.
2. Under increased Syrian withdrawals, energy generation at the Al-Wehdah and King Talal Dams is slightly decreased with respect to the baseline. The pumping energy is slightly affected (.7% and .48%) for the two levels of withdrawals

Table 5.4.4a: Syrian irrigation withdrawals, constrained GW drawdown

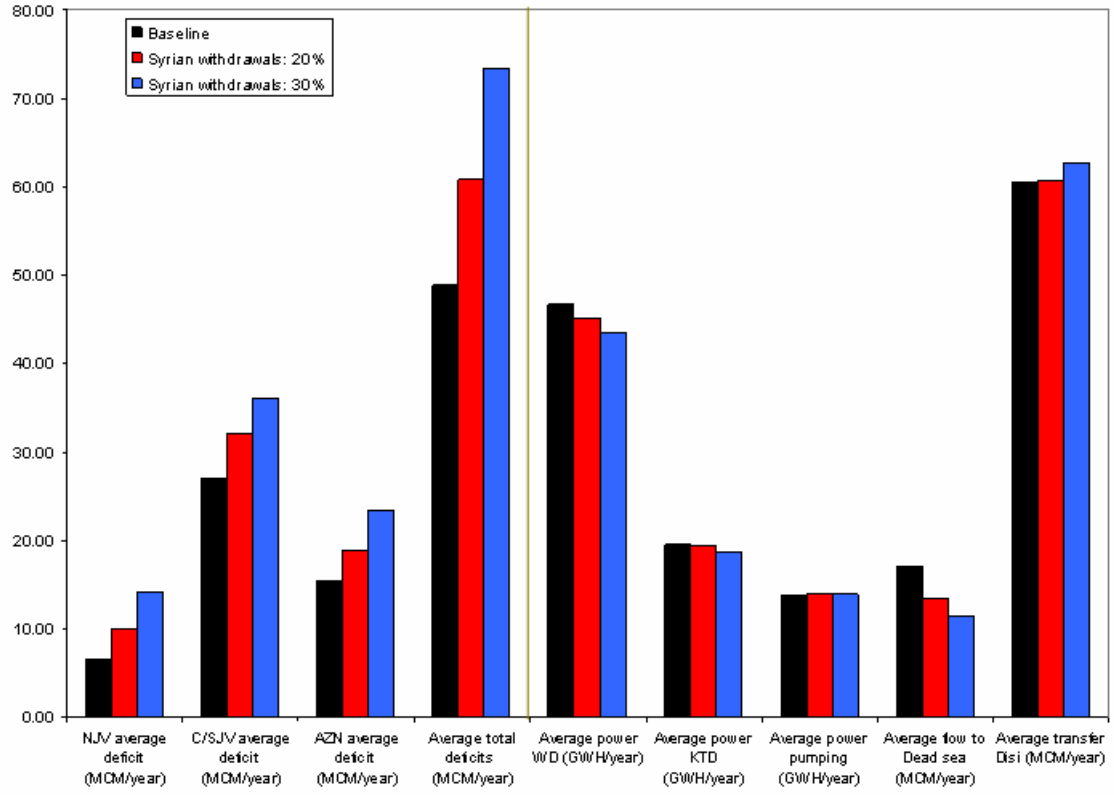

Criteria / Run	NJV average deficit (MCM/year)	C/SJV average deficit (MCM/year)	AZN average deficit (MCM/year)	Average total deficits (MCM/year)	Average power WD (GWH/year)	Average power KTD (GWH/year)	Average power pumping (GWH/year)	Average flow to Dead sea (MCM/year)	Average transfer Disi (MCM/year)
Baseline	6.48	26.92	15.38	48.79	46.73	19.52	13.79	17.0	60.44
20% NJV	9.96 (53.68%)	32.07 (19.12%)	18.86 (22.62%)	60.90 (24.83%)	45.09 (-3.49%)	19.34 (-.90%)	13.88 (0.7%)	13.44 (-21.11%)	60.73 (.48%)
30% NJV	14.10 (117.53%	36.02 (33.8%)	23.31 (51.48%)	73.44 (50.52%)	43.57 (-6.75%)	18.69 (-4.23%	13.85 (.48%)	11.48 (-32.59%)	62.65 (3.66%)

Table 5.4.4b: Syrian irrigation withdrawals, unconstrained GW drawdown

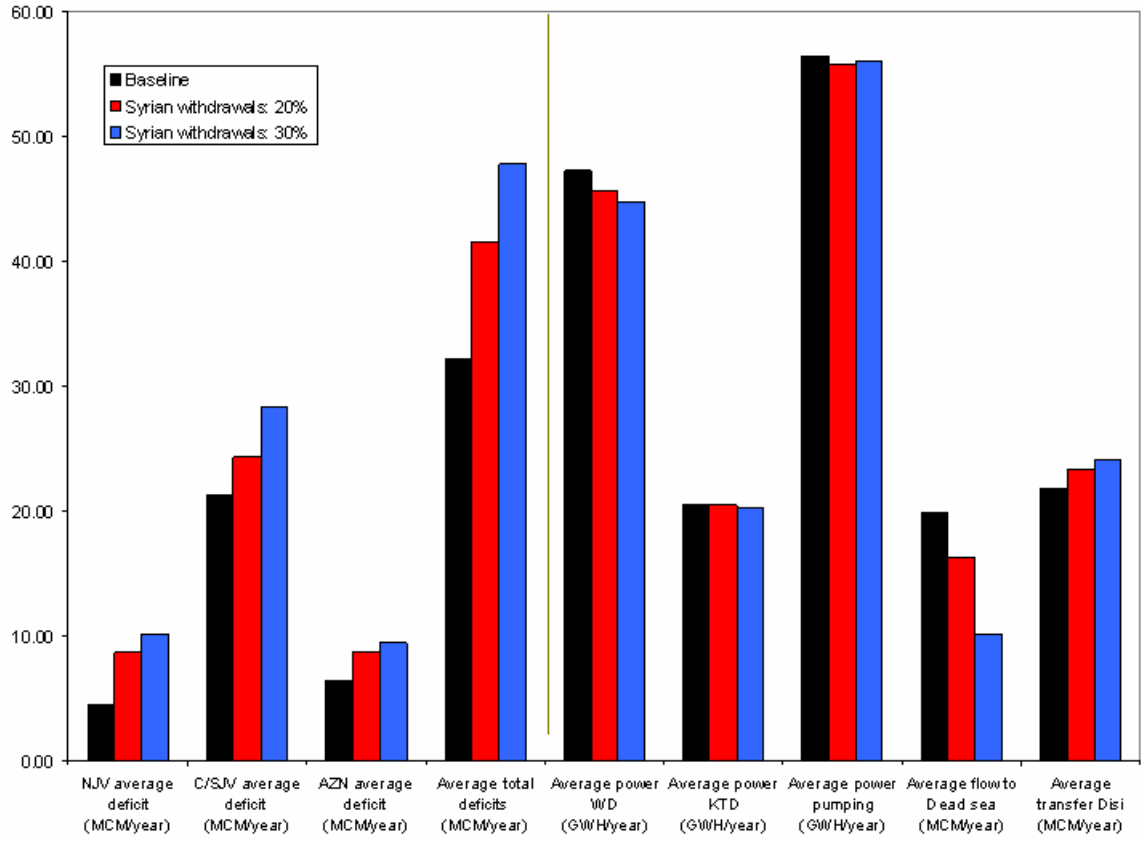

Criteria / Run	NJV average deficit (MCM/year)	C/SJV average deficit (MCM/year)	AZN average deficit (MCM/year)	Average total deficits (MCM/year)	Average power WD (GWH/year)	Average power KTD (GWH/year)	Average power pumping (GWH/year)	Average flow to Dead sea (MCM/year)	Average transfer Disi (MCM/year)
Baseline	4.43	21.32	6.46	32.23	47.26	20.49	56.40	19.91	21.74
20% NJV	8.58 (93.34%)	24.26 (13.78%)	8.72 (35.01%)	41.57 (28.99%)	45.67 (-3.36%)	20.43 (-.26%)	55.76 (-1.13%)	16.22 (-18.57%)	23.29 (7.09%)
30% NJV	10.11 (127.95%)	28.25 (32.45%)	9.42 (45.70%)	47.81 (48.34%)	44.73 (-5.35%)	20.15 (-1.63%)	56.06 (-.61%)	10.08 (-49.35%)	24.09 (10.80%)

3. Residual flow to the Dead Sea is decreased by 21% and 32% respectively for 20% and 30% withdrawal increases. The Disi Aquifer transfer to Amman is affected only slightly.

In the unconstrained case, total deficits decreased with respect to the constrained case by about 30% and 29% respectively for the 20% and 30% withdrawal increase levels. The largest reduction occurs in the Amman-Zarqa area. The Disi Aquifer water transfer is reduced by 50% in the unconstrained run for both levels of withdrawals. Similar conclusions can be drawn when comparing the unconstrained case of this scenario with the unconstrained case of the baseline

Scenario 4: Minimum Flow to the Dead Sea

This scenario aims at assessing the water resources impacts of a minimum flow requirement to the Dead Sea. The Dead Sea is an environmentally sensitive area suffering from excessive evaporation losses and falling water levels. The minimum flow requirement was taken as a fraction (5% or 10%) of the monthly averaged surface water inflows. Detailed results of this scenario are shown in appendix H for the constrained and unconstrained groundwater runs. . Tables 5.4.5a and 5.4.5b compare this scenario with the baseline.

Constrained groundwater case:

1. At the 5% and 10% minimum flow requirement, all demand areas show increased deficits with respect to the baseline case by 23% and 46% respectively.

Table 5.4.5a: Dead Sea residual flow, constrained GW drawdown

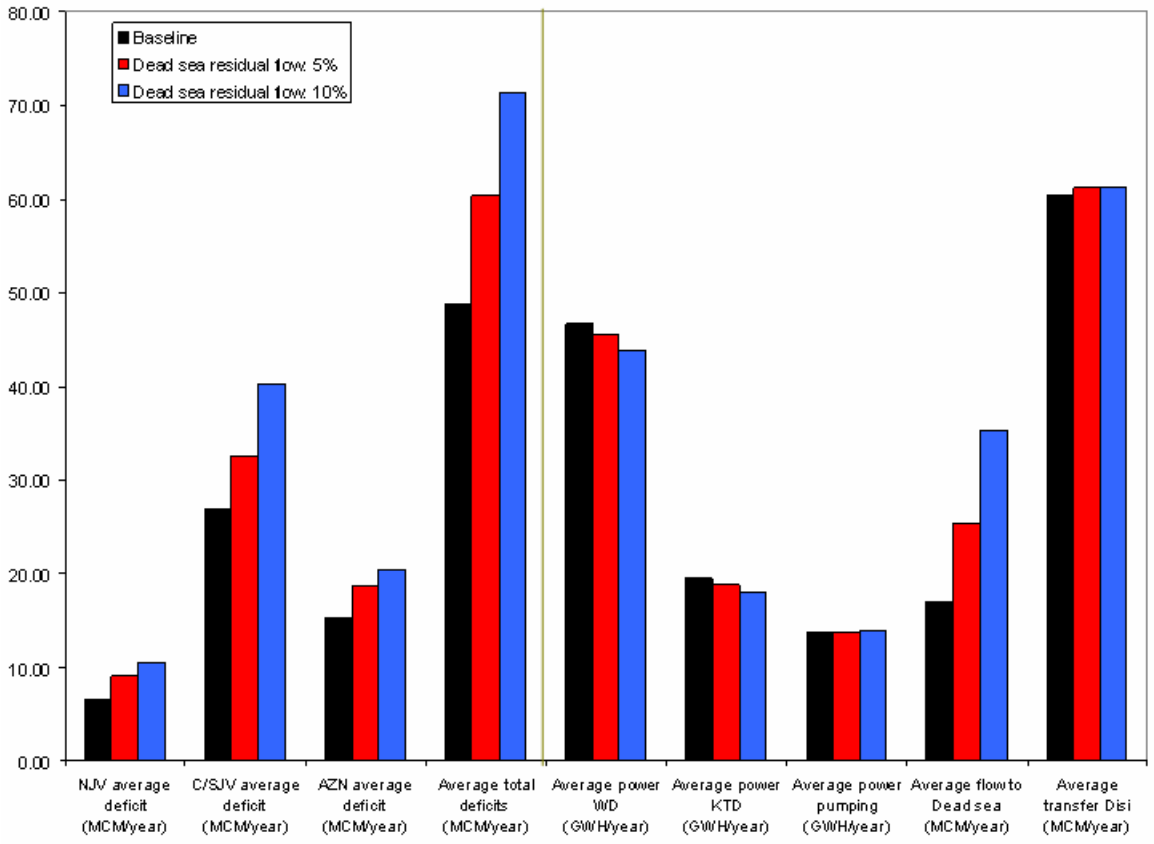

Criteria / Run	NJV average deficit (MCM/year)	C/SJV average deficit (MCM/year)	AZN average deficit (MCM/year)	Average total deficits (MCM/year)	Average power WD (GWH/year)	Average power KTD (GWH/year)	Average power pumping (GWH/year)	Average flow to Dead sea (MCM/year)	Average transfer Disi (MCM/year)
Baseline	6.48	26.92	15.38	48.79	46.73	19.52	13.79	17.0	60.44
5% Residual flow	9.08 (40.07%)	32.53 (20.83%)	18.70 (21.54%)	60.31 (23.62%)	45.44 (-2.75%)	18.84 (-3.47%)	13.81 (.14%)	25.39 (48.96%)	61.15 (1.18%)
10% Residual flow	10.58 (63.21%)	40.346 (49.87%)	20.42 (32.73%)	71.35 (46.24%)	43.76 (-6.35%)	17.92 (-8.116%	13.91 (.92%)	35.23 (106.72%)	61.32 (1.46%)

Table 5.4.5b: Dead Sea residual flow, unconstrained GW drawdown

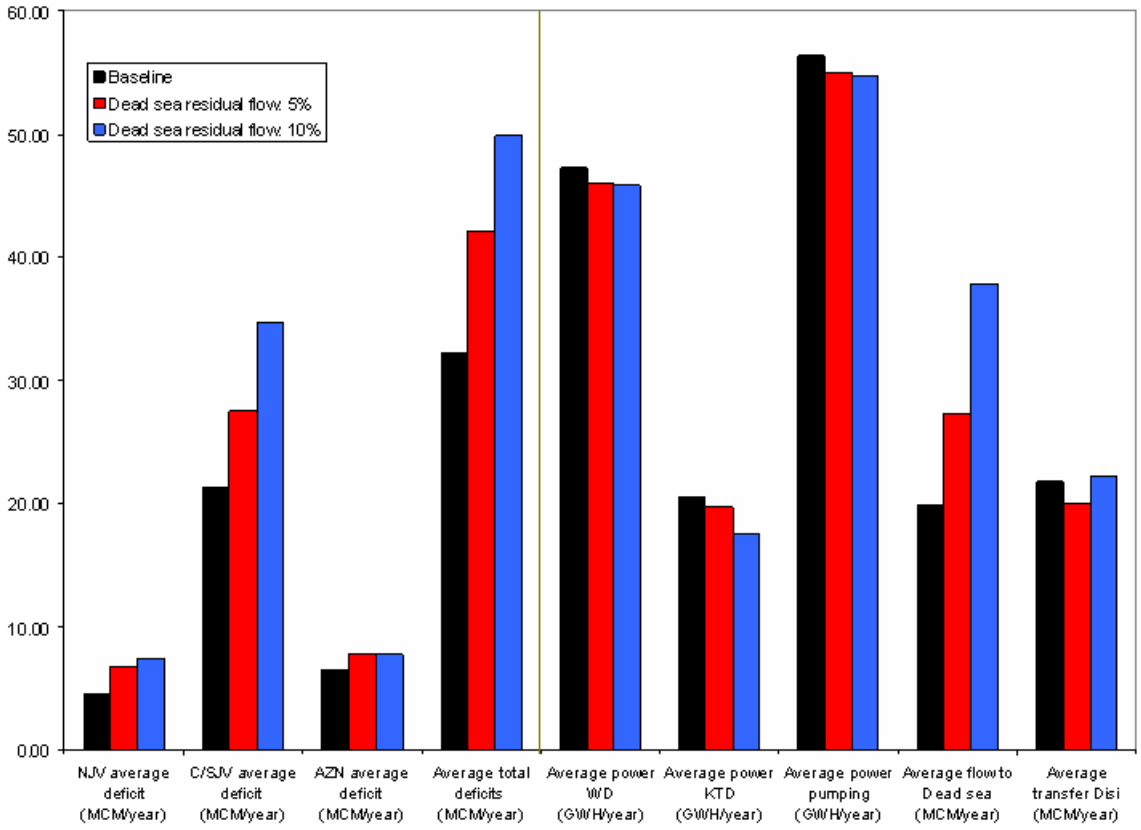

Criteria / Run	NJV average deficit (MCM/year)	C/SJV average deficit (MCM/year)	AZN average deficit (MCM/year)	Average total deficits (MCM/year)	Average power WD (GWH/year)	Average power KTD (GWH/year)	Average power pumping (GWH/year)	Average flow to Dead sea (MCM/year)	Average transfer Disi (MCM/year)
Baseline	4.43	21.32	6.46	32.23	47.26	20.49	56.40	19.91	21.74
5% Residual flow	6.7 (52.67%)	27.56 (29.22%)	7.80 (20.69%)	42.14 (30.74%)	45.90 (-2.86%)	19.73 (-3.67%)	55.01 (-2.47%)	27.21 (36.63%)	20.01 (-7.99%)
10% Residual flow	7.44 (67.83%)	34.66 (62.5%)	7.72 (19.50%)	49.84 (54.63%)	45.85 (-2.98%)	17.49 (-14.62%)	54.69 (-3.03%)	37.83 (89.95%)	22.11 (1.70%)

2. At the 10% minimum flow requirement, energy generation at the King Talal Dam and Al Wehdah Dam decreased with respect to the baseline by 8% and 6% respectively. The effect on pumping energy is small.
3. As expected, the residual flow to the Dead Sea increases with respect to the baseline by 48% and 106% for the 5% and 10% minimum flow requirement respectively. The Disi Aquifer water transfer is not changed significantly.

Unconstrained groundwater case:

Comparing the unconstrained results with the constrained results, total deficits are reduced by about 31% for both the 5% and 10% requirement levels of residual flow. Also, the Disi transfer to Amman decreases by about 66% for both the 5% and 10% minimum flow requirement levels.

Similar observations can be noted when comparing the unconstrained run of this scenario with the unconstrained run of the baseline.

Scenario 5: Increased Municipal and Industrial Demands (Amman)

The Amman-Zarqa area houses the capital city of Jordan as well as several of its industries. This scenario aims at assessing the implications of Amman's increasing demands.

Detailed results of this scenario are shown in Appendix I. Tables 5.4.6a and 5.4.6b compare this scenario to the baseline. The municipal and industrial demand targets in the baseline and this scenario are different. Thus, to compare the deficits on an equal basis a normalized deficit change measure was introduced by dividing the average annual

Table 5.4.6a: Municipal and industrial demands increase, constrained GW drawdown

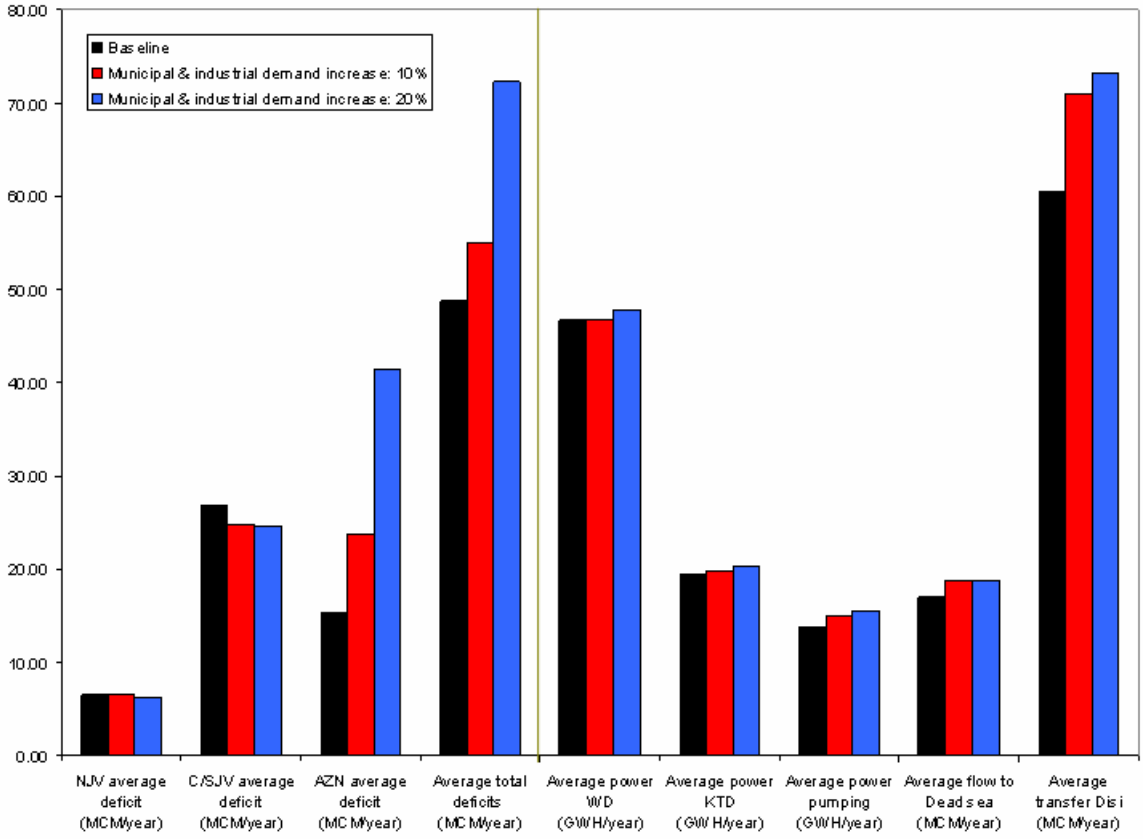

Criteria / Run	NJV average deficit (MCM/year)	C/SJV average deficit (MCM/year)	AZN average deficit (MCM/year)	Average total deficits (MCM/year)	Average power WD (GWH/year)	Average power KTD (GWH/year)	Average power pumping (GWH/year)	Average flow to Dead sea (MCM/year)	Average transfer Disi (MCM/year)
Baseline	6.48	26.92	15.38	48.79	46.73	19.52	13.79	17.0	60.44
10% M&I increase	6.49 (.12%)	24.72 (-8.14%)	23.75 (40.34%)	54.97 (8.40%)	46.78 (.11%)	19.78 (1.36%)	14.89 (8.03%)	18.68 (9.62%)	70.98 (17.44%)
20% M&I increase	6.31 (-2.55%)	24.63 (-8.49%)	41.40 (124.21%)	72.35 (37.45%)	47.77 (2.23%)	20.36 (4.34%)	15.50 (12.44%)	18.78 (10.19%)	73.17 (21.07%)

Table 5.4.6b: Municipal and industrial demands increase, unconstrained GW drawdown

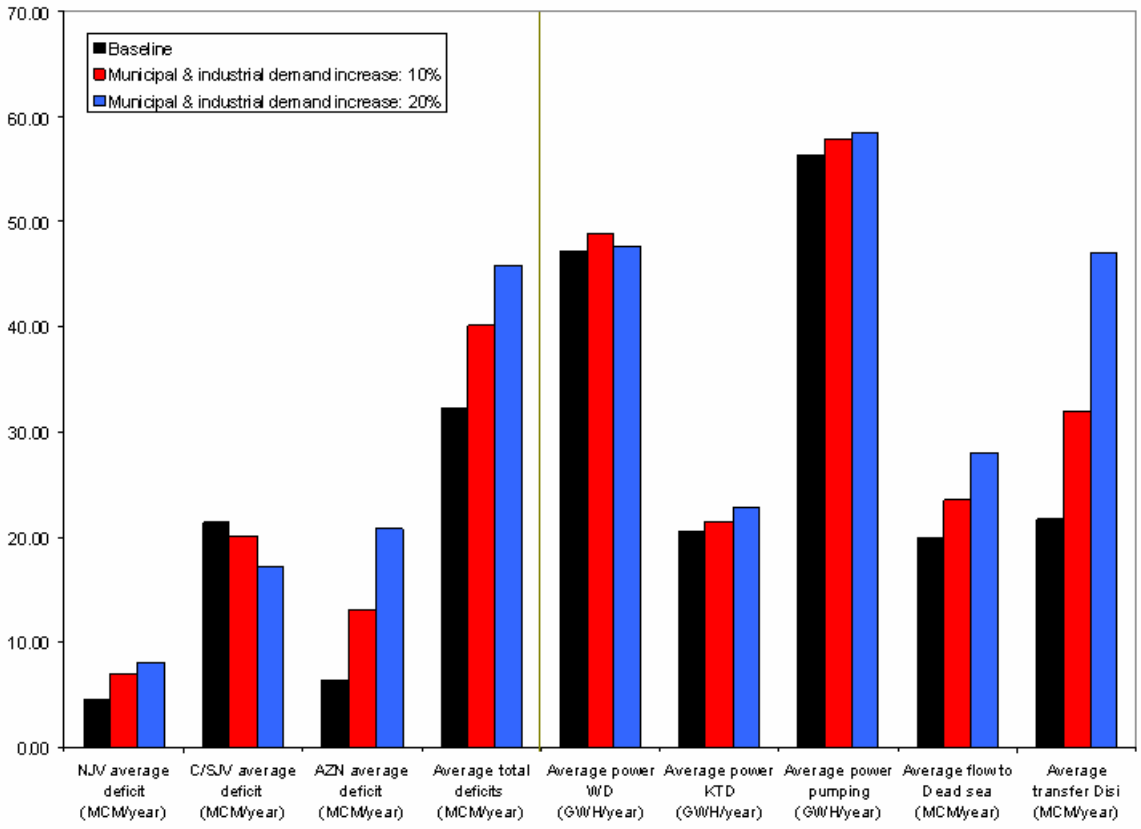

Criteria / Run	NJV average deficit (MCM/year)	C/SJV average deficit (MCM/year)	AZN average deficit (MCM/year)	Average total deficits (MCM/year)	Average power WD (GWH/year)	Average power KTD (GWH/year)	Average power pumping (GWH/year)	Average flow to Dead sea (MCM/year)	Average transfer Disi (MCM/year)
Baseline	4.43	21.32	6.46	32.23	47.26	20.49	56.40	19.91	21.74
10% M&I increase	6.96 (56.97%)	20.10 (-5.71%)	13.06 (83.69%)	40.14 (19.80%)	48.81 (3.28%)	21.45 (4.71%)	57.93 (2.71%)	23.56 (18.30%)	31.96 (46.97%)
20% M&I increase	8.02 (80.90%)	17.07 (-19.96%)	20.83 (168.61%)	45.93 (32.10%)	47.67 (.86%)	22.78 (11.20%)	58.59 (3.87%)	28.05 (40.85%)	46.98 (116.03%)

deficits by the annual municipal and industrial demand target for each case. Namely, Equation 5.1 is modified for the Amman-Zarqa deficits as follows:

$$(Y')\% = ((X'_{scenario} - X'_{baseline}) / X'_{baseline}) * 100\% \quad (5.2)$$

Where :

$X'_{scenario}$: is the Amman-Zarqa deficit value divided by the Amman-Zarqa total annual demand used in the scenario;

$X'_{baseline}$: is the Amman-Zarqa deficit value divided by the Amman-Zarqa total annual demand used in the baseline case;

Y': percentage change of the ratio $X'_{scenario}$ from the baseline ratio $X'_{baseline}$.

However, except for the the deficits in the Amman-Zarqa area, the other comparison measures are computed based on Equation 5.1.

Constrained groundwater case:

1. Average total deficits increase by 8% and 37% respectively for the 10% and 20% demand increase levels. More specifically, the Amman-Zarqa deficit ratio increased by about 40% and 124% for the 10% and 20% demand increase levels respectively. By comparison, the deficits of the Central and South Jordan Valley decreased by about 8% for both the levels of demand increase, the reason being the increase in return flow to the Zarqa River.
2. Energy generation increased slightly at Al-Wehdah (.1% and 2.2%) for the 10% and 20% demand increase levels respectively. King Talal Dam energy generation increased by (1.3% and 4.3%) for the 10% and 20% demand increase levels respectively. Pumping energy increased as a result of the increase in demand (8% and 12%) for the 10% and 20% demand increase levels.

3. As expected, the Disi transfer to Amman increases by about 17% and 21% respectively for the 10% and 20% demand increase levels. Furthermore, as a result of the increased return flow, the residual flow entering the Dead Sea also increased by about 10% for both demand increase levels.

Unconstrained groundwater case:

In the unconstrained case, the deficits in the Amman-Zarqa area decrease by 45% and 50% as compared to the constrained case for the two levels of demand increase. Also, total deficits decrease by 27% and 36% as compared to the constrained scenario. The drawdown frequency curves indicate that almost 85% of the time the aquifer levels dropped significantly higher than 10 meters, with drawdowns of 15 to 16 meters being common.

Similar comparisons can be made for the unconstrained run of this scenario and the unconstrained run of the baseline. The most notable difference is that in this scenario the North Jordan Valley area starts to experience higher deficits as compared to the baseline by as much as 57% and 81% for the 10% and 20% demand increase levels respectively.

Scenario 6: Increased Agricultural Demands

This scenario analyzes the effects of increased agricultural demands (by 10% and 20%) in the North Jordan Valley and the Central/South Jordan Valley areas. Detailed results of this scenario are shown in Appendix J. Tables 5.4.7a and 5.4.7b compare this scenario to the baseline. In Tables 5.4.7a and 5.4.7b, the

Table 5.4.7a: Agricultural demands increase, constrained GW drawdown

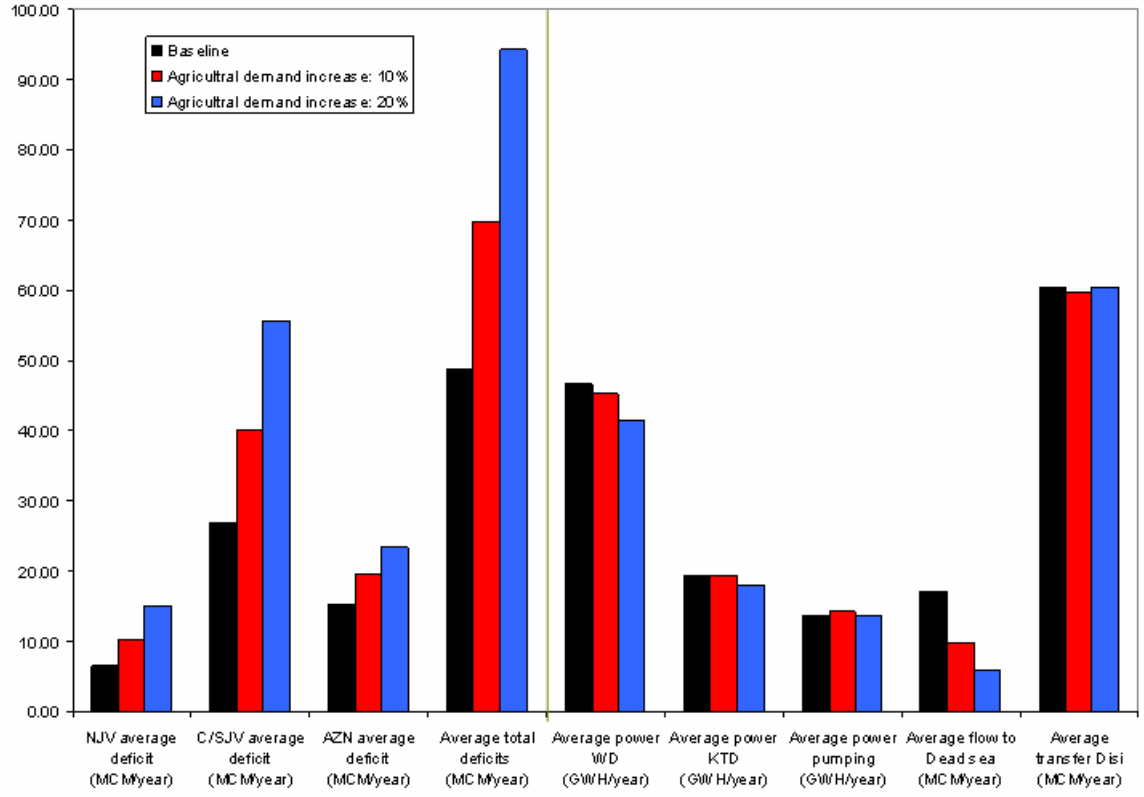

Criteria / Run	NJV average deficit (MCM/year)	C/SJV average deficit (MCM/year)	AZN average deficit (MCM/year)	Average total deficits (MCM/year)	Average power WD (GWH/year)	Average power KTD (GWH/year)	Average power pumping (GWH/year)	Average flow to Dead sea (MCM/year)	Average transfer Disi (MCM/year)
Baseline	6.48	26.92	15.38	48.79	46.73	19.52	13.79	17.0	60.44
10% Agricult. increase	10.23 (43.5%)	39.96 (34.96%)	19.54 (27.01%)	69.74 (34.78%)	45.19 (-3.29%)	19.35 (-.85%)	14.16 (2.70%)	9.77 (-42.64%)	59.77 (-1.09%)
20% Agricult. increase	15.01 (93.01%)	55.75 (72.57%)	23.46 (52.47%)	94.23 (72.27%)	41.43 (-11.33)	18.03 (-7.6%)	13.76 (-.21%)	5.93 (-65.16%)	60.47 (0.05%)

Table 5.4.7b: Agricultural demands increase, unconstrained GW drawdown

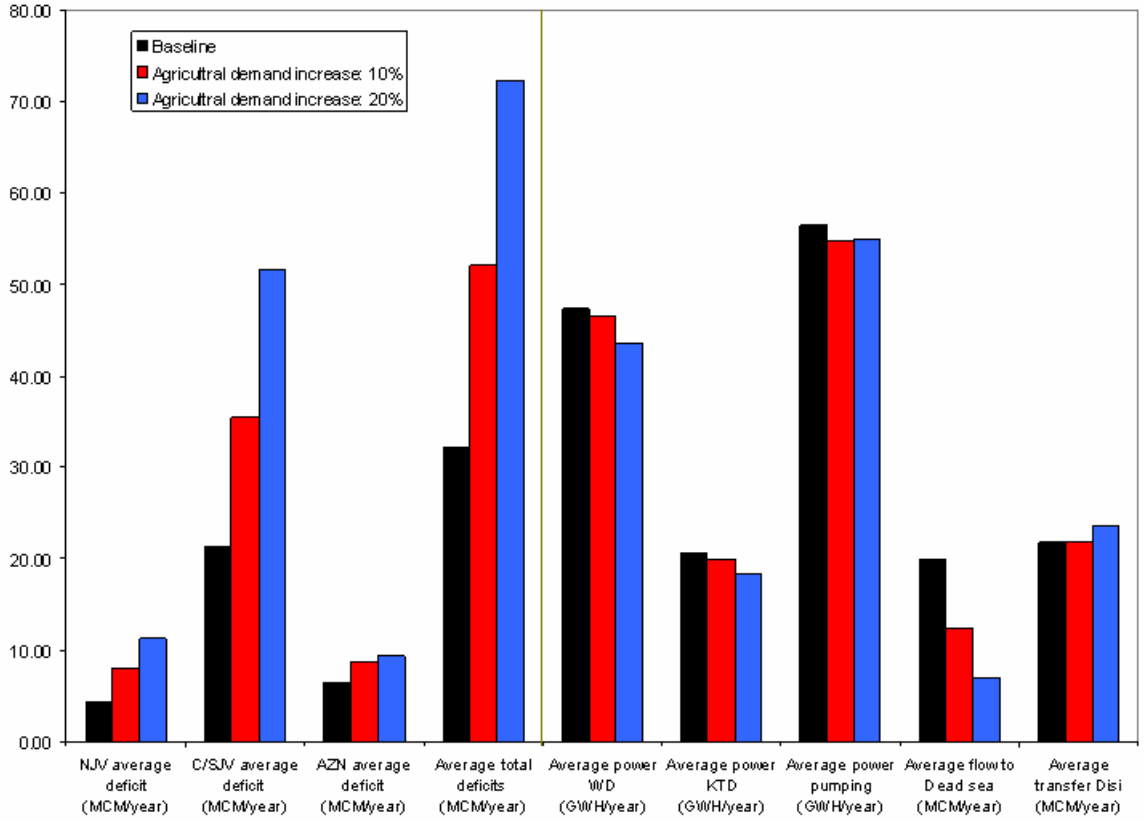

Criteria / Run	NJV average deficit (MCM/year)	C/SJV average deficit (MCM/year)	AZN average deficit (MCM/year)	Average total deficits (MCM/year)	Average power WD (GWH/year)	Average power KTD (GWH/year)	Average power pumping (GWH/year)	Average flow to Dead sea (MCM/year)	Average transfer Disi (MCM/year)
Baseline	4.43	21.32	6.46	32.23	47.26	20.49	56.40	19.91	21.74
10% Agricult. increase	7.98 (63.48%)	35.40 (50.90%)	8.71 (34.76%)	52.09 (52.40%)	46.45 (-1.70%)	19.94 (-2.64%)	54.73 (-2.96%)	12.37 (-37.89%)	21.92 (.80%)
20% Agricult. increase	11.28 (111.82%)	51.59 (101.58%)	9.39 (45.37%)	72.27 (100.01%)	43.61 (-7.71%)	18.31 (-10.60%)	54.84 (-2.77%)	6.97 (-64.99%)	23.51 (8.11%)

quantities in the brackets for the deficit criteria in the North Jordan Valley and Central/South Jordan Valley areas are computed based on Equation 5.2. The remaining quantities between brackets in the table are computed based on Equation 5.1.

Constrained groundwater case:

1. All areas of demand show an increase in deficits as compared to the baseline. Total deficits increase by 34% and 72% respectively for the 10% and 20% increase levels.
2. Energy generation slightly decreases at Al-Wehdah and King Talal dams, at the 20% increase level the reduction with respect to the baseline at King Talal Dam and Al Wehdah Dam is 7% and 11% respectively. Pumping energy is similar to the baseline case, the changes from the constrained baseline are 2.7% and -.21% for the 10% and 20% demand increase levels respectively.
3. The residual flow to the Dead Sea decreases considerably by about 42% and 65% for the 10% and 20% demand increase levels respectively. The Disi Aquifer transfer is similar to the constrained baseline, the changes being -1.1% and .06 % respectively for the 10% and 20% increase levels.

Unconstrained groundwater case:

As expected, the unconstrained case results in less total deficits. However, this occurs at the expense of higher groundwater drawdowns (as shown in Appendix J). Also, the Disi transfer is reduced by 65% as compared to the constrained run.

The comparison of this scenario (unconstrained case) and the unconstrained baseline run lead to similar conclusions.

Perfect Forecast Scenario:

This scenario is designed to quantify the value of perfect forecasts with respect to the previous performance criteria. The detailed results are shown in Appendix K. Tables 5.4.8a and 5.4.8b compare this case with the baseline which uses imperfect forecasts.

Comparison with baseline; Constrained groundwater case:

1. Total deficits are reduced by about 26% compared to the constrained baseline, with the largest decrease occurring in Central and South Jordan Valley where a 32% decrease is reported.
2. Energy generation at Al-Wehdah and King Talal dams are similar to the constrained baseline. However, pumping energy increases by 32% as a result of increased pumping. This happens because in the baseline case the management model meets the groundwater drawdown constraint (10 meters) in a probabilistic sense, meaning that 90% of the drawdown ensemble is less than 10 meters. By contrast, in the perfect forecast case, there is only one drawdown sequence per monitoring location, and the management scheme is only required to keep it less than 10 meters. The Disi transfer is not affected appreciably.
3. The residual flow to the Dead Sea decreases as compared to the constrained baseline case (35%). This occurs because the control model has perfect knowledge of the system inflows and boundary conditions and

Table 5.4.8a: Perfect forecast scenario, constrained GW drawdown

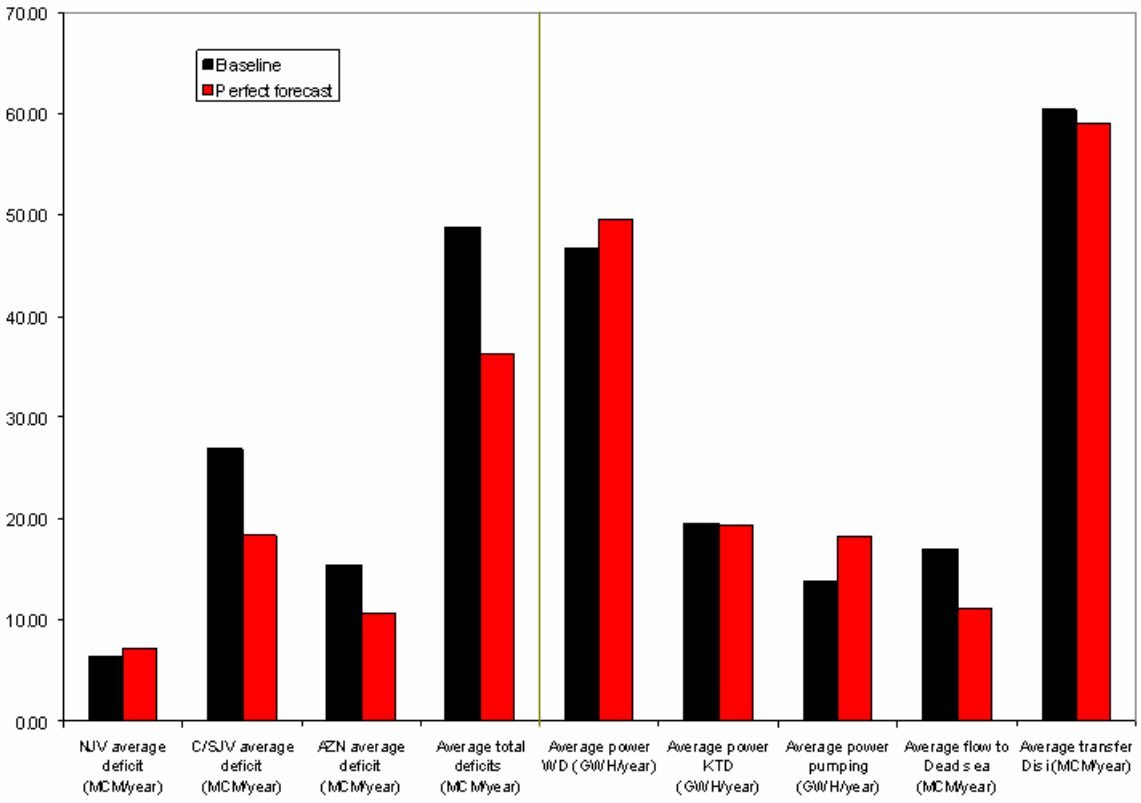

Criteria / Run	NJV average deficit (MCM/year)	C/SJV average deficit (MCM/year)	AZN average deficit (MCM/year)	Average total deficits (MCM/year)	Average power WD (GWH/year)	Average power KTD (GWH/year)	Average power pumping (GWH/year)	Average flow to Dead sea (MCM/year)	Average transfer Disi (MCM/year)
Baseline	6.48	26.92	15.38	48.79	46.73	19.52	13.79	17.0	60.44
Perfect forecast	7.20 (11.08%)	18.38 (-31.7%)	10.71 (-30.38%)	36.29 (-25.60%)	49.54 (6.02%)	19.34 (-.92%)	18.22 (32.18%)	11.13 (-34.67%)	59.04 (-2.3%)

Table 5.4.8b: Perfect forecast scenario, unconstrained GW drawdown

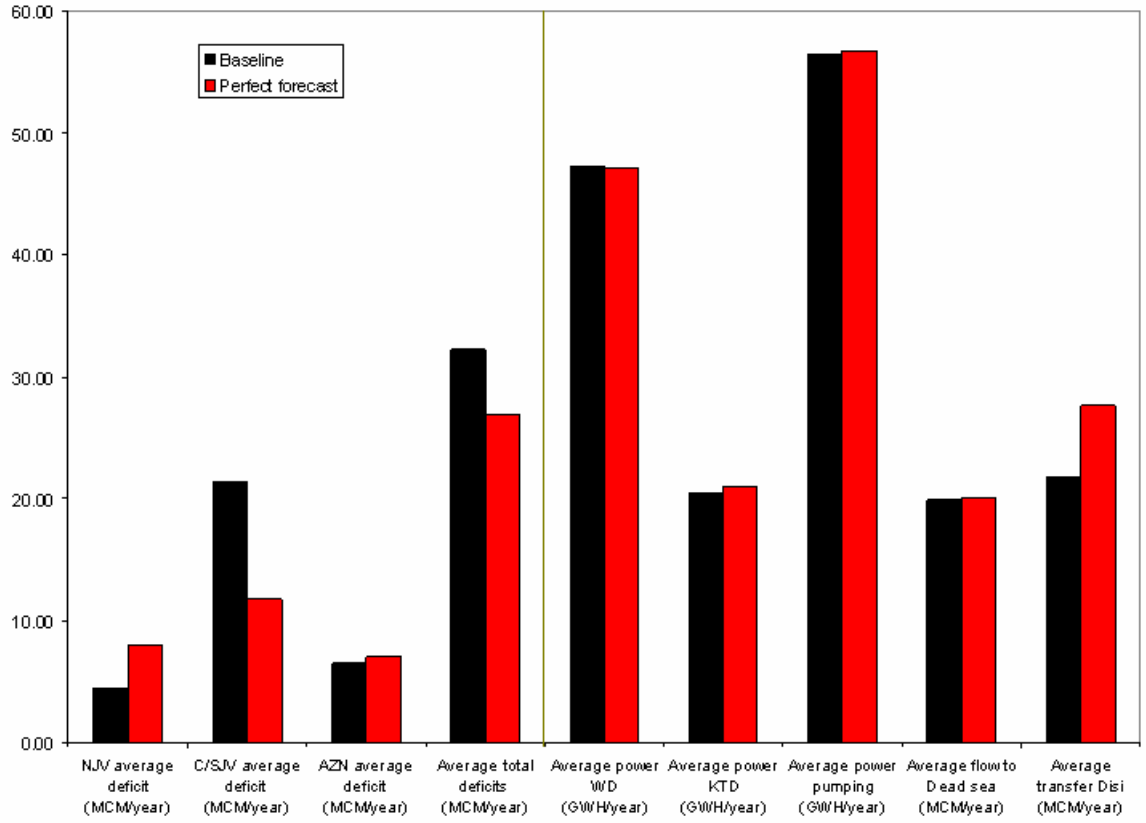

Criteria / Run	NJV average deficit (MCM/year)	C/SJV average deficit (MCM/year)	AZN average deficit (MCM/year)	Average total deficits (MCM/year)	Average power WD (GWH/year)	Average power KTD (GWH/year)	Average power pumping (GWH/year)	Average flow to Dead sea (MCM/year)	Average transfer Disi (MCM/year)
Baseline	4.43	21.32	6.46	32.23	47.26	20.49	56.40	19.91	21.74
Perfect forecast	8.01 (80.57%)	11.74 (-44.92%)	7.04 (9.01%)	26.80 (-16.82%)	47.09 (-.34%)	20.98 (2.42%)	56.73 (.58%)	19.99 (.38%)	27.57 (26.79%)

manages to meet more of the water demands. As a consequence, the residual flow decreases.

Comparison with baseline; Unconstrained groundwater case

Comparing the unconstrained perfect forecast case with the unconstrained baseline case:

1. Total water deficits are reduced by 17% compared to the unconstrained baseline. North Jordan Valley deficits increase by 80% as compared to the baseline. The reason for this is associated with the storage frequency curves of the Karameh Dam. This dam maintains higher storages in the perfect forecast case than in the unconstrained baseline 80% of the time. This happens because the Al-Wehdah Dam releases more in the perfect forecast case to reduce the water deficits of the Central/South Jordan Valley area. However in the long run—since there is not enough water to meet all demands—the total system deficits are reduced, and the deficits of the North Jordan Valley area are increased.
2. Energy generation at Al-Wehdah and King Talal dams is similar to the unconstrained baseline. Pumping energy is slightly different compared to the baseline case, because the system is allowed to pump as much as possible to meet the demands for both cases (in the perfect forecast and in the baseline case).
3. The Disi water transfer to the Amman-Zarqa node is 26% more as compared to the unconstrained baseline case. The reason for this increase is because the Al-Wehdah Dam releases are used to reduce the deficits in the Central/South Jordan Valley and is unable to also meet Amman's demands.

4. The residual flow to the Dead Sea increases slightly (.4%) with respect to the unconstrained baseline case. As noted earlier, however, the constrained perfect forecast case reports a reduction in the residual flow by about 30% with respect to the constrained baseline. This difference between the two ratios is due to the increase of return flow to King Talal Dam from the Amman-Zarqa area. More specifically, the deficits in the Amman-Zarqa area in the unconstrained perfect forecast case are reduced by 52% with respect to the constrained perfect forecast case. More water in the Amman –Zarqa area means more water into King Talal Dam and more water available to become residual flow to the Dead Sea.

Comparison of constrained and unconstrained perfect forecast scenarios:

Comparing the unconstrained perfect forecast case with the constrained perfect forecast case, the following can be noted: The unconstrained case shows a reduction in the resulting deficits with respect to the constrained case. The deficits for the Amman-Zarqa area, Central/South Jordan Valley, and total deficits are reduced by 34% , 36% ,and 26% respectively compared to the constrained case. As expected, the transfer from the Disi Aquifer to Amman is reduced compared to the constrained case (-53%). The residual flow to the Dead Sea increases by 79% due to the increase in the return flow from the Amman-Zarqa area. Aquifer drawdowns also increase in the unconstrained case due to increased pumping. Appendix (K) shows that in the unconstrained case, 80% of the time the maximum drawdown is between than 18.8 and 21.5 meters, while in the constrained case 80% of the time the maximum drawdown is between 9.4 and 10 meters. The constrained and unconstrained perfect forecast scenarios, show the importance of good forecasting in reducing water deficits. In the constrained case, the resulting total

deficits reduction with respect to the constrained baseline case is 26%, while in the unconstrained case the ratio is 17% . This suggests that the importance of forecasting in a constrained system, such as the Jordanian system, increases. Since groundwater drawdowns are constrained, pumping can not be increased arbitrarily to make up for any lost water due to inaccurate forecasting.

Non-conjunctive Management Scenario:

This scenario is designed to assess the benefits of conjunctive water resources management versus separate management of the surface and ground water systems. Detailed graphs of this scenario are shown in Appendix L. Tables 5.4.9a and 5.4.9b compare this case with the baseline.

Constrained groundwater case:

1. Total deficits increase by about 62% with respect to the constrained baseline case. The Amman-Zarqa node deficits increase significantly by 295% with respect to the constrained baseline. North Jordan Valley and Central/South Jordan Valley deficits decrease by about 44% and 45% respectively. This deficit reduction in the North and Central/South Jordan Valleys is due to more water availability to the Jordan Valley to transfer a fixed amount of water to the Amman-Zarqa area
2. Energy generation at the Al Wehdah Dam increases slightly by 4% with respect to the constrained baseline. Energy at the King Talal Dam decreases by about 13% with respect to the constrained baseline due to the reduction in return flow from the Amman-Zarqa area. Pumping energy is slightly increased

Table 5.4.9a: Non-conjunctive management scenario, constrained GW drawdown

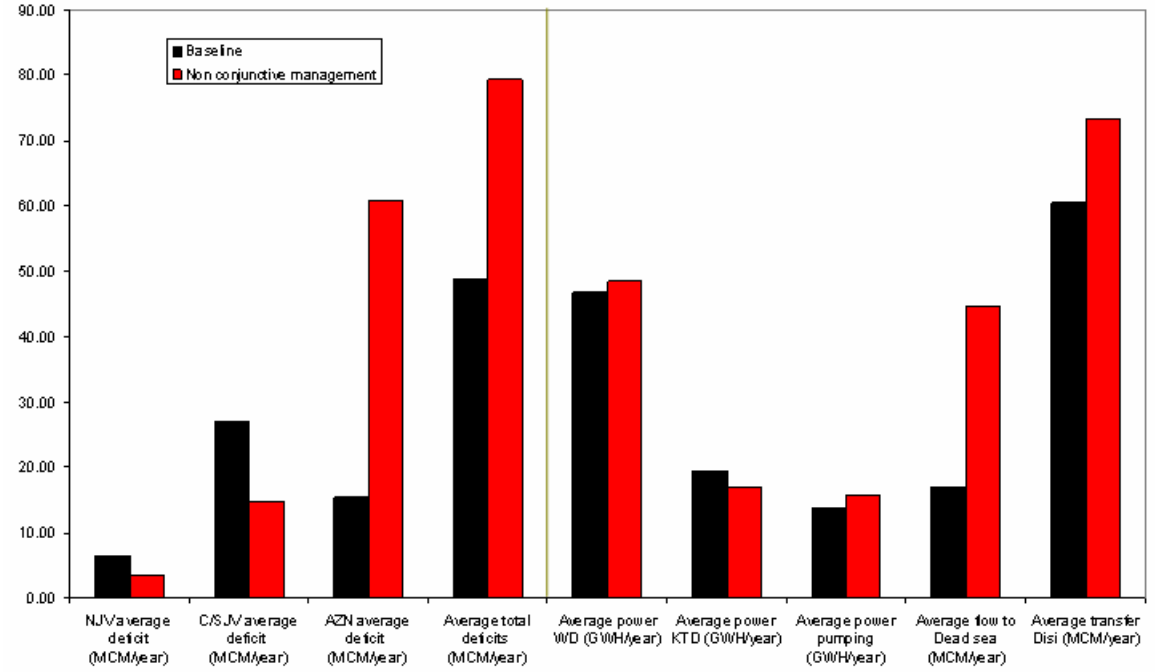

Run \ Criteria	NJV average deficit (MCM/year)	C/SJV average deficit (MCM/year)	AZN average deficit (MCM/year)	Average total deficits (MCM/year)	Average power WD (GWH/year)	Average power KTD (GWH/year)	Average power pumping (GWH/year)	Average flow to Dead sea (MCM/year)	Average transfer Disi (MCM/year)
Baseline	6.48	26.92	15.38	48.79	46.73	19.52	13.79	17.0	60.44
Separate management	3.62 (-44.11%)	14.78 (-45.08%)	60.88 (295.65%)	79.29 (62.51%)	48.48 (3.75%)	16.91 (-13.33%)	15.73 (14.13%)	44.61 (161.75%)	73.28 (21.24%

Table 5.4.9b: Non-conjunctive management scenario, unconstrained GW drawdown

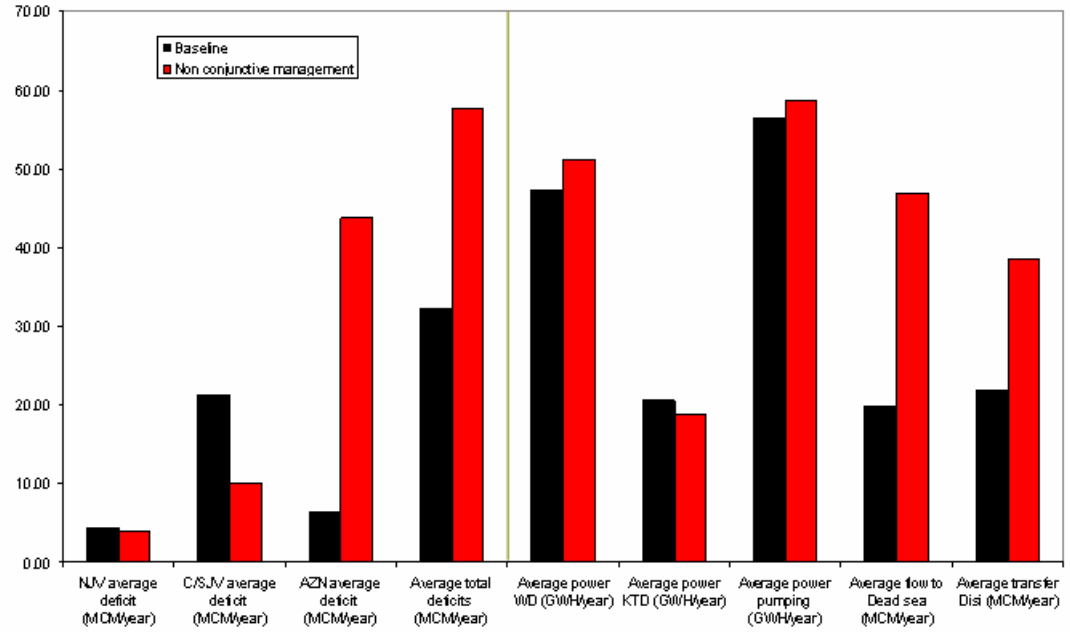

Criteria / 1	NJV average deficit (MCM/year)	C/SJV average deficit (MCM/year)	AZN average deficit (MCM/year)	Average total deficits (MCM/year)	Average power WD (GWH/year)	Average power KTD (GWH/year)	Average power pumping (GWH/year)	Average flow to Dead sea (MCM/year)	Average transfer Disi (MCM/year)
seline	4.43	21.32	6.46	32.23	47.26	20.49	56.40	19.91	21.74
parate management	3.86 (-12.8%)	10.01 (-53.0%)	43.71 (576%)	57.58 (78.6%)	51.09 (8.1%)	18.71 (-8.6%)	58.73 (4.12%)	46.85 (135.2%)	38.66 (77.6%)

by about 14% due to the increase in pumping to make up the difference from the KAC water transfer.

3. The residual flow to the Dead Sea increases with respect to the constrained baseline by 161%.
4. Water transfer from the Disi to the Amman-Zarqa area increases by about 21% with respect to the constrained baseline. This increase implies higher drawdowns in Disi, and higher conveyance costs

Overall, the comparison of the constrained scenarios (conjunctive and non-conjunctive cases) shows that conjunctive management decreases total and individual water deficits and reduces the stresses in the groundwater aquifers. Figure (5.4.1a) depicts the pumping and drawdown frequency curves at two monitoring locations for both cases (conjunctive and non-conjunctive). The figure shows that conjunctive pumping is lower by about 10% than non-conjunctive pumping. As a result, non-conjunctive drawdowns are higher than conjunctive drawdowns nearly throughout the simulation horizon.

Unconstrained groundwater case:

1. Total deficits increase by about 78% with respect to the unconstrained baseline. The Amman-Zarqa node deficits increase by 576% with respect to the unconstrained baseline case.The deficits in the North and Central/South Jordan Valleys decrease by about 13% and 53% respectively.
2. Energy generation at the Al Wehdah Dam increases by 8% with respect to the unconstrained baseline. Energy generation at the King Talal Dam decreases by.

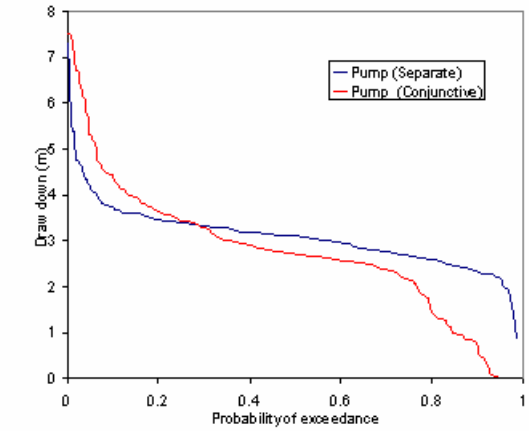

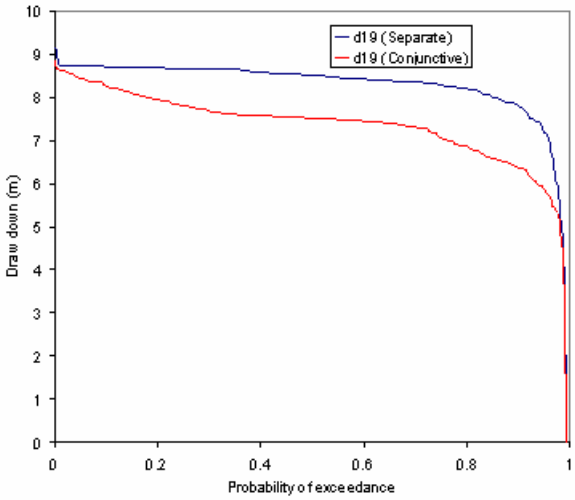

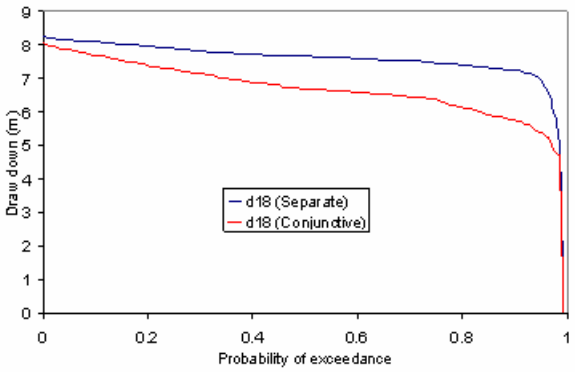

Figure 5.4.1a: Non-conjunctive management scenario, constrained GW drawdown

about 9% relative to the unconstrained baseline. Pumping energy increases by about 4% with respect to the unconstrained baseline.

3. Residual flow to the Dead Sea increases with respect to the unconstrained baseline by about 135%. This change is analogous to the constrained case.
4. The water transfer from the Disi to the Amman-Zarqa area increases by about 77% with respect to the unconstrained baseline.

These comparisons lead demonstrate the value of conjunctive management. As in the constrained case, total and individual deficits decrease and the stresses in the groundwater aquifers are reduced. For example, figure 5.4.1b shows the pumping and drawdown frequency curves at two monitoring locations. The figure shows that non-conjunctive pumping proceeds at full capacity during the entire simulation horizon. By contrast, conjunctive pumping is at capacity only 75% of the time. The resulting drawdowns are higher in the non-conjunctive case.

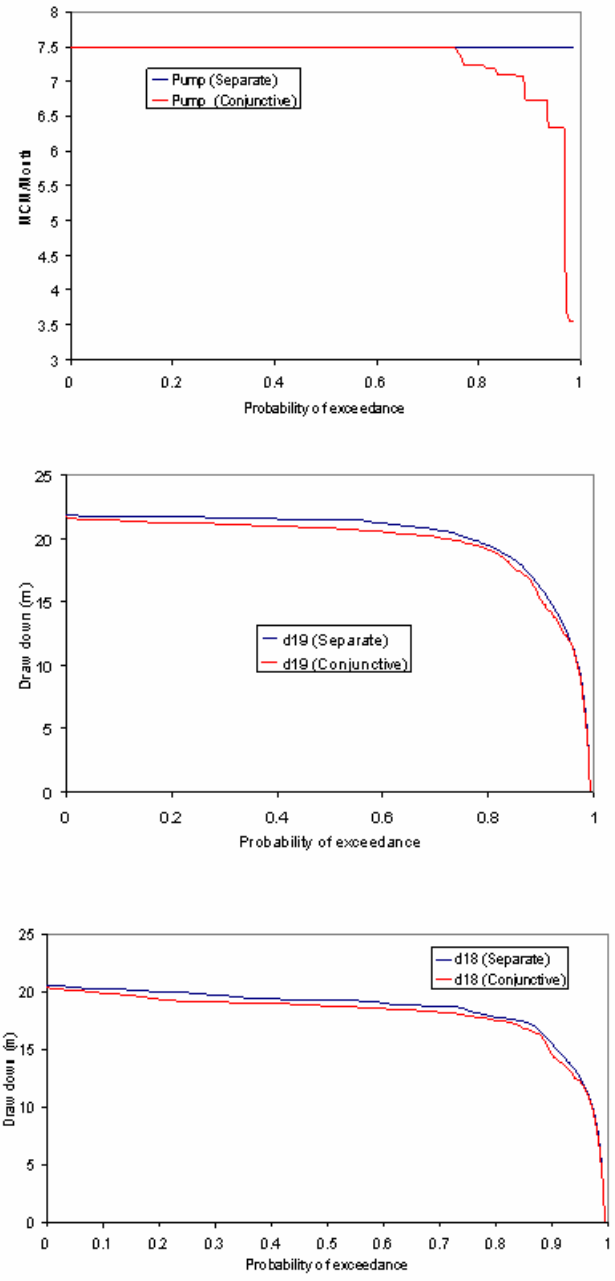

Figure 5.4.1b: Non-conjunctive management scenario, unconstrained GW drawdown

5.5 Conclusions and Recommendations

This chapter describes an assessment for Jordan's water resources using the integrated tools developed in the Thesis. The assessment evaluates the impact of various infrastructure changes of the Jordanian system, water demand increases, improved forecasting methods, and conjunctive versus non-conjunctive management methods. The following general conclusions and recommendations can be drawn from the study:

1. The Al-Wehdah Dam would be a valuable project for Jordan as well as for Syria, and Israel. Specifically for Jordan, this dam would reduce water deficits in all demand areas and would generate energy needed for future economic growth.
2. The Disi Aquifer project also reduces water deficits in the major demand areas. However a more comprehensive assessment is required to assess the impact of the transfer on the Disi Aquifer. Given adequate data, the tools developed herein can be expanded to include a complete model for the Disi aquifer that can assess the project implications for the benefit of Jordan, Israel, and Saudi Arabia, the three stakeholder states. This is especially important as the Disi aquifer contains fossil, unreplenishable water.
3. The Syrian irrigation withdrawals should be the considered and agreed upon by Jordan and Syria in a way that is equitable to both. Once such agreements are in place, the decision tools developed herein can be used to manage the system.
4. The Dead Sea presents environmental concerns that are in competition with the other water demands. This was shown by requiring increased minimum flows in the Dead Sea and assessing the impacts on water deficits. However, in addition to surface inflow, the Dead Sea also receives groundwater contributions. If data are

available, this component should also be modeled, and the management of the Dead Sea should consider both surface and groundwater resources.

5. Increasing demands are shown to increase water resources stresses throughout the system. It is clear that additional water resources, beyond the Disi Aquifer and the Al-Wehdah Dam, would be needed to sustain Jordan's needs. Desalinazation is a definite option, but water transfers from major nearby rivers in the neighboring countries may also be an alternative.
6. Groundwater is over-exploited in Jordan. Continuing to over-draw the aquifers is unsustainable both quantitatively as well qualitatively. Strong evidence of this can be seen in the Wadi Arab area where intense aquifer pumping (to meet demands in north Jordan) has resulted in drying up most of the springs in the area that provide inflow to Wadi Arab (Ministry of Water and Irrigation, report2000). Furthermore, brine water intrusion into the aquifers is wide spread in the country (Ministry of Water and Irrigation, report2000). Brine intrusion occurs because large groundwater drawdowns reverse or change groundwater gradients between aquifers, allowing leakage of brine water. Thus, Jordan must balance the short term need to meet the ever-increasing water demands in the Amman-Zarqa area against the long run threat of serious aquifer deterioration.
7. Improved forecasting in combination with adaptive control methods leads to more effective water resources management. Furthermore, improved forecasting is more critical in constrained systems. Forecasting can be improved by enhancing the existing hydro-climatic measurement network and by developing and using climate and hydrologic models.

8. Conjunctive management of surface water and groundwater resources entails clear advantages over non-conjunctive methods. Conjunctive management facilitates optimal coordination of all surface and ground water resources and reduces water shortages and system stresses. The method developed herein enables conjunctive water resources management for system of realistic complexity and size.

CHAPTER 6

CONCLUSIONS AND FUTURE WORK RECOMMENDATIONS

This dissertation presents new methodologies for conjunctive water resources management, an issue of critical importance worldwide. It is becoming increasingly clear that sustainable management of surface and ground water resources requires integrated management strategies.

The conjunctive management problem is complex for several reasons:

1. Complicated and dimensionally high dynamics that can easily overwhelm the capacity of management methods.
2. Constraints on reservoir storages, groundwater draw downs, and supply/demand targets. These nonlinearities can be nonlinear- nonquadratic terms, which produce complications to the solution if standard control methods are used like linear and nonlinear programming methods.
3. Multiple objectives.
4. Uncertain surface water inflows, groundwater parameters, and boundary conditions.

The research presented herein addresses these challenges, as indicated below.

1. The transfer function approach is employed to represent the groundwater dynamics within the conjunctive management system. Transfer functions were

converted into simpler state space forms that are compatible with the representation of the surface system and the optimization (control) technique used to derive management policies. This approach is shown to be both accurate and at the same time effective in reducing the problem dimensionality.

2. An additional dimensionality reduction approach was developed to represent transfer functions based on a limited set of base locations. The computational savings of this approach are very significant for large systems.
3. Uncertainty characterization was achieved by generating transfer function ensembles that account for parameter uncertainty. This approach is general and can be applied to any groundwater aquifer that has distinct zones of constant (but uncertain) parameters.
4. A conjunctive management optimization procedure was implemented to derive solutions to the integrated problem. This procedure is explicitly stochastic and is able to observe probabilistic constraints. The application for the Jordanian water resources system indicates that the method is reliable and computationally efficient.
5. The application to the Jordanian water resources system demonstrates that conjunctive water resources management is preferable to the separate management of surface and ground water systems. The underlying reason is that conjunctive management leverages all existing opportunities for storing and allocating water be they in the surface or the ground water system. This conclusion is expected to be valid for all systems where surface and ground water

resources are linked by hydraulic means or by the need to meet common objectives.

Two important extensions of the work presented herein are as follows:

1. *Conjunctive management for unconfined and transient aquifer systems:* As indicated earlier, unconfined aquifers can also be modeled under the current framework if their response is linearized around nominal pumping sequences. The effectiveness of this approach would depend on the rate at which aquifer response deviates from the nominal sequences.
2. *Conjunctive management for flow and groundwater solute transport:* This can also be accomplished by the methods developed herein by deriving and using transfer functions characteristic of solute transport processes.

CONJUNCTIVE MANAGEMENT OF SURFACE WATER AND GROUNDWATER RESOURCES

VOLUME II

A Dissertation Presented to
The Academic Faculty

By

Malek Abu Rumman

In Partial Fulfillment of the
Requirements for the Degree
Doctor of Philosophy in Civil Engineering

Georgia Institute of Technology
May 2005

Appendix A

STATE SPACE REPRESENTATION OF TRANSFER FUNCTIONS WITH DIFFERENT COEFFICIENTS RATIOS

APPENDIX A:

TRANSFER FUNCTION STATE SPACE REPRESENTATION

A.1 Overview

In Chapter 3, it was shown that if the ratio between any two consecutive transfer function coefficients is constant (i.e., $\frac{Tp(i)}{Tp(i-1)} = \alpha$, i= 2, 3, …, n), then the drawdown equation at time step (k+1),

$$dp(k+1)= Tp(1)\, P(k) + Tp(2)\, P(k-1) + Tp(3)\, P(k-2)+\ldots+ Tp(n)\, P(k-n+1), \quad (A.1)$$

can be written as

$$dp(k+1)= Tp(1)\, P(k) + \alpha\, Tp(1)\, P(k-1) + \alpha^2\, Tp(1)\, P(k-2)+\ldots+ \alpha^{n-1}\, Tp(1)\, P(k-n+1). \quad (A.2)$$

Rearranging terms, (A.2) yields:

$$dp(k+1)= Tp(1)\, P(k) + \alpha\, \{Tp(1)\, P(k-1)+ \alpha\, Tp(1)\, P(k-2)+\ldots+ \alpha^{n-2}\, Tp(1)\, P(k-n+1)\}. \quad (A.3)$$

In (A.3), the term in the brackets,

$$\{Tp(1)\, P(k-1)+ \alpha\, Tp(1)\, P(k-2)+\ldots+ \alpha^{n-2}\, Tp(1)\, P(k-n+1)\},$$

is the drawdown at time step (k). Thus, equation (A.3) assumes the simpler form

$$dp(k+1)= Tp(1)\, P(k) + \alpha\, dp(k). \quad (A.3a)$$

This appendix generalizes the previous result and shows that if the ratio between two consecutive transfer function coefficients is constant *beyond* a certain time step k > M, then, the transfer function simplifies as follows:

$$dp(k+1)= \lambda_1\, P(k) + \lambda_2\, dp(k) + \lambda_3\, P(k-1) + \lambda_4\, dp(k-1) + \ldots.+ \lambda_{2M-1}\, P(k-M+1) + \lambda_{2M}\, dp(k-M+1) \quad (A.4)$$

where: $\lambda_1, \lambda_2, \ldots, \lambda_{2M-1}$, and λ_{2M} are constants.

A.2 The Case of M=2

This case pertains to a situation where the ratio between any two consecutive coefficients {Tp(k), Tp(k+1)}of the transfer function is equal to a constant α for $k > 2$, while the ratio of the first two coefficients {Tp(2), Tp(1)} is appreciably different and equal to $\alpha + \Delta\alpha 1$:

$$\frac{Tp(2)}{Tp(1)} = \alpha + \Delta\alpha 1,\ \frac{Tp(3)}{Tp(2)} = \alpha,\quad \frac{Tp(4)}{Tp(3)} = \alpha,\ \ldots \frac{Tp(n)}{Tp(n-1)} = \alpha\ . \tag{A.5}$$

As a result of (A.5),

$Tp(2)= (\alpha + \Delta\alpha 1)\ Tp(1)$,

$Tp(3)= \alpha\ Tp(2)$,

$Tp(4)= \alpha\ Tp(3)$,

⋮

$Tp(n)= \alpha\ Tp(n-1)$.

Substituting recursively,

$Tp(2)= (\alpha + \Delta\alpha 1)\ Tp(1)$,

$Tp(3)= (\alpha^2 + \alpha\ \Delta\alpha 1\ )\ Tp(1)$,

$Tp(4)= (\alpha^3 + \alpha^2\ \Delta\alpha 1\ )\ Tp(1)$,

⋮

$$Tp(n)= (\alpha^{n-1} + \alpha^{n-2}\ \Delta\alpha 1\ )\ Tp(1). \tag{A.6}$$

Therefore, the drawdown at time step (k+1) can be written as follows:

$$dp(k+1)= Tp(1)\ P(k) + (\alpha + \Delta\alpha 1)\ Tp(1)\ P(k-1) + (\alpha^2 + \alpha\ \Delta\alpha 1\ )\ Tp(1)\ P(k-2) + (\alpha^3 + \alpha^2\ \Delta\alpha 1\ )\ Tp(1)\ P(k-3) + \ldots..+ (\alpha^{n-1} + \alpha^{n-2}\ \Delta\alpha 1\ )\ T(1)\ P(k-n+1) \tag{A.7}$$

Rearrange terms in (A.7),

$$dp(k+1)= Tp(1)\,P(k) + \alpha\,Tp(1)\,P(k-1) + \alpha^2\,Tp(1)\,P(k-2) + \alpha^3\,Tp(1)\,P(k-3) + \ldots.. + \alpha^{n-1}\,Tp(1)\,P(k-n+1) +$$

$$\Delta\alpha 1\,Tp(1)\,P(k-1) + \alpha\,\Delta\alpha 1\,Tp(1)\,P(k-2) + \alpha^2\,\Delta\alpha\,Tp(1)\,P(k-3) + \ldots.. + \alpha^{n-2}\,\Delta\alpha 1\,Tp(1)\,P(k-n+1). \quad (A.8)$$

Grouping together terms with common powers of α and $\alpha\,\Delta\alpha 1$, yields:

$$dp(k+1)= Tp(1)\,P(k) + \alpha\,\{Tp(1)\,P(k-1) + \alpha\,Tp(1)\,P(k-2) + \alpha^2\,Tp(1)\,P(k-3) + \ldots.. + \alpha^{n-2}\,Tp(1)\,P(k-n+1)\} + \Delta\alpha 1\,Tp(1)\,P(k-1) + \alpha\,\Delta\alpha 1\{Tp(1)\,P(k-2) + \alpha\,Tp(1)\,P(k-3) + \ldots.. + \alpha^{n-3}\,Tp(1)\,P(k-n+1)\} \quad (A.9)$$

Consider the terms in the brackets, namely,

$\{Tp(1)\,P(k-1) + \alpha\,Tp(1)\,P(k-2) + \alpha^2\,Tp(1)\,P(k-3) + \ldots.. + \alpha^{n-2}\,T(1)\,P(k-n+1)\}$ and

$\{Tp(1)\,P(k-2) + \alpha\,Tp(1)\,P(k-3) + \ldots.. + \alpha^{n-3}\,T(1)\,P(k-n+1)\}$.

Since, the first bracket represents the drawdown at time step (k), and the second represents the drawdown at time step (k-1), the equation (A.9) simplifies to

$$dp(k+1)= Tp(1)\,P(k) + \alpha\,dp(k) + \Delta\alpha 1\,Tp(1)\,P(k-1) + \alpha\,\Delta\alpha 1\,dp(k-1). \quad (A.10)$$

Thus, the original drawdown equation is shown to have the equivalent form

$$dp(k+1)= \lambda_1\,P(k) + \lambda_2\,dp(k) + \lambda_3\,P(k-1) + \lambda_4\,dp(k-1) \quad (A.10a)$$

where λ_1, λ_2, λ_3, and λ_4 are constants.

A.3 The Case of M=3, M=4, …

This case pertains to a situation where the ratio between any two consecutive coefficients $\{Tp(k), Tp(k+1)\}$ of the transfer function is equal to a constant α for $k > 3$,

while the ratios of the first two coefficient pairs {Tp(2), Tp(1)} and {Tp(3), Tp(2)} are respectively equal to $\alpha + \Delta\alpha 1$ and $\alpha + \Delta\alpha 2$. Namely,

$$\frac{Tp(2)}{Tp(1)} = \alpha + \Delta\alpha 1,\ \frac{Tp(3)}{Tp(2)} = \alpha + \Delta\alpha 2,\ \frac{Tp(4)}{Tp(3)} = \alpha,\ \ldots,\ \frac{Tp(n)}{Tp(n-1)} = \alpha. \qquad (A.11)$$

Relationships (A.11) imply

$Tp(2)= (\alpha + \Delta\alpha 1)\ Tp(1)$,

$Tp(3)= (\alpha+ \Delta\alpha 2\ )\ Tp(2)$,

$Tp(4)= \alpha\ Tp(3)$,

⋮

$Tp(n)= \alpha\ Tp(n-1)$.

Or, after substitution,

$Tp(2)= (\alpha + \Delta\alpha 1)\ Tp(1)$,

$Tp(3)= (\alpha^2 + \alpha\ (\Delta\alpha 1 + \Delta\alpha 2\ ) + \Delta\alpha 1\ \Delta\alpha 2)\ Tp(1)$,

$Tp(4)= (\alpha^3 + \alpha^2\ (\Delta\alpha 1 + \Delta\alpha 2\ ) + \alpha\ \Delta\alpha 1\ \Delta\alpha 2)\ Tp(1)$,

⋮

$Tp(n)= (\alpha^{n-1} + 2\ \alpha^{n-2}\ (\Delta\alpha 1 + \Delta\alpha 2) + \alpha^{n-3}\ \Delta\alpha 1\ \Delta\alpha 2)\ Tp(1)$. (A.12)

Substituting equation (A.12) in (A.1) yields:

$dp(k+1)= Tp(1)\ P(k) + (\alpha + \Delta\alpha 1)\ Tp(1)\ P(k-1) + (\alpha^2 + \alpha\ (\Delta\alpha 1 + \Delta\alpha 2\ ) + \Delta\alpha 1\ \Delta\alpha 2)$

$Tp(1)\ P(k-2) + (\alpha^3 + \alpha^2\ (\Delta\alpha 1 + \Delta\alpha 2) + \alpha\ \Delta\alpha 1\ \Delta\alpha 2)\ Tp(1)\ P(k-3) + \ldots + (\alpha^{n-1} + \alpha^{n-2}\ (\Delta\alpha 1$

$+ \Delta\alpha 2) + \alpha^{n-3}\ \Delta\alpha 1\ \Delta\alpha 2)\ T(1)\ P(n+1)$ (A.13)

Rearranging,

$dp(k+1)= Tp(1)\ P(k) + \alpha\ Tp(1)\ P(k-1) + \alpha^2\ Tp(1)\ P(k-2) + \alpha^3\ Tp(1)\ P(k-3) + \ldots + \alpha^{n-1}$

$T(1)P(n+1)$ +

$\Delta\alpha 1\ Tp(1)\ P(k-1) + \alpha\ (\Delta\alpha 1 + \Delta\alpha 2\ )\ Tp(1)\ P(k-2) + \alpha^2\ (\Delta\alpha 1 + \Delta\alpha 2\ )\ Tp(1)\ P(k-3) +$

$\ldots + \alpha^{n-2}\ (\Delta\alpha 1 + \Delta\alpha 2\ )\ T(1)\ P(n+1)\ +$

$\Delta\alpha 1\ \Delta\alpha 2\ Tp(1)\ P(k-2) + \alpha\ \Delta\alpha 1\ \Delta\alpha 2\ Tp(1)\ P(k-3) + \alpha^2\ \Delta\alpha 1\ \Delta\alpha 2\ Tp(1)\ P(k-4)\ + \ldots$

$+ \alpha^{n-3}\ \Delta\alpha 1\ \Delta\alpha 2\ T(1)\ P(n+1)$ (A.14)

Grouping terms with common powers of α, $\alpha\ (\Delta\alpha 1 + \Delta\alpha 2)$, and $\alpha\ \Delta\alpha 1\ \Delta\alpha 2$ yields

$dp(k+1) = Tp(1)\ P(k) + \alpha\ \{Tp(1)\ P(k-1) + \alpha\ Tp(1)\ P(k-2) + \alpha^2\ Tp(1)\ P(k-3) + \ldots + \alpha^{n-2}$

$T(1)P(kn+1)\}\ +\ \Delta\alpha 1\ Tp(1)\ P(k-1) + \alpha\ (\Delta\alpha 1 + \Delta\alpha 2\ )\ \{\ Tp(1)\ P(k-2) + \alpha\ Tp(1)\ P(k-3) +$

$\ldots + \alpha^{n-3}\ T(1)\ P(n+1)\} + \Delta\alpha 1\ \Delta\alpha 2\ Tp(1)\ P(k-2) + \alpha\ \Delta\alpha 1\ \Delta\alpha 2\ \{Tp(1)\ P(k-3) + \alpha\ Tp(1)$

$P(k-4)\ + \ldots + \alpha^{n-4}\ T(1)\ P(n+1)\}$ (A.15)

In (A.15), the bracket

$\{Tp(1)\ P(k-1) + \alpha\ Tp(1)\ P(k-2) + \alpha^2\ Tp(1)\ P(k-3) + \ldots + \alpha^{n-2}\ T(1)\ P(n+1)\}$ represents the drawdown at time step (k), the bracket

$\{Tp(1)\ P(k-2) + \alpha\ Tp(1)\ P(k-3) + \ldots + \alpha^{n-3}\ T(1)P(n+1)\}$ represents the drawdown at time step (k-1), and the bracket

$\{Tp(1)\ P(k-3) + \alpha\ Tp(1)\ P(k-4)\ + \ldots + \alpha^{n-4}\ T(1)P(n+1)\}$ represents the drawdown at time step (k-2).

Using these associations, (A.15) yields:

$dp(k+1) = Tp(1)\ P(k) + \alpha\ dp(k) +\ \Delta\alpha 1\ Tp(1)\ P(k-1) + \alpha\ (\Delta\alpha 1 + \Delta\alpha 2\ )\ dp(k-1) +\ \Delta\alpha 1$

$\Delta\alpha 2\ Tp(1)\ P(k-2) +\ \alpha\ \Delta\alpha 1\ \Delta\alpha 2\ dp(k-2).$ (A.16)

Thus, equation (A.16) can be written as:

$dp(k+1) = \lambda_1\ P(k) + \lambda_2\ dp(k) + \lambda_3\ P(k-1) + \lambda_4\ dp(k-1) + \lambda_5\ P(k-2) +\ \lambda_6\ dp(k-2).$ (A.16a)

where λ_1, λ_2, λ_3, λ_4, λ_5, and λ_6 are constants.

Repeating the previous analysis in the case where M=4, namely when

$$\frac{Tp(2)}{Tp(1)} = \alpha + \Delta\alpha 1,\ \frac{Tp(3)}{Tp(2)} = \alpha + \Delta\alpha 2,\ \frac{Tp(4)}{Tp(3)} = \alpha + \Delta\alpha 3,$$

$$\frac{Tp(5)}{Tp(4)} = \alpha,\ \ldots,\ \frac{Tp(n)}{Tp(n-1)} = \alpha, \qquad \text{(A.17)}$$

leads to the following representation of the drawdown at time step (k+1):

$$dp(k+1) = \lambda 1\, P(k) + \lambda 2\, dp(k) + \lambda 3\, P(k-1) + \lambda 4\, dp(k-1) + \lambda 5\, P(k-2) + \lambda 6\, dp(k-2) + \lambda 7\, P(k-3) + \lambda 8\, dp(k-3) \qquad \text{(A.18)}$$

where λ_1, λ_2, λ_3, λ_4, λ_5, λ_6, λ_7, and λ_8 are constants and equal to

$\lambda_1 = Tp(1)$,

$\lambda_2 = \alpha$,

$\lambda_3 = \Delta\alpha 1\ Tp(1)$,

$\lambda_4 = \alpha\ (\Delta\alpha 1 + \Delta\alpha 2 + \Delta\alpha 3)\ Tp(1)$,

$\lambda_5 = (\Delta\alpha 1\ \Delta\alpha 2 - \alpha\ \Delta\alpha 3)\ Tp(1)$,

$\lambda_6 = \alpha\ (\Delta\alpha 1\ \Delta\alpha 2 + \Delta\alpha 3\ \Delta\alpha 1 + \Delta\alpha 3\ \Delta\alpha 2)\ Tp(1)$,

$\lambda_7 = \Delta\alpha 3\ \Delta\alpha 2\ \Delta\alpha 1\ Tp(1)$, and

$\lambda_8 = \alpha\ (\Delta\alpha 3\ \Delta\alpha 2\ \Delta\alpha 1)\ Tp(1)$.

Thus, in the general case where the ratio of two consecutive transfer function coefficients $\{Tp(k+1), Tp(k)\}$ is constant for $k > M$, it can be stated that the drawdown equation (A.1) assumes the following equivalent form:

$$dp(k+1) = \lambda_1 P(k) + \lambda_2 dp(k) + \lambda_3 P(k-1) + \lambda_4 dp(k-1) + \ldots + \lambda_{2M-1} P(k-M+1) + \lambda_{2M} dp(k-M+1) \qquad \text{(A.19)}$$

where $\lambda_1, \lambda_2, \ldots, \lambda_{2M-1}$, and λ_{2M} are constant coefficients.

APPENDIX B

ELQG CONTROL METHOD

APPENDIX B:

EXTENDED LINEAR QUADRATIC GAUSSIAN (ELQG) CONTROL METHOD

This appendix describes the ELQG control algorithm used to solve the conjunctive management problem formulated in Chapter 4. The method was developed by A.P. Georgakakos (1984, 1987, 1988, and 1989); the description herein follows A.P Georgakakos 1988:

1. Let $\{u^{nom}(n), n = k, k+1,\ldots, N-1\}$ be a nominal control sequence and $\{\overline{s^{nom}}(n), n = k, k+1,\ldots, N-1\}$ the associated (through the system dynamics) mean state sequence. Generate a second order Taylor expansion of the cost terms g[ ] around the previous control and state sequences. Denote $N_s(n)$, $N_u(n)$, $N_{ss}(n)$, $N_{uu}(n)$, $N_{us}(n)$, n= k, k+1, …, N-1, the first and second order coefficient of this Taylor expansion.

2. Compute the gradient vector $\partial J^{old}/\partial u(n)$, n = k, …, N-1, and Hessian matrices $\partial^2 J^{old} / \partial u(n)\, \partial u(n)$, n = k, …, N-1, of the performance index around the nominal control sequence by the following recursive procedure (backward time pass):

$P(N)= N_s(N)$

$P(n)= N_s(n) + A^T(n)P(n+1)$

$$\partial J^{old}/ \partial u(n) = N_u(n) + B^T(n)P(n+1), \qquad \text{(B.1)}$$

$n=N-1, N-2,\ldots., k$

$H(N)= N_{ss}(N)$

$H(N)= N_{ss}(n) + A^T(n)H(n+1)\, A(n)$

$$\{\partial^2 J^{old} / \partial u(n)\, \partial u(n)\}= N_{uu}(n) + B^T(n)H(n+1)\, B(n) \qquad \text{(B.2)}$$

n=N-1, N-2,….,k

3. Determine the binding control constraint set U^+ :

Compute $u_j'(n) = u_j^{nom}(n) - [\{\partial^2 J^{old}/ \partial u(n)\, \partial u(n)]^{-1}\ [\partial Jold/ \partial u(n)]$ (B.3)

j=1,…., M (dimension of the control vector), and n = k, …, N-1.

The set of binding control variables U^+ includes all variables $u_j(n)$ for which

$u_j^{min}(n) \le u_j'(n)$, $u_j^{nom}(n) \le u_j^{min}(n) + \varepsilon$, or

$u_j^{max}(n) - \varepsilon \le u_j'(n)$, $u_j^{nom}(n) \le u_j^{max}(n)$ (B.4)

where ε is a small positive number.

4. Compute the projected Newton direction d(n), n = k, …, N-1, for the nonbinding control elements as follows:

4.1 Determine the sequence of positive semi-definite matrices K(n), n = k, …, N, and vectors λ(n), n = k, …, N-1, by the following recursive computation:

$K(N)= N_{ss}(n)$

$K(n)= N_{ss}(n) + A^T(n)K(n+1)\ A(n) - [\{B^T(n)K(n+1)\ A(n) + N_{us}(n)\}^r]^T$

$[\{B^T(n)K(n+1)\ B(n) + N_{uu}(n)\}^{rc}]^{-1}\ [\{B^T(n)K(n+1)\ A(n) + N_{us}(n)\}^r]$

(B.5)

n = N-1, N-2,…., k,

and

$\lambda(N) = N_s(N)$

$\lambda(n) = N_s(n) + A^T(n)\ \lambda\ (n+1) - [\{B^T(n)K(n+1)\ A(n) + N_{us}(n)\}^r]^T\ [\{B^T(n)K(n+1)$

$B(n) + N_{uu}(n)\}^{rc}]^{-1}\ [\{B^T(n)\ \lambda\ (n+1) + N_u(n)\}^r]$

(B.6)

n= N-1, N-2, …., k,

4.2 Compute the projected Newton optimization direction from

$d(n)= -D(n)[L(n)\,\delta s'(n) + \Lambda(n)]$, $n=k,k+1,\ldots, N-1$,

where $D(n)= [BT(n)K(n+1)B(n) + N_{uu}(n)\}^{rc}]^{-1}$,

$L(n)= [\{B^T(n)\,K(n+1)\,A(n) + N_{us}(n)\}^{r}]$,

$\Lambda(n)= [\{B^T(n)\,\lambda\,(n+1) + N_{u}(n)\}^{r}]$,

$\delta s'(n+1) =A(n)\,\delta s'(n)+ B(n)d'(n)$, $n = k, k+1, \ldots, N-1$, $\delta s'(k)=0$.

(B.7)

In the last equation, $d'(n)$ is the direction $d(n)$ augmented with zeros at the positions of the binding control elements. The notation $(x)^r$ or $(x)^{rc}$ respectively indicates that the rows or the rows and columns of matrix x corresponding to binding control elements have been deleted. (x may be a vector).

5. Compute the direction $dj^+(n)$ for the binding control elements from

$$dj^+(n)= [\{\partial^2 J^{old}/ \partial u(n)\,\partial u(n)]^{-1}\ [\partial\, Jold/ \partial u(n)] \qquad (B.8)$$

Use the modified Armijo Rule to select the step size α as follows:

$\alpha = \beta^m$, where $\beta \in (0,1)$,

and m is the smallest non-negative integer for which

$$Jold- Jnew \geq -\sigma\{\ \beta^m\ \sum_n [(\partial\, Jold/ \partial u(n))^r]^T\, d(n) + \sum_n \sum_{j \in U+} [(\partial\, Jold/ \partial u_j(n))]^T\, [dj^+(n)]^+ \qquad (B.9)$$

In the above equation, $[dj^+(n)]^+$ is equal to $dj^+(n)$ if the resulting control variables, $u_j'(n) = u_j^{nom}(n) + \alpha\, dj^+(n)$, are feasible, or equal to the distance of $u_j^{nom}(n)$ from the violated bound otherwise.

6. Compute the new nominal control sequence based on the following iteration:

$u_j(n) = u_j^{nom}(n) + \alpha\, dj^+(n)$, if the control is not binding, and

$u_j(n) = u_j^{nom}(n) + \alpha\ [dj^+(n)]^+$, if the control is binding.

7. Recompute the nominal control and mean state sequences and repeat Steps 1 through 6. Terminate if the criterion

$$w = \{ \sum_{n,j} [u_j^{nom}(n) - \{u_j^{nom}(n) - [\{\partial^2 J^{old} / \partial u(n)\ \partial u(n)]^{-1}\ [\partial Jold / \partial u(n)]\}^+]^2 \}^{.5} \quad \text{(B.10)}$$

is negligibly small.

APPENDIX C

THE ANALOG ESP FORECAST MODEL

APPENDIX C:

THE HISTORICAL ANALOG FORECASTING MODEL

Inflow and groundwater input forecasts are obtained by the Historical Analog forecasting model (Yao and Georgakakos, 2001). This model produces forecasts based on information derived from the historical record. The underlying idea is that similar climatic and hydrologic conditions are followed by similar conditions for some time in the future. More specifically, streamflows and other hydrologic quantities materialize as a result of a nonlinear hydro-climatic process orbiting around an unknown attractor set. Although this set is not easily definable, this premise leads to the following conjecture: If the process is presently at a certain point in its orbit, its position in the near future can potentially be inferred by observing the movement it experienced on similar occasions in the past.

For example, streamflows are the result of the rainfall-runoff process, and the values they assume over a certain time period depend on various hydro-climatic factors including watershed rainfall, temperature, and soil moisture conditions. Thus, if the climate-watershed system tends to revisit the neighborhood of certain conditions (states), it should also tend to generate similar streamflow patterns.

In keeping with the above, the historical analog model "searches" the historical record and selects several inflow traces which, at some time in the past, have started from conditions similar to those of the current inflow sequence. Each one of these traces is a

possible future realization of the inflow process and all together constitute a set on which to base probabilistic, multi-lead forecasts.

Thus, suppose that the present time is April 1st, and the previous days' inflows were W_1, W_2,...,W_n , where subscript "1" represents the last day in March, "2" the day before that, etc., and n is a parameter related to the process memory. Namely, [W_1, W_2,...,W_n] is the most recent inflow sequence to April 1st. The next step in the implementation of the historical analog model is to retrieve all inflow traces of the same month and date as the W_1, W_2,...,W_n from the historical record and compute their Euclidian distance, E_j , from the current sequence:

$E_j = [(W_1 - W_{1,j})+ (W_2 - W_{2,j})\ldots+ (W_n - W_{n,j})]^{0.5}$, j=1, 2, ….., m,

where $W_{i,j}$ is the historical inflow of year j at the same calendar date as W_i; m is the number of years in the historical record; and E_j measures the proximity of [$W_{i,j}$, i=1, 2, ..., n] to the most recent inflows [W_i , i=1, 2, ..., n]. A small value of E_j implies that the $W_{i,j}$ sequence is in the neighborhood of W_i. The inflows following $W_{i,j}$ are known (as part of the historical record) and can be used as the forecasts of the inflows following W_i. To generate multiple forecast traces, one can rank the E_j's from smallest to largest, select the top portion of the ranked list, and use the corresponding historical inflows following $W_{i,j}$ as possible future inflow realizations. It is noted that several other ways may be used to measure the proximity of the historical to the most recent streamflow sequences. The reasons for using this particular scheme are that it is easy to implement and it has been effective in several other applications.

APPENDIX D

BASELINE CASE

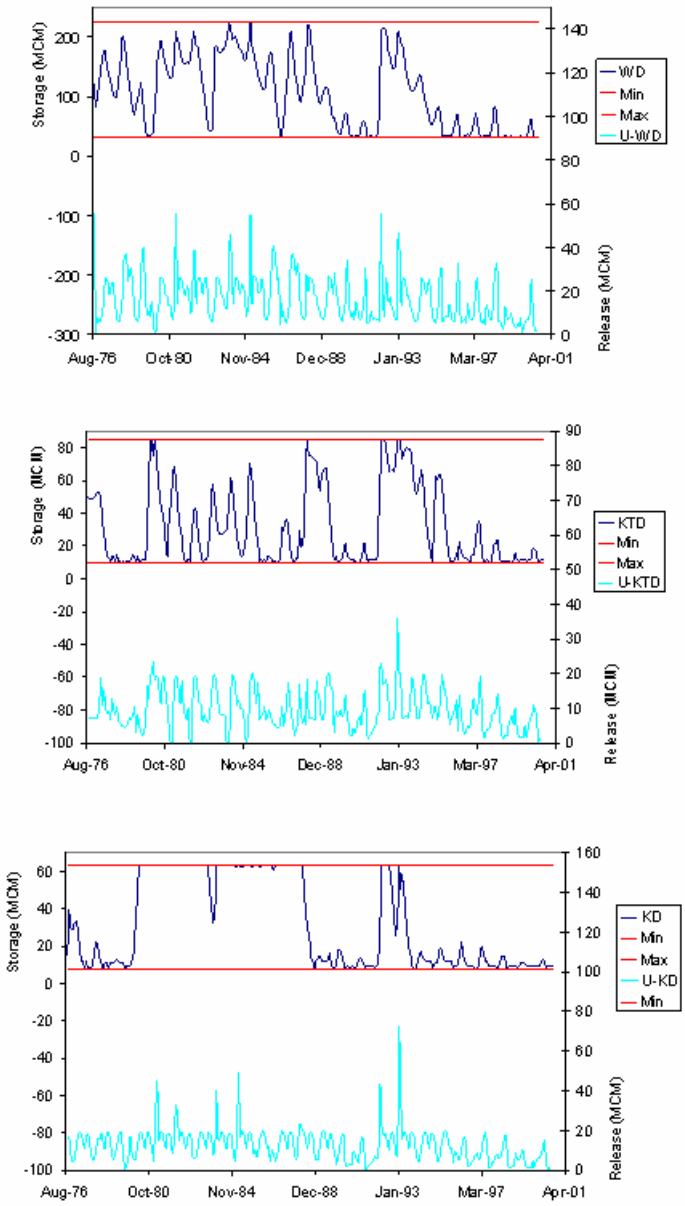

Figure D.1: Assessment model, baseline case, constrained GW drawdown, WD, KTD, and KD storage and release sequences

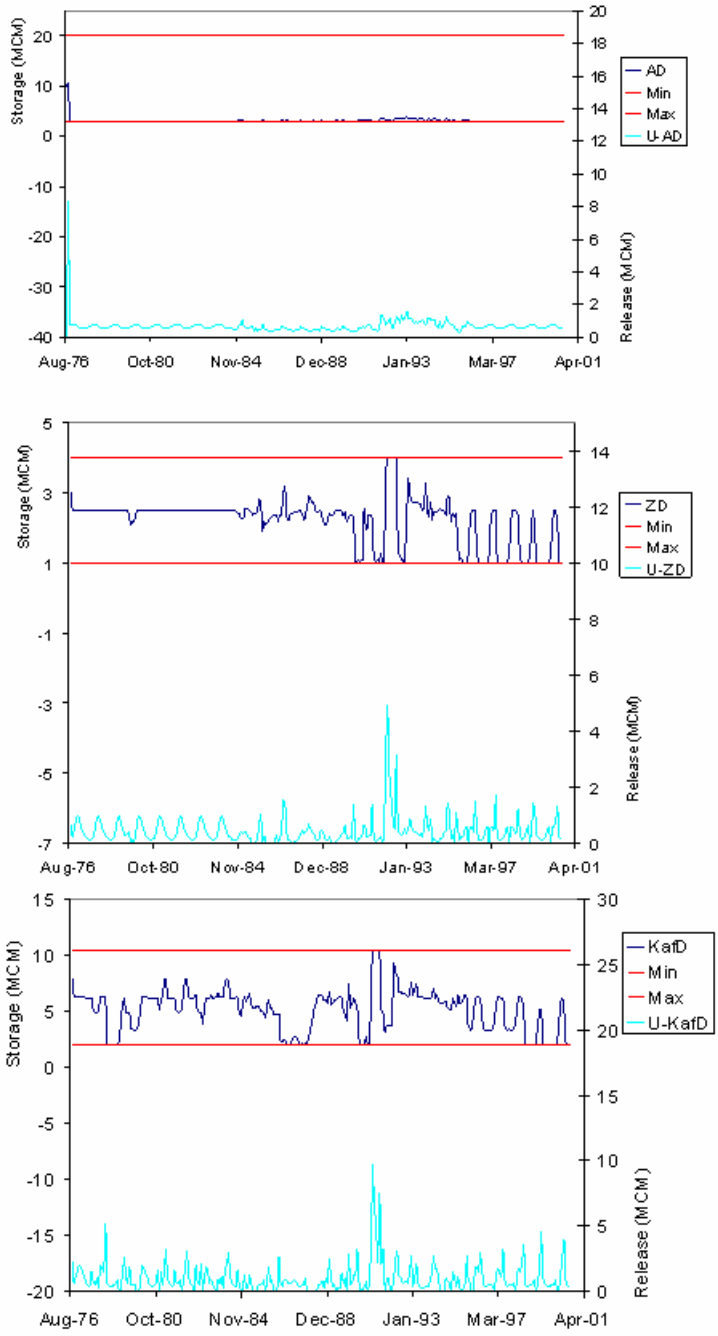

Figure D.2: Assessment model, baseline case, constrained GW drawdown, AD, ZD, and KafD storage and release sequences

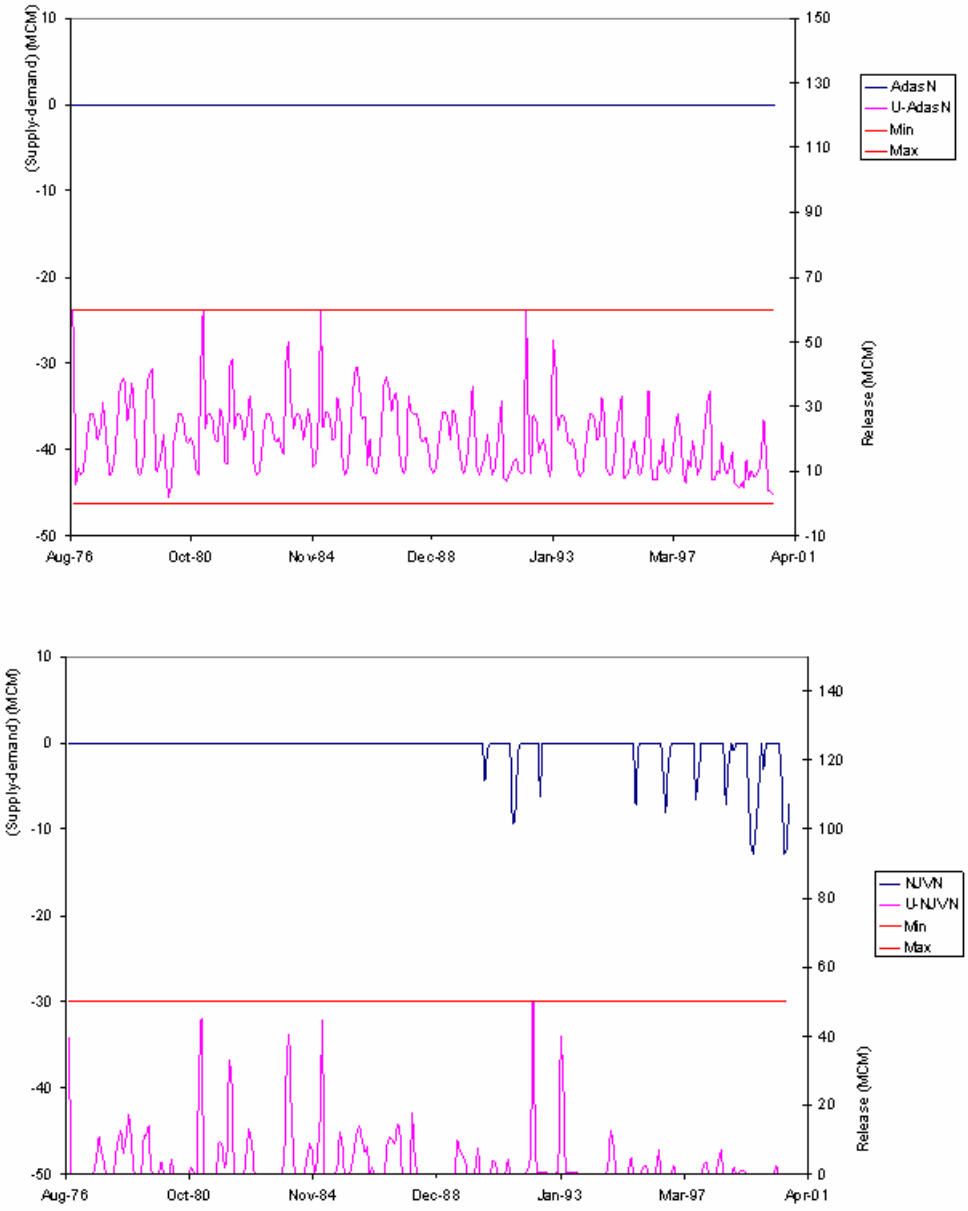

Figure D.3: Assessment model, baseline case, constrained GW drawdown, monthly water deficit and release sequences at Adasiya and North Jordan Valley nodes

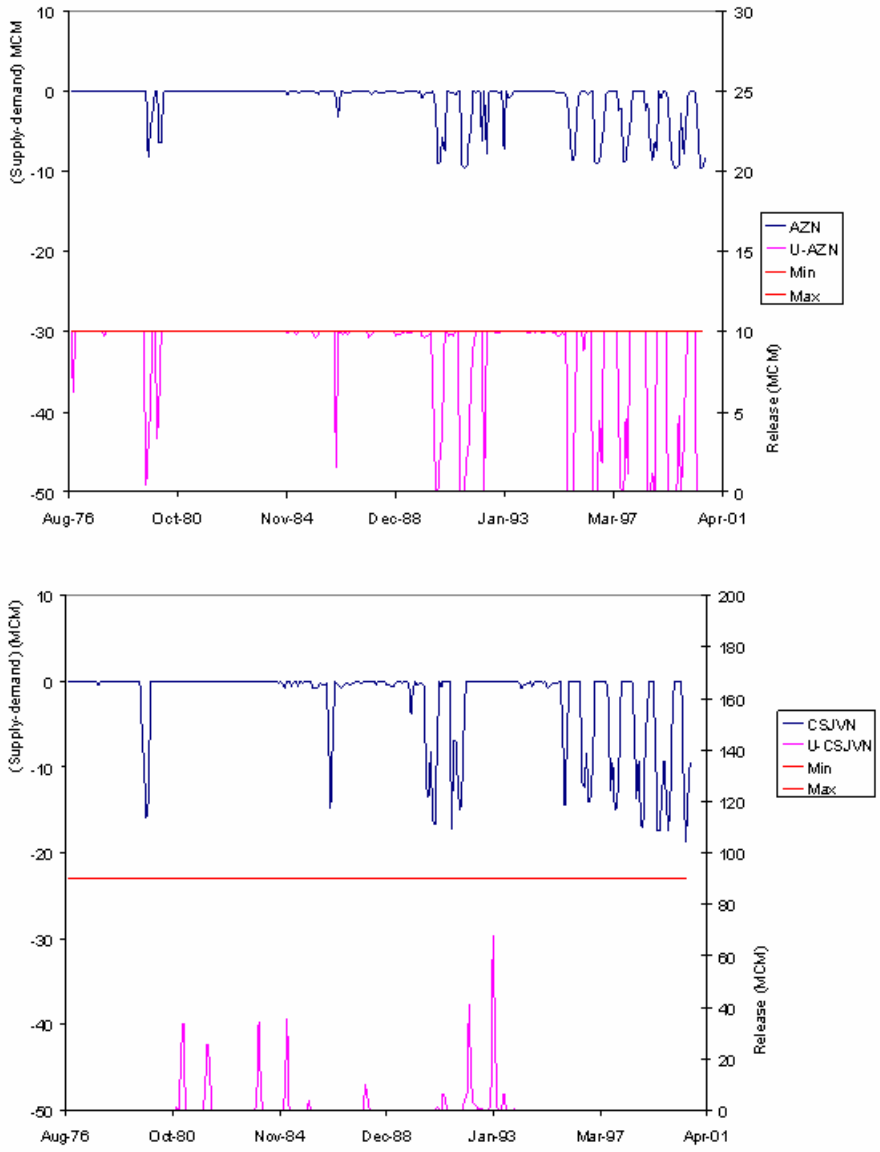

Figure D.4: Assessment model, baseline case, constrained GW drawdown, monthly water deficit and release sequences at Amman-Zarqa and C/S Jordan Valley nodes

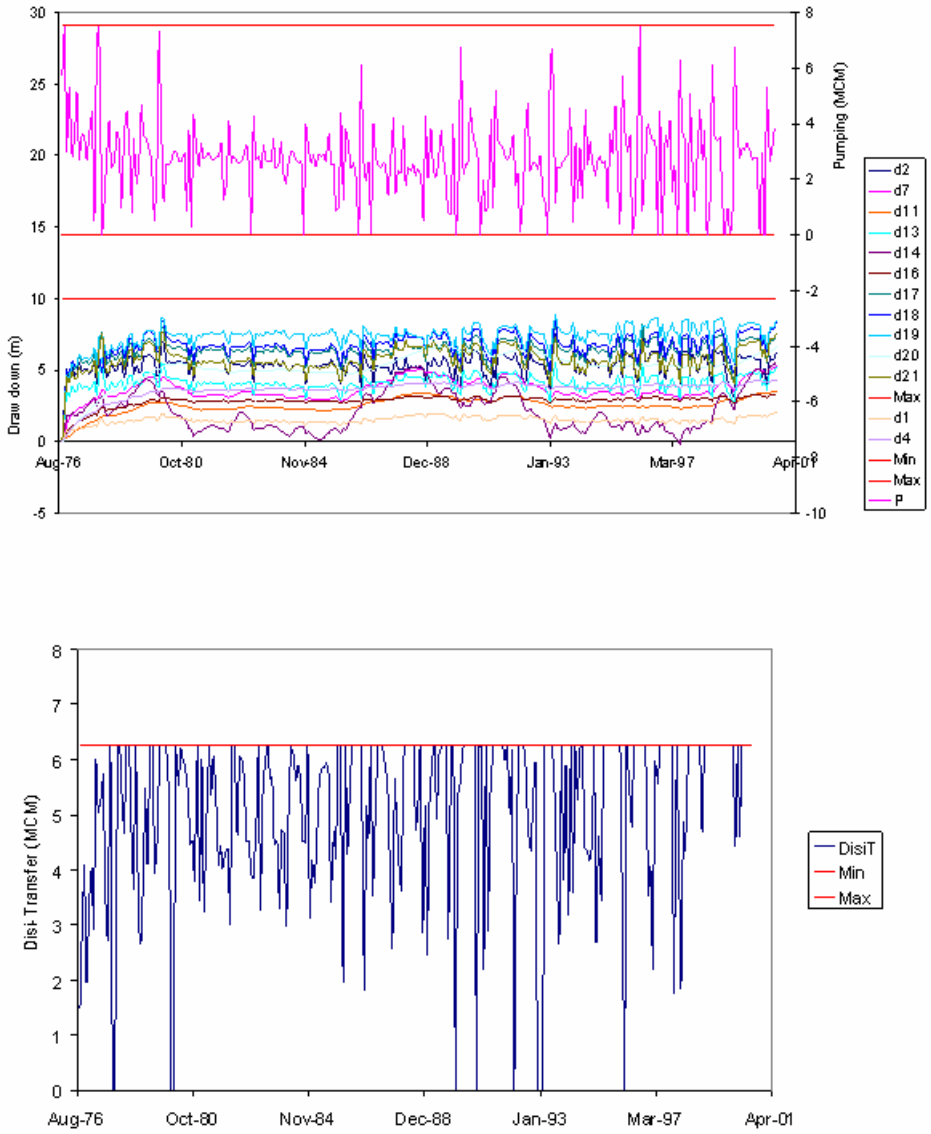

Figure D.5: Assessment model, baseline case, constrained GW drawdown, monthly pumping, drawdown and Disi transfer sequences

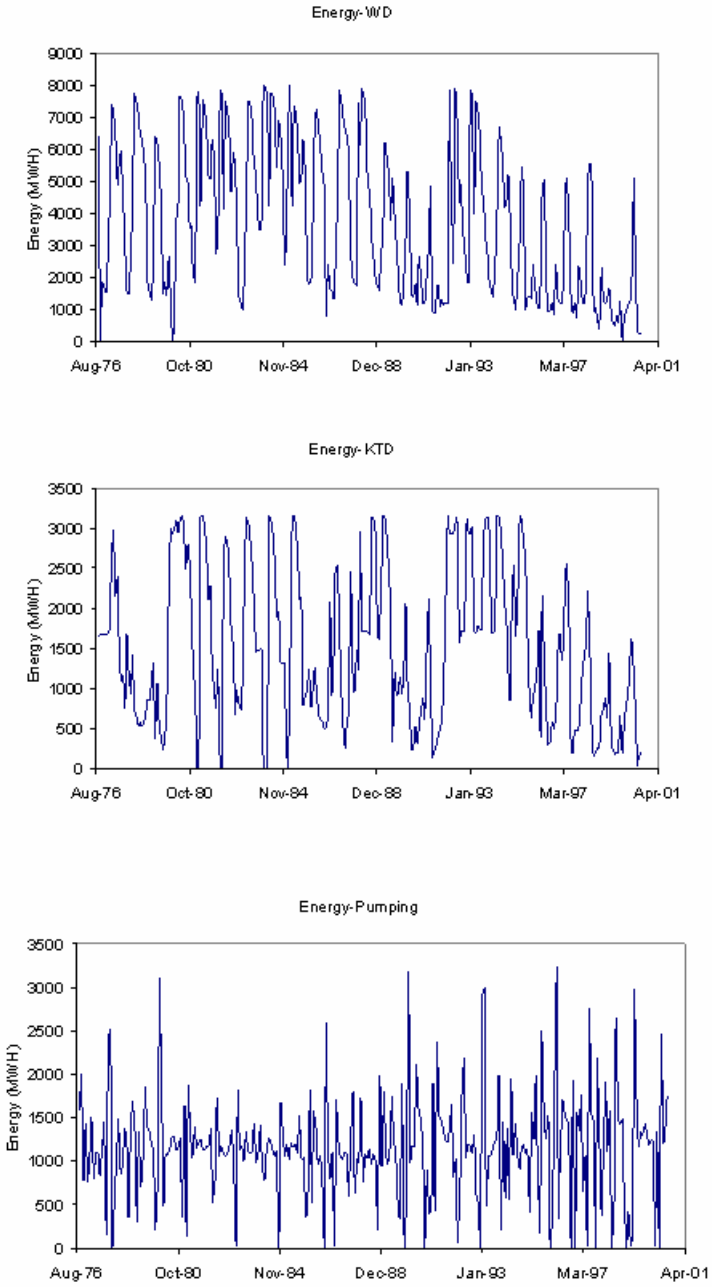

Figure D.6: Assessment model, baseline case, constrained GW drawdown, WD, KTD and pumping energy sequences

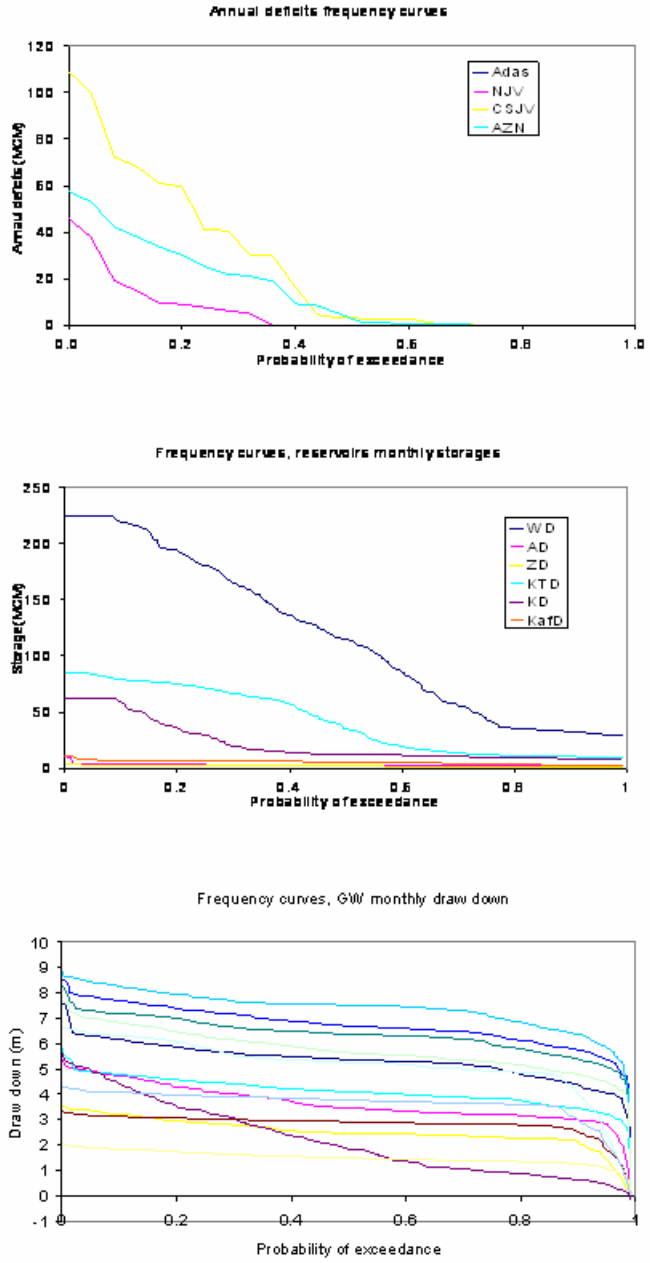

Figure D.7: Assessment model, baseline case, constrained GW drawdown, annual deficits, storages, and drawdowns frequency curves

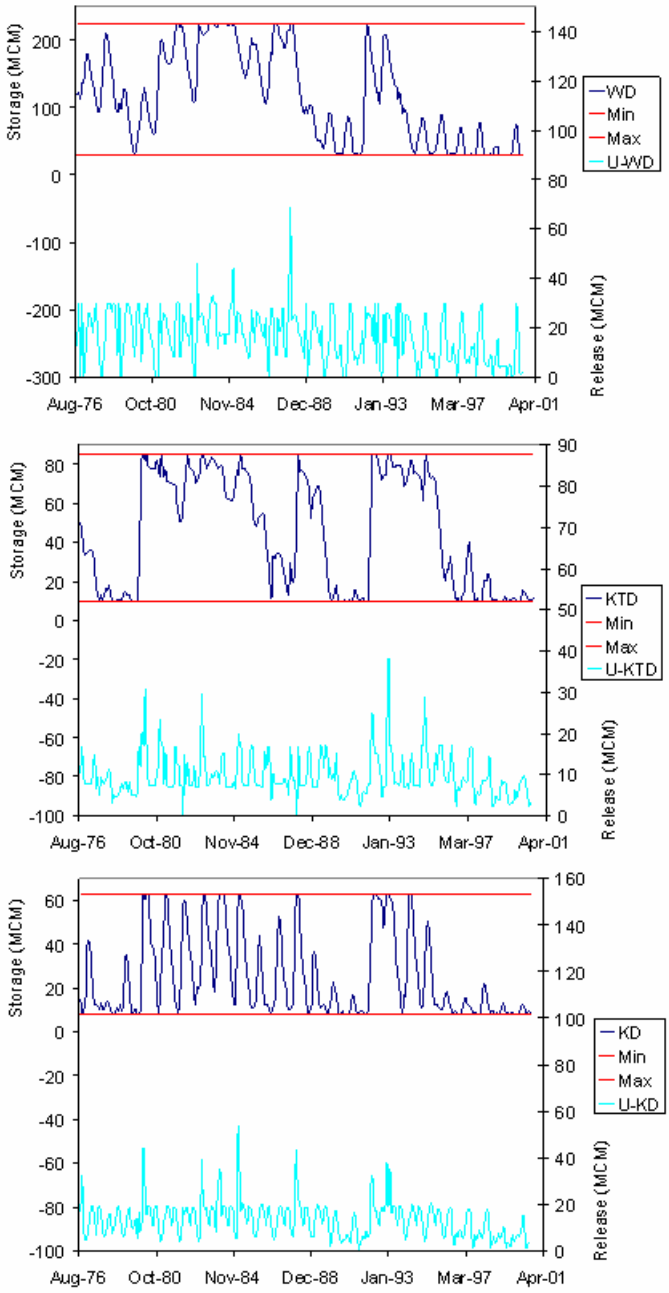

Figure D.8: Assessment model, baseline case, unconstrained GW drawdown , WD, KTD, and KD storage and release sequences

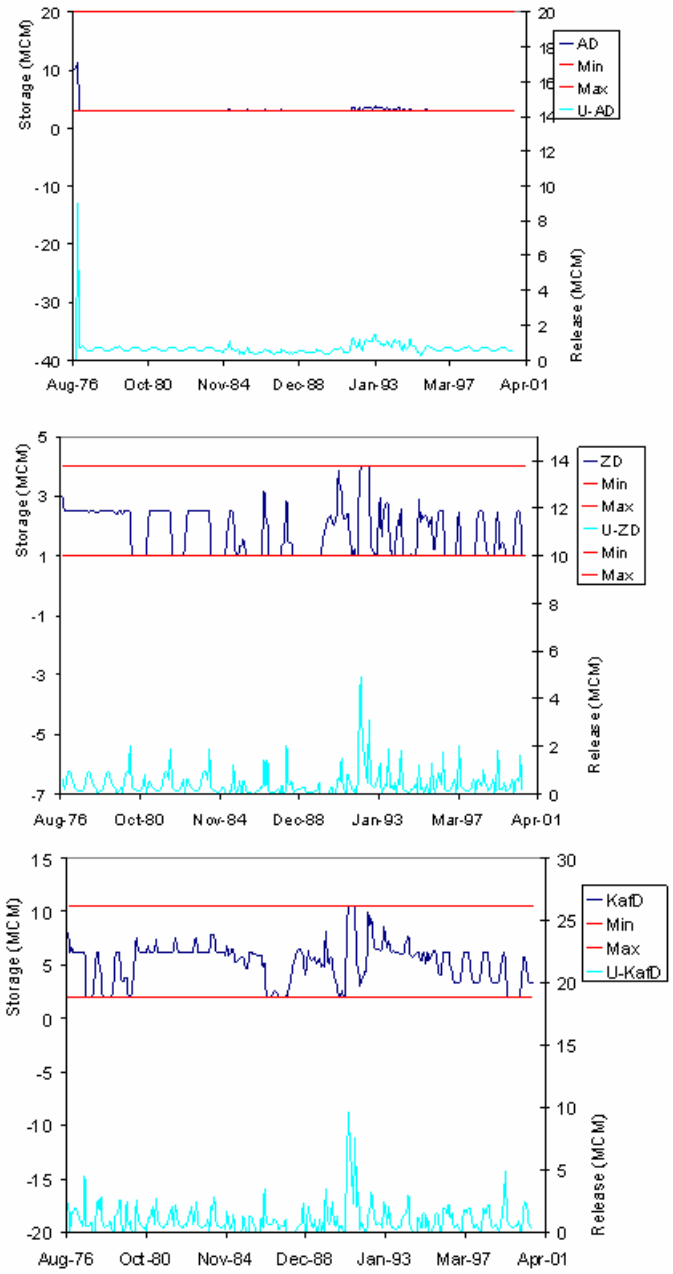

Figure D.9: Assessment model, baseline case, unconstrained GW drawdown, AD, ZD, and KafD storage and release sequences

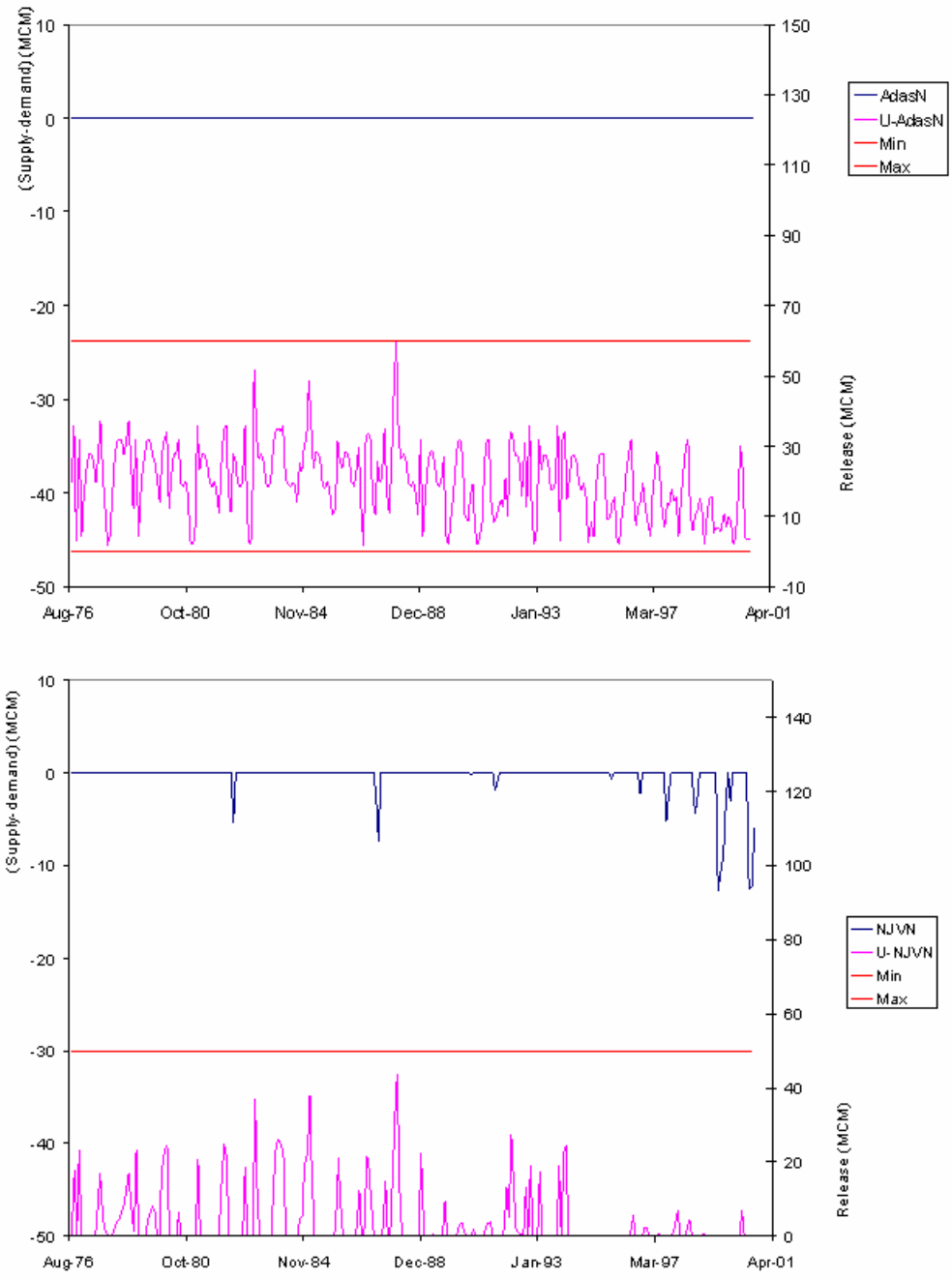

Figure D.10: Assessment model, baseline case, unconstrained GW drawdown, monthly water deficit and release sequences at Adasiya and North Jordan Valley nodes

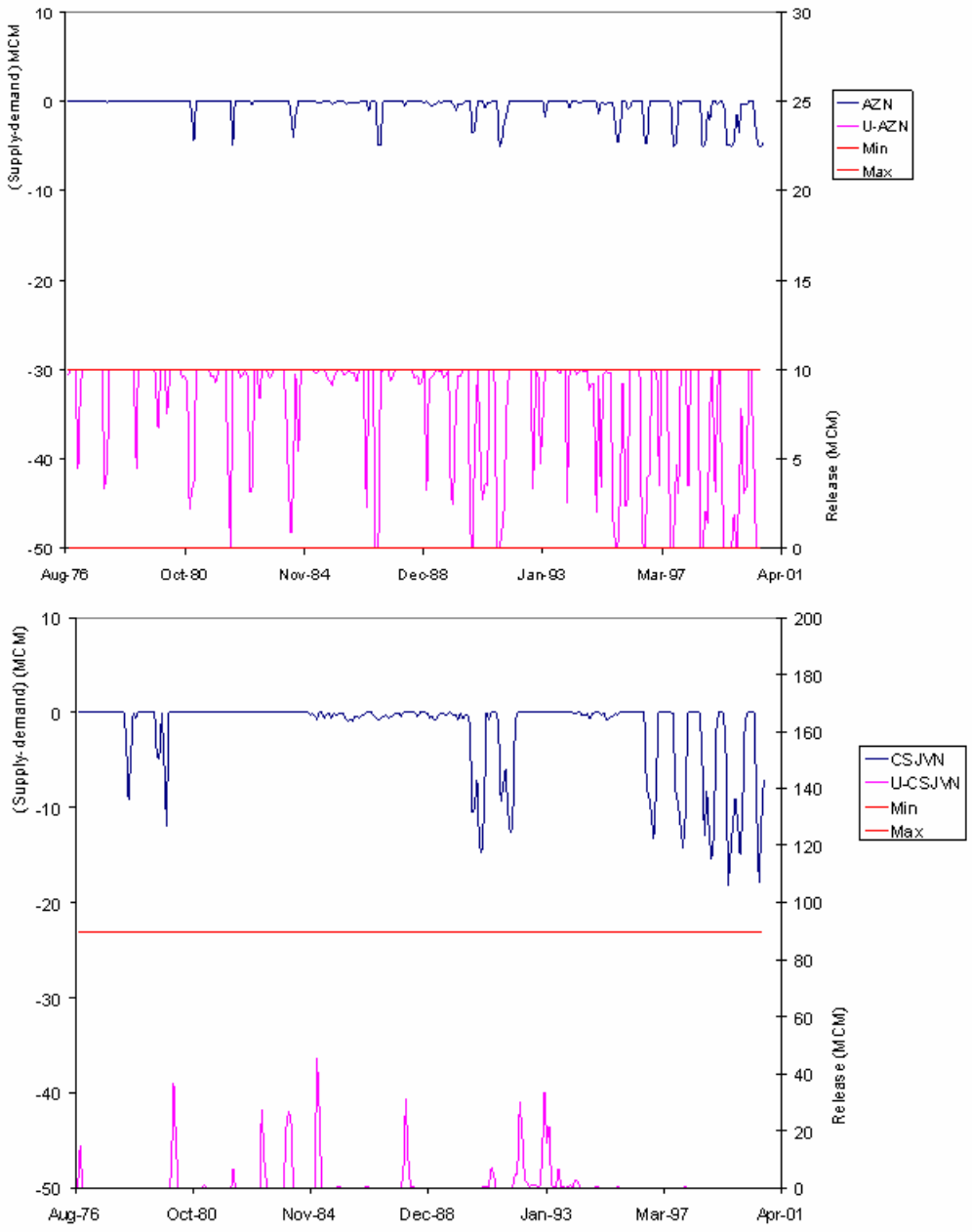

Figure D.11: Assessment model, baseline case, unconstrained GW drawdown, monthly water deficit and release sequences at Amman-Zarqa and C/S Jordan Valley nodes

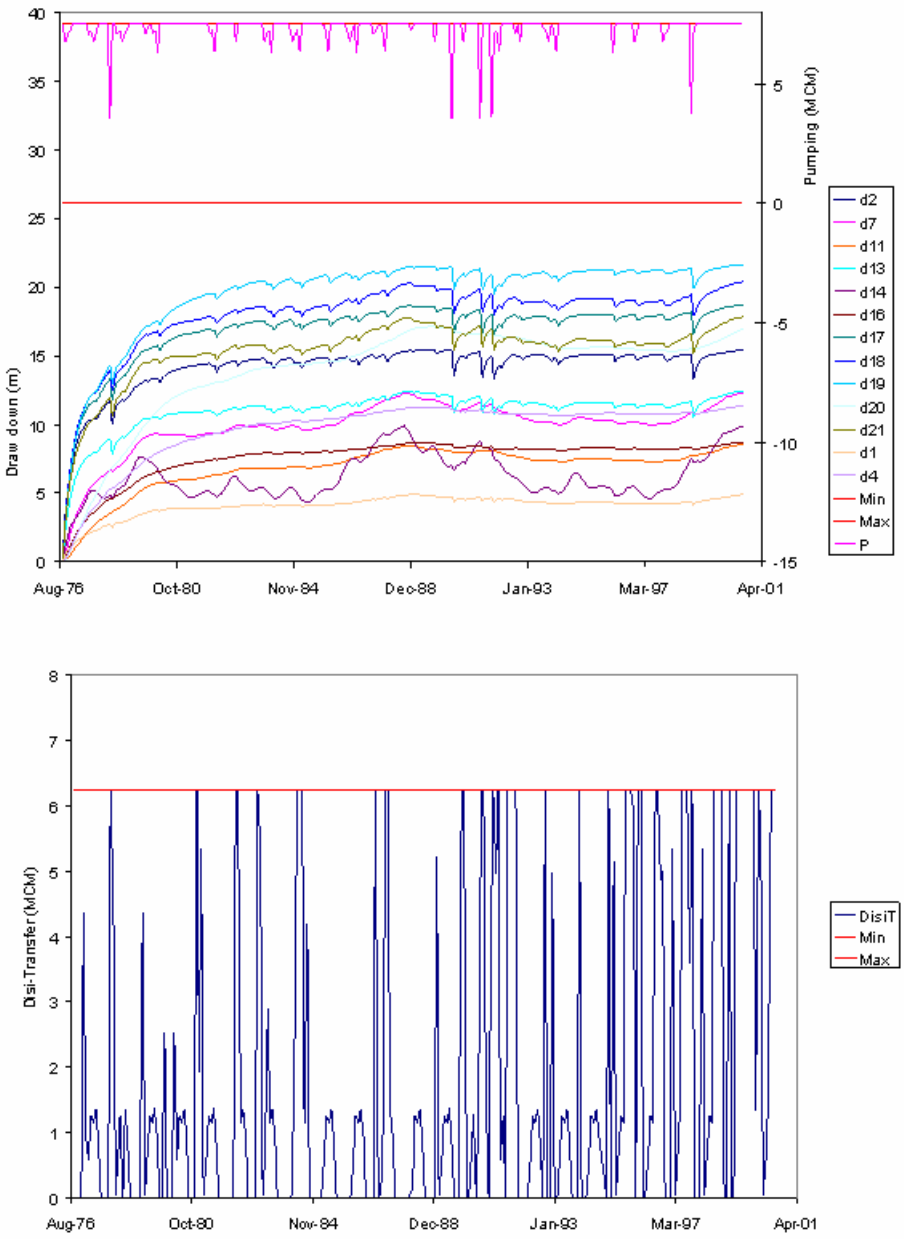

Figure D.12: Assessment model, baseline case, unconstrained GW drawdown, monthly pumping, drawdown and Disi transfer sequences

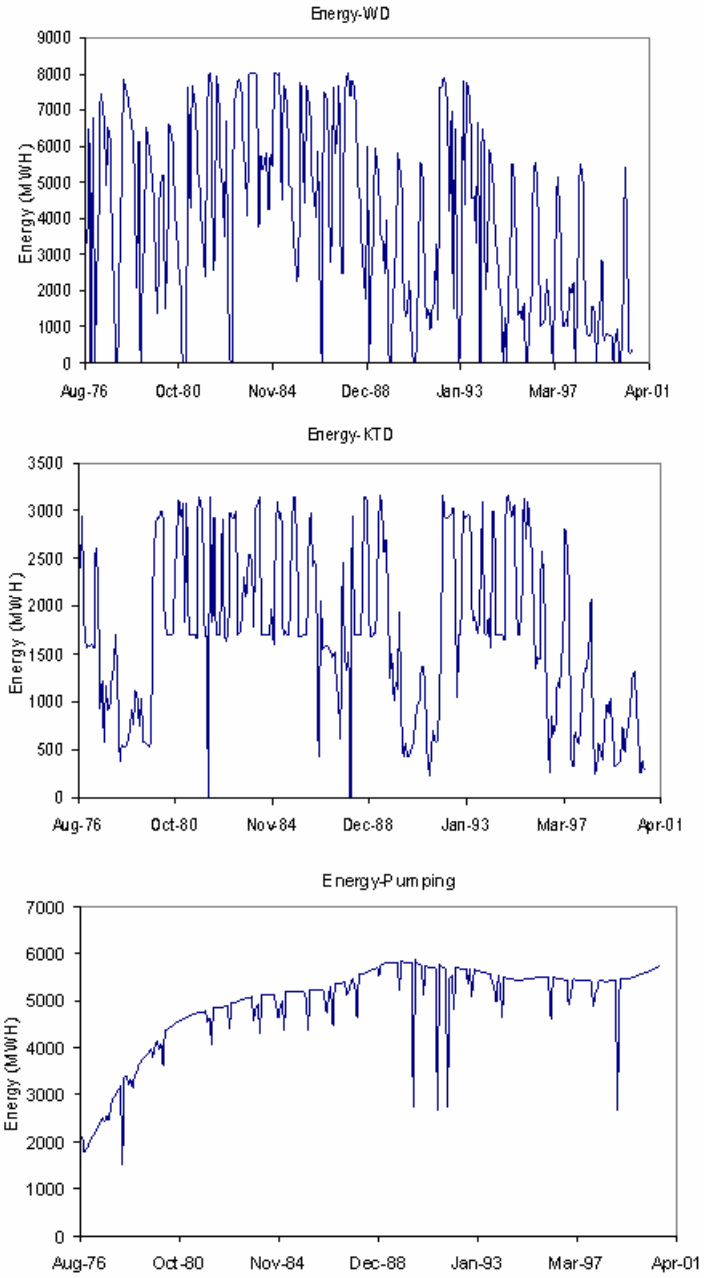

Figure D.13: Assessment model, baseline case, unconstrained GW drawdown , WD, KTD and pumping energy sequences

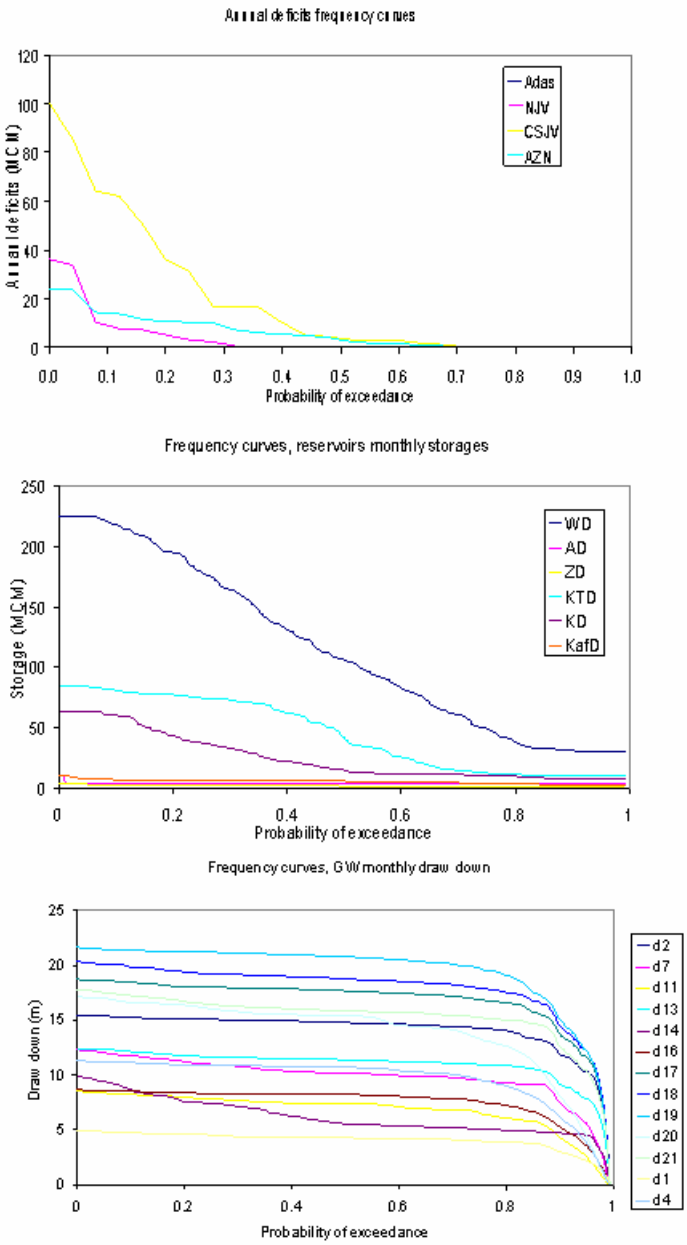

Figure D.14: Assessment model, baseline case, unconstrained GW drawdown, annual deficits, storages, and drawdowns frequency curves

APPENDIX E

SCENARIO 1: EXISTING CONDITIONS

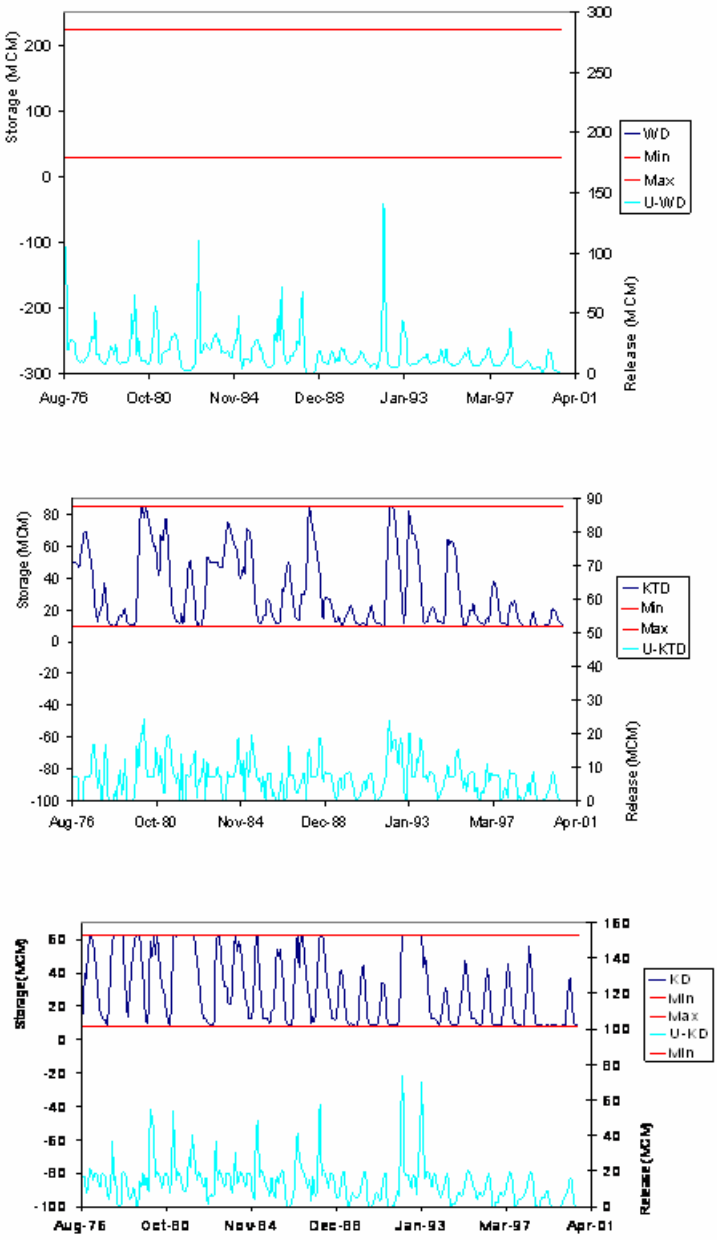

Figure E.1: Assessment model, scenario1, constrained GW drawdown , WD, KTD, and KD storage and release sequences

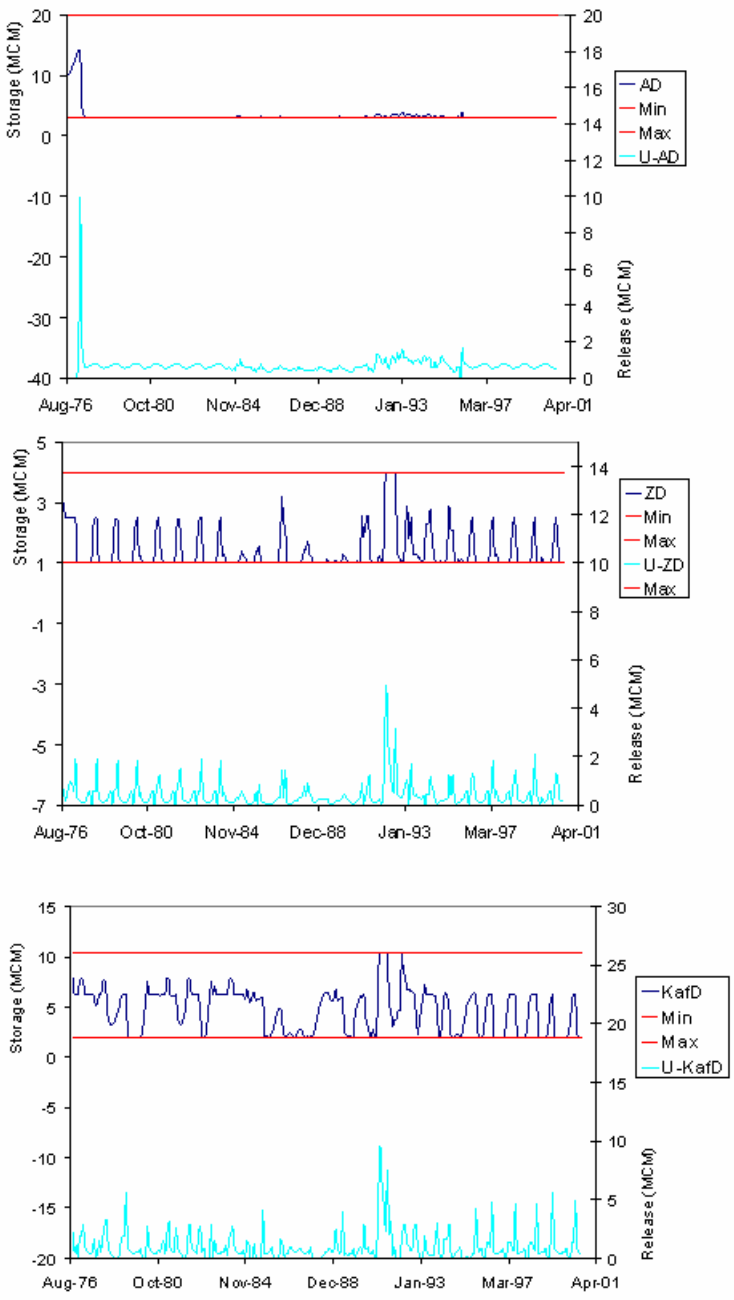

Figure E.2 :Assessment model, scenario1, constrained GW drawdown, AD, ZD, and KafD storage and release sequences

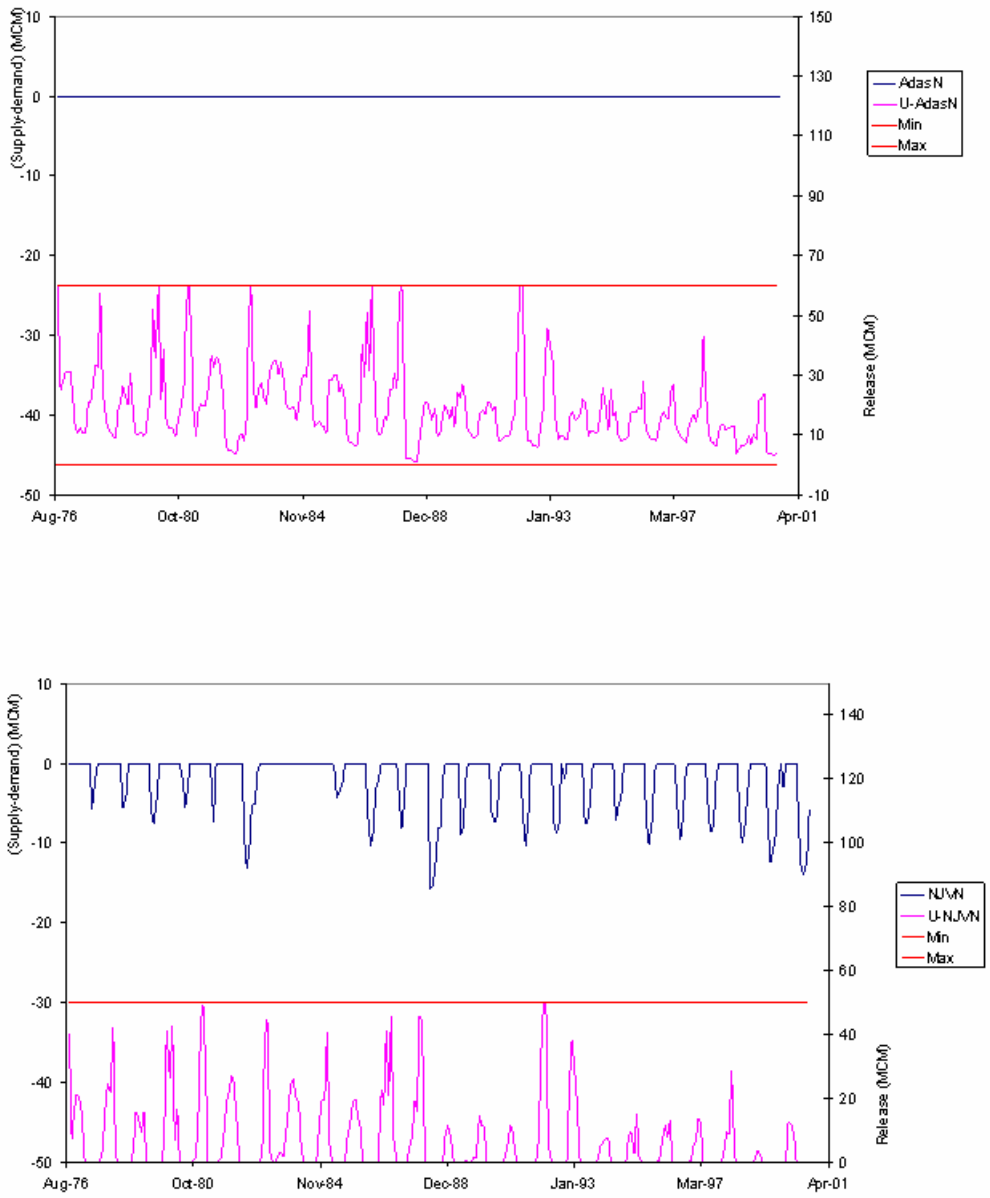

Figure E.3: Assessment model, scenario1, constrained GW drawdown, monthly water deficit and release sequences at Adasiy and North Jordan Valley nodes

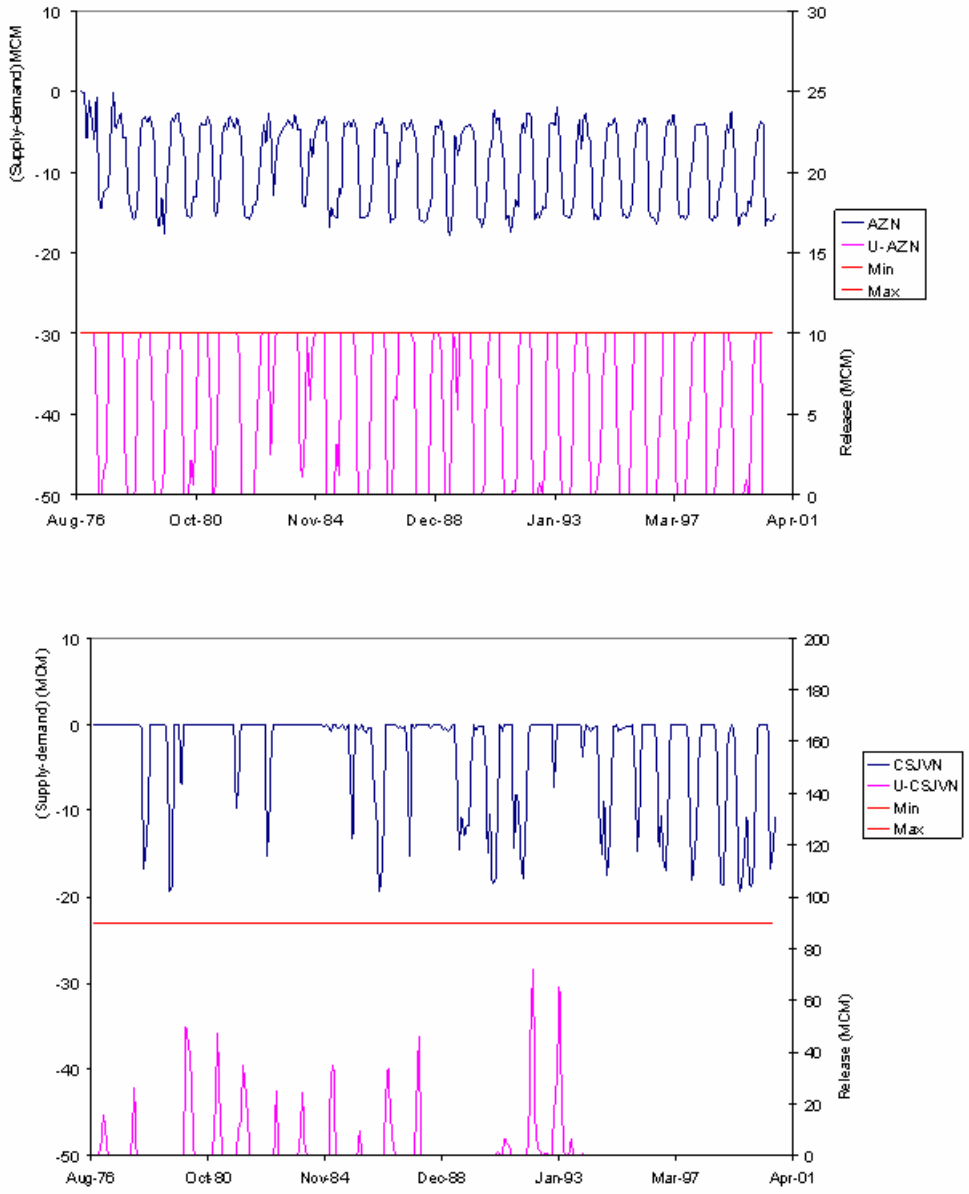

Figure E.4: Assessment model, scenario1, constrained GW drawdown, monthly water deficit and release sequences at Amman Zarqa and C/S Jordan Valley nodes

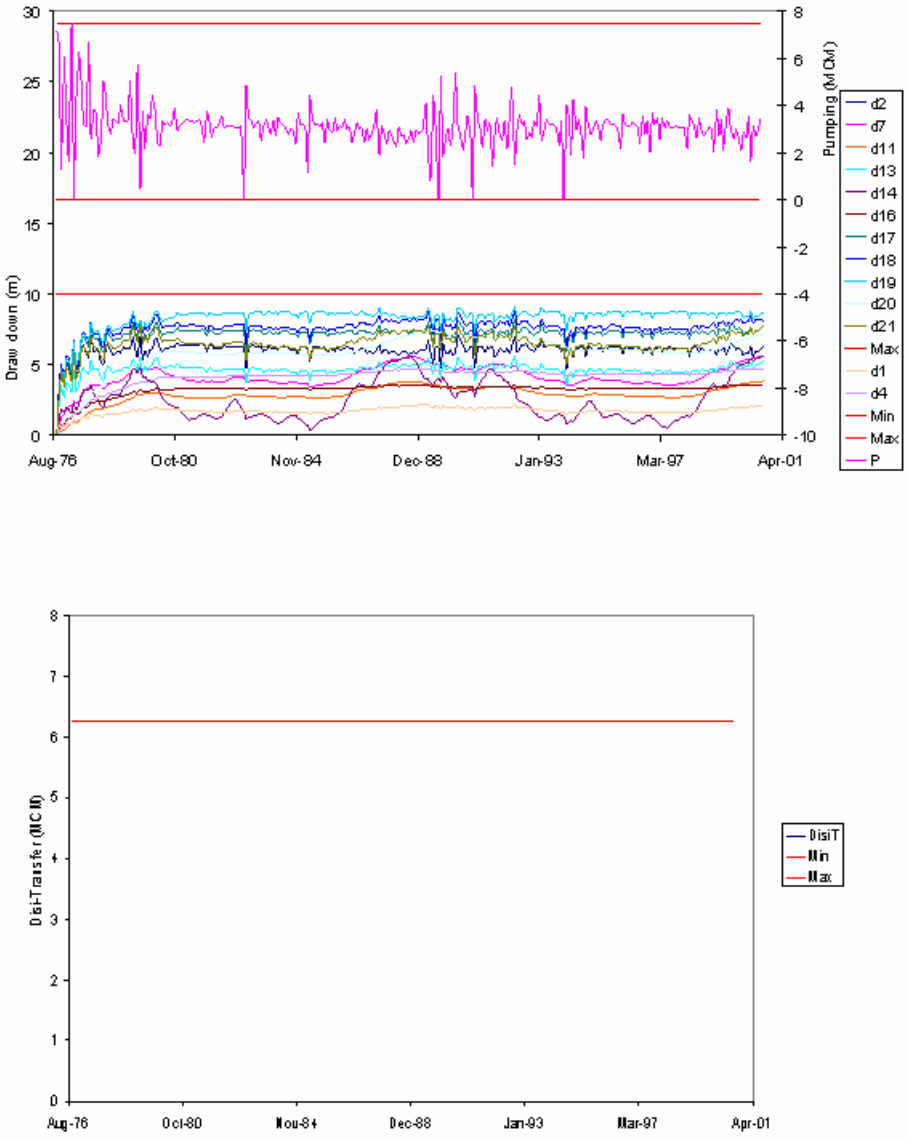

Figure E.5: Assessment model, scenario1, constrained GW drawdown, monthly pumping, drawdown and Disi transfer sequences

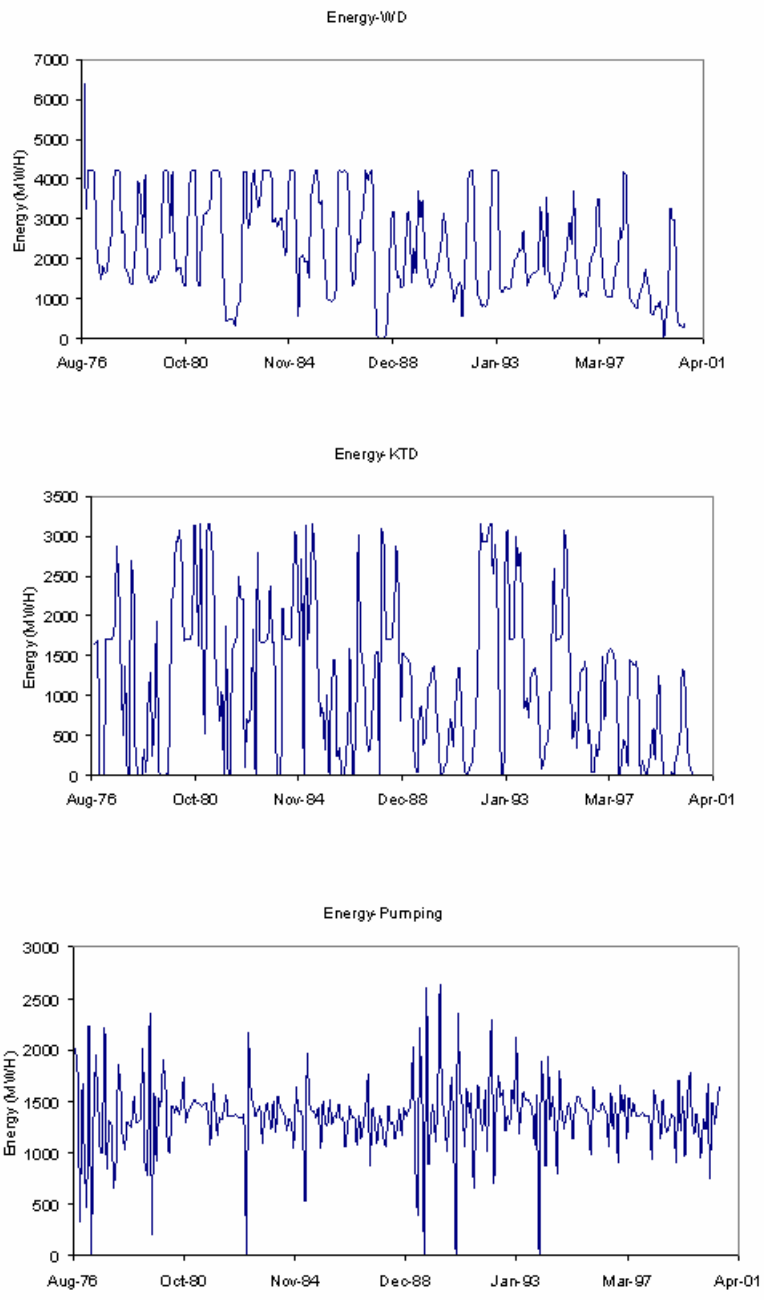

Figure E.6: Assessment model, scenario1, constrained GW drawdown , WD, KTD and pumping energy sequences

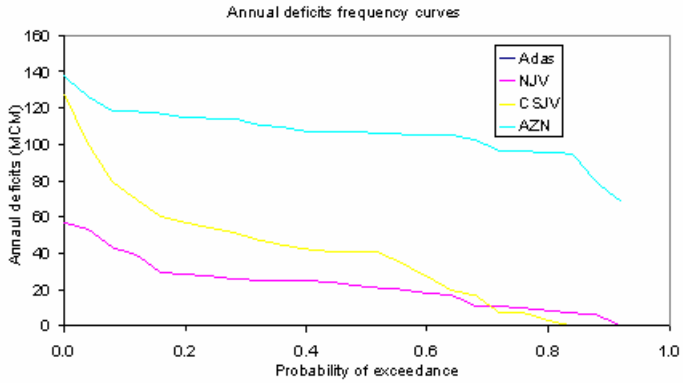

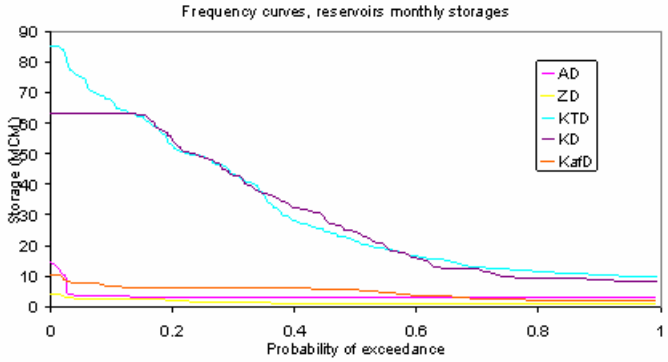

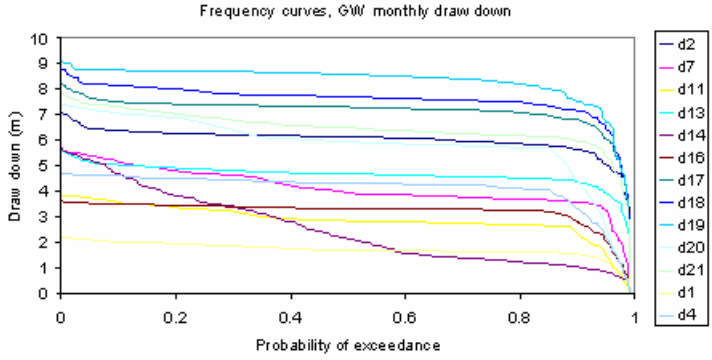

Figure E.7: Assessment model, scenario1, constrained GW drawdown, annual deficits, storages, and drawdowns frequency curves

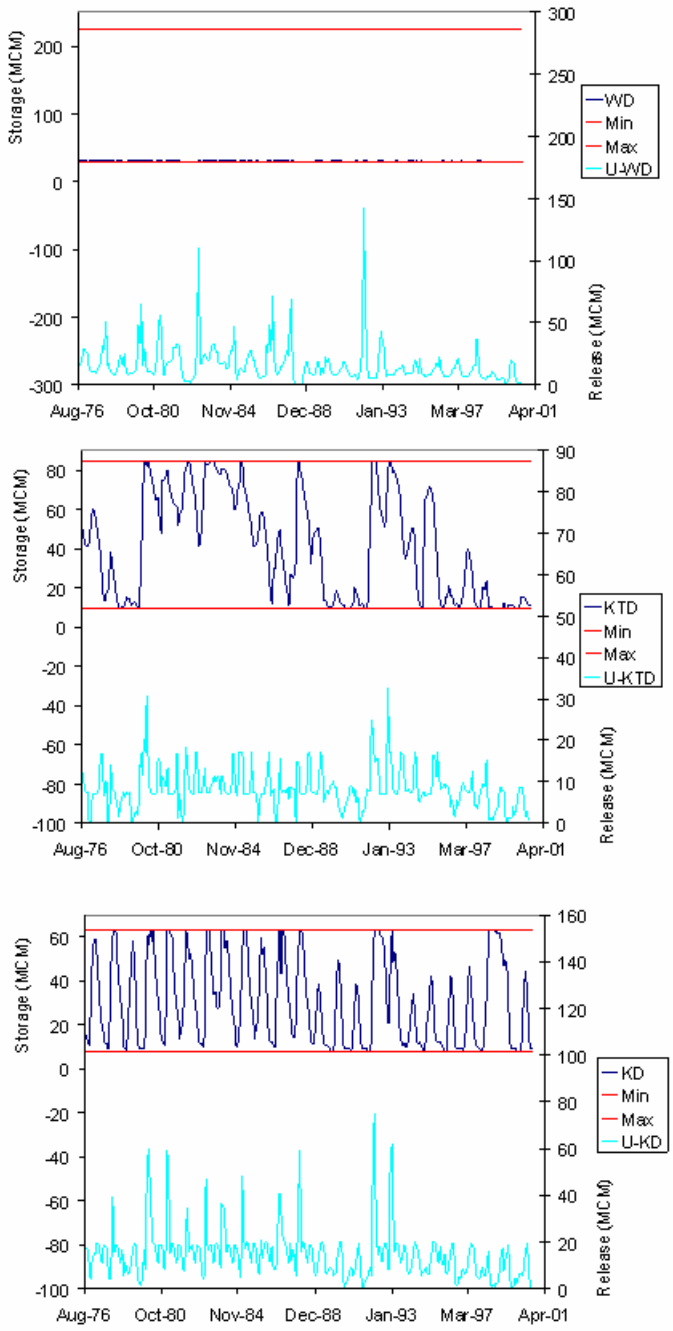

Figure E.8: Assessment model, scenario1, unconstrained GW drawdown,WD, KTD, and KD storage and release sequences

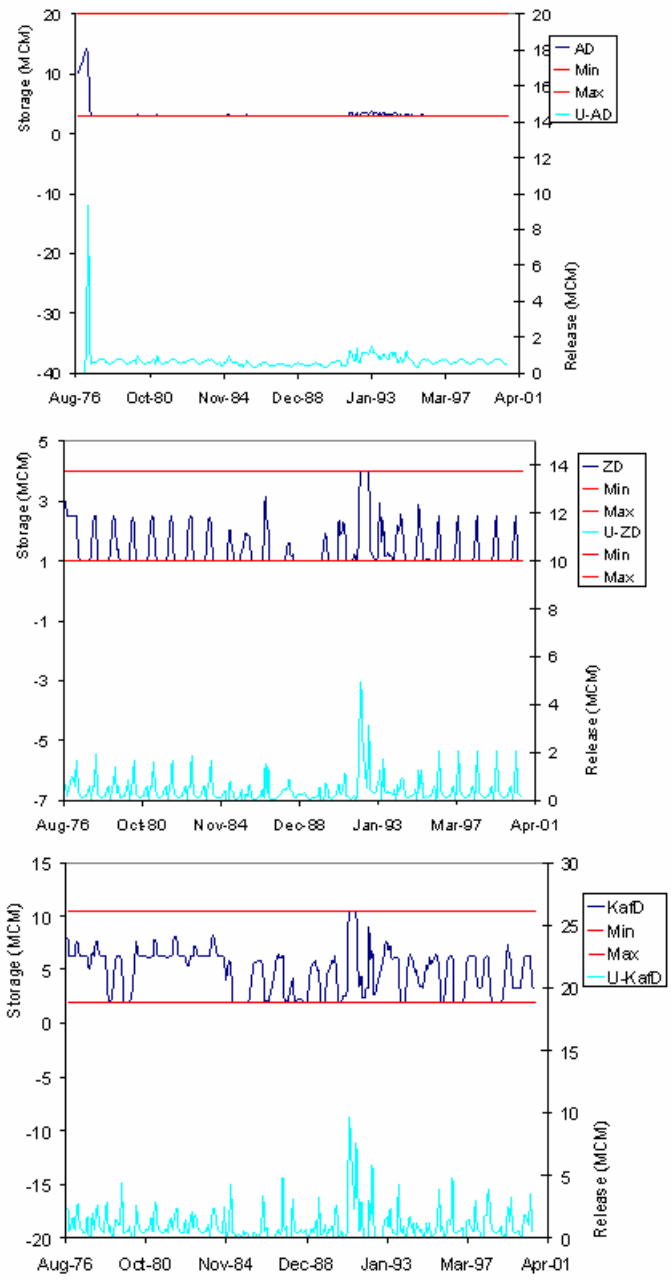

Figure E.9: Assessment model, scenario1, unconstrained GW drawdown, AD, ZD, and KafD storage and release sequences

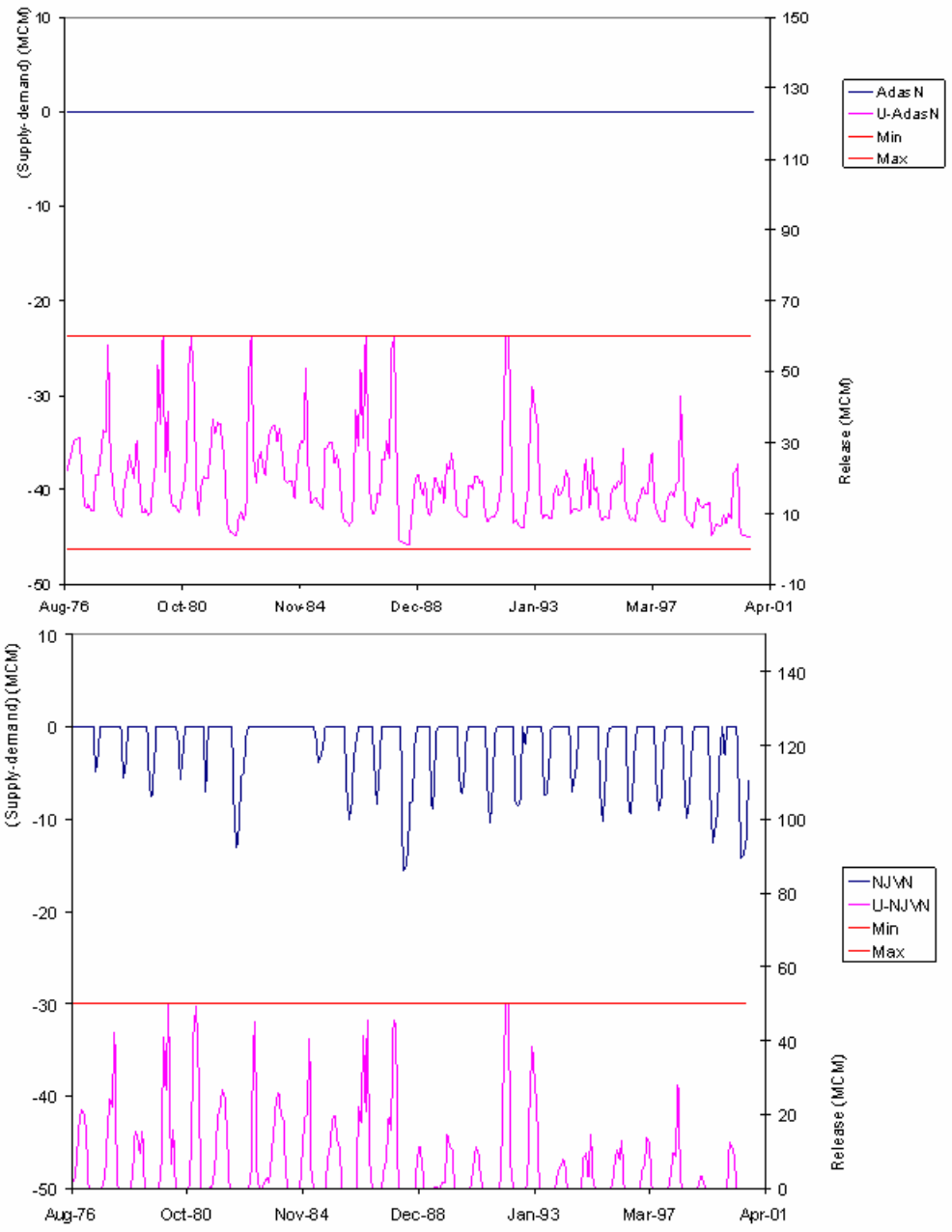

Figure E.10: Assessment model, scenario1, unconstrained GW drawdown , monthly water deficit and release sequences at Adasiya and North Jordan Valley nodes

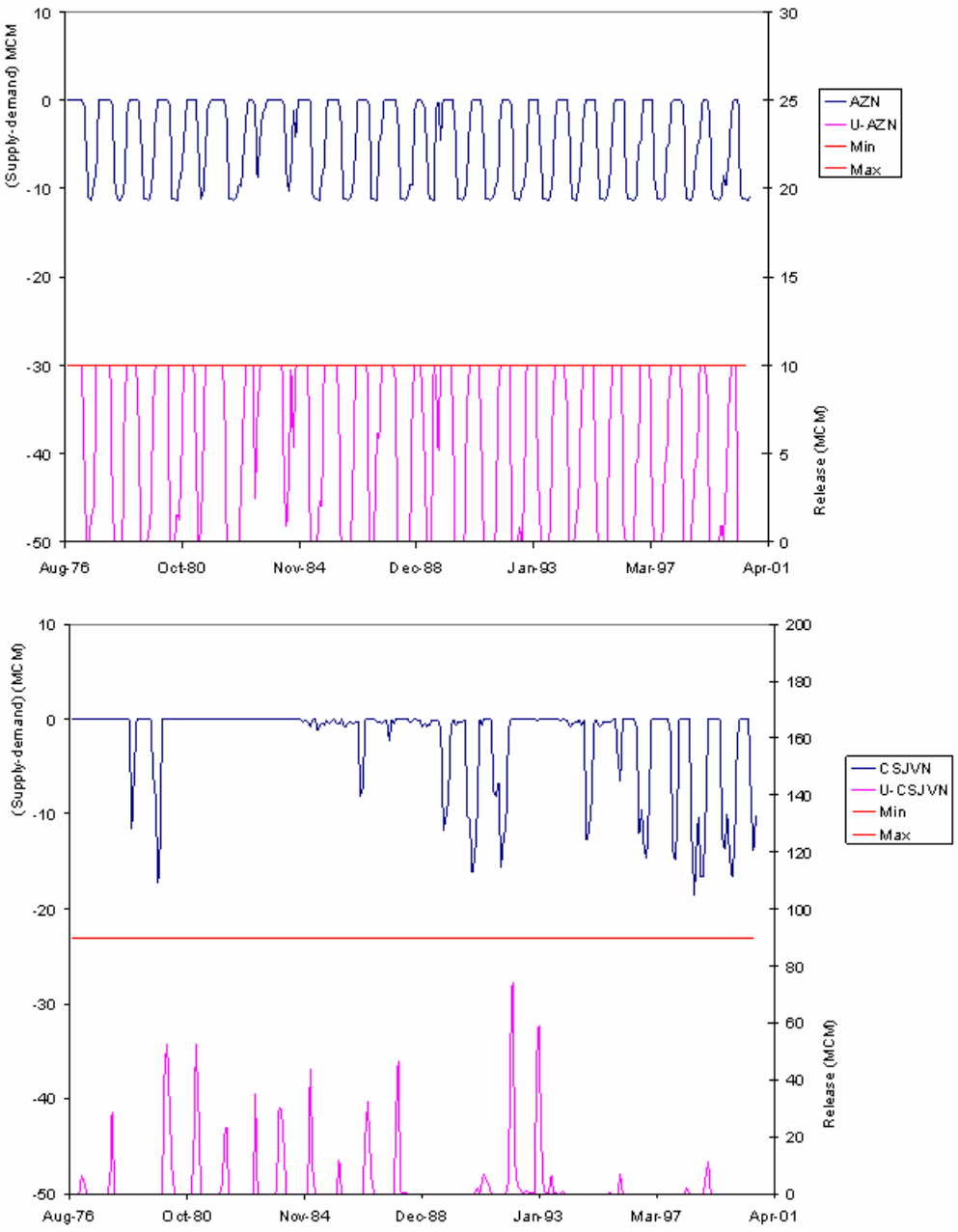

Figure E.11: Assessment model, scenario1, unconstrained GW drawdown, monthly water deficit and release sequences at Amman Zarqa and C/S Jordan Valley nodes

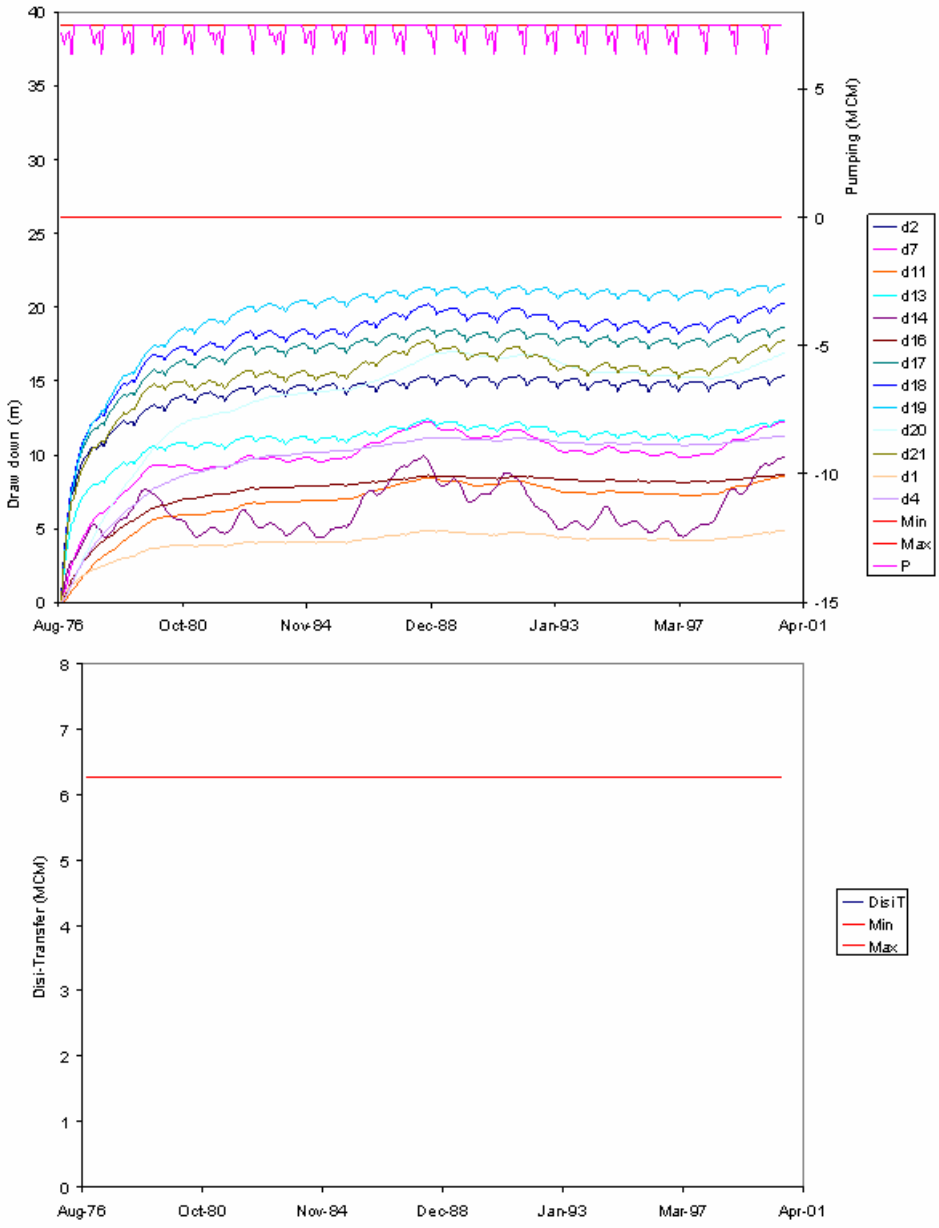

Figure E.12: Assessment model, scenario1, unconstrained GW drawdown, monthly pumping, drawdown and Disi transfer sequences

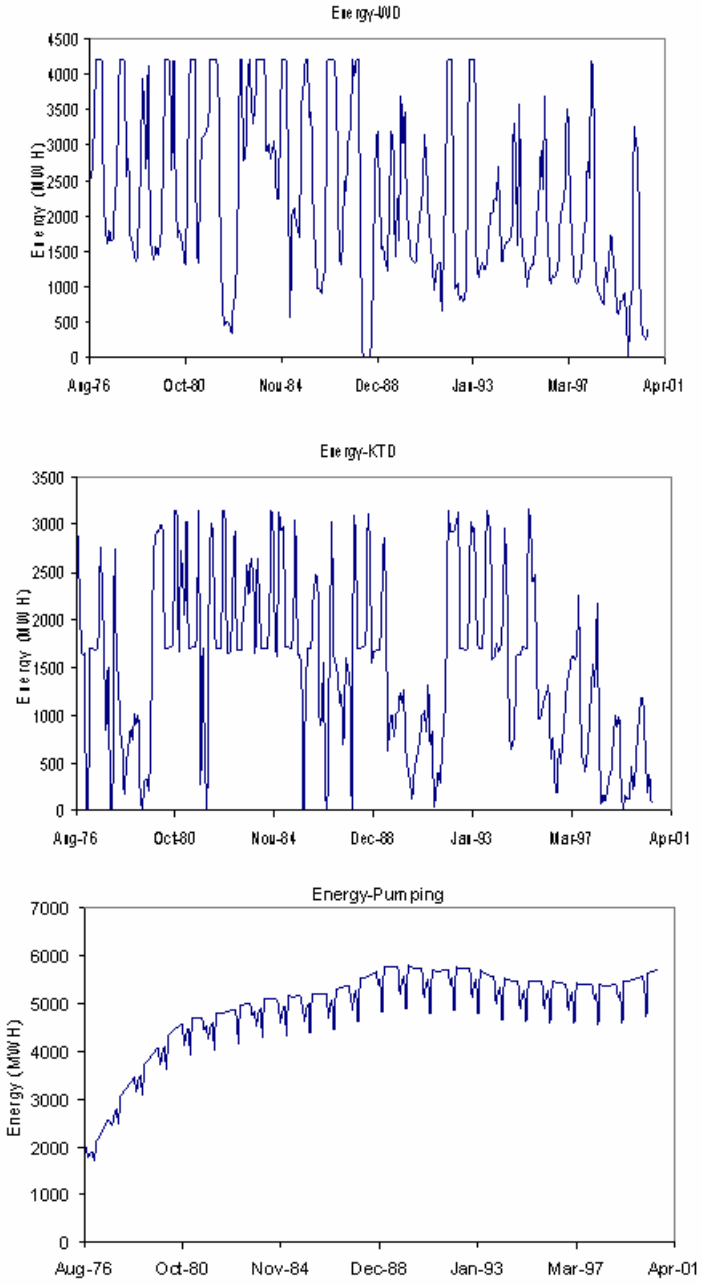

Figure E.13: Assessment model, scenario1, unconstrained GW drawdown , WD, KTD and pumping energy sequences

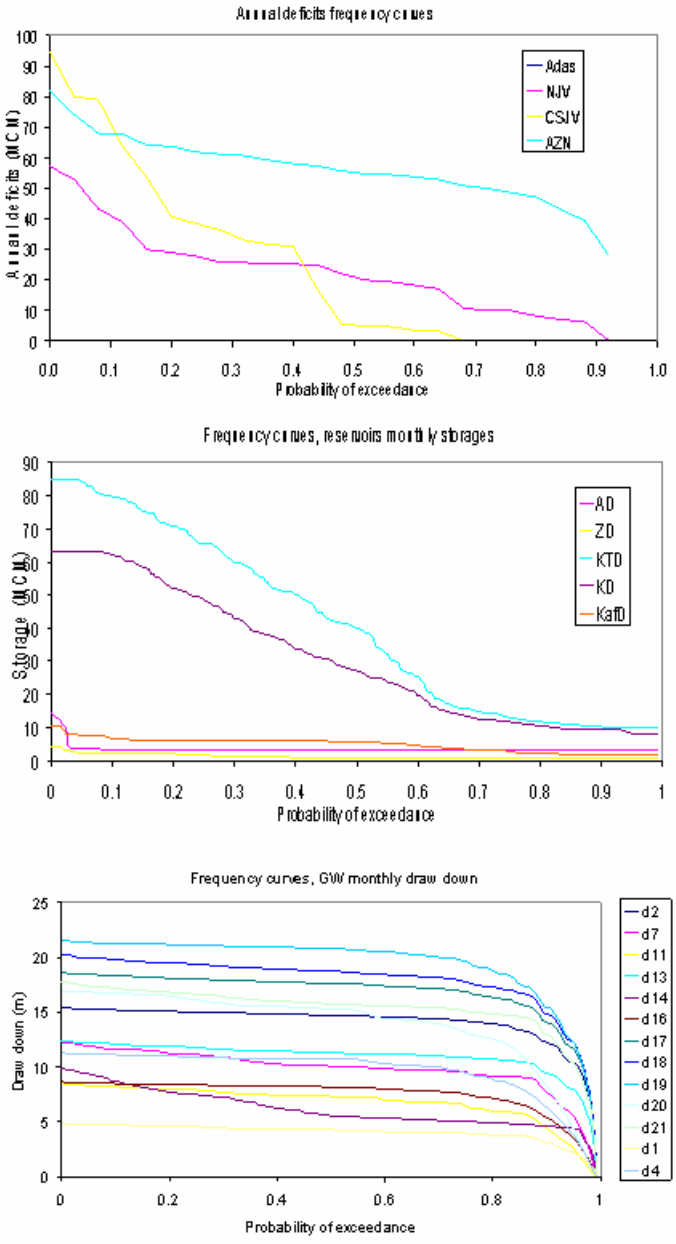

Figure E.14: Assessment model, scenario1, unconstrained GW drawdown, annual deficits, storages, and drawdowns frequency curves

APPENDIX F

SCENARIO 2: EXISTING CONDITIONS+ Al WEHDAH DAM

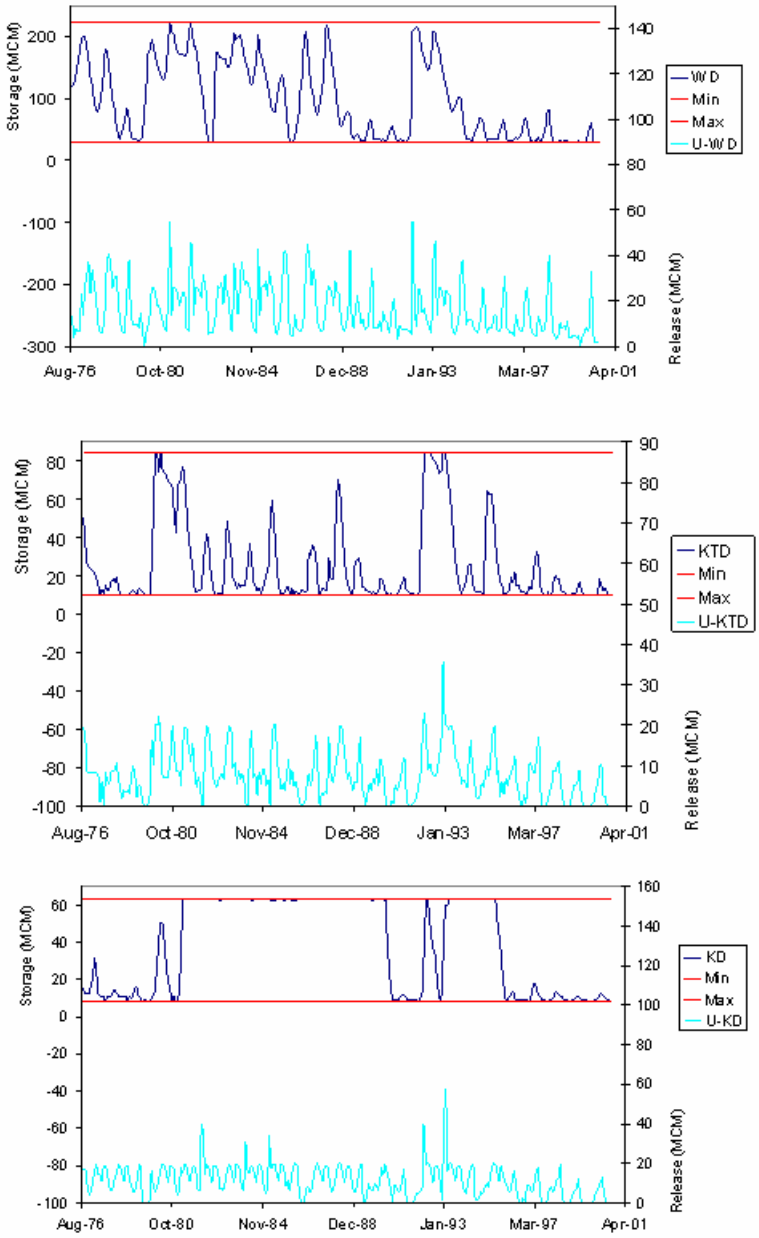

Figure F.1: Assessment model, scenario2, constrained GW drawdown, WD, KTD, and KD storage and release sequences

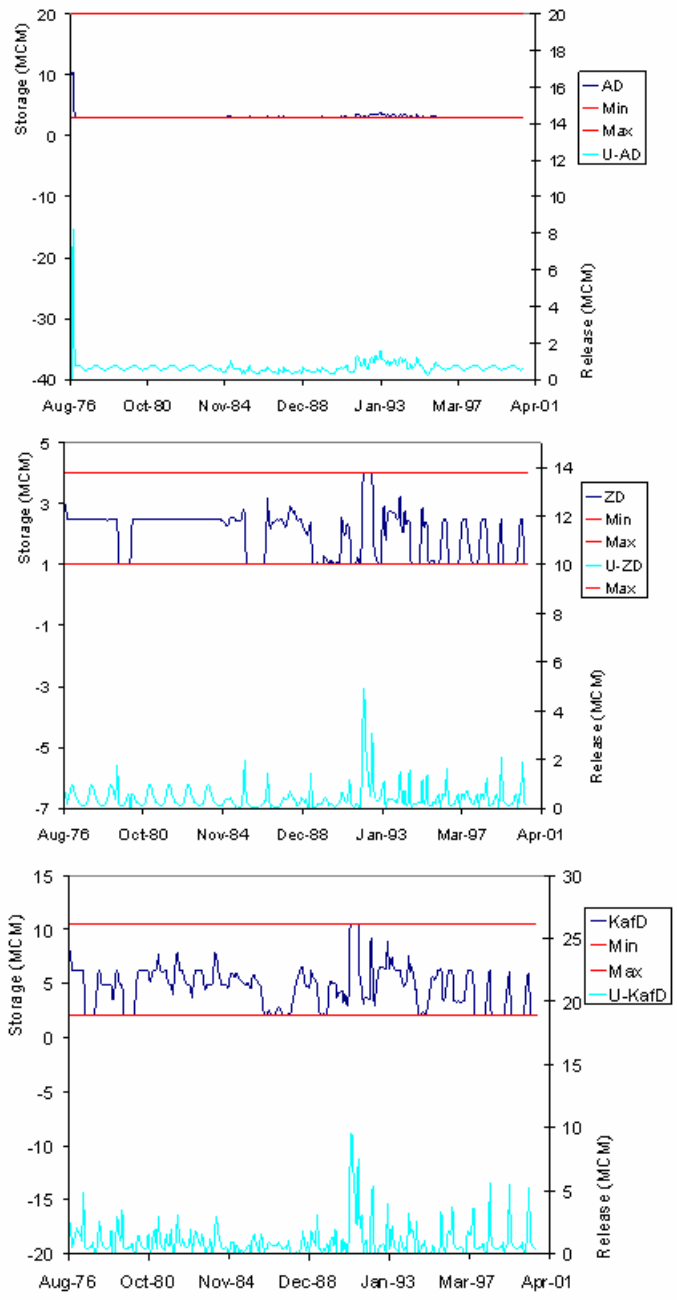

Figure F.2: Assessment model, scenario2, constrained GW drawdown, AD, ZD, and KafD storage and release sequences

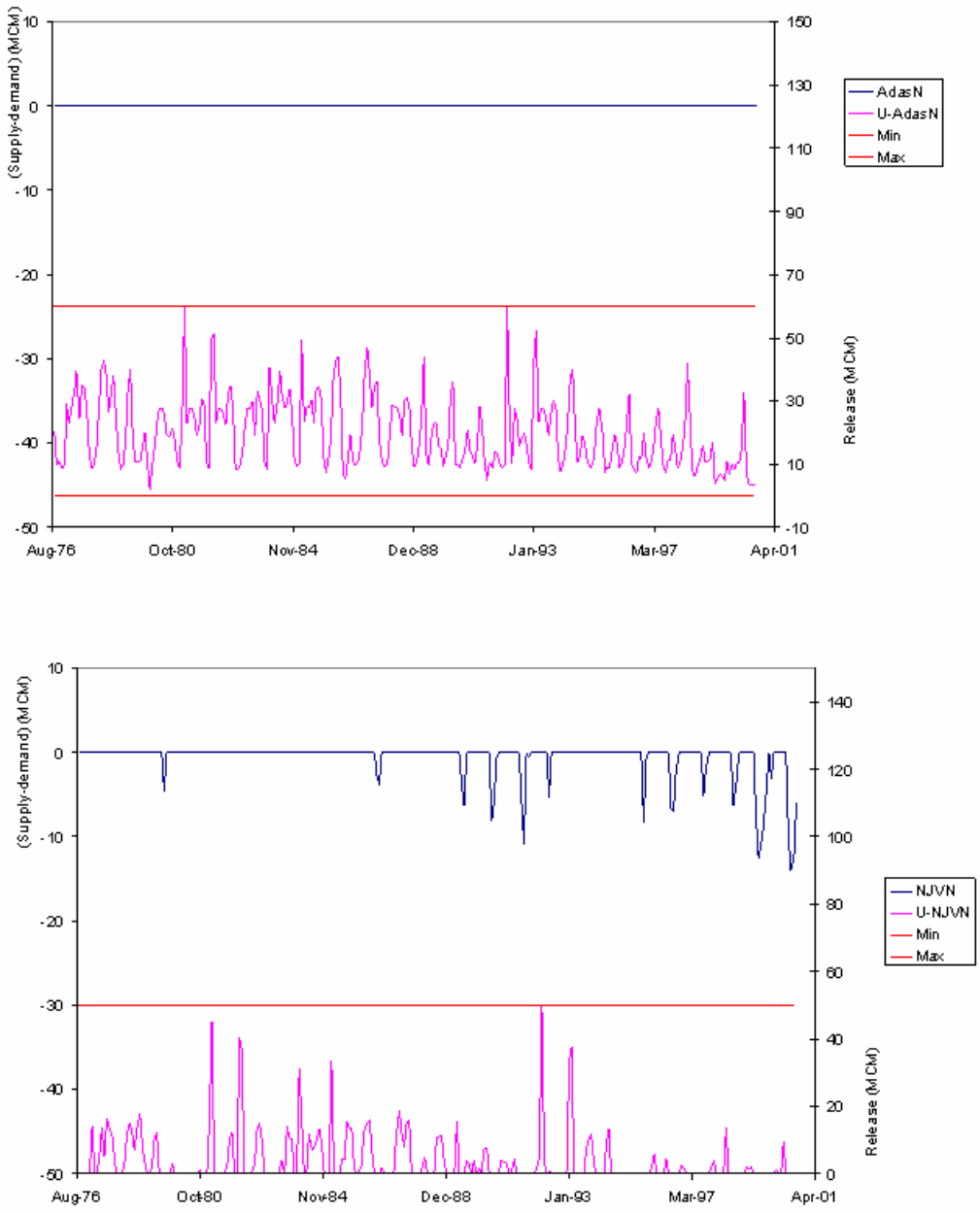

Figure F.3: Assessment model, scenario2, constrained GW drawdown, monthly water deficit and release sequences at Adasiya and North Jordan Valley nodes

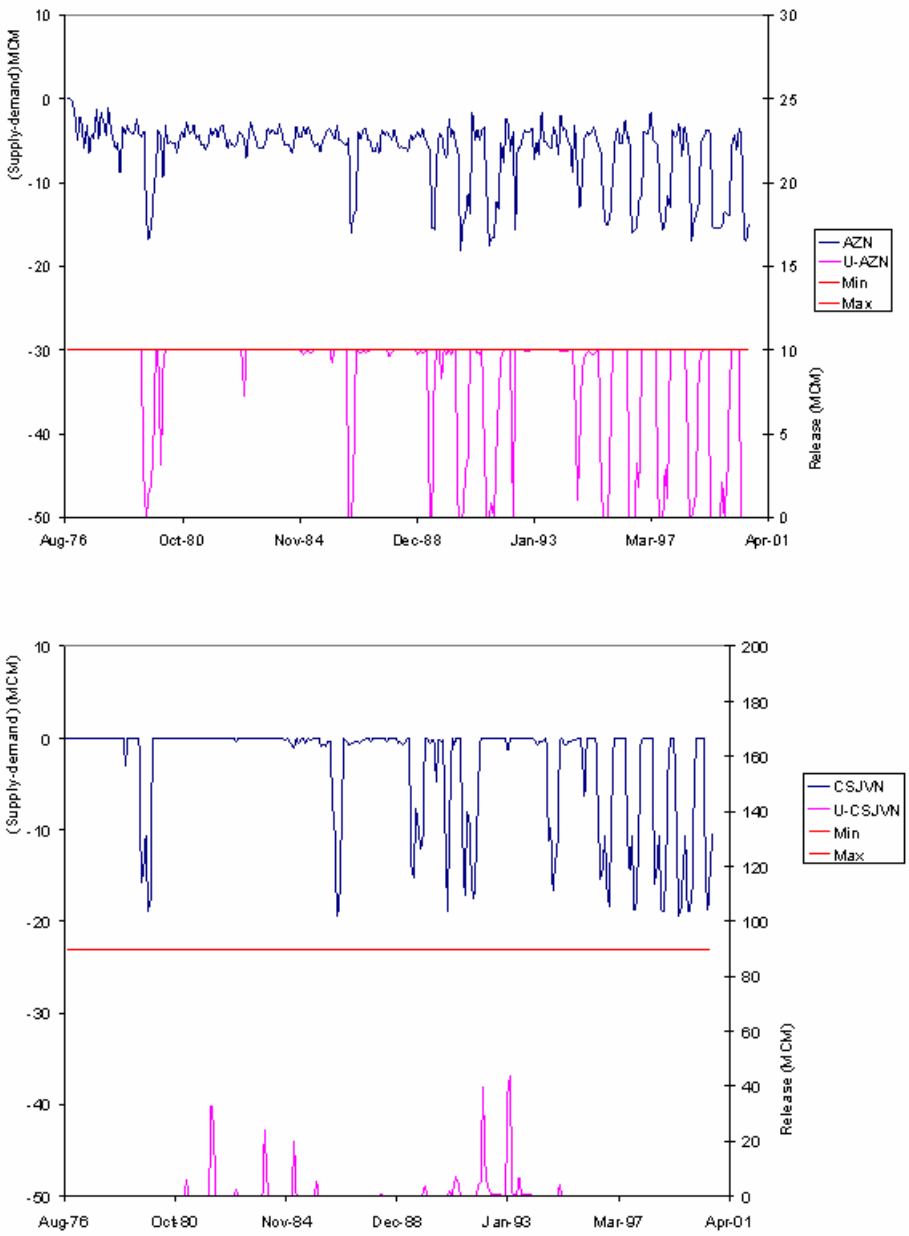

Figure F.4: Assessment model, scenario2, constrained GW drawdown , monthly water deficit and release sequences at Amman-Zarqa and C/S Jordan Valley nodes

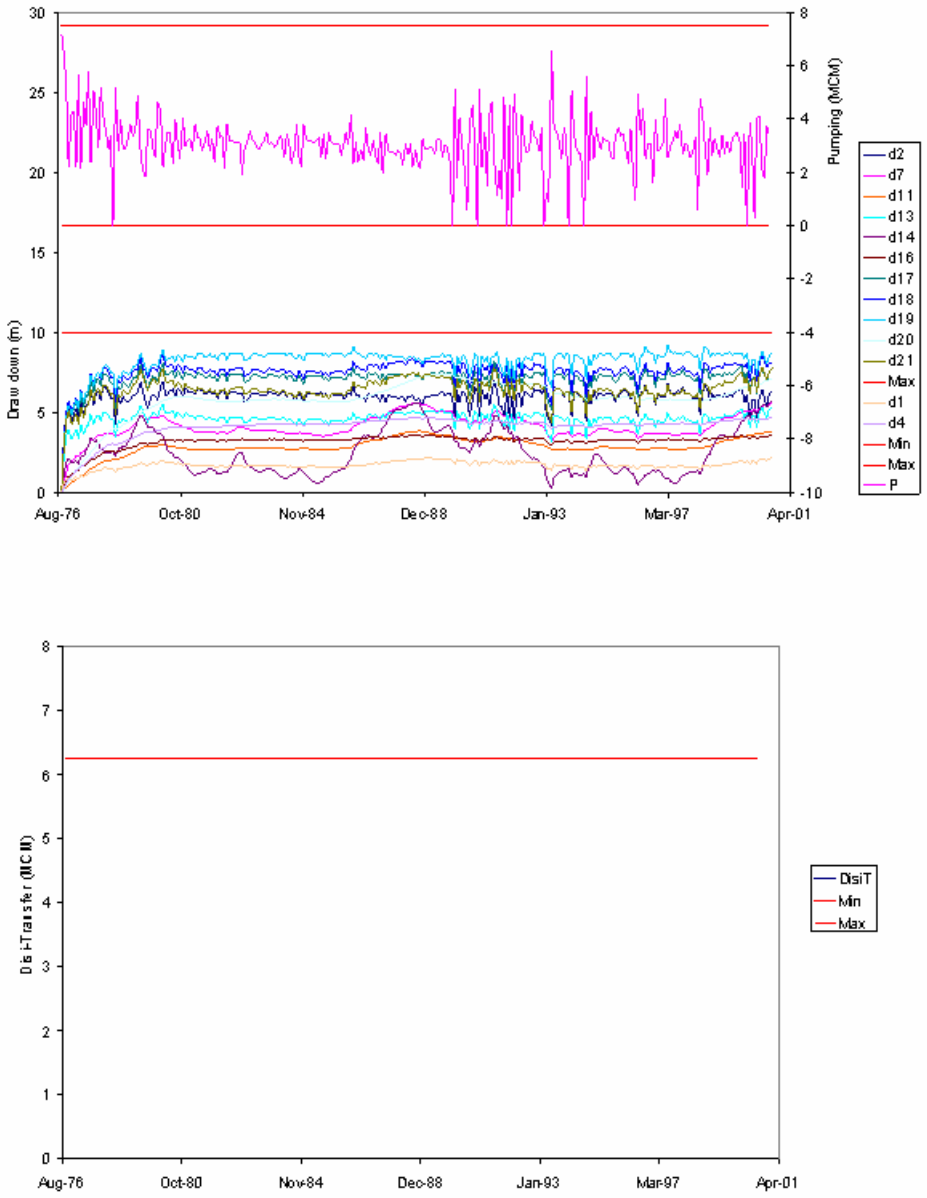

Figure F.5: Assessment model, scenario2, constrained GW drawdown, monthly pumping, drawdown and Disi transfer sequences

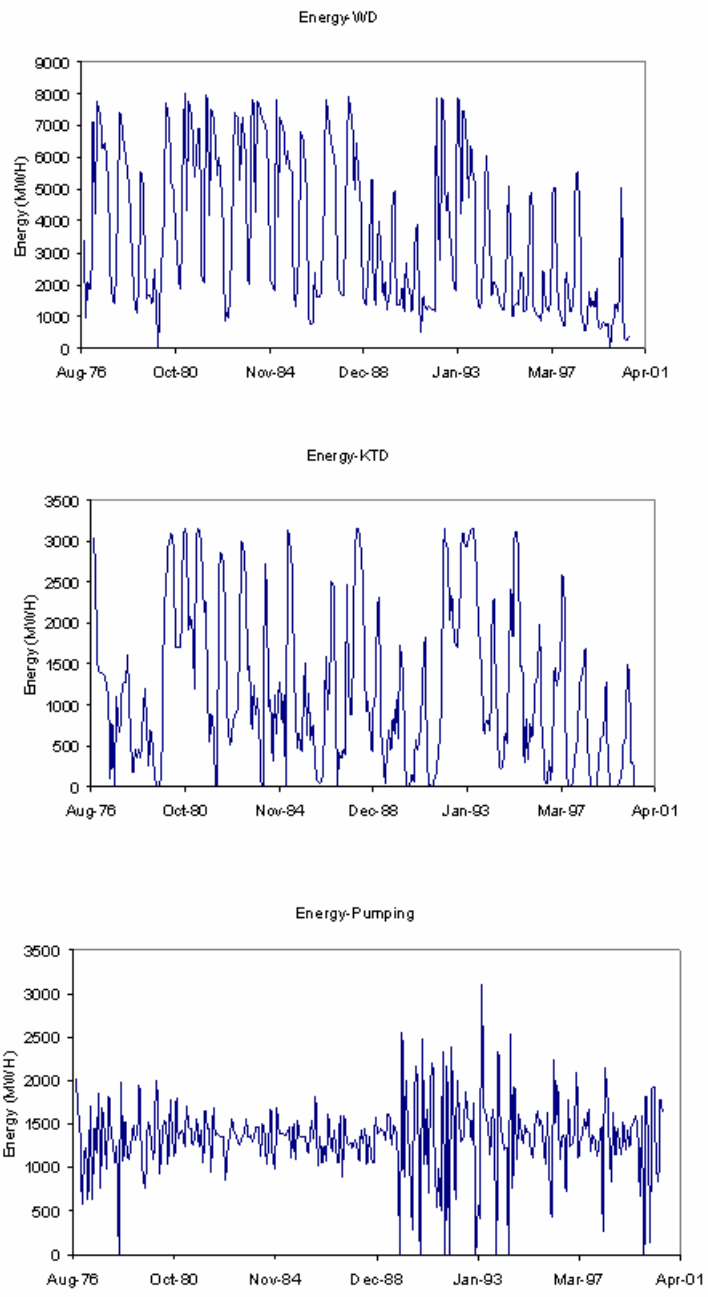

Figure F.6: Assessment model, scenario2, constrained GW drawdown , WD, KTD and pumping energy sequences

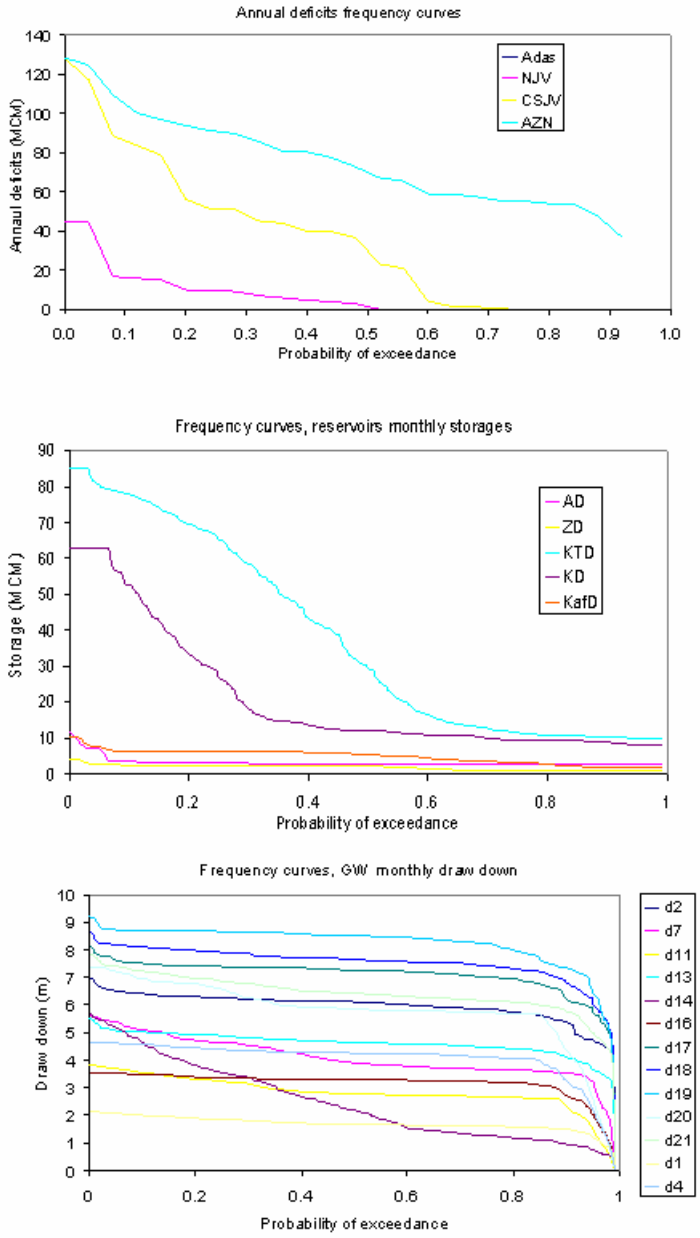

Figure F.7: Assessment model, scenario2, constrained GW drawdown, annual deficits, storages, and drawdowns frequency curves

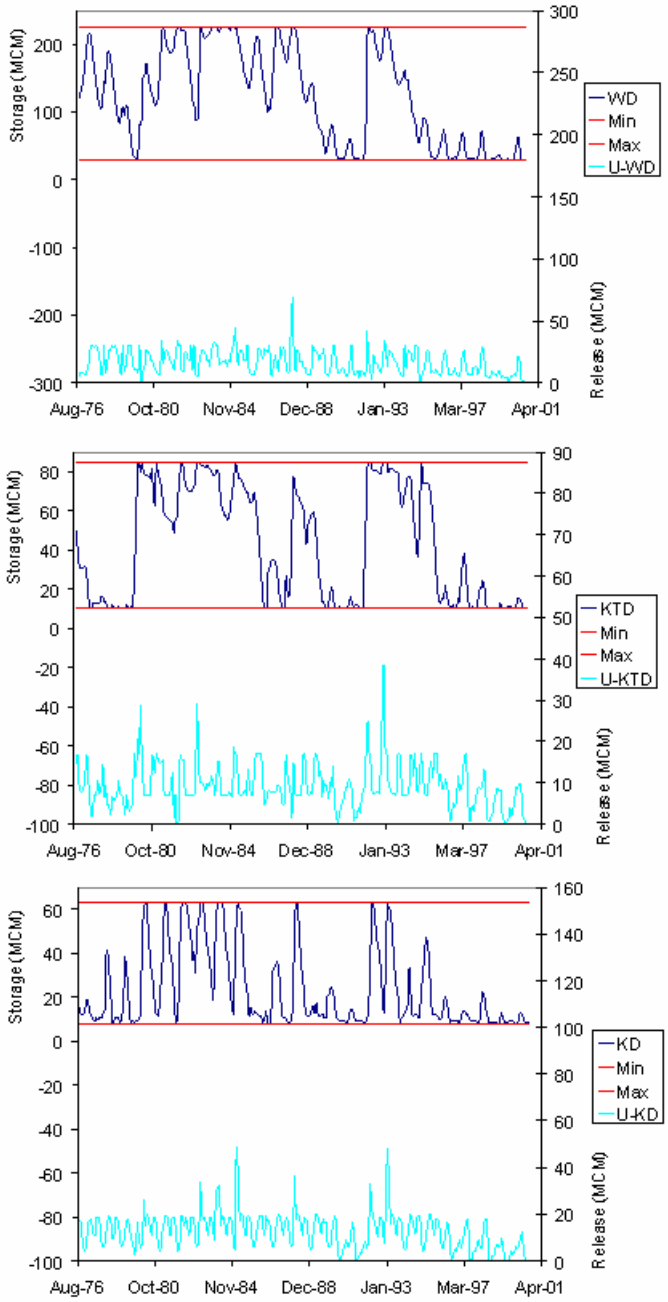

Figure F.8: Assessment model, scenario2, unconstrained GW drawdown, WD, KTD, and KD storage and release sequences

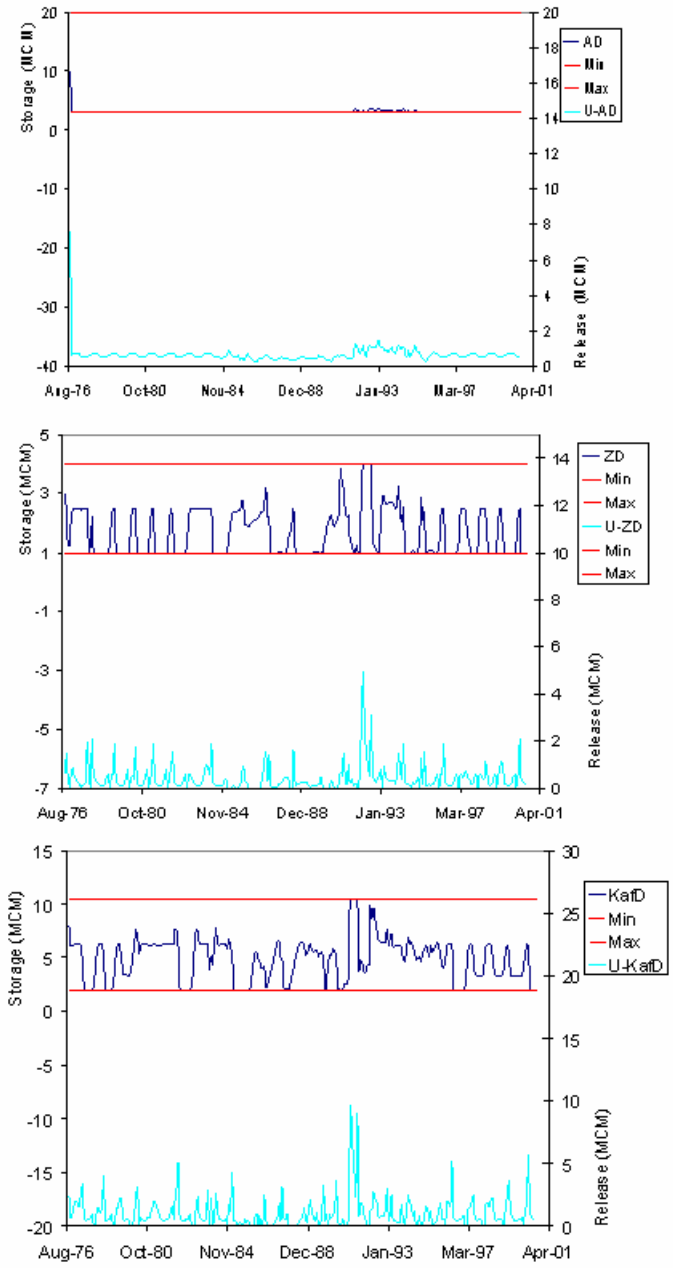

Figure F.9: Assessment model, scenario2, unconstrained GW drawdown, AD, ZD, and KafD storage and release sequences

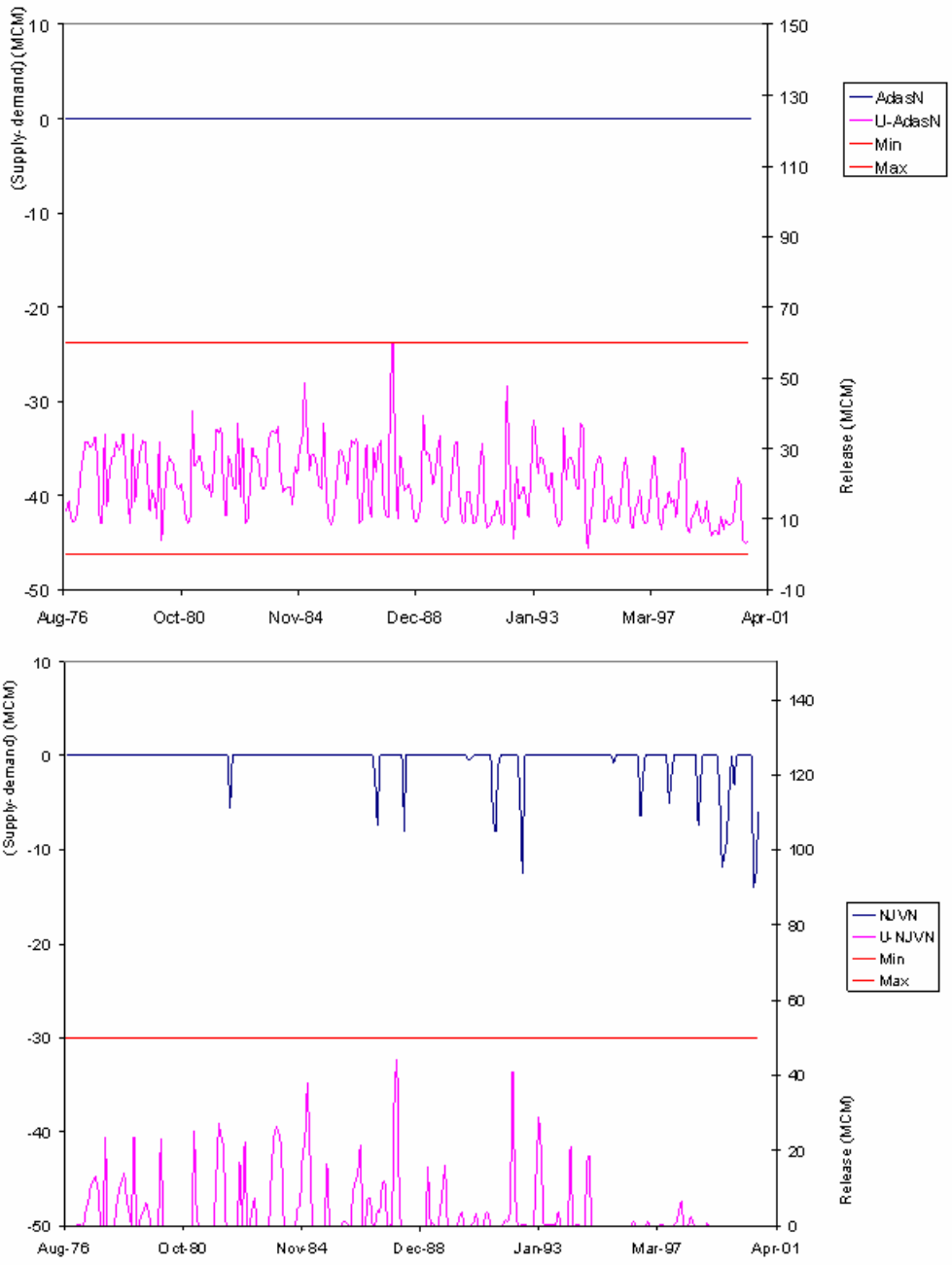

Figure F.10: Assessment model, scenario2, unconstrained GW drawdown, monthly water deficit and release sequences at Adasiya and North Jordan Valley nodes

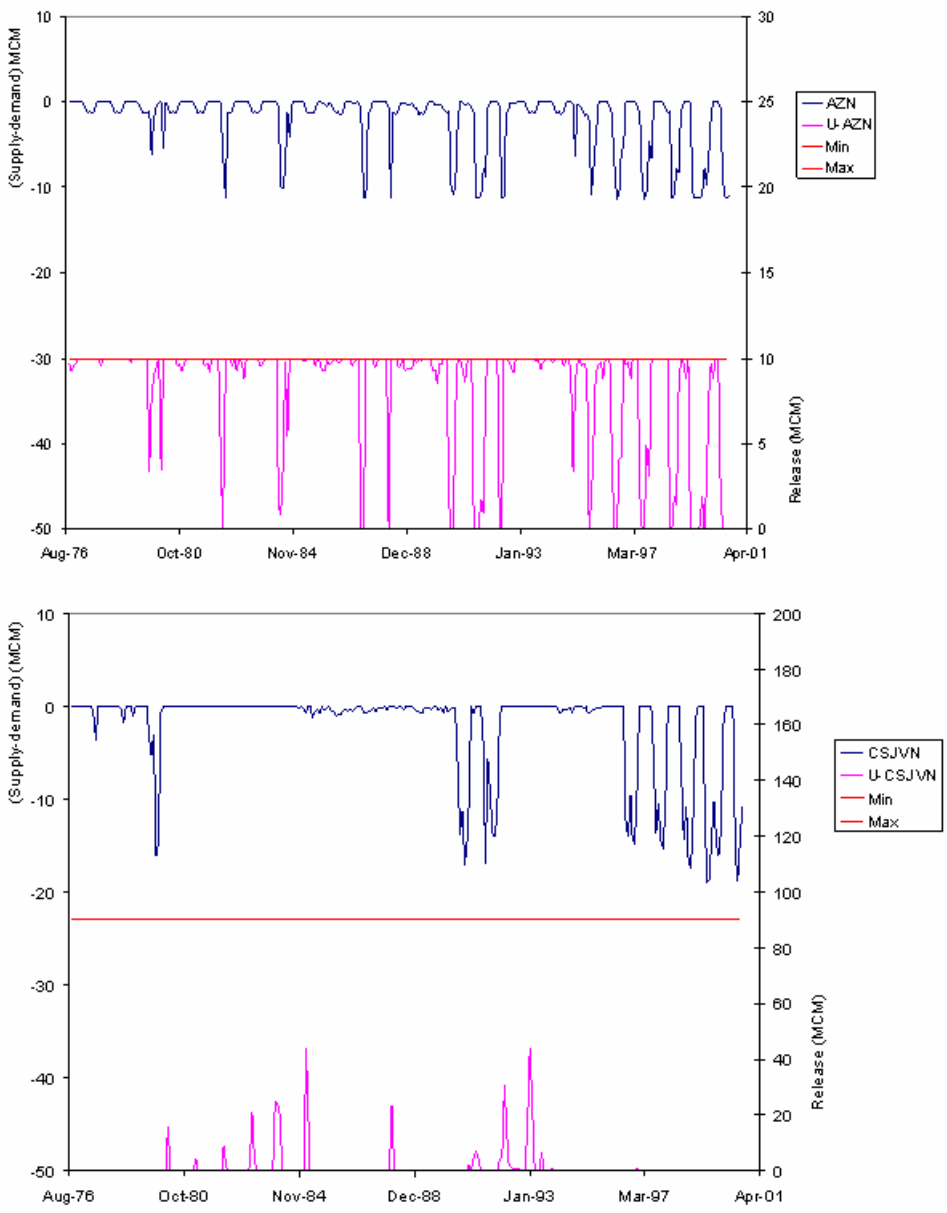

Figure F.11: Assessment model, scenario2, unconstrained GW drawdown, monthly water deficit and release sequences at Amman-Zarqa and C/S Jordan Valley nodes

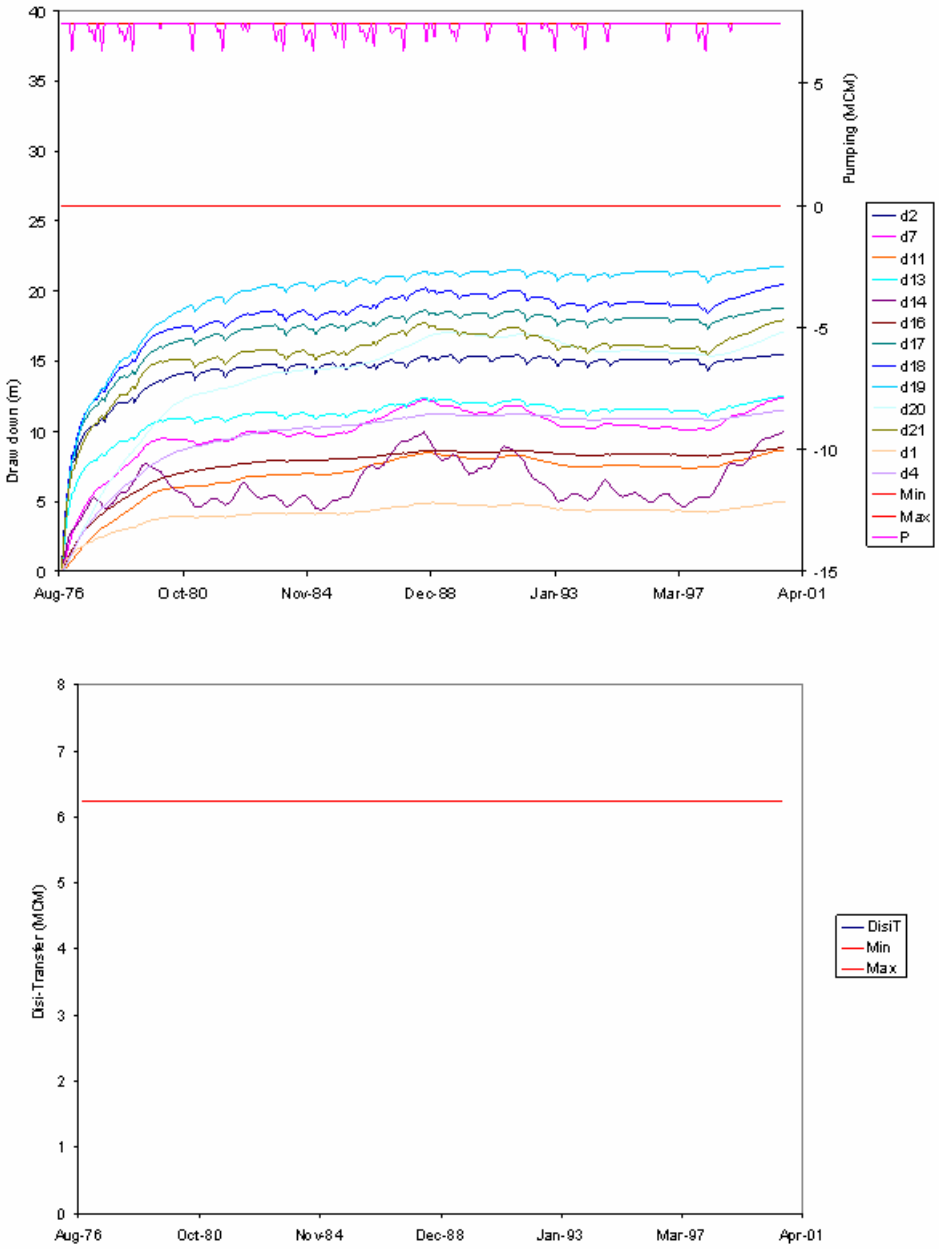

Figure F.12: Assessment model, scenario2, unconstrained GW drawdown, monthly pumping, drawdown and Disi transfer sequences

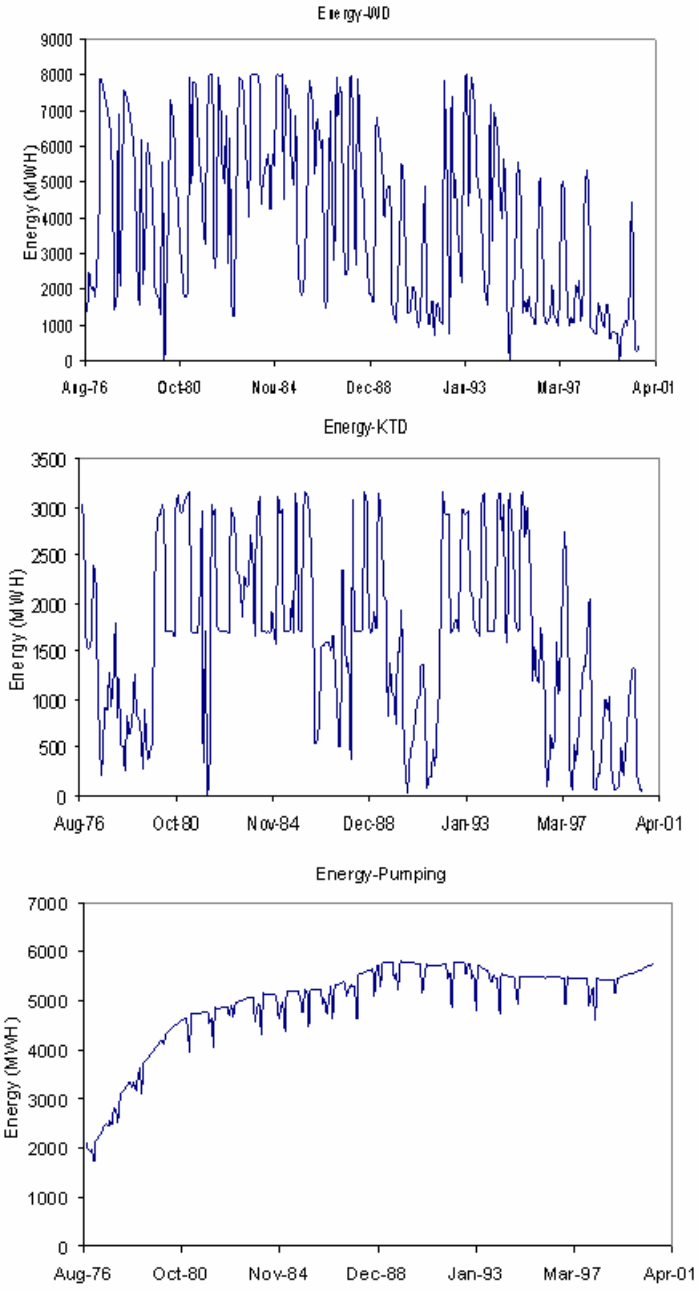

Figure F.13: Assessment model, scenario2, unconstrained GW drawdown , WD, KTD and pumping energy sequences

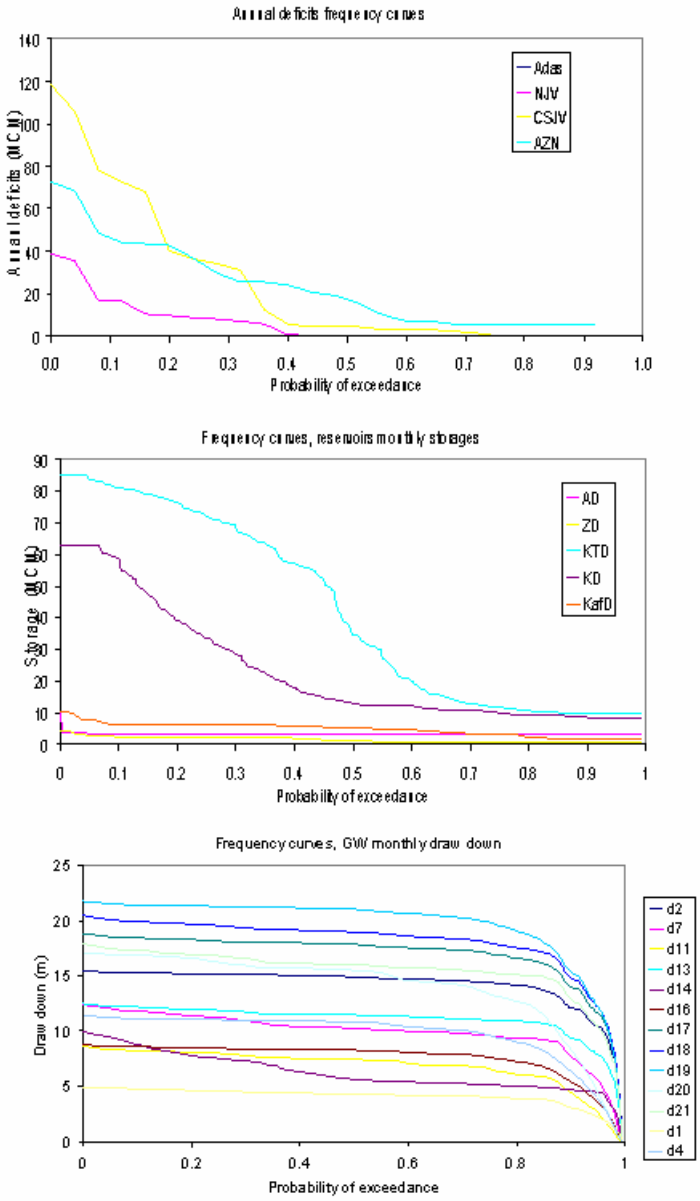

Figure F.14: Assessment model, scenario2, unconstrained GW drawdown, annual deficits, storages, and drawdowns frequency curves

APPENDIX G

SCENARIO 3: SYRIAN IRRIGATION WITHDRAWALS

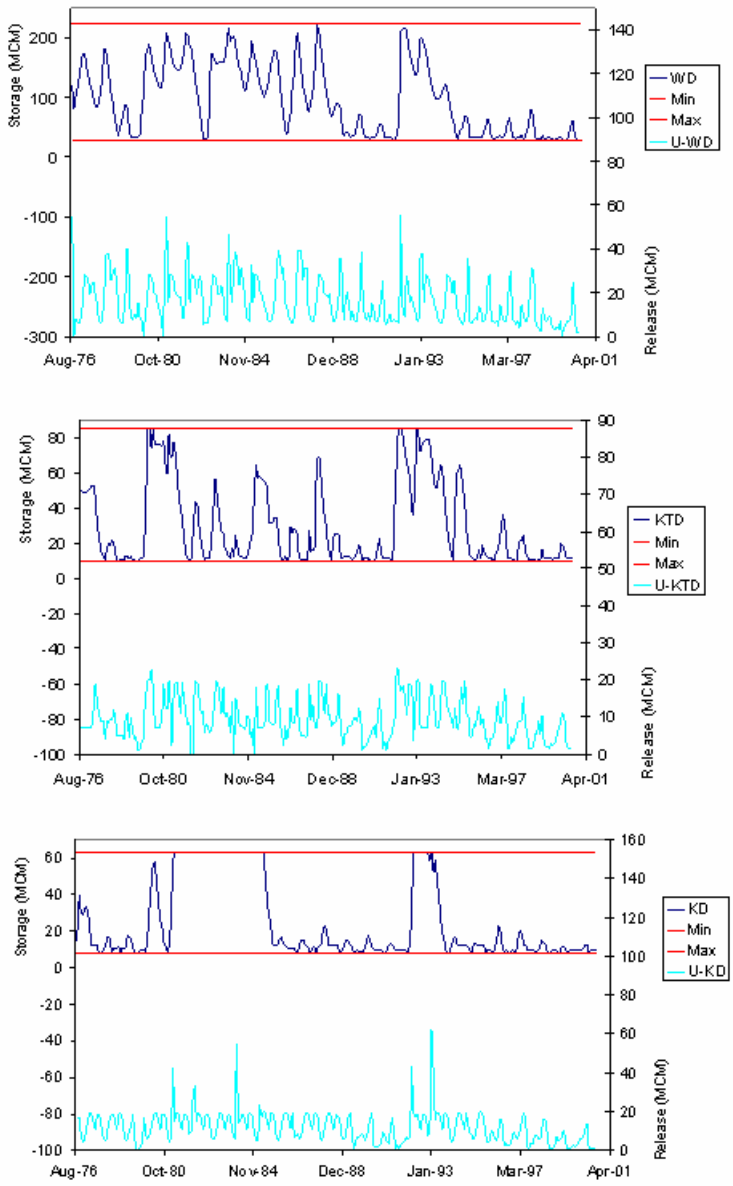

Figure G.1: Assessment model, scenario3, Syrian withdrawals 20%, constrained GW drawdown, WD, KTD, and KD storage and release sequences

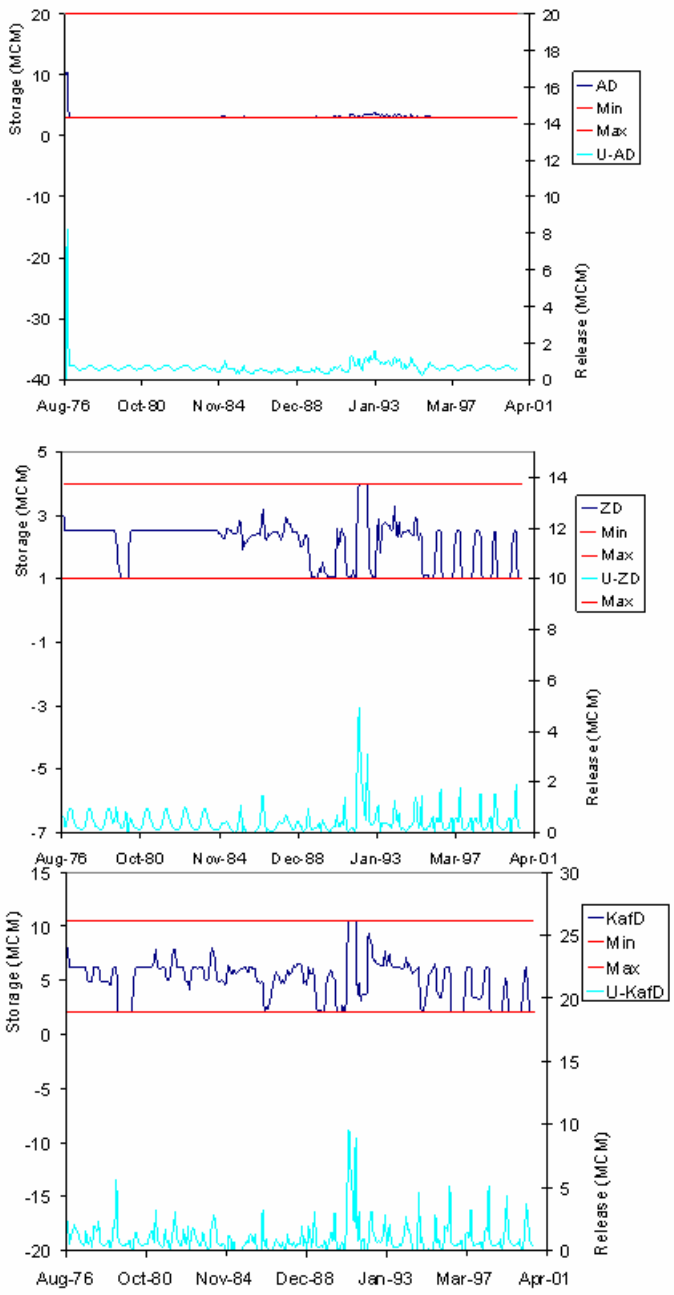

Figure G.2: Assessment model, scenario3, Syrian withdrawals 20%, constrained GW drawdown, AD, ZD, and KafD storage and release sequences

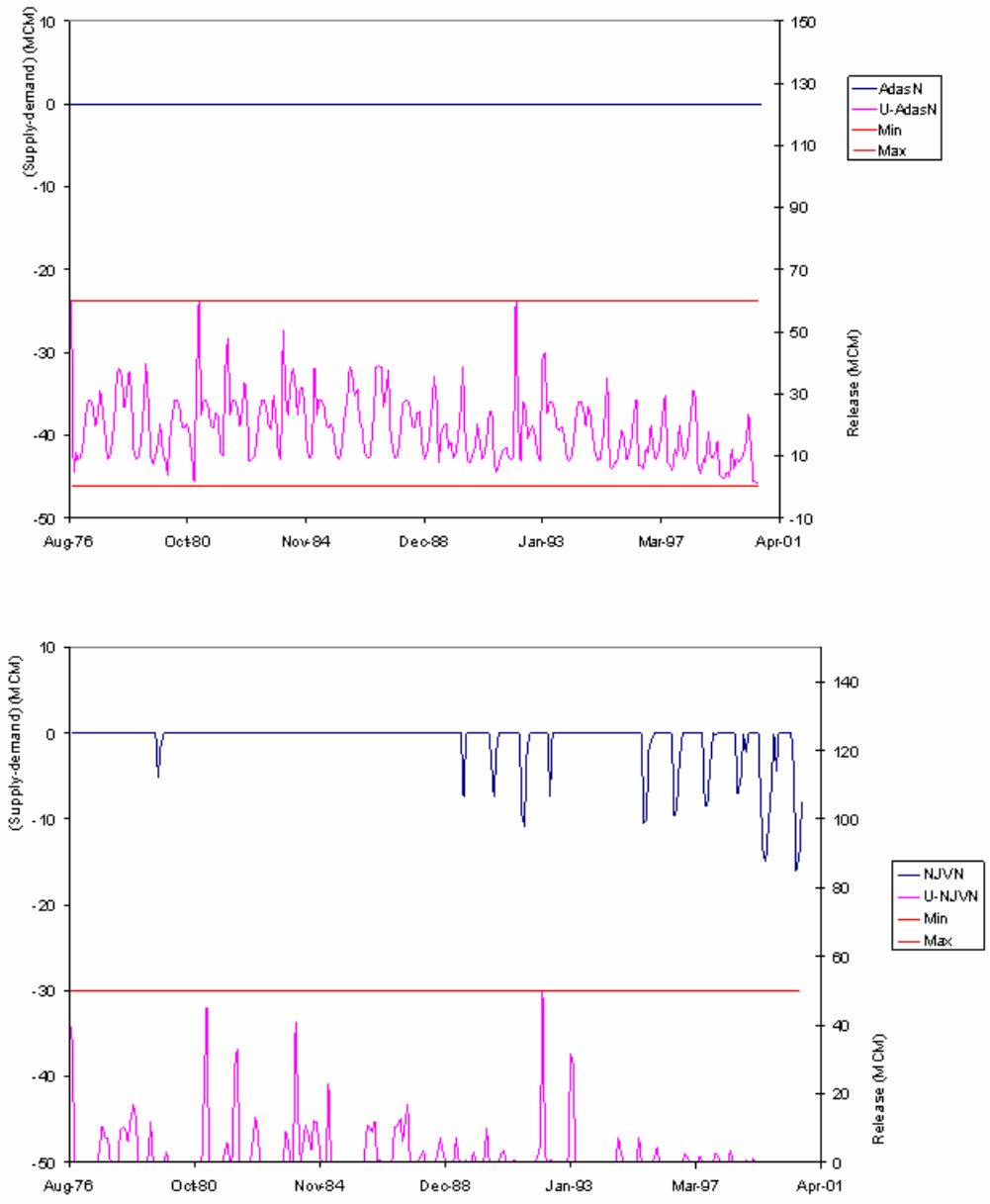

Figure G.3: Assessment model, scenario3, Syrian withdrawals 20%, constrained GW drawdown, monthly water deficit and release sequences at Adasiya and North Jordan Valley nodes

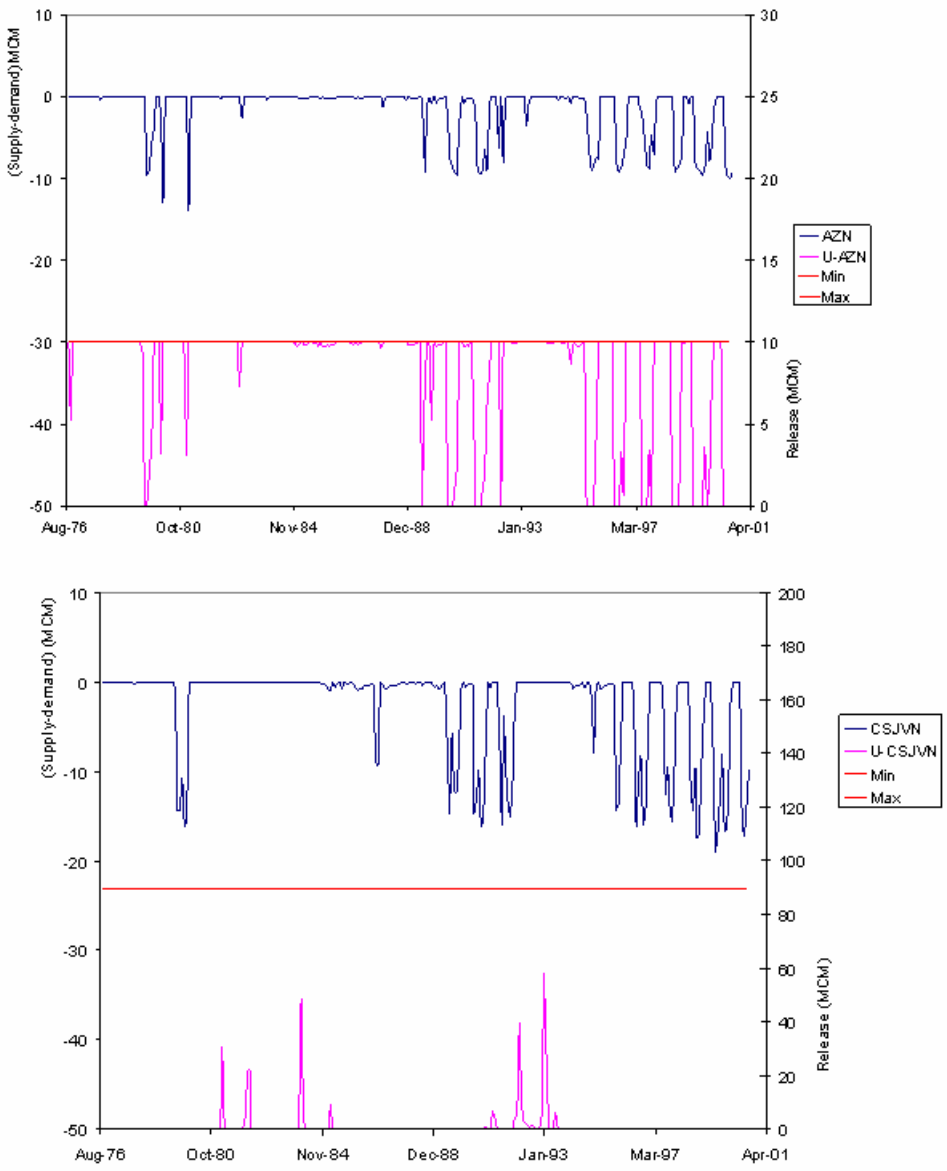

Figure G.4: Assessment model, scenario3, Syrian withdrawals 20%, constrained GW drawdown, monthly water deficit and release sequences at Amman-Zarqa and C/S Jordan Valley nodes

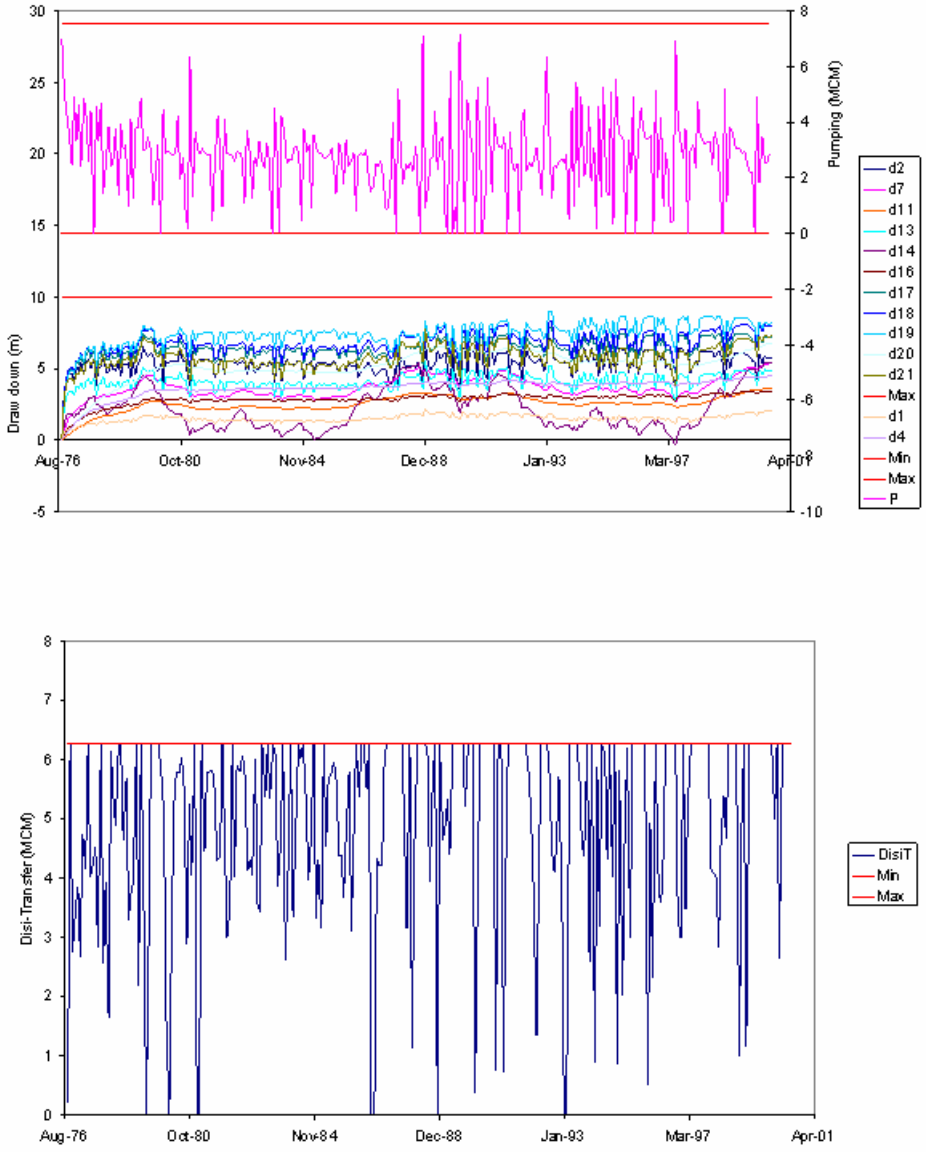

Figure G.5: Assessment model, scenario3, Syrian withdrawals 20%, constrained GW drawdown, monthly pumping, drawdown and Disi transfer sequences

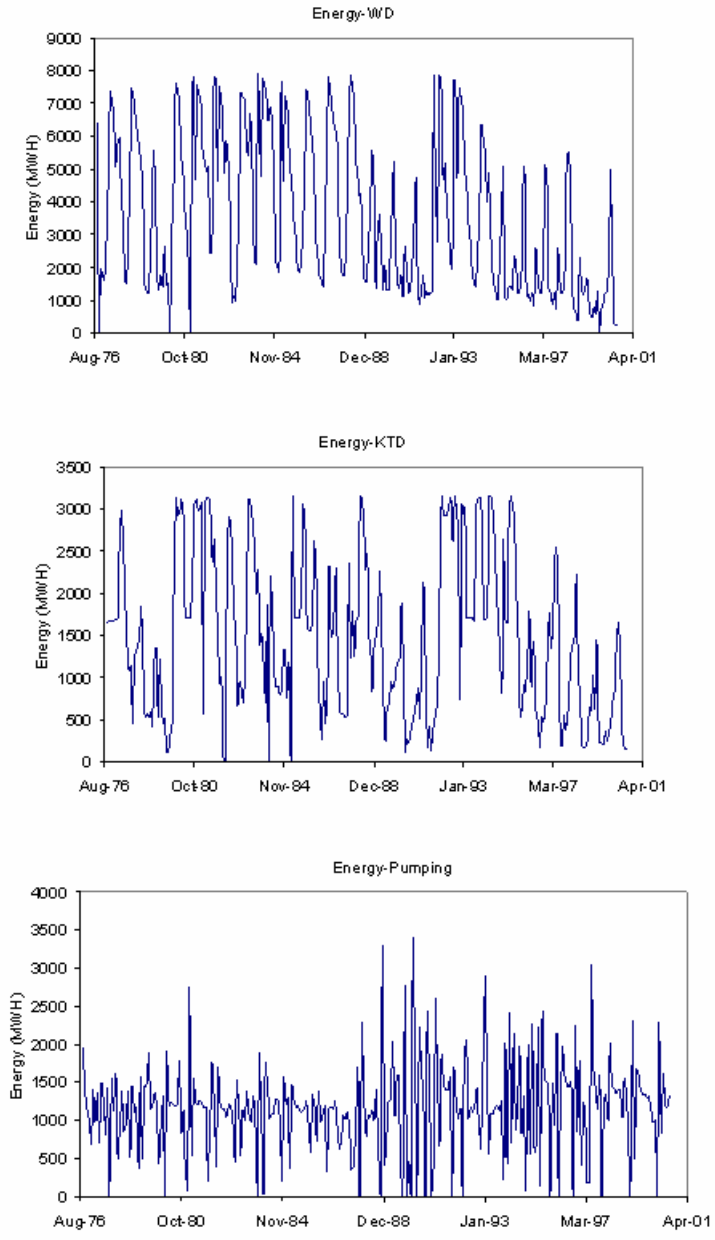

Figure G.6: Assessment model, scenario3, Syrian withdrawals 20%, constrained GW drawdown, WD, KTD and pumping energy sequences

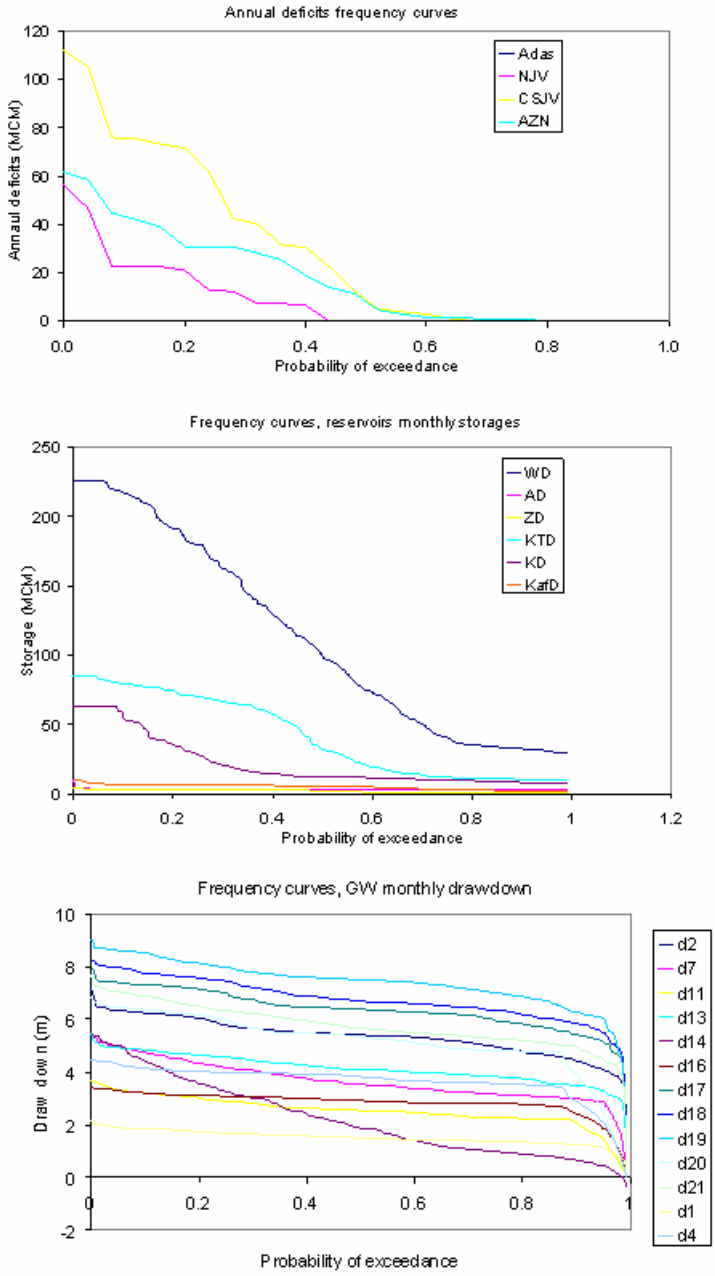

Figure G.7: Assessment model, scenario3, Syrian withdrawals 20%, constrained GW drawdown, annual deficits, storages, and drawdowns frequency curves

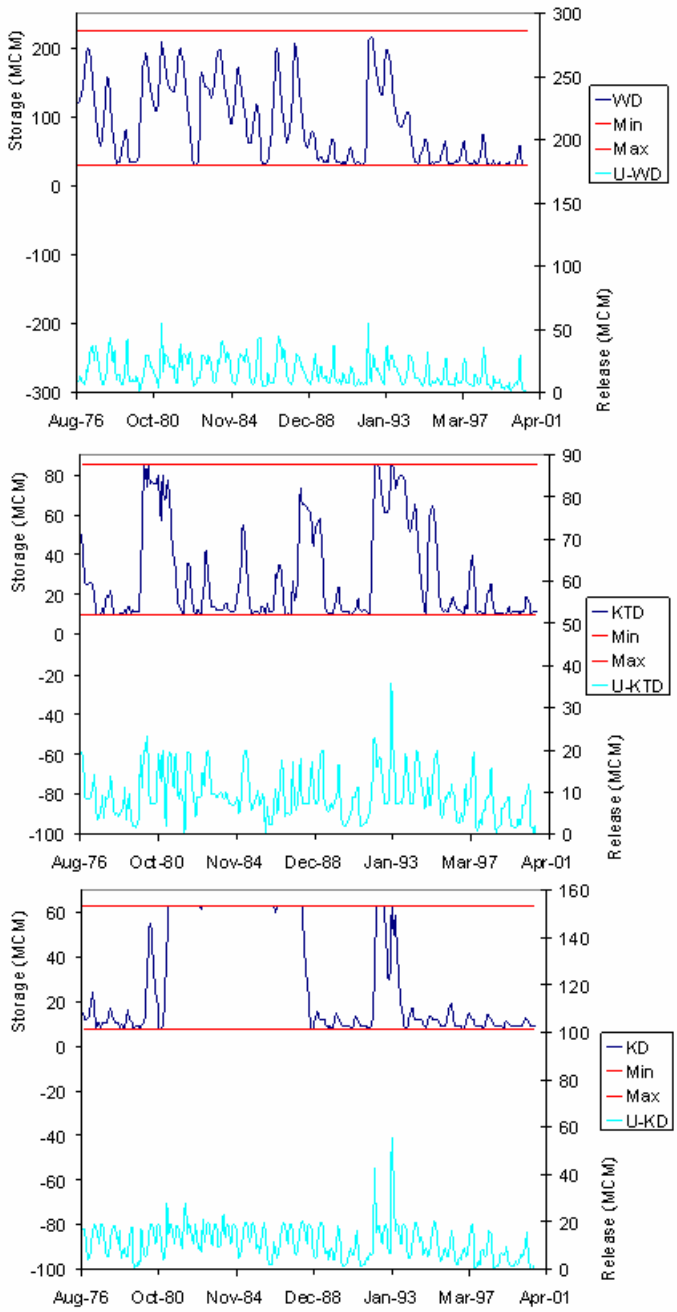

Figure G.8: Assessment model, scenario3, Syrian withdrawals 30%, constrained GW drawdown, WD, KTD, and KD storage and release sequences

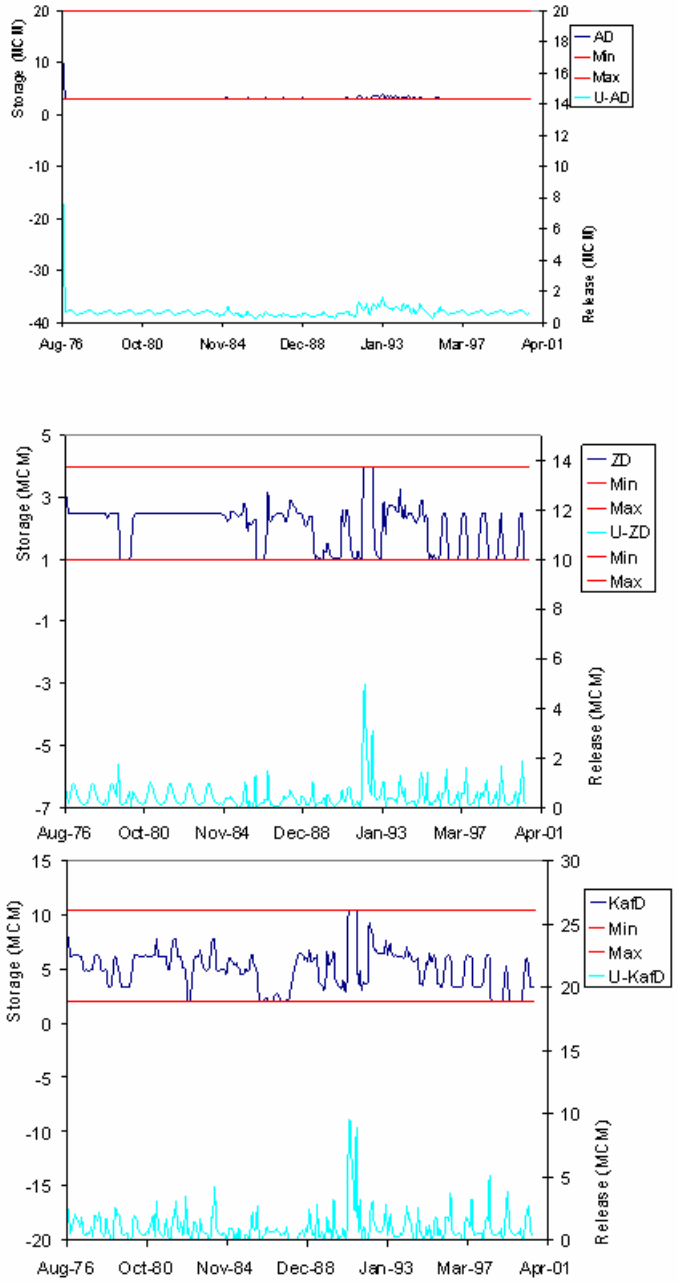

Figure G.9: Assessment model, scenario3, Syrian withdrawals 30%, constrained GW drawdown, AD, ZD, and KafD storage and release sequences

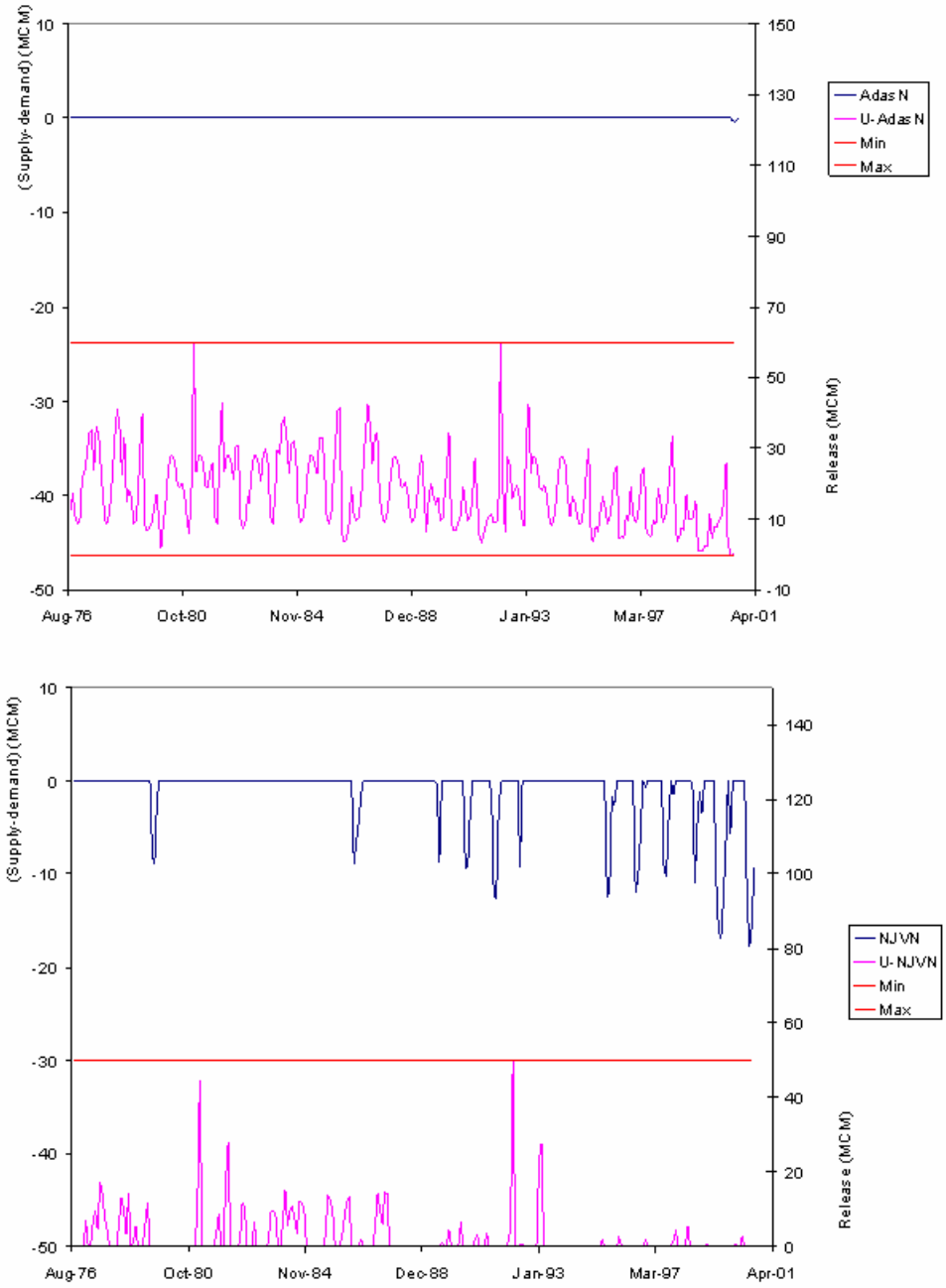

Figure G.10: Assessment model, scenario3, Syrian withdrawals 30%, constrained GW drawdown, monthly water deficit and release sequences at Adasiya and North Jordan Valley nodes

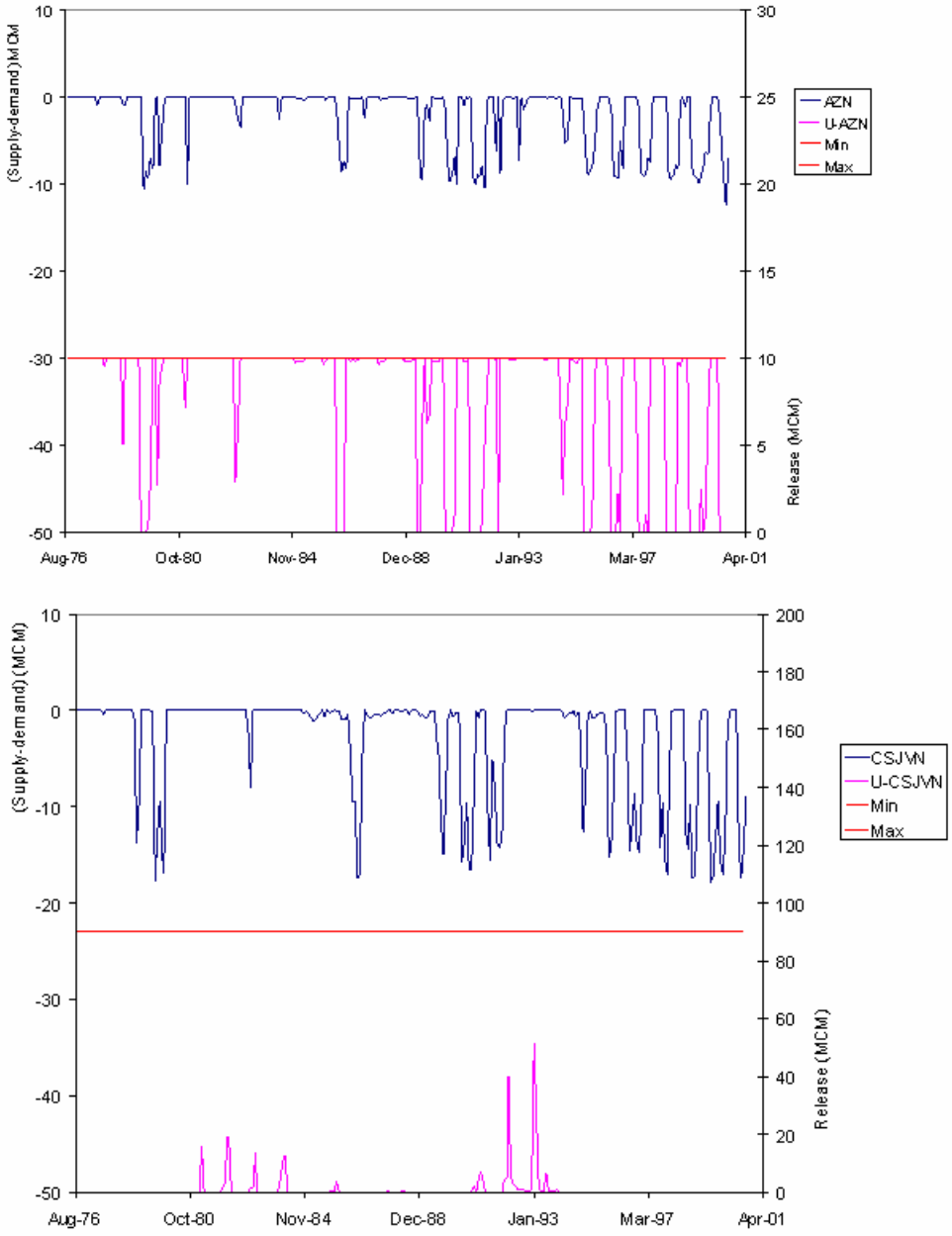

Figure G.11: Assessment model, scenario3, Syrian withdrawals 30%, constrained GW drawdown, monthly water deficit and release sequences at Amman-Zarqa and C/S Jordan Valley nodes

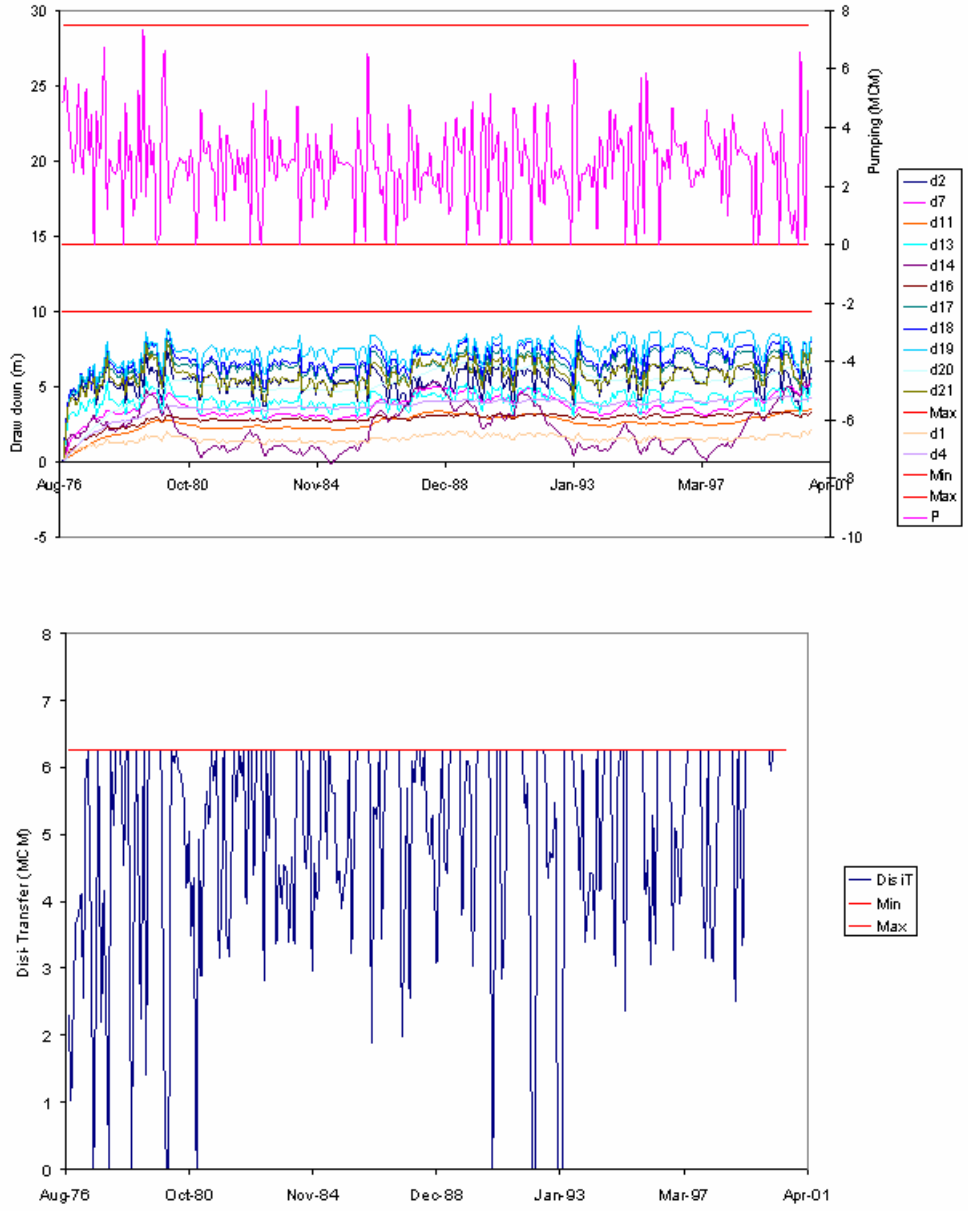

Figure G.12: Assessment model, scenario3, Syrian withdrawals 30%, constrained GW drawdown, monthly pumping, drawdown and Disi transfer sequences

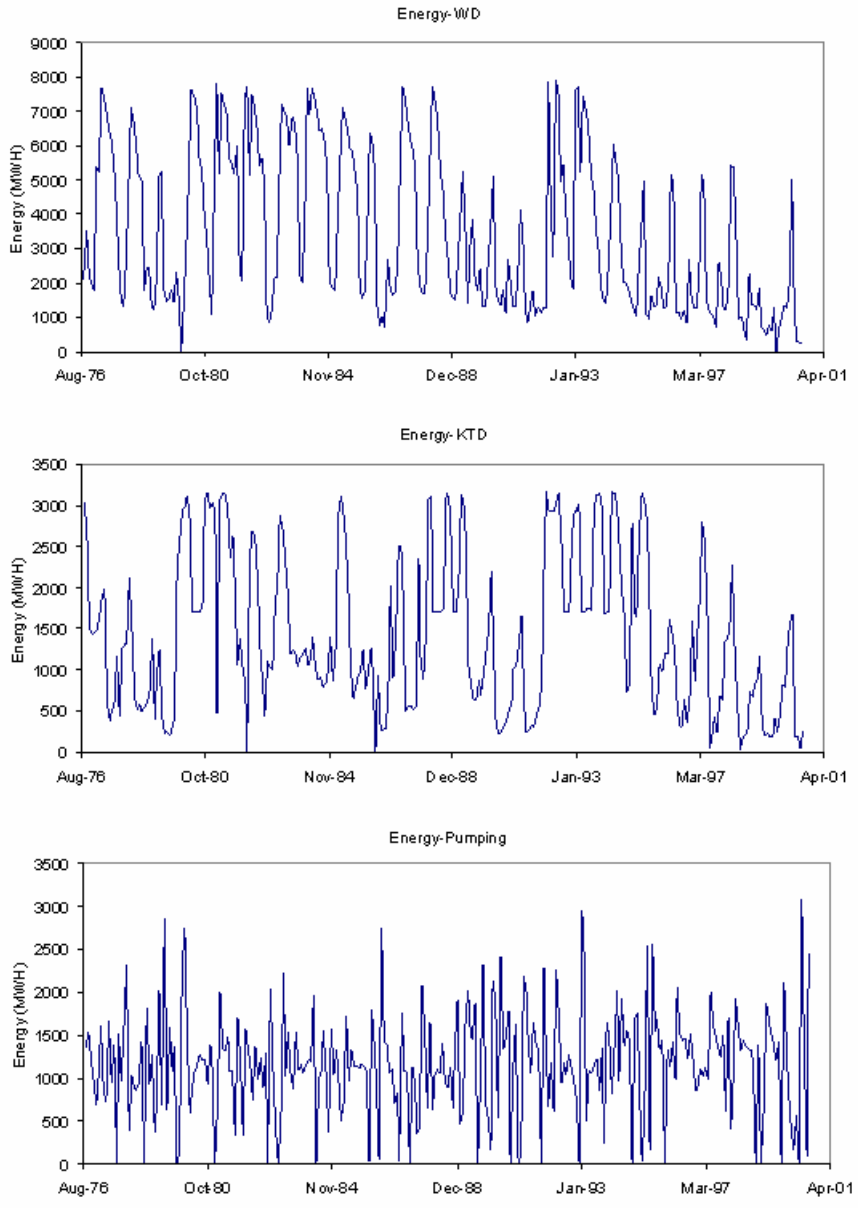

Figure G.13: Assessment model, scenario3, Syrian withdrawals 30%, constrained GW drawdown, WD, KTD and pumping energy sequences

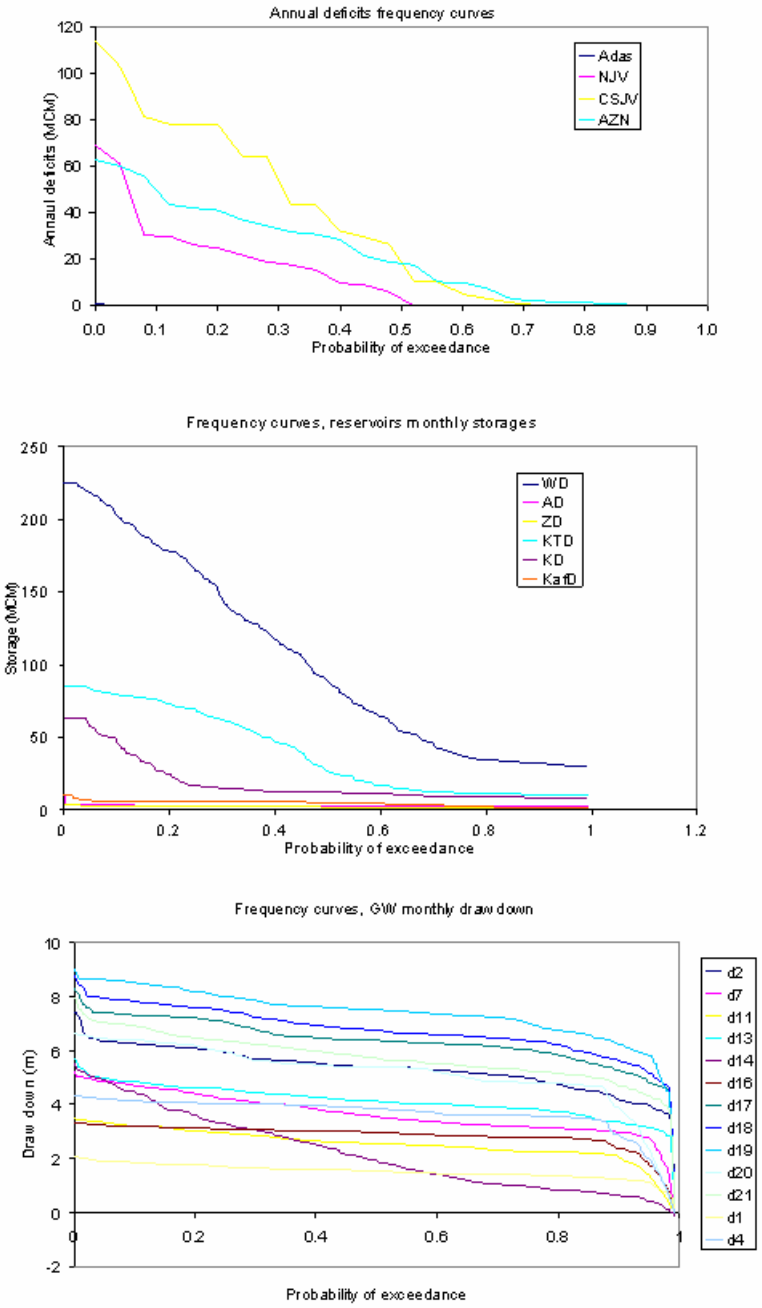

Figure G.14: Assessment model, scenario3, Syrian withdrawals 30%, constrained GW drawdown, annual deficits, storages, and drawdowns frequency curves

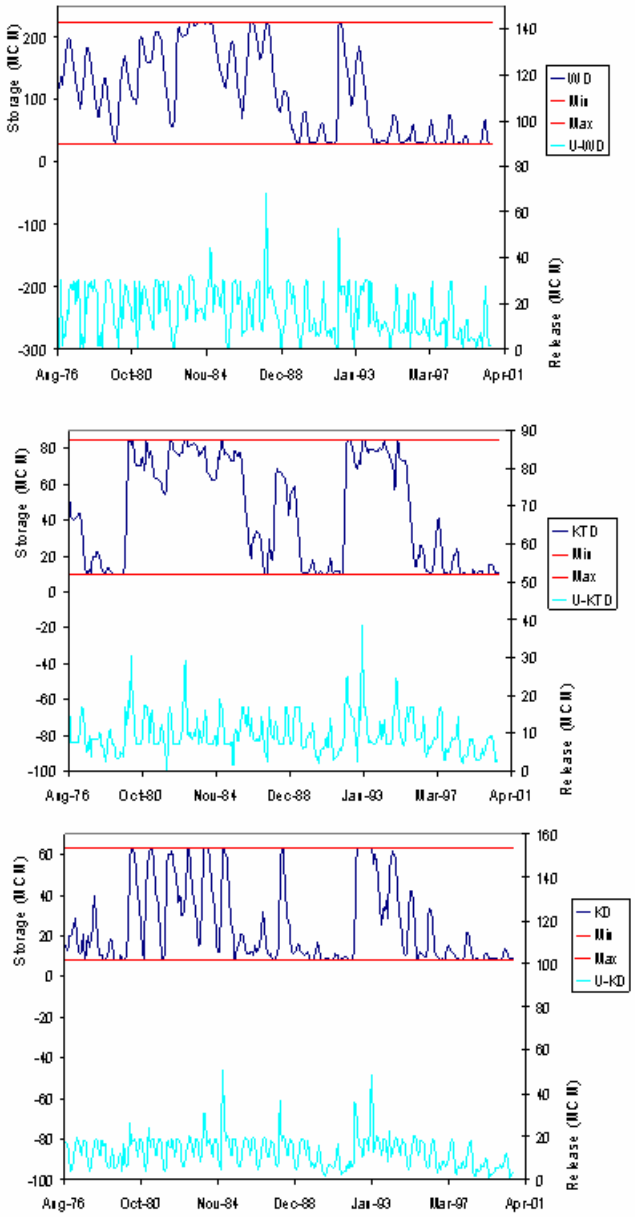

Figure G.15: Assessment model, scenario3, Syrian withdrawals 20%, unconstrained GW drawdown, WD, KTD, and KD storage and release sequences

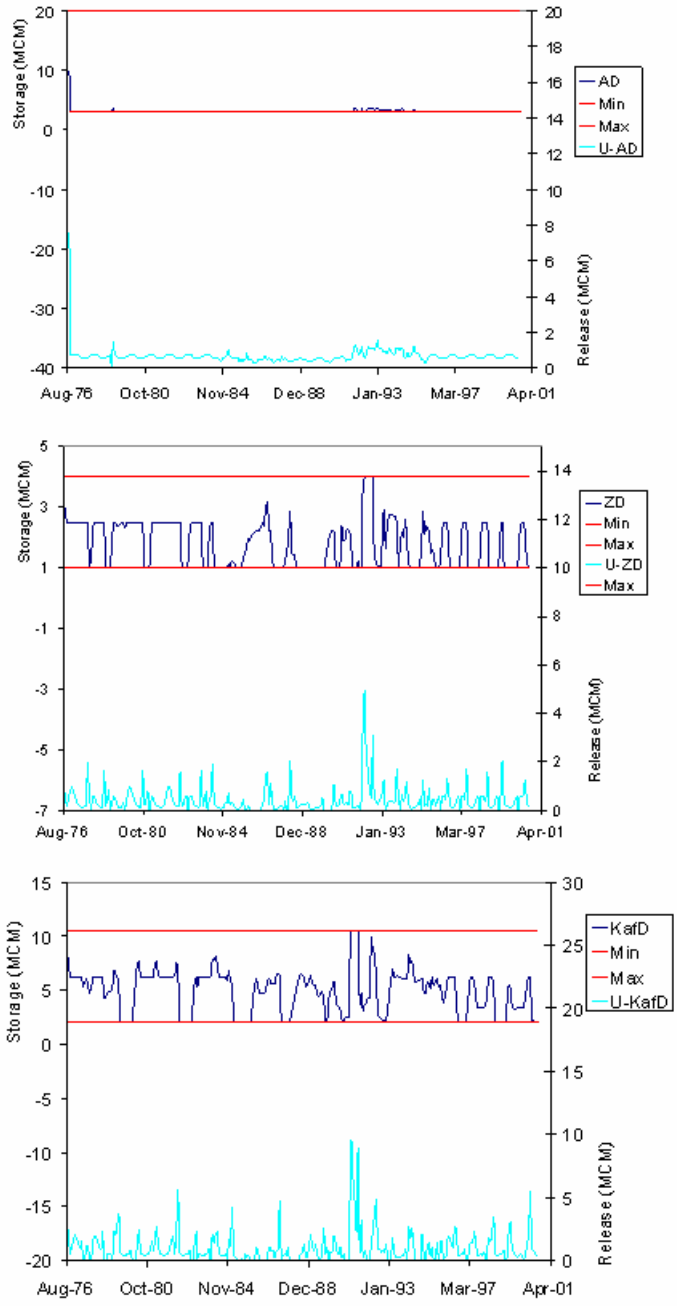

Figure G.16: Assessment model, scenario3, Syrian withdrawals 20%, unconstrained GW drawdown, AD, ZD, and KafD storage and release sequences

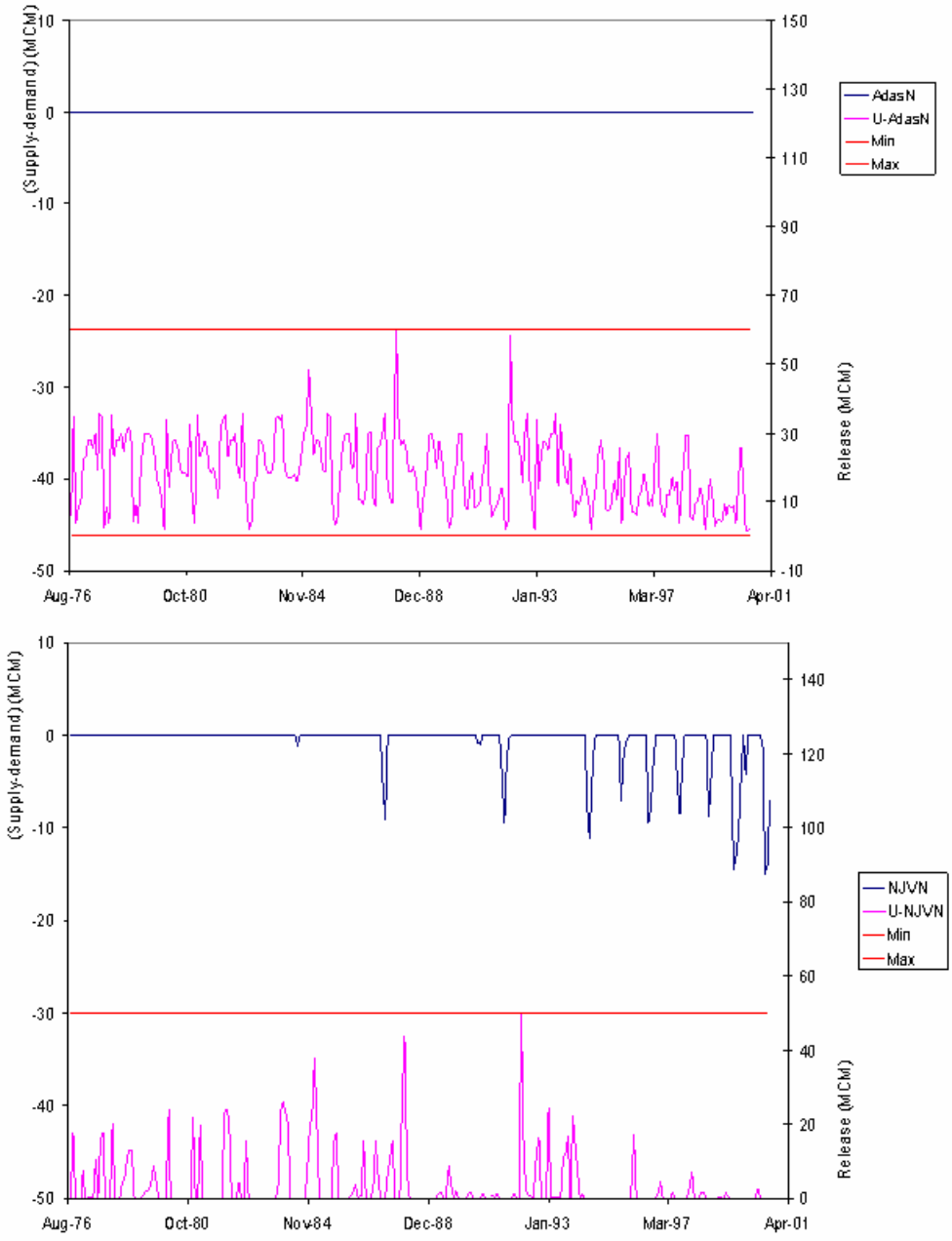

Figure G.17: Assessment model, scenario3, Syrian withdrawals 20%, unconstrained GW drawdown, monthly water deficit and release sequences at Adasiya and North Jordan Valley nodes

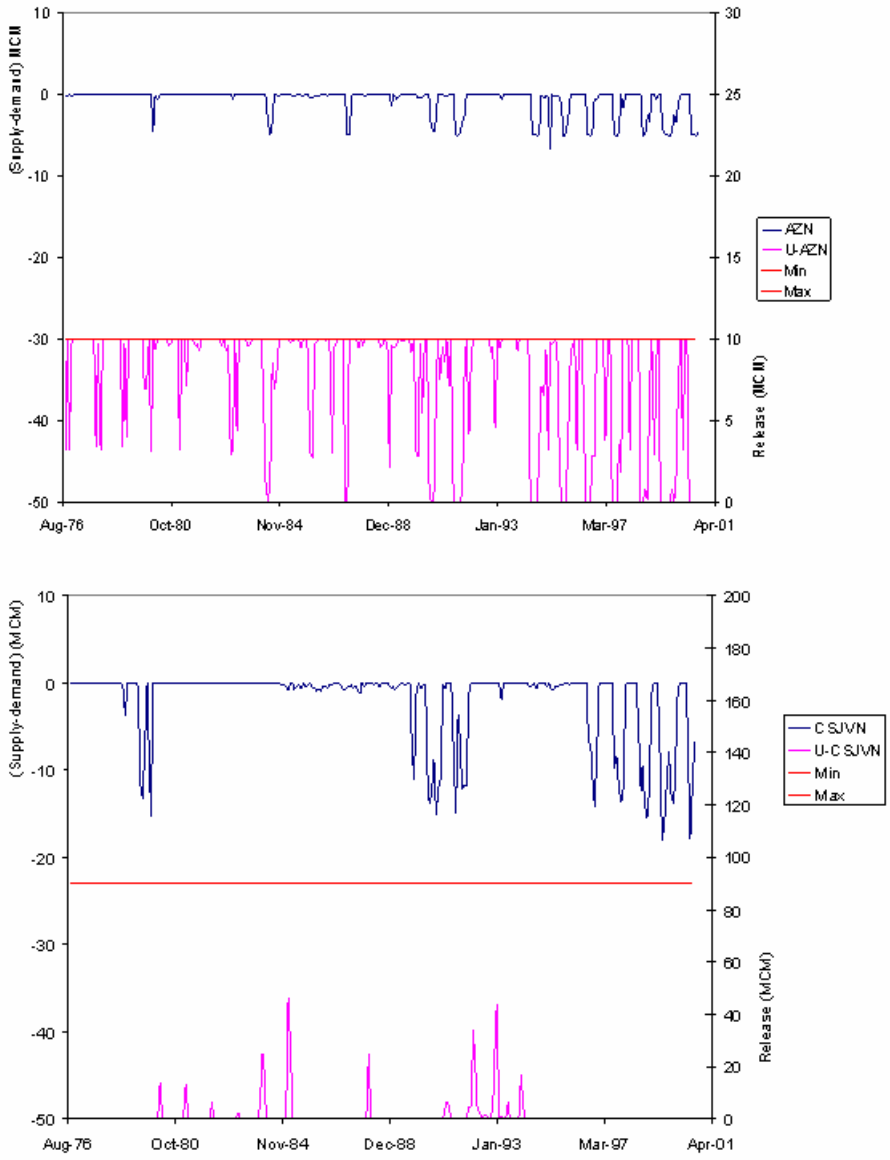

Figure G.18: Assessment model, scenario3, Syrian withdrawals 20%, unconstrained GW drawdown, monthly water deficit and release sequences at Amman-Zarqa and C/S Jordan Valley nodes

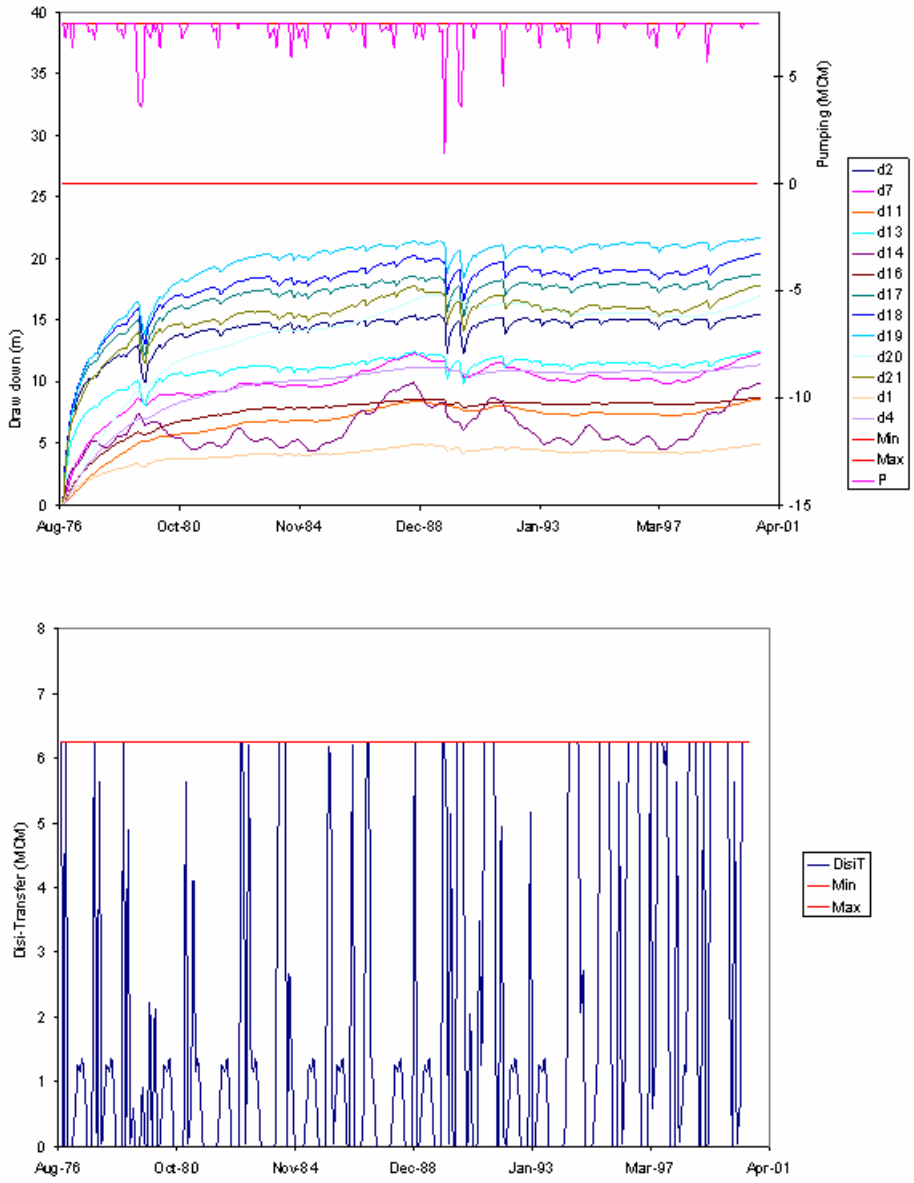

Figure G.19: Assessment model, scenario3, Syrian withdrawals 20%, unconstrained GW drawdown, monthly pumping, drawdown and Disi transfer sequences

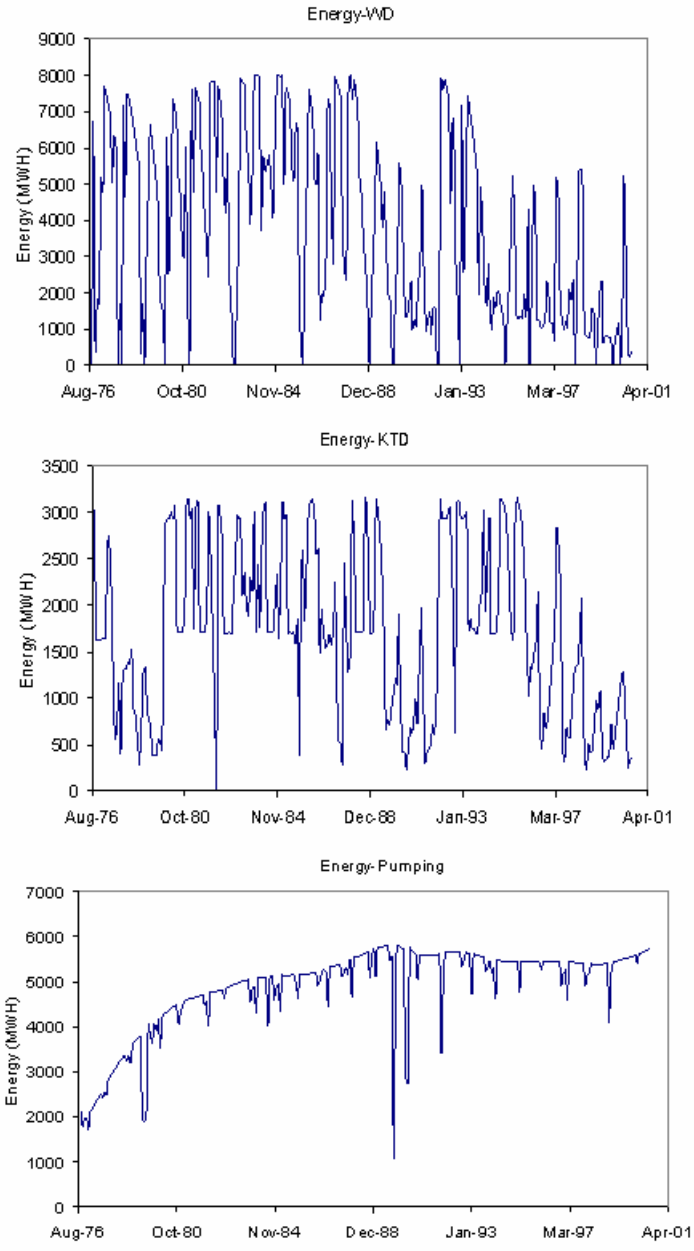

Figure G.20: Assessment model, scenario3, Syrian withdrawals 20%, unconstrained GW drawdown, WD, KTD and pumping energy sequences

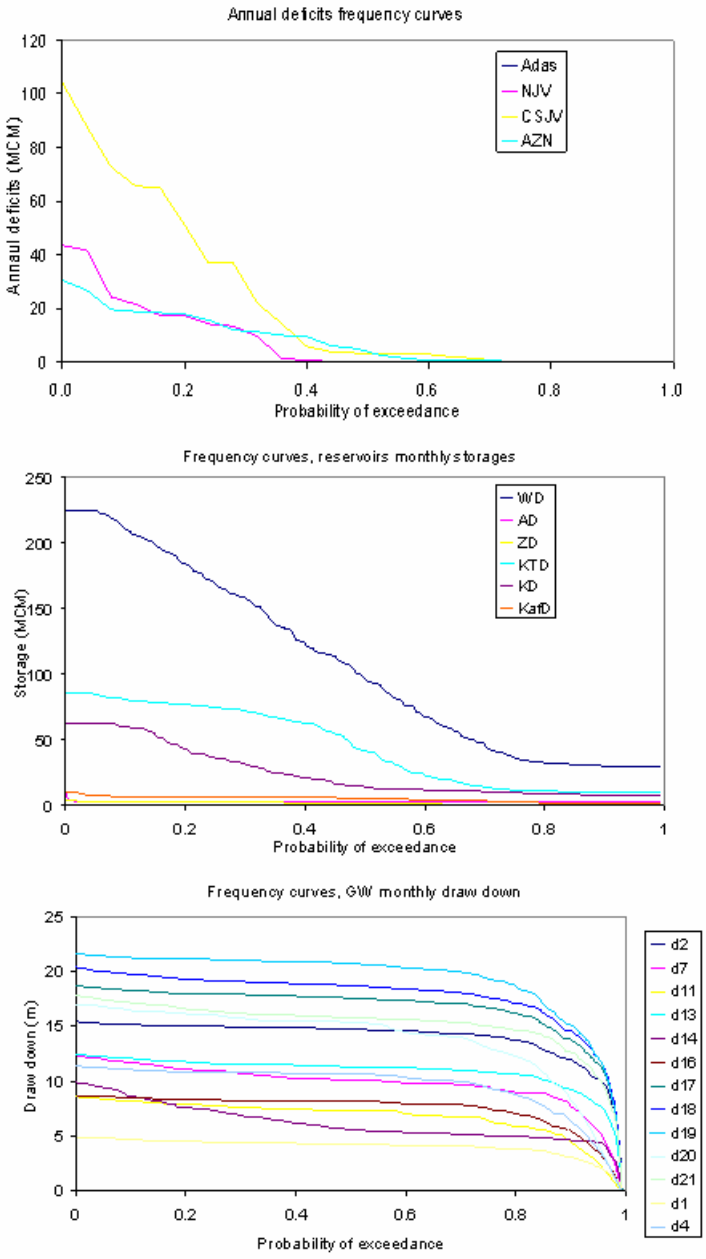

Figure G.21: Assessment model, scenario3, Syrian withdrawals 20%, unconstrained GW drawdown, annual deficits, storages, and drawdowns frequency curves

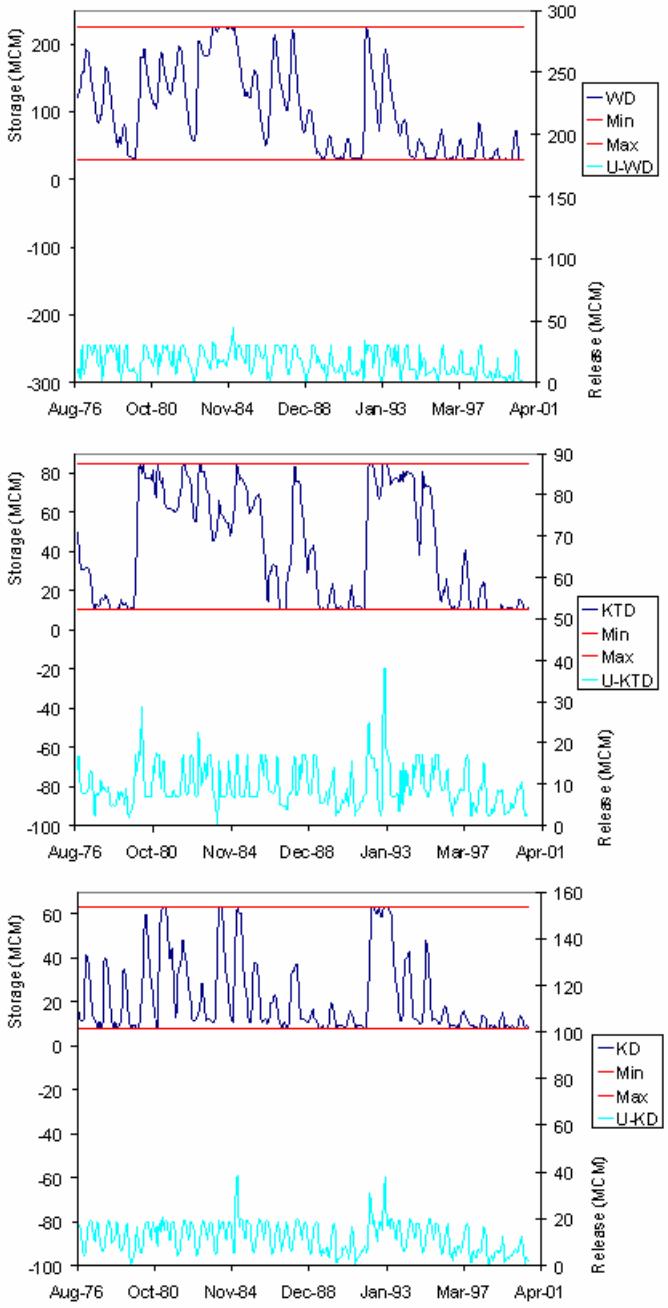

Figure G.22: Assessment model, scenario3, Syrian withdrawals 30%, unconstrained GW drawdown, WD, KTD, and KD storage and release sequences

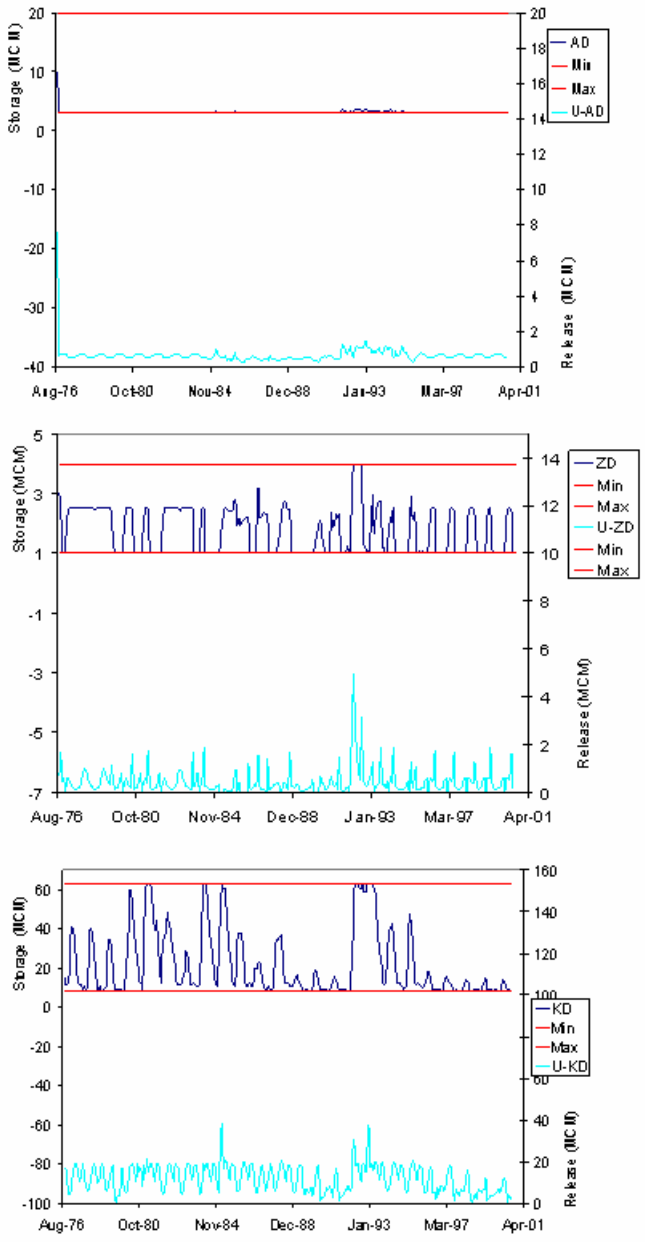

Figure G.23: Assessment model, scenario3, Syrian withdrawals 30%, unconstrained GW drawdown, AD, ZD, and KafD storage and release sequences

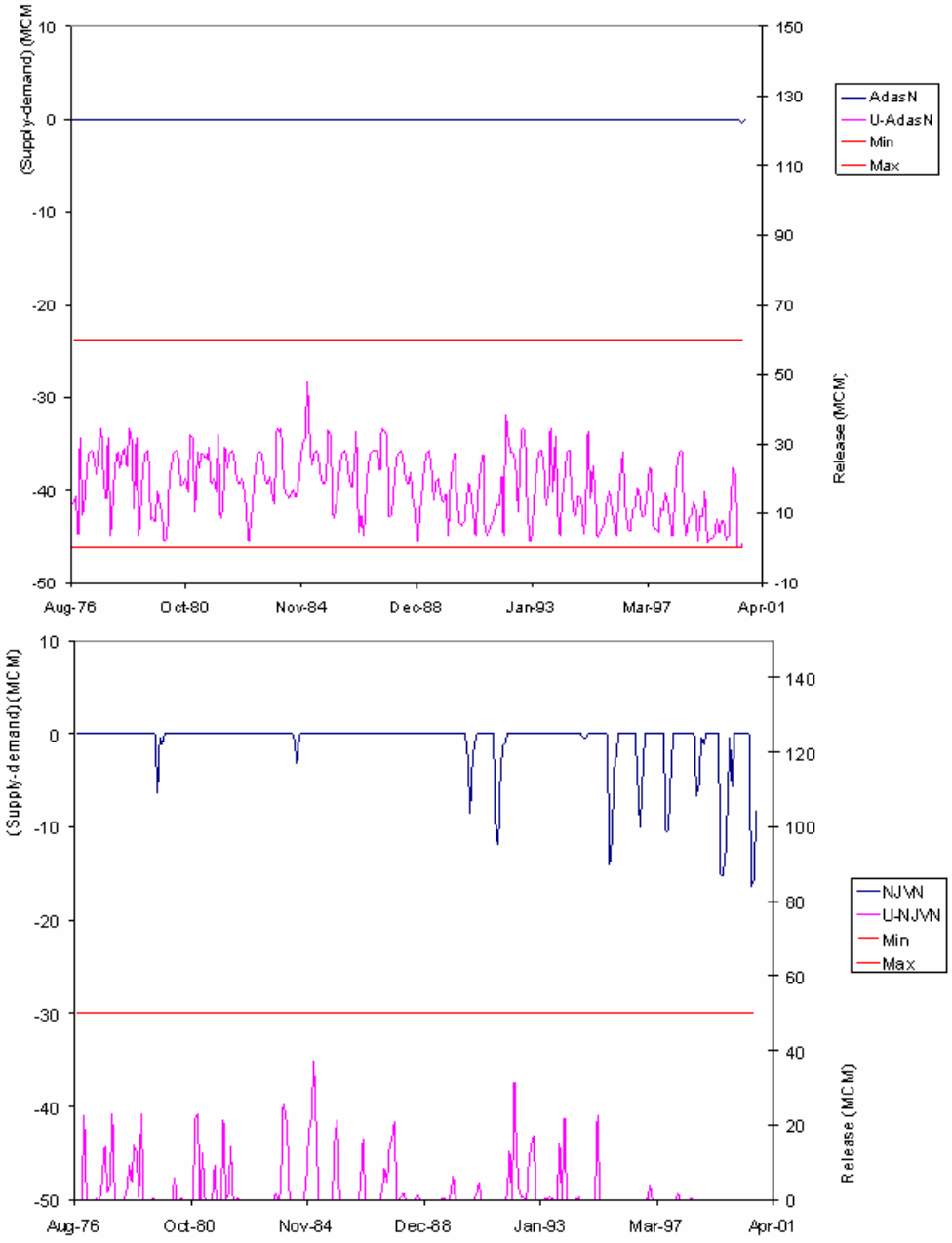

Figure G.24: Assessment model, scenario3, Syrian withdrawals 30%, unconstrained GW drawdown, monthly water deficit and release sequences at Adasiya and North Jordan Valley nodes

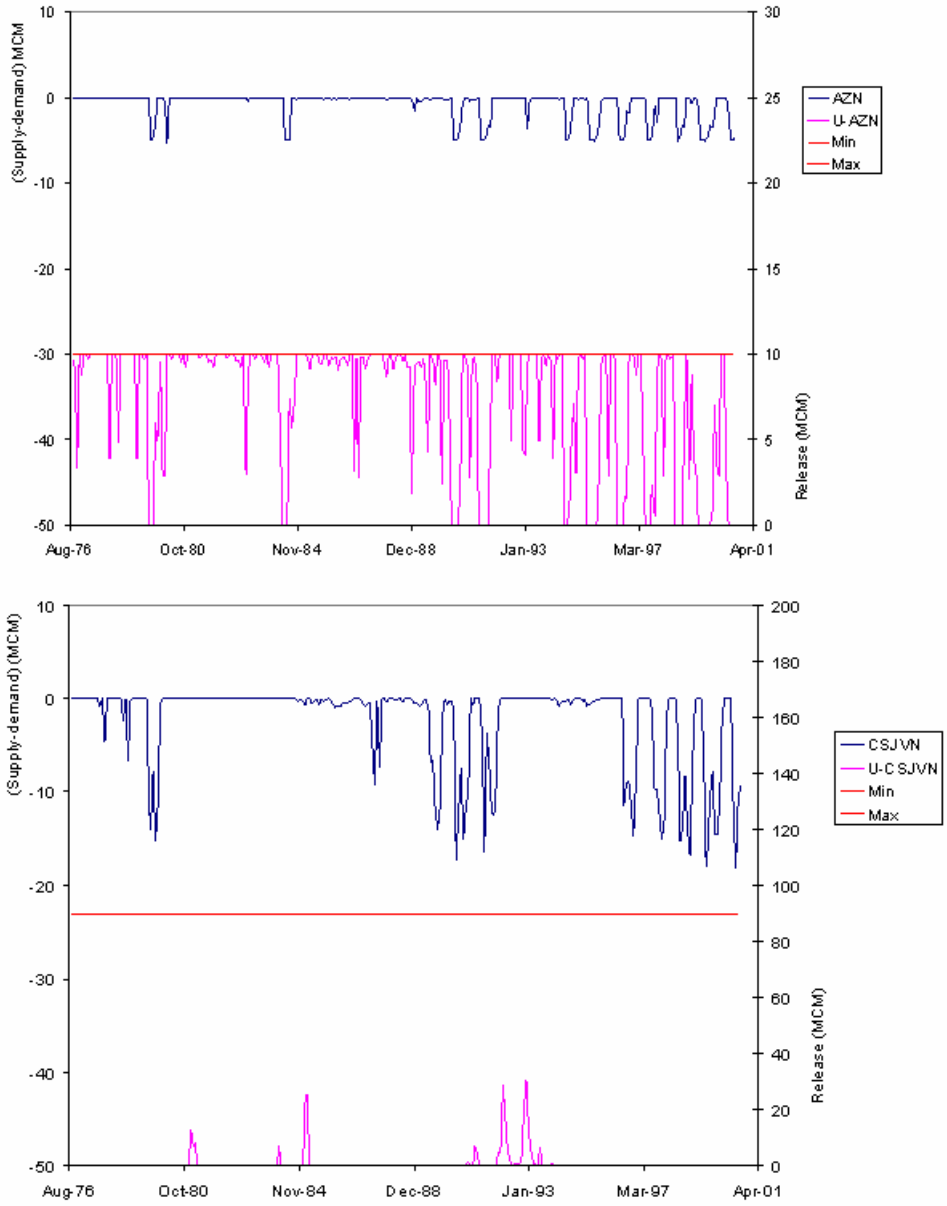

Figure G.25: Assessment model, scenario3, Syrian withdrawals 30%, unconstrained GW drawdown, monthly water deficit and release sequences at Amman-Zarqa and C/S Jordan Valley nodes

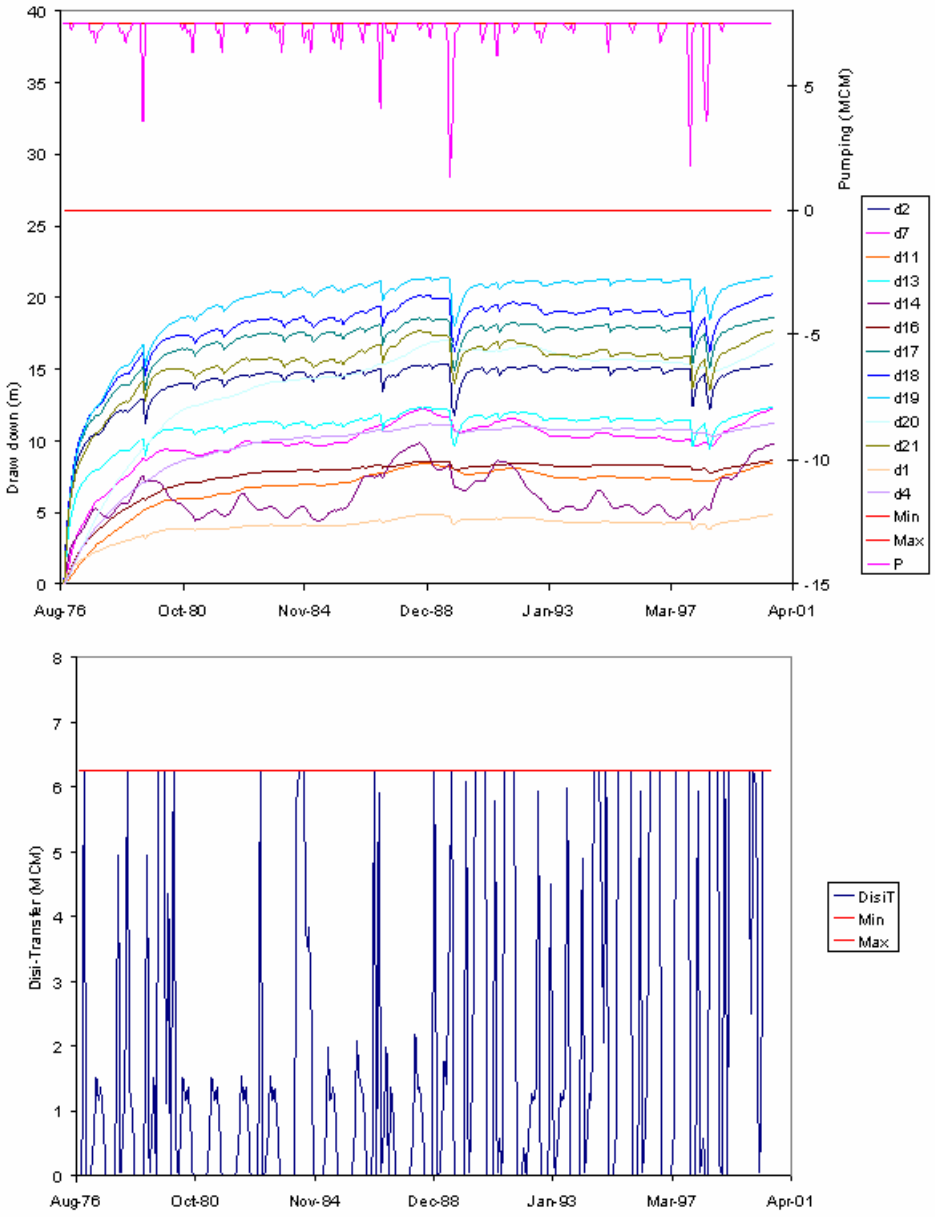

Figure G.26: Assessment model, scenario3, Syrian withdrawals 30%, unconstrained GW drawdown, monthly pumping, drawdown and Disi transfer sequences

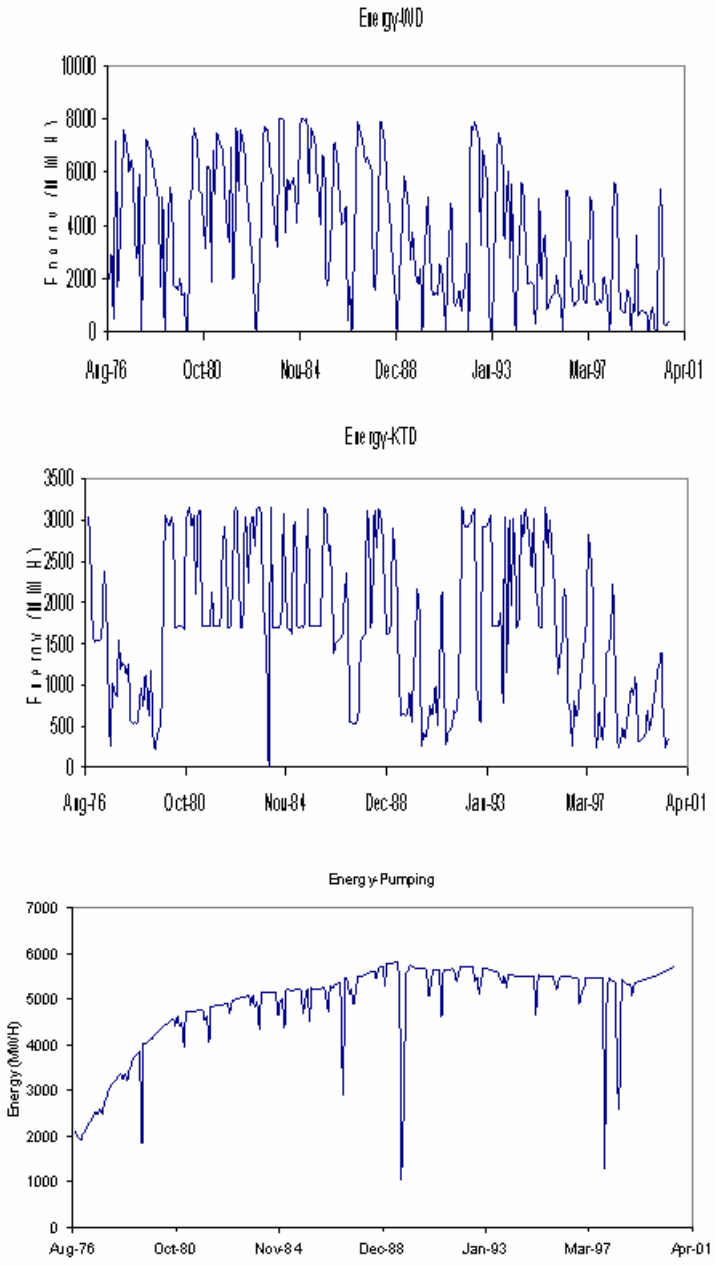

Figure G.27: Assessment model, scenario3, Syrian withdrawals 30%, unconstrained GW drawdown, WD, KTD and pumping energy sequences

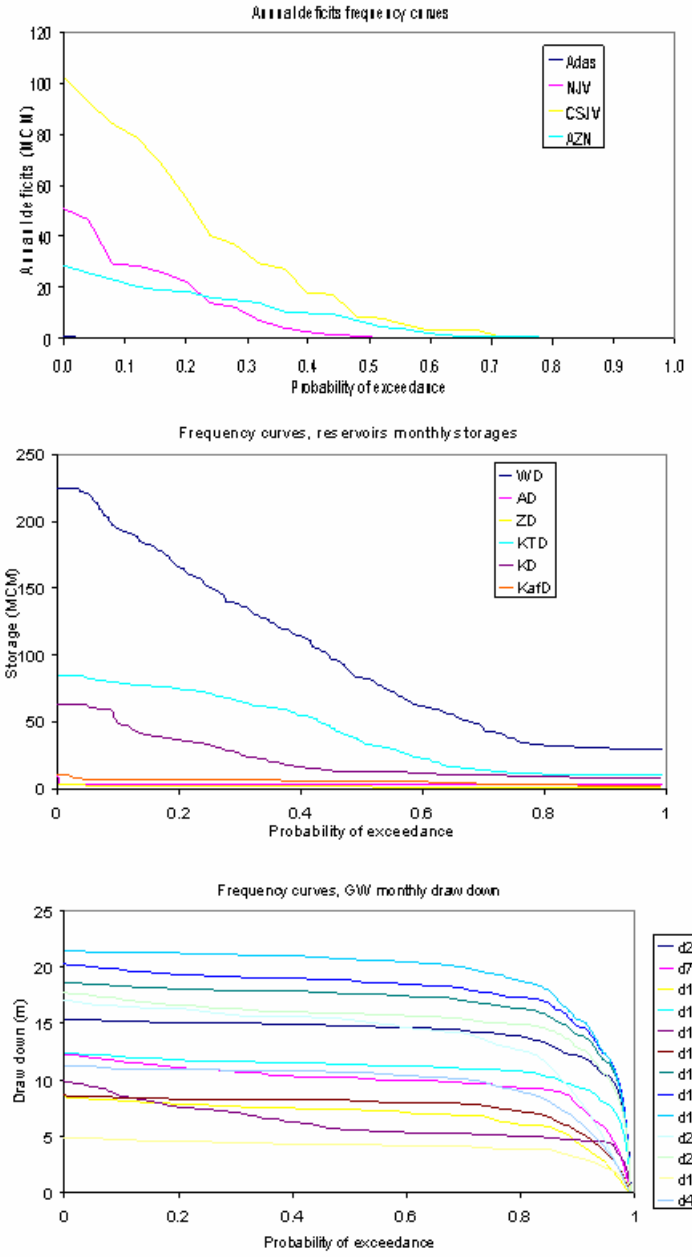

Figure G.28: Assessment model, scenario3, Syrian withdrawals 30%, unconstrained GW drawdown, annual deficits, storages, and drawdowns frequency curves

APPENDIX H

SCENARIO 4: RESIDUAL FLOW TO DEAD SEA

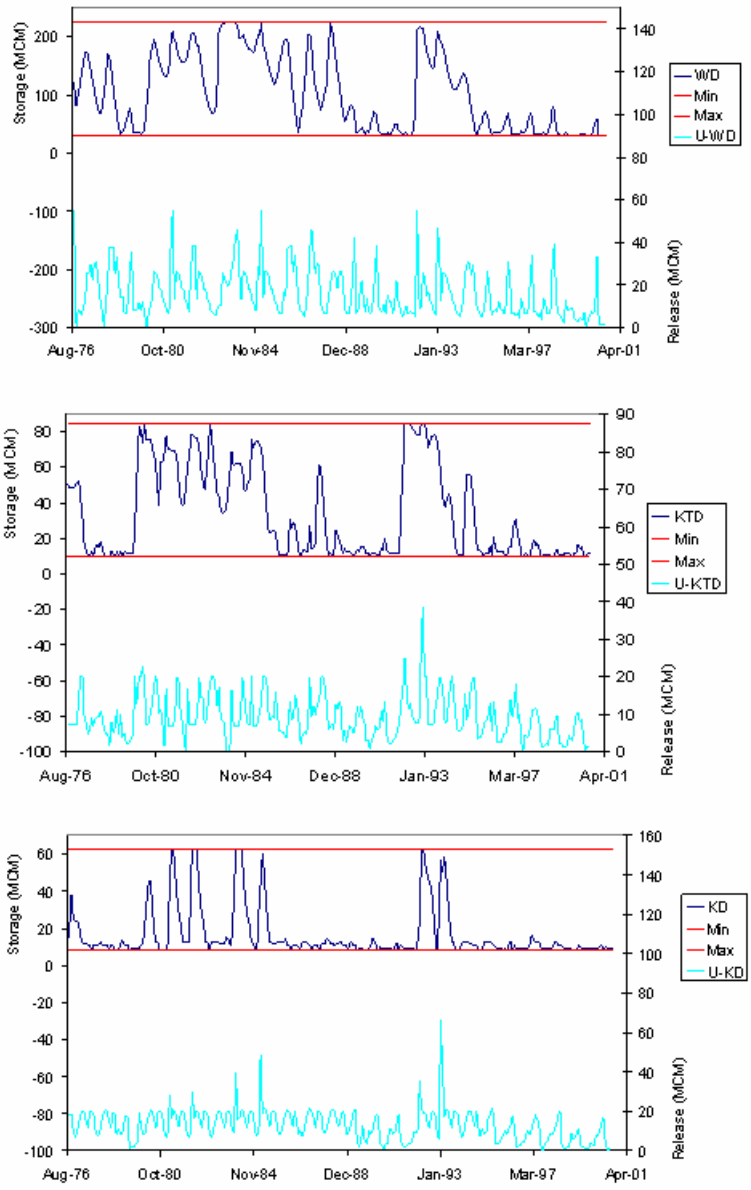

Figure H.1: Assessment model, scenario4, residual flow to Dead Sea 5%, constrained GW drawdown, WD, KTD, and KD storage and release sequences

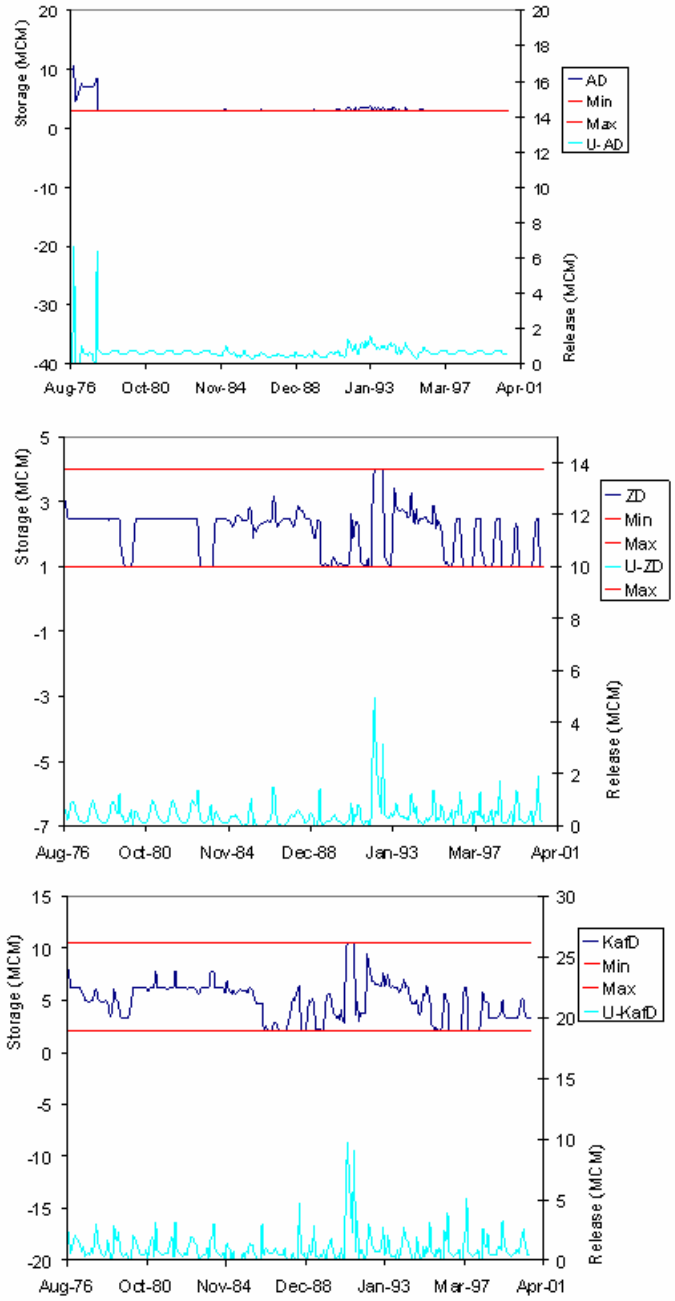

Figure H.2: Assessment model, scenario4, residual flow to Dead Sea 5%, constrained GW drawdown, AD, ZD, and KafD storage and release sequences

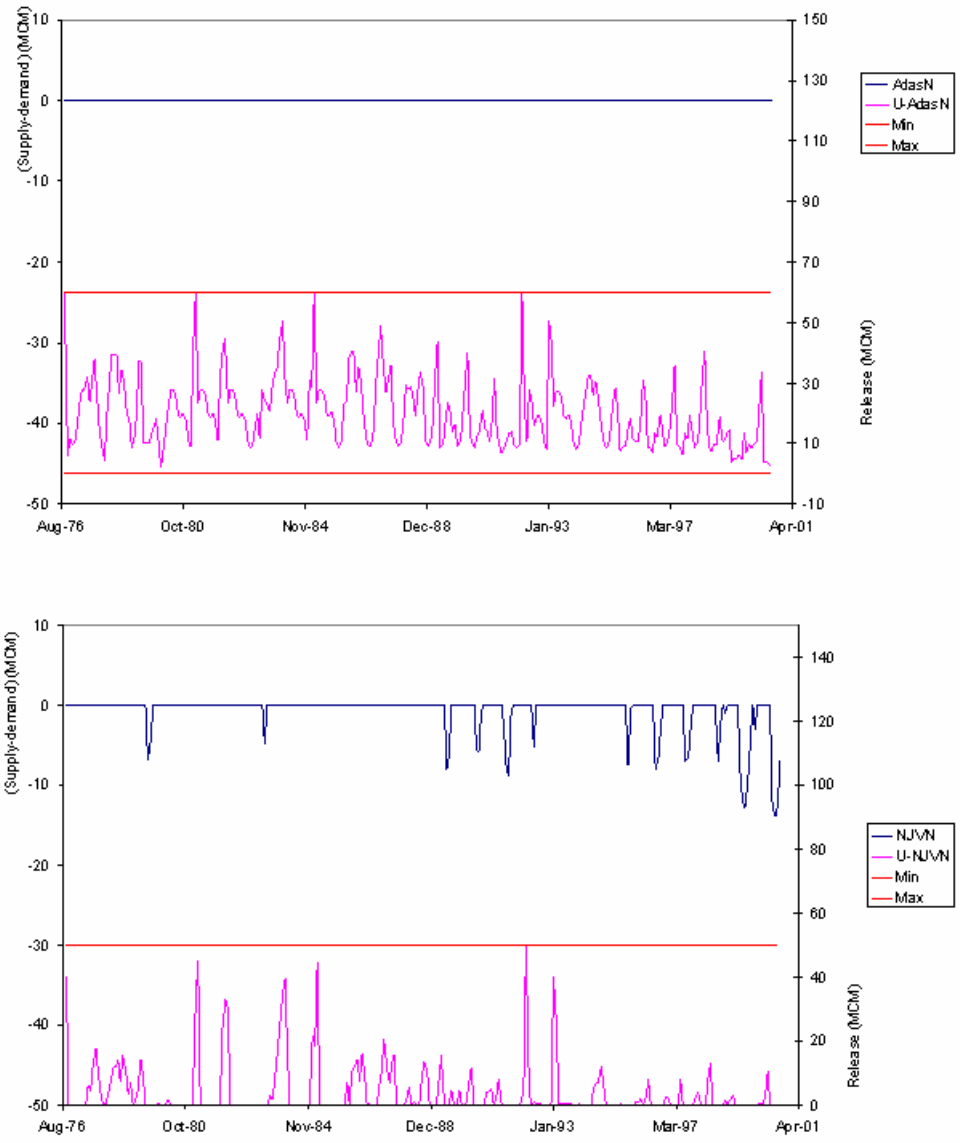

Figure H.3: Assessment model, scenario4, residual flow to Dead Sea 5%, constrained GW drawdown, monthly water deficit and release sequences at Adasiya and North Jordan Valley nodes

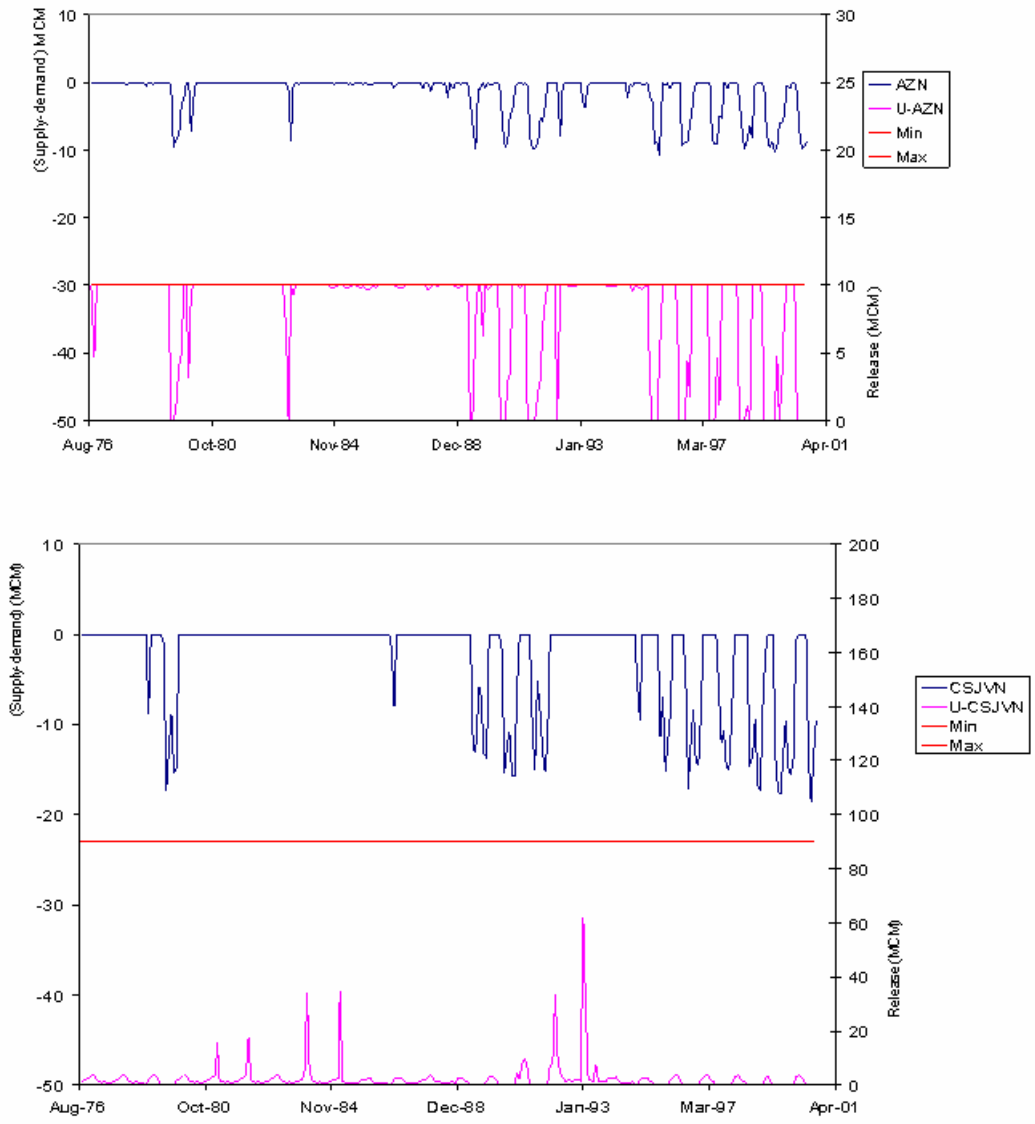

Figure H.4: Assessment model, scenario4, residual flow to Dead Sea 5%, constrained GW drawdown, monthly water deficit and release sequences at Amman-Zarqa and C/S Jordan Valley nodes

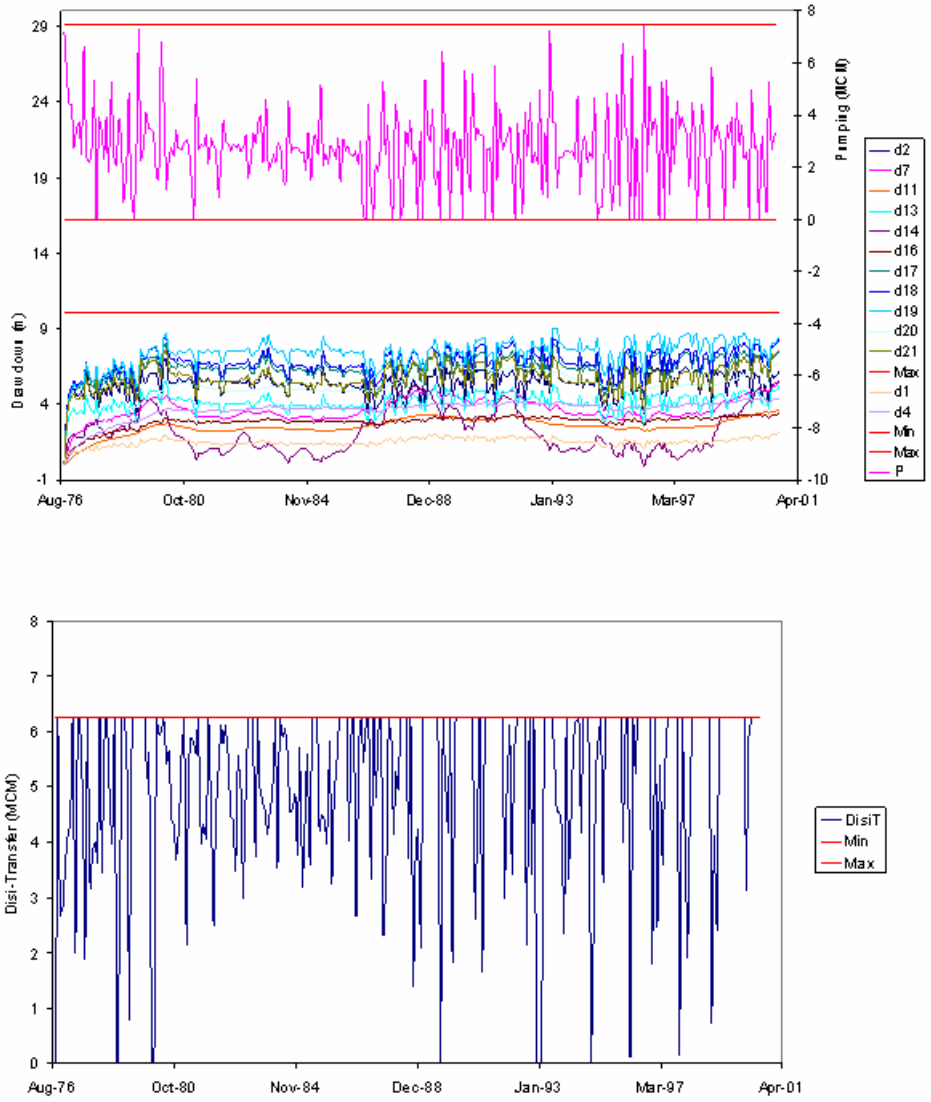

Figure H.5: Assessment model, scenario4, residual flow to Dead Sea 5%, constrained GW drawdown, monthly pumping, drawdown and Disi transfer sequences

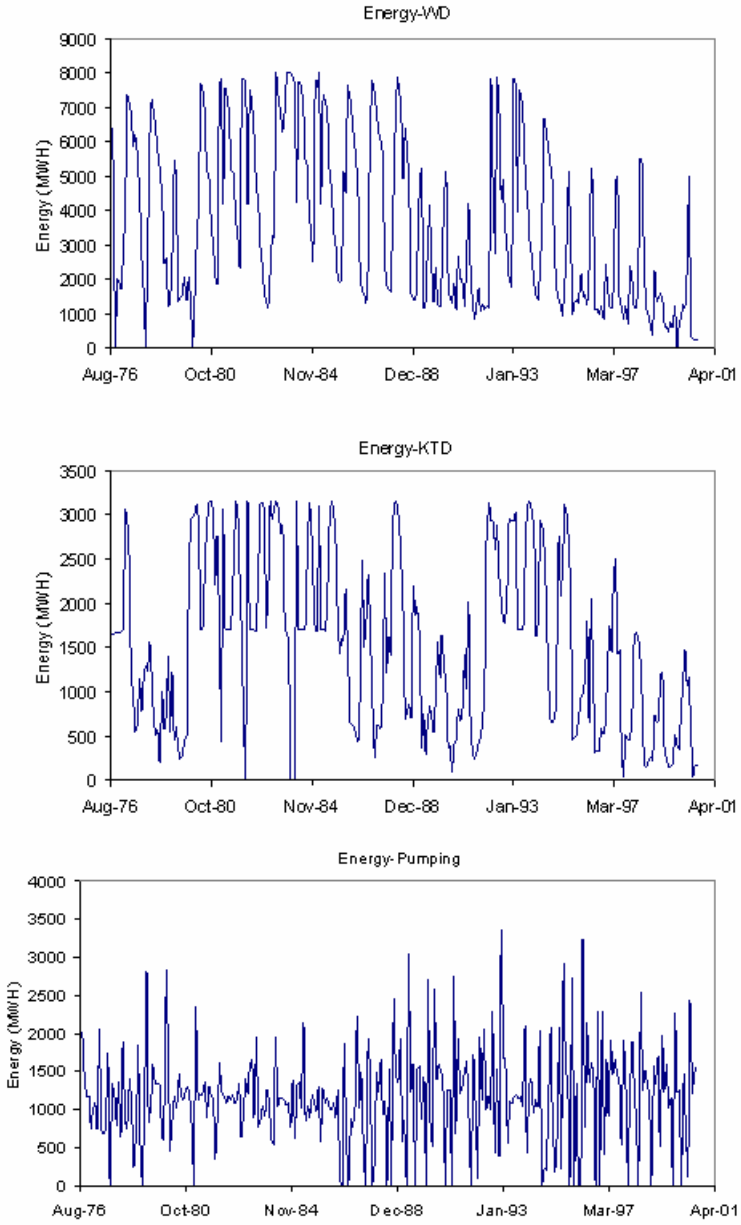

Figure H.6: Assessment model, scenario4, residual flow to Dead Sea 5%, constrained GW drawdown, WD, KTD and pumping energy sequences

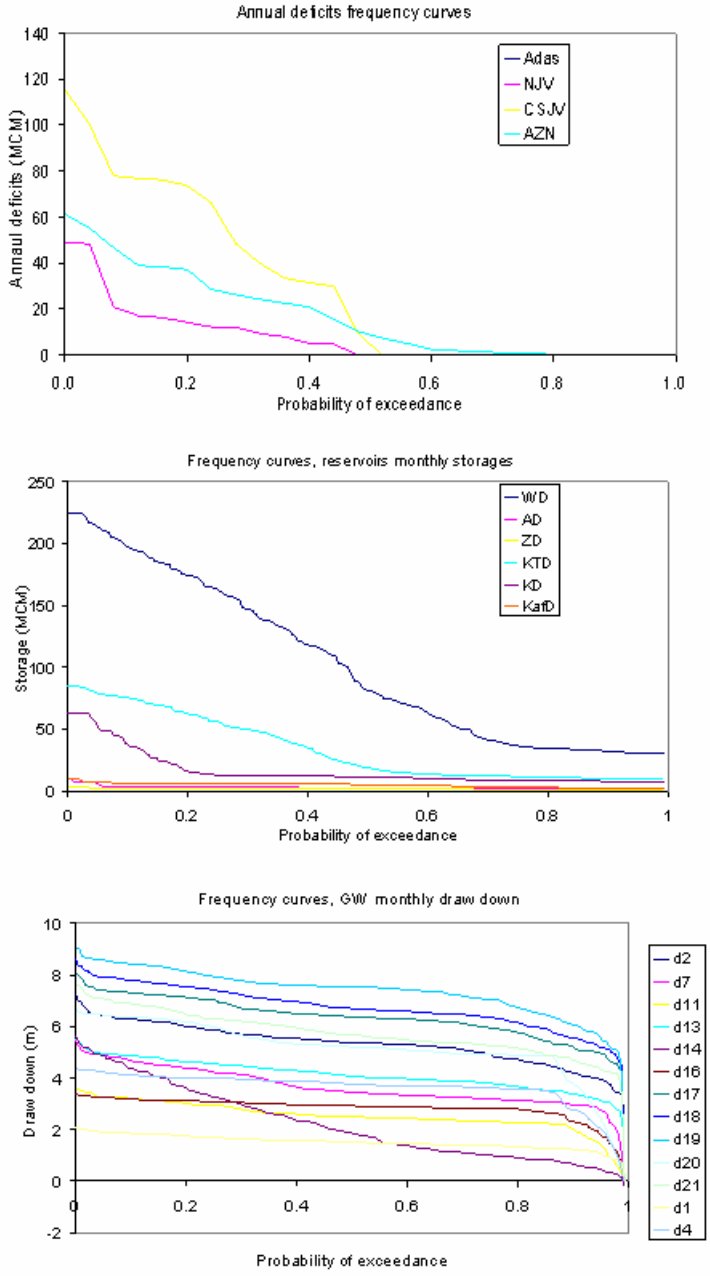

Figure H.7: Assessment model, scenario4, residual flow to Dead Sea 5%, constrained GW drawdown, annual deficits, storages, and drawdowns frequency curves

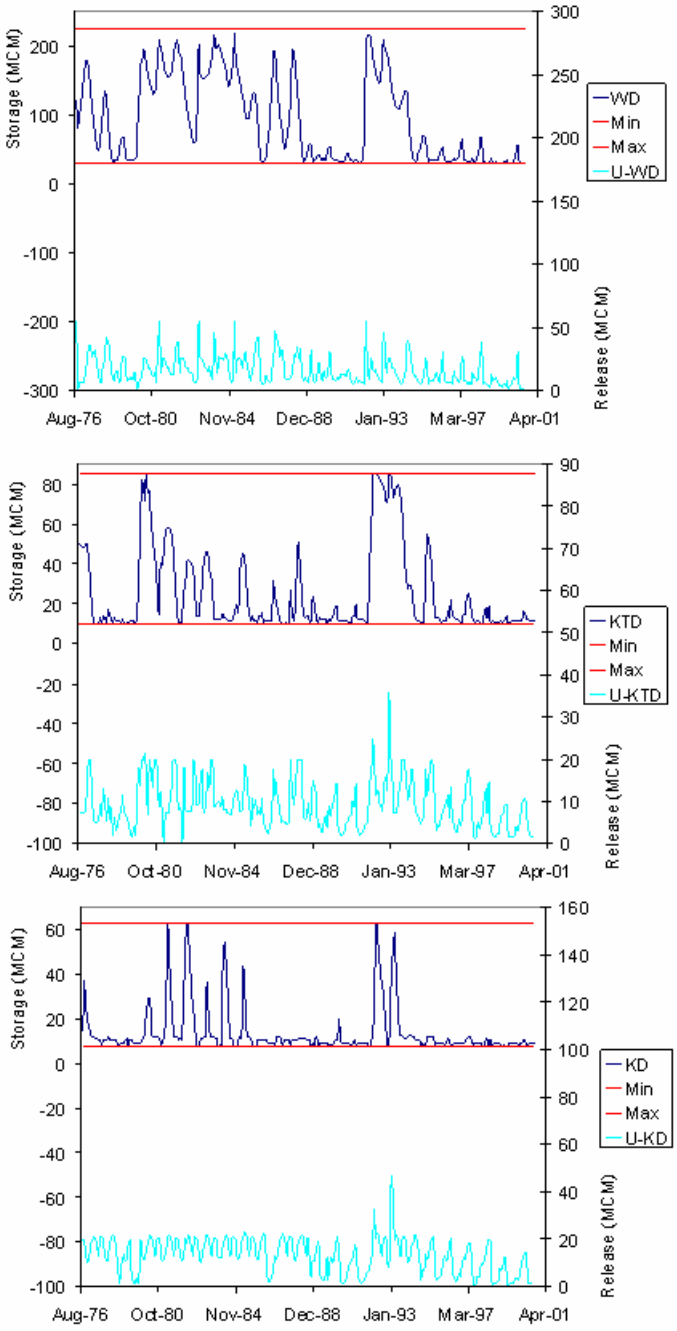

Figure H.8: Assessment model, scenario4, residual flow to Dead Sea 10%, constrained GW drawdown, WD, KTD, and KD storage and release sequences

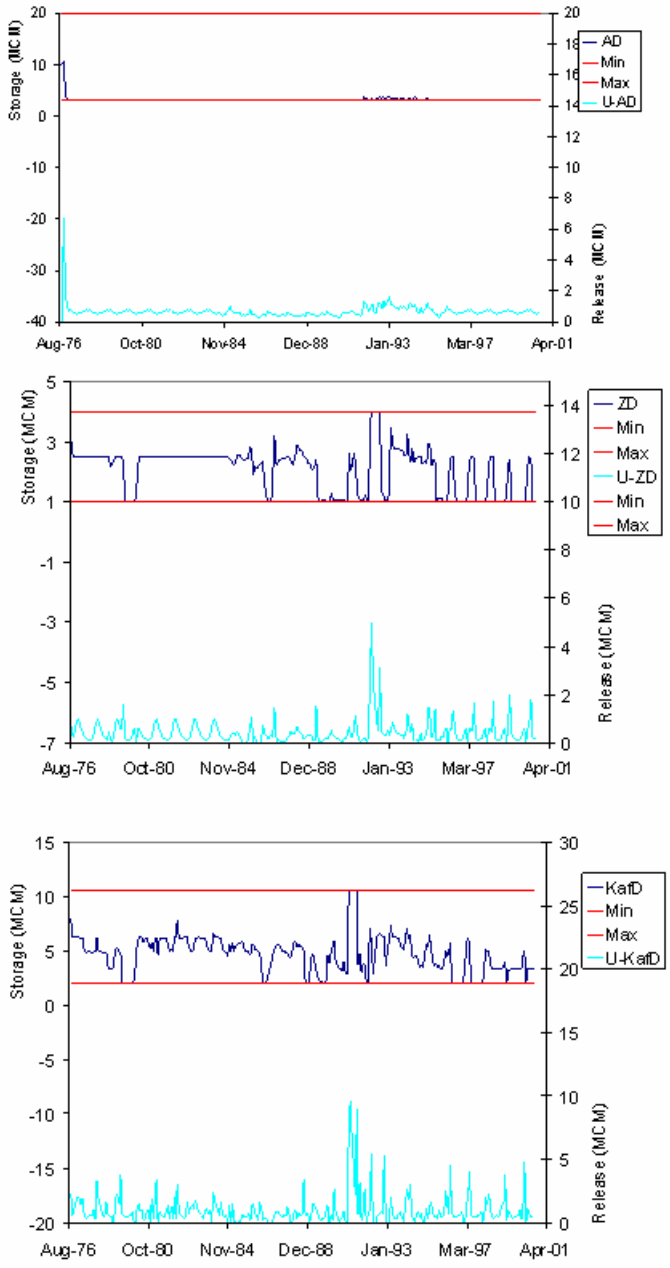

Figure H.9: Assessment model, scenario4, residual flow to Dead Sea 10%, constrained GW drawdown, AD, ZD, and KafD storage and release sequences

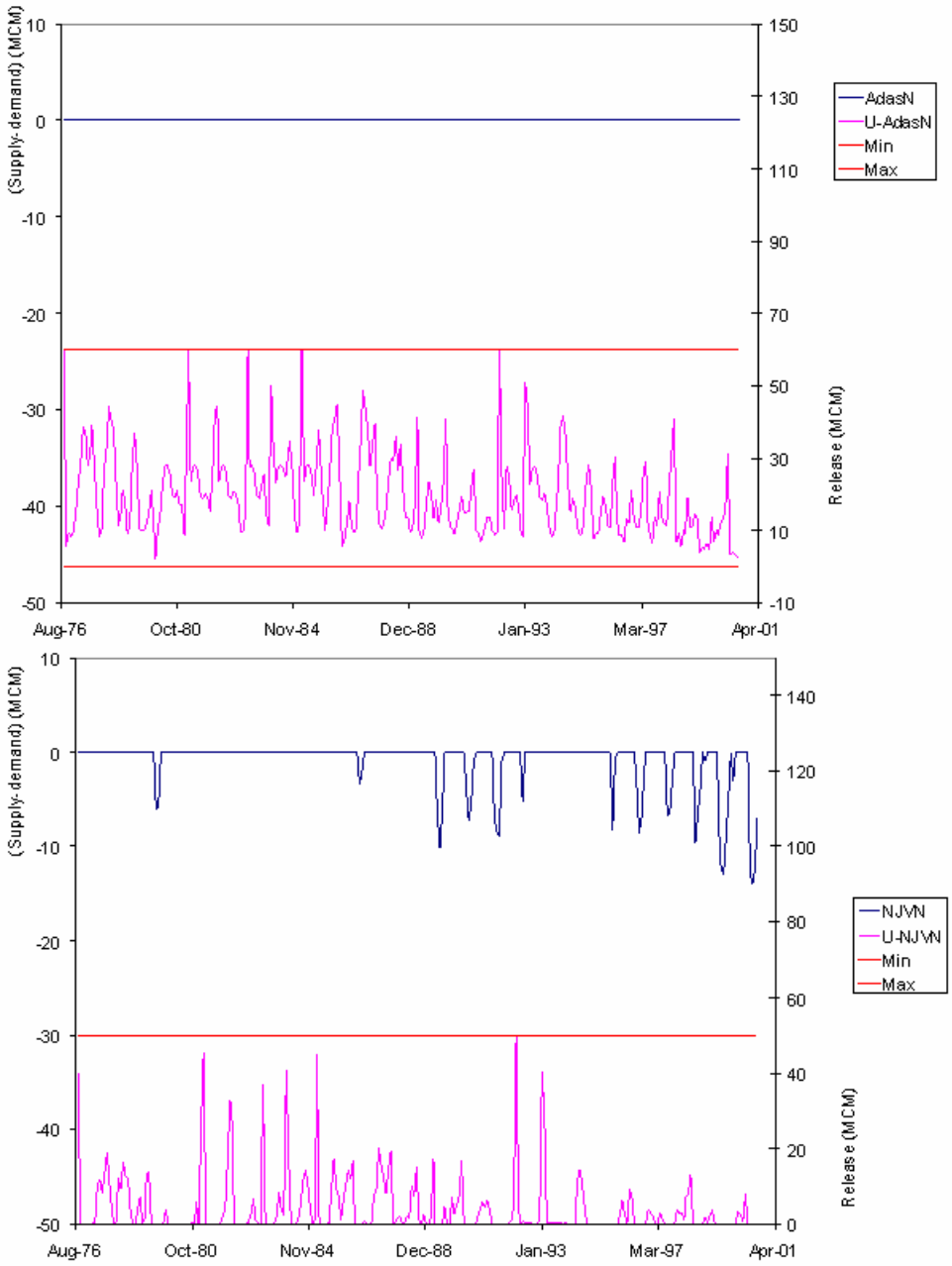

Figure H.10: Assessment model, scenario4, residual flow to Dead Sea 10%, constrained GW drawdown, monthly water deficit and release sequences at Adasiya and North Jordan Valley nodes

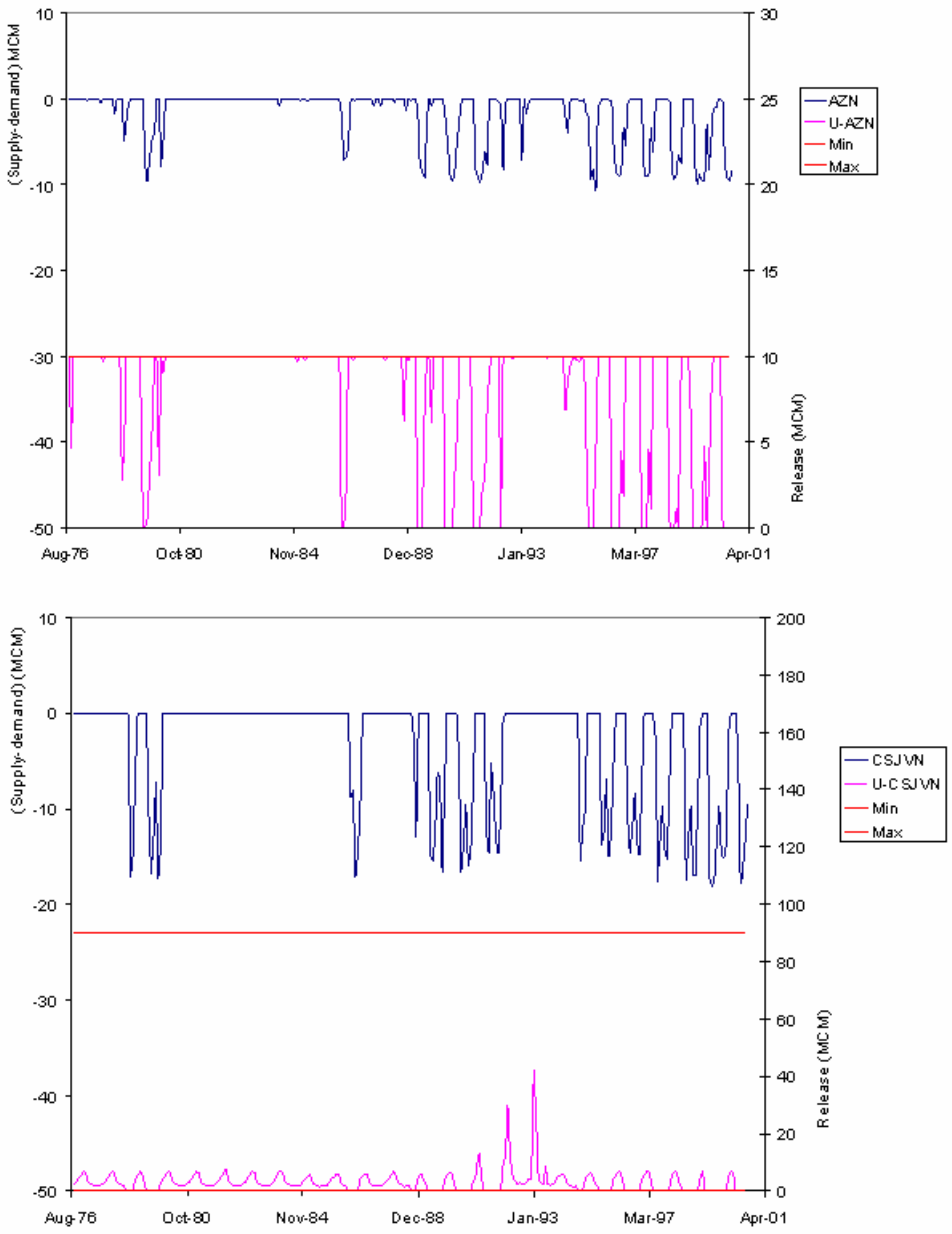

Figure H.11: Assessment model, scenario4, residual flow to Dead Sea 10%, constrained GW drawdown, monthly water deficit and release sequences at Amman-Zarqa and C/S Jordan Valley nodes

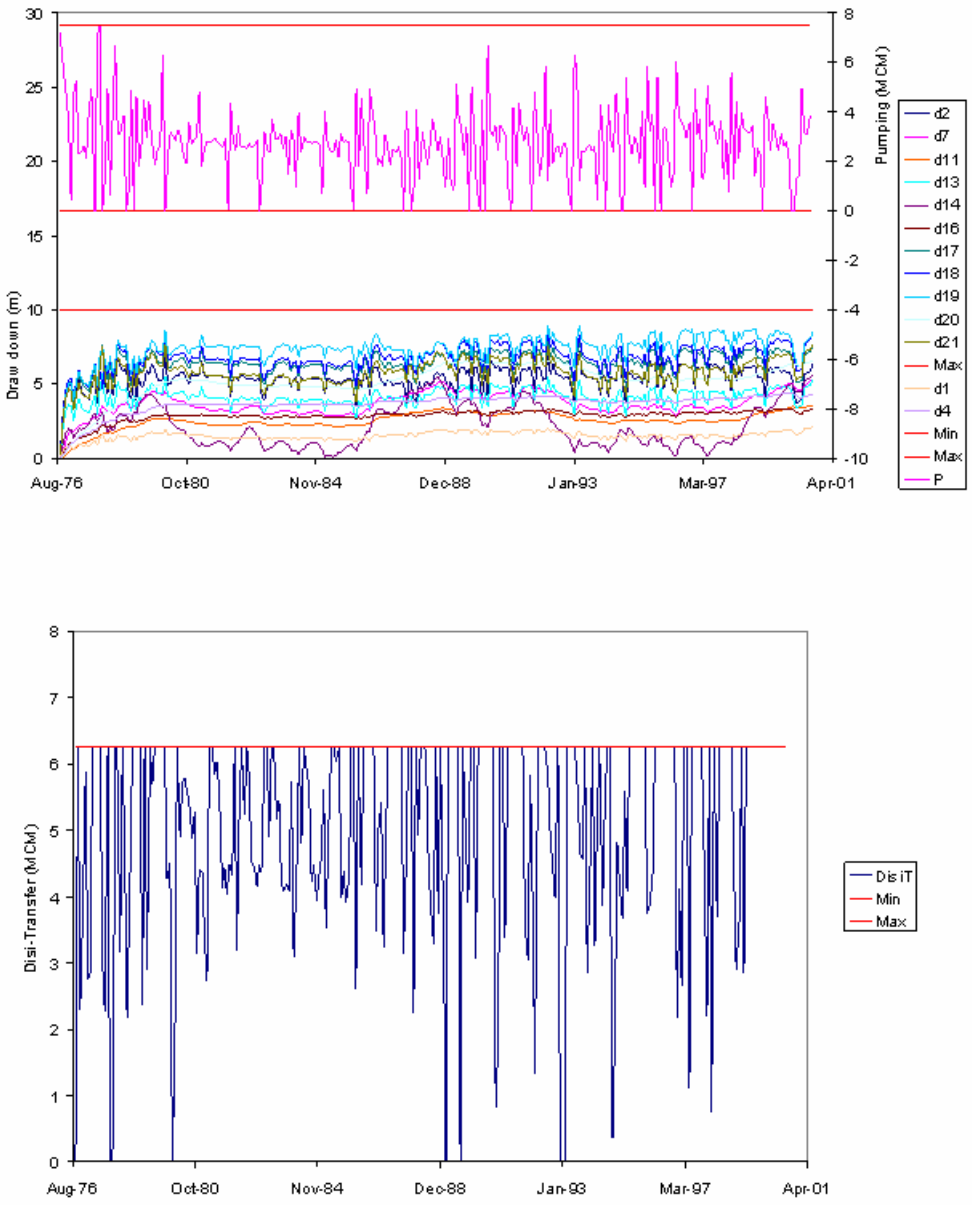

Figure H.12: Assessment model, scenario4, residual flow to Dead Sea 10%, constrained GW drawdown, monthly pumping, drawdown and Disi transfer sequences

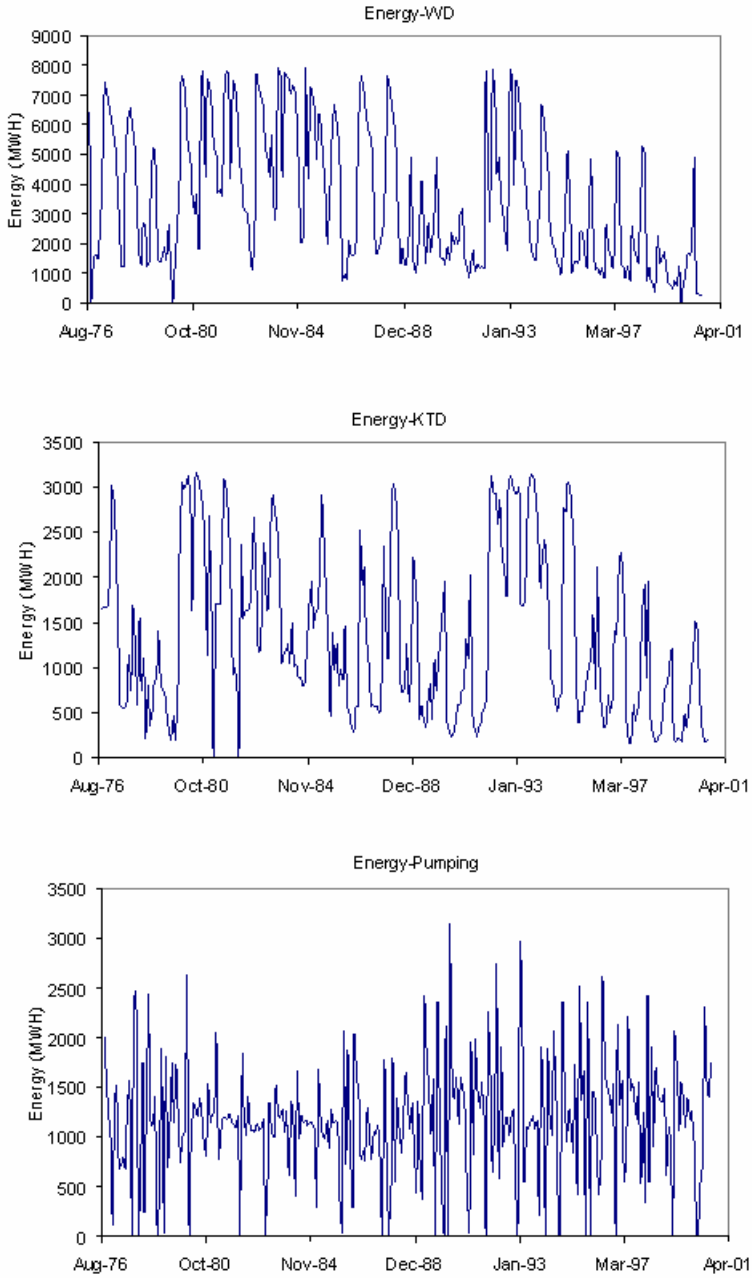

Figure H.13: Assessment model, scenario4, residual flow to Dead Sea 10%, constrained GW drawdown, WD, KTD and pumping energy sequences

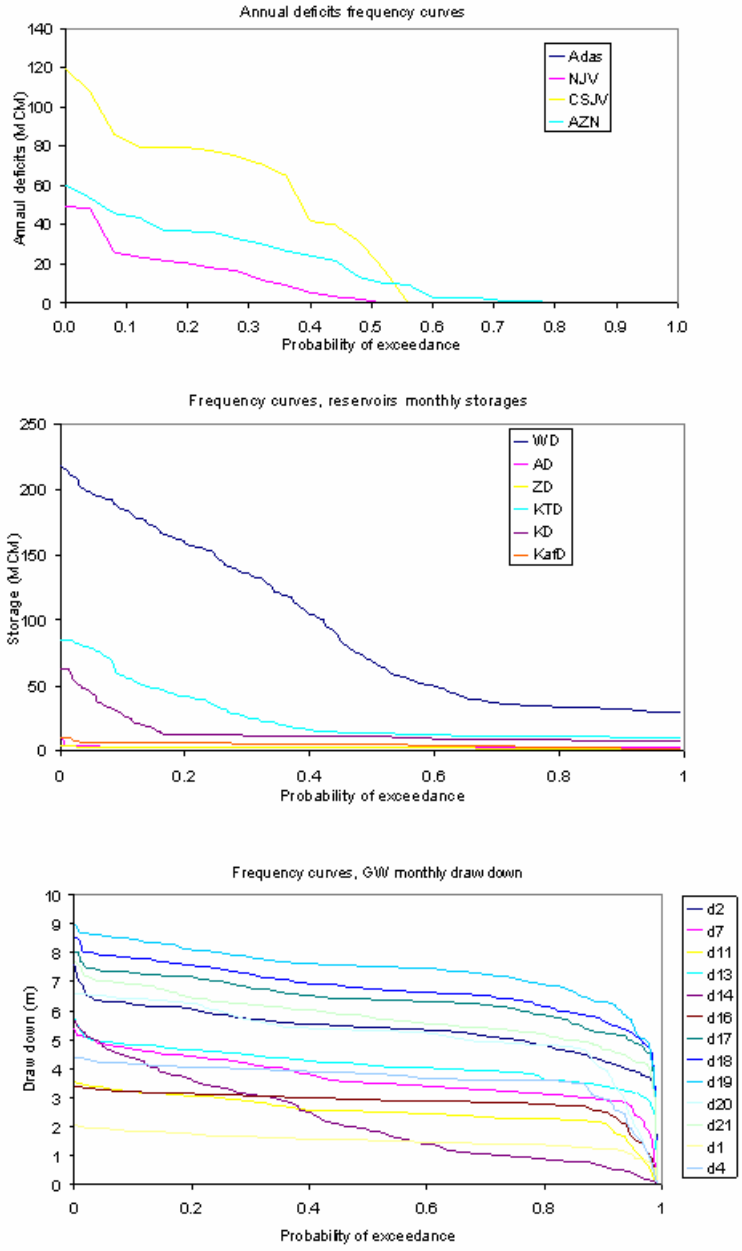

Figure H.14: Assessment model, scenario4, residual flow to Dead Sea 10%, constrained GW drawdown, annual deficits, storages, and drawdowns frequency curves

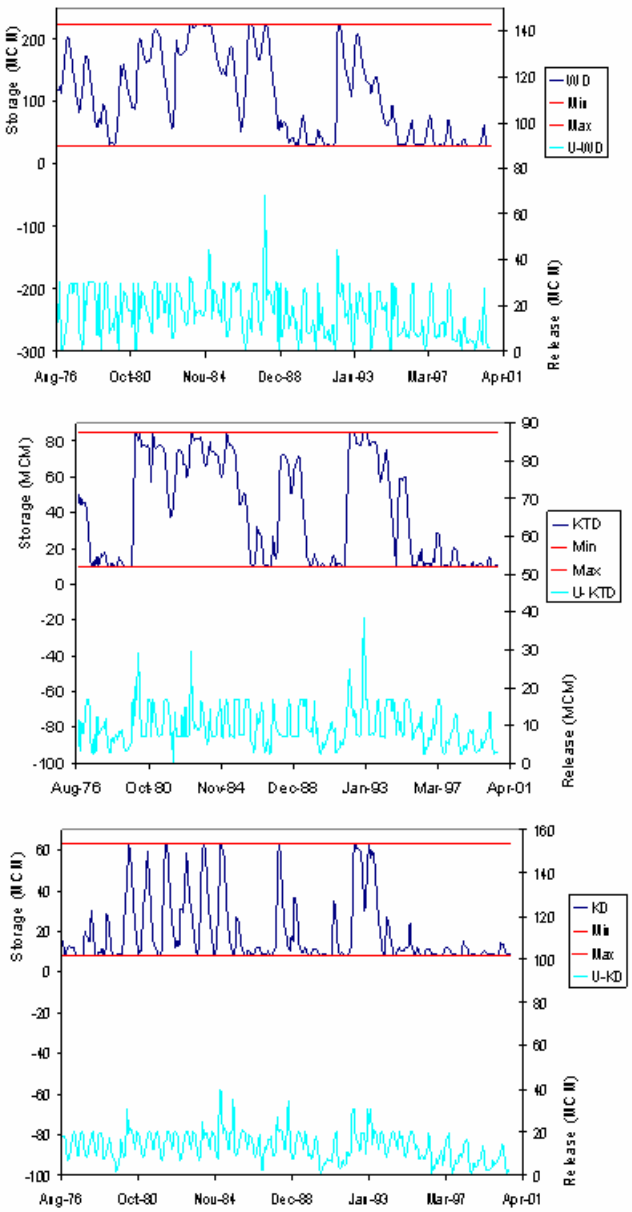

Figure H.15: Assessment model, scenario4, residual flow to Dead Sea 5%, unconstrained GW drawdown, WD, KTD, and KD storage and release sequences

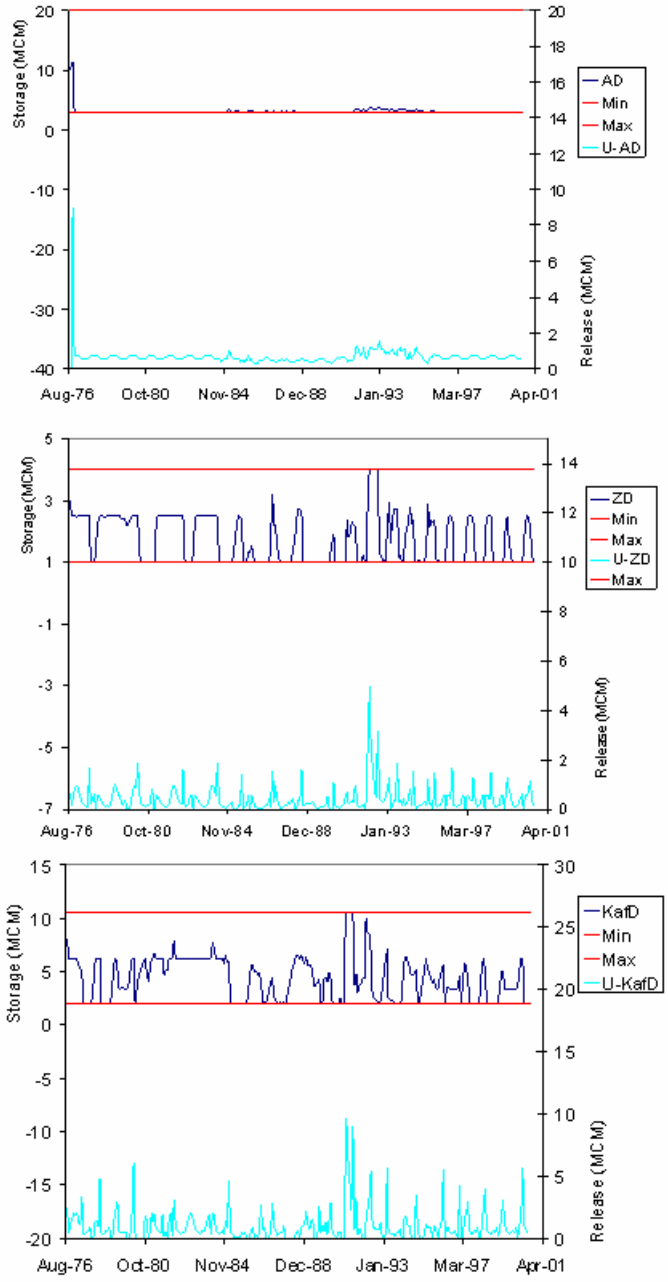

Figure H.16: Assessment model, scenario4, residual flow to Dead Sea 5%, unconstrained GW drawdown, AD, ZD, and KafD storage and release sequences

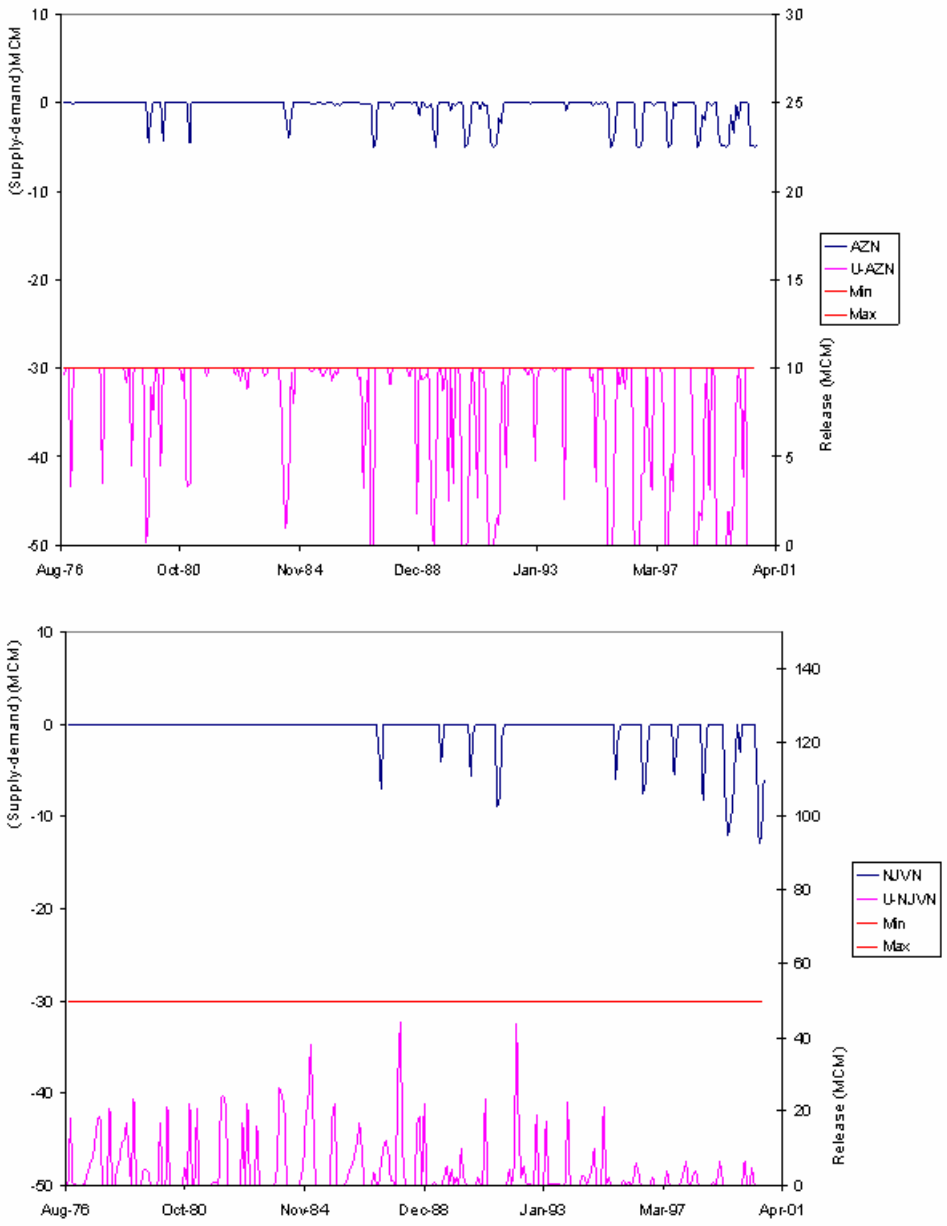

Figure H.17: Assessment model, scenario4, residual flow to Dead Sea 5%, unconstrained GW drawdown, monthly water deficit and release sequences at Adasiya and North Jordan Valley nodes

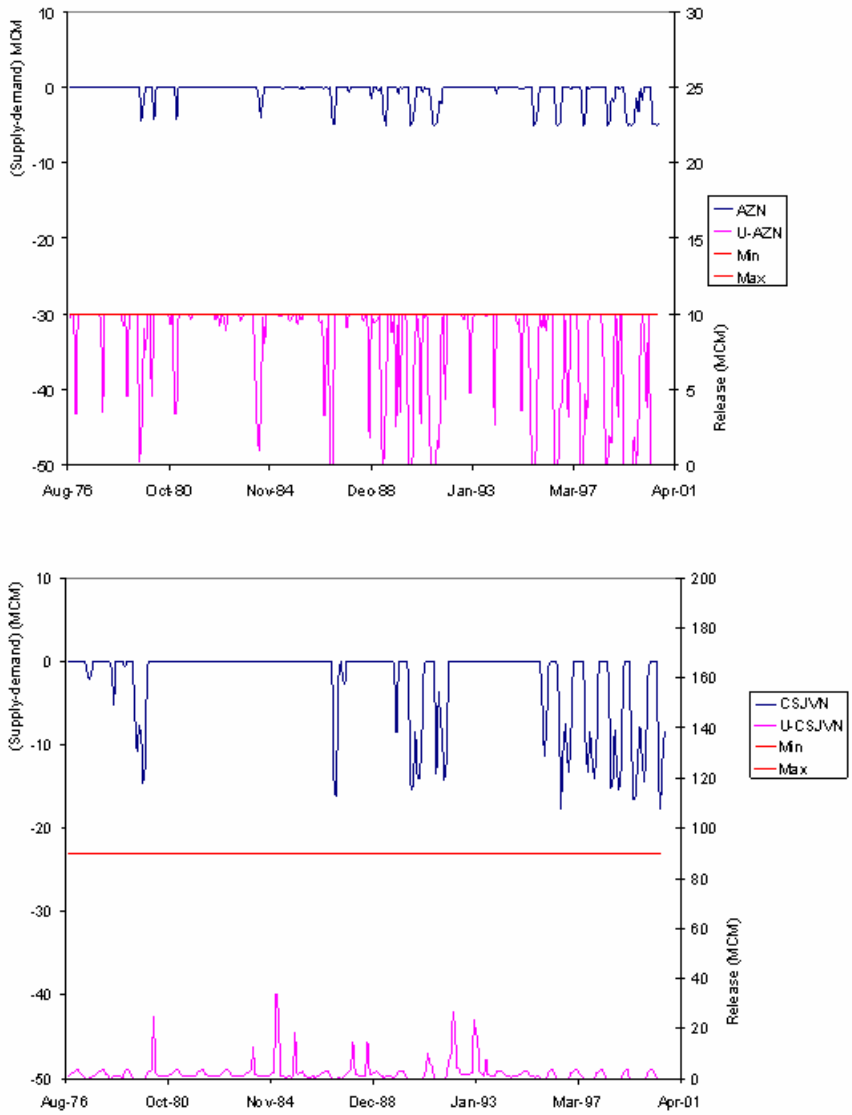

Figure H.18: Assessment model, scenario4, residual flow to Dead Sea 5%, unconstrained GW drawdown, monthly water deficit and release sequences at Amman-Zarqa and C/S Jordan Valley nodes

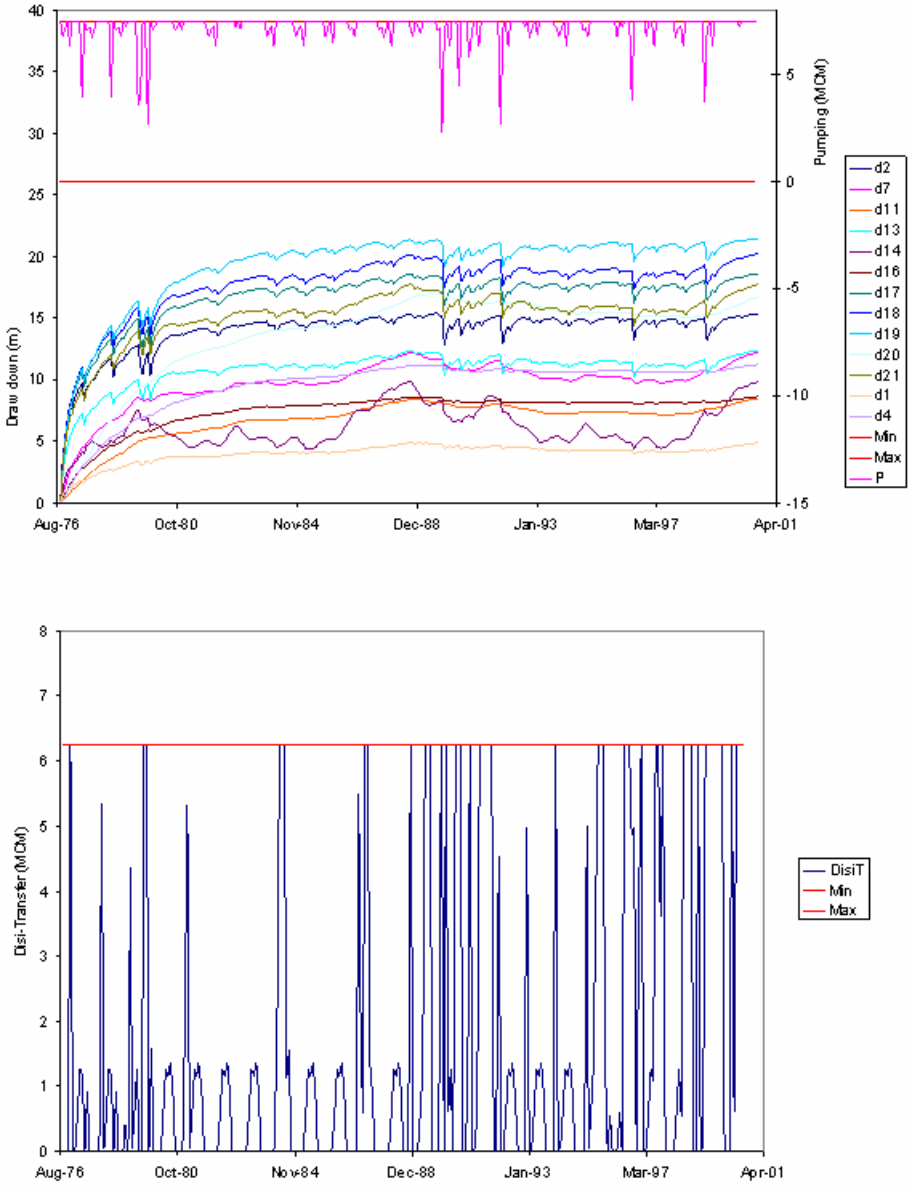

Figure H.19: Assessment model, scenario4, residual flow to Dead Sea 5%, unconstrained GW drawdown, monthly pumping, drawdown and Disi transfer sequences

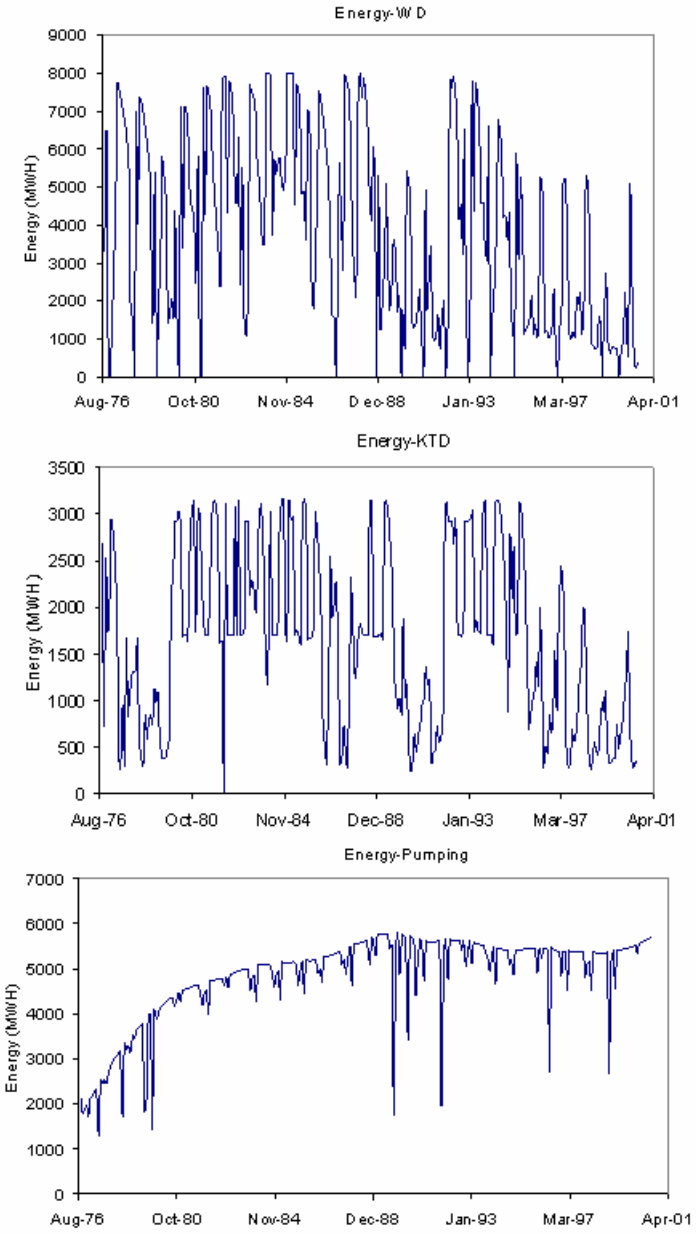

Figure H.20: Assessment model, scenario4, residual flow to Dead Sea 5%, unconstrained GW drawdown, WD, KTD and pumping energy sequences

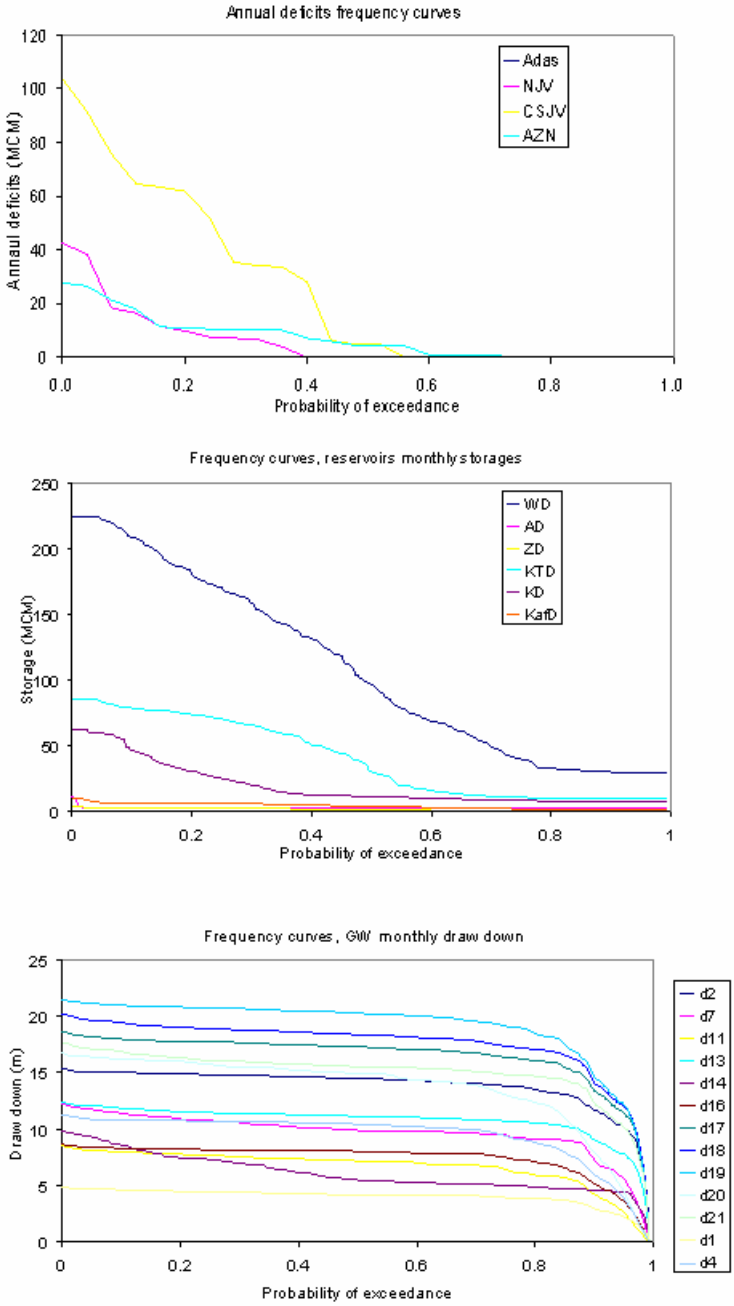

Figure H.21: Assessment model, scenario4, residual flow to Dead Sea 5%, unconstrained GW drawdown, annual deficits, storages, and drawdowns frequency curves

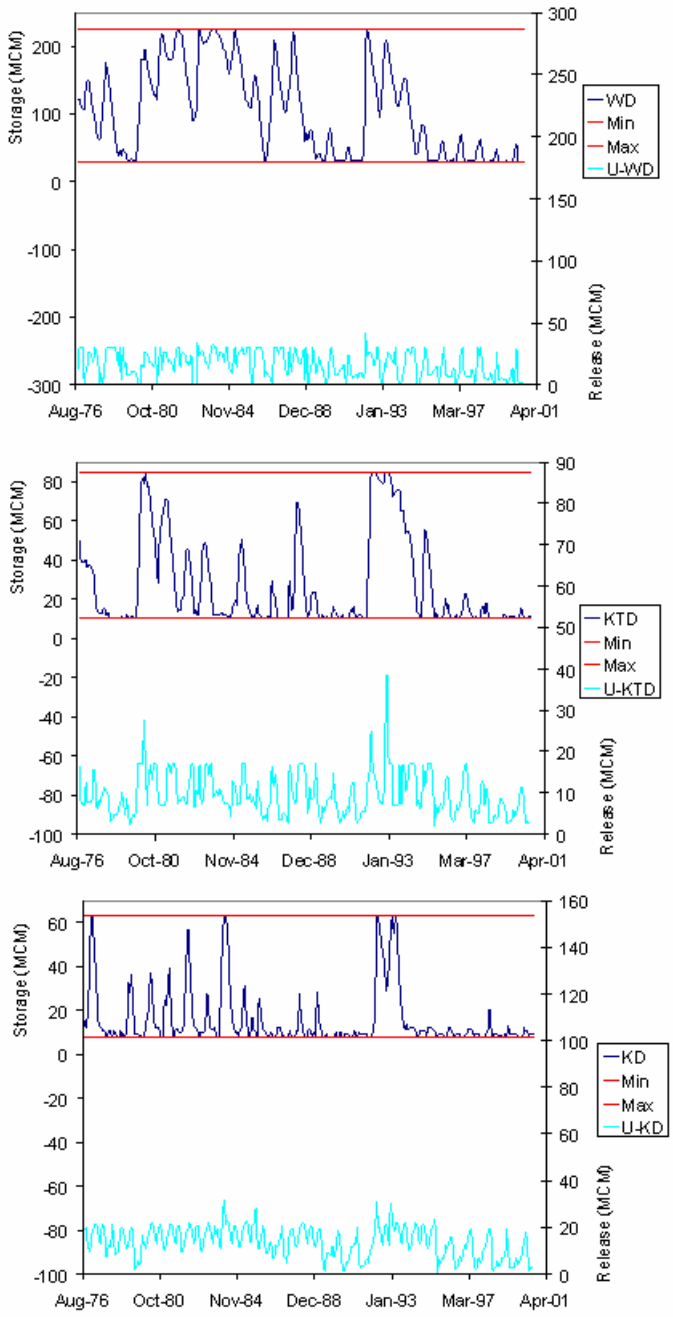

Figure H.22: Assessment model, scenario4, residual flow to Dead Sea 10%, unconstrained GW drawdown, WD, KTD, and KD storage and release sequences

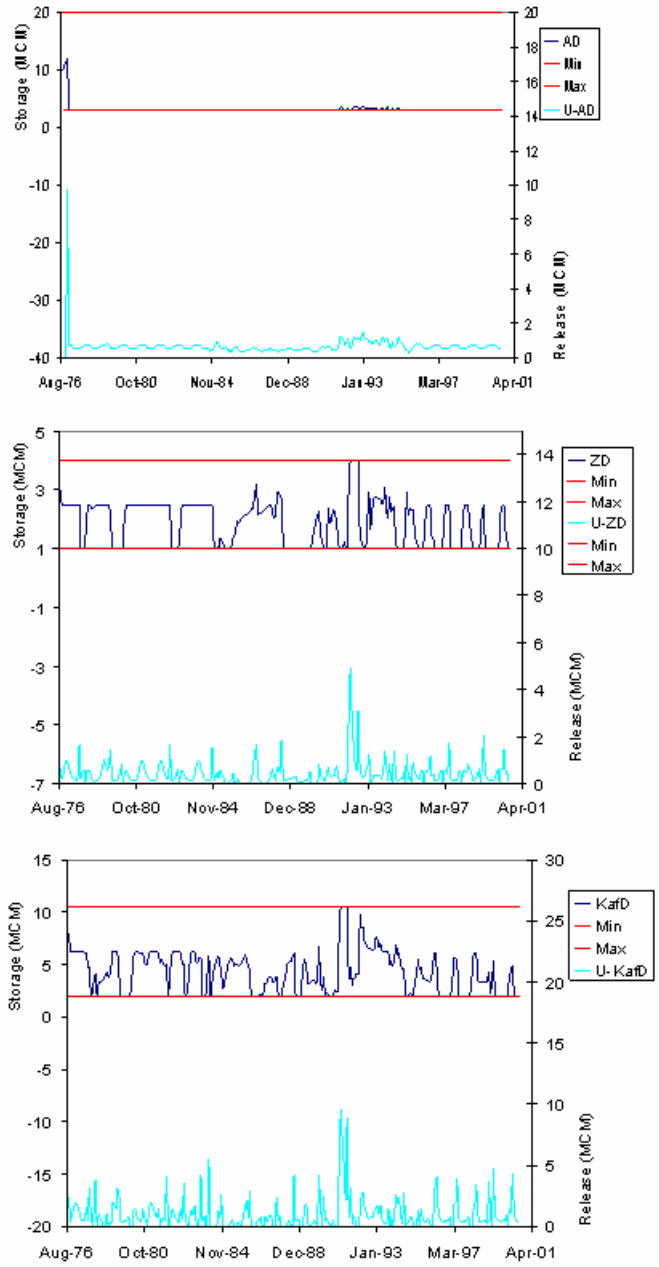

Figure H.23: Assessment model, scenario4, residual flow to Dead Sea 10%, unconstrained GW drawdown, AD, ZD, and KafD storage and release sequences

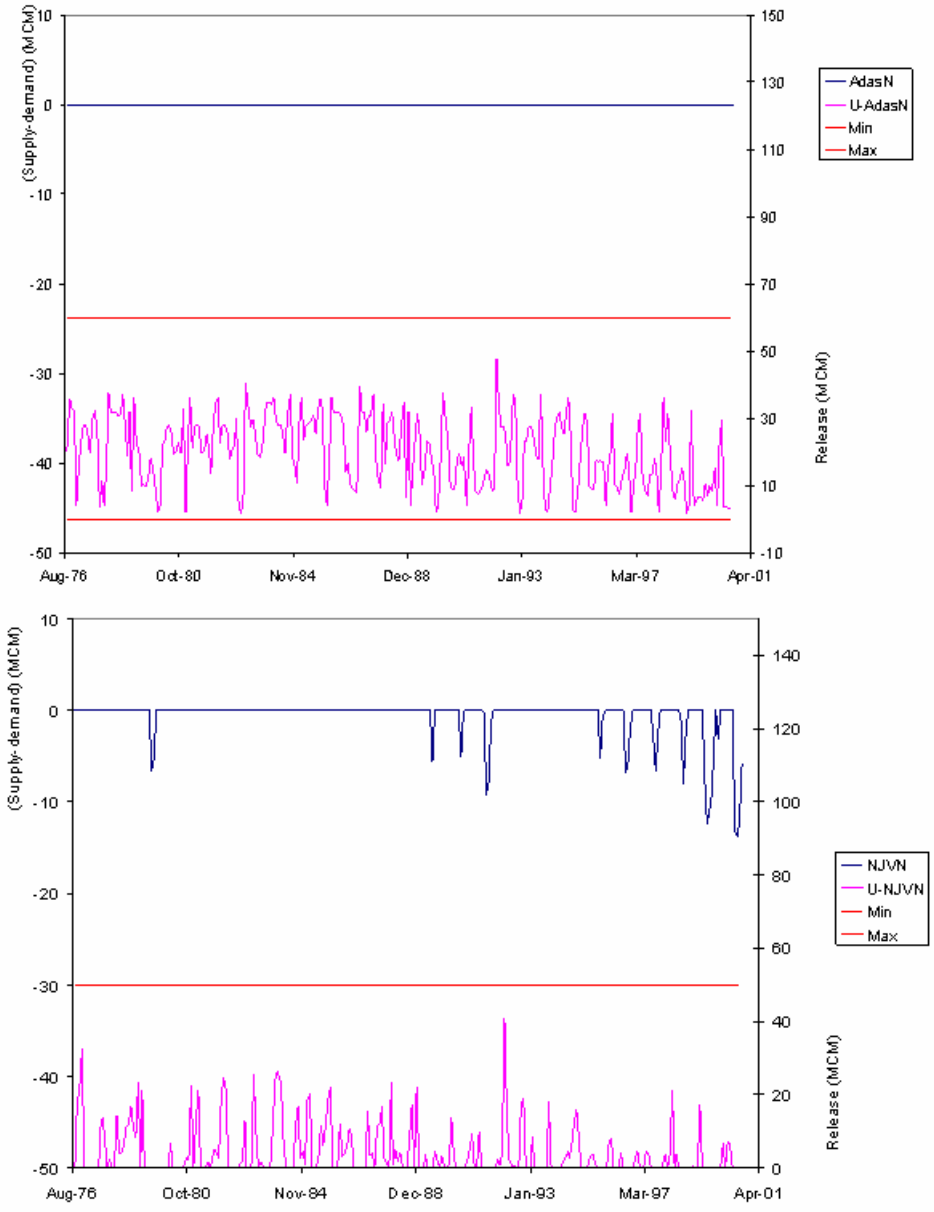

Figure H.24: Assessment model, scenario4, residual flow to Dead Sea 10%, unconstrained GW drawdown, monthly water deficit and release sequences at Adasiya and North Jordan Valley nodes

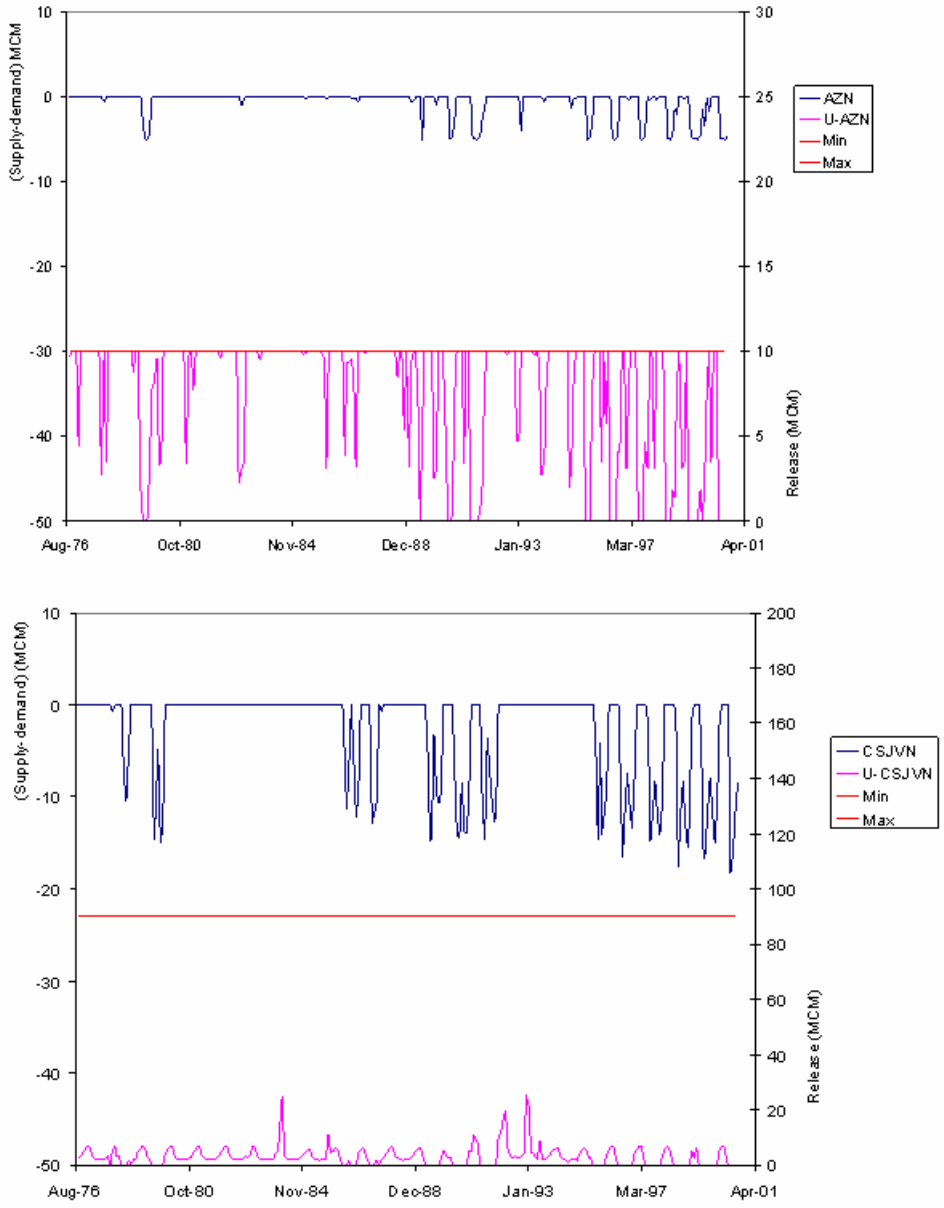

Figure H.25: Assessment model, scenario4, residual flow to Dead Sea 10%, unconstrained GW drawdown, monthly water deficit and release sequences at Amman-Zarqa and C/S Jordan Valley nodes

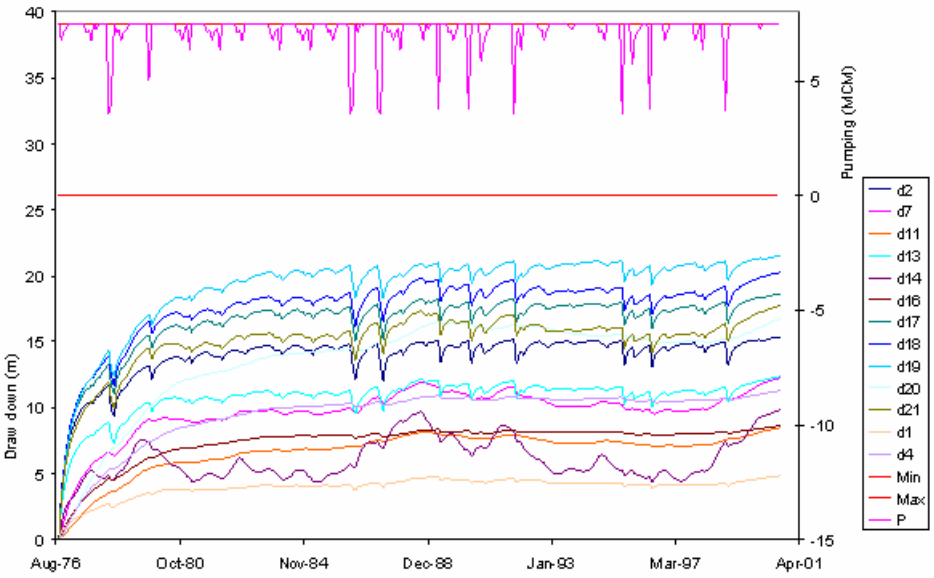

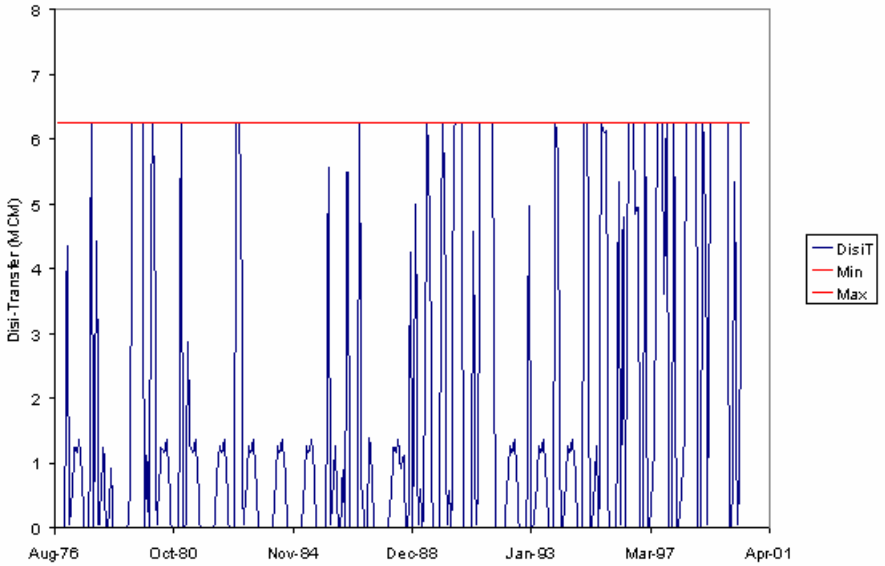

Figure H.26: Assessment model, scenario4, residual flow to Dead Sea 10%, unconstrained GW drawdown, monthly pumping, drawdown and Disi transfer sequences

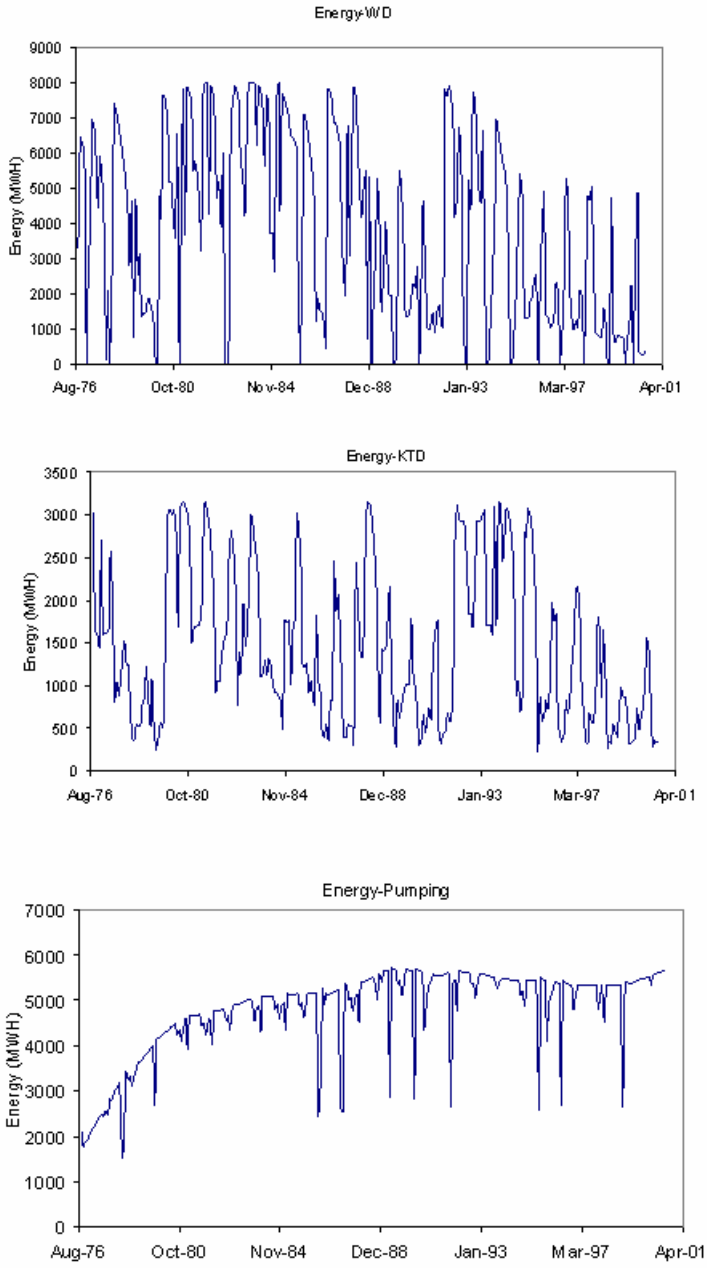

Figure H.27: Assessment model, scenario4, residual flow to Dead Sea 10%, unconstrained GW drawdown, WD, KTD and pumping energy sequences

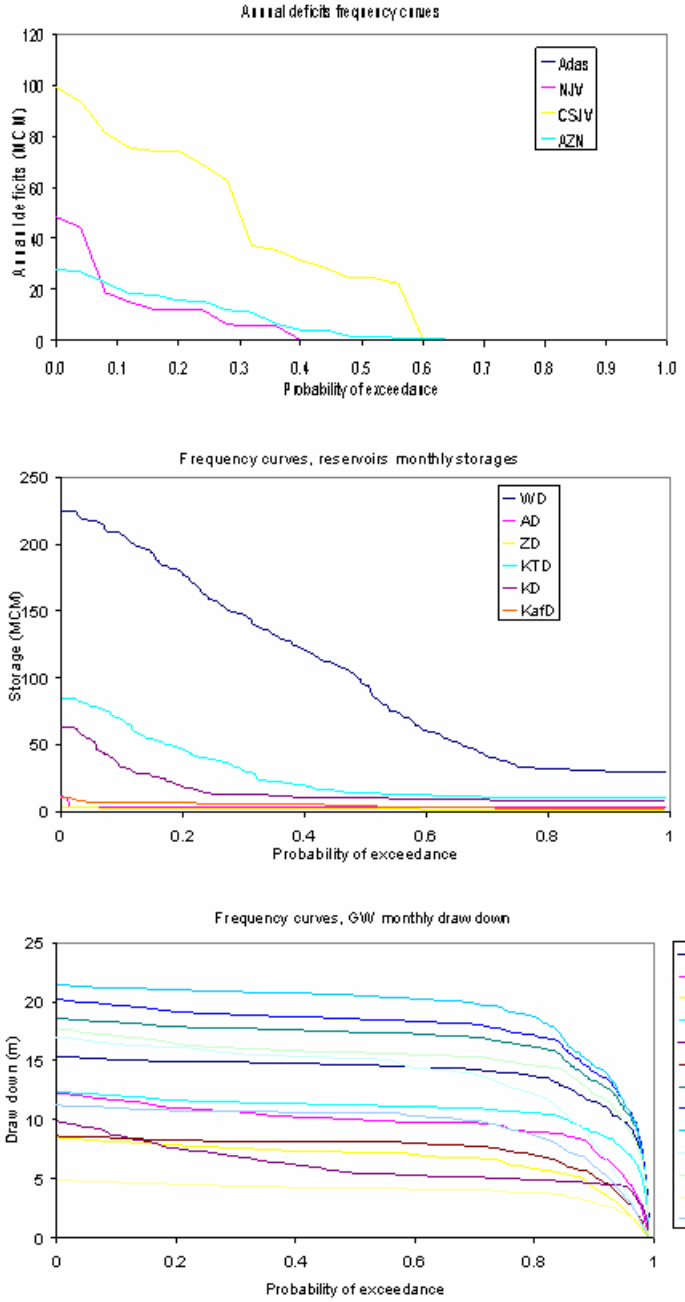

Figure H.28: Assessment model, scenario4, residual flow to Dead Sea 10%, unconstrained GW drawdown, annual deficits, storages, and drawdowns frequency curves

APPENDIX I

SCENARIO 5: M&I DEMANDS INCREASE

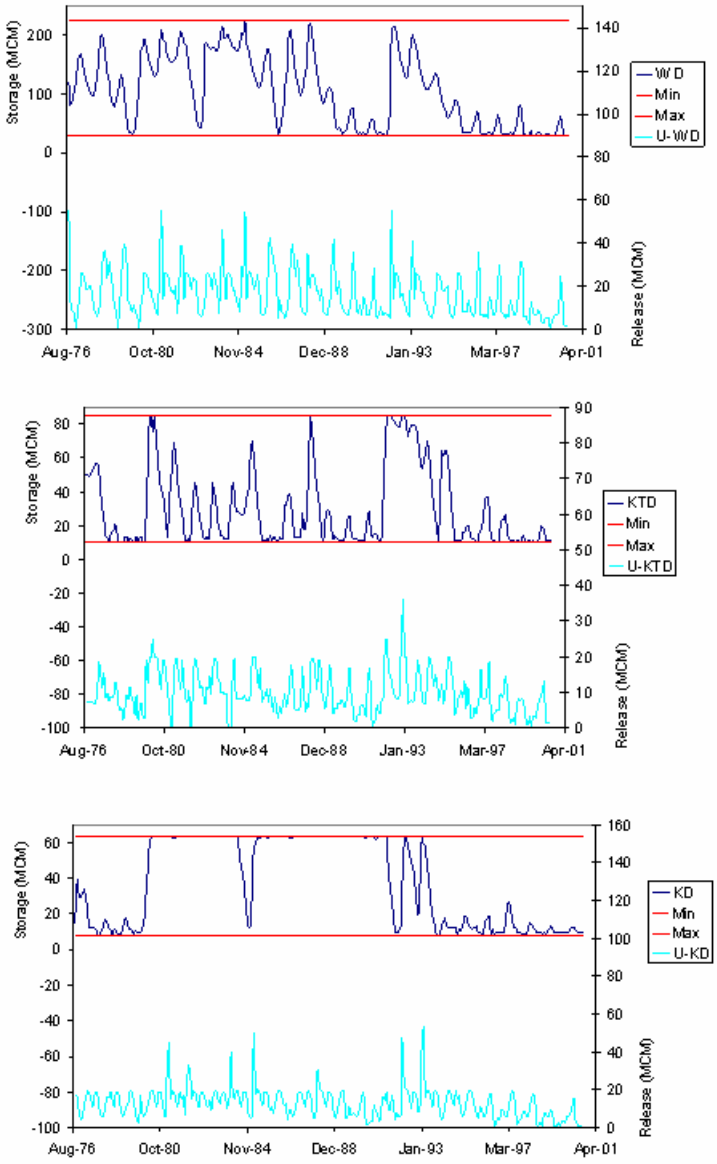

Figure I.1: Assessment model, scenario5, M&I demand increase 10%, constrained GW drawdown, WD, KTD, and KD storage and release sequences

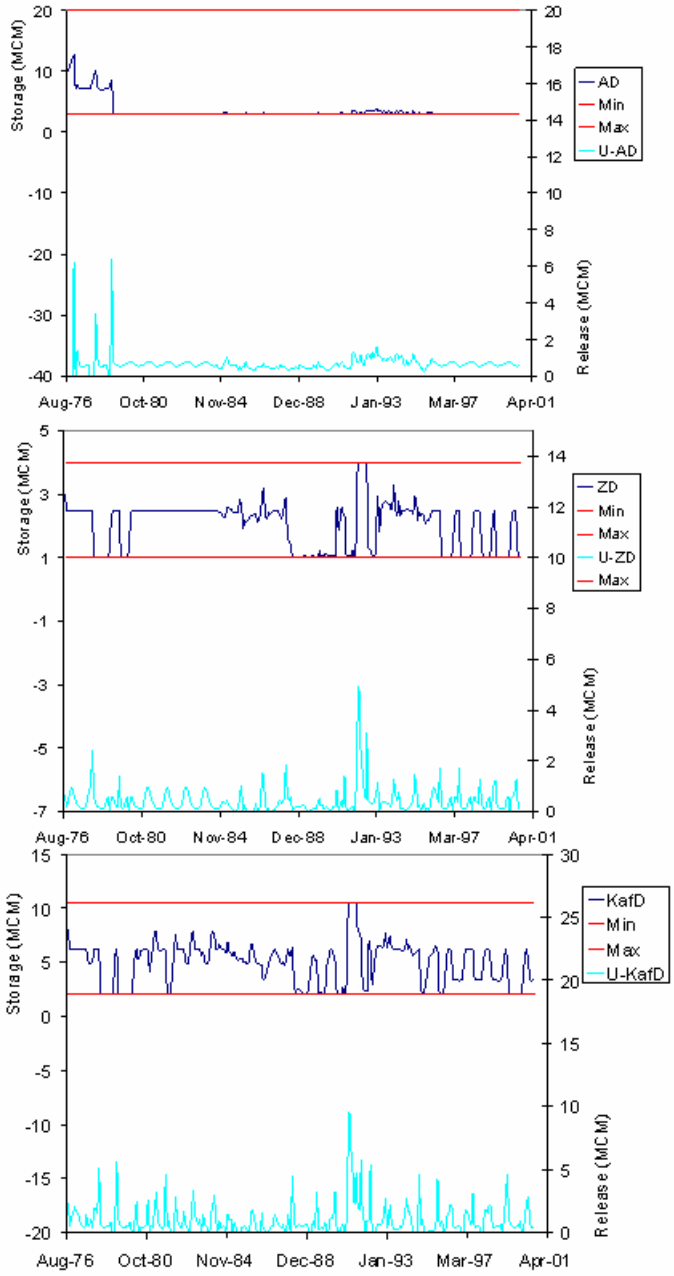

Figure I.2: Assessment model, scenario5, M&I demand increase 10%, constrained GW drawdown, AD, ZD, and KafD storage and release sequences

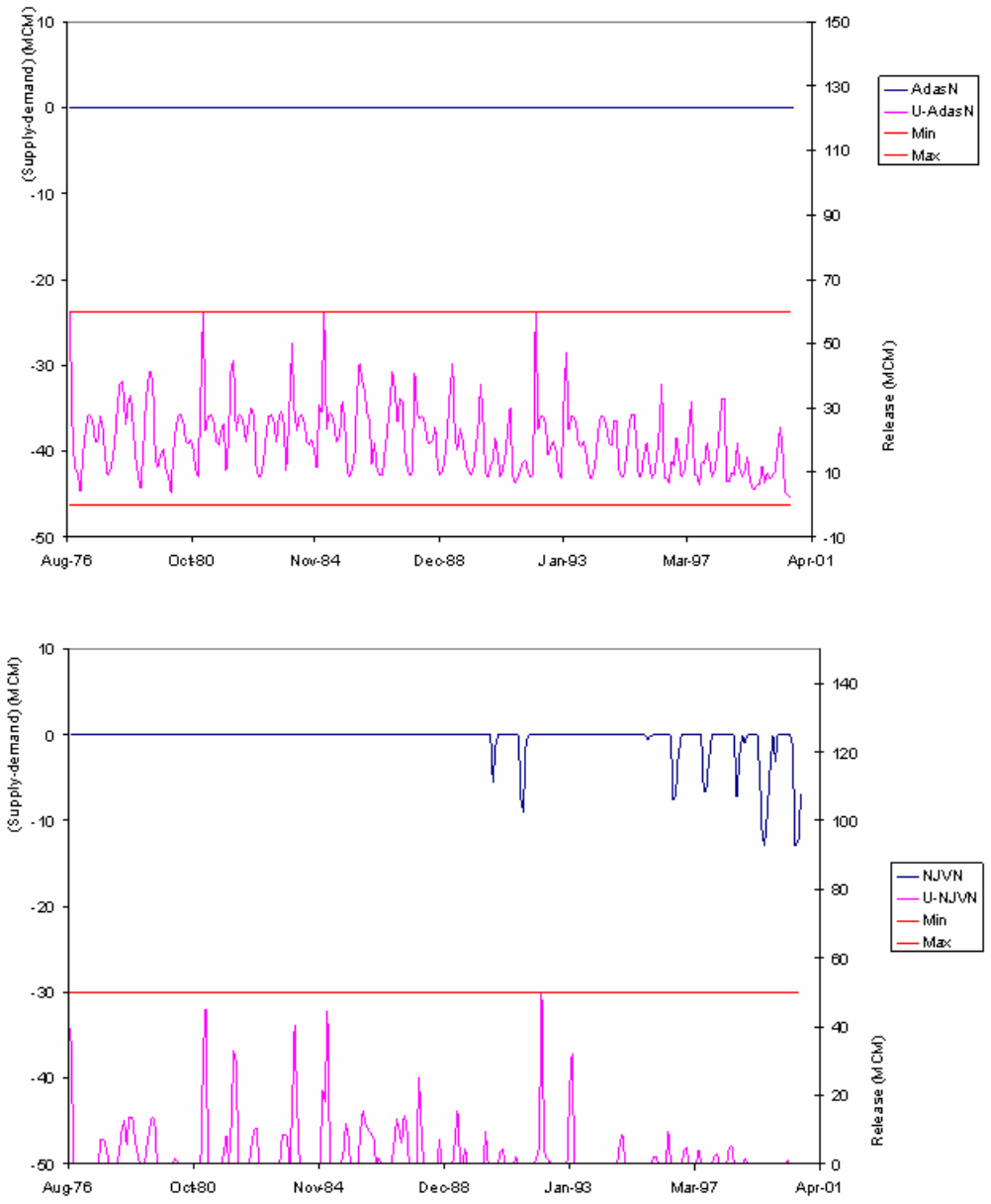

Figure I.3: Assessment model, scenario5, M&I demand increase 10%, constrained GW drawdown, monthly water deficit and release sequences at Adasiya and North Jordan Valley nodes

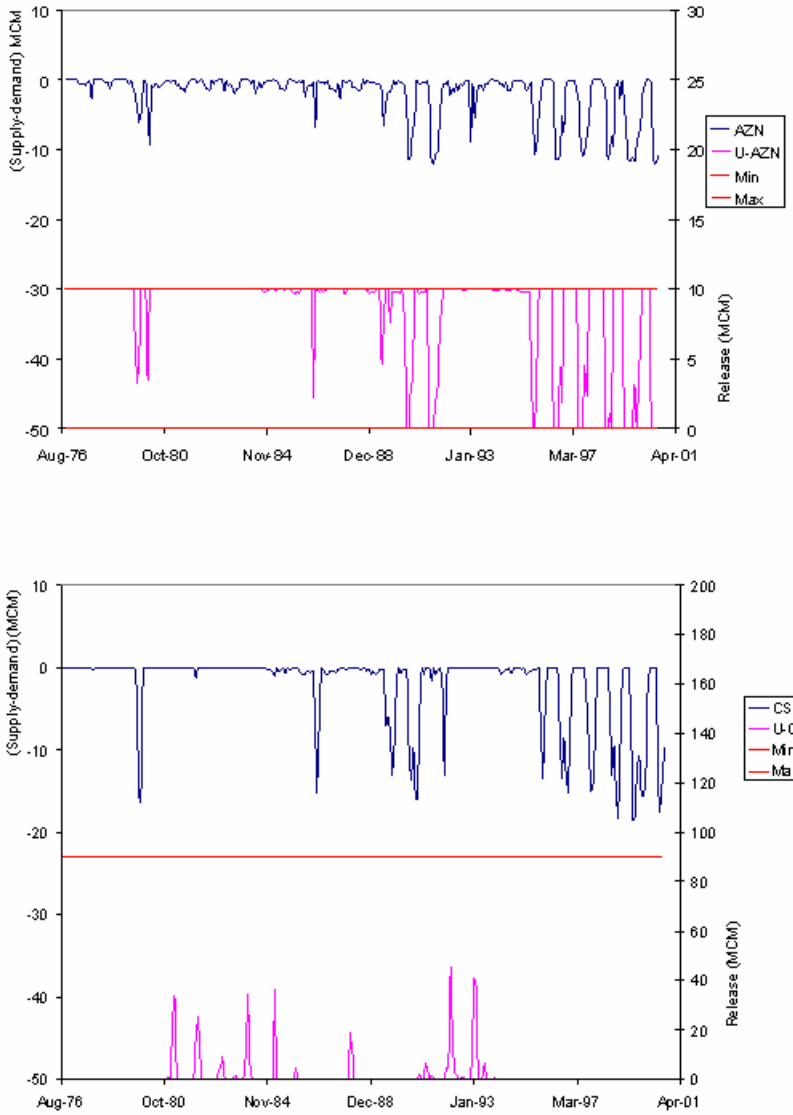

Figure I.4: Assessment model, scenario5, M&I demand increase 10%, constrained GW drawdown, monthly water deficit and release sequences at Amman-Zarqa and C/S Jordan Valley nodes

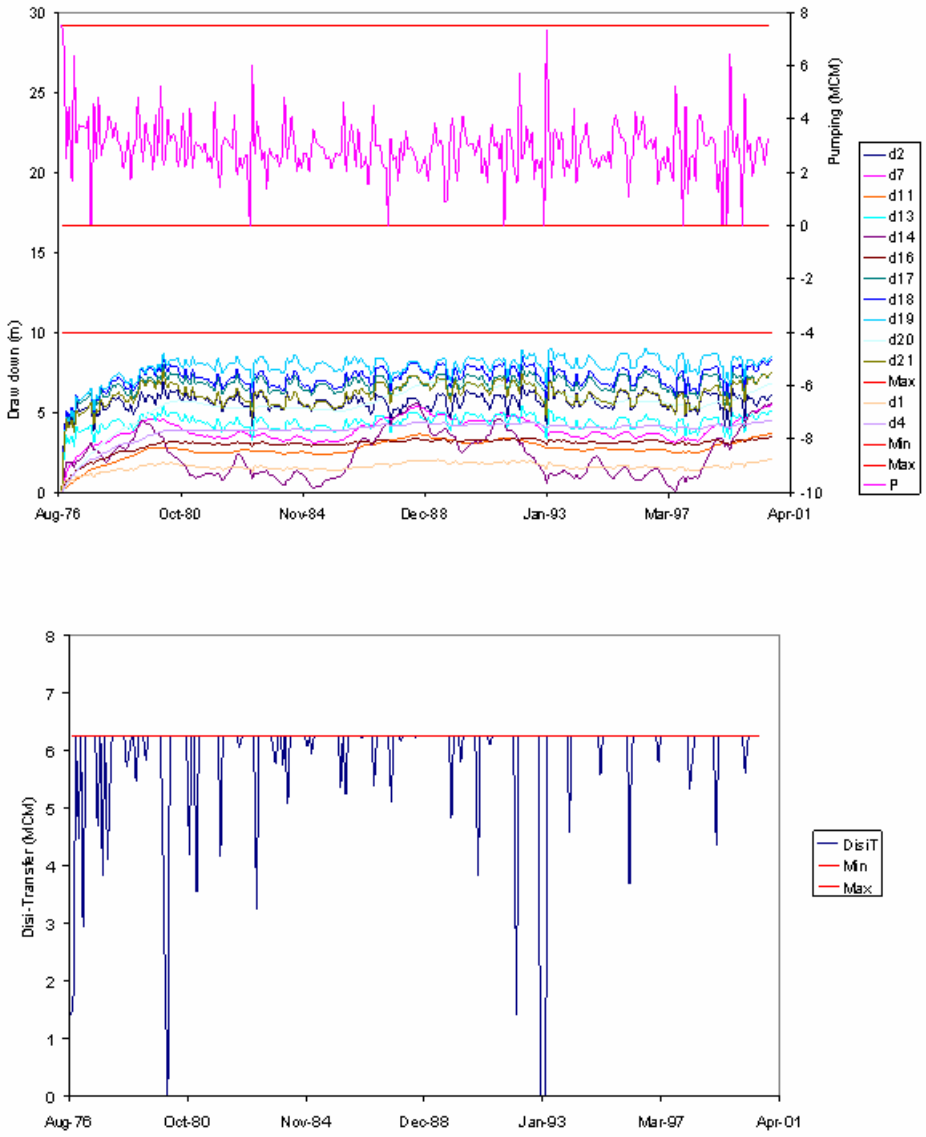

Figure I.5: Assessment model, scenario5, M&I demand increase 10%, constrained GW drawdown, monthly pumping, drawdown and Disi transfer sequences

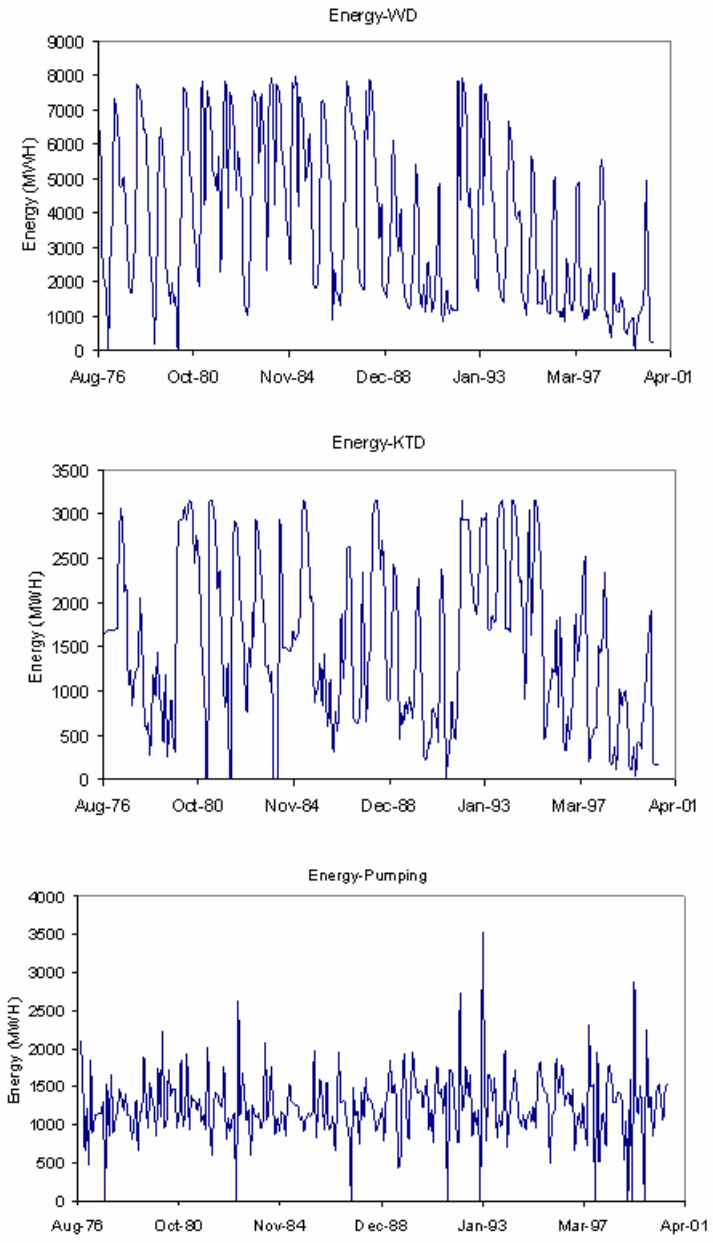

Figure I.6: Assessment model, scenario5, M&I demand increase 10%, constrained GW drawdown, WD, KTD and pumping energy sequences

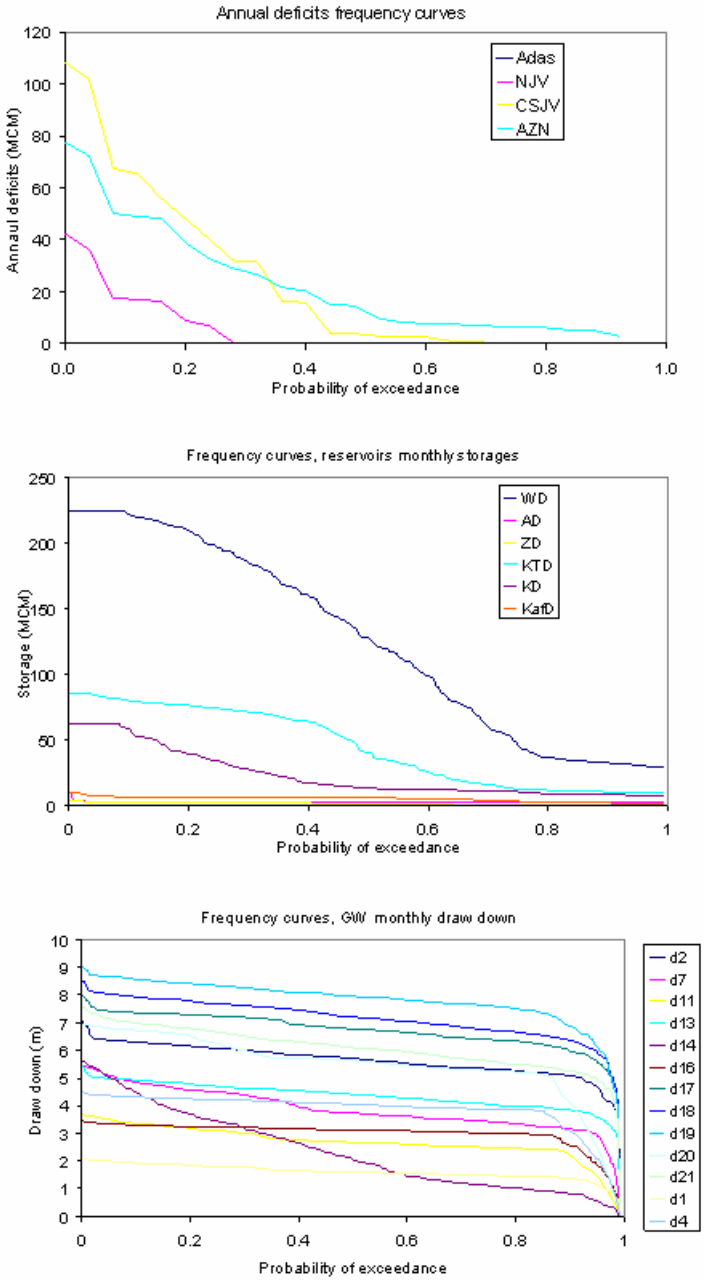

Figure I.7: Assessment model, scenario5, M&I demand increase 10%, constrained GW drawdown, annual deficits, storages, and drawdowns frequency curves

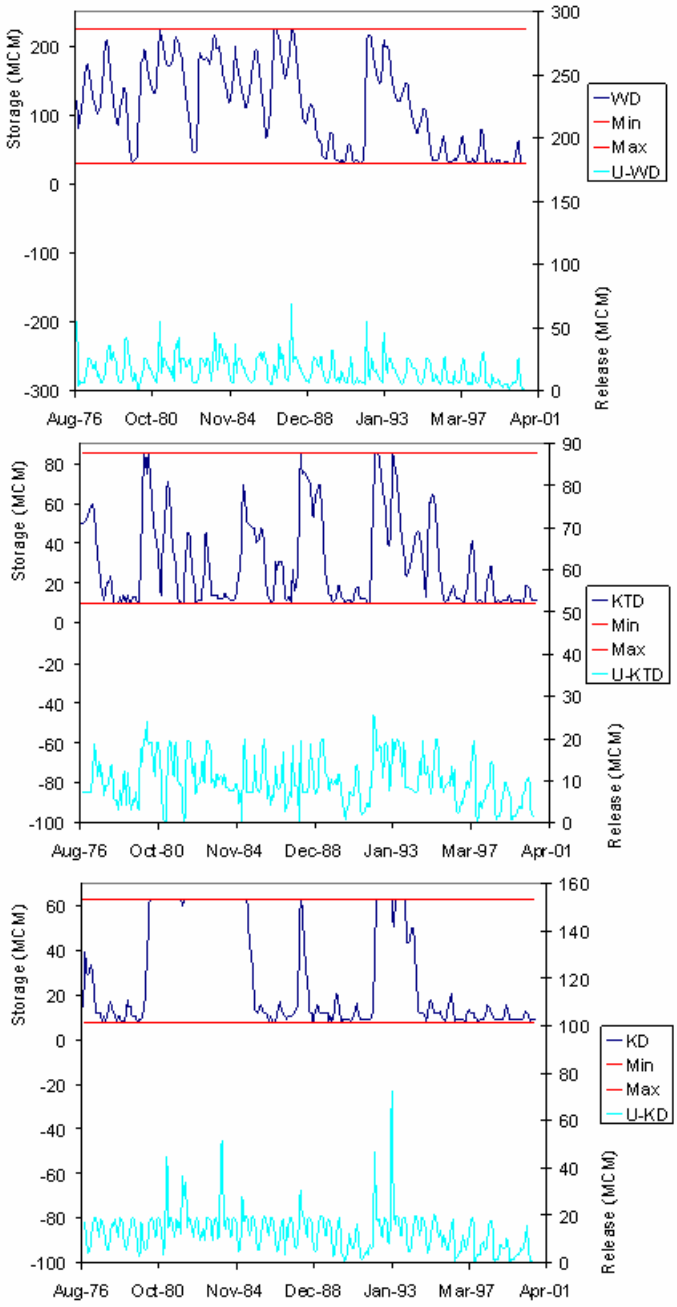

Figure I.8: Assessment model, scenario5, M&I demand increase 20%, constrained GW drawdown, WD, KTD, and KD storage and release sequences

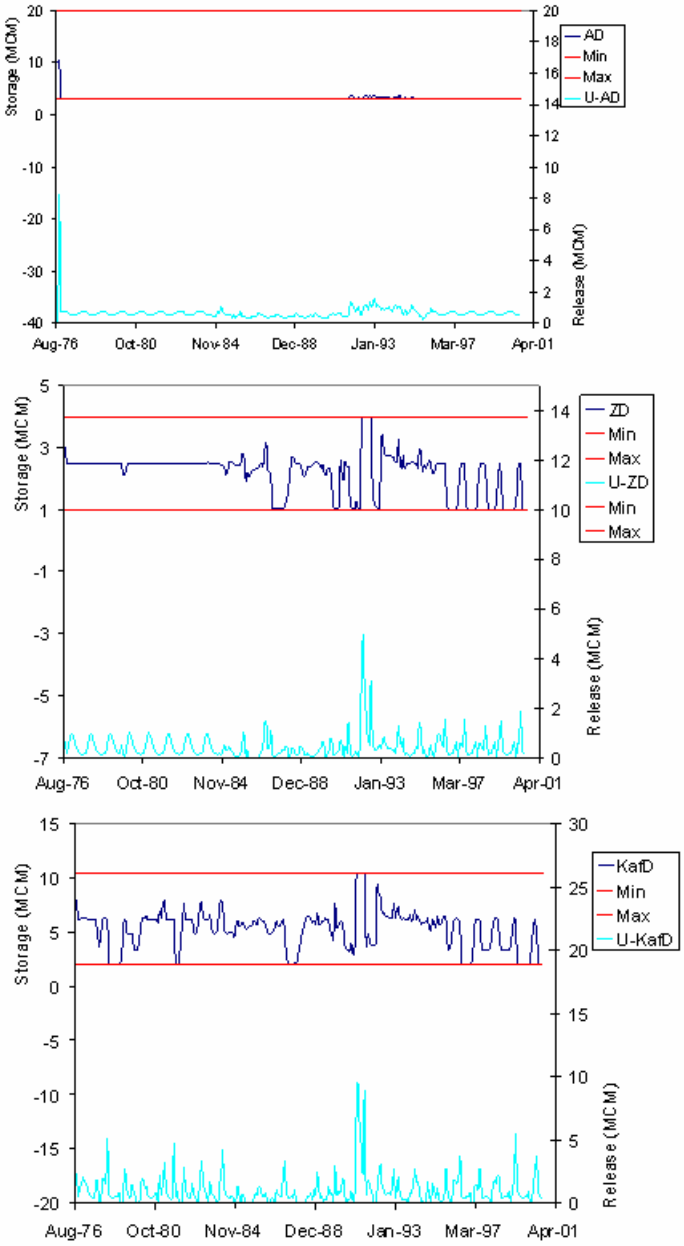

Figure I.9: Assessment model, scenario5, M&I demand increase 20%, constrained GW drawdown, AD, ZD, and KafD storage and release sequences

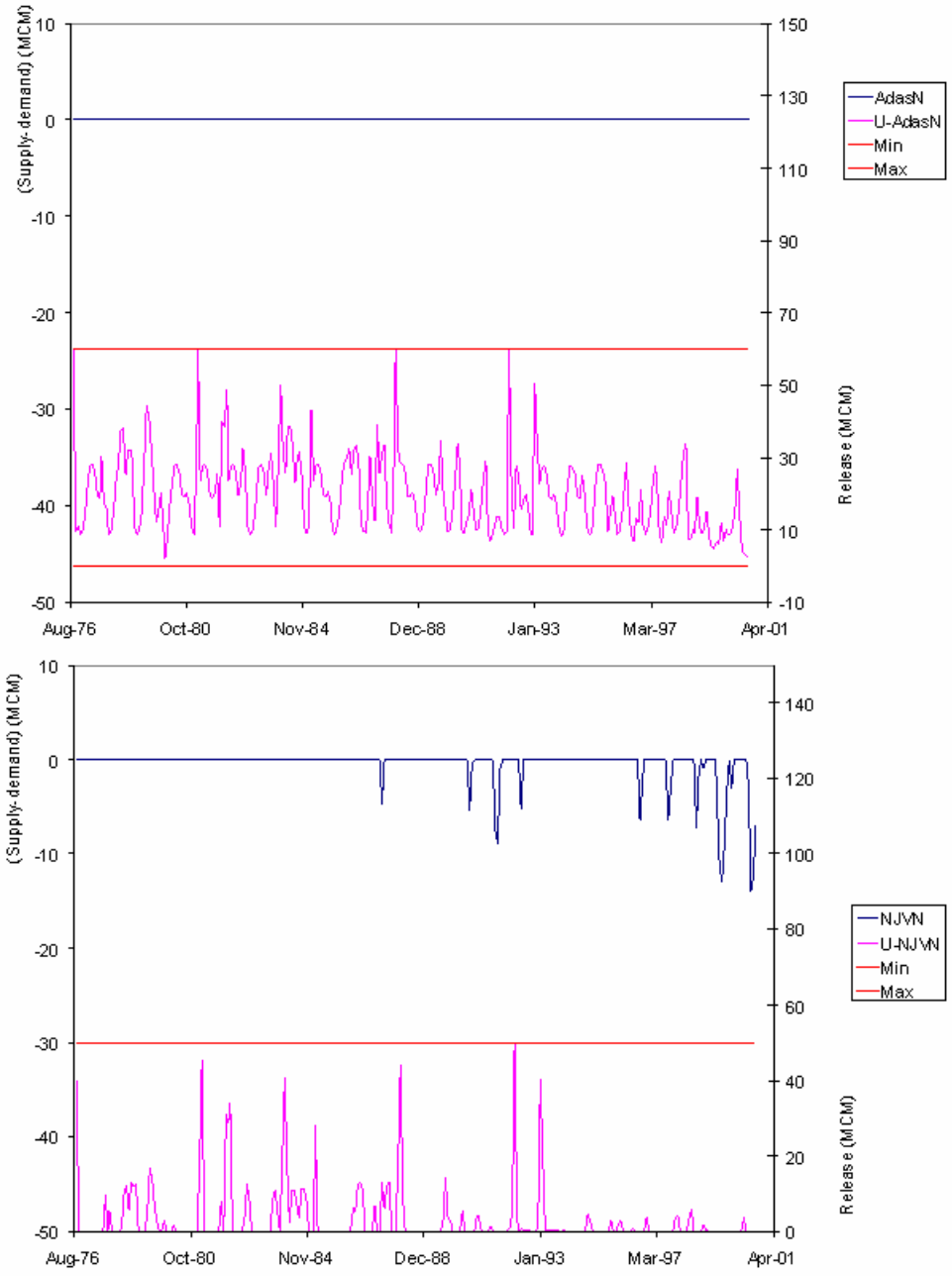

Figure I.10: Assessment model, scenario5, M&I demand increase 20%, constrained GW drawdown, monthly water deficit and release sequences at Adasiya and North Jordan Valley nodes

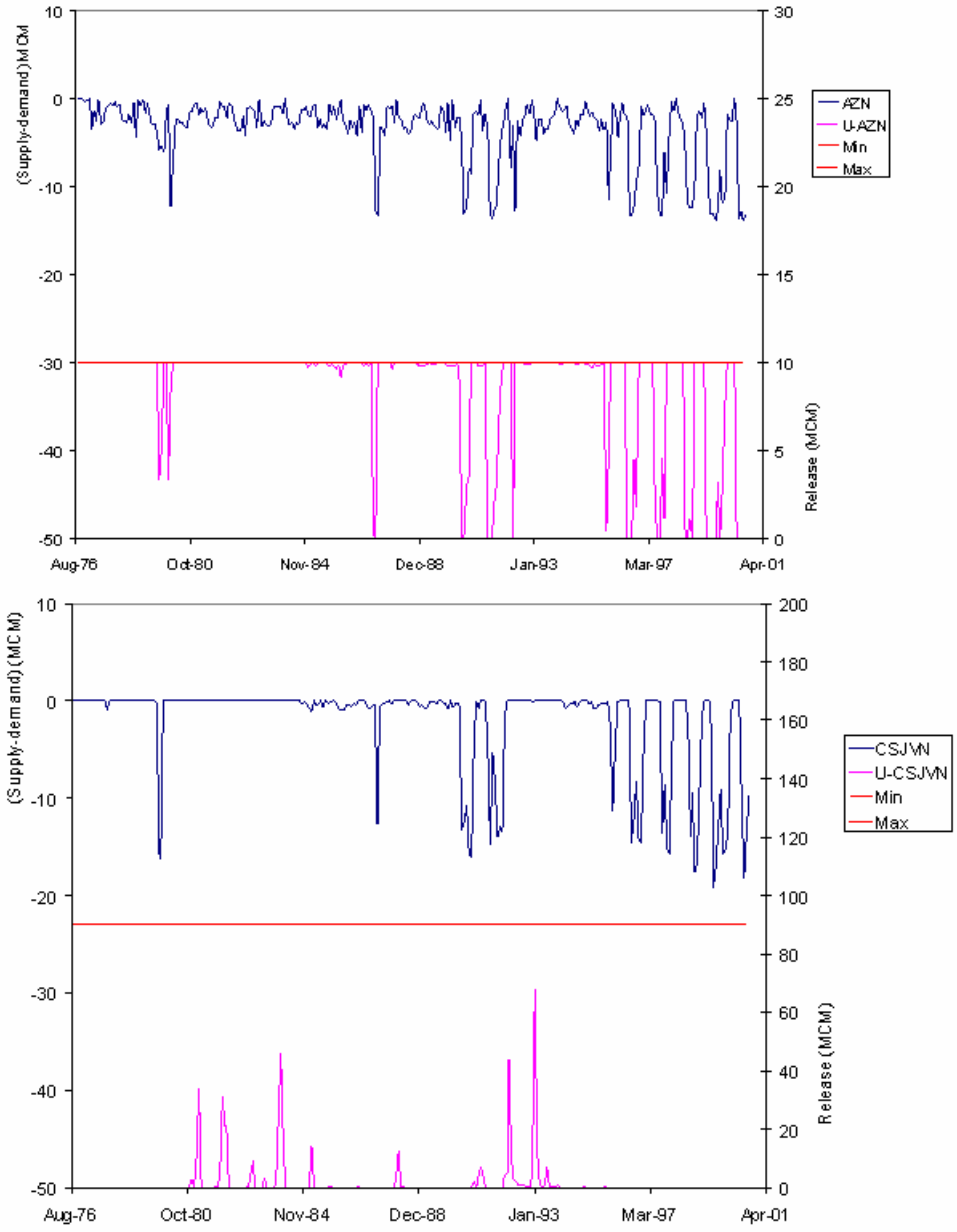

Figure I.11: Assessment model, scenario5, M&I demand increase 20%, constrained GW drawdown, monthly water deficit and release sequences at Amman-Zarqa and C/S Jordan Valley nodes

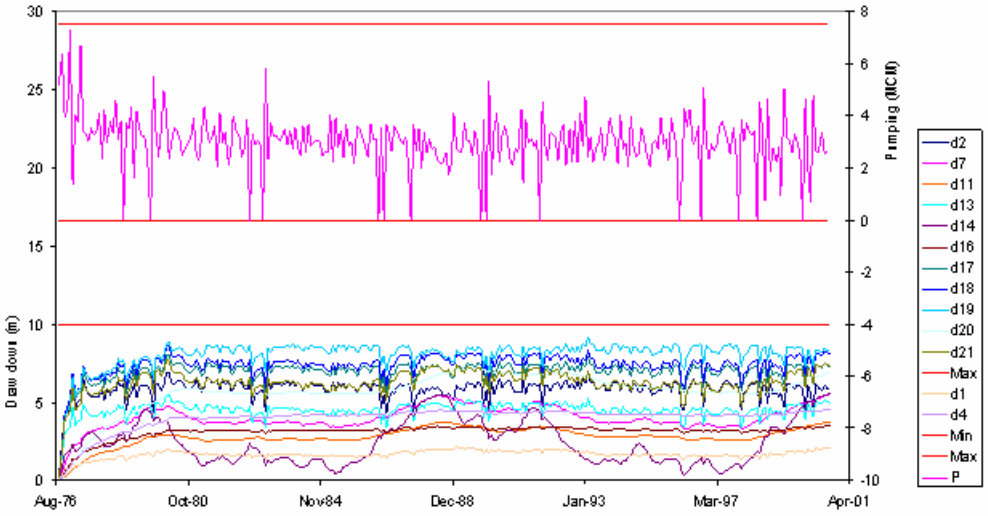

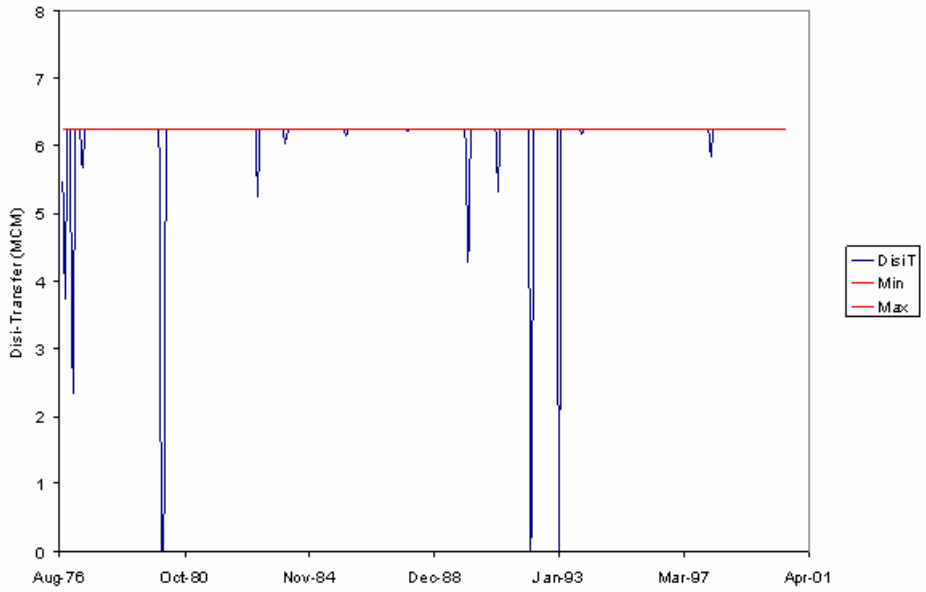

Figure I.12: Assessment model, scenario5, M&I demand increase 20%, constrained GW drawdown, monthly pumping, drawdown and Disi transfer sequences

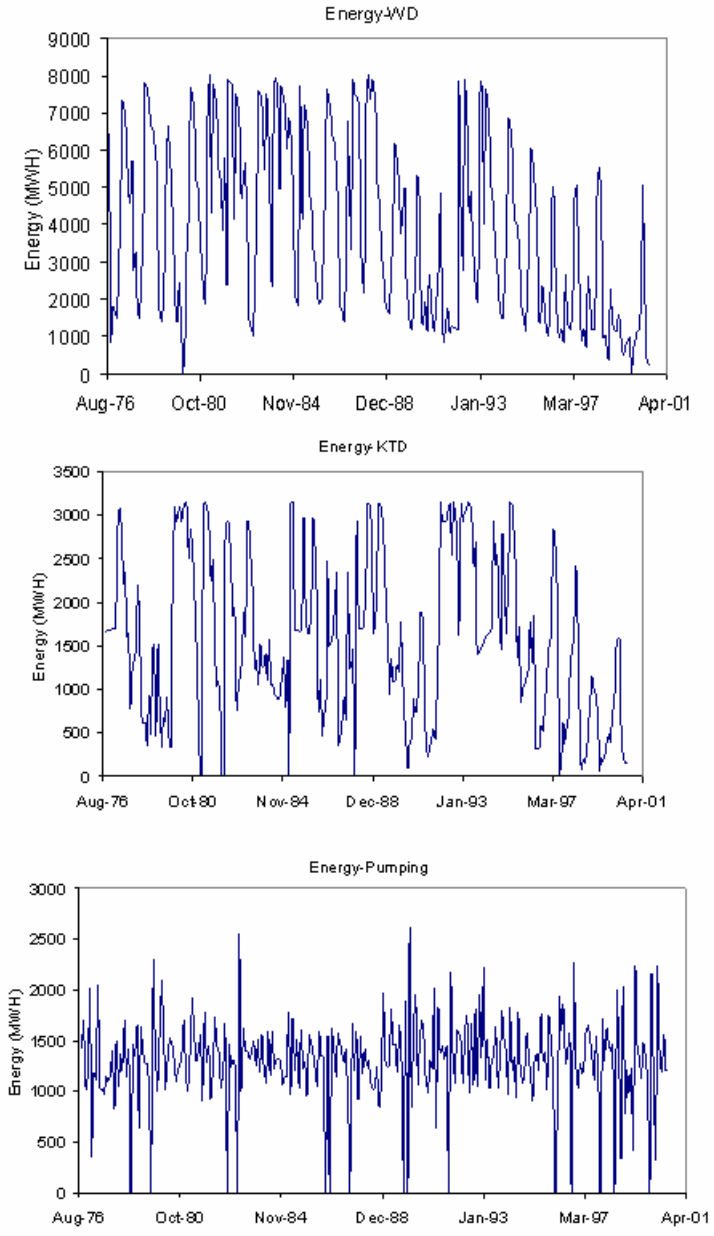

Figure I.13: Assessment model, scenario5, M&I demand increase 20%, constrained GW drawdown, WD, KTD and pumping energy sequences

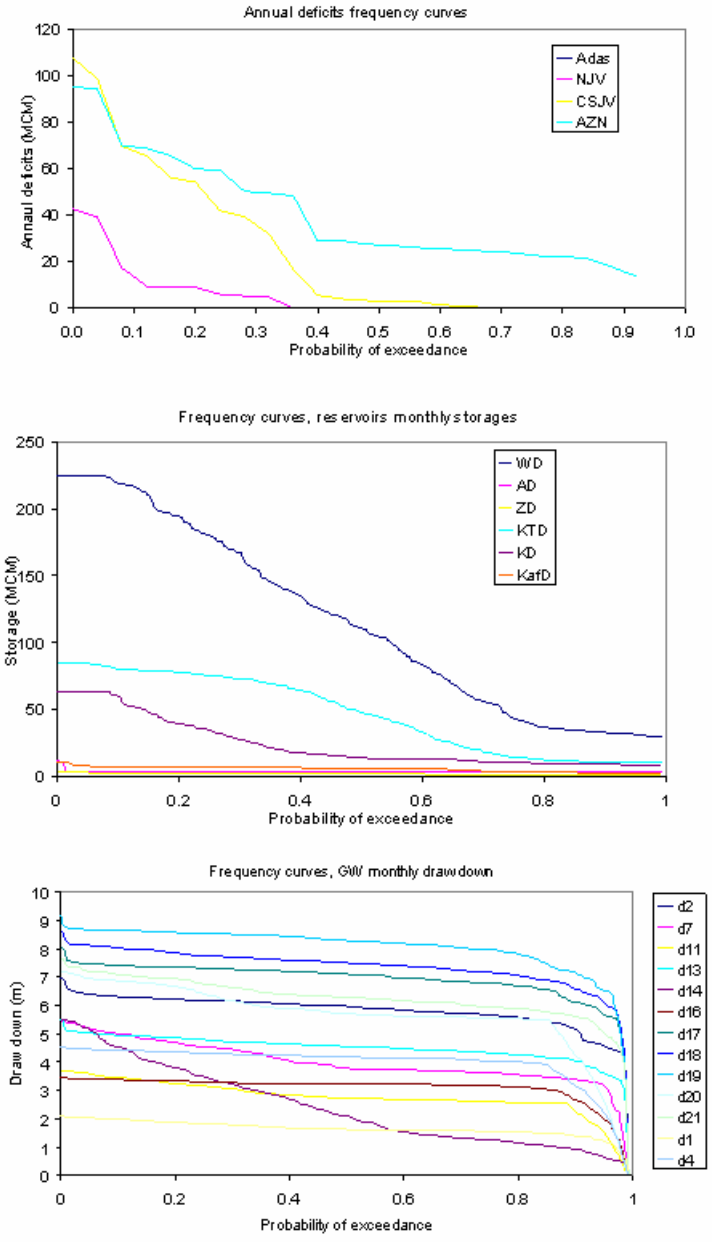

Figure I.14: Assessment model, scenario5, M&I demand increase 20%, constrained GW drawdown, annual deficits, storages, and drawdowns frequency curves

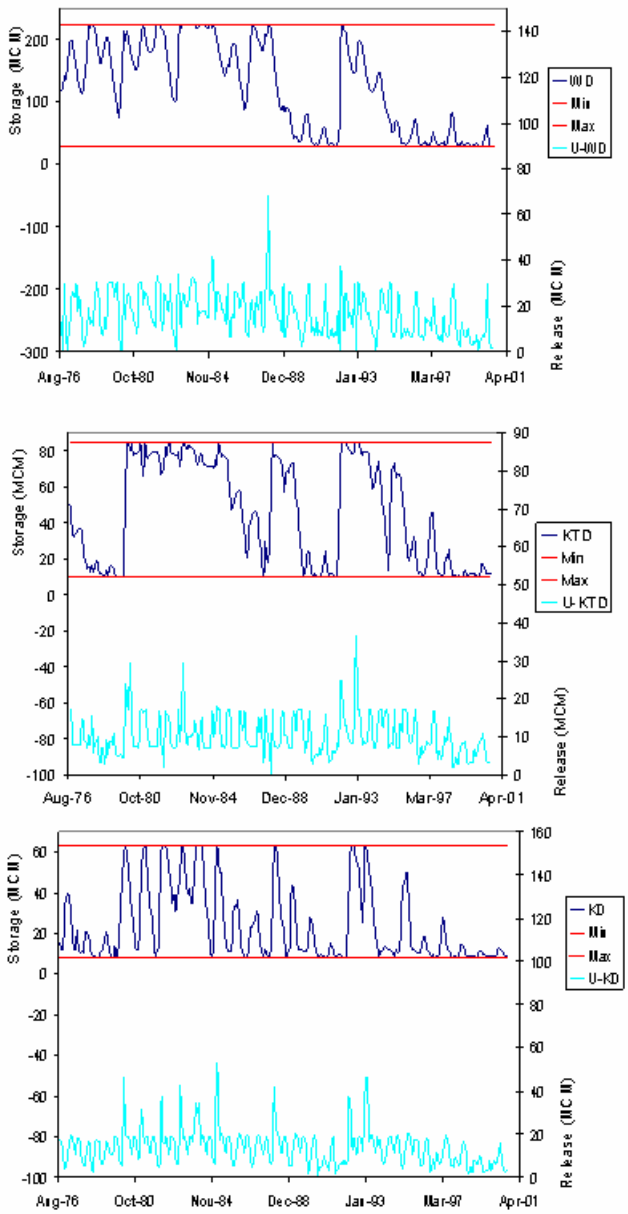

Figure I.15: Assessment model, scenario5, M&I demand increase 10%, unconstrained GW drawdown, WD, KTD, and KD storage and release sequences

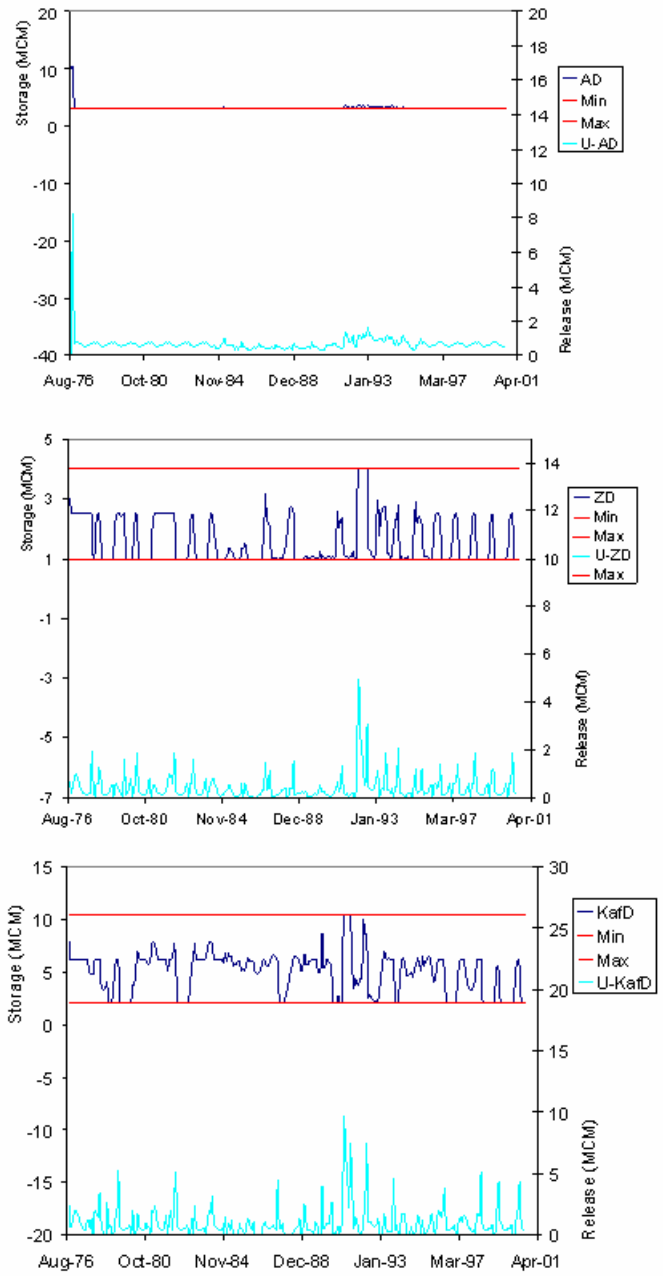

Figure I.16: Assessment model, scenario5, M&I demand increase 10%, unconstrained GW drawdown, AD, ZD, and KafD storage and release sequences

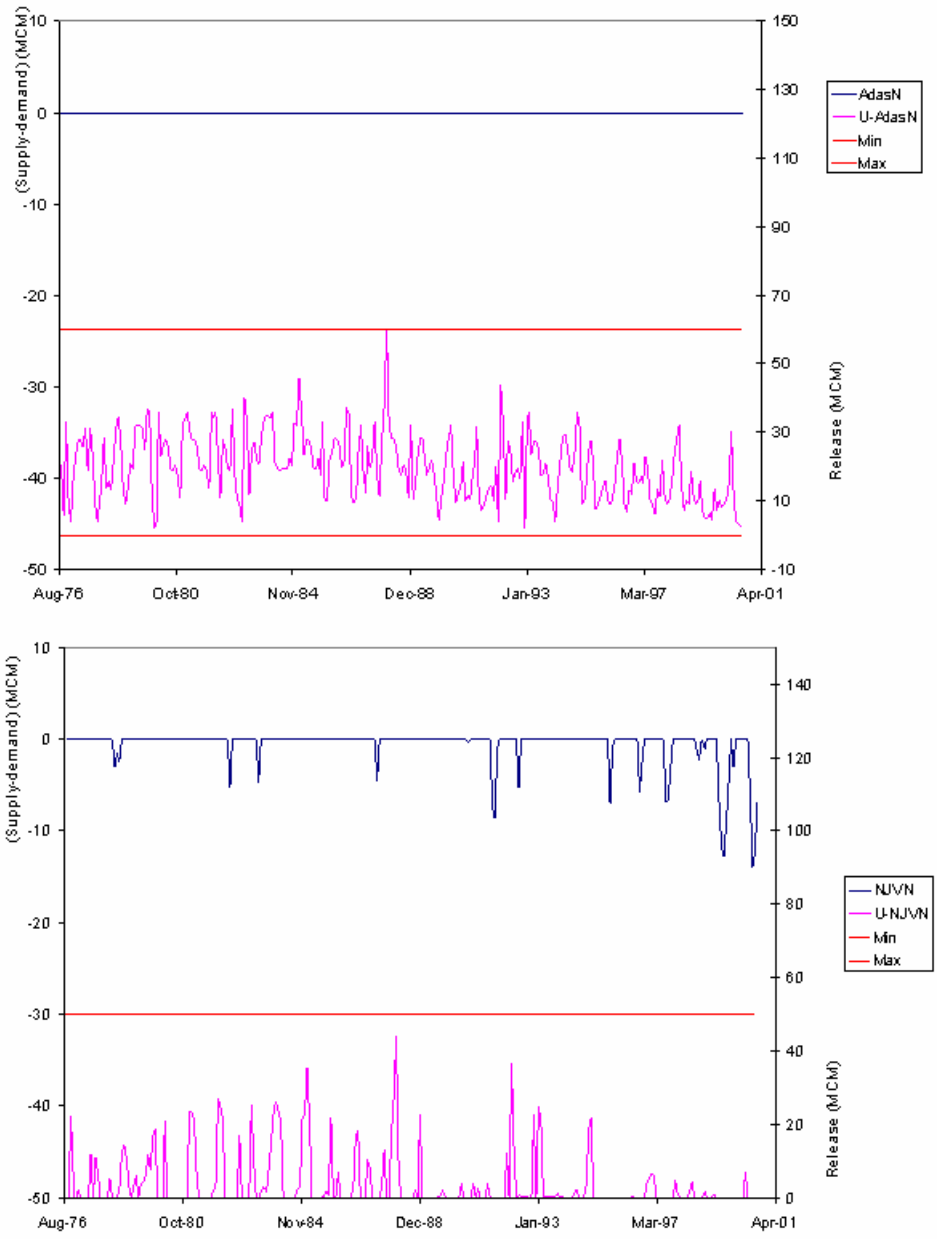

Figure I.17: Assessment model, scenario5, M&I demand increase 10%, unconstrained GW drawdown, monthly water deficit and release sequences at Adasiya and North Jordan Valley nodes

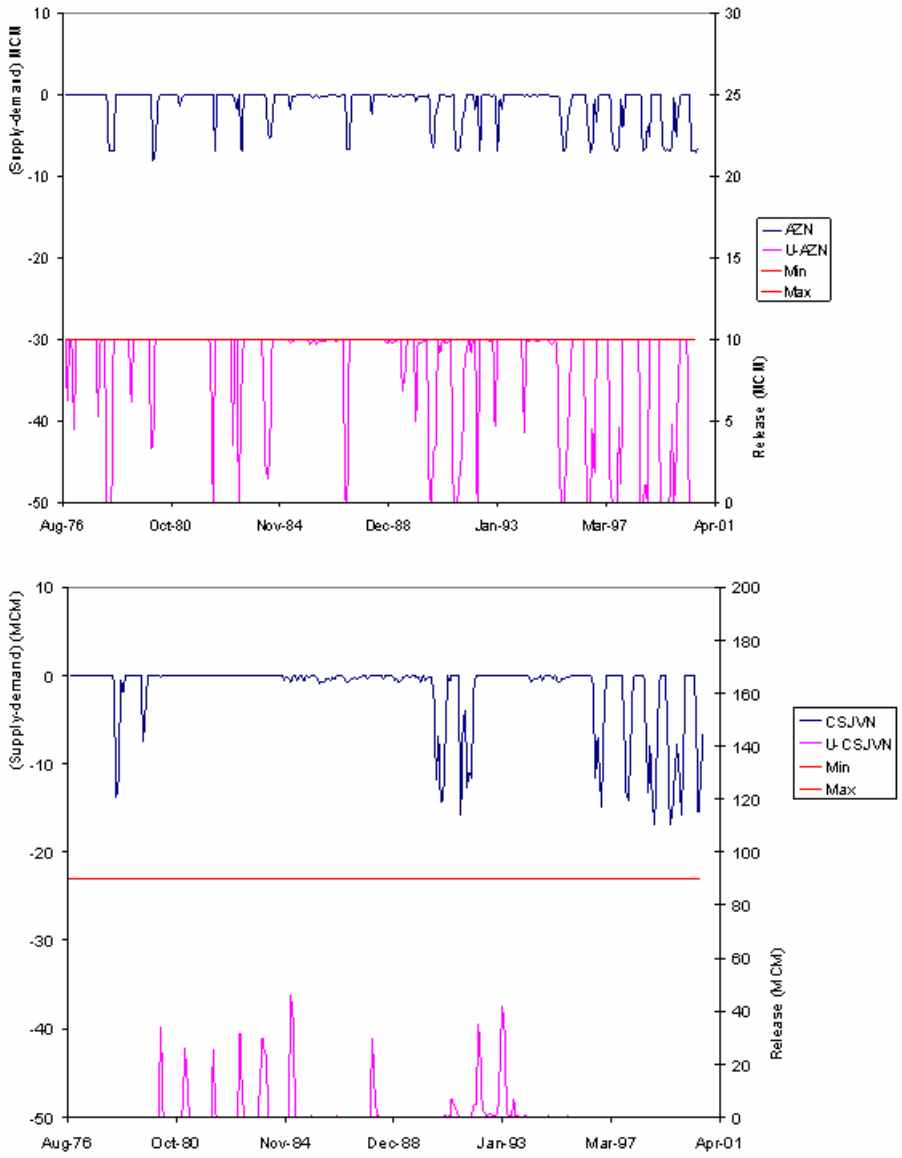

Figure I.18: Assessment model, scenario5, M&I demand increase 10%, unconstrained GW drawdown, monthly water deficit and release sequences at Amman-Zarqa and C/S Jordan Valley nodes

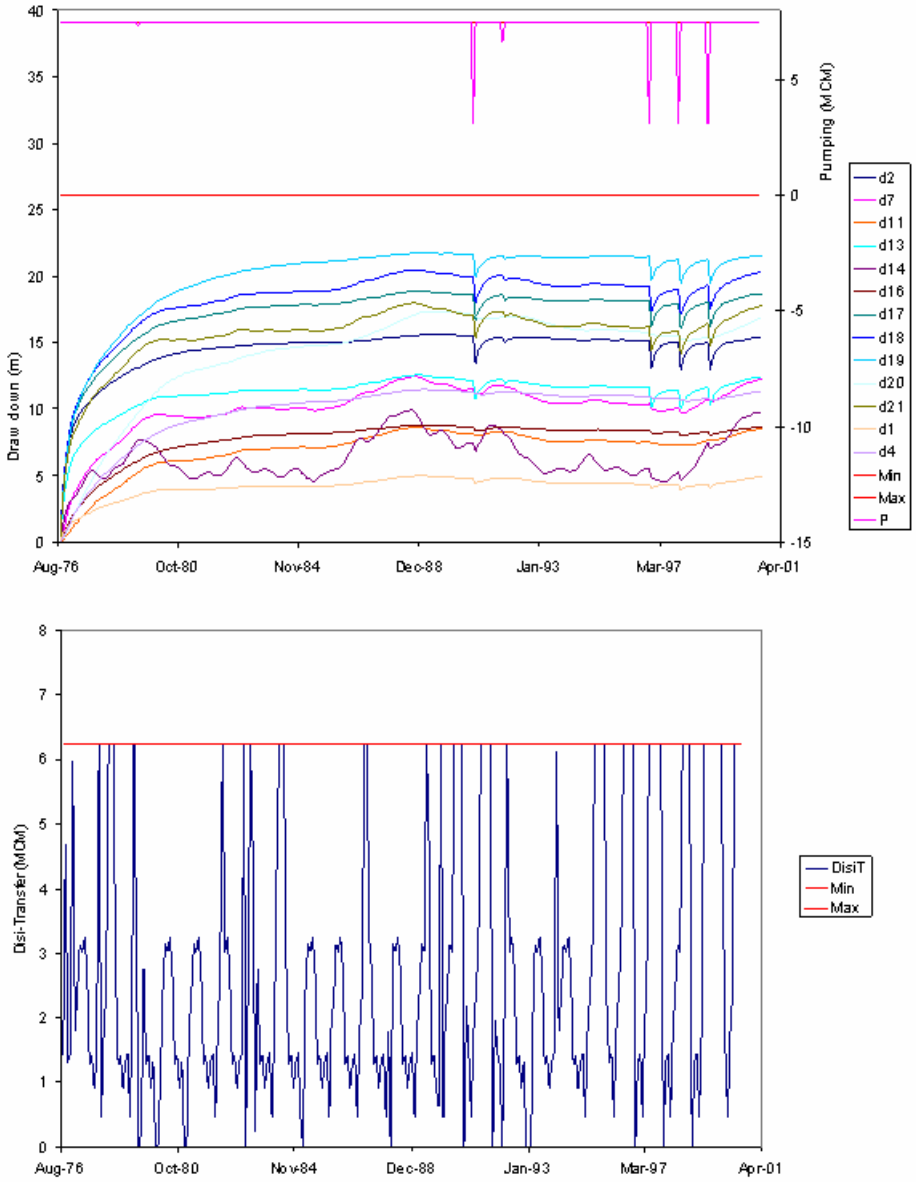

Figure I.19: Assessment model, scenario5, M&I demand increase 10%, unconstrained GW drawdown, monthly pumping, drawdown and Disi transfer sequences

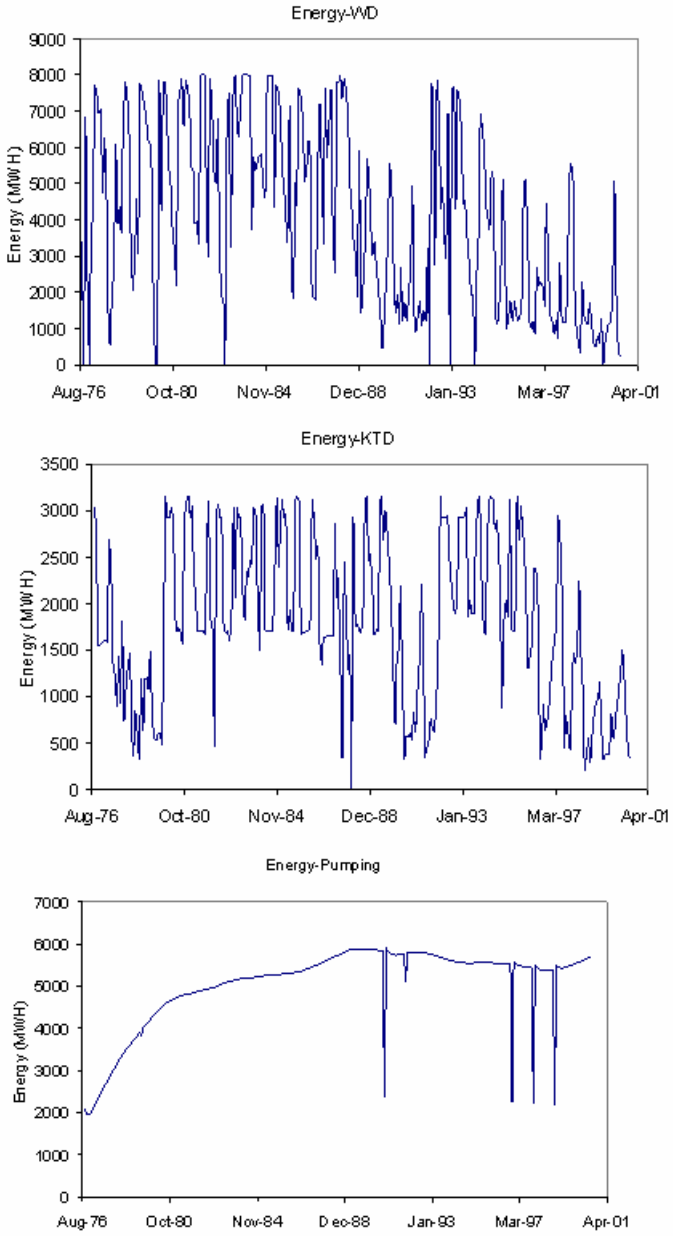

Figure I.20: Assessment model, scenario5, M&I demand increase 10%, unconstrained GW drawdown, WD, KTD and pumping energy sequences

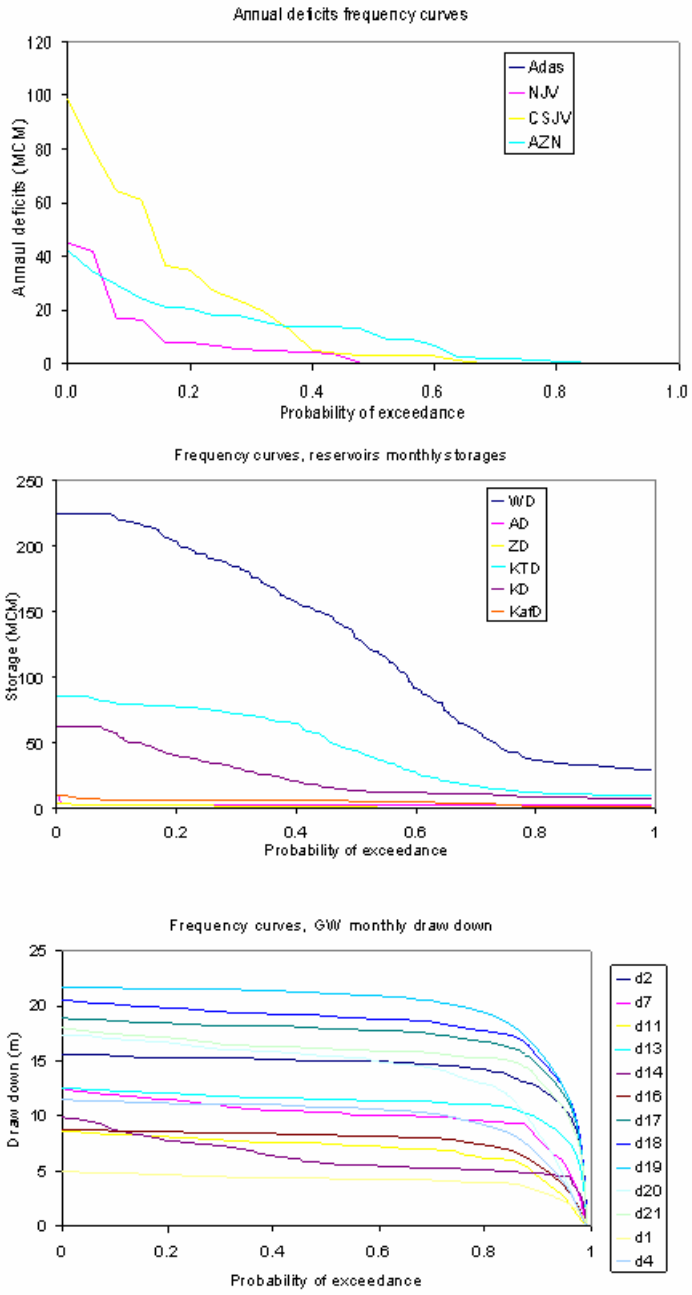

Figure I.21: Assessment model, scenario5, M&I demand increase 10%, unconstrained GW drawdown, annual deficits, storages, and drawdowns frequency curves

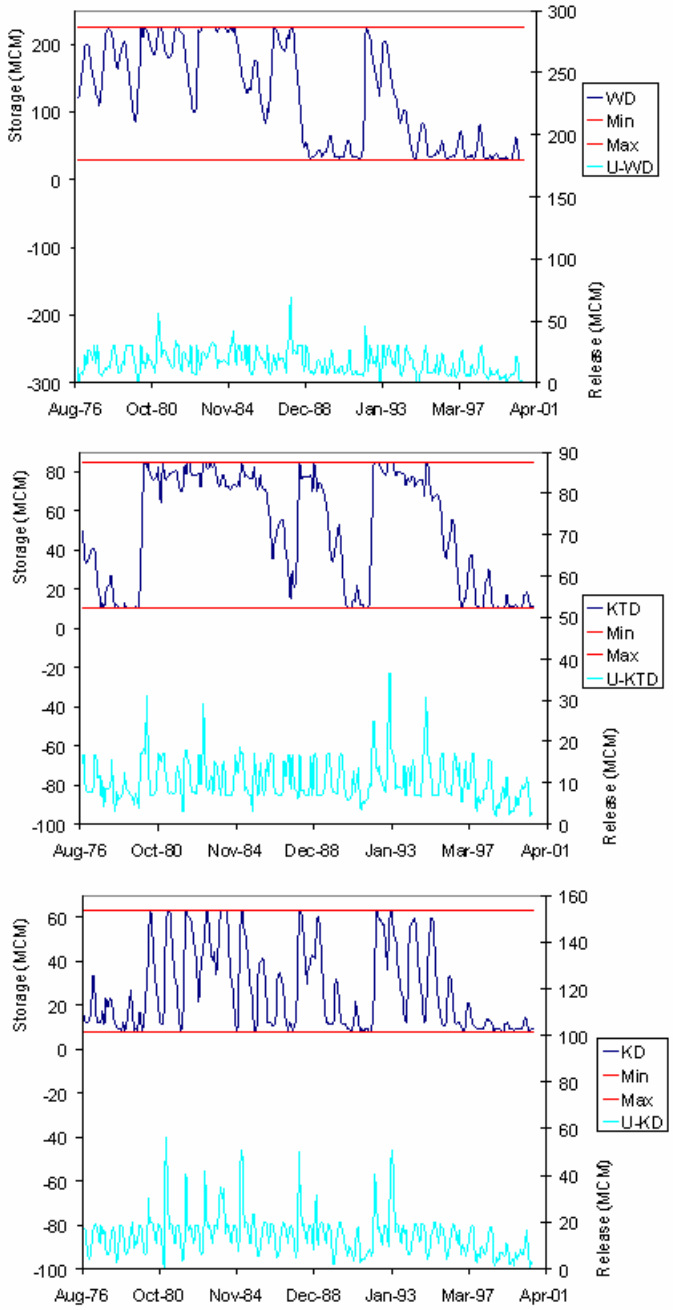

Figure I.22: Assessment model, scenario5, M&I demand increase 20%, unconstrained GW drawdown, WD, KTD, and KD storage and release sequences

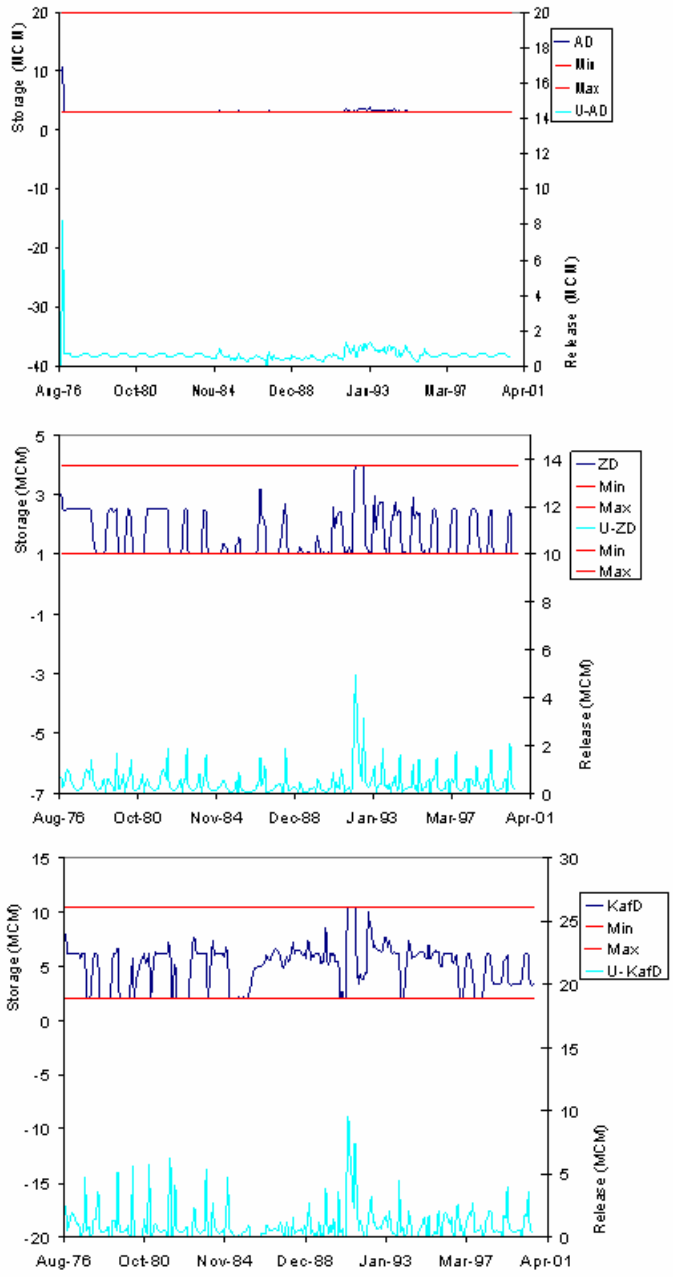

Figure I.23: Assessment model, scenario5, M&I demand increase 20%, unconstrained GW drawdown, AD, ZD, and KafD storage and release sequences

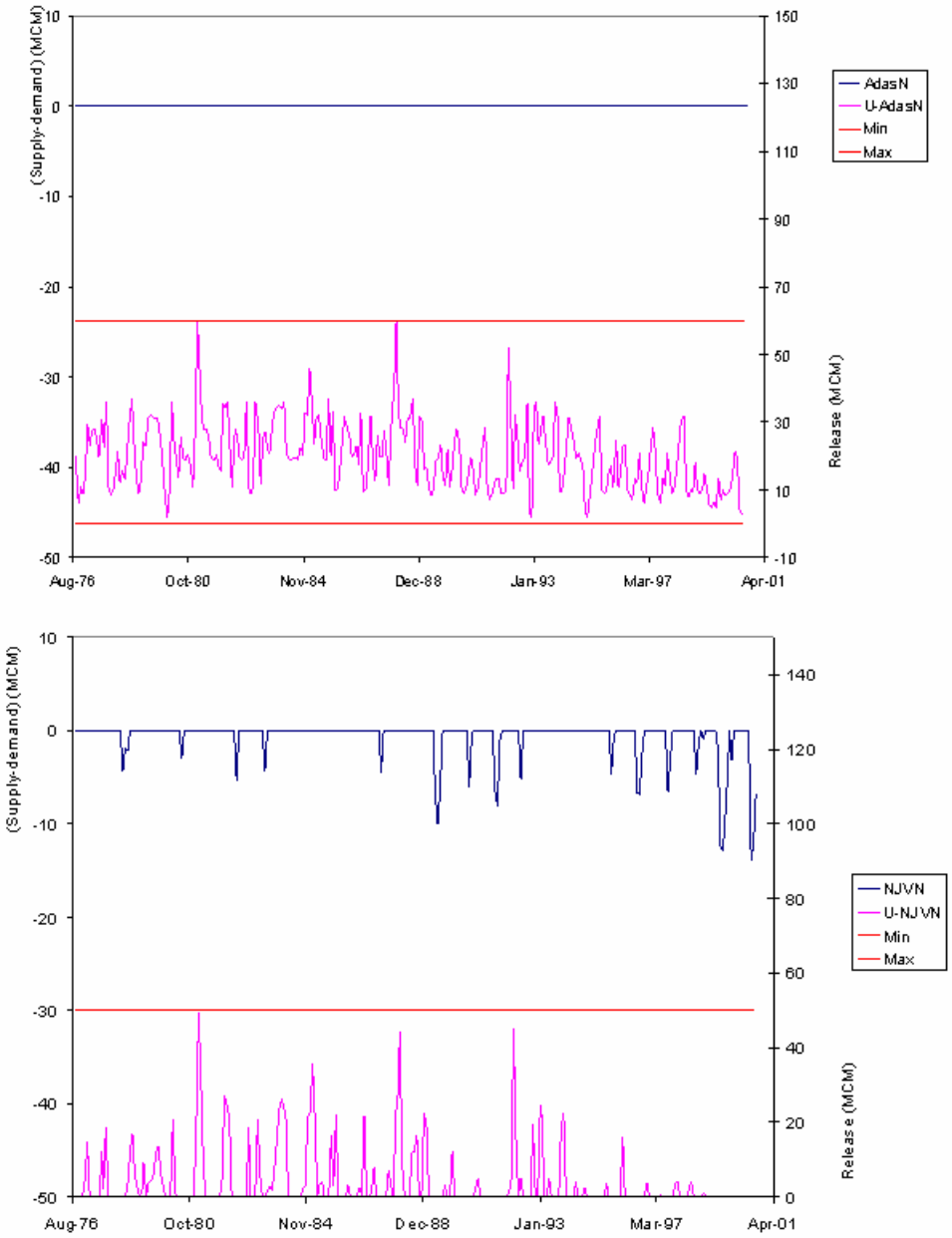

Figure I.24: Assessment model, scenario5, M&I demand increase 20%, unconstrained GW drawdown, monthly water deficit and release sequences at Adasiya and North Jordan Valley nodes

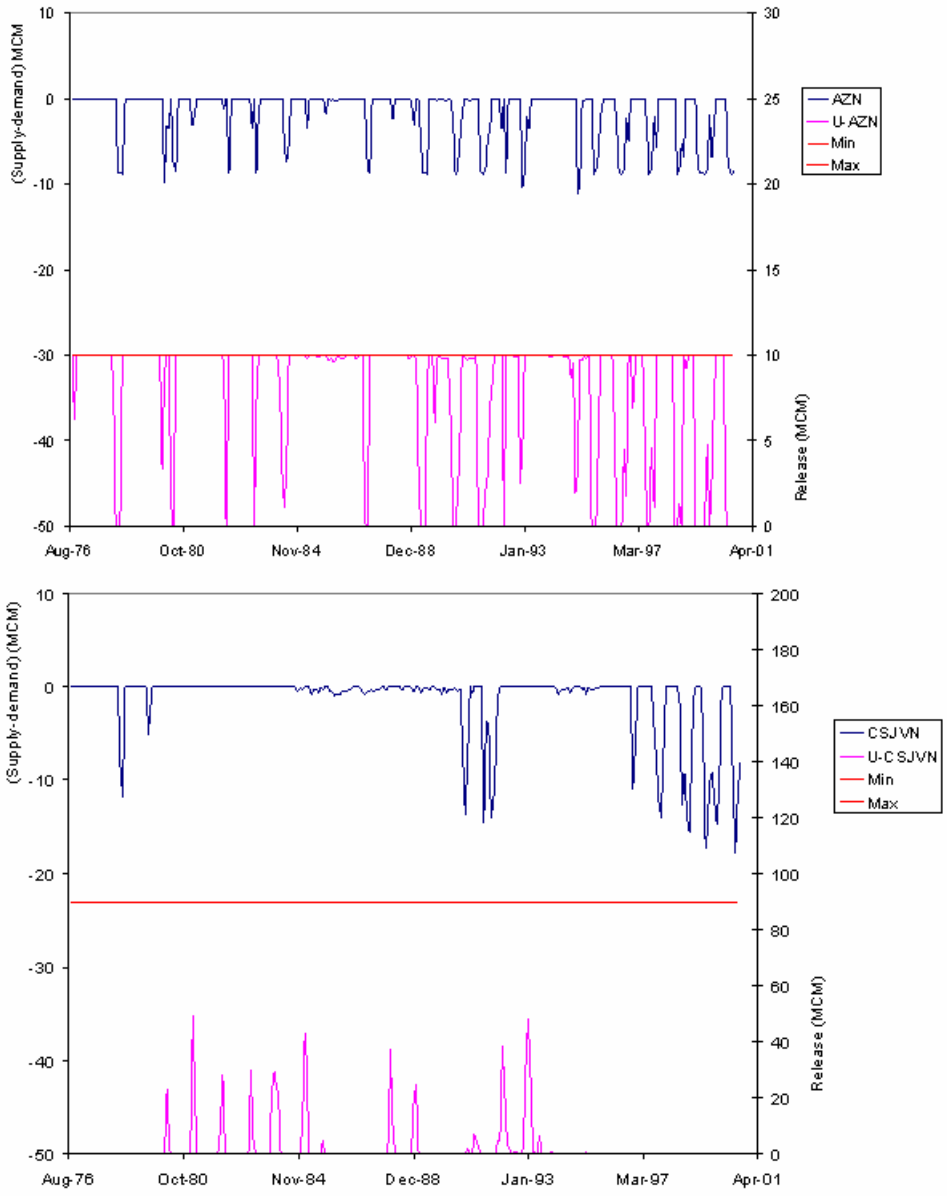

Figure I.25: Assessment model, scenario5, M&I demand increase 20%, unconstrained GW drawdown, monthly water deficit and release sequences at Amman-Zarqa and C/S Jordan Valley nodes

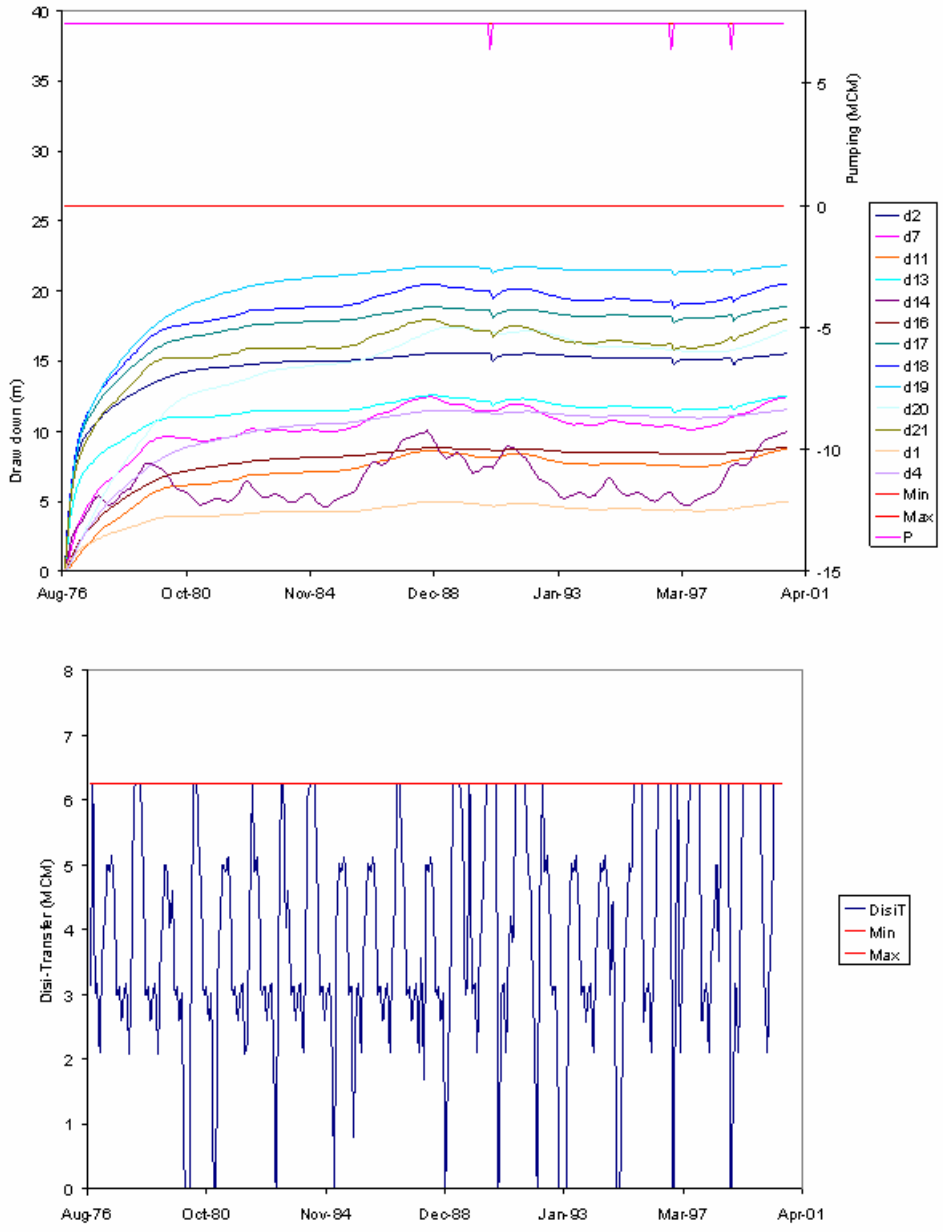

Figure I.26: Assessment model, scenario5, M&I demand increase 20%, unconstrained GW drawdown, monthly pumping, drawdown and Disi transfer sequences

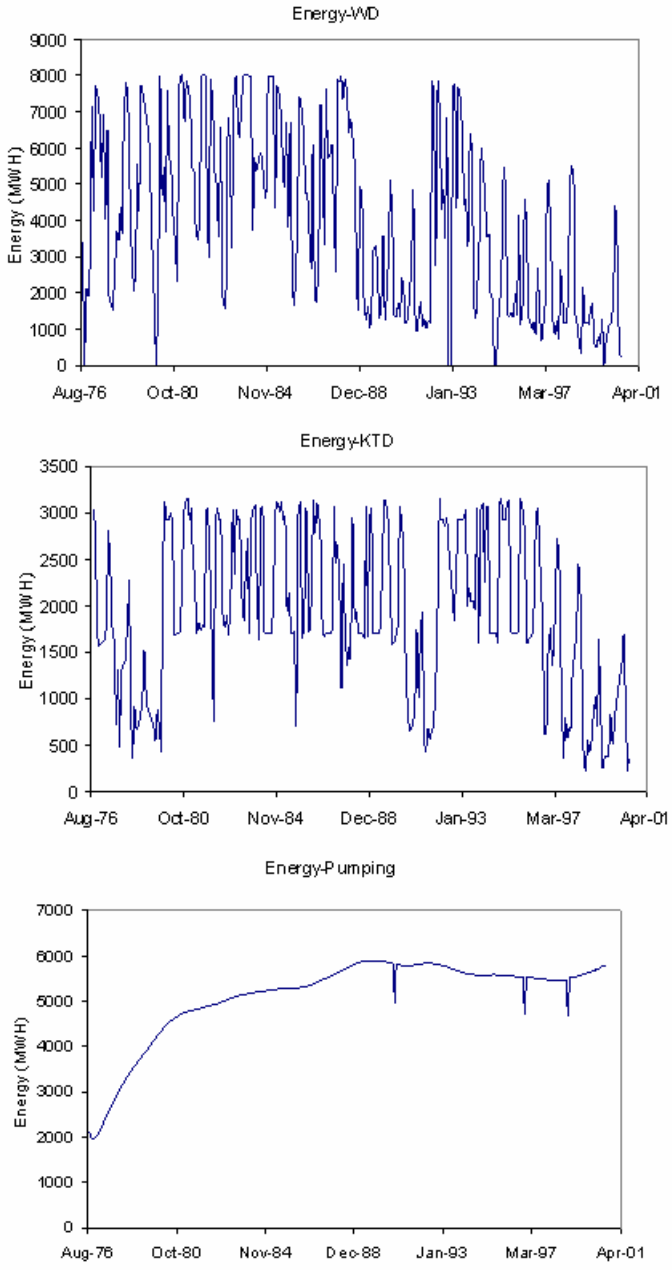

Figure I.27: Assessment model, scenario5, M&I demand increase 20%, unconstrained GW drawdown, WD, KTD and pumping energy sequences

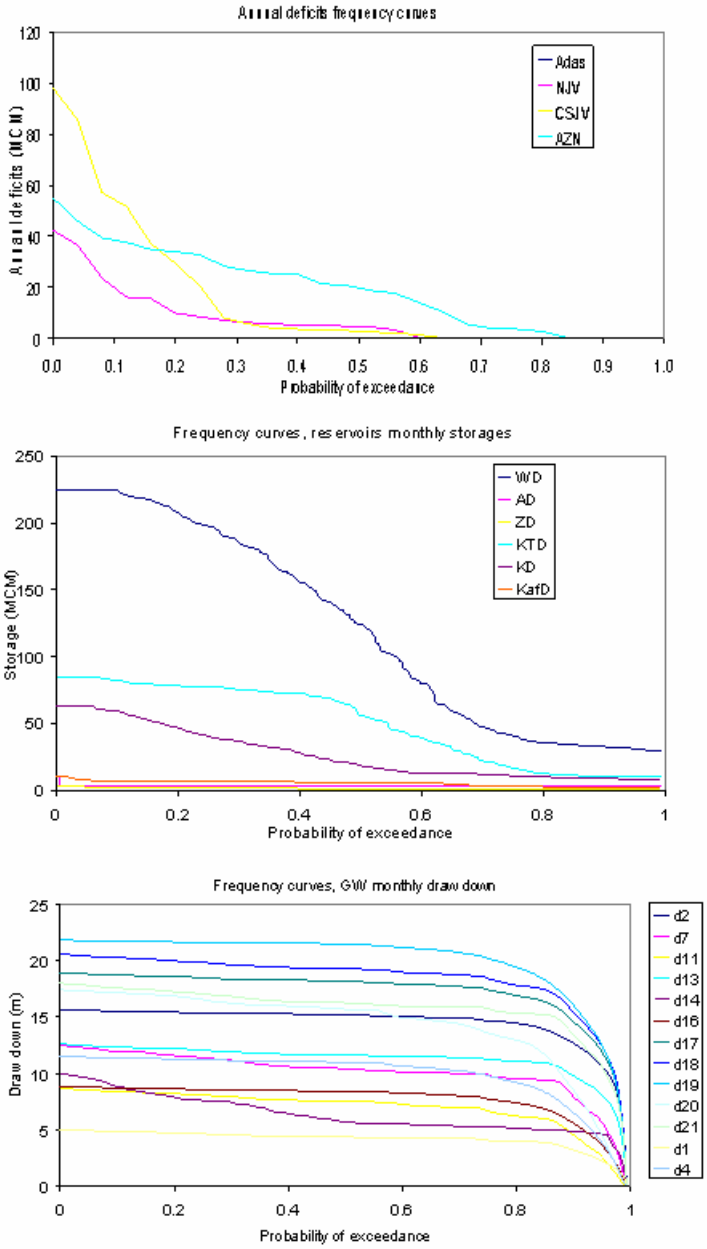

Figure I.28: Assessment model, scenario5, M&I demand increase 20%, unconstrained GW drawdown, annual deficits, storages, and drawdowns frequency curves

APPENDIX J

SCENARIO 6: AGRICULTURAL DEMAND INCREASE

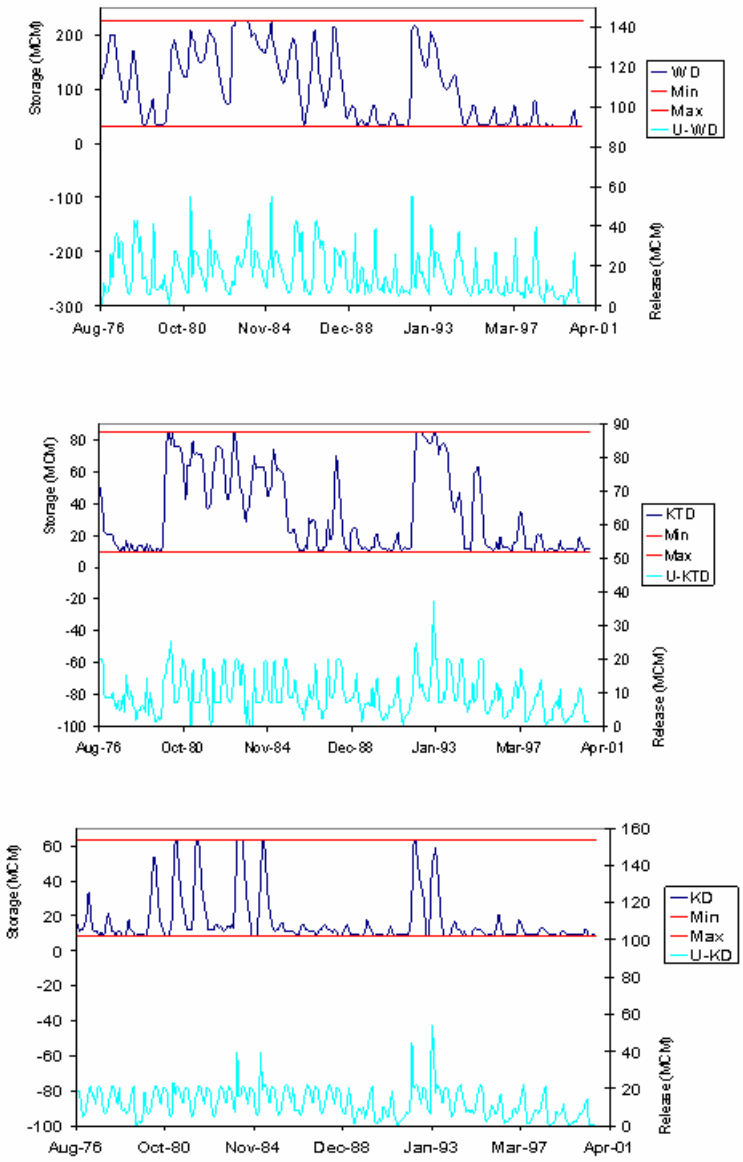

Figure J.1: Assessment model, scenario6, agricultural demand increase 10%, constrained GW drawdown, WD, KTD, and KD storage and release sequences

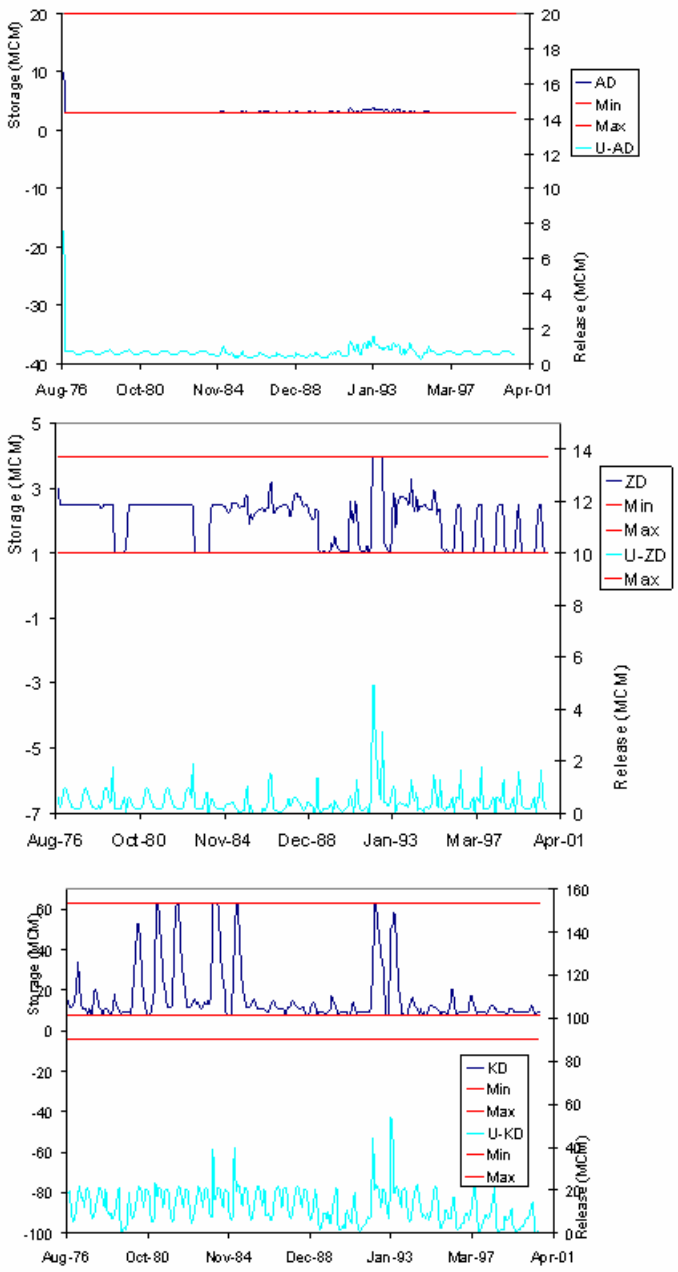

Figure J.2: Assessment model, scenario6, agricultural demand increase 10%, constrained GW drawdown, AD, ZD, and KafD storage and release sequences

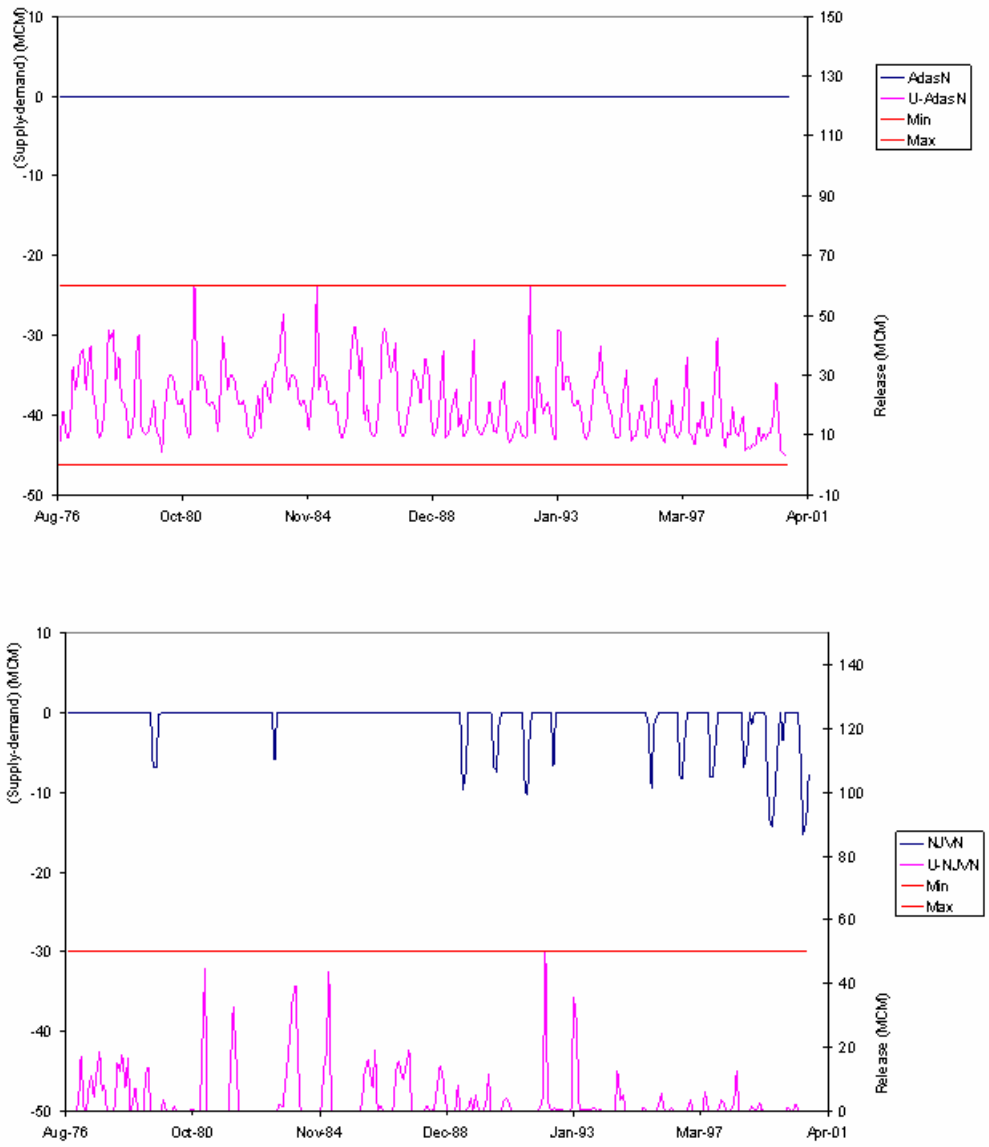

Figure J.3: Assessment model, scenario6, agricultural demand increase 10%, constrained GW drawdown, monthly water deficit and release sequences at Adasiya and North Jordan Valley nodes

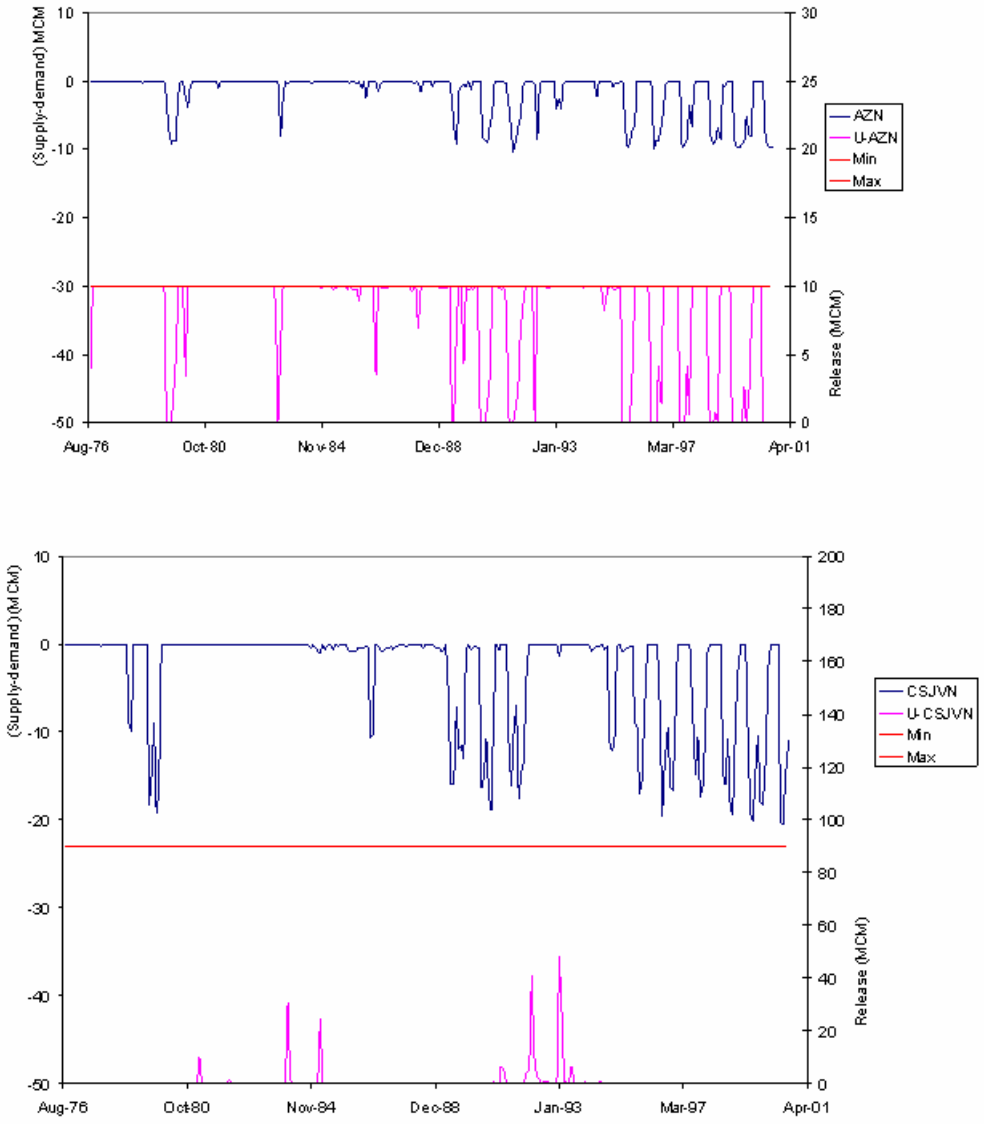

Figure J.4: Assessment model, scenario6, agricultural demand increase 10%, constrained GW drawdown, monthly water deficit and release sequences at Amman-Zarqa and C/S Jordan Valley nodes

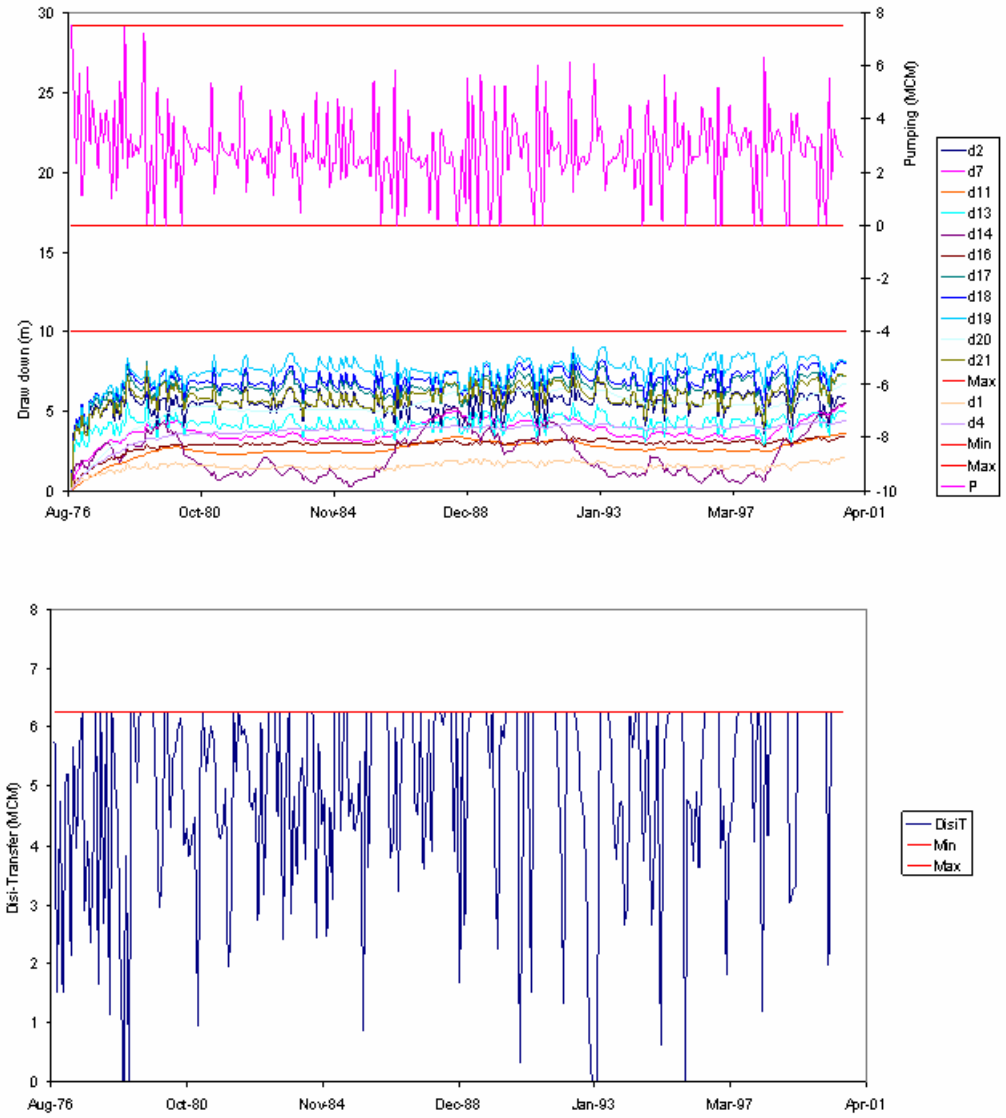

Figure J.5: Assessment model, scenario6, agricultural demand increase 10%, constrained GW drawdown, monthly pumping, drawdown and Disi transfer sequences

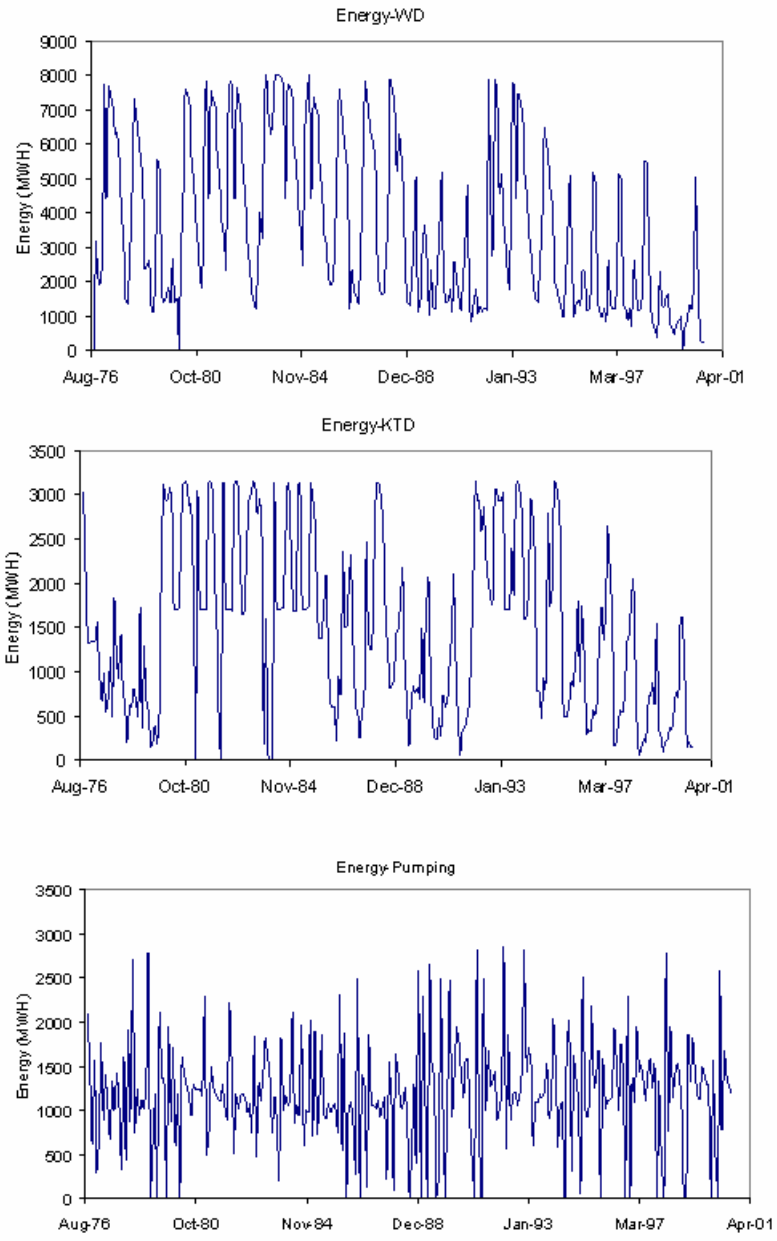

Figure J.6: Assessment model, scenario6, agricultural demand increase 10%, constrained GW drawdown, WD, KTD and pumping energy sequences

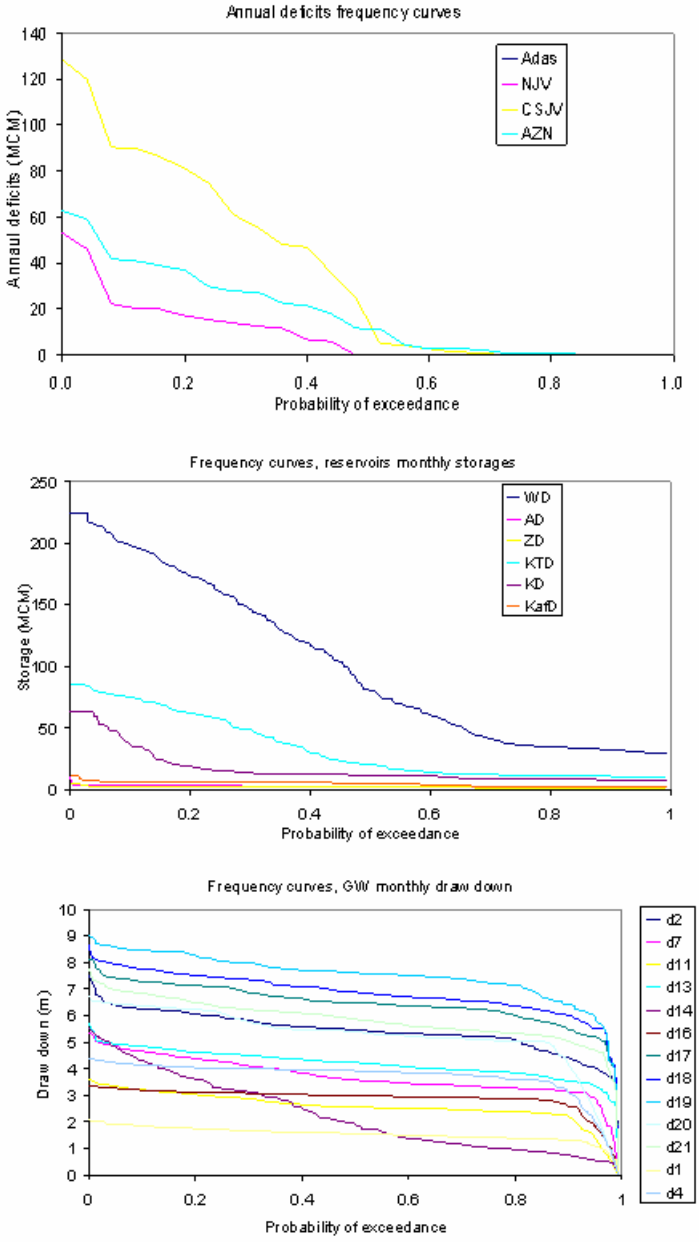

Figure J.7: Assessment model, scenario6, agricultural demand increase 10%, constrained GW drawdown, annual deficits, storages, and drawdowns frequency curves

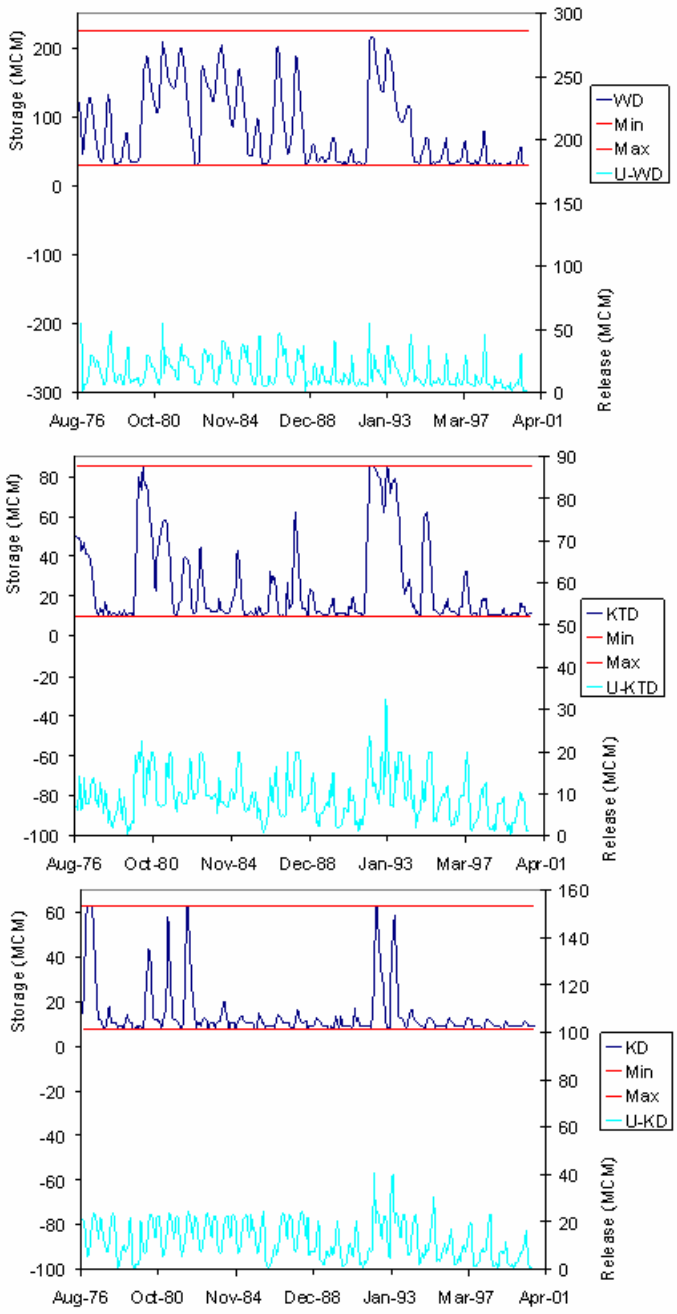

Figure J.8: Assessment model, scenario6, agricultural demand increase 20%, constrained GW drawdown, WD, KTD, and KD storage and release sequences

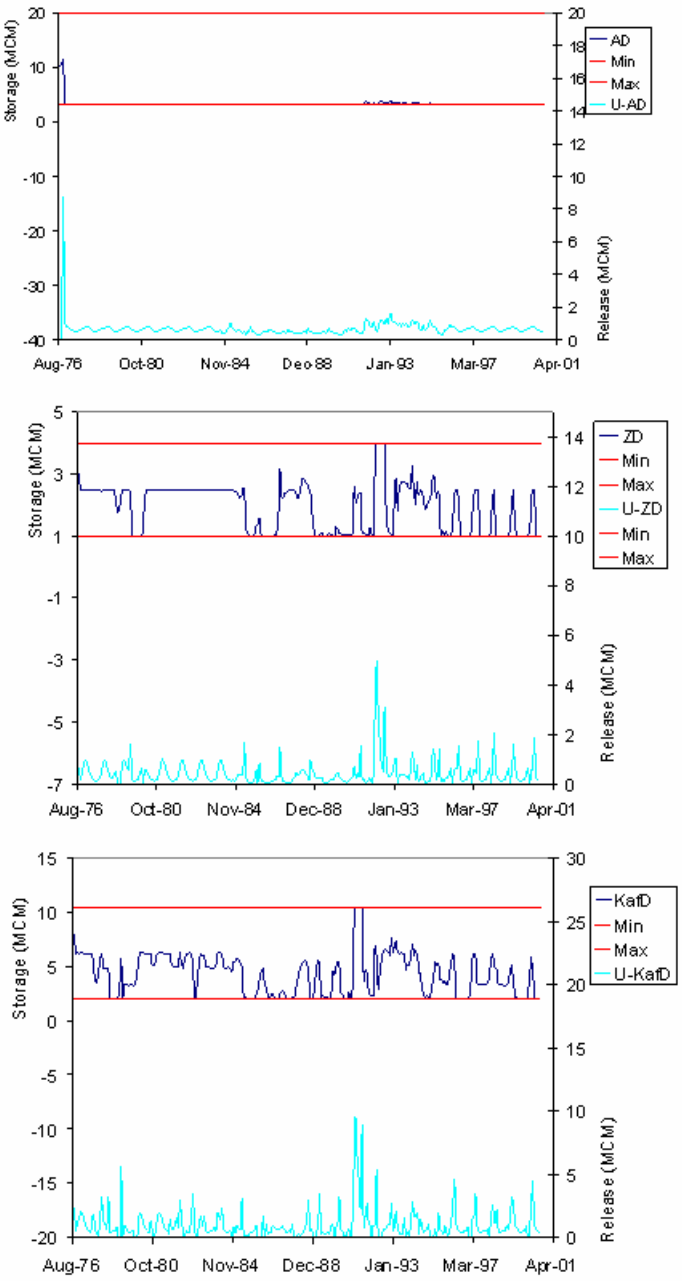

Figure J.9: Assessment model, scenario6, agricultural demand increase 20%, constrained GW drawdown, AD, ZD, and KafD storage and release sequences

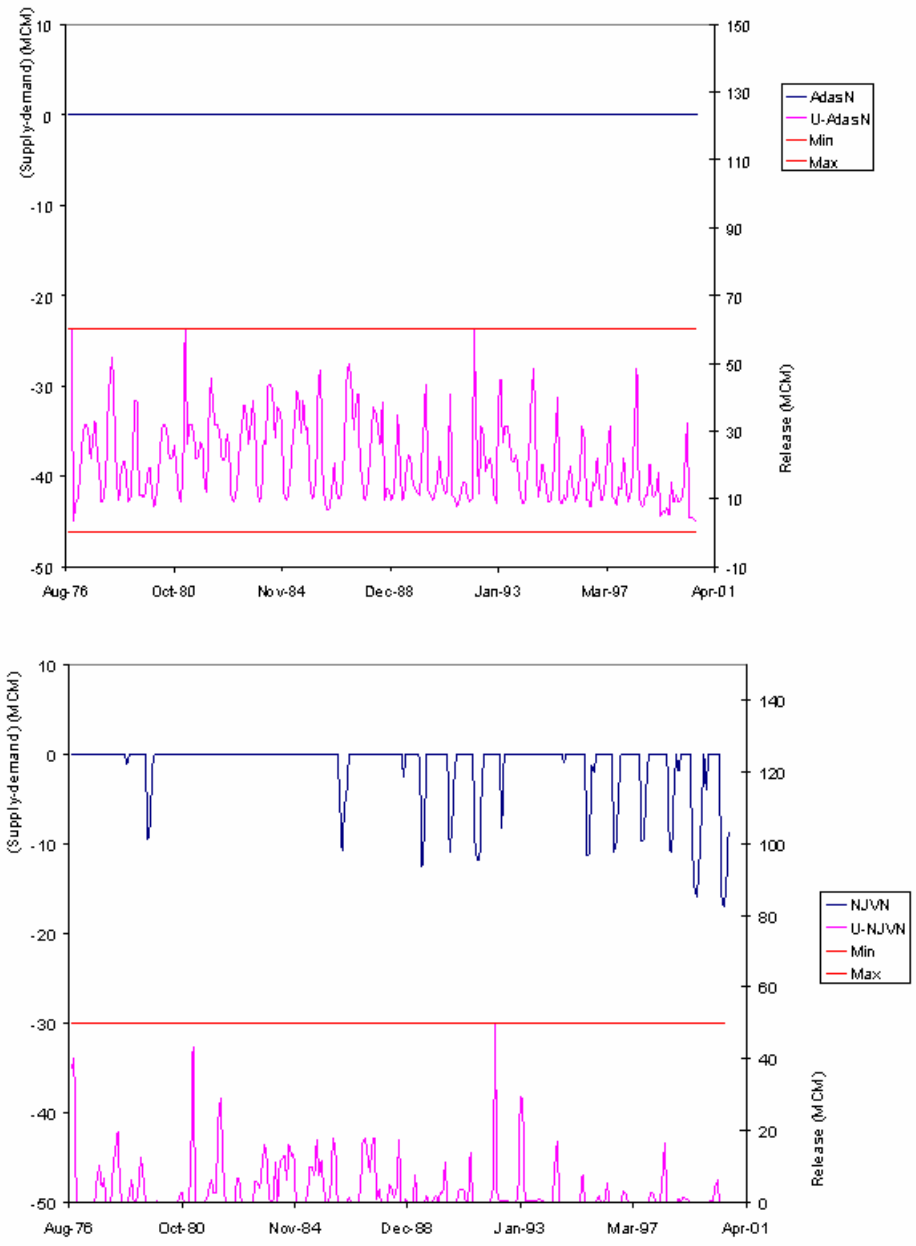

Figure J.10: Assessment model, scenario6, agricultural demand increase 20%, constrained GW drawdown, monthly water deficit and release sequences at Adasiya and North Jordan Valley nodes

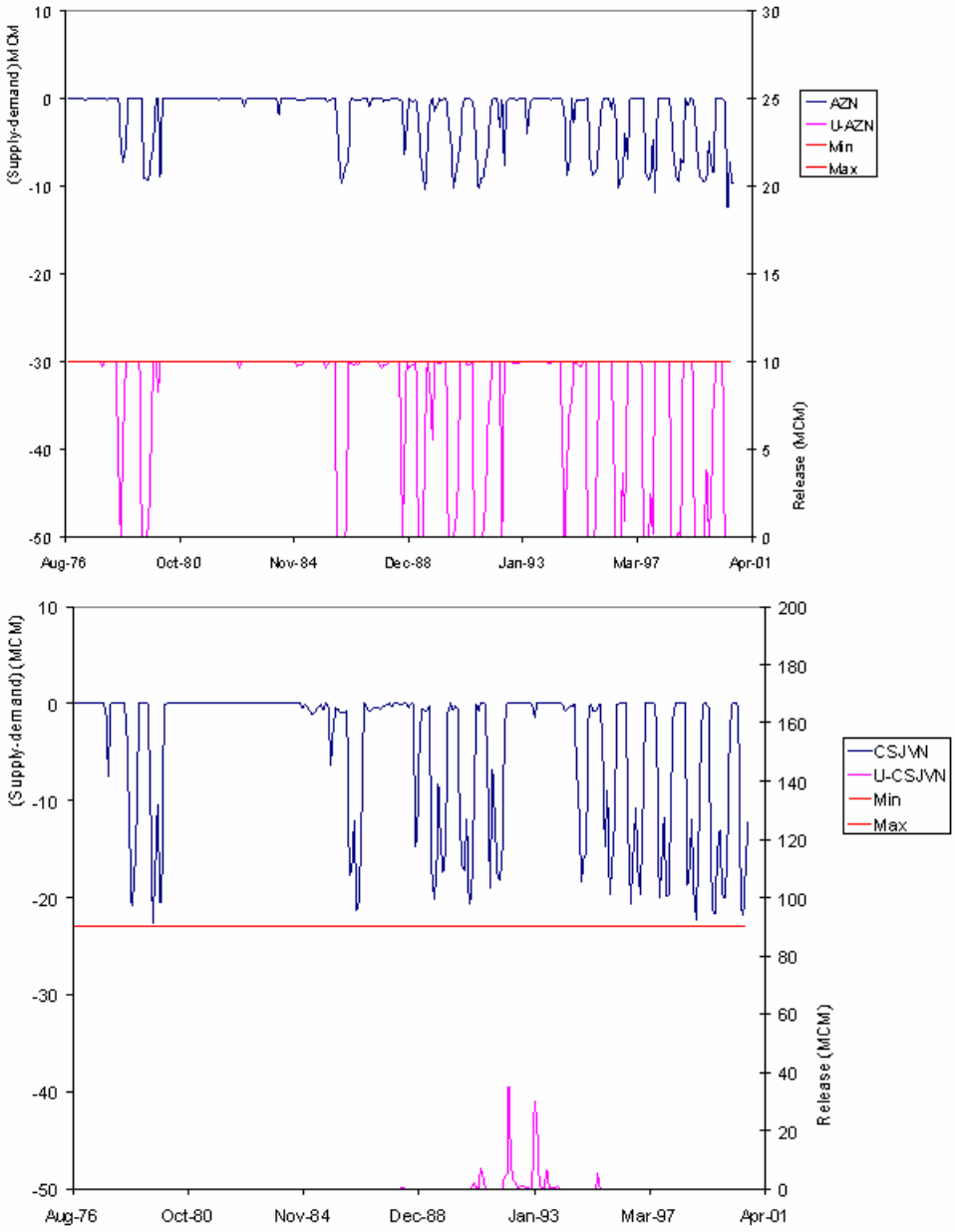

Figure J.11: Assessment model, scenario6, agricultural demand increase 20%, constrained GW drawdown, monthly water deficit and release sequences at Amman-Zarqa and C/S Jordan Valley nodes

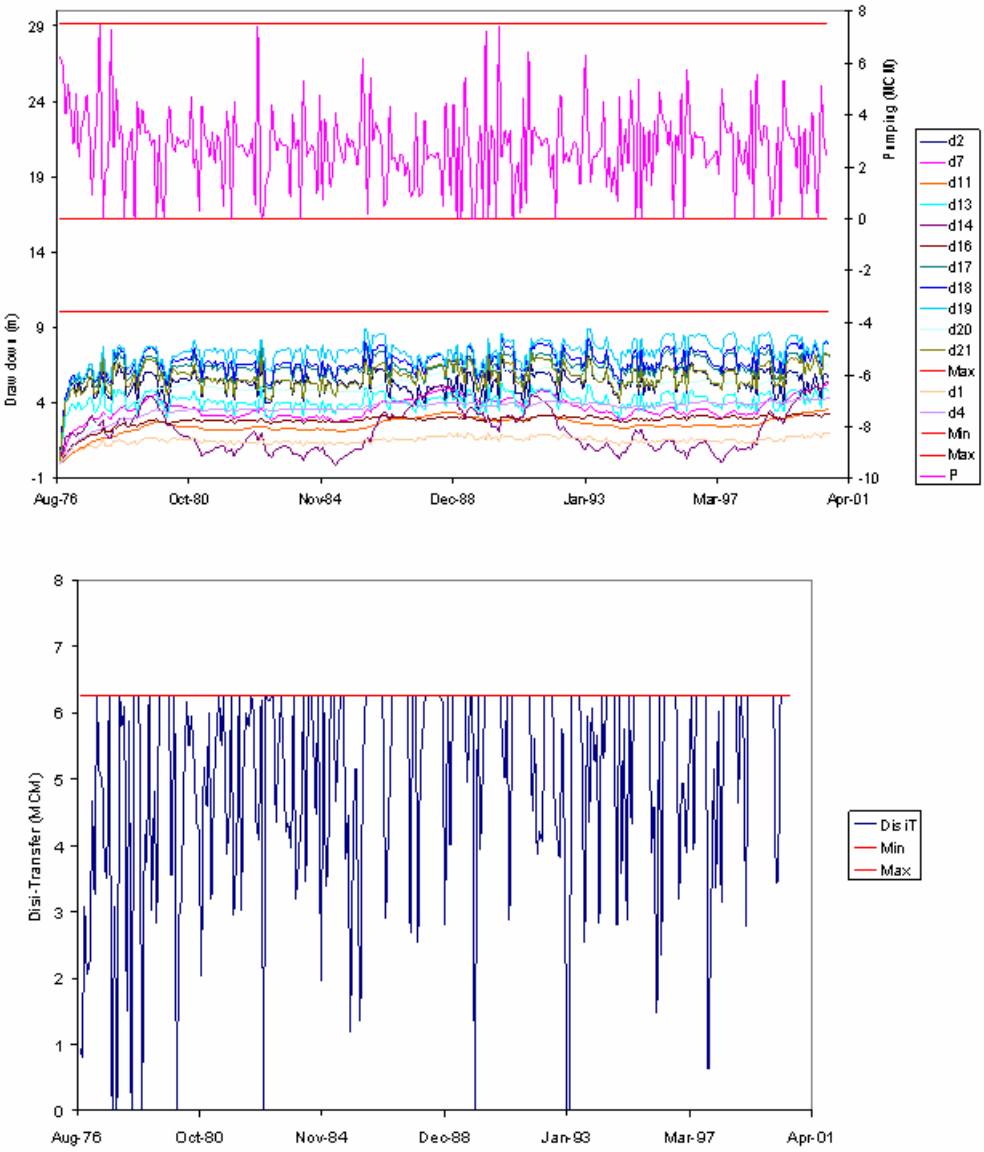

Figure J.12: Assessment model, scenario6, agricultural demand increase 20%, constrained GW drawdown, monthly pumping, drawdown and Disi transfer sequences

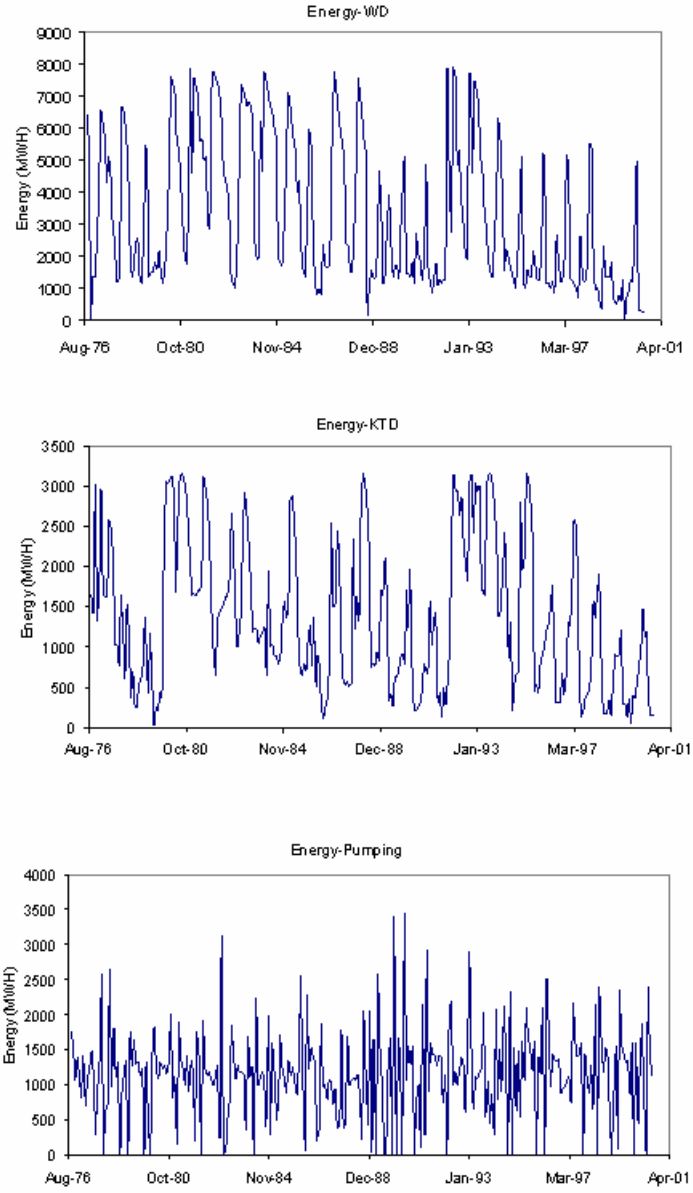

Figure J.13: Assessment model, scenario6, agricultural demand increase 20%, constrained GW drawdown, WD, KTD and pumping energy sequences

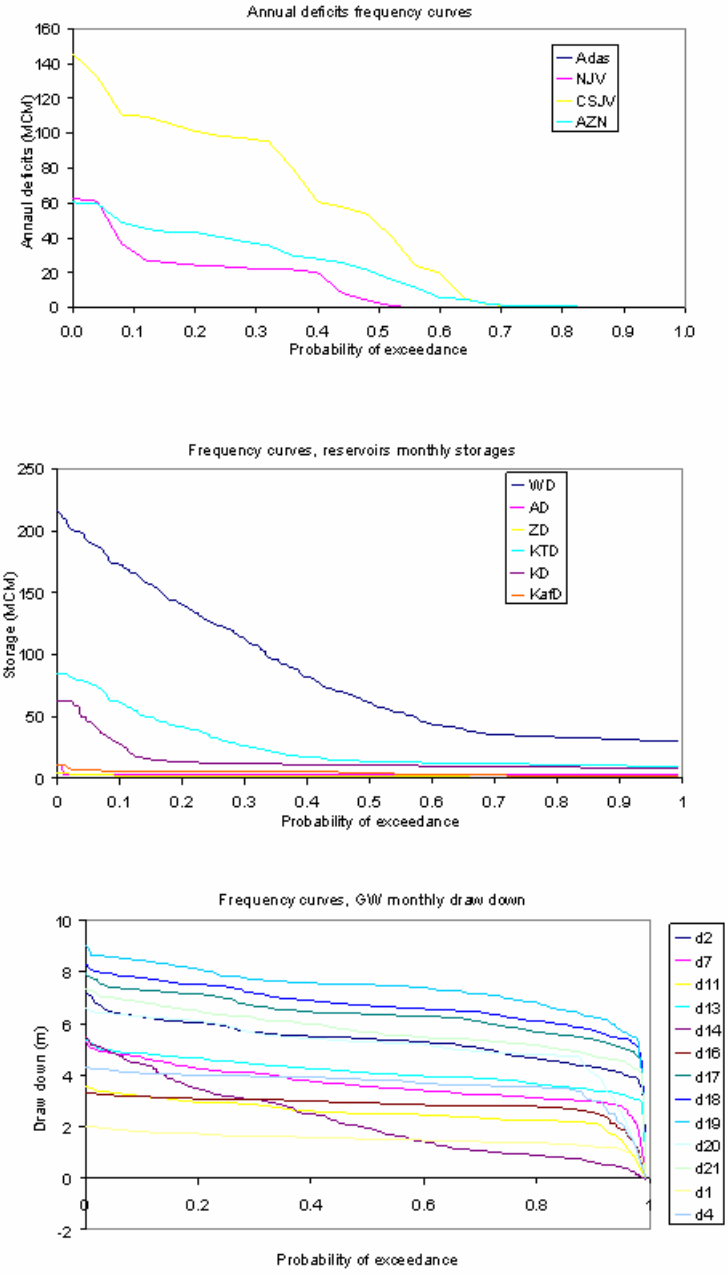

Figure J.14: Assessment model, scenario6, agricultural demand increase 20%, constrained GW drawdown, annual deficits, storages, and drawdowns frequency curves

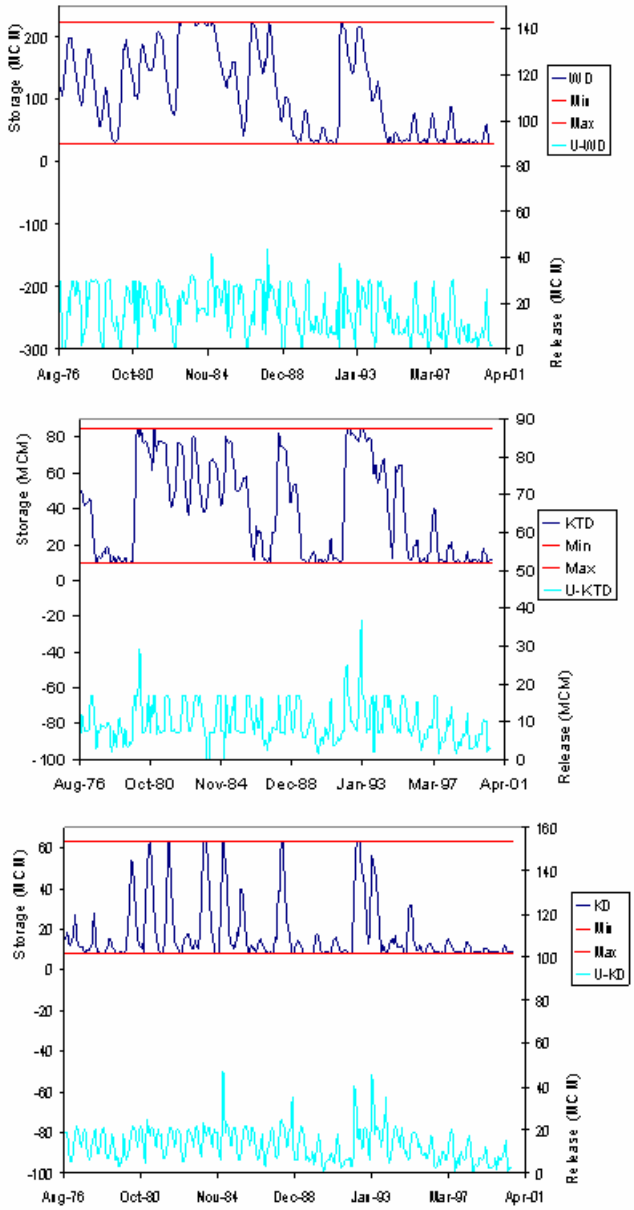

Figure J.15: Assessment model, scenario6, agricultural demand increase 10%, unconstrained GW drawdown, WD, KTD, and KD storage and release sequences

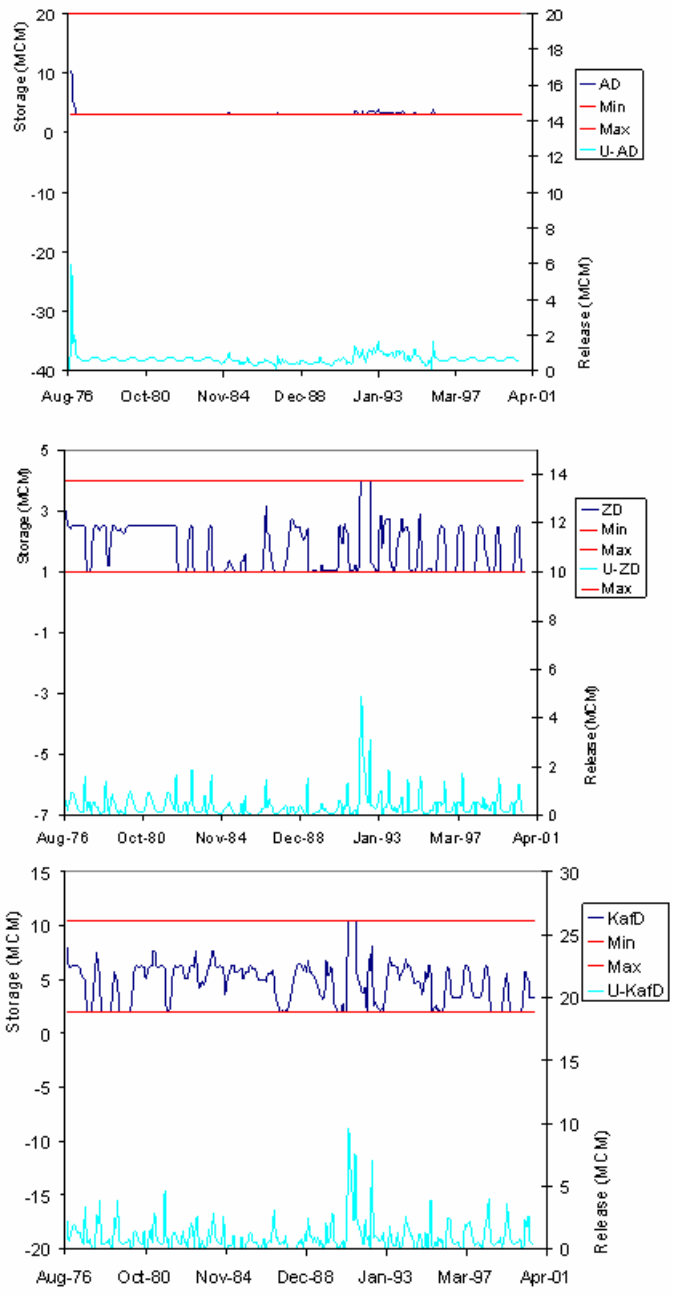

Figure J.16: Assessment model, scenario6, agricultural demand increase 10%, unconstrained GW drawdown, AD, ZD, and KafD storage and release sequences

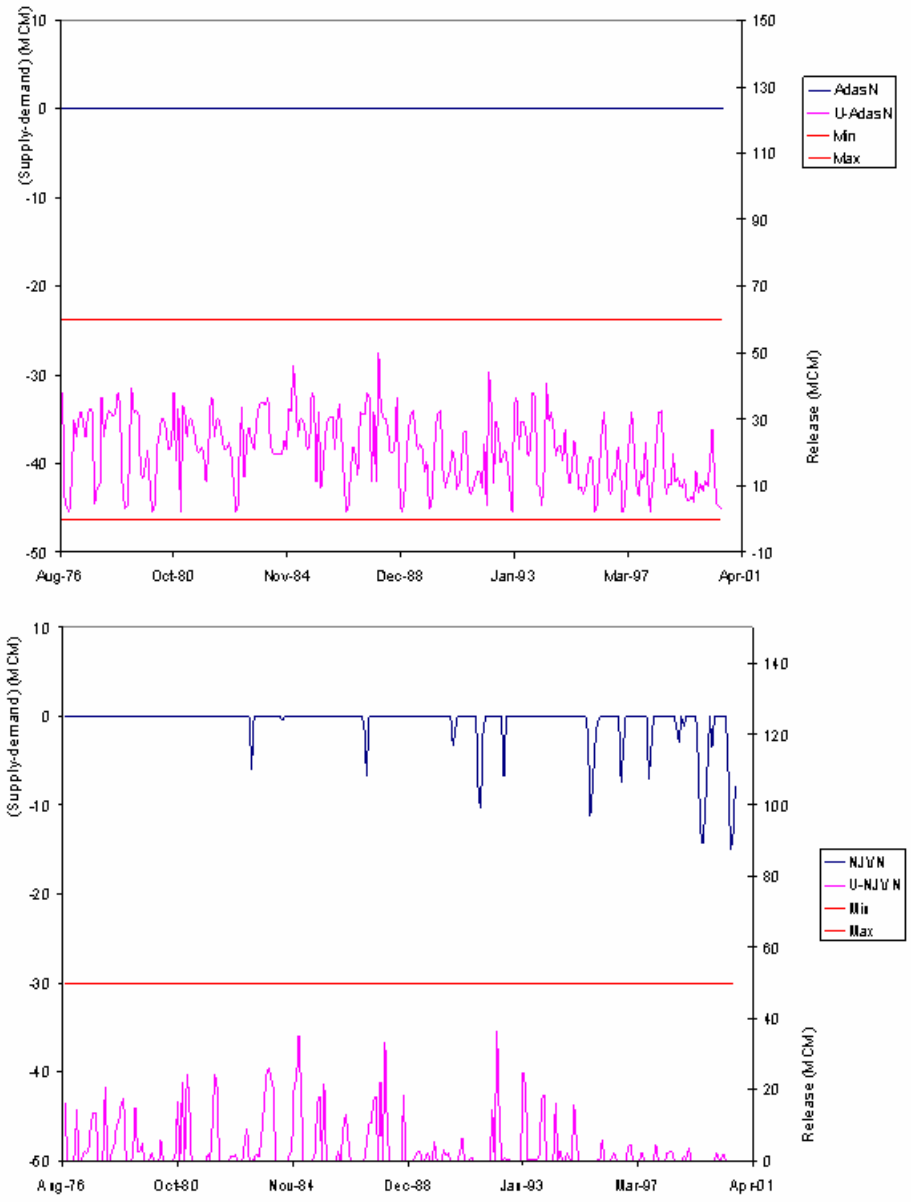

Figure J.17: Assessment model, scenario6, agricultural demand increase 10%, unconstrained GW drawdown, monthly water deficit and release sequences at Adasiya and North Jordan Valley nodes

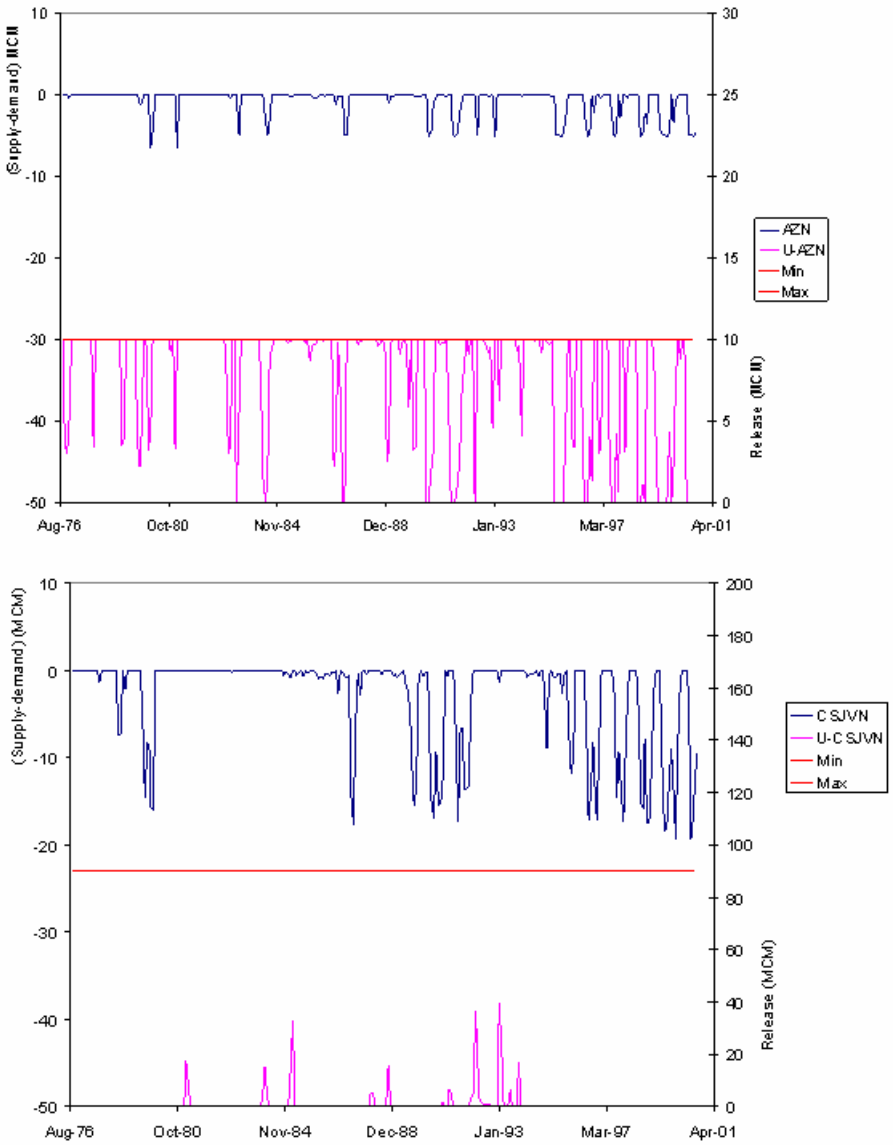

Figure J.18: Assessment model, scenario6, agricultural demand increase 10%, unconstrained GW drawdown, monthly water deficit and release sequences at Amman-Zarqa and C/S Jordan Valley nodes

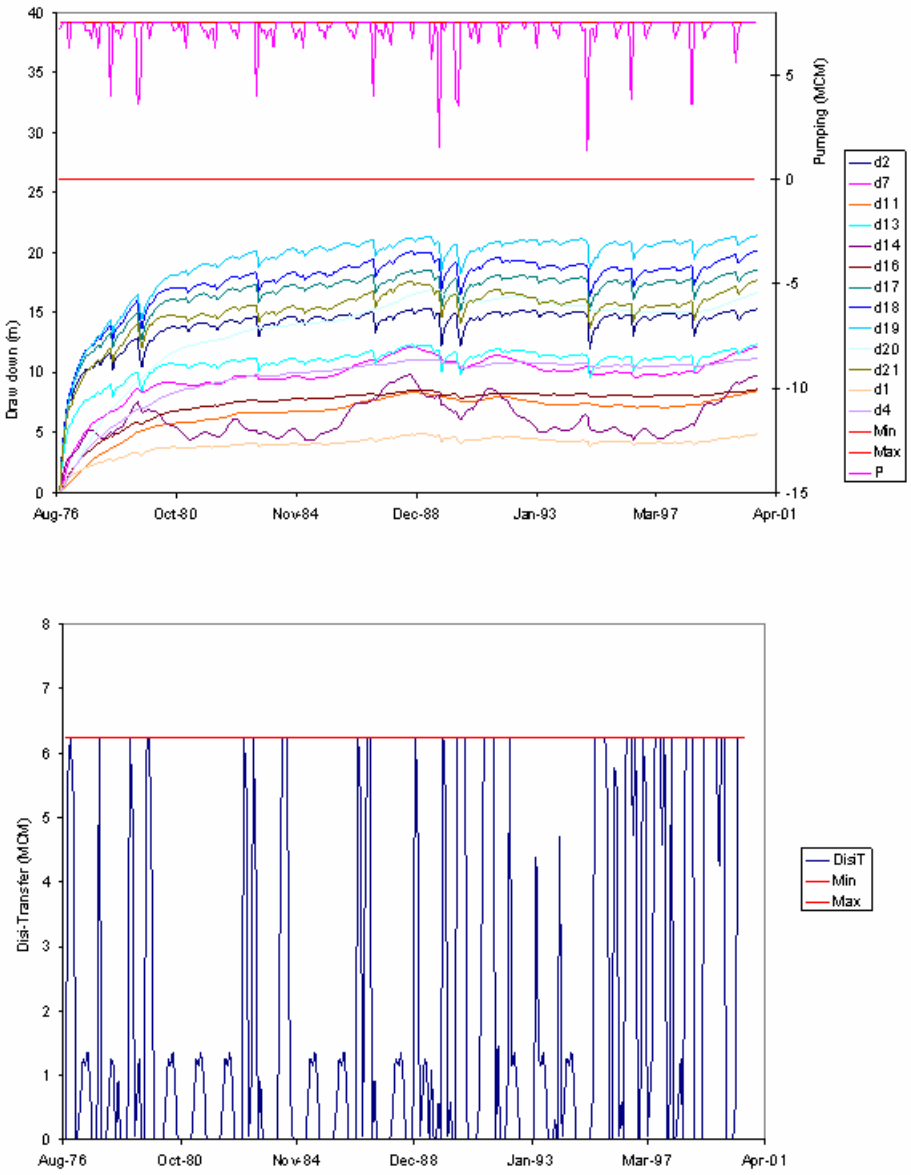

Figure J.19: Assessment model, scenario6, agricultural demand increase 10%, unconstrained GW drawdown, monthly pumping, drawdown and Disi transfer sequences

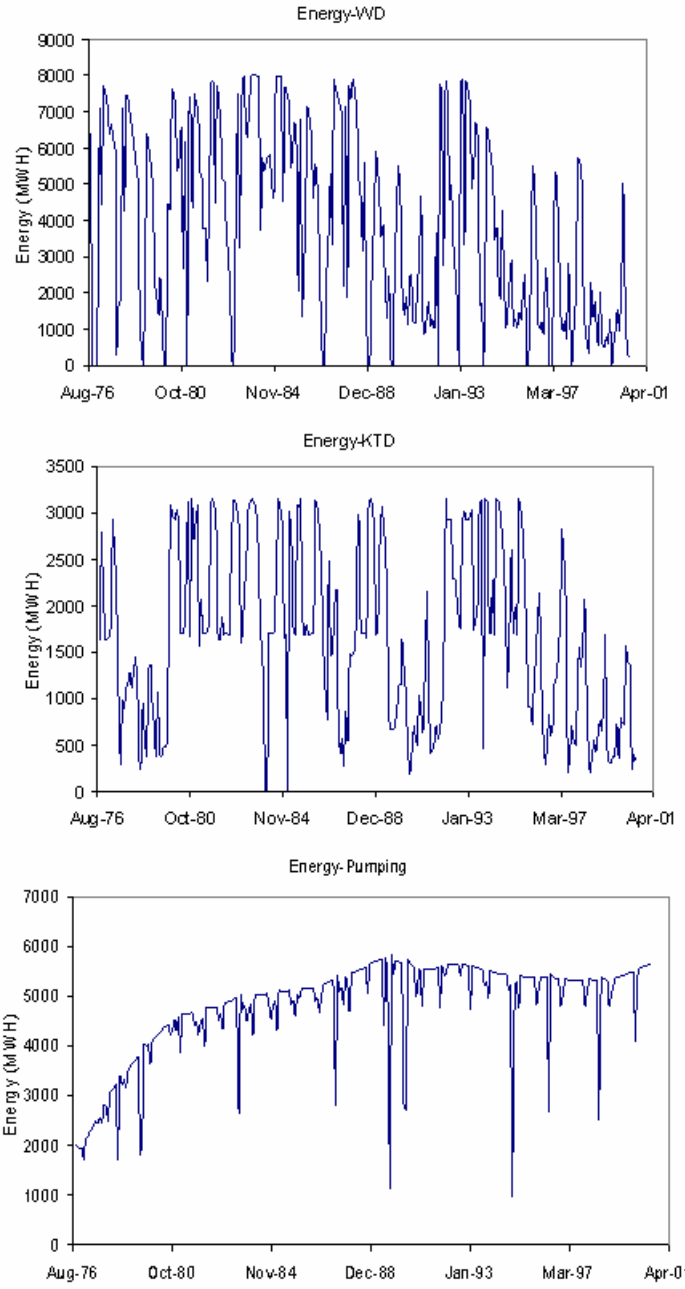

Figure J.20: Assessment model, scenario6, agricultural demand increase 10%, unconstrained GW drawdown, WD, KTD and pumping energy sequences

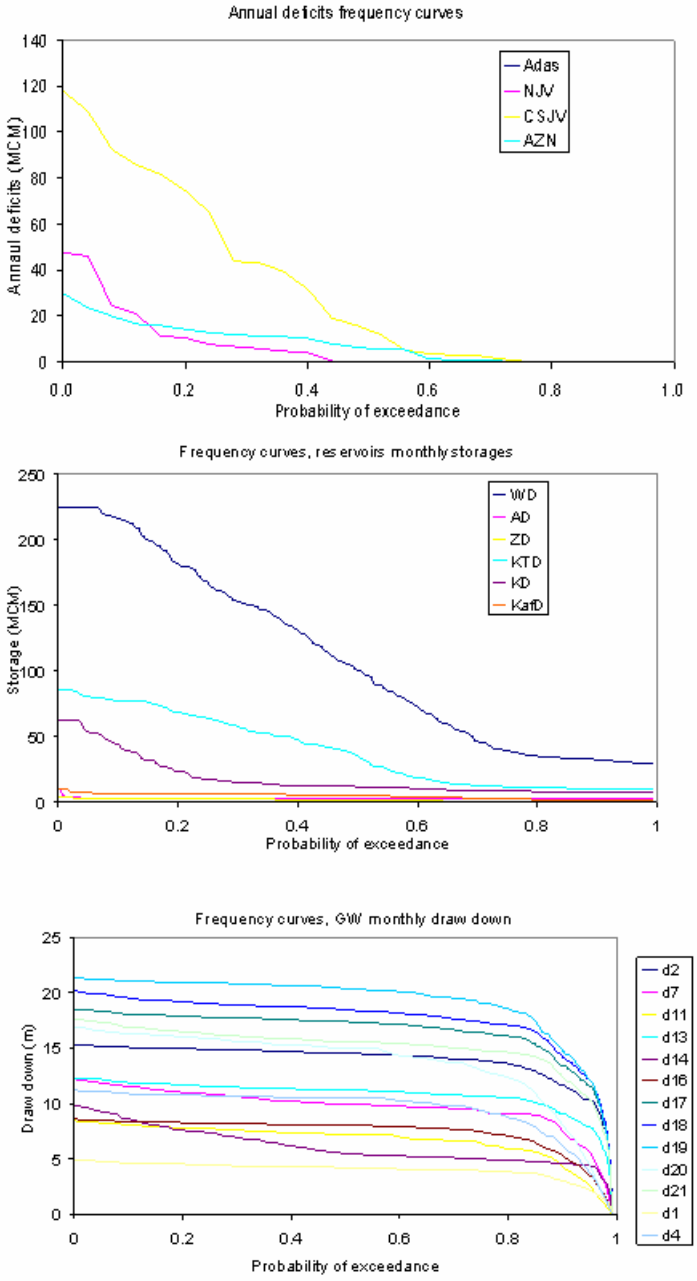

Figure J.21: Assessment model, scenario6, agricultural demand increase 10%, unconstrained GW drawdown, annual deficits, storages, and drawdowns frequency curves

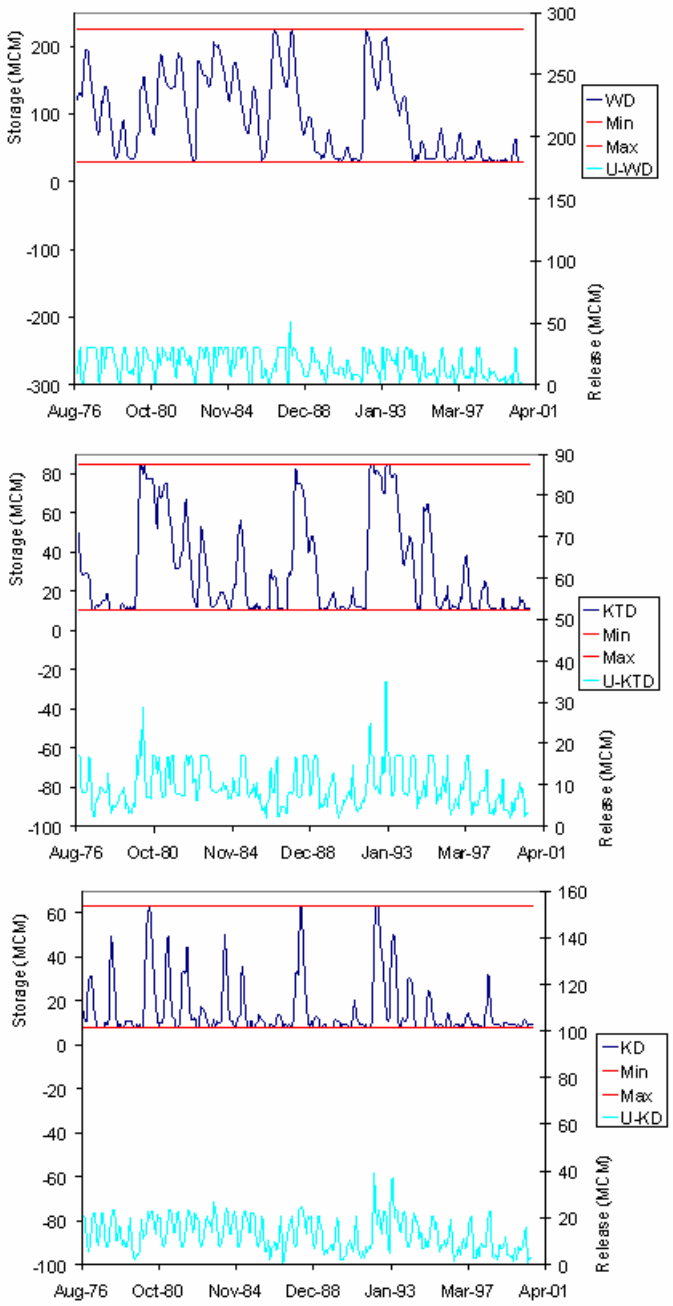

Figure J.22: Assessment model, scenario6, agricultural demand increase 20%, unconstrained GW drawdown, WD, KTD, and KD storage and release sequences

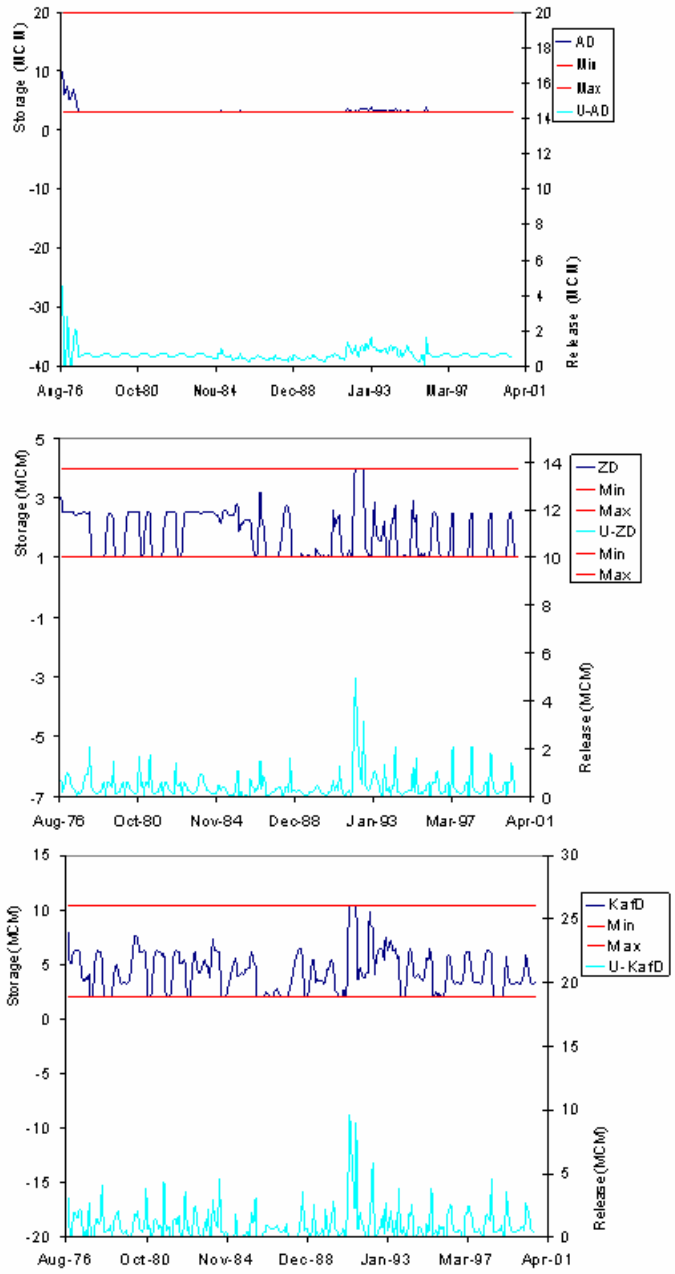

Figure J.23: Assessment model, scenario6, agricultural demand increase 20%, unconstrained GW drawdown, AD, ZD, and KafD storage and release sequences

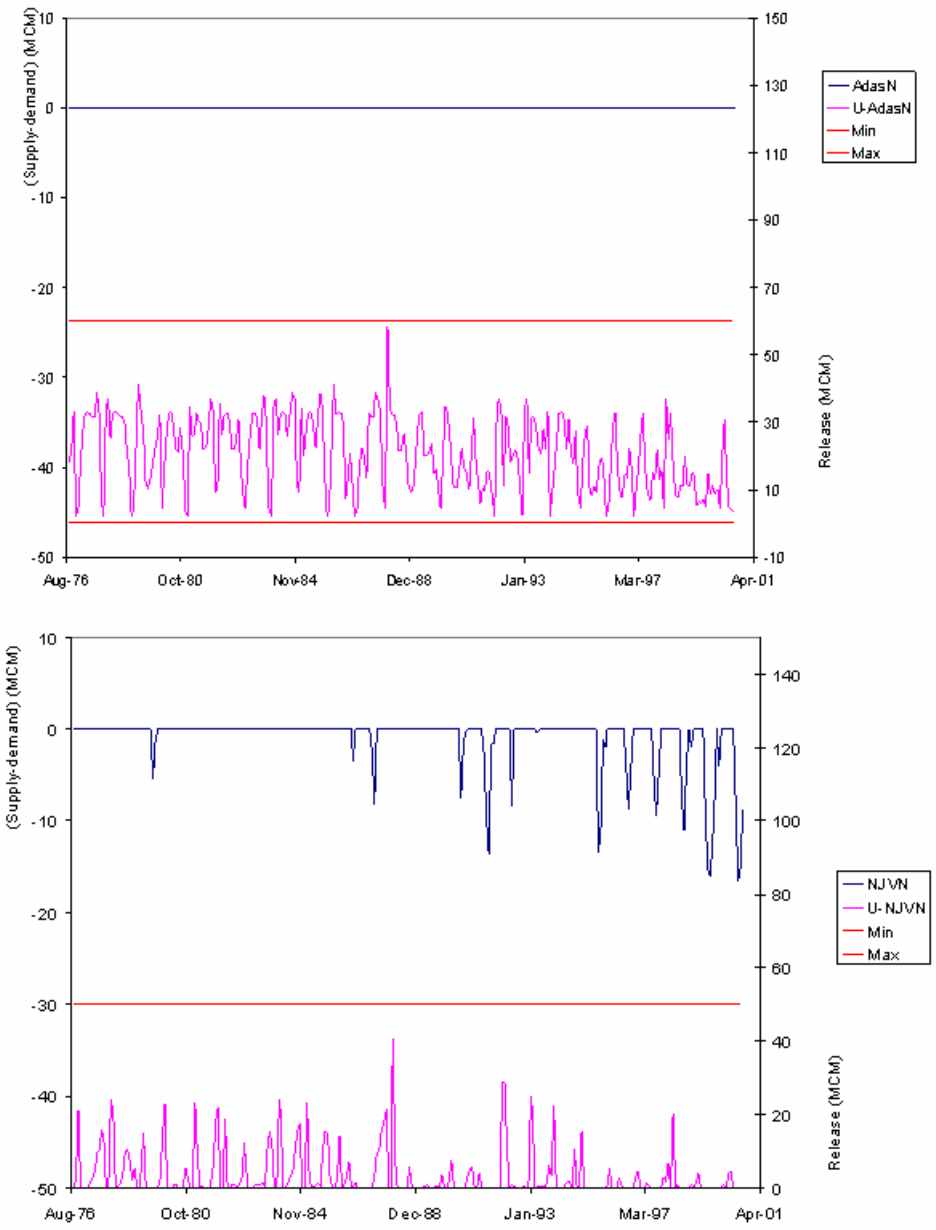

Figure J.24: Assessment model, scenario6, agricultural demand increase 20%, unconstrained GW drawdown, monthly water deficit and release sequences at Adasiya and North Jordan Valley nodes

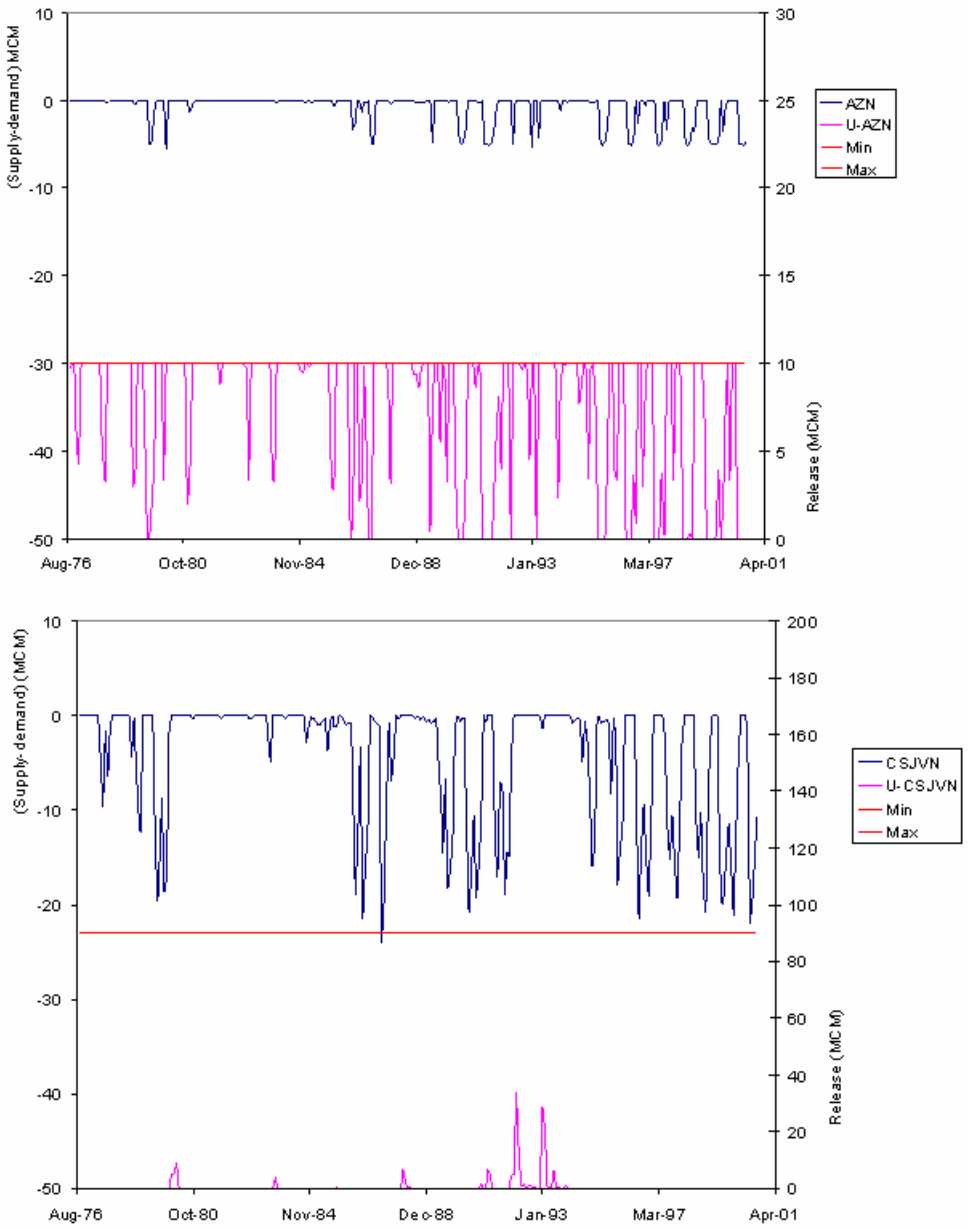

Figure J.25: Assessment model, scenario6, agricultural demand increase 20%, unconstrained GW drawdown, monthly water deficit and release sequences at Amman-Zarqa and C/S Jordan Valley nodes

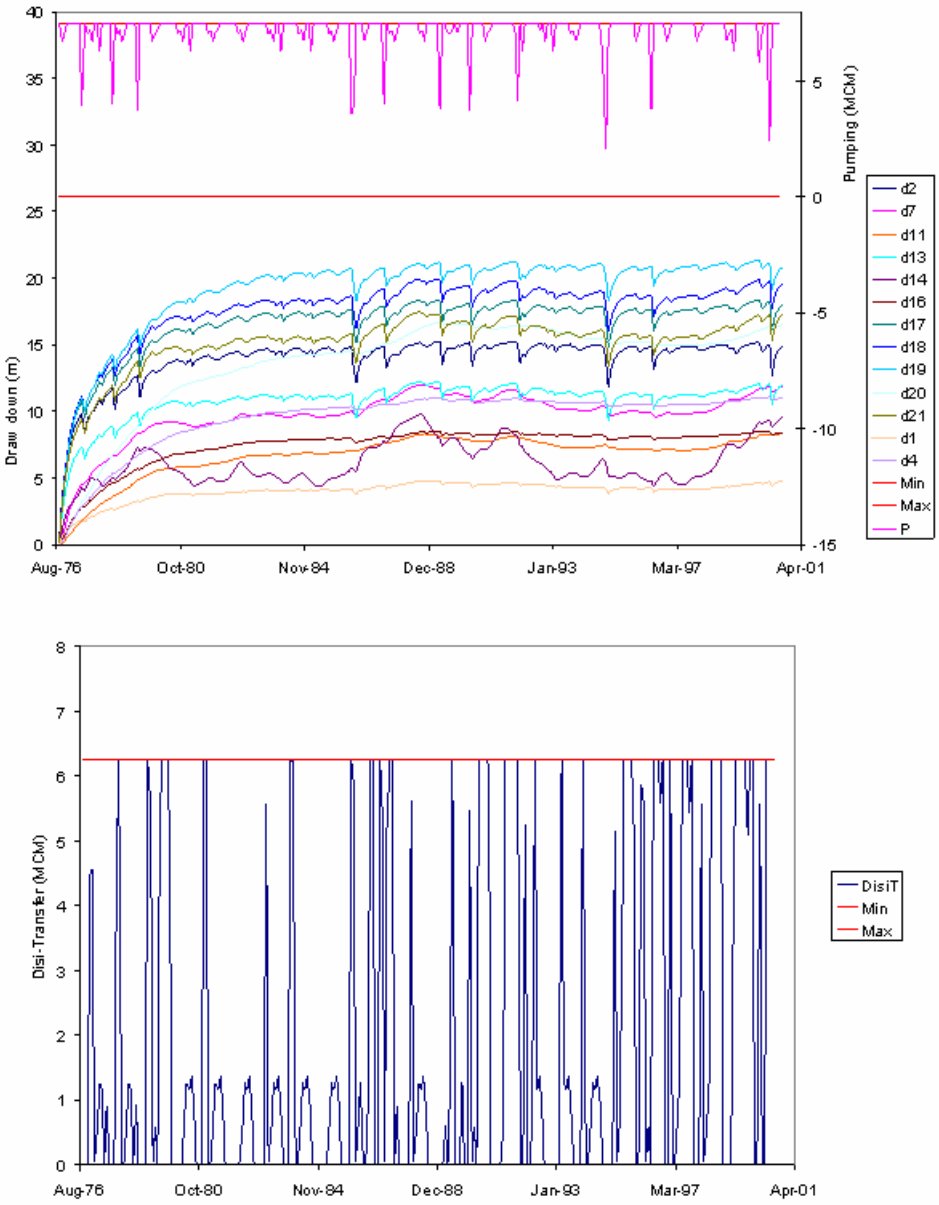

Figure J.26: Assessment model, scenario6, agricultural demand increase 20%, unconstrained GW drawdown, monthly pumping, drawdown and Disi transfer sequences

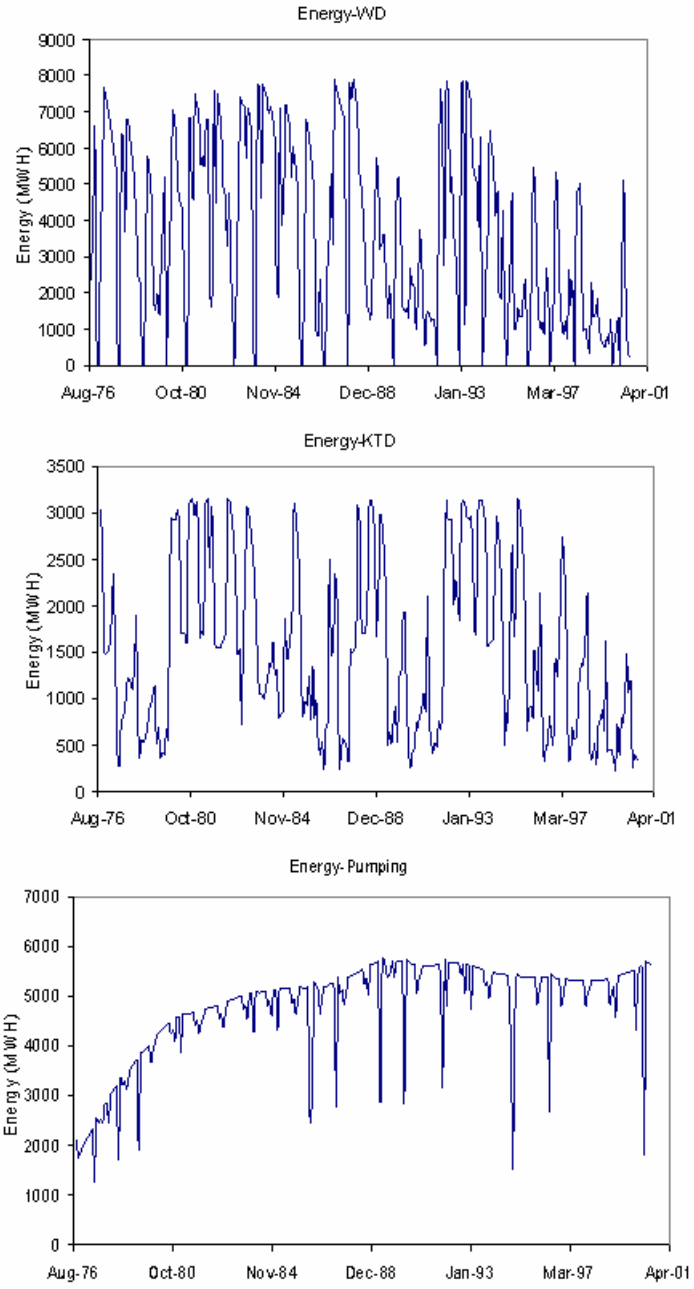

Figure J.27: Assessment model, scenario6, agricultural demand increase 20%, unconstrained GW drawdown, WD, KTD and pumping energy sequences

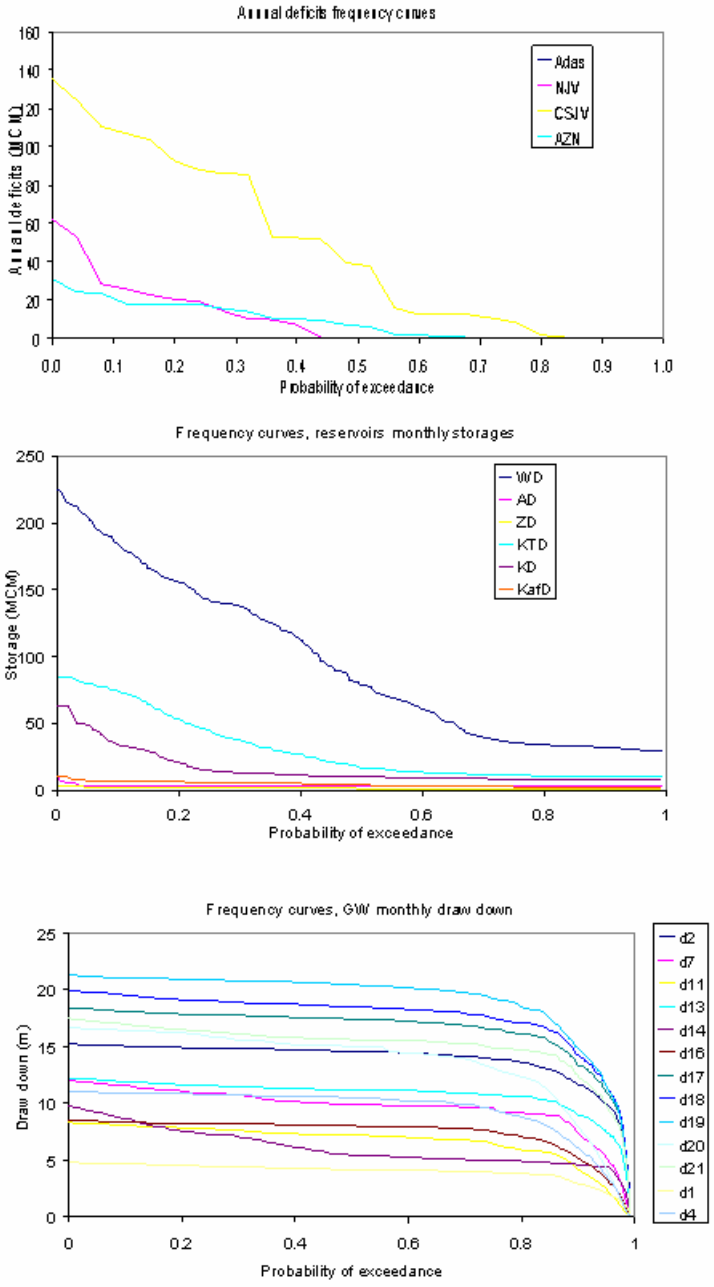

Figure J.28: Assessment model, scenario6, agricultural demand increase 20%, unconstrained GW drawdown, annual deficits, storages, and drawdowns frequency curves

APPENDIX K

PERFECT FORECAST SCENARIO

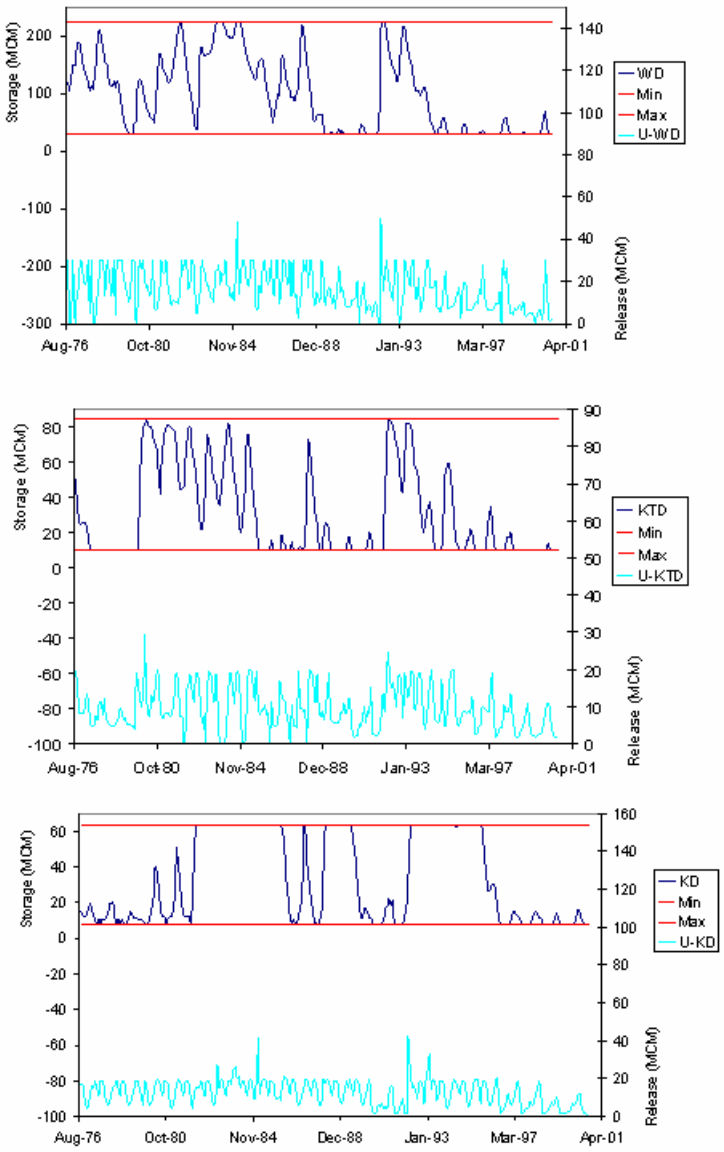

Figure K1: Assessment model, perfect forecast scenario, constrained GW drawdown, WD, KTD, and KD storage and release sequences

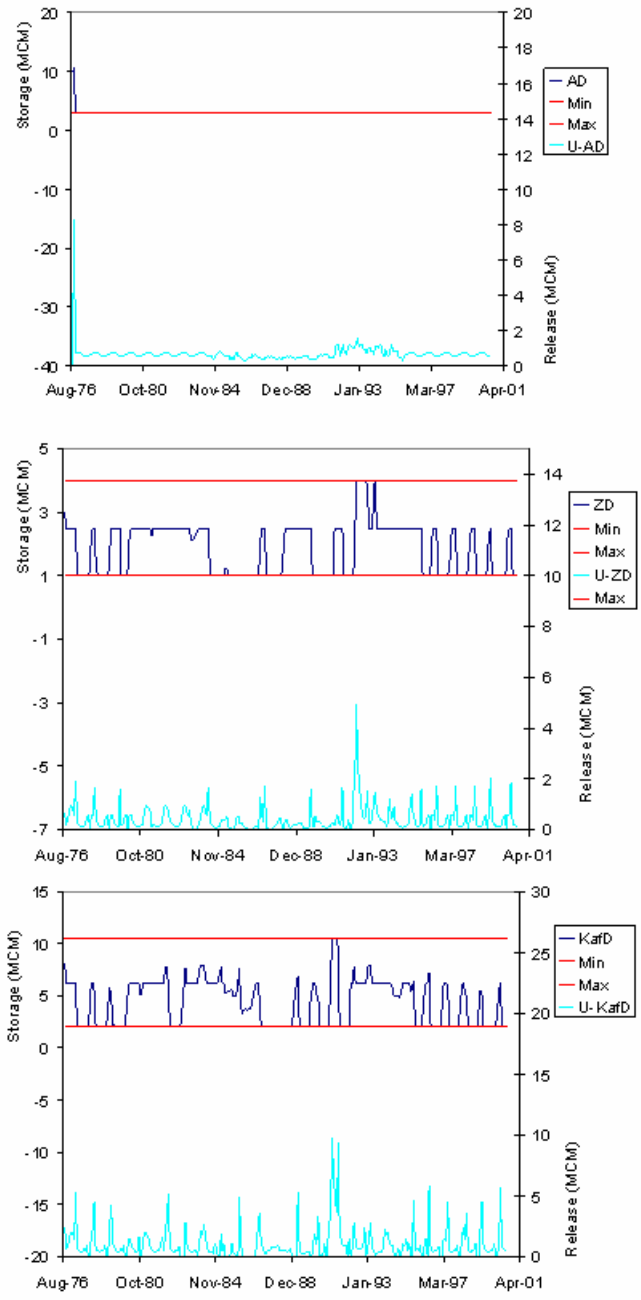

Figure K2: Assessment model, perfect forecast scenario, constrained GW drawdown, AD, ZD, and KafD storage and release sequences

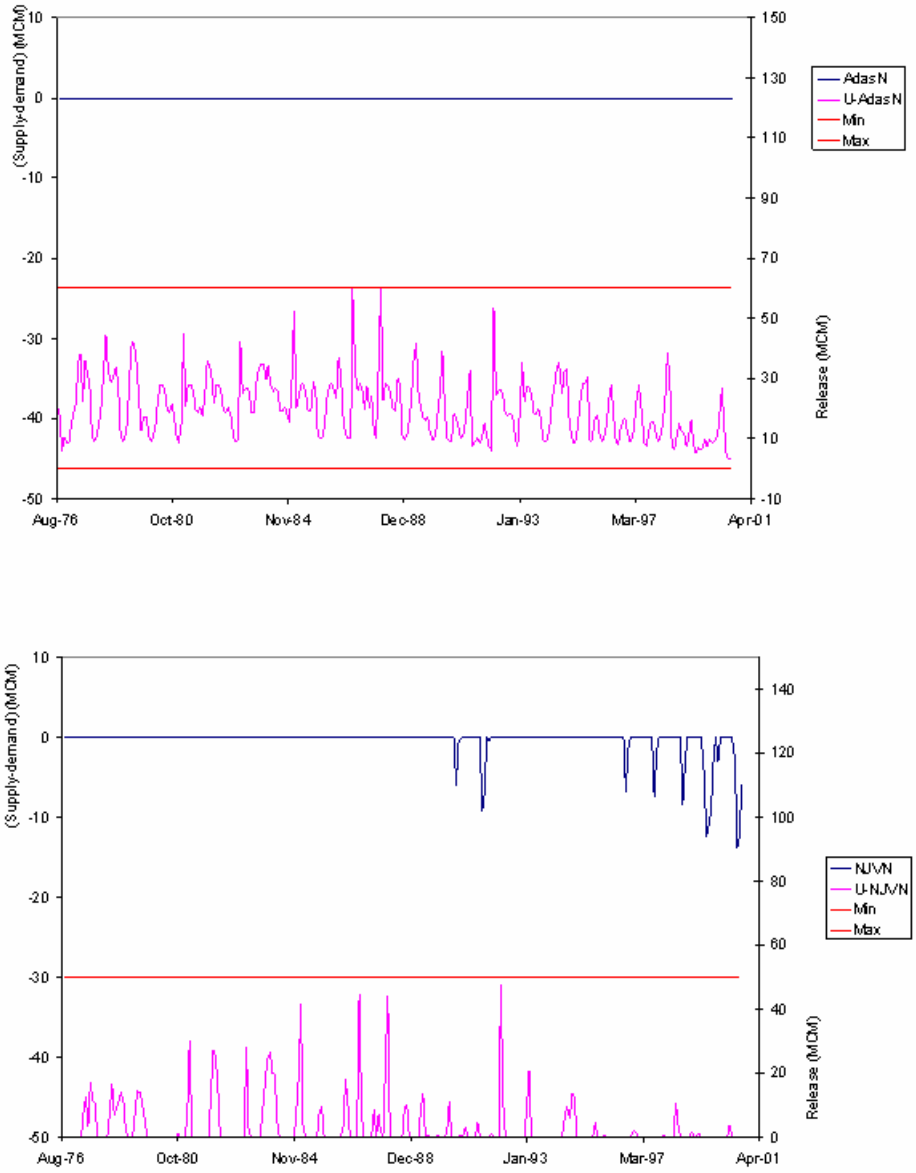

Figure K3: Assessment model, perfect forecast scenario, constrained GW drawdown, monthly water deficit and release sequences at Adasiya and North Jordan Valley nodes

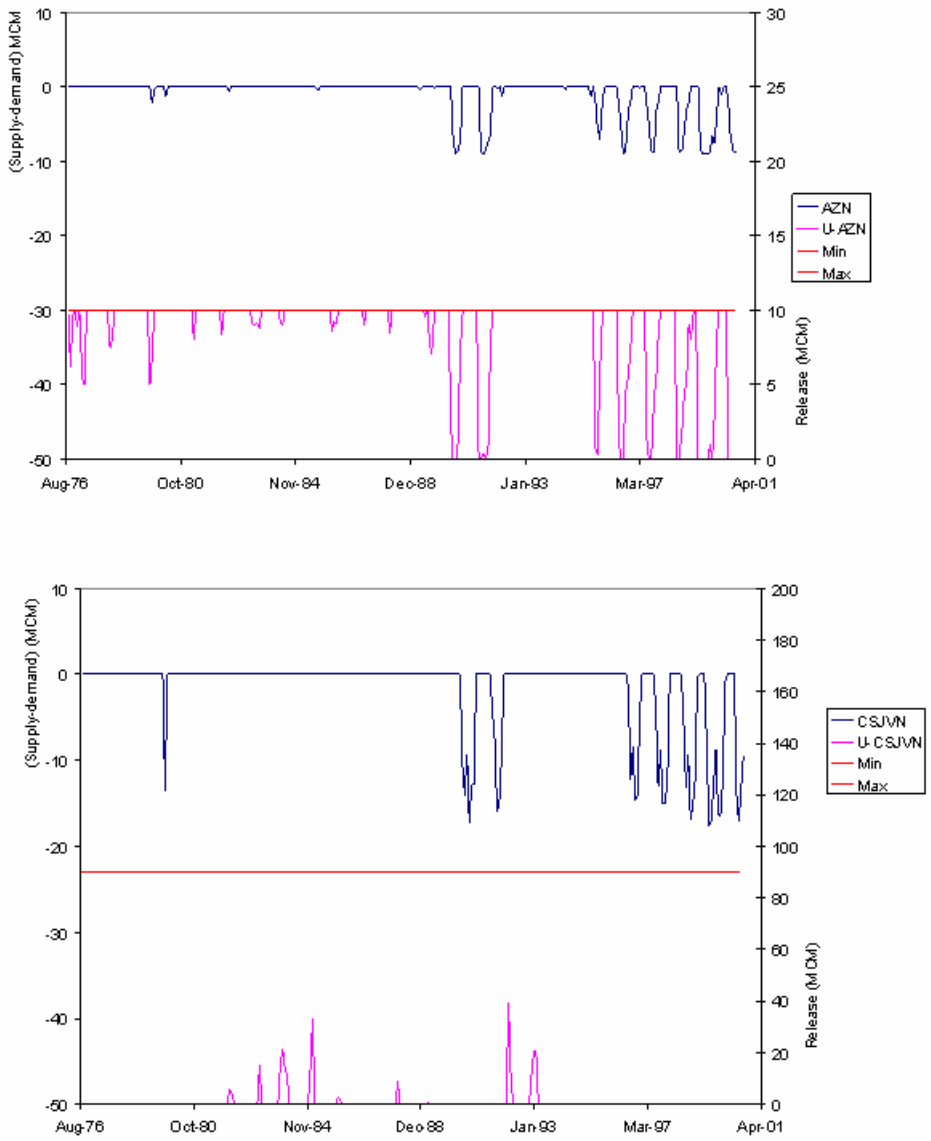

Figure K4: Assessment model, perfect forecast scenario, constrained GW drawdown, monthly water deficit and release sequences at Amman-Zarqa and C/S Jordan Valley nodes

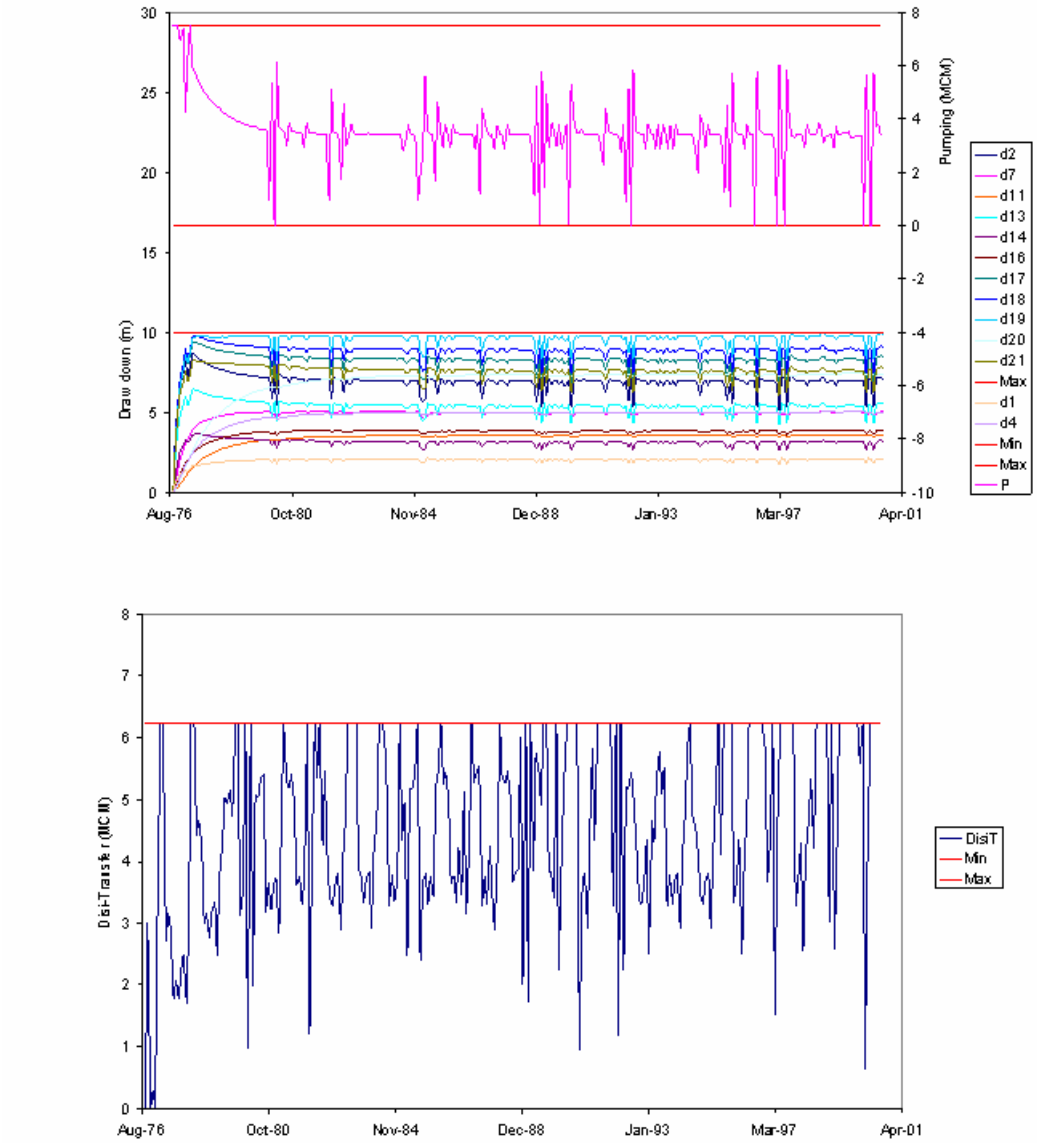

Figure K5: Assessment model, perfect forecast scenario, constrained GW drawdown, monthly pumping, drawdown and Disi transfer sequences

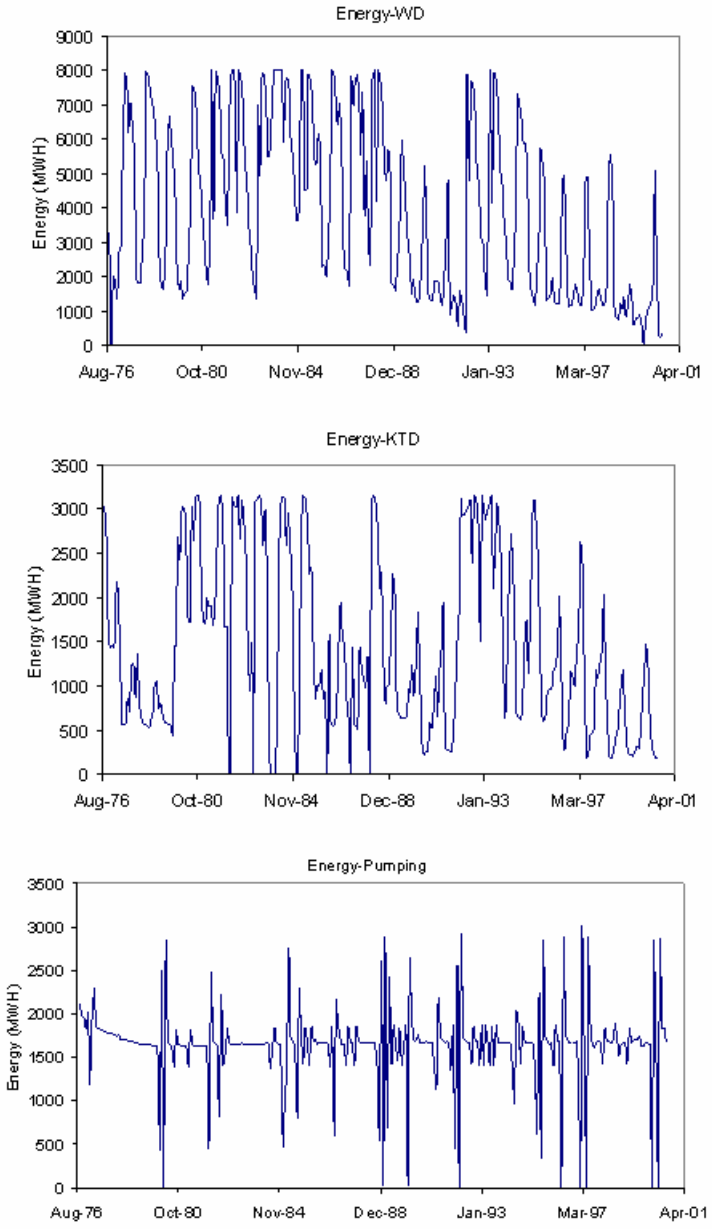

Figure K6: Assessment model, perfect forecast scenario, constrained GW drawdown, WD, KTD and pumping energy sequences

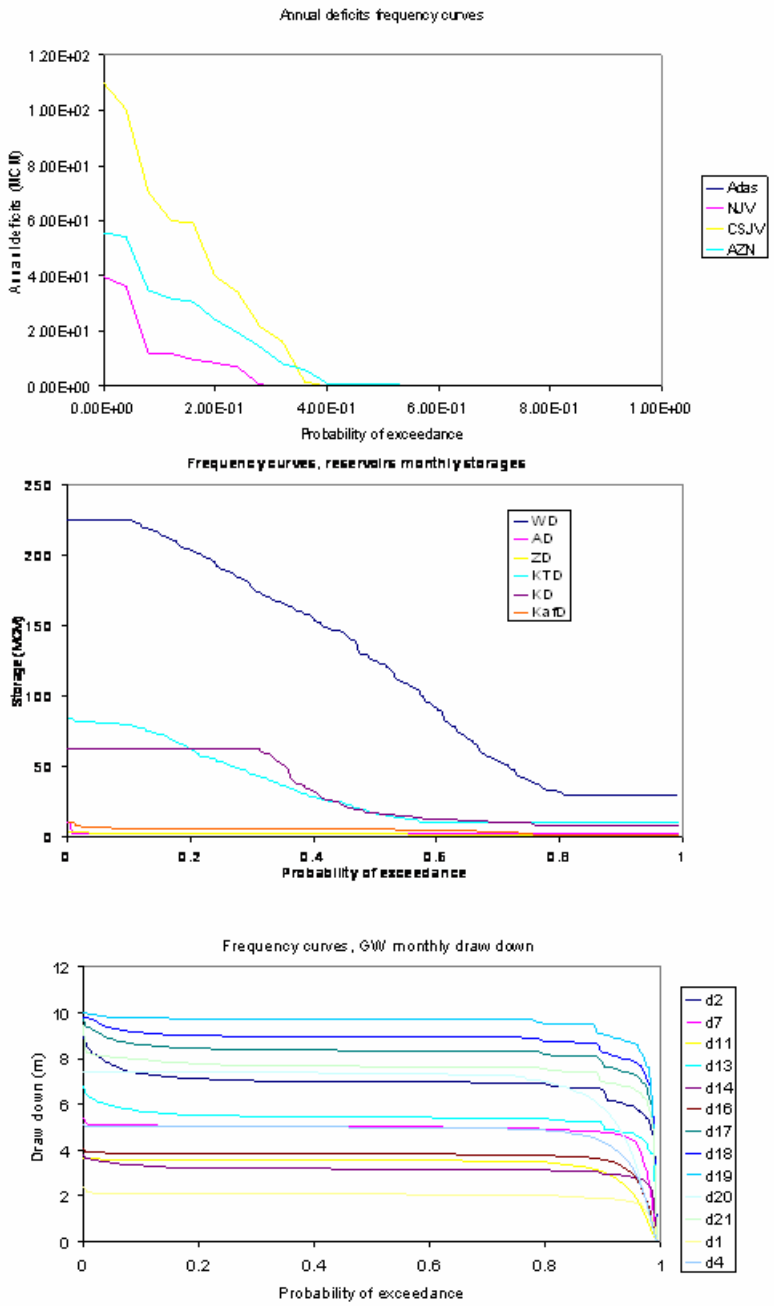

Figure K7: Assessment model, perfect forecast scenario, constrained GW drawdown, annual deficits, storages, and drawdowns frequency curves

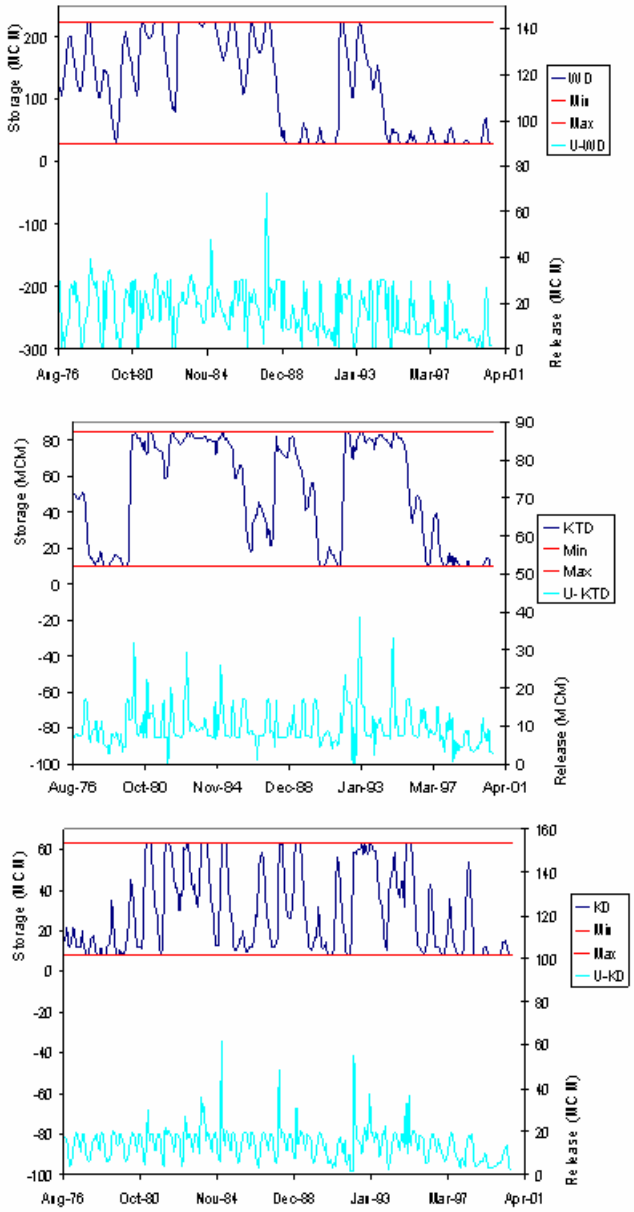

Figure K8: Assessment model, perfect forecast scenario, unconstrained GW drawdown, WD, KTD, and KD storage and release sequences

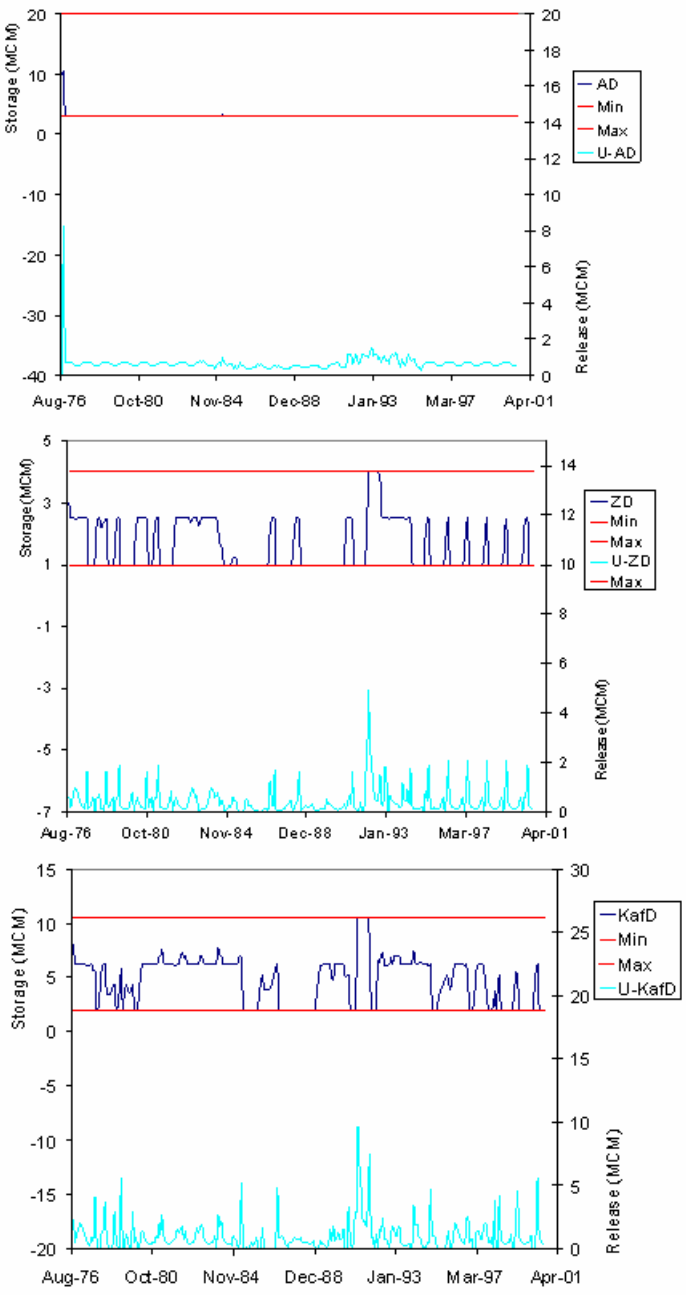

Figure K9: Assessment model, perfect forecast scenario, unconstrained GW drawdown, AD, ZD, and KafD storage and release sequences

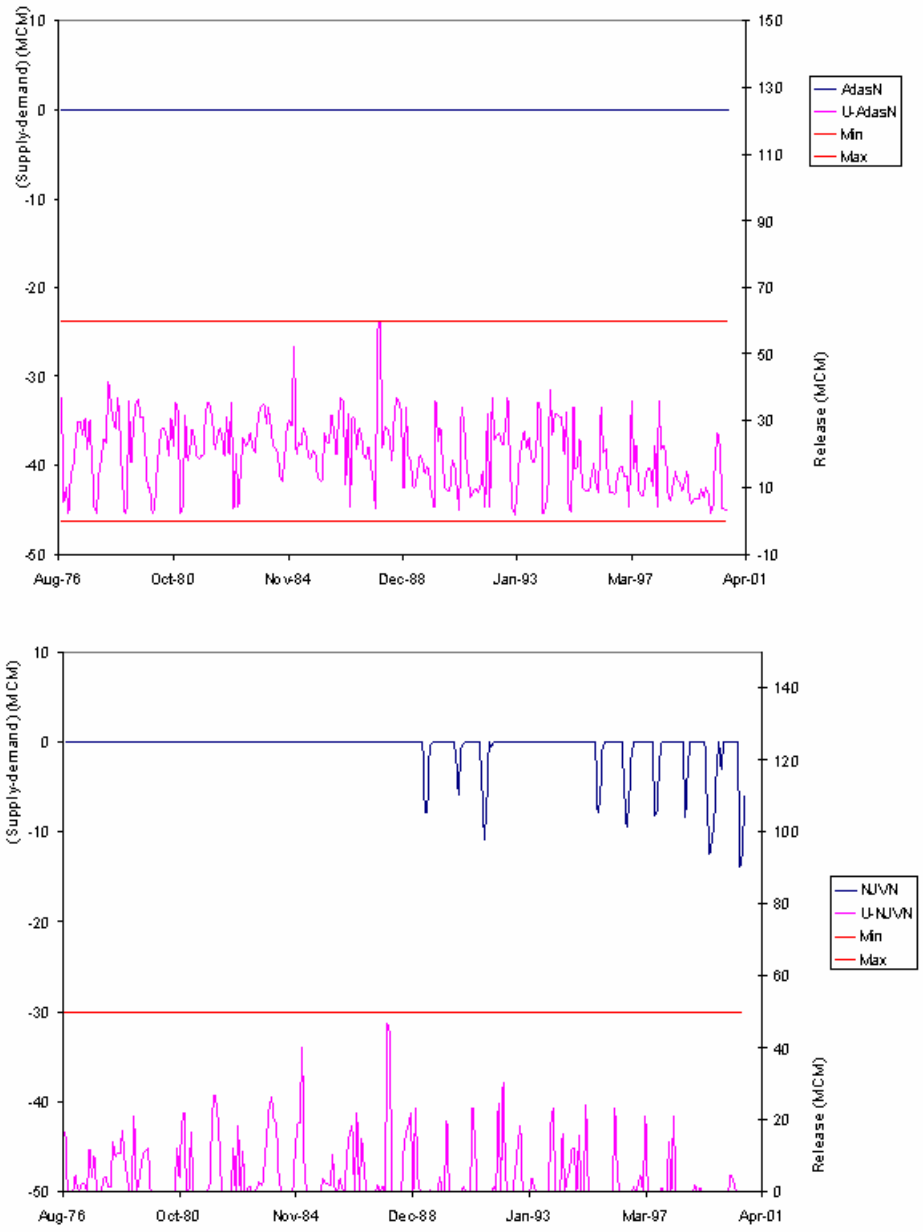

Figure K10: Assessment model, perfect forecast scenario, unconstrained GW drawdown, monthly water deficit and release sequences at Adasiya and North Jordan Valley nodes

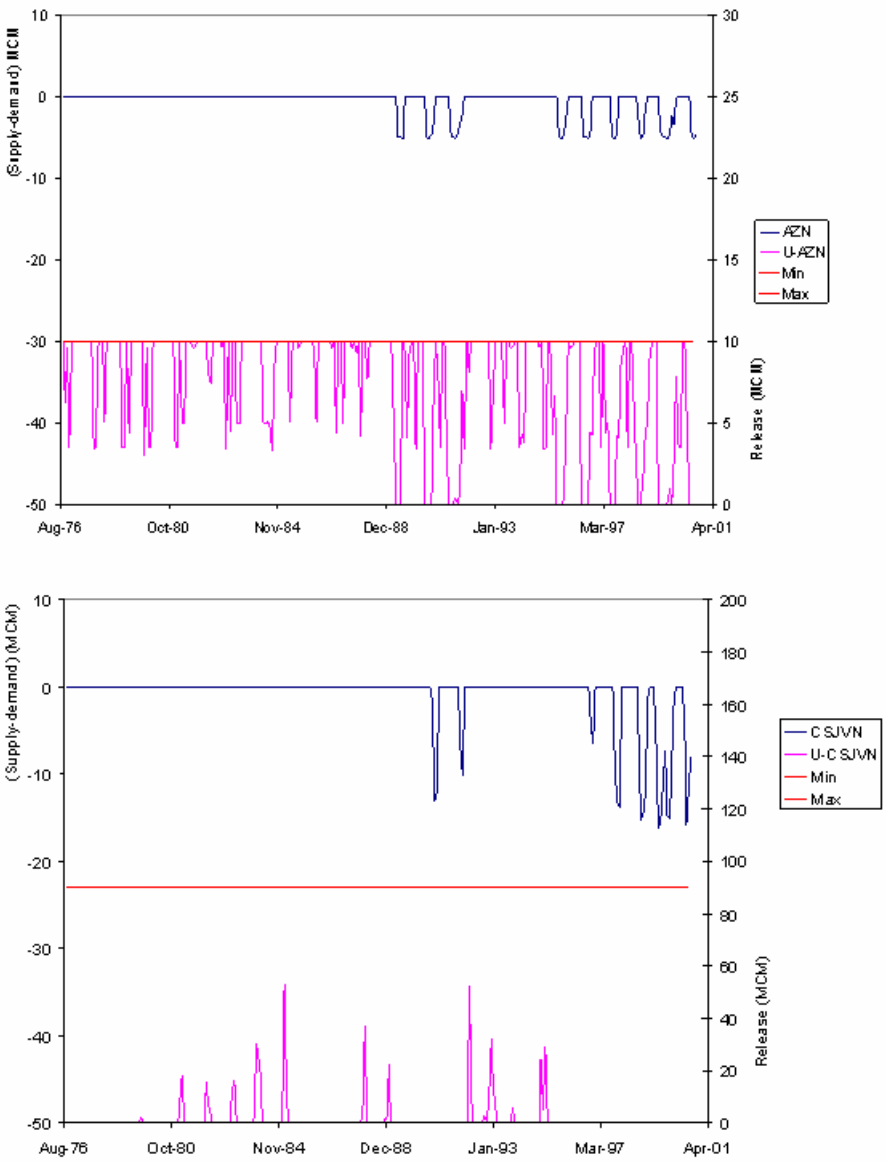

Figure K11: Assessment model, perfect forecast scenario, unconstrained GW drawdown, monthly water deficit and release sequences at Amman-Zarqa and C/S Jordan Valley nodes

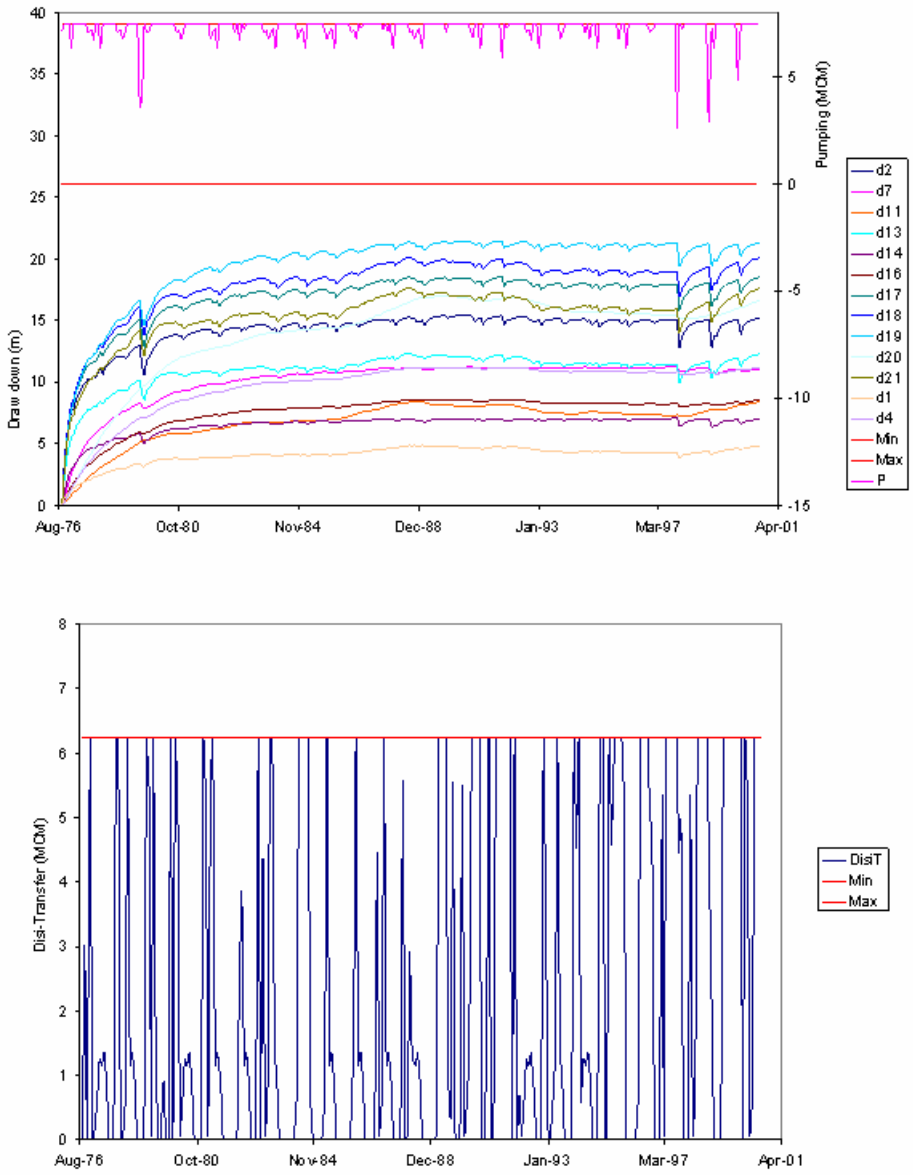

Figure K12: Assessment model, perfect forecast scenario, unconstrained GW drawdown, monthly pumping, drawdown and Disi transfer sequences

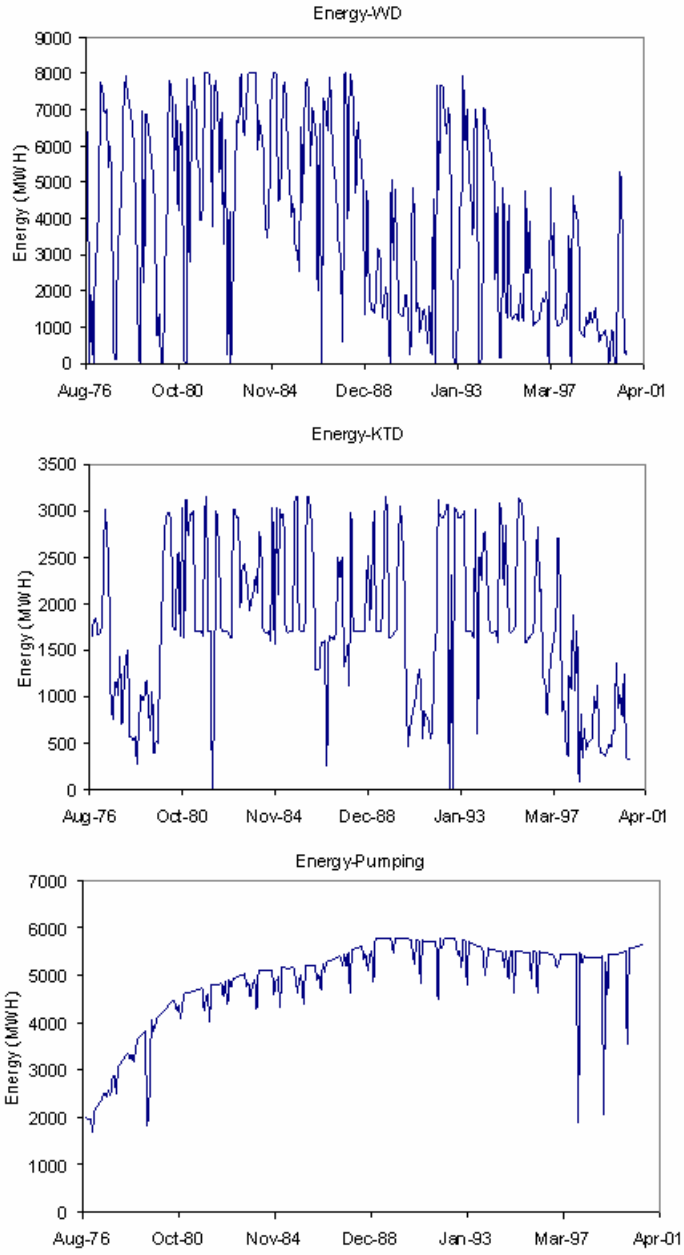

Figure K13: Assessment model, perfect forecast scenario, unconstrained GW drawdown, WD, KTD and pumping energy sequences

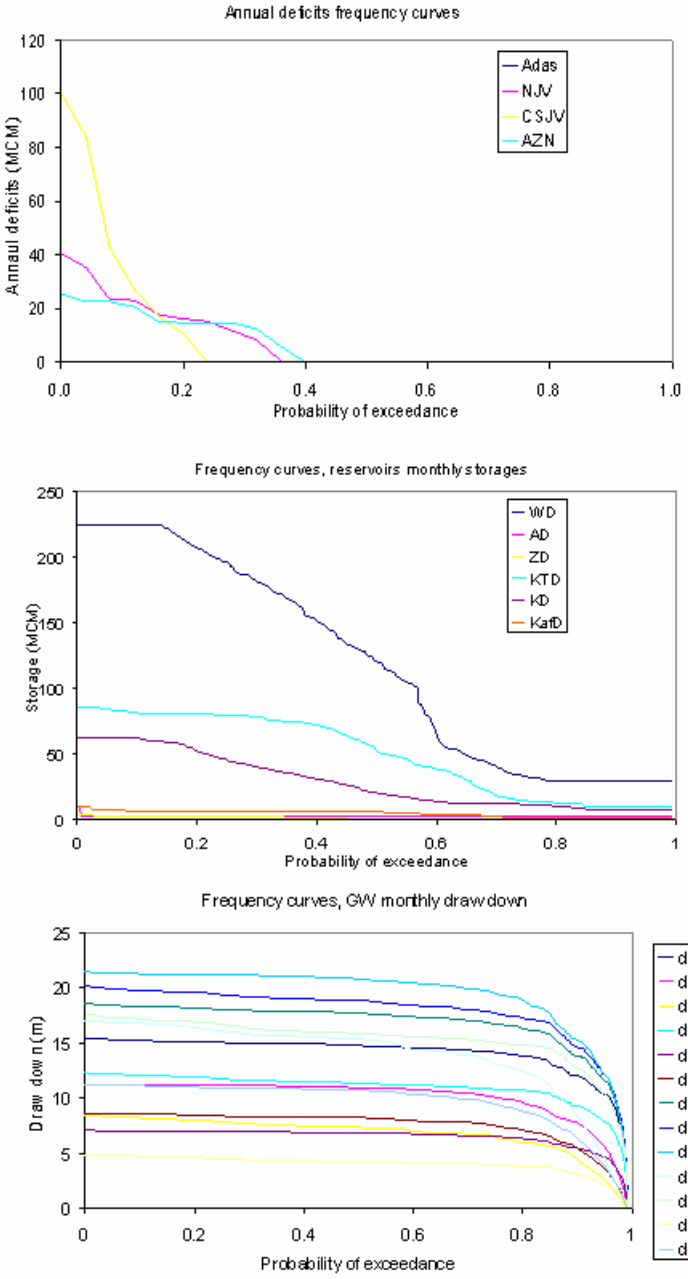

Figure K14: Assessment model, perfect forecast scenario, unconstrained GW drawdown, annual deficits, storages, and drawdowns frequency curves

APPENDIX L

NON-CONJUNCTIVE MANAGEMENT SCENARIO

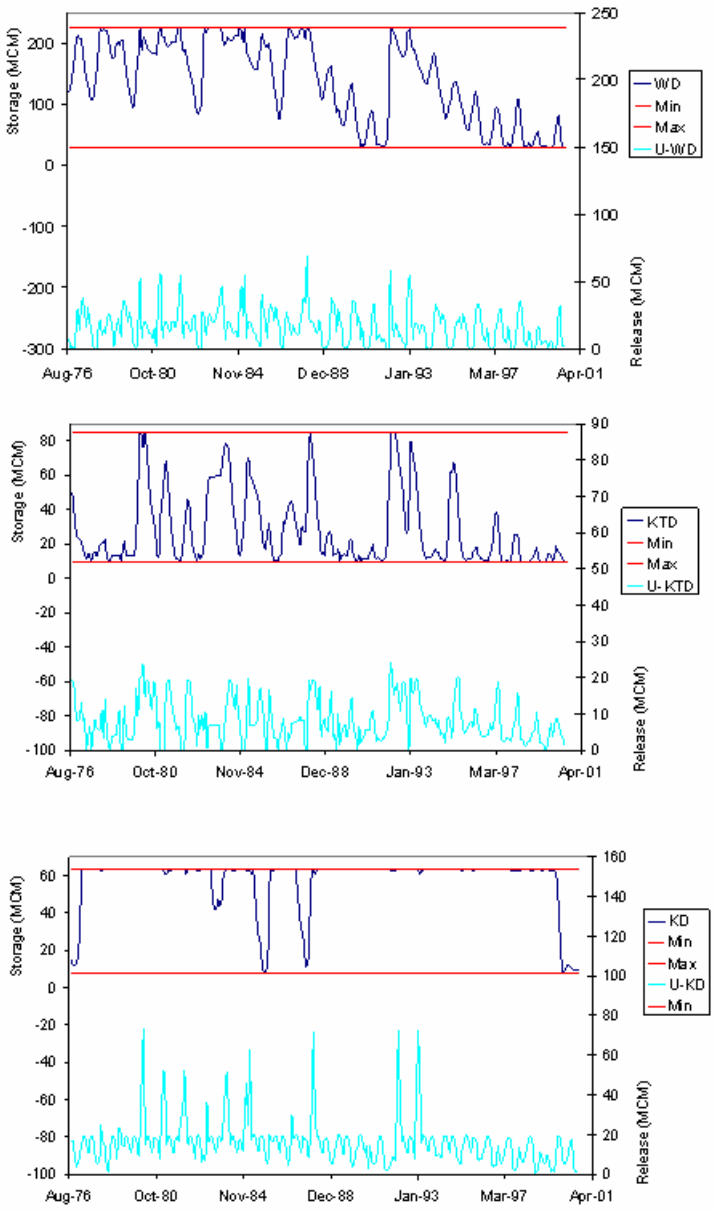

Figure L1: Assessment model, non-conjunctive management, constrained GW drawdown, WD, KTD, and KD storage and release sequences

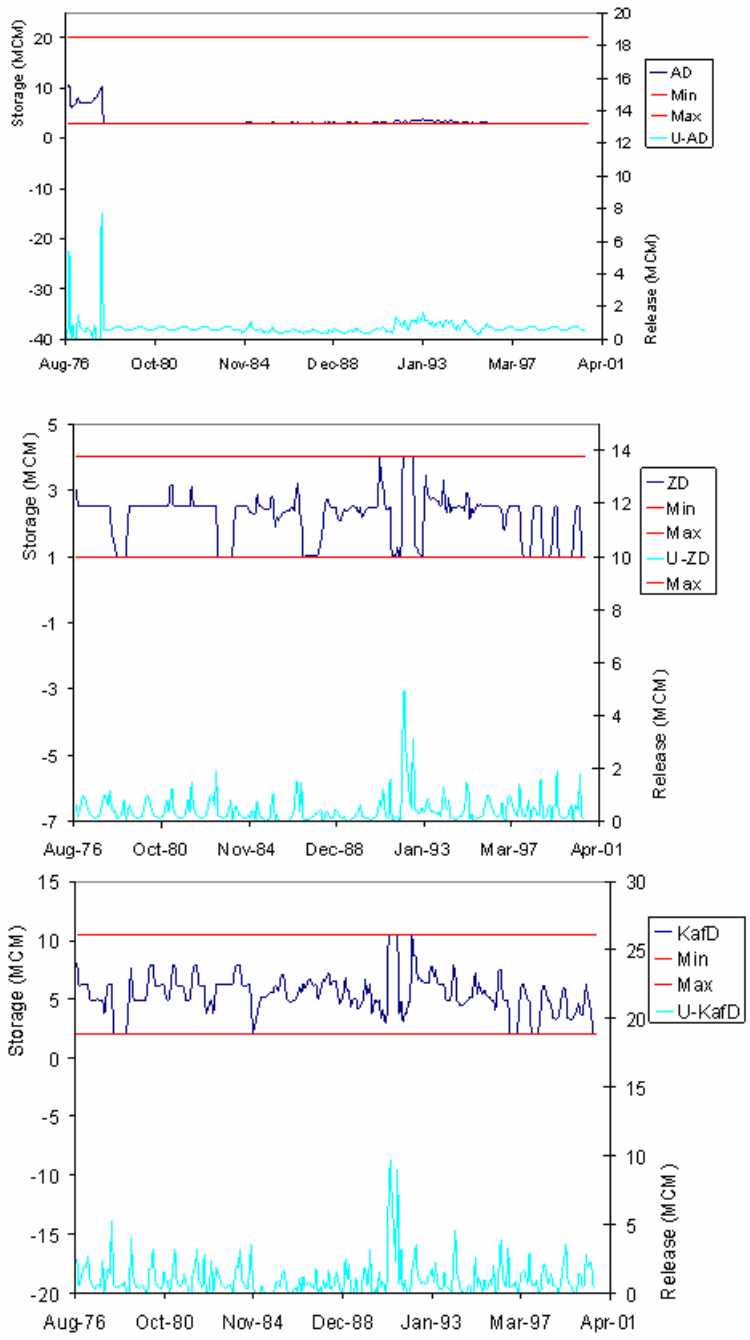

Figure L2: Assessment model, non-conjunctive management, constrained GW drawdown, AD, ZD, and KafD storage and release sequences

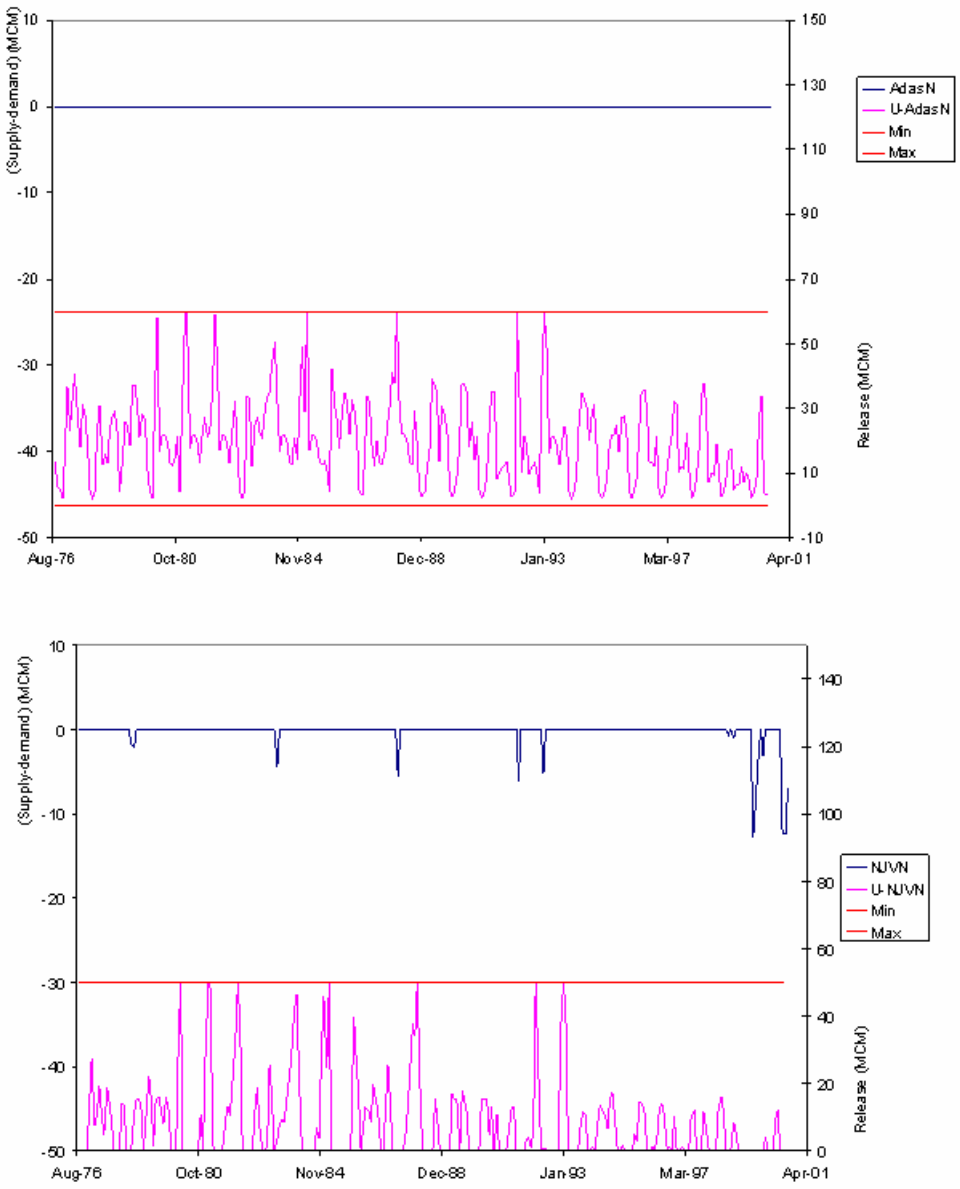

Figure L3: Assessment model, non-conjunctive management, constrained GW drawdown, monthly water deficit and release sequences at Adasiya and North Jordan Valley nodes

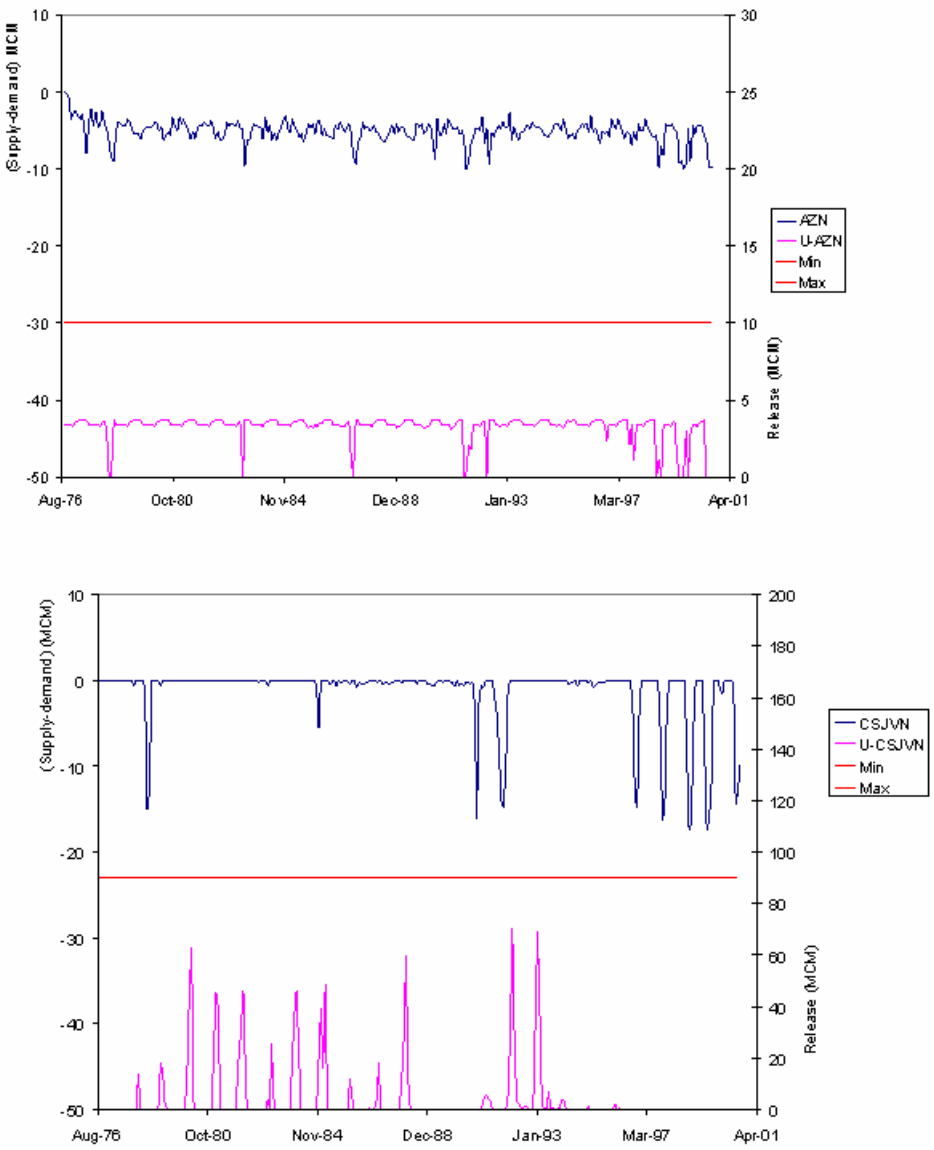

Figure L4: Assessment model, non-conjunctive management, constrained GW drawdown, monthly water deficit and release sequences at Amman-Zarqa and C/S Jordan Valley nodes

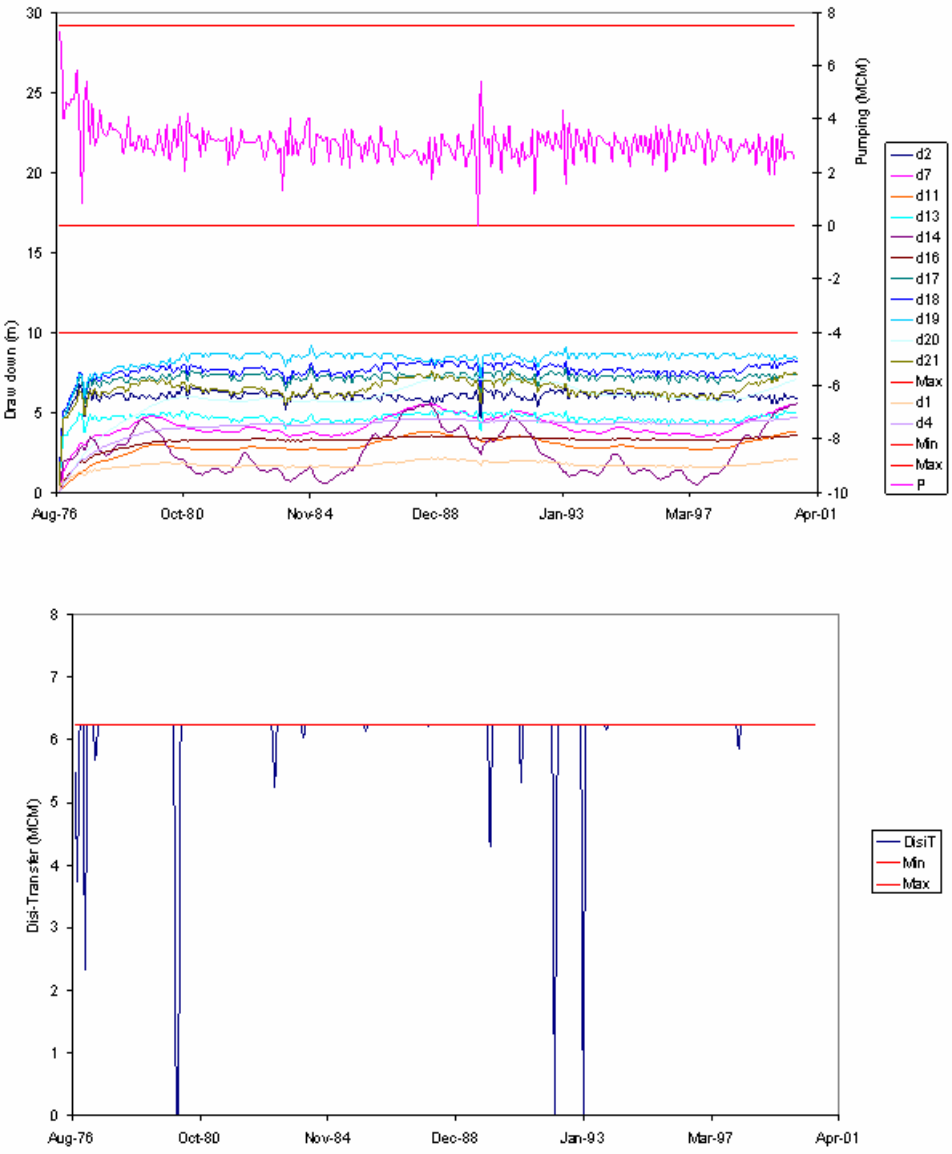

Figure L5: Assessment model, non-conjunctive management, constrained GW drawdown, monthly pumping, drawdown and Disi transfer sequences

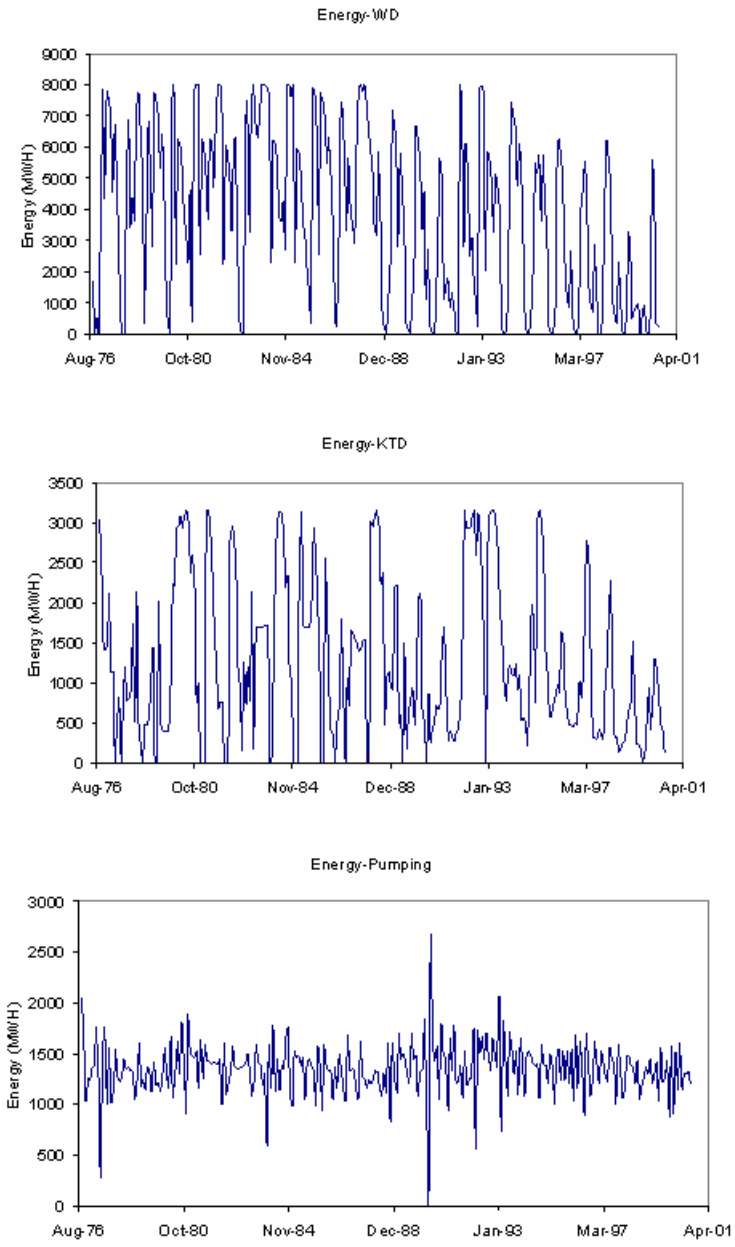

Figure L6: Assessment model, non-conjunctive management, constrained GW drawdown, WD, KTD and pumping energy sequences

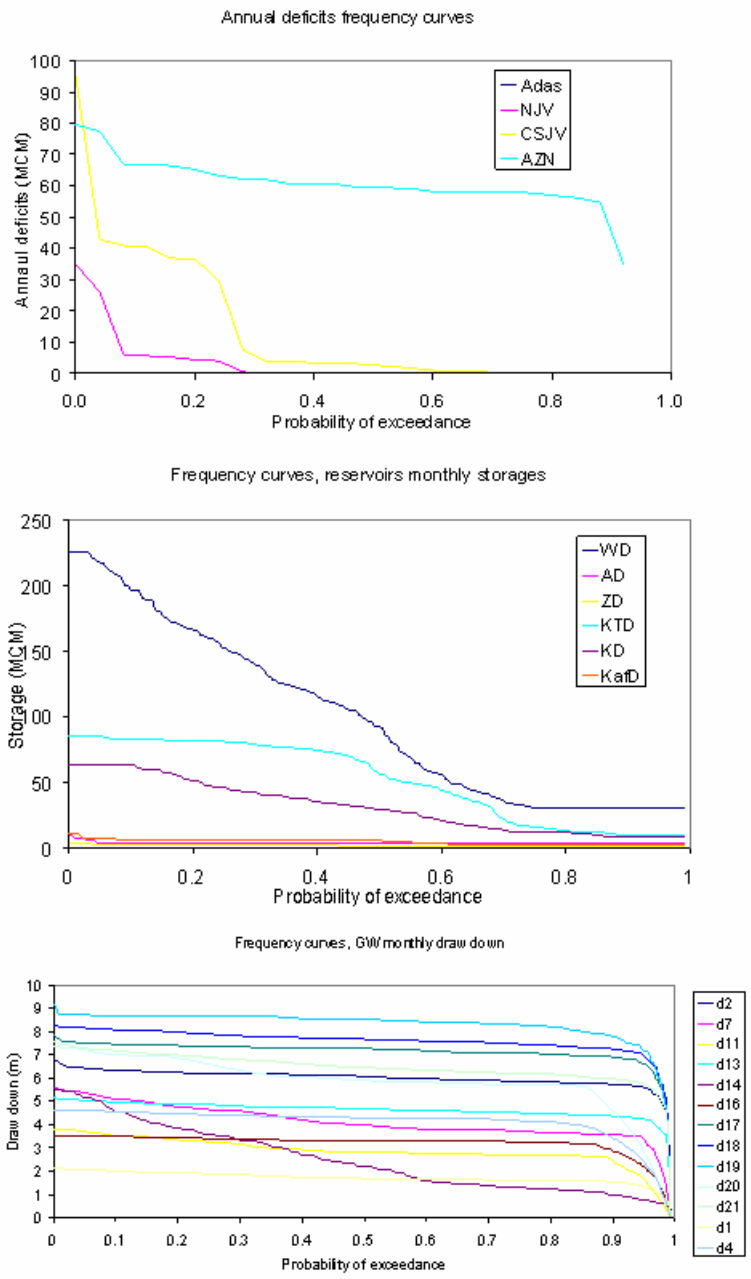

Figure L7: Assessment model, non-conjunctive management, constrained GW drawdown, annual deficits, storages, and drawdowns frequency curves

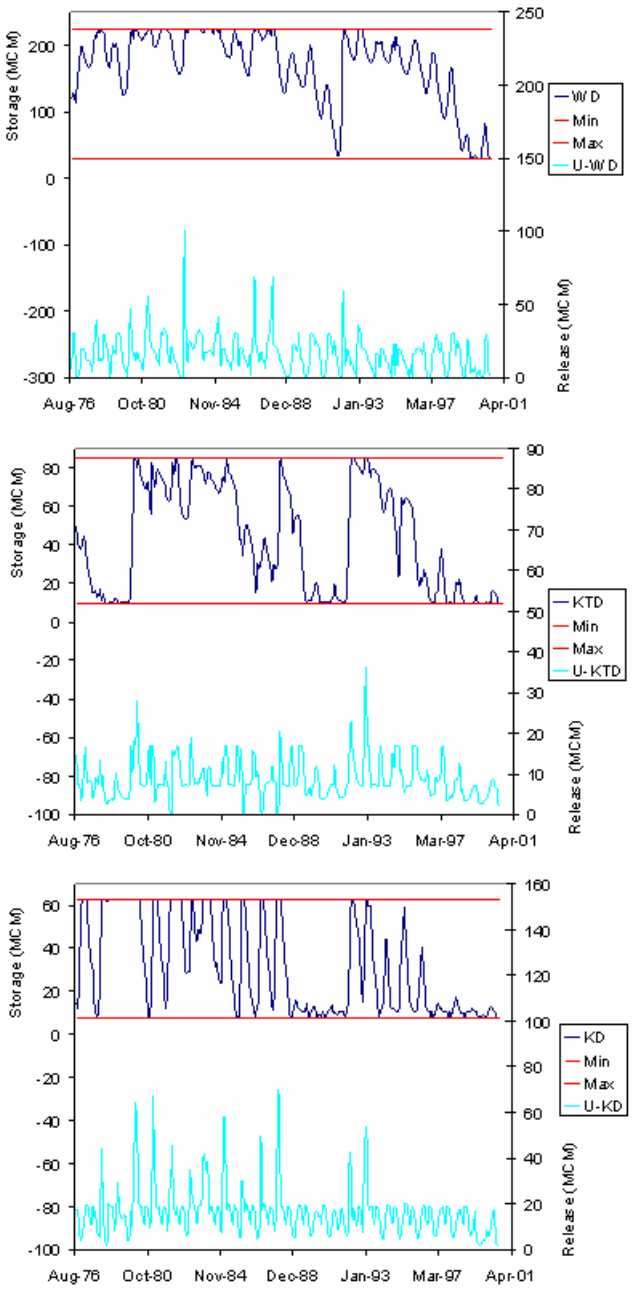

Figure L8: Assessment model, non-conjunctive management, unconstrained GW drawdown , WD, KTD, and KD storage and release sequences

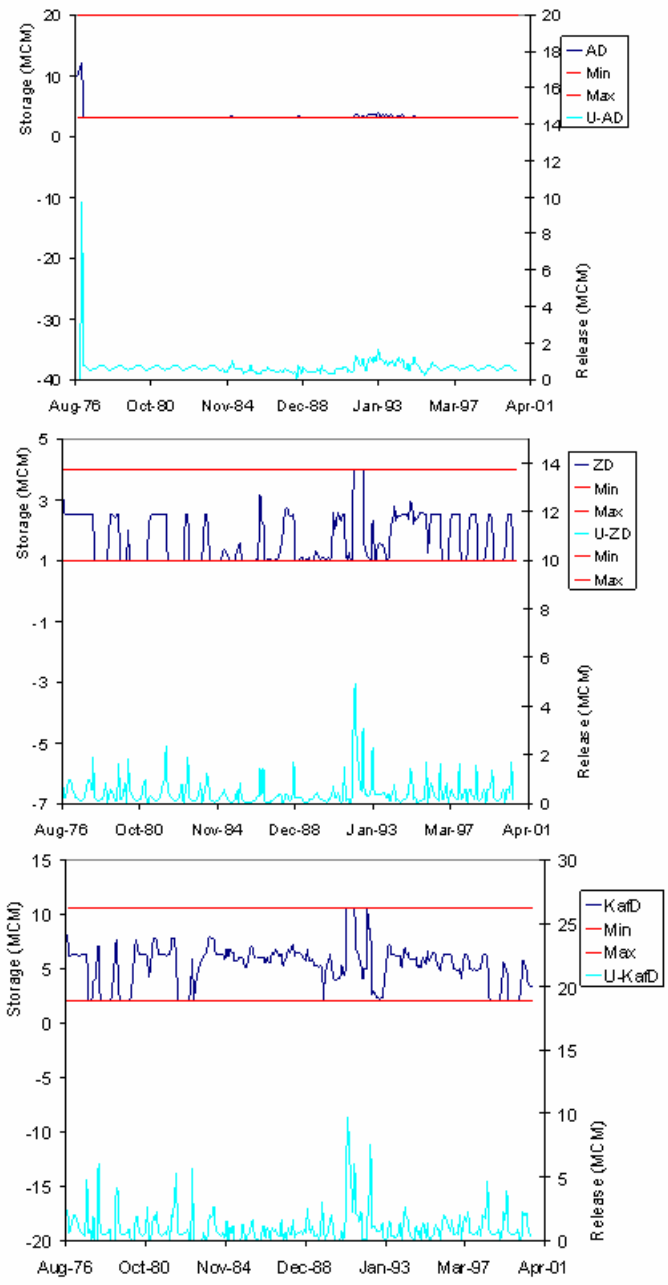

Figure L9: Assessment model, non-conjunctive management, unconstrained GW drawdown, AD, ZD, and KafD storage and release sequences

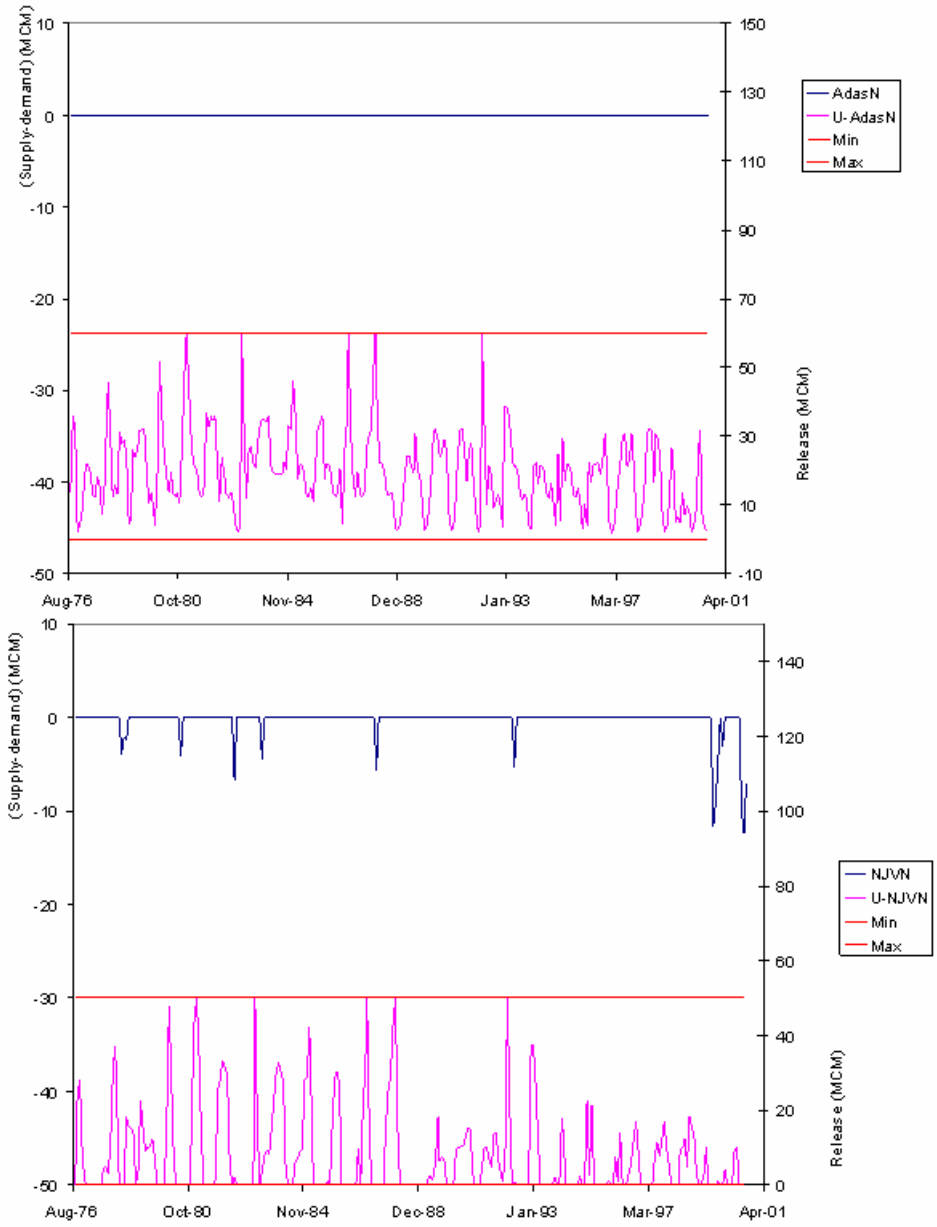

Figure L10: Assessment model, non-conjunctive management, unconstrained GW drawdown, monthly water deficit and release sequences at Adasiya and North Jordan Valley nodes

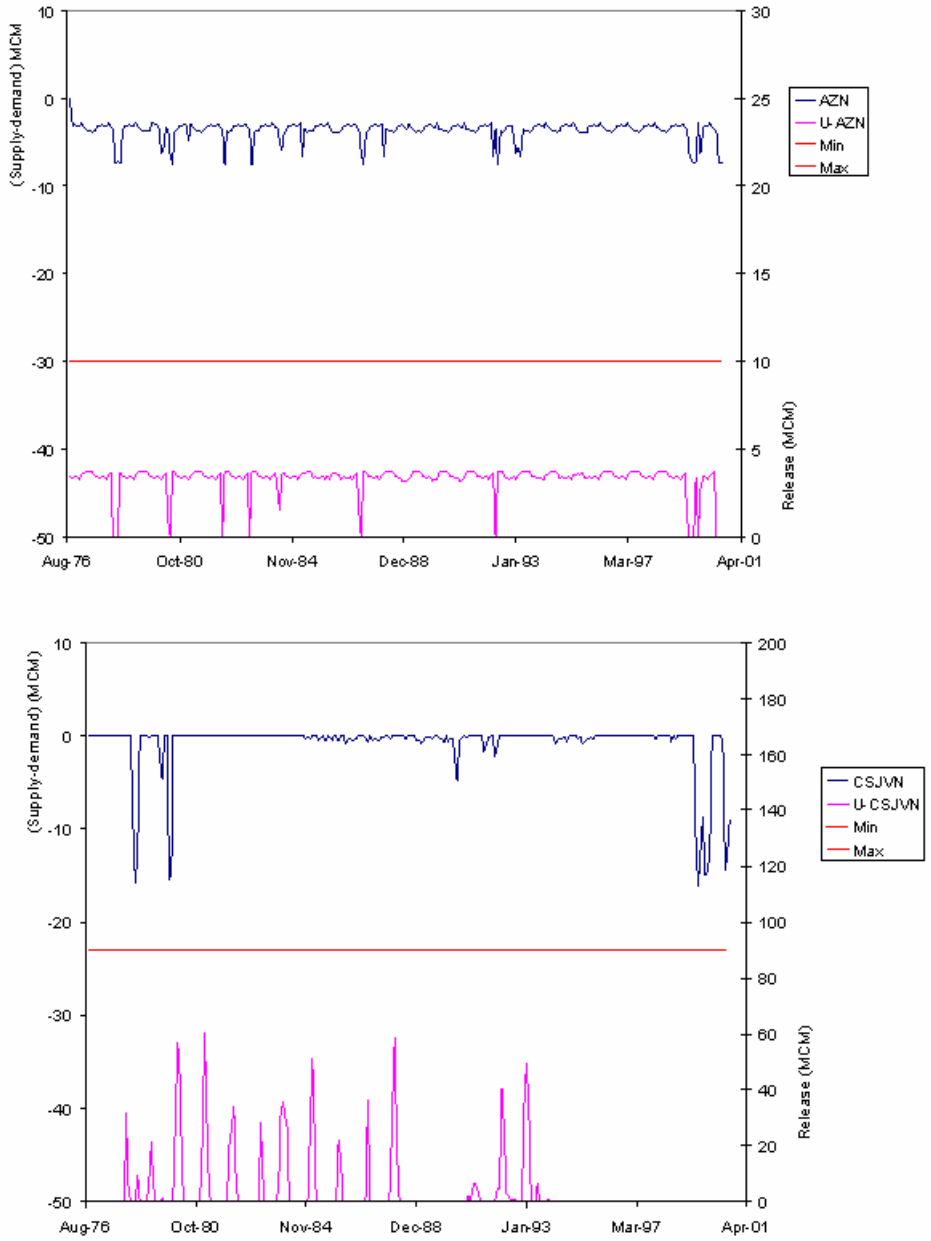

Figure L11: Assessment model, non-conjunctive management, unconstrained GW drawdown, monthly water deficit and release sequences at Amman-Zarqa and C/S Jordan Valley nodes

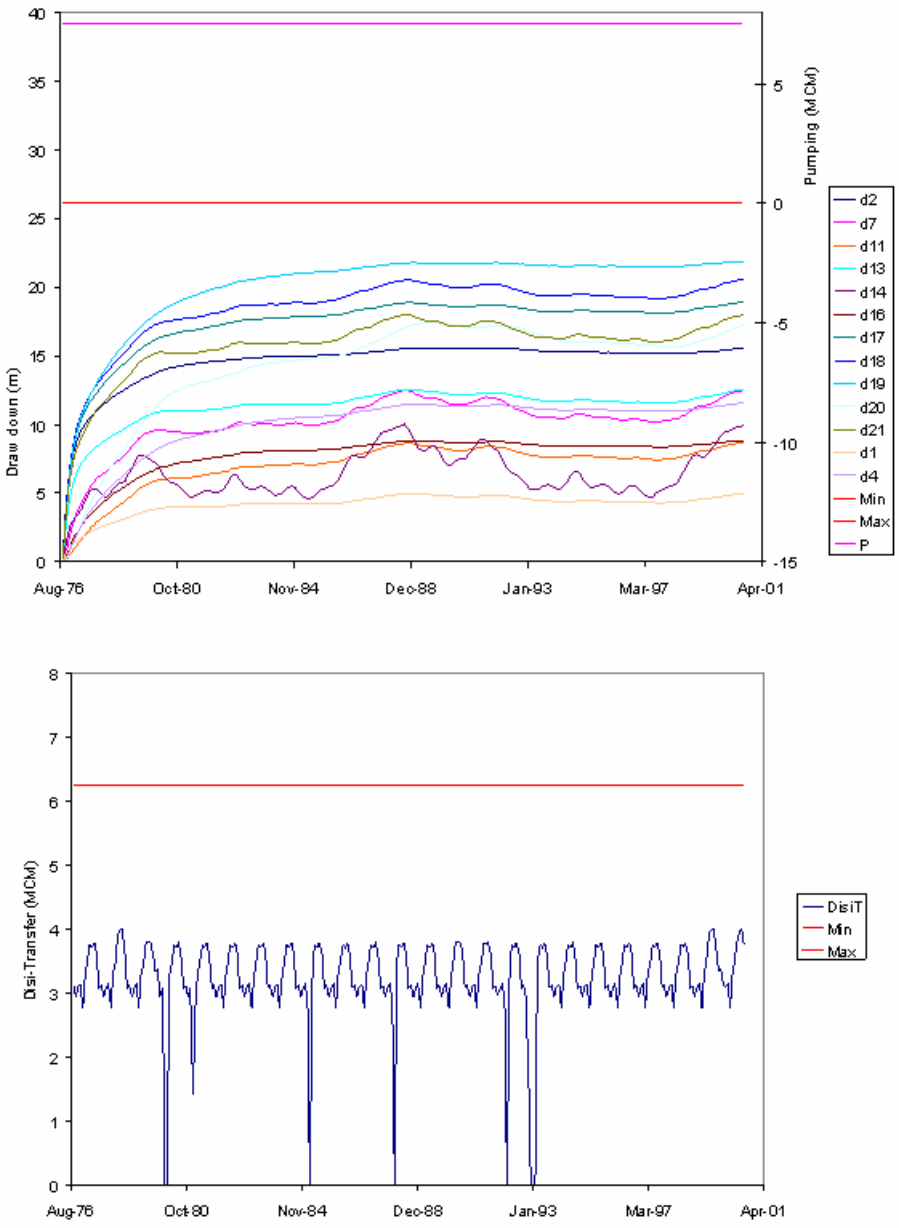

Figure L12: Assessment model, non-conjunctive management, unconstrained GW drawdown, monthly pumping, drawdown and Disi transfer sequences

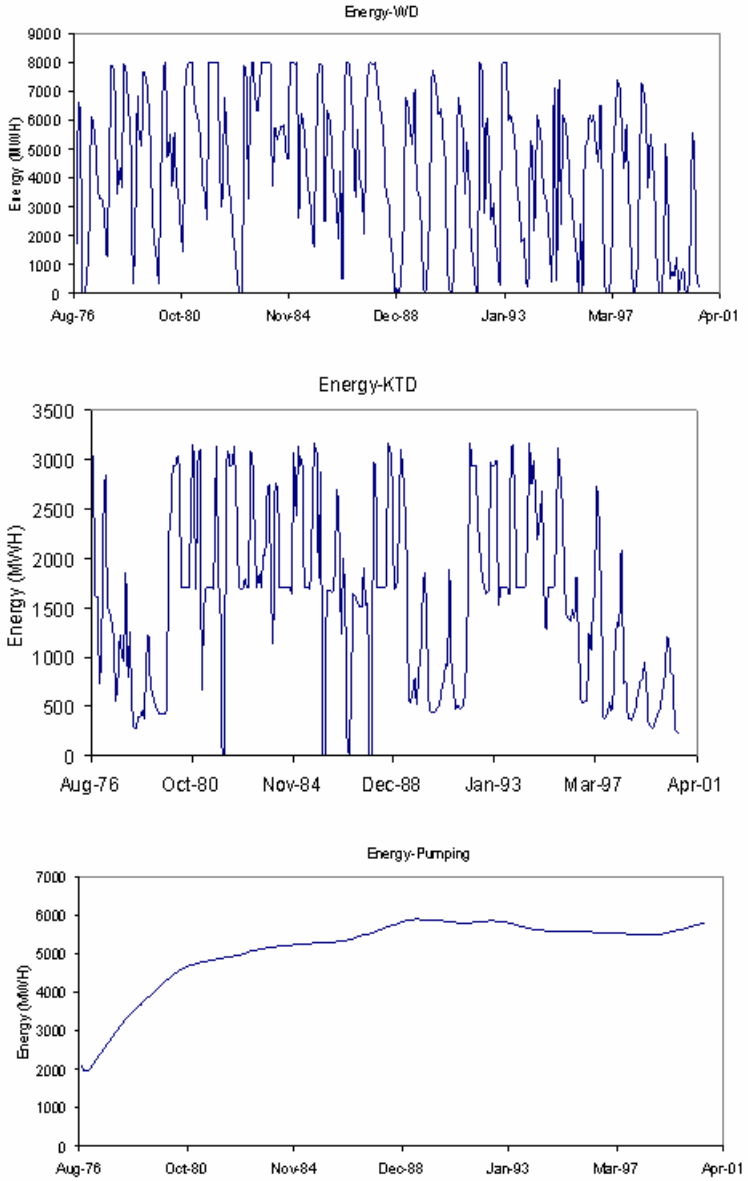

Figure L13: Assessment model, non-conjunctive management, unconstrained GW drawdown , WD, KTD and pumping energy sequences

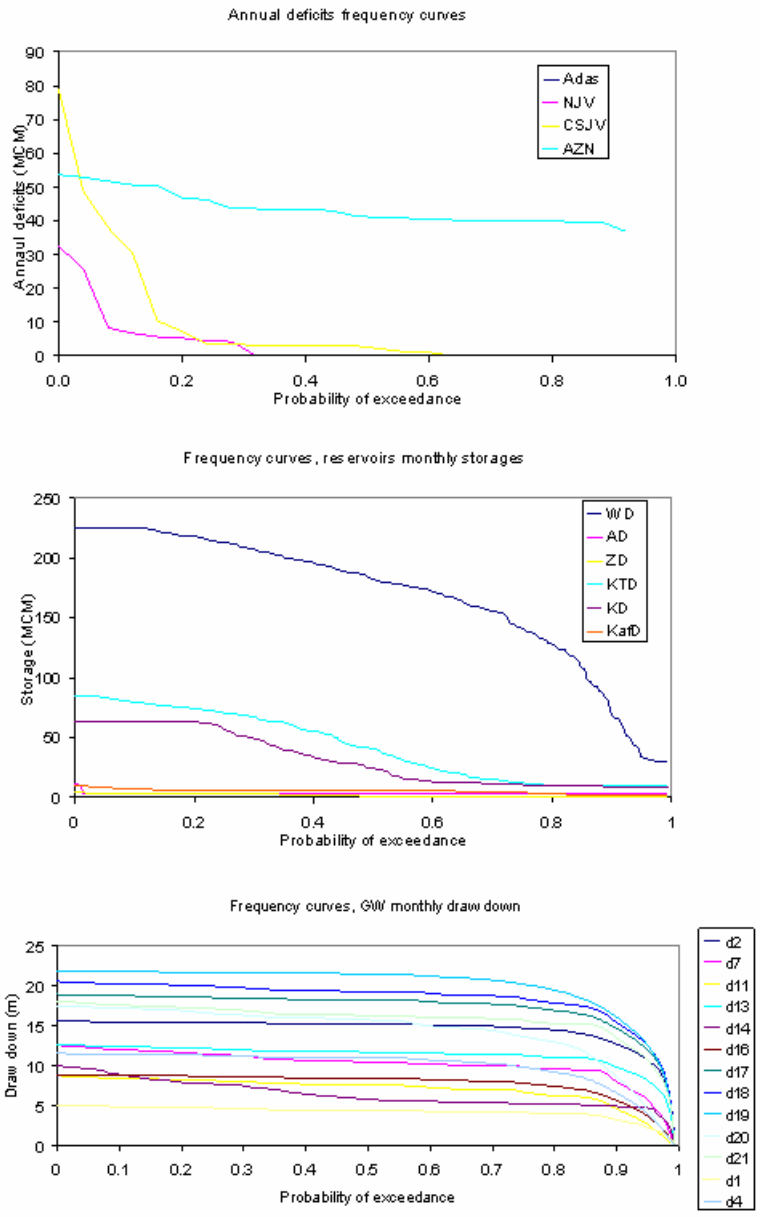

Figure L14: Assessment model, non-conjunctive management, unconstrained GW drawdown, annual deficits, storages, and drawdowns frequency curves

References

Ahlfeld, D.P. 1994. “Applications of Optimal Hydraulic Control to Ground-Water Systems.” *Journal of Water Resources Planning and Management*. Vol. **120(**3). pp. 350-365.

Ahlfeld, D. P. and Mulligan, A.E. 2000. Optimal Management of Flow in Groundwater Systems. Academic Press publishing company, California.

Ahlfeld, D.P., Zafirakou, A., and Riefler, R.G. 1997. “Solution of the Groundwater Transport Management Problem by Sequential Relaxation.”*Advances in Water Resources*. Vol. **21**. pp. 591-604.

Anderson, M. P., and , Woessner, W. W. 1992. Applied Groundwater Modeling. Academic Press Publishing Company, New York.

Chvatal V., 1980. Linear Programming. Freeman publishing company, New York.

Conover, W.J. 1999. Practical Nonparametric Statistics. Willey & Sons publishing company, New York.

Dagan, G., 1982. “Stochastic Modeling of Groundwater Flow by Unconditional and Conditional Probabilities, 2, The Solute Transport.” *Water Resources Research*. Vol. **18**, pp. 835- 842.

Dagan, G., 1990. “Transport in Heterogeneous Formations: Spatial Moments, ergodicity, and effective dispersion.” *Water Resources Research*. Vol. **26**, pp. 1281- 1290.

Dettinger, M.D., and J.L. Wilson, 1981. “First Order Analysis of Uncertainty in Numerical Models of Groundwater Flow, 1, Mathmatical development.“ *Water Resources Research*. Vol. **17**(1), pp. 149- 161.

Donald J. Polmann, Dennis McLaughilin, Steve Luis, Lynn W. Gelhar, and Rachid Ababou. 1991. “Stochastic Modeling of Large-Scale Flow in Heterogeneous Unsaturated Soils.” *Water Resources Research*. Vol.**27**(7), pp. 1447-1458.

El-Nasser, H., 1997. "The Partition of Water Resources in the Jordan River Basin: History and Current Development," Proceedings of the International Conference on "The Water in the Mediterranean Countries: Management Problems of a Scarce Resource," Naples.

Food and Agricultural Organization of the United Nations, 1993. " Water Policies and Agriculture, " in " The State of Food and Agriculture, FAO Agriculture Series No. 26, FAO, Rome, Italy.

Freeze, R. A., and J. A. Cherry, 1979. Groundwater. Prentice Hall publishing company, Englewood Cliffs, N. J.

Georgakakos, A. P., Optimal Control of Water Resources Systems, Lecture Presented at Short Course on Water Resources systems, Environ. Syst. Anal. Group, New Univ. of Lisbon, Portugal, 1988

Georgakakos, A. P., and D. H. Marks, 1987. "A New Method for the Real Time Operation of Reservoir Systems." *Water Resources Research*. Vol. **23**(7), pp. 1376- 1390.

Georgakakos, A.P., and Vlatsa, D.A. 1991. "Stochastic Control of Groundwater Systems." *Water Resources Research.* Vol. **27**(8). pp. 2077-2090.

Georgakakos, A. P. and Yao, H., 2001. "Assessment of Folsom Lake Response to Historical and Potential Future Climate Scenarios. 2. Reservoir Management" *Journal of Hydrology*. Vol **249**. pp. 176-196

Gorelick, S.M., and Remson, I. 1982. "Optimal Dynamic Management of Groundwater Pollutant Sources." *Water Resources Research.* Vol. **18**(1). pp. 71-76.

Gorelick, S.M., and Voss, C.I. 1984. "Aquifer Reclamation Design: The Use of Contaminant Transport Simulation Combined With Nonlinear Programing." *Water Resources Research.* Vol. **20**(4). pp. 415-427.

Haimes, Y.Y., and Dreizin, Y.C. 1977. "Management of Groundwater and Surface Water Via Decomposition." *Water Resources Research*. Vol. **13**(1). pp. 69-77.

Harza Engineering Company. 1988a. "Technical and Economic Feasibity of the Al Wehdah Dam Project, Volume 1- Main Report." Ministry of Water and Irrigation, Amman, Jordan

Harza Engineering Company. 1988b. "Raising King Talal Dam Project ; Operations and Maintenance Manual ." Ministry of Water and Irrigation, Amman, Jordan

Herrling, B., and Heckele, A. 1986. "Coupling of Finite Element and Optimization Methods for the Management of Groundwater Systems." *Advances in Water Resources.* Vol. **9**. pp. 190-195.

Hoeksema, R.J., and Kitanidis, P.K. 1984. "An Application of the

Geostatistical Approach to the Inverse Problem in Two-Dimensional Groundwater Modeling." *Water Resources Research.* Vol. **20**(7). pp. 1003-1020.

Hoeksema, R.J., and Kitanidis, P.K. 1985. "Analysis of the Spatial Structure of Properties of Selected Aquifers." *Water Resources Research*. Vol. **21**(4). pp. 563-572.

Hoeksema, R.J., and Kitanidis, P.K. 1985. "Comparison of Gaussian Conditional Mean and Estimation in the Geostatistical Solution of the Inverse Problem." *Water Resources Research*. Vol. **21**(6). pp. 825-836.

Hoeksema, R.J., and Kitanidis, P.K. 1989. "Prediction of Transmissivities, Heads, and Seepage Velocities Using Mathematical Modeling and Geostatistics." *Advances in Water Resources*. Vol. **12**. pp. 90-101.

James, A. L. and C. M. Oldenburg, 1997. " Linear and Monte Carlo Uncertainty analysis for Subsurface Contaminant Transport Simulation." *Water Resources Research*. Vol. **33**(11), pp. 2495- 2508.

Jones, L., Willis, R., and Yeh, W. 1987. "Optimal Control of Nonlinear Groundwater Hydraulics Using Differential Dynamic Programming." *Water Resources Research.* Vol. **23**(11). pp. 2097-2106.

Keshari, A.K., and Datta, B. 1995. "Integrated Optimal Management of Ground-Water Pollution and Withdrawal." *Ground Water*. Vol. **34**(1). pp. 104-113.

Kunstmann, H., Kinzelbach, W., and Siegfried, T. 2002. "Conditional First Order Second-Moment Method and its Application to the Quantification of Uncertainty in Groundwater Modeling." *Water Resources Research*. Vol. **38**(4). pp. 1-14.

Lefkoff, L.J., and Gorelick, S.M. 1986. "Design and Cost Analysis of Rapid Aquifer Restoration Systems Using Flow Simulation and Quadratic Programming." *Ground Water*. Vol. **24**(6). pp. 777-790.

Livezey, R.E., and Chen, W.Y. 1982. "Statistical Field Significance and its Determination by Monte Carlo Techniques." *Monthly Weather Review*. Vol. **111**. pp. 46-59.

Maddock, T. 1973. "Management Model as a Tool for Studying the Worth of Data." *Water Resources Research*. Vol. **9**(2). pp. 270-280.

Mantoglou, A., and L. W. Gelhar, 1987a. "Large-Scale Models of Transient Unsaturated Flow Systems." *Water Resources Research*. Vol. **23**(1), pp. 37- 46.

Mantoglou, A., and L. W. Gelhar, 1987b. “Capillary Tension Head Variance, Mean Soil Moisture Content , and Effective Specific Soil Moisture. Capacity of Transient Unsaturated Flow in Stratified Soils .” *Water Resources Research*. Vol. **23**(1), pp. 47- 56.

Mantoglou, A., and L. W. Gelhar, 1987c. “Effective Hydraulic Conductivities of Transient Unsaturated Flow in Stratified Soils.” *Water Resources Research*. Vol. **23**(1), pp. 57- 68.

Mcdonald M. G. and A. W. Harbaugh, 1988. A Modular Three- Dimensional Finite-Difference Groundwater Flow Model. USGS, Virginia.

Ministry of Water and Irrigation, Amman, Jordan. 2000. “Hydrogeology of the Amman-Zarqa Groundwater Basin.”

Ministry of Water and Irrigation, Amman, Jordan. 2000. “Ministry of Water and Irrigation Annual Report 2000.”

Ministry of Water and Irrigation, Amman, Jordan. The Website For the Water Industry. World Wide Web Browser: www.water-technology.net/projects/greater_amman/specs.html

Ministry of Water and Irrigation, “Treaty of Peace Between the Hashemite Kingdom of Jordan and the State of Israel , Annex ||: Water Related Matters.” Amman, Jordan

Murtagh, B. A., and M. A. Saunders, 1987, MINOS 5.1 Users Guide, SOL Rep 83-20R, Revised 1987, Stanford Univ., Stanford, Calif.

Reichard, E.G., 1995. “ Groundwater-Surface Water Management With Stochastic Surface Water Supplies: A simulation optimization Approach.“ *Water Resources Research*. Vol. **31**(11), pp. 2845- 2865.

U.S. Geological Survey, 1998. “Overview of Middle East Water Resources.” Middle East Water Data Banks Project.

Vivek Kapoor and Lynn W. Gelhar. 1994. “Transport in Three-Dimensional Heterogeneous Aquifers. 1. Dynamics of concentration fluctuations.” *Water Resources Research*. Vol. **30**(6), pp. 1775- 1788.

Wagner, B.J. 1999. “Evaluation Data Worth for Ground-Water Management Under Uncertainty.” *Journal of Water Resources Planning and Management*. Vol. **125(**5). pp. 281-288.

Wagner, B.J., and Gorelick, S.M. 1986. “A Statistical Methodology for

Estimating Transport Parameters: Theory and Applications to One-Dimensional Advective-Dispersive Systems." *Water Resources Research*. Vol. **22**(8). pp. 1303-1315.

Wagner, B.J., and Gorelick, S.M. 1987. "Optimal Groundwater Quality Management Under Parameter Uncertainty." *Water Resources Research.* Vol. **23**(7). pp. 1162-1174.

Wagner, B.J., and Gorelick, S.M. 1989. "Reliable Aquifer Remediation in the Presence of Spatially Variable Hydraulic Conductivity: From Data to Design." *Water Resources Research*. Vol. **25**(10). pp. 2211-2225.

Wilks, D. S., 2000. Statistical Methods in Atmospheric Sciences. Academic Press publishing company, California.

Willis, R., and Finney, B.A. 1985. "Optimal Control of Nonlinear Groundwater Hydraulics: Theoretical Development and Numerical Experiments." *Water Resources Research*. Vol. **21**(10). pp. 1476-1482.

Yazicigil, H., and Rasheeduddin, M. 1987. "Optimization Model for Groundwater Management in Multi-Aquifer Systems." *Journal of Water Resources Planning and Management*. Vol. **113(**2). pp. 257-273.

Vita

Malek Mohammad Abu Rumman was born in Amman, Jordan on April 19, 1974. He graduated from high school in 1992. At the same year he started his B.S. in Civil Engineering at the University of Jordan. He finished his undergraduate degree 1n 1996 with the highest honors, ranked third among the 1996 graduating class. At the end of his undergraduate studies, Malek got an engineering training assistantship in Sweden.

From March 1997 to December 1997, Malek worked as a consultant engineer at an engineering company in Dubai, United Arab Emirates.

From January 1998 to the present, Malek has attended graduate studies at the School of Civil and Environmental Engineering, Environmental Fluid Mechanics and water resources program at Georgia Institute of Technology (GA Tech). During this period Malek worked as a research associate in the Georgia Water Resources Institute. Also From July 1999 to the present, Malek has started working part time with the United States Geological Survey (USGS) on groundwater related modeling problems.

In December 2002 Malek married Taroub Al-Zubi, the couple have one daughter Amal Abu Rumman, born in 2003. Malek Loves hiking and camping, and enjoys nature.